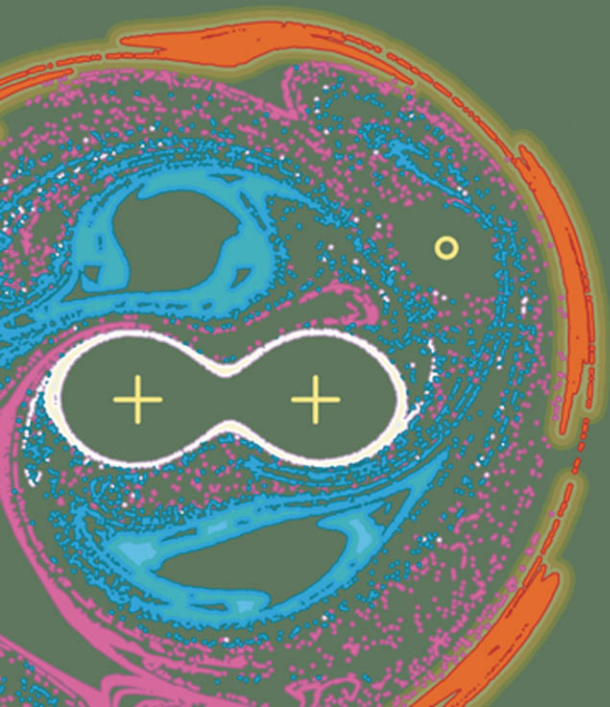


OXFORD

George M. Zaslavsky

# Hamiltonian Chaos & Fractional Dynamics



# HAMILTONIAN CHAOS AND FRACTIONAL DYNAMICS

*This page intentionally left blank*

# Hamiltonian Chaos and Fractional Dynamics

---

GEORGE M. ZASLAVSKY

*Department of Physics and Courant Institute of  
Mathematical Sciences, New York University*

OXFORD  
UNIVERSITY PRESS



# OXFORD

UNIVERSITY PRESS

Great Clarendon Street, Oxford OX2 6DP

Oxford University Press is a department of the University of Oxford.  
It furthers the University's objective of excellence in research, scholarship,  
and education by publishing worldwide in

Oxford New York

Auckland Cape Town Dar es Salaam Hong Kong Karachi

Kuala Lumpur Madrid Melbourne Mexico City Nairobi

New Delhi Shanghai Taipei Toronto

With offices in

Argentina Austria Brazil Chile Czech Republic France Greece

Guatemala Hungary Italy Japan Poland Portugal Singapore

South Korea Switzerland Thailand Turkey Ukraine Vietnam

Oxford is a registered trade mark of Oxford University Press  
in the UK and in certain other countries

Published in the United States  
by Oxford University Press Inc., New York

© Oxford University Press 2005

The moral rights of the author have been asserted

Database right Oxford University Press (maker)

First published 2005

Reprinted 2006

All rights reserved. No part of this publication may be reproduced,  
stored in a retrieval system, or transmitted, in any form or by any means,  
without the prior permission in writing of Oxford University Press,  
or as expressly permitted by law, or under terms agreed with the appropriate  
reprographics rights organization. Enquiries concerning reproduction  
outside the scope of the above should be sent to the Rights Department,  
Oxford University Press, at the address above

You must not circulate this book in any other binding or cover  
and you must impose this same condition on any acquirer

A catalogue record for this title is available from the  
British Library

Library of Congress Cataloging in Publication Data  
Zaslavsky, George M.  
Hamiltonian chaos and fractional dynamics/George M. Zaslavsky.  
p. cm.

Includes bibliographical references and index.

ISBN 0-19-852604-0 (alk. paper)

1. Hamiltonian systems. 2. Chaotic behavior in systems. I. Title.

QC174.85.H35Z37 2005

530.15'474-dc22

2004018403

10 9 8 7 6 5 4 3 2

Typeset by Newgen Imaging Systems (P) Ltd., Chennai, India

Printed in Great Britain

on acid-free paper by Biddles Ltd, King's Lynn

## PREFACE

Non-linear dynamics had always been an important subject of study in different physical and mathematical disciplines, but its real success and a radically new understanding of non-linear processes occurred in the last 40 years. This understanding was inspired by the discovery and insight of a new phenomenon known as dynamical chaos, or simply chaos. The reason for that is easy to understand, since any typical system with more than one degree of freedom possesses chaotic motion for some initial conditions. We still do not know what is the measure of chaotic trajectories, but it seems that it is non-zero, and that makes the study of chaos important for constructing the models of dynamical processes in nature.

Chaotic dynamics has a rigorous definition, or more precisely, definitions that may be not equivalent but which nevertheless have one common feature: none of these definitions can be applied to typical or realistic Hamiltonian dynamics. In other words, all rigorous models of chaos should be considered as strong, and sometimes too strong, idealizations of what we find in the theoretical models of nature. The reason for this is that we never have real chaotic dynamics for all possible initial conditions and, in fact, non-chaotic orbits are always neighbouring the chaotic ones. The mixture of chaotic and non-chaotic domains in the phase space does not have a simple pattern and the understanding of interaction of these domains remains incomplete.

A much more serious difficulty in the investigation of realistic systems is that chaos, in its rigorous definition, is not the only way in which the randomness of trajectories can occur in the solutions of regular non-random equations of motion. This means that the randomness of the dynamics may have different representations where the chaos is one of several possible ways of realization of random dynamics. The well-known euphemism of chaos—the ‘butterfly effect’—which originated from the earliest period of study of chaotic dynamics looks oversimplified now. The research which followed, along with deeper investigations, has involved new ideas of fractal time, non-Gaussian distributions, non-ergodic dynamics, non-Kolmogorov–Arnold–Moser theory analysis of stability, non-exponential divergence of trajectories, and many other ‘nons’.

This book turns the attention to the new and realistic image of the origin of dynamical chaos and randomness, considering the basic principles of the Hamiltonian theory of chaos and some applications that include such entities as cooling of particles and signals, control and erasing of chaos, polynomial complexity, and Maxwell’s Demon. An insight into the origin of randomness in

dynamical systems, which can be not of the same type as chaos, reveals new possibilities in physics, biology, chemistry, engineering, and other disciplines.

A more general approach to the randomness of dynamics requires new vision of the dynamical objects and new tools. For example, a typical negligence of zero measure sets in the ergodic theory can not be applied to realistic systems in general, since some zero measure domains in the phase space are responsible for the system evolution, particle transport, character of statistical laws, and many other important features of the dynamics. A typical Gaussian process, used to describe kinetics due to chaos, is too rough an approximation that has not worked for a fairly long time. The properties of random trajectories, which typically are assigned to non-zero Lyapunov exponents, may not be related to these exponents, and the random behaviour of the system may be governed by zero-Lyapunov-exponent theory rather than the non-zero one. Last, but not least, the dynamics of realistic Hamiltonian systems has unusual microscopic features that are a direct consequence of its fractal space-time structures and super-complicated phase space topologies. Fractality of the chaotic dynamics and kinetics is the dominant part of the book that also includes some existing material on the Hamiltonian dynamics that are non-ergodic and do not mix well.

The book consists of 4 parts which comprise of 24 chapters with appendices. The first part, 'Chaotic Dynamics', is the largest. In this part the reader is provided with some basic information about typical Hamiltonian models of the dynamics, perturbed dynamics, definitions and examples of the chaotic dynamics, and physical models of chaos. More detailed description is given for separatrix chaos, stochastic webs, and the perturbation theory beyond the KAM-theory for infinitesimal non-linearity. Phase space topology, symmetry of webs, and renormalization group theory of the near separatrix dynamics are specific features of the first section. The second part is 'Fractality of Chaos'. In addition to the more or less usual material on the fractal features of the chaotic trajectories, this part includes Poincaré recurrences analysis, fractal time structures of trajectories, and descriptions of different dynamical quasi-traps. The third part is 'Kinetics'. Beginning with the traditional description of chaotic dynamics using the diffusion equation, there is a detailed motivation and conditions of the failure of this description. We include the auxiliary material on Levy processes and Levy flights. The basic essence of this part is devoted to fractional kinetics, its foundation, description, modification, solutions, and the renormalization group analysis. A special chapter in this part is 'Pseudochaos', i.e. kinetics of a system with weak mixing and zero Lyapunov exponents. The fourth part is 'Applications', which is mainly devoted to application of the theory of chaos to some fundamental problems of dynamics: complexity and entropy of systems, foundation of statistical physics on the basis of chaos theory, and dynamics of advected tracers and vortices. This part considers dynamical cooling, the construction of Maxwell's Demon, and interplay between exponential and polynomial instabilities in different models of dynamics. Four appendices should help the readers with elliptic functions and fractional calculus.

The material of the book, as is clear from the above description, does not follow the traditional scheme of the majority of the existing literature on chaos. The intention of the author was to put together the most difficult and not yet clear problems of the general theory of chaotic systems. The readers will find here some discussions that are not typically included in the standard texts: Poincaré recurrences and Maxwell's Demon, non-ergodicity, log-periodicity, dynamical quasi-traps, dynamical cooling and chaos erasing, space-time fractality, directional complexity and entropy, chaos and origin of statistical laws, symmetric and quasi-symmetric tilings, oriental patterns, and many others. The importance of the discussed issues and understanding of their origins should inspire the researchers and students to touch the most intimate areas of non-linear dynamics.

The majority of the material in the book is based on the lecture courses and research of the author and his colleagues in the Courant Institute of Mathematical Sciences and Physics Department of New York University. Parts of the material were published in (Zaslavsky, *et al.* (1991); Zaslavsky (1998), (2002)). The book can be read by researchers and students of physics, mathematics, and engineering who have a university-level knowledge of contemporary dynamics and an elementary knowledge of chaos theory. The material of the book is self-contained and may serve as an introduction to difficult problems on the contemporary theory of Hamiltonian chaotic dynamics in systems with few degrees of freedom, while a more comprehensive study will require more specialized sources. Some derivations of the basic material are included in the problems. We deliberately include a few long derivations as an inspirational challenge for those who would like to work in the area of chaotic dynamics. Although the book considers the material related to Hamiltonian systems, some tools we discuss can be applied to a very broad class of dynamical systems such as the stock market or the Internet.

It is my great pleasure to express the deep appreciation and gratitude to all those who have helped me in working on this book. I had numerous inspiring discussions with Michael Shlesinger on fractal time, Weierstrass, and continuous time random walks, and with Valentine Afraimovich and Lai-Sang Young on complexity, entropy, and contemporary ergodic theory. I do not think that I could have gone successfully through different problems without their help. Many results and achievements are shared with my co-authors: Sadrilla Abdullaev, Valentine Afraimovich, Valery Beloshapkin, Sadrudin Benkadda, Benjamin Carreras, Mark Edelman, Serge Kassibrakis, Leonid Kuznetsov, Xavier Leoncini, Anatoly Neishtadt, Boris Niyasov, Sergei Prants, Vered Rom-Kedar, Roald Sagdeev, Alexander Saichev, Don Stevens, Michael Shlesinger, Alexander Tretiakov, Daniel Usikov, Harold Weitzner, and Roscoe White. I also have made important results with my close collaborator Alexander Chernikov and student Oleg Lyubomudrov who have tragically since died. Different results of the book were discussed with Maurice Courbage, John Lowenstein, Dimitri Treschev, and

Yasha Sinai. Mark Edelman has helped with preparing the pictures for publication. Pat Sruse has printed the text of the book, while Mark Edelman, Rong Fan, and Caroline Muller have helped with the final editing of the text. My special thanks to the staff of Oxford University Press for their help in preparing the book for publication, and particularly I wish to thank Sonke Adlung for the enthusiastic support of the idea to write the book, and to Anita Petrie for the thorough editing work.

During the days of working on the book I received warm hospitality from Vered Rom-Kedar at the Weitzmann Institute of Science (Rehovot, Israel), Sadri Benkadda at the Division of Complex Systems, CNRS (Marseille, France), Vladimir Zeitlin at the École Normale Supérieure (Paris, France), Vitali Milman at Tel-Aviv University (Tel-Aviv, Israel), and Mark Green at IPAM, UCLA (Los Angeles, USA). I also appreciate the U.S. Navy and the U.S. Department of Energy for supporting a significant part of my research.

The book includes numerous figures obtained with my colleagues and published in my papers and books. Kind permissions were received from the publishers World Scientific, American Physical Society, American Institute of Physics, and Elsevier Science B.V. for the reproduction of the following figures of this book: Figs. 9.2, 9.6, 9.7, 12.4, 12.6, 15.2, 16.1, 16.2, 17.1 from (Zaslavsky *et al.*, 1997); Figs. 11.5–11.7 from (Zaslavsky and Edelman, 2000); Figs. 6.2, 12.1, 12.3, 22.9 from (Zaslavsky, 1995); Figs. 9.5, 19.14, 19.15, 22.1, 22.4–22.6 from (Zaslavsky and Edelman, 2004); Figs. 6.3, 6.5–6.10 from (Kuznetsov and Zaslavsky, 1997); Figs. 9.9, 12.7, 19.1, 19.2, 22.7, 22.8 from (Zaslavsky, 2002b); Figs. 9.3, 15.3, 15.4, 22.2, 22.3 from (Zaslavsky and Edelman, 1997); Figs. 19.6, 19.7, 19.9–19.12 from (Zaslavsky and Edelman, 2001); Figs. 20.1, 21.1, 21.2 from (Afraimovich and Zaslavsky, 2003); Figs. 23.1, 23.3–23.5 from (Govorukhin *et al.*, 1999); Figs. 24.1–24.3 from Kuznetsov and Zaslavsky, 1998); Figs. 24.4–24.6 from (Kuznetsov and Zaslavsky, 2000); Fig. 24.7 from (Leoncini *et al.*, 2001); Figs. 24.8–24.11 from (Leoncini and Zaslavsky, 2002).

A color picture on the cover shows an advected particle in a flow of three vortices. It was obtained from (Leoncini *et al.*, 2001) and modified to the present form by M. Zaslavski.

*George Moiseevich  
Zaslavsky  
New York, 2004*

# CONTENTS

## Part 1 Chaotic Dynamics

<b>1</b>	<b>Hamiltonian dynamics</b>	<b>3</b>
1.1	Hamiltonian equations	3
1.2	Phase space dynamics	5
1.3	Action-angle variable (one degree of freedom)	8
	Notes	
	Problems	
<b>2</b>	<b>Examples of Hamiltonian dynamics</b>	<b>13</b>
2.1	Pendulum	13
2.2	Oscillations in the infinite potential well	16
2.3	Magnetic moments	17
2.4	Field line behaviour	18
2.5	Hamiltonian equations for the ABC-flow	20
	Problems	22
<b>3</b>	<b>Perturbed dynamics</b>	<b>23</b>
3.1	The Liouville–Arnold theorem on integrability	23
3.2	Consequences of the integrability	25
3.3	Non-integrability and the Kozlov condition	26
3.4	Resonances	28
3.5	Non-linear resonance and chain of islands	29
3.6	Kolmogorov–Arnold–Moser (KAM) theory	32
	Notes	
	Problems	
<b>4</b>	<b>Chaotic dynamics</b>	<b>37</b>
4.1	Natural measure	37
4.2	Ergodicity, mixing, and weak mixing	39
4.3	Local instability and Lyapunov exponents	42
4.4	Hyperbolic systems	46
4.5	Entropy of dynamical systems	48
4.5.1	Partitioning and coarse-graining	48
4.5.2	Kolmogorov–Sinai (KS) entropy	49
4.5.3	Topological entropy	51
4.5.4	Physical interpretation	51
4.5.5	Entropy and Lyapunov exponents	53

4.6	Definition of chaotic dynamics	53
4.7	Chirikov resonance overlapping criteria	54
	Notes	
	Problems	
<b>5</b>	<b>Physical models of chaos</b>	<b>57</b>
5.1	Mapping the dynamics	57
5.2	Universal and standard map	60
5.3	Web map (kicked oscillator)	64
5.4	Kepler map	68
	Notes	
	Problems	
<b>6</b>	<b>Separatrix chaos</b>	<b>73</b>
6.1	Description of models	73
6.2	Separatrix map	76
6.3	The stochastic layer	78
6.4	The stochastic layer of the standard map	81
6.5	Hidden renormalization group near the separatrix	83
6.6	Renormalization of resonances	89
6.7	Hidden renormalization for coupled oscillators	91
	Notes	
	Problems	
<b>7</b>	<b>Weak chaos and symmetry</b>	<b>97</b>
7.1	Stochastic webs	97
7.2	Stochastic webs with quasi-crystalline symmetry	99
7.3	Stochastic web skeleton	102
7.4	Symmetries and their dynamical generation	110
7.5	Width of the stochastic web	114
7.6	Symmetry in art and nature	117
	7.6.1 Symmetry and chaos	117
	7.6.2 Ornamental patterns	118
	7.6.3 Patterns in nature	120
	Notes	
	Problems	
<b>8</b>	<b>Beyond the KAM-theory</b>	<b>125</b>
8.1	Small non-linearity	125
8.2	Web-Tori	127
8.3	Width of the stochastic web	134
8.4	Transition from KAM-Tori to Web-Tori	135
	Notes	
	Problems	

<b>9</b>	<b>Phase space of chaos</b>	<b>139</b>
9.1	Topological non-universality of chaos	139
9.2	Examples with billiards	142
9.3	Accelerator mode islands	143
9.4	Ballistic mode islands	151
9.5	Cantori	152
9.6	Sticky domains and escapes	154
	Notes	
	Problems	
 <b>Part 2 Fractality of Chaos</b>		
<b>10</b>	<b>Fractals and chaos</b>	<b>159</b>
10.1	Fractal dynamics	159
10.2	Generalized fractal dimension	161
10.3	Renormalization group and generalized fractal dimension	162
10.4	Multifractal spectra	164
10.5	Thermodynamic interpretation	167
10.6	Complex dimension and log-periodicity	169
	Notes	
	Problems	
<b>11</b>	<b>Poincaré recurrences</b>	<b>173</b>
11.1	Poincaré theorem on recurrences	173
11.2	Recurrence time distributions and Kac lemma	174
11.3	Distribution of recurrences in uniform mixing	177
11.4	More asymptotics on recurrences	180
	Notes	
	Problems	
<b>12</b>	<b>Dynamical traps</b>	<b>187</b>
12.1	Definition of the dynamical trap	187
12.2	Hierarchical-islands trap (HIT)	189
12.3	Renormalization for the exit time distribution	193
12.4	Stochastic layer trap	196
	Notes	
<b>13</b>	<b>Fractal time</b>	<b>201</b>
13.1	Fractal time	201
13.2	Fractal and multifractal recurrences	204
13.3	Multifractal space-time and its dimension spectrum	207
13.4	Critical exponent for the Poincaré recurrences	209
	Notes	
	Problems	



## Part 3 Chaotic kinetics

<b>14 General principles of kinetics</b>	215
14.1 Time scales	215
14.2 Fokker–Planck–Kolmogorov (FPK) equation	217
14.3 Detailed balance principle	220
14.4 Solutions and normal transport	221
14.5 Growth of entropy	222
14.6 Kolmogorov conditions and conflict with dynamics	223
14.7 Truncated distributions	225
Notes	
Problems	
<b>15 Lévy process, Lévy flights, and Weierstrass random walk</b>	229
15.1 Lévy distribution	230
15.2 Lévy process	231
15.3 Poincaré recurrences and Feller’s theorems	234
15.4 Lévy flights and conflict with dynamics	235
15.5 Weierstrass random walks (WRW)	240
Notes	
Problems	
<b>16 Fractional kinetic equation (FKE)</b>	245
16.1 Derivation of FKE	245
16.2 Conditions for the FKE	249
16.3 Evolution of moments (transport)	250
16.4 Conflict with dynamics	252
16.5 Dynamical origin of critical exponents	253
16.6 Principles of simulations	257
Notes	
Problems	
<b>17 Renormalization group of kinetics (RGK)</b>	261
17.1 Space-time scalings	261
17.2 Log-periodicity	263
17.3 Duality of the dynamics and the origin of multi-fractality	265
17.4 Multifractional kinetics	267
Notes	
<b>18 Fractional kinetic equation: solutions and modifications</b>	273
18.1 Solutions to FKE (series)	273
18.2 Solutions to FKE (separation of variables)	275
18.3 Continuous time random walk (CTRW)	276
18.4 Lévy walks and other generalizations of CTRW	279
18.5 Conflict with dynamics	281
18.6 Subdiffusion and superdiffusion	281

Notes

Problems

<b>19 Pseudochaos</b>	287
19.1 Billiards in polygons	287
19.2 Continued fractions and scalings of trajectories	291
19.3 Fractional kinetics of irrational trajectories	296
19.4 More examples of pseudochaos	303
19.4.1 Rhombic billiard	303
19.4.2 More billiards	303
19.4.3 Saw-tooth web map	306
Notes	
Problems	
 <b>Part 4 Applications</b>	
<b>20 Complexity and entropy of dynamics</b>	315
20.1 Complexity in phase space	316
20.2 Symbolic and topological complexities	317
20.3 Topological and metric entropies	320
20.4 Conflict with dynamics	323
Notes	
Problems	
 <b>21 Complexity and entropy functions</b>	325
21.1 Definitions of complexity function	325
21.2 Probability of $\epsilon$ -divergence	328
21.3 Calculation of local complexity function	329
21.4 Flight complexity function	331
21.5 Entropy function	333
21.6 Polynomial and mixed complexities and anomalous transport	335
21.7 Travelling waves and Riemann invariants of entropy and complexity	337
Notes	
Problems	
 <b>22 Chaos and foundation of statistical mechanics</b>	341
22.1 Zermelo's and Loschmidt's paradoxes	341
22.1.1 Historical comments	341
22.1.2 Paradox of recurrence	342
22.1.3 Paradox of reversibility	343
22.1.4 Boltzmann's comments	343
22.2 Chaos and the paradoxes	344
22.3 Anomalous properties of the Sinai and Bunimovich billiards	344
22.4 Maxwell's Demon and Chaos	346

22.5	Maxwell's Demon as a dynamical model	348
22.6	Comments on the application of Ergodic Theory	352
22.7	Comments on dynamical cooling and chaos erasing	352
	Notes	
<b>23</b>	<b>Chaotic advection (dynamics of tracers)</b>	<b>357</b>
23.1	Beltrami flows with $q$ -symmetry	357
23.2	Compressible helical flows	359
23.3	Compressible flow with quasi-symmetry	367
	Notes	
	Problems	
<b>24</b>	<b>Advection by point vortices</b>	<b>373</b>
24.1	Basic equations for point vortices and for advection	373
24.2	Advection in three vortices	376
24.3	Transport of advected particles (vortices)	383
	Notes	
	Problems	
<b>Appendices</b>		<b>393</b>
A	Elliptic integrals and elliptic functions	393
B	Spectrum of the Kepler problem	394
C	Fractional integro-differentiation	396
D	Formulas of fractional calculus	399
<b>References</b>		<b>403</b>
<b>Index</b>		<b>417</b>

PART 1

CHAOTIC DYNAMICS

*This page intentionally left blank*

## HAMILTONIAN DYNAMICS

A wide class of physical phenomena can be described by Hamiltonian equations. This class includes particles, fields, classical and quantum objects, and it makes up a significant part of our knowledge of the basics of dynamics in nature. Hamiltonian dynamics is very different from, for example, dissipative dynamics, and its analysis uses specific tools that cannot be applied in other cases. Discovery of chaotic dynamics is a result of discovering new features in Hamiltonian dynamics and new types of solutions of the dynamical equations. Complementary to the chaotic dynamics, results on the stability of dynamics, known as Kolmogorov–Arnold–Moser (KAM) theory, have added significantly to the contemporary structure of the theory of Hamiltonian systems. In this chapter we are presenting some information on Hamiltonian dynamics that is important for the description of the so-called Hamiltonian chaos (*Note 1.1*).

### 1.1 Hamiltonian equations

A Hamiltonian system with  $N$  degrees of freedom is characterized by a generalized coordinate vector  $\mathbf{q} \in \mathbb{R}^N$ , generalized momentum vector  $\mathbf{p} \in \mathbb{R}^N$ , and a Hamiltonian  $H = H(\mathbf{p}, \mathbf{q})$  such that the equations of motion are:

$$\dot{p}_i \equiv \frac{dp_i}{dt} = -\frac{\partial H}{\partial q_i}; \quad \dot{q}_i \equiv \frac{dq_i}{dt} = \frac{\partial H}{\partial p_i}, \quad (i = 1, \dots, N). \quad (1.1)$$

The space  $(\mathbf{p}, \mathbf{q})$  is  $2N$ -dimensional phase space and a pair  $(p_i, q_i)$ ,  $\forall i$  is called the canonically conjugate variables.

The Hamiltonian can depend explicitly on time, i.e.  $H = H(\mathbf{p}, \mathbf{q}, t)$ . Then the system can be considered in an extended space of  $2(N + 1)$  variables  $(\mathbf{p}, \mathbf{q}; p_0, q_0)$  with

$$p_0 = -H, \quad q_0 = t \quad (1.2)$$

as a new canonical pair, and with a new Hamiltonian

$$\mathcal{H} = H(p, q, q_0) + p_0. \quad (1.3)$$

Indeed, the Hamiltonian dynamical equations

$$\begin{aligned}\dot{p}_i &= -\frac{\partial \mathcal{H}}{\partial q_i} = -\frac{\partial H}{\partial q_i}; & \dot{q}_i &= \frac{\partial \mathcal{H}}{\partial p_i} = \frac{\partial H}{\partial p_i}, & (i = 1, \dots, N), \\ \dot{p}_0 &= -\frac{\partial \mathcal{H}}{\partial q_0} = -\frac{\partial H}{\partial t}; & \dot{q}_0 &= \frac{\partial \mathcal{H}}{\partial p_0} = 1\end{aligned}\tag{1.4}$$

coincide with (1.1) and definitions (1.2). It follows from (1.3) that  $\mathcal{H} \equiv 0$ , and the equation  $p_0 = -H$  does not provide any information. Due to that, the system with the Hamiltonian  $H = H(\mathbf{p}, \mathbf{q}, t)$  is called to have  $(N + 1/2)$  degrees of freedom.

An important notion of Hamiltonian dynamics is the *Poisson bracket* defined for two arbitrary smooth functions  $A = A(\mathbf{p}, \mathbf{q})$  and  $B = B(\mathbf{p}, \mathbf{q})$  as

$$[A, B] = \sum_{i=1}^N \left( \frac{\partial A}{\partial q_i} \frac{\partial B}{\partial p_i} - \frac{\partial A}{\partial p_i} \frac{\partial B}{\partial q_i} \right).\tag{1.5}$$

Particularly, equations

$$\dot{p}_i = [p_i, H], \quad \dot{q}_i = [q_i, H], \quad (i = 1, \dots, N)\tag{1.6}$$

coincide with the Hamiltonian equations (1.1). In general case, for any differentiable  $A = A(\mathbf{p}, \mathbf{q}, t)$  we have

$$\dot{A} = \frac{\partial A}{\partial t} + [A, H].\tag{1.7}$$

The following properties of the Poisson bracket are valid (see Problem 1.1):

(a) bilinearity

$$[aA + bB, C] = a[A, C] + b[B, C],\tag{1.8}$$

where  $a$  and  $b$  are constants.

(b) skewness

$$[A, B] = -[B, A],\tag{1.9}$$

which cannot be satisfied for an odd dimension of phase space.

(c) Leibniz identity

$$[AB, C] = B[A, C] + A[B, C].\tag{1.10}$$

(d) Jakobi identity

$$[A, [B, C]] + [C, [A, B]] + [B, [C, A]] = 0. \quad (1.11)$$

Using the Poisson brackets and their generalizations, one can formulate Hamiltonian dynamics for many different types of systems (*Note 1.2*).

## 1.2 Phase space dynamics

It is useful to say that equations (1.1) define a *phase flow*, or simply a *flow*, in phase space. Let

$$d\Gamma_t = d\mathbf{p}_t d\mathbf{q}_t \quad (1.12)$$

be an element of the phase volume  $\Gamma_t$  at time  $t$ , i.e.

$$\Gamma_t = \int_{\hat{\sigma}_t} d\mathbf{p}_t d\mathbf{q}_t \quad (1.13)$$

and integration is performed over the volume bounded by a hypersurface  $\hat{\sigma}_t$ . The evolution of the initial phase volume  $\Gamma_0$  to  $\Gamma_t$  during the time interval  $(0, t)$  is shown in Fig. 1.1.

An important property of Hamiltonian dynamics is the Liouville theorem on the preservation of phase volume, i.e.

$$\Gamma_t = \text{const} = \Gamma_0. \quad (1.14)$$

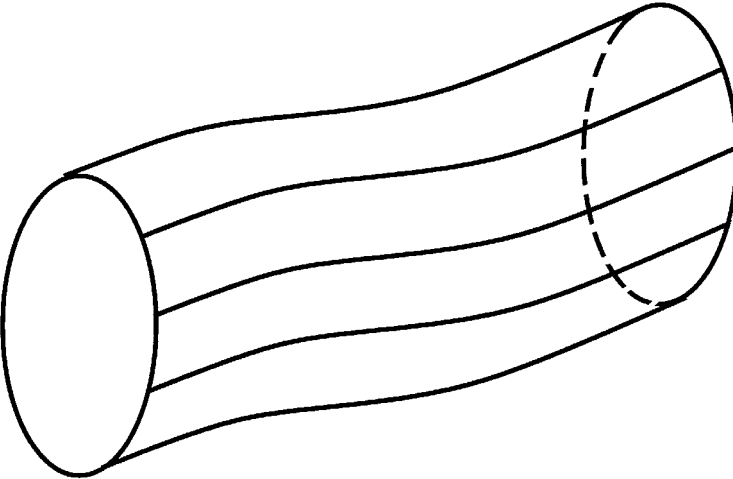


FIG. 1.1. Evolution of a phase volume.



(See proof, for example, in Arnold (1978) even for a time-dependent Hamiltonian.) The Liouville theorem can also be interpreted as incompressibility of the phase liquid

$$\operatorname{div}_{(\mathbf{p}, \mathbf{q})} \mathbf{J} = \frac{\partial \dot{\mathbf{q}}}{\partial \mathbf{q}} + \frac{\partial \dot{\mathbf{p}}}{\partial \mathbf{p}} = 0, \quad (1.15)$$

where  $(\dot{\mathbf{p}}, \dot{\mathbf{q}})$  satisfy the Hamiltonian equation (1.1) and  $\mathbf{J}$  is the current vector in  $2N$ -dimensional space (see Problem 1.2).

Let  $f = f(\mathbf{p}, \mathbf{q}, t)$  be a distribution function of particles in phase space. It is normalized as

$$\int_{\Gamma} f(\mathbf{p}, \mathbf{q}, t) d\Gamma = 1. \quad (1.16)$$

Condition (1.16) corresponds to the conservation of the number of particles (one in this case). The differential form of (1.16) is the equation of continuity

$$\frac{\partial f}{\partial t} + \operatorname{div}_{(\mathbf{p}, \mathbf{q})}(\mathbf{J}f) = 0 \quad (1.17)$$

or following from (1.15)

$$\frac{\partial f}{\partial t} + \dot{\mathbf{q}} \frac{\partial f}{\partial \mathbf{q}} + \dot{\mathbf{p}} \frac{\partial f}{\partial \mathbf{p}} = 0 \quad (1.18)$$

also known as the Liouville equation.

The results (1.15) and (1.18) are different representations of the conservation of the phase volume in the process of dynamics. Any deformation of the phase volume is permitted (Fig. 1.2) but there are no sources and sinks (Fig. 1.3)—in other words, attractors and repellers are forbidden due to the phase volume conservation.

Systems with one degree of freedom can be analysed fairly simply by drawing their *phase portrait* or a family of possible orbits  $p = p(q)$  on the phase plane  $(p, q)$ . Consider for example a Hamiltonian

$$H = \frac{p^2}{2m} + V(q), \quad (1.19)$$

where  $V(q)$  is potential energy and full energy  $E = H(p, q)$  doesn't depend on time. The dynamics can be presented through the quadrature

$$t = \int^q \frac{dq}{p(q, E)} = \pm \int^q \frac{dq}{[2m(E - V(q))]^{1/2}} \quad (1.20)$$

that defines in an implicit way a solution

$$q = q(t; q_0, p_0), \quad p = p(t; q_0, p_0) \quad (1.21)$$

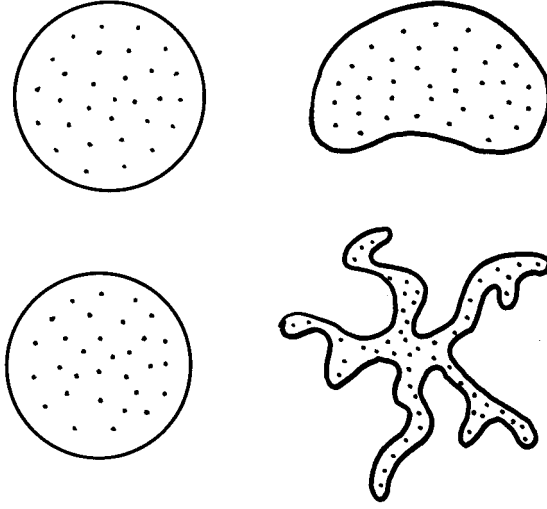


FIG. 1.2. Stable (upper) and unstable (lower) evolution of phase volume.

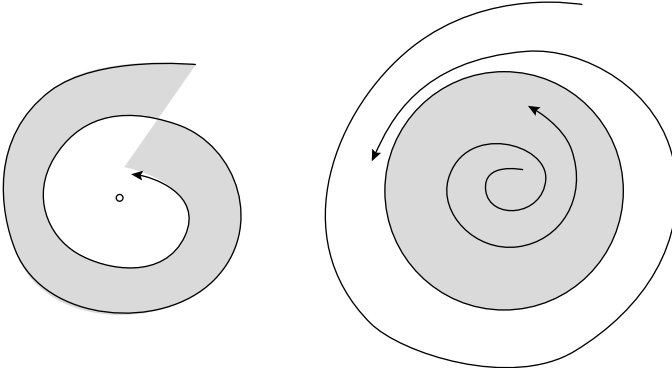


FIG. 1.3. Trajectories attraction to a point or to a cycle.

that satisfies the initial conditions  $q = q_0$ ,  $p = p_0$  for  $t = t_0$  and particularly  $H(p_0, q_0) = E$ . The phase portrait (Fig. 1.4) is the topological structure of a family of trajectories with different initial conditions in the  $(p, q)$ -plane. For the example in Fig. 1.4 we have open trajectories, closed (*periodic*) trajectories, and *separatrices* that go through the *stationary points* with

$$\dot{q}^* = 0, \quad \dot{p}^* = -\frac{\partial V(q^*)}{\partial q} = 0, \quad \frac{\partial^2 V(q^*)}{\partial q^2} < 0. \quad (1.22)$$

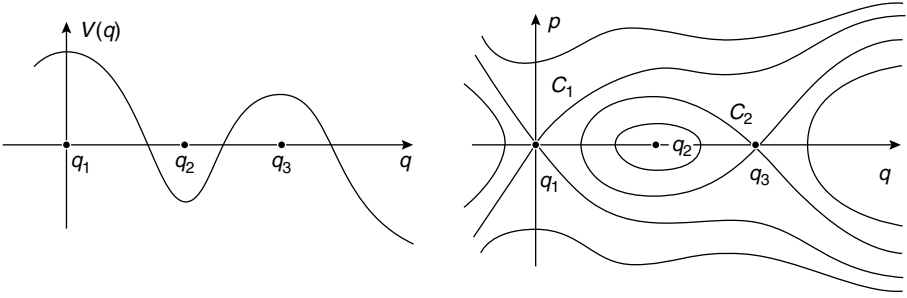


FIG. 1.4. Potential  $V(q)$  and the corresponding phase portrait with the stationary points  $q_1, q_2, q_3$ , and separatrices  $C_1, C_2$ .

Dynamics in the vicinity of a stationary point  $(p^*, q^*)$  can be found by an expansion near the point. From (1.19) and (1.21) we have

$$\frac{1}{2m}(p - p_s^*)^2 + \frac{1}{2}V''(q^*)(q - q^*)^2 = E - E^*, \quad V''(q^*) \neq 0, \quad E^* = H(p^*, q^*). \quad (1.23)$$

The behaviour of trajectories near the stationary point depends on the sign of  $V''(q^*)$  (see Fig. 1.5); it is a family of hyperbolas for  $V''(q^*) < 0$  and ellipses for  $V''(q^*) > 0$ . The point  $(p^*, q^*)$  is called the hyperbolic (saddle) or elliptic point respectively. Separatrices are trajectories that go through the saddle points.

### 1.3 Action-angle variables (one degree of freedom)

Action ( $I$ )-angle or phase ( $\vartheta$ ) variables are canonically conjugate and convenient in use for different problems. They are introduced through the *generating function*

$$S(q, I) = S(q, H(I)) = \int^q p(q, H) dq \quad (1.24)$$

in the following way

$$I = \frac{1}{2\pi} \oint p(q, H) dq = I(H), \quad (1.25)$$

$$\vartheta = \frac{\partial S(q, I)}{\partial I}.$$

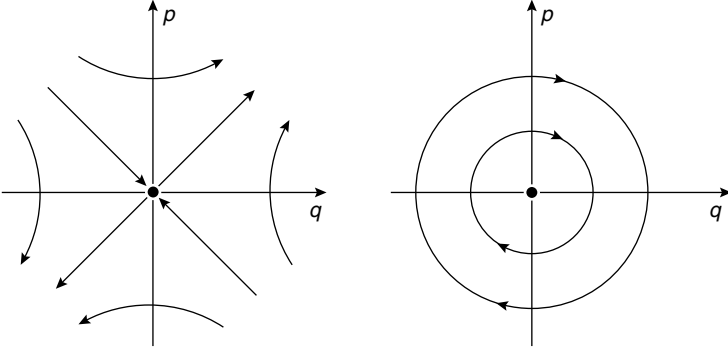


FIG. 1.5. Phase trajectories near the hyperbolic (saddle) point and elliptic point.

Variables  $(I, \vartheta)$  satisfy the equations

$$\begin{aligned} \dot{I} &= -\frac{\partial H(I)}{\partial \vartheta} = 0, \\ \dot{\vartheta} &= \frac{\partial H(I)}{\partial I} = \frac{dH(I)}{dI} \equiv \omega(I), \end{aligned} \tag{1.26}$$

where  $\omega$  is a frequency of non-linear oscillations since its dependence on  $I$ . Equations (1.25) can be simply solved

$$\begin{aligned} I &= \text{const} = I(E), \\ \vartheta &= \omega(I)t + \text{const} \end{aligned} \tag{1.27}$$

with an energy

$$E = H(I) = \text{const} \tag{1.28}$$

that can be obtained by the inversion of the first equation in (1.25).

The cyclic feature of the phase  $\vartheta$  follows from the definitions (1.24) and (1.25). A change  $\Delta\vartheta$  per period of oscillations is

$$\begin{aligned} \Delta S &= \oint p \, dq = 2\pi I, \\ \Delta\vartheta &= \frac{\partial \Delta S}{\partial I} = 2\pi. \end{aligned} \tag{1.29}$$

These expressions allow us to consider a spectral decomposition of the old variables  $(p, q)$ :

$$\begin{aligned} q &= q(I, \vartheta) = \sum_{n=-\infty}^{\infty} q_n(I) e^{in\vartheta}, \quad q_{-n} = q_n^*, \\ p &= p(I, \vartheta) = \sum_{n=-\infty}^{\infty} p_n(I) e^{in\vartheta}, \quad p_{-n} = p_n^* \end{aligned} \quad (1.30)$$

with

$$\begin{aligned} q_n &= \frac{1}{2\pi} \int_0^{2\pi} q(I, \vartheta) e^{-in\vartheta} d\vartheta, \\ p_n &= \frac{1}{2\pi} \int_0^{2\pi} p(I, \vartheta) e^{-in\vartheta} d\vartheta. \end{aligned} \quad (1.31)$$

For the quadratic Hamiltonian

$$H = \frac{1}{2}p^2 + \frac{1}{2}\omega_0^2 q^2 \quad (1.32)$$

with mass  $m = 1$  we have

$$H(I) = \omega_0 I, \quad \omega(I) = \omega_0 \quad (1.33)$$

and the oscillations are linear, i.e. consist of only one harmonic:

$$\begin{aligned} q &= \left( \frac{2I}{\omega_0} \right)^{1/2} \sin(\omega_0 t + \vartheta_0), \\ p &= \left( \frac{2I}{\omega_0} \right)^{1/2} \cos(\omega_0 t + \vartheta_0). \end{aligned} \quad (1.34)$$

Let  $p(I, \vartheta)$ ,  $q(I, \vartheta)$  be good functions without singularities on the real axis. Then they can have singularity in the complex plane and asymptotics of  $p_n, q_n$  for  $n \gg 1$  may be of the form

$$p_n \sim \exp\left(-\frac{n}{N^*}\right), \quad q_n \sim \exp\left(-\frac{n}{N^*}\right) \quad (1.35)$$

with  $N^* \gg 1$ . The number  $N^*$  defines a characteristic spectral width of oscillations. It will be calculated in an explicit way for some examples later.

## Notes

### Note 1.1

There are indispensable books that review the fundamental features of contemporary Hamiltonian dynamics, which we recommend for more detailed reading: Arnold (1978); Arnold *et al.* (1993); Kozlov (1996).

### Note 1.2

We will provide some examples in the following chapter. A detailed description of different generalizations can be found in Dubrovin *et al.* (1984).

## Problems

More complicated problems are marked by (\*).

1.1 Prove (1.8)–(1.11) using the definition (1.5).

1.2 Prove that (1.14) follows from (1.15).

1.3 Draw the phase portrait for the Hamiltonian

$$H = \cos p + \cos q.$$

1.4 Draw the phase portrait for the Hamiltonian

$$H = \cos p + \cos \left( p + \left( \frac{\sqrt{3}}{2} \right) x \right) + \cos \left( p - \left( \frac{\sqrt{3}}{2} \right) x \right).$$

1.5 For an arbitrary, smooth potential  $V(q)$  find particle dynamics near a turning point  $q^*$ :

$$V(q^*) = E \text{ (particle energy); } V'(q^*) \neq 0.$$

1.6 The same as in Problem 1.5 when  $q^*$  is a hyperbolic point:

$$V'(q^*) = 0, \quad V''(q^*) < 0.$$

1.7\* Prove that for analytical  $p(t), q(t)$  on the real axis  $t$  the spectral width is finite, i.e.  $N^* < \infty$  in (1.35).

*This page intentionally left blank*

## EXAMPLES OF HAMILTONIAN DYNAMICS

### 2.1 Pendulum

This is a standard and classical example of non-linear and unharmonic dynamics governed by the Hamiltonian

$$H = \frac{1}{2}p^2 - \omega_0^2 \cos x, \quad p = \dot{x}. \quad (2.1)$$

Its phase space is shown in Fig. 2.1 with the potential  $V = -\omega_0^2 \cos x$  and the stationary points  $\dot{x}_r = 0$ ,  $x_r = n\pi$  ( $n = 0, \pm 1, \dots$ ). Trajectories for (2.1) are defined from the equation

$$\ddot{x} + \omega_0^2 \sin x = 0 \quad (2.2)$$

and they correspond to oscillations for  $H = E < \omega_0^2$  or rotations  $H = E > \omega_0^2$ . A special, singular, trajectory with  $H_s = E_s = \omega_0^2$  is the pendulum *separatrix*. The corresponding solution on the separatrix is

$$\begin{aligned} \dot{x}_s &= \pm 2\omega_0 \cos\left(\frac{x}{2}\right) = \pm \frac{2\omega_0}{\cosh \omega_0 t}, \\ x_s &= 4 \arctan e^{\omega_0 t} - \pi. \end{aligned} \quad (2.3)$$

The profile of  $v_s = \dot{x}_s$  is called a soliton while the profile of  $x$  is called a kink.

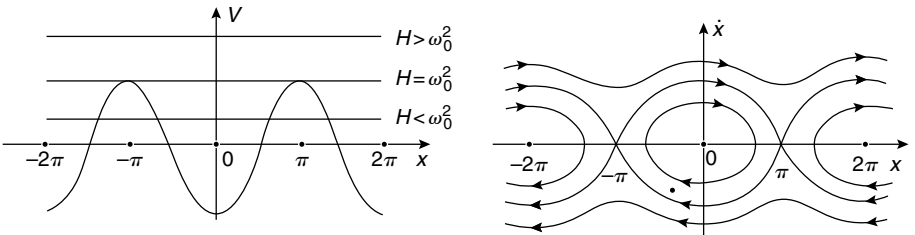


FIG. 2.1. Potential  $V(x)$  and the phase space of a pendulum.



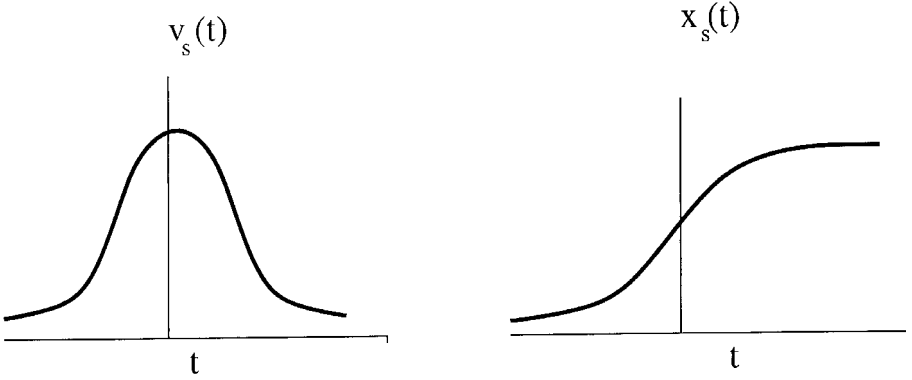


FIG. 2.2. Dynamics on the separatrix: soliton-type (left) and kink-type (right).

In the case  $H > \omega_0^2$ , the solution is not bounded but periodic. In this case the formula (1.25) for the action variable can be replaced by

$$I = \frac{1}{2\pi} \int_{-\pi}^{\pi} p dx = \frac{1}{2\pi} \int_{x_0}^{x_0+2\pi} p dx \quad (2.4)$$

with an arbitrary  $x_0$ . Let us introduce a parameter  $\kappa$ :

$$\kappa^2 = \frac{1 + H/\omega_0^2}{2}, \quad 1 \leq \kappa < \infty, \quad (2.5)$$

which defines oscillations for  $\kappa < 1$ , rotations for  $\kappa > 1$ , and the separatrix for  $\kappa = 1$ .

Using expression for  $p$  from (2.1) and calculating (2.4) we obtain:

$$\begin{aligned} I = I(H) &= \frac{2}{\pi} \int_0^{x_0} dx [2(H + \omega_0^2 \cos x)]^{1/2} \\ &= \frac{8}{\pi} \omega_0 \begin{cases} E\left(\frac{\pi}{2}; \kappa\right) - (1 - \kappa^2)F\left(\frac{\pi}{2}; \kappa\right), & (\kappa \leq 1), \\ \kappa E\left(\frac{\pi}{2}; \frac{1}{\kappa}\right), & (\kappa \geq 1), \end{cases} \end{aligned} \quad (2.6)$$

where  $x_0$  corresponds to 1/4 of the period of oscillations and satisfies the equation  $\cos x_0 = -H/\omega_0^2$  and  $F(\pi/2; \kappa)$ ;  $E(\pi/2; \kappa)$  are full elliptic integrals of the 1st and 2nd kind respectively (see Appendix A).

The frequency, defined in (1.26), is

$$\begin{aligned}\omega(H) &= \frac{dH(I)}{dI} = \frac{1}{dI(H)/dH} \\ &= \frac{\pi}{2}\omega_0 \begin{cases} \frac{1}{F(\pi/2; \kappa)}, & (\kappa \leq 1), \\ \frac{\kappa}{F}\left(\frac{\pi}{2}; \frac{1}{\kappa}\right), & (\kappa \geq 1). \end{cases}\end{aligned}\quad (2.7)$$

Using the asymptotic expressions for  $F$  (see Appendix A) we have for  $H = E$

$$\omega(E) \approx \begin{cases} \omega_0, & (\kappa \ll 1), \\ \frac{\pi\omega_0}{\ln(32E_s/|E_s - E|)}, & (1 - \kappa^2 \ll 1) \end{cases}\quad (2.8)$$

with

$$E_s = \omega_0^2 \quad (2.9)$$

as an energy value on the separatrix.

The spectral decomposition (1.30) for the velocity  $v = \dot{x} = p$  has the form:

$$\begin{aligned}v = \dot{x} &= 8\omega \sum_{n=1}^{\infty} \frac{a^{n-1/2}}{1 + a^{2n-1}} \cos[(2n-1)\omega t], & (\kappa \leq 1), \\ v = \dot{x} &= 8\omega \left\{ \frac{1}{4} + \sum_{n=1}^{\infty} \frac{a^n}{1 + a^{2n}} \cos(n\omega t) \right\}, & (\kappa \geq 1)\end{aligned}\quad (2.10)$$

with

$$\begin{aligned}a &= \exp\left(-\frac{\pi\bar{F}'}{\bar{F}}\right), \quad \bar{F} = F\left(\frac{\pi}{2}; \bar{\kappa}\right), \\ \bar{F}' &= F\left(\frac{\pi}{2}; (1 - \bar{\kappa}^2)^{1/2}\right), \quad \bar{\kappa} = \begin{cases} \kappa, & (\kappa \leq 1), \\ \frac{1}{\kappa}, & (\kappa \geq 1). \end{cases}\end{aligned}\quad (2.11)$$

It follows from (2.11) that

$$a \sim \begin{cases} \frac{\kappa^2}{32}, & (\kappa \ll 1), \\ \exp\left(-\frac{\pi}{N^*}\right), & (1 - \kappa^2 \ll 1) \end{cases}\quad (2.12)$$

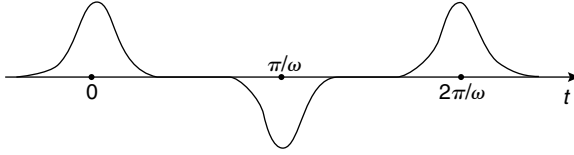


FIG. 2.3. Time dependence of the pendulum velocity near the separatrix ( $\kappa \leq 1$ ).

with

$$N^* = \frac{1}{\pi} \ln \frac{32E_s}{|E_s - E|} = \frac{\omega_0}{\omega(E)}. \quad (2.13)$$

Near the separatrix  $\kappa \rightarrow 1$  and  $\omega \rightarrow 0$ , i.e.  $N^* \rightarrow \infty$ . Velocity behaviour is a periodic set of the soliton-like pulses (Fig. 2.3). For  $\kappa \geq 1$  the velocity behaviour is similar to Fig. 2.3 (see Problem 2.2).

## 2.2 Oscillations in the infinite potential well

This case corresponds to a particle that moves between two walls with ideal reflections from them.

The corresponding Hamiltonian is:

$$H = \frac{p^2}{2} + V(x), \quad V(x) = 0, \quad |x| \leq \frac{a}{2}, \quad V(x) = \infty, \quad |x| > \frac{a}{2}. \quad (2.14)$$

Along the trajectories

$$p = \dot{x} = \text{const} = (2H)^{1/2} \quad (2.15)$$

and for the frequency we have

$$\omega = \omega(H) = \frac{2\pi}{T} = \frac{\dot{x}}{2a} = \frac{(2H)^{1/2}}{2a}. \quad (2.16)$$

The action is

$$I = 2pa = 2a(2H)^{1/2} \quad (2.17)$$

and, comparing to (2.16),

$$\omega = \omega(I) = \frac{I}{(2a)^2}. \quad (2.18)$$

Finally

$$\dot{x} = \frac{I}{2a} \theta_{2\pi}(t) = \sum_{n=-\infty}^{\infty} p_n(I) e^{in\vartheta} \quad (2.19)$$

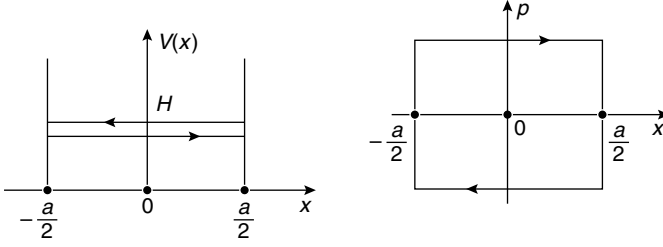


FIG. 2.4. Particle oscillations between two walls (left) and the corresponding phase space (right).

with  $\theta_{2\pi}$  as a periodic step-function and

$$\begin{aligned} p_n(I) &= p_{-n}^*(I) = \frac{i}{2an} I, \\ \theta_{2\pi}(t) &= \theta_{2\pi}(t + T) = \pm 1. \end{aligned} \quad (2.20)$$

Since the trajectories are singular (see Fig. 2.4), the Fourier coefficients  $p_n$  do not have exponential decay and the finite  $N^*$  does not exist.

### 2.3 Magnetic moments

Consider a particle with a magnetic moment  $\mathbf{M} = (M_x, M_y, M_z)$  and

$$\mathbf{M}^2 = M_x^2 + M_y^2 + M_z^2. \quad (2.21)$$

The particle, imbedded into a media with external magnetic field, can get an energy

$$W = W(M_x, M_y, M_z). \quad (2.22)$$

Dynamics of the magnetic moment are then defined by the so-called Landau-Lifshits equation

$$\dot{\mathbf{M}} = -g \mathbf{M} \times \frac{\partial W}{\partial \mathbf{M}}, \quad (2.23)$$

where  $g$  is a constant factor.

Equation (2.23) has two integrals of motion:  $\mathbf{M}^2$  and  $W$ , that can be verified by their direct differentiation. Let us show how equation (2.23) can be written in a Hamiltonian form. First, introduce new variables:

$$M^\pm = M_x \pm iM_y. \quad (2.24)$$

Equation (2.23) can be rewritten as:

$$\frac{d}{dt}M^\pm = \pm igM^\pm \frac{\partial W}{\partial M_z} \mp 2igM_z \frac{\partial W}{\partial M^\mp}. \quad (2.25)$$

The equation for  $\dot{M}_z$  can be obtained from (2.25) if we use

$$M_z = (\mathbf{M}^2 - M^+M^-)^{1/2}. \quad (2.26)$$

Now replace

$$W(M_x, M_y, M_z) \rightarrow \mathcal{W}(M^+, M^-; (M^2 - M^+M^-)^{1/2}). \quad (2.27)$$

Then equation (2.25) transforms into:

$$\frac{dM^\pm}{dt} = \mp 2igM_z(M^+, M^-) \frac{\partial \mathcal{W}}{\partial M^\mp}, \quad (2.28)$$

where  $M_z$  should be replaced by (2.26).

Equation (2.27) is related to the generalized Hamiltonian system (Dubrovin *et al.* (1984)). To see this, let us introduce a new time variable  $\tau$  by the equation:

$$\frac{d\tau}{dt} = 2igM_z(M^+(t), M^-(t)) \quad (2.29)$$

and rewrite (2.28) as:

$$\frac{dM^\pm}{d\tau} = \mp \frac{\partial \mathcal{W}}{\partial M^\mp}, \quad (2.30)$$

which defines the canonical pair  $(M^+, M^-)$  and the Hamiltonian  $\mathcal{W}$  in the form of (2.27). The obtained Hamiltonian presentation of equation (2.23) is not unique and a choice of one or another set of canonical variables is a matter of convenience.

## 2.4 Field line behaviour

The problem to be considered here is fairly old and has numerous applications. Let  $\mathbf{v} = \mathbf{v}(\mathbf{r})$  be a vector field defined in three-dimensional space  $\mathbf{r} = (x, y, z)$ . The set of equations:

$$\frac{dx}{v_x} = \frac{dy}{v_y} = \frac{dz}{v_z} \quad (2.31)$$

defines field line behaviour in space and can be rewritten in a parametric form

$$\dot{\mathbf{r}} \equiv \frac{d\mathbf{r}}{dt} = \mathbf{v}(\mathbf{r}), \quad (2.32)$$

where the parameter  $t$  can represent a length along the field line. For any given initial point  $\mathbf{r}_0 = (x_0, y_0, z_0)$ , equation (2.32) defines the solution:

$$\mathbf{r} = \mathbf{r}(x, y, z; x_0, y_0, z_0) \quad (2.33)$$

that shows a coordinate of the field line that passes through the point  $\mathbf{r}_0$ . In fact, the system (2.32) has only two independent equations:

$$\begin{aligned} \frac{dx}{dz} &= \frac{v_x}{v_z} = f_1(x, y, z), \\ \frac{dy}{dz} &= \frac{v_y}{v_z} = f_2(x, y, z). \end{aligned} \quad (2.34)$$

One can assume a point massless particle that moves along field lines following equation (2.32) or, using a ‘time’  $z$ , one can consider a trajectory in space:

$$x = x(z; x_0, y_0, z_0), \quad y = y(z; x_0, y_0, z_0) \quad (2.35)$$

obtained from ‘dynamical’ equation (2.34). Both forms (2.33) and (2.35) are equivalent.

The most important applications of the problem (2.31), (2.32) occur for advected particles in fluids (tracers) and for magnetic field lines with respect to the fusion devices. In Fig. 2.5 we present different possible behaviours of field lines. Evidently the problem of the field line behaviour can be considered as a dynamical problem and the unstable behaviour can occur as chaos of field lines, but, for the cases of absence of real time dependence, equation (2.32) or (2.34) would be formulated in a Hamiltonian form.

Consider the case of incompressible fluid:

$$\operatorname{div} \mathbf{v} = 0 \quad (2.36)$$

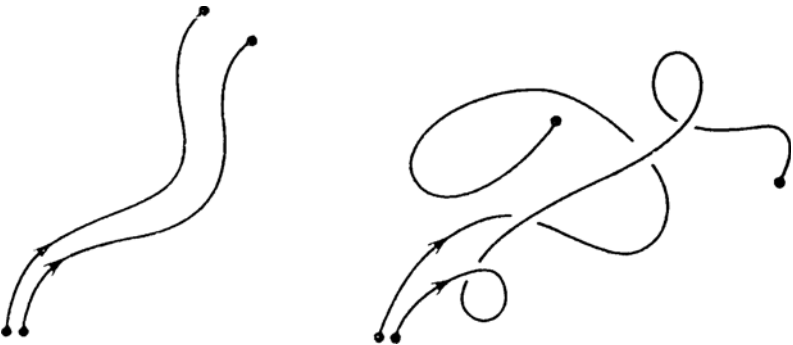


FIG. 2.5. Stable (left) and unstable (right) behaviour of field lines.

for which the tracers follow *streamlines* (the case of compressible fluid is in Chapter 23.2). Let us introduce a variable  $\xi$  (vector potential) by the equation:

$$\mathbf{v} = \text{curl } \xi \quad (2.37)$$

and put

$$\xi_y = 0, \quad \xi_z = H, \quad p = \int^y v_z dy. \quad (2.38)$$

Then it is simple to verify that:

$$\frac{dx}{dz} = \frac{\partial H}{\partial p}, \quad \frac{dp}{dz} = -\frac{\partial H}{\partial x}, \quad (2.39)$$

which are Hamiltonian equations with respect to ‘time’  $z$  and canonical pair  $(p, x)$ . There are other ways of introducing Hamiltonian form for streamlines. Particularly, in the two-dimensional case  $\mathbf{r} = (x, y)$ ,  $\mathbf{v} = (v_x, v_y)$  we can introduce the so-called *stream function*  $\Psi$ :

$$v_x = \frac{\partial \Psi}{\partial y}, \quad v_y = -\frac{\partial \Psi}{\partial x} \quad (2.40)$$

to satisfy the continuity equation (2.36). Then equation (2.32) takes the canonical form:

$$\dot{x} = \frac{\partial \Psi}{\partial y}, \quad \dot{y} = -\frac{\partial \Psi}{\partial x} \quad (2.41)$$

with Hamiltonian  $\Psi = \Psi(x, y)$  and  $(x, y)$  as a canonical pair. The same equations can be generalized for the case when  $\Psi = \Psi(x, y; t)$  where  $t$  is a real time. Then the dot in (2.41) can be taken as the real time and system (2.41) together with  $\Psi = \Psi(x, y; t)$  is the Hamiltonian one.

## 2.5 Hamiltonian equations for the ABC-flow

A stationary non-dissipative flow satisfies the so-called Beltrami condition:

$$\mathbf{v} = c \text{curl } \mathbf{v} \quad (2.42)$$

with a free *helicity* parameter  $c$  that can be a function of  $\mathbf{r}$ . This type of field was considered much with respect to many different physical problems. Particularly, if we replace  $\mathbf{v}$  by the magnetic field  $\mathbf{B}$ , then the direct consequence from (2.42):

$$\mathbf{B} \times \text{curl } \mathbf{B} = 0 \quad (2.43)$$

is the condition of the force-free field.

In 1965 V. I. Arnold (see Arnold (1965)) suggested that the following steady state flow:

$$\begin{aligned} v_x &= A \sin z + C \cos y, \\ v_y &= B \sin x + A \cos z, \\ v_z &= C \sin y + B \cos x \end{aligned} \tag{2.44}$$

would possess a non-trivial topology of streamlines since it satisfies the Beltrami condition (with  $c = 1$ ). The flow (2.44) was called ABC (Arnold–Beltrami–Childress)-flow, and the non-trivial topology appears to be a streamline chaos (more detailed discussion is in Chapter 23).

In this section we want to present an explicit form of the Hamiltonian equation for (2.44) (see Zaslavsky *et al.* (1988, 1991)).

Let us rewrite (2.44) in the form

$$\frac{dx}{dz} = \frac{1}{\Psi} \frac{\partial H}{\partial y}, \quad \frac{dy}{dz} = -\frac{1}{\Psi} \frac{\partial H}{\partial x} \tag{2.45}$$

with

$$\begin{aligned} \Psi &= \Psi(x, y) = C \sin y + B \cos x, \\ H &= H(x, y, z) = \Psi(x, y) + A(y \sin z - x \cos z). \end{aligned} \tag{2.46}$$

Following (2.38), define

$$p = p(x, y) = \int_0^y dy' \Psi(x, y') \tag{2.47}$$

and that gives instead of (2.45)

$$\frac{dx}{dz} = \frac{\partial H}{\partial p}, \quad \frac{dp}{dz} = -\frac{\partial H}{\partial x} \tag{2.48}$$

with the Hamiltonian

$$H = B \cos x + C \sin y + A (y \sin z - x \cos z) \tag{2.49}$$

and

$$p = y \cos x + \sin y, \tag{2.50}$$

Equation (2.50) can be inverted with the Bessel–Fubini integral

$$y(x, p) = \frac{p}{\cos x} + 2 \sum_{n=1}^{\infty} \frac{1}{n} (-1)^n J_n \left( \frac{n}{\cos x} \right) \sin \frac{np}{\cos x}. \tag{2.51}$$



This gives the Hamiltonian (2.49) in an explicit form

$$H(x, p, z) = Cy + B \cos x - Ax \cos z + y(x, p)(A \sin z - C \cos x), \quad (2.52)$$

where  $y(x, p)$  should be taken from (2.51).

Let us note that the Hamiltonian form of equations with a time-periodic perturbation implies an immediate conclusion of the existence of chaotic trajectories (streamlines) as will be clear later. This demonstrates how the Hamiltonian form of a problem provides some general conclusion on orbits and their properties.

## Problems

More complicated problems are marked by (\*).

2.1 Using a reference book, prove the expressions (2.6)–(2.8) and (2.10)–(2.13).

2.2 Find and draw the pendulum velocity  $\dot{x} = \dot{x}(t)$  and coordinate  $x = x(t)$  near the separatrix for  $\kappa < 1$  and  $\kappa > 1$ . Compare the results to Fig. 2.2.

2.3 A particle is moving in the potential

$$V(q) = \omega_0^2 q^2 + a q^4.$$

Find for  $a > 0$

(a) solutions  $q(t)$ ,  $p(t)$ ;

(b) action  $I = I(E)$ ;

(c) frequency  $\omega = \omega(I)$ ;

(d) spectral decomposition  $p_n$ ,  $q_n$ ;

(e) find asymptotics of solutions  $q$ ,  $p$  and  $I$ ,  $\omega$  for  $E \gg \omega_0^2$ .

2.4 The same as in Problem 2.3 for the potential

$$V(q) = -\omega_0^2 q^2 + a q^4, \quad a > 0.$$

Find also the asymptotics of the dynamics near the separatrix.

2.5\* The same as in (b)–(d) of Problem 2.3 but for the Hamiltonian

$$H = \cos p + \cos q.$$

Also find the dynamics near the separatrix and on the separatrix.

2.6 Prove the correctness of equations (2.39) using the transition from variables  $(x, y)$  to  $\xi = \xi(x, y)$ ,  $p = p(x, y)$  with  $\xi = x$ .

2.7 Show that (2.40) follows from the condition of incompressibility (2.36).

# 3

## PERTURBED DYNAMICS

A typical approach to general study of dynamical systems is to split the system's Hamiltonian in two parts: unperturbed Hamiltonian  $H_0$  and perturbation  $\epsilon V$ , i.e.

$$H = H_0 + \epsilon V \quad (3.1)$$

with  $\max V \sim H_0$  and a dimensionless perturbation parameter  $\epsilon$  that is assumed to be small ( $\epsilon \ll 1$ ). It is also typical to consider the unperturbed system as an integrable one and present

$$H_0 = H_0(I_1, \dots, I_N) \quad (3.2)$$

as a function of actions  $\mathbf{I} = (I_1, \dots, I_N)$ . Then we can write for a general situation

$$V = V(I_1, \vartheta_1; \dots; I_N, \vartheta_N), \quad (3.3)$$

where  $\boldsymbol{\vartheta} = (\vartheta_1, \dots, \vartheta_N)$  are phases canonically conjugated to  $\mathbf{I}$ . Perturbation  $V$  can be incorporated into  $H_0$  if it does not depend on phases  $(\vartheta_1, \dots, \vartheta_N)$ , and there is no force if  $V$  does not depend on actions  $(I_1, \dots, I_N)$ . Thus a perturbation in the form (3.3) makes a non-trivial case.

Perturbed problems are the most difficult part of the theory of dynamical systems and a possibility of solution of (3.1) or even a description of some features of the solution is still far from complete.

### 3.1 The Liouville–Arnold theorem on integrability

This theorem was formulated in its contemporary form by Arnold (1978) and then appeared with different modifications in Kozlov (1996) and Dubrovin *et al.* (1984).

Consider a Hamiltonian system with  $N$  degrees of freedom and  $N$  first integrals of motion  $F_j$ , ( $j = 1, \dots, N$ )

$$[H, F_j] = 0, \quad (\forall j), \quad (3.4)$$

which mutually commute

$$[F_j, F_k] = 0, \quad (\forall j, k). \quad (3.5)$$

It is also assumed that the level set of  $F_j$  forms a smooth compact connected manifold  $\mathcal{M} \subset \mathbb{R}^{2N}$ , and the functions  $F_j(\forall j)$  are linearly independent on  $\mathcal{M}$ .

Then trajectories wind the invariant surface which is  $N$ -dimensional torus  $\mathbf{T}^N$  with phase (angles)

$$\vartheta_j = \omega_j t + \vartheta_j^{(0)}, \quad \omega_j = \omega_j(\mathbf{I}) = \text{const}, \quad (\forall j), \quad (3.6)$$

where  $\omega_j(\mathbf{I})$  are defined below and the Hamiltonian equations integrated in quadratures. Without loss of generality, one can consider  $F_1 = H$ . The main point of the theorem is the possibility to introduce  $N$  actions  $I_j$  ( $\forall j$ ), similar to Section 1.3, as integrals of motion instead of  $F_j$  ( $\forall j$ ).

Let the initial Hamiltonian be

$$H_0 = H_0(\mathbf{p}, \mathbf{q}), \quad \mathbf{p} = (p_1 \dots, p_N), \quad \mathbf{q} = (q_1 \dots, q_N). \quad (3.7)$$

Consider a generating function

$$S(\mathbf{I}, \mathbf{q}) = \int_{\mathbf{q}^{(0)}}^{\mathbf{q}} \mathbf{p}(\mathbf{I}, \mathbf{q}) \cdot d\mathbf{q}, \quad \mathbf{I} = (I_1, \dots, I_N) \quad (3.8)$$

in a vicinity of the initial point  $\mathbf{q}^{(0)}$ , which is single-valued in the simply connected neighbourhood. A canonical transformation from  $(\mathbf{p}, \mathbf{q})$  to  $(\mathbf{I}, \boldsymbol{\vartheta})$  is

$$p_j = \frac{\partial S}{\partial q_j}, \quad \vartheta_j = \frac{\partial S}{\partial I_j}, \quad \mathbf{I} = (I_1, \dots, I_N), \quad (3.9)$$

where the actions are defined as

$$I_j = \frac{1}{2\pi} \oint_{C_j} \mathbf{p} \cdot d\mathbf{q} = I_j(F_1, \dots, F_N), \quad (\forall j), \quad (3.10)$$

and  $C_j$  are basic contours of a torus  $\mathbf{T}^N$ . The torus is defined by the initial conditions, i.e. by the integrals of motion  $(F_1, \dots, F_N)$ , and the canonical equations are

$$\begin{aligned} \dot{I}_j &= -\frac{\partial H}{\partial \vartheta_j}, \quad \dot{\vartheta}_j = \frac{\partial H}{\partial I_j}, \quad (\forall j), \\ H &= H(I_1, \dots, I_N) = H(\mathbf{I}). \end{aligned} \quad (3.11)$$

The quantities

$$\omega_j(\mathbf{I}) = \frac{\partial H(\mathbf{I})}{\partial I_j} \quad (3.12)$$

are called frequencies, and they define the angles  $\vartheta_j$  (compare to (3.6)).

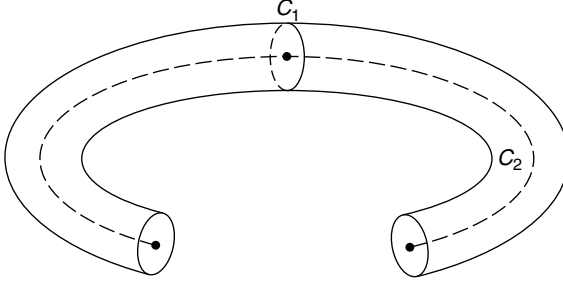


FIG. 3.1. Basic contours  $C_1, C_2$  for a 2-dimensional torus.

Since (3.11),  $\dot{I}_j = 0$  ( $\forall j$ ) and  $I_j$  are integrals of motion as they also follow from (3.10) (*Note 3.1*).

### 3.2 Consequences of the integrability

If  $N = 2$  and there exists an integral of motion  $F$  independent on  $H$ , then the system is integrable since it has two integrals:  $F$  and  $H$ . A more specific question is how unique is the definition of actions (3.10) as canonical variables. In general, actions are not defined uniquely but the invariant tori are defined uniquely if the condition of non-degeneracy is valid

$$\det \left| \frac{\partial^2 H(\mathbf{I})}{\partial I_j \partial I_k} \right| = \det \left| \frac{\partial \omega_j(\mathbf{I})}{\partial I_k} \right| \neq 0 \quad (3.13)$$

(see Arnold, 1978). This comment shows that the behaviour of trajectories in phase space does not depend on the choice of variables.

The angle variables are cyclic. Let us consider a change  $\Delta S_j$  after performing the integration in (3.8) along a contour  $C_j$ . Due to definition (3.10) it gives

$$\Delta S_j = 2\pi I_j, \quad (3.14)$$

and from (3.9) we obtain  $\Delta \vartheta_j = 2\pi$ , i.e. each cycle over a contour  $C_j$  changes  $\vartheta_j$  by  $2\pi$ , ( $\forall j$ ), and this explains the name of the angle variables. It follows immediately the spectral decomposition

$$\begin{aligned} \mathbf{p} &= \sum_{\mathbf{m}=-\infty}^{\infty} p_{\mathbf{m}}(\mathbf{I}) \exp(i\mathbf{m} \cdot \boldsymbol{\vartheta}), \quad \mathbf{m} = (m_1, \dots, m_N), \\ \mathbf{q} &= \sum_{\mathbf{m}=-\infty}^{\infty} q_{\mathbf{m}}(\mathbf{I}) \exp(i\mathbf{m} \cdot \boldsymbol{\vartheta}), \quad \mathbf{m} = (m_1, \dots, m_N), \end{aligned} \quad (3.15)$$

which is analogous to the case  $N = 1$ . Formulas (3.15) show that integrable systems perform a conditionally periodic motion.

One more generalization can be considered for the case  $N = 1\ 1/2$ , i.e. for a Hamiltonian

$$H = H(p, q; t) = H(p, q; t + T) \quad (3.16)$$

with a periodic dependence on time and period  $T$ . One can consider dynamics in a cylindric space  $\mathbb{R}^2\mathbb{L}_t$  with  $\mathbb{L}_t$  along the  $t$ -axis. Due to periodicity along  $t$ , one can consider trajectories within an interval  $(0, T)$  of  $\mathbb{L}_t$  and construct the corresponding mapping (see Chapter 4).

It is important to remark that the Liouville–Arnold theorem does not assume the separation of variables when the Hamiltonian can be written as

$$H(\mathbf{I}) = \sum_{j=1}^N H^{(j)}(I_j). \quad (3.17)$$

This situation will be considered as a trivial one.

### 3.3 Non-integrability and the Kozlov condition

The notion of integrability and its counter-notion, non-integrability, has no unique definition. Different details are discussed in Kozlov (1996) and Arnold *et al.* (1993). One of the possibilities is that a system is integrable if its solutions  $(\mathbf{p}(t), \mathbf{q}(t))$  can be expressed through quadratures. We will use here the following definition: a system is not integrable if the number  $M$  of independent commuting integrals satisfies the condition

$$M \leq N, \quad (3.18)$$

but the family of trajectories of the system cannot be displayed on an invariant  $N$ -torus. In a simplified way, we can state a system is *completely integrable* if its Hamiltonian can be presented in the form (3.11). Here is the motivation for this definition. The symplectic property of Hamiltonian dynamics permits us to reduce the order of differential equations by  $2M$  if there is  $M \leq N$  single-valued independent integrals of motion, i.e. effectively the original system with  $N$  degrees of freedom can be transformed to a system with  $N - M$  degrees of freedom. At the moment, we do not have an example of the Hamiltonian system with  $M < N$  and with no randomness (*Note 3.2*).

Few important examples of the non-integrability were shown in Kozlov (1983, 1996) and Arnold *et al.* (1993). Consider a compact analytical surface of the topological genus  $g_t$ . It is equivalent to a sphere with  $g_t$  handles and, particularly, the torus has  $g_t = 1$ . The result of Kozlov (1983) is that for  $g_t \geq 2$  the system is not integrable. In Fig. 3.2 we present an example of non-integrability for  $N = 2$ .

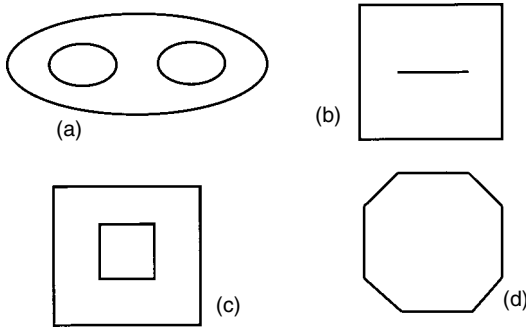


FIG. 3.2. Examples of non-integrable systems with 2 degrees of freedom ( $N = 2$ ): (a) invariant surface with  $g_t = 2$  and a trajectory that winds the surface; (b)–(d) 2-dimensional billiards, similar to the case (a).

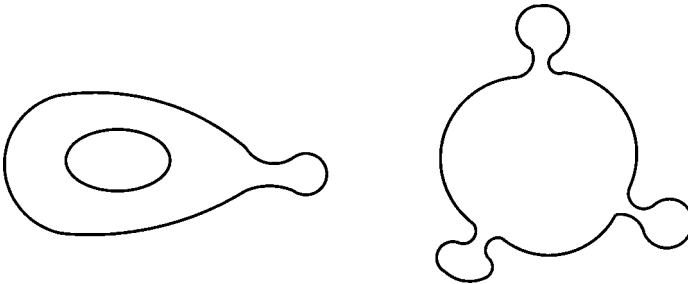


FIG. 3.3. Invariant surfaces in phase space, that have stable close contours, are wound by trajectories which are not integrable.

All these examples have interesting physical interpretations (see Chapter 19).

Less evident examples, obtained also in Kozlov (1983, 1996) are shown in Fig. 3.3.

The important part of these results is that the analysis of the integrability is non-local.

The origin of an indefiniteness in all these examples can be explained in the following qualitative way (see Fig. 3.4: after winding the middle part of the surface with  $g_t = 2$ , the next part of the trajectory, upper or lower level, is sensitive to small perturbations) (*Note 3.3*).

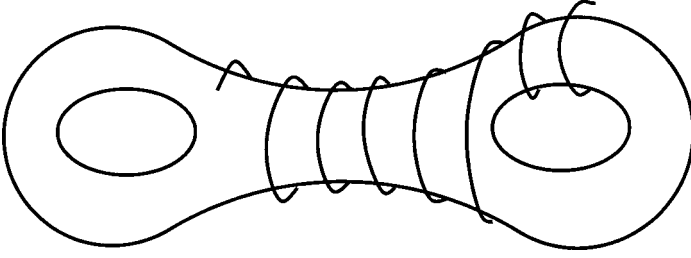


FIG. 3.4. Indefiniteness of a trajectory to wind upper/lower part of the surface.

### 3.4 Resonances

Expansion (3.15) provides a fairly simple understanding of the main difficulty of perturbation theories. Consider the perturbed Hamiltonian (3.1) and present it in the form

$$H(\mathbf{I}, \boldsymbol{\vartheta}) = H_0(\mathbf{I}) + \epsilon V(\mathbf{I}, \boldsymbol{\vartheta}) = H_0(\mathbf{I}) + \epsilon \sum_{\mathbf{m}} V_{\mathbf{m}}(\mathbf{I}) \exp(i\mathbf{m} \cdot \boldsymbol{\vartheta}) \quad (3.19)$$

with  $m_j \in \mathbb{N}$  and

$$V_{-\mathbf{m}} = V_{\mathbf{m}}^* . \quad (3.20)$$

The Hamiltonian equations can be written as

$$\begin{aligned} \dot{I}_j &= -\frac{\partial H}{\partial \vartheta_j} = -\epsilon \frac{\partial V}{\partial \vartheta_j} = -i\epsilon \sum_{\mathbf{m}} m_j V_{\mathbf{m}} \exp(i\mathbf{m} \cdot \boldsymbol{\vartheta}), \\ \dot{\vartheta}_j &= \frac{\partial H}{\partial I_j} = \frac{\partial H_0}{\partial I_j} + \epsilon \frac{\partial V}{\partial I_j} = \omega_j + \epsilon \sum_{\mathbf{m}} \frac{\partial V_{\mathbf{m}}}{\partial I_j} \exp(i\mathbf{m} \cdot \boldsymbol{\vartheta}). \end{aligned} \quad (3.21)$$

Until now the expressions (3.21) are exact. Assume that  $\epsilon \ll 1$  and that in the right-hand side of the first equation one can substitute the zero-approximation term, i.e.  $I_j = I_j^{(0)}$ ,  $\vartheta_j = \omega_j^{(0)} t + \vartheta_j^{(0)}$ ,  $\omega_j^{(0)} = \omega_j^{(0)}(\mathbf{I})$ . Then it gives

$$I_j(t) = I_j^{(0)} - \epsilon \sum_{\mathbf{m}} \frac{m_j}{(\mathbf{m} \cdot \boldsymbol{\omega}^{(0)})} V_{\mathbf{m}}(\mathbf{I}^{(0)}) \cdot \exp(i\mathbf{m} \cdot (\boldsymbol{\omega}^{(0)} t + \boldsymbol{\vartheta}^{(0)})). \quad (3.22)$$

The obtained expression shows the so-called small denominator problem since the expression  $\mathbf{m} \cdot \boldsymbol{\omega}$  depends on  $\mathbf{I}^{(0)}$  and for some values of  $\mathbf{I}^{(0)}$  it can be close to the resonant condition

$$\mathbf{m} \cdot \boldsymbol{\omega}^{(0)} = m_1 \omega_1^{(0)} + \dots + m_N \omega_N^{(0)} = 0 . \quad (3.23)$$

For  $N = 2$  this equation can be satisfied when two non-zero frequencies are in the rational connection.

A role of the resonances can be understood in the following way. Let (3.23) be valid for some set of values of  $\mathbf{I}^{(0)}$ . Then the perturbation term does not depend on time in zero-approximation, and integration of (3.21) gives terms proportional to  $t$ . This is an instability which appears due to a bad approximation approach. A better approximation is in Section 3.5.

### 3.5 Non-linear resonance and chain of islands

This section describes the structure of the resonances by an approach that is more appropriate than just the perturbation method of Section 3.4. For the sake of simplicity, consider a system of 1 1/2 degrees of freedom

$$H = H_0(I) + \epsilon V(I, \theta, t), \quad (3.24)$$

where  $\epsilon \ll 1$  and  $V$  is periodic in time with the period  $T = 2\pi/\nu$ . Therefore,  $V$  can be expanded in a double Fourier series in  $\theta$  and  $t$ :

$$V(I, \theta, t) = \frac{1}{2} \sum_{k, \ell} V_{k, \ell}(I) e^{i(k\theta - \ell\nu t)}, \quad V_{k, \ell}^* = V_{-k, -\ell}. \quad (3.25)$$

Using expressions (3.24) and (3.25), the Hamiltonian equations of motion can be transformed into

$$\begin{aligned} \dot{I} &= -\epsilon \frac{\partial V}{\partial \theta} = -\frac{i\epsilon}{2} \sum_{k, \ell} k V_{k, \ell}(I) e^{i(k\theta - \ell\nu t)}, \\ \dot{\theta} &= \frac{\partial H}{\partial I} = \frac{dH_0}{dI} + \epsilon \frac{\partial V(I, \theta, t)}{\partial I} = \omega(I) + \frac{1}{2} \epsilon \sum_{k, \ell} \frac{\partial V_{k, \ell}(I)}{\partial I} e^{i(k\theta - \ell\nu t)}, \end{aligned} \quad (3.26)$$

where we use the frequency of oscillations for the unperturbed motion:

$$\omega(I) = \frac{dH_0}{dI}. \quad (3.27)$$

The resonance condition implies

$$k\omega(I) - \ell\nu = 0 \quad (3.28)$$

with integers  $k$  and  $\ell$ . Let us specify a pair of integers,  $(k_0, \ell_0)$ , and the corresponding value,  $I_0$ , such that (3.28) converts into the identity

$$k_0\omega(I_0) = \ell_0\nu. \quad (3.29)$$

Due to the system non-linearity there are many possible values  $(k, \ell; I)$  that satisfy the condition (3.28). For the beginning we analyse a simplified situation of an isolated resonance (3.29) and ignore all other possible resonances. This



means that in the equations of motion (3.26), only terms with  $k = \pm k_0$ ,  $\ell = \pm \ell_0$  should be retained, which satisfy the resonance condition at  $I = I_0$ :

$$\begin{aligned}\dot{I} &= \epsilon k_0 V_0 \sin(k_0 \theta - \ell_0 \nu t + \phi), \\ \dot{\theta} &= \omega(I) + \epsilon \frac{\partial V_0}{\partial I} \cos(k_0 \theta - \ell_0 \nu t + \phi),\end{aligned}\tag{3.30}$$

where

$$V_{k_0, \ell_0} = |V_{k_0, \ell_0}| e^{i\phi} = V_0 e^{i\phi}.\tag{3.31}$$

It is also assumed that the value

$$\Delta I = I - I_0\tag{3.32}$$

is small, i.e. (3.26) is considered in the vicinity of the resonance value of the action  $I_0$ .

A list of typical approximations is as follows:

- (i) Put  $V_0 = V_0(I_0)$  on the right-hand sides of (3.30);
- (ii) Expand the frequency  $\omega(I)$  using (3.32):

$$\omega(I) = \omega_0 + \omega' \Delta I,\tag{3.33}$$

where

$$\omega_0 = \omega(I_0), \quad \omega' = \frac{d\omega(I_0)}{dI};\tag{3.34}$$

- (iii) Neglect the second term of the order of  $\epsilon$  in the second equation of (3.30) for the angle.

Finally, we reduce the system (3.30) to its simplified version:

$$\begin{aligned}\frac{d}{dt}(\Delta I) &= -\epsilon k_0 V_0 \sin \psi \\ \frac{d}{dt}\psi &= k_0 \omega' \Delta I,\end{aligned}\tag{3.35}$$

where a new phase is introduced:

$$\psi = k_0 \theta - \ell_0 \nu t + \phi - \pi\tag{3.36}$$

assuming that  $\omega' > 0$ . In the case that  $\omega' < 0$  a corresponding phase shift in the definition of  $\psi$  should be applied. The set of equations (3.35) has a Hamiltonian form:

$$\frac{d}{dt}(\Delta I) = -\frac{\partial \bar{H}}{\partial \psi}; \quad \frac{d}{dt}\psi = \frac{\partial \bar{H}}{\partial(\Delta I)},\tag{3.37}$$

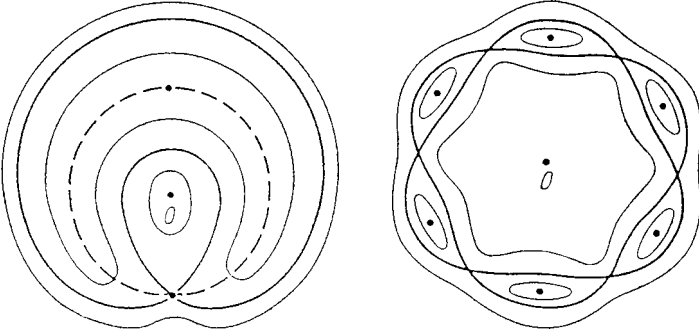


FIG. 3.5. Non-linear resonances on the phase plane  $(p, q)$ . The dashed line is the unperturbed trajectory with  $I = I_0$ . The thick line is a new separatrix of phase oscillations: (a)  $k_0 = \ell_0 = 1$ ; (b)  $k_0 = 6, \ell_0 = 1$ .

where

$$\bar{H} = \frac{1}{2}k_0\omega'(\Delta I)^2 - \epsilon k_0 V_0 \cos \psi. \quad (3.38)$$

Expression (3.38) is an effective Hamiltonian describing dynamics of the system in a neighbourhood of the resonance. Variables  $(\Delta I, \psi)$  form a canonically conjugate pair.

A comparison of expressions (3.38) and (2.1) shows that the Hamiltonian  $\bar{H}$  describes the oscillations of a nonlinear pendulum. It follows from (3.35) that

$$\ddot{\psi} + \Omega_0^2 \sin \psi = 0, \quad (3.39)$$

where the frequency of ‘small amplitude’ oscillation is

$$\Omega_0 = (\epsilon k_0^2 V_0 |\omega'|)^{1/2}. \quad (3.40)$$

The quantity  $\Omega_0$  is also the frequency of phase oscillations. The formulas obtained in Section 2.1 and Appendix A for the non-linear pendulum can be automatically applied to Hamiltonian (3.38).

On the phase plane  $(p, q)$ , a phase curve defined by the action  $I_0$  (see Fig. 3.5) corresponds to an exact resonance. The transform (3.36), from polar angle  $\theta$  to phase  $\psi$ , corresponds to the transform of a coordinate frame of reference rotating with a frequency  $\ell_0\nu$ . It follows that for the resonance with an order  $k_0$ , there is a chain of islands with  $k_0$  separatrix cells,  $k_0$  hyperbolic singular points, and  $k_0$  elliptic ones. Thus, the topology of phase space is changed in the vicinity of the resonance value  $I_0$ .

Let us determine the conditions under which the system is ‘trapped’ by a non-linear resonance. The dimensionless parameter  $\alpha$  characterizes a degree of

non-linearity of oscillations:

$$\alpha \equiv \frac{I_0}{\omega_0} \left| \frac{d\omega(I_0)}{dI} \right| = \frac{I_0}{\omega_0} |\omega'|. \quad (3.41)$$

The three approximations mentioned above are valid if the following conditions are satisfied:

$$\epsilon \ll \alpha \ll \frac{1}{\epsilon}. \quad (3.42)$$

The first inequality means that the non-linearity must be fairly strong while the second inequality restricts the time of the approximation.

To determine the validity of the Hamiltonian (3.38), we need to estimate the amplitude of the phase oscillations:

$$\frac{\max \Delta I}{I_0} \sim \left( \epsilon \frac{V_0}{|\omega'|} \right)^{1/2} \frac{1}{I_0} \sim \left( \frac{\epsilon}{\alpha} \right)^{1/2}, \quad (3.43)$$

where we put  $V_0 \sim H_0 \sim \omega_0 I_0$ . In the same way, we derive the frequency width of the resonance from the definition (3.40):

$$\frac{\max \Delta \omega}{\omega_0} = \frac{\Omega_0}{\omega_0} = (\epsilon \alpha)^{1/2}. \quad (3.44)$$

Expression (3.43) provides the meaning for the first inequality in (3.42) and expression (3.44) gives the meaning of the second one, i.e., the relative changes in action and frequency must be small due to the non-linear resonance approximation.

The described set of islands will be called *resonant islands* or *chain of islands*. Their study leaves aside many questions, and particularly the question of a role of all other possible resonances. We will discuss them in the forthcoming sections (*Note 3.4*).

### 3.6 Kolmogorov–Arnold–Moser (KAM) theory

Sections 3.3 and 3.4 describe how the perturbation theory works, at least in a simplified way. The role of neglected terms can be estimated for a finite time. The approach to the stability problem, developed by the KAM theory, is very different and it establishes stability results for an *infinite time* (*Note 3.5*).

The crucial idea of the KAM theory is to consider invariant tori rather than trajectories and to study a perturbation of the tori rather than stability of trajectories. A simplified formulation of the KAM theory results is the following: consider a system with a Hamiltonian of the form (3.1)–(3.3). Then for  $\epsilon \rightarrow 0$  and some conditions formulated below the majority of the invariant unperturbed tori

persists under the perturbation in a slightly deformed way, and the rest of the tori that can be destroyed by the perturbation is of a small measure  $\delta\Gamma(\epsilon)$  and

$$\delta\Gamma(\epsilon) \rightarrow 0, \quad (\epsilon \rightarrow 0). \quad (3.45)$$

The main conditions of the theory are: condition of the system *non-degeneracy*

$$\hat{\alpha} \equiv \det \left| \frac{\partial^2 H_0}{\partial I_j \partial I_k} \right| \neq 0 \quad (3.46)$$

(compare to (3.13)), and condition of the isoenergetic non-degeneracy:

$$\det \left| \begin{array}{c} \frac{\partial^2 H}{\partial I_j \partial I_k} \\ \boldsymbol{\omega} \end{array}, \begin{array}{c} \boldsymbol{\omega} \\ 0 \end{array} \right| \neq 0, \quad \boldsymbol{\omega} = (\omega_1, \dots, \omega_N). \quad (3.47)$$

The physical meaning of these conditions is the following. Condition (3.46) means that the unperturbed system is essentially non-linear. Let, for example,  $\omega_1 = \partial H_0 / \partial I_1$  correspond to linear oscillations, i.e.  $\omega_1 = \text{const}$  and it does not depend on any action  $I_k$ . To understand the second condition (3.47), consider the case  $N = 2$  and let the resonant condition  $n_1\omega_1 + n_2\omega_2 = 0$  be valid for some values of  $n_1, n_2$  and  $(I_1, I_2)$ . Then  $\omega_1/\omega_2 = -n_2/n_1$  and due to a perturbation  $I_1, I_2$  will change with time. This should lead the system to escape from the resonance unless

$$\frac{\omega_1}{\omega_2} = \text{const}. \quad (3.48)$$

The condition (3.48) leads to

$$d \left( \frac{\omega_1}{\omega_2} \right) = 0 \quad (3.49)$$

or

$$\begin{aligned} \frac{\partial \omega_1}{\partial I_1} \omega_2 - \frac{\partial \omega_2}{\partial I_1} \omega_1 &= 0, \\ \frac{\partial \omega_1}{\partial I_2} \omega_2 - \frac{\partial \omega_2}{\partial I_2} \omega_2 &= 0 \end{aligned} \quad (3.50)$$

that can be written in a form (3.47). Thus the condition (3.47), due to (3.48) and (3.50), means that the system can escape fairly fast from the resonance domain.

In real systems we have finite  $\epsilon$  and finite  $\hat{\alpha}$  (3.46) that can be arbitrarily small. The problem of finding some critical values  $\epsilon_c$  and  $\hat{\alpha}_c$ , such that the invariant tori persists for  $\epsilon < \epsilon_c$  and  $\hat{\alpha} < \hat{\alpha}_c$ , is beyond the KAM theory and it will be discussed in Chapter 8. In the Kolmogorov–Arnold publication, functions  $H_0(\mathbf{I})$  and  $V(\mathbf{I}, \boldsymbol{\vartheta}, t)$  were assumed to be analytical ones on their arguments, while Moser assumed these functions to have a finite number of derivatives.

## Notes

### Note 3.1

Transformation  $(F_1, \dots, F_N) \rightarrow (I_1, \dots, I_N)$  with the same definition of actions  $I_j$  as in (3.10) was used in Einstein (1917) with respect to a problem of quantization of systems with  $N$  non-separated degrees of freedom. Einstein conjectured the formula

$$I_j = \frac{1}{2\pi} \oint_{C_j} \sum_{k=1}^N p_k dq_k = n_j \hbar, \quad n_j \in \mathbf{N}, \quad (\forall j)$$

with  $N$  independent quantum numbers  $n_j$ . It was also mentioned in Einstein (1917) that a deficit of independent integrals of motion, comparing to  $N$ , makes a problem for quantization. This problem is known now as a part of the quantum chaos manifestations (see more in Zaslavsky (1981)).

### Note 3.2

The last statement is not sufficient since the randomness is not defined yet. We will discuss this point later in corresponding sections.

### Note 3.3

More discussions of the conditions of non-integrability can be found in Kozlov (1996) and Arnold *et al.* (1993).

### Note 3.4

The chain of resonance islands was investigated in Chirikov (1979). Islands-around-islands were introduced in Meiss (1986). A detailed review and rigorous results can be found in Meiss (1992).

### Note 3.5

KAM-theory is an abbreviation used for the results that have been published in Kolmogorov (1954); Arnold (1961, 1963); Moser (1962, 1967). More discussions can be found in Arnold (1978) and Arnold *et al.* (1993).

## Problems

More complicated problems are marked by (\*).

3.1\* Find a set of resonances for weakly coupled oscillators:

$$H = 1/2(p_1^2 + p_2^2) + V_1(q_1) + V_2(q_2) + \epsilon q_1 q_2$$

with  $V_1(q_1) = 1/2q_1^2 + 1/4q_1^4$ ,  $V_2(q_2) = 1/2q_2^2$  and  $\epsilon \ll 1$ .

3.2 Find the conserving quantity in non-linear resonances of the Problem 3.1.

3.3 A particle is moving between two walls located at  $q = \pm a$ , without gravity, and with absolute elastic collision with walls. The Hamiltonian is:

$$H = \frac{p^2}{2} + V_0(q),$$

where  $V_0(q) = \infty$  if  $q = \pm a$ , and  $V_0(q) = b|q|$  if  $-a < q < a$ .

(a) Find the action and frequency of oscillations.

(b) Find the solutions  $q(t)$ ,  $p(t)$ .

(c) Find the spectrum  $q_n$ ,  $p_n$ .

3.4 In the Problem 3.3, add perturbation to the potential

$$V(q) = V_0(q) + \epsilon ab \cos(\nu t), \quad \epsilon \ll 1.$$

(a) Find all possible resonances between the perturbation and unperturbed motion.

(b) Find the width of resonances.

*This page intentionally left blank*

## CHAOTIC DYNAMICS

Speaking about ‘chaotic dynamics’, we have in mind a kind of randomness or, more accurately, the idea that trajectories of particles or systems can be indistinguishable from some random process. This means that there exists an exact or approximate equivalent between solutions of some stochastic equation and, for example, the Newton equation, without anything random in the latter one. Surprisingly, it seems to be correct in spite of the paradoxical statement and numerous obstacles on the way to find the adequacy. The main trouble with the definition of chaotic dynamics for realistic physical situations, i.e. the description of trajectories as solutions of physically reasonable dynamical equations appears due to the imperfectness of the statistical analysis with the presence of strong ‘dynamical elements’ and due to insufficiency of the dynamical analysis with the presence of strong ‘statistical elements’. In this chapter we start the discussion of chaotic dynamics, or simply chaos, and different continuations and generalizations will appear later.

### 4.1 Natural measure

A typical physical way to describe randomly moving particles in phase space  $(\mathbf{p}, \mathbf{q}) \in \Gamma$  is to use a distribution function  $\rho(\mathbf{p}, \mathbf{q}; t)$  which is a normalized particle density

$$\int \rho(\mathbf{p}, \mathbf{q}; t) d\mathbf{p} d\mathbf{q} = 1. \quad (4.1)$$

Particularly, for one particle, one can use

$$\rho(\mathbf{p}, \mathbf{q}; t) = \delta(\mathbf{p} - \mathbf{p}(t))\delta(\mathbf{q} - \mathbf{q}(t)), \quad (4.2)$$

where  $\mathbf{p}(t), \mathbf{q}(t)$  are solutions of the dynamical equations and  $\delta$  is the Dirac function. The distribution (4.2) is singular and it does not have any information except the solutions  $\mathbf{p}(t), \mathbf{q}(t)$ . There are different ways how one can introduce smoothed distributions in phase space.

Consider finite dynamics in the phase space  $\Gamma$  and let  $\Pi_\epsilon$  be a partitioning of  $\Gamma$  by hypercubes of the volume  $\epsilon^{2N}$ .

We can introduce the number  $M(\Pi_\epsilon)$  which is a minimal number of the hypercubes that cover full  $\Gamma$ . Let us label all hypercubes by  $k$  and  $\mathbf{p}^{(k)}, \mathbf{q}^{(k)}$  are



coordinates of the centre of the  $k$ -hypercube. Evidently,

$$M(\Pi_\epsilon) \cdot \epsilon^{2N} \geq \Gamma \quad (4.3)$$

and the equality occurs as  $\epsilon \rightarrow 0$ . Consider  $\mathcal{N}$  initial trajectories (particles) and make a snapshot at time instant  $t$ . We will have some number of particles  $\mathcal{N}_j(t)$  in  $j$ -th hypercube. Then the function

$$\rho_j(t) = \frac{\mathcal{N}_j(t)}{\mathcal{N}} \quad (4.4)$$

corresponds to the particle density at the  $j$ -th hypercube at time instant  $t$ . The value of  $\epsilon$  shows an accuracy of the determination of coordinates of a particle. The smaller  $\epsilon$  is, the larger  $\mathcal{N}$  should be. In the case that the limit exists

$$\rho(\mathbf{p}, \mathbf{q}; t) = \lim_{\mathcal{N} \rightarrow \infty} \lim_{\epsilon \rightarrow 0} \rho_j(t) \quad (4.5)$$

the function  $\rho(\mathbf{p}, \mathbf{q}; t)$  with omitted subscript  $j$  will be called *coarse-grained* distribution function, and

$$dm(\mathbf{p}, \mathbf{q}, t) = \rho(\mathbf{p}, \mathbf{q}; t) d\Gamma = \rho(\mathbf{p}, \mathbf{q}; t) d\mathbf{p} d\mathbf{q} \quad (4.6)$$

will be called *natural measure* or *physical measure*. The latter notion is simply a probability to find a particle in the volume  $d\Gamma(\mathbf{p}, \mathbf{q})$  with coordinates  $(\mathbf{p}, \mathbf{q})$  at time  $t$ . In Hamiltonian systems there is already, in some sense, a natural measure called the *Liouville measure* that satisfies the Liouville equation and the coarse-grained distribution function captures different parts of the Liouville measure.

There are some points in the definition (4.5), (4.6) that should be considered cautiously when applied to Hamiltonian dynamics. Their origin is imposed by our incomplete understanding of how the real dynamics appears. Here they are:

(a) Any real situation suggests

$$\mathcal{N} \neq \infty, \quad \epsilon \neq 0 \quad (4.7)$$

and in reality we do not know how big  $\mathcal{N}$  and how small  $\epsilon$  should be to represent a real situation.

- (b) Selection of  $\mathcal{N}$  trajectories (particles) means selection of an ensemble and we do not have in hand any rigorous definition of a ‘good’ or well-representative ensemble.
- (c) Later, we will show some examples of dynamics for which the ensembles and limit (4.7) should be defined in different ways. For example, these different classes can be distinguished by a pair constant  $(\delta_\epsilon, \delta_{\mathcal{N}})$  such that

$$\epsilon^{\delta_\epsilon} \cdot \mathcal{N}^{\delta_{\mathcal{N}}} = \text{const}, \quad \epsilon \rightarrow 0, \quad \mathcal{N} \rightarrow \infty.$$

The pair  $(\delta_\epsilon, \delta_{\mathcal{N}})$  is defined by a singularity of the phase space.

- (d) Depending on the singularity of phase space, not all partitions  $\Pi_\epsilon$  are equivalent: they should be adjusted to a corresponding class of the ensemble. In future we will always assume that the ensemble of a problem is selected correctly.

The stationary distribution  $\rho_0(\mathbf{p}, \mathbf{q})$  does not depend on time. It is evident that the coarse-grained function loses some information related to fluctuations of  $\mathcal{N}_j(t)$ . Another way of introducing a stationary measure, if it exists, is the following: consider one trajectory during a large time  $t$  and the value  $t_j$  that this trajectory spends in the  $j$ -th hypercube. It is evident that

$$t = \sum_j t_j.$$

Then

$$\rho_t(\mathbf{p}, \mathbf{q}) = \lim_{t \rightarrow \infty} \left( \frac{t_j}{t} \right)$$

can be considered as particle density with a coordinate  $(\mathbf{p}, \mathbf{q})$  where the subscript  $j$  is omitted.

In some cases

$$\rho_0(\mathbf{p}, \mathbf{q}) = \rho_t(\mathbf{p}, \mathbf{q}), \quad (4.8)$$

known as the property of *ergodicity*. We will see that the behaviour of real trajectories is much more complicated and needs more subtle description. Even when the property (4.8) exists, in many typical situations it cannot be applied since the limits  $\mathcal{N} \rightarrow \infty$  or  $t \rightarrow \infty$  are not accessible.

In concluding of this section, let us add that a typical problem for applications is to define the evolution of systems, i.e.  $\rho(\mathbf{p}, \mathbf{q}; t)$ , rather than  $\rho_0(\mathbf{p}, \mathbf{q})$ , that may not exist in non-stationary systems.

All the comments related to the definition of the density function  $\rho$  will be discussed more in the corresponding sections (*Note 4.1*).

## 4.2 Ergodicity, mixing, and weak mixing

Here are some basic notions used in the ergodic theory of dynamical systems. Let us simplify notations and put  $x(t; x_0) \in \mathbb{R}^{2N}$  for the canonical pair  $\mathbf{p}(t; \mathbf{p}_0, \mathbf{q}_0)$  and  $\mathbf{q}(t; \mathbf{p}_0, \mathbf{q}_0)$ . Then

$$\overline{f(x)} = \lim_{T \rightarrow \infty} \frac{1}{T} \int_0^T f(x(t; x_0)) dt \quad (4.9)$$

is mean time value of function  $f(x)$ . Consider an ensemble of  $\mathcal{N}$  initial points  $x_0^{(j)}$ ,  $j = 1, \dots, \mathcal{N}$  in phase space, and the function  $f(x(t; x_0^{(j)}))$  along each

trajectory. Then

$$\langle f(x) \rangle = \lim_{\mathcal{N} \rightarrow \infty} \frac{1}{\mathcal{N}} \sum_{j=1}^{\mathcal{N}} f(x(t; x_0^{(j)})) \quad (4.10)$$

is *ensemble average of  $f(x)$* .

The ergodic theorem states that for typical Hamiltonian systems with finite dynamics  $\Gamma$  can be decomposed into possibly infinitely many subdomains  $\Gamma_k$ :

$$\cup_k \Gamma_k = \Gamma, \quad \Gamma_k \cap_{k \neq \ell} \Gamma_\ell = 0, \quad (4.11)$$

such that for each subdomain  $\Gamma_k$  the following equality is valid:

$$\overline{f(x \in \Gamma_k)} = \langle f(x \in \Gamma_k) \rangle = \int_{\Gamma_k} f(x) \rho(x, t) dx, \quad (\forall k), \quad (4.12)$$

where  $\rho(x, t) = \rho(\mathbf{p}, \mathbf{q}; t)$  is the same as in (4.6). The property (4.12) is also known as the equality of *time average* and *ensemble average* (*Note 4.2*).

The notion of mixing has better physical understanding and a more important application. Let  $f(x), g(x)$  be two arbitrary square integrable functions, and let the dynamics be finite and ergodic. The correlation function, or correlator, of  $f(x)$  and  $g(x)$  is:

$$\mathcal{R}(f, g; t) = \langle f(x(t + \tau; x_0)) g(x(\tau; x_0)) \rangle - \langle f(x) \rangle \langle g(x) \rangle. \quad (4.13)$$

Due to the ergodicity  $\langle f(x) \rangle$  and  $\langle g(x) \rangle$  do not depend on time. The property

$$\lim_{t \rightarrow \infty} \mathcal{R}(f, g; t) = 0 \quad (4.14)$$

is known as the correlation decay. The value of  $\mathcal{R}$  depends on time  $t$  and on the choice of functions  $f(x)$  and  $g(x)$ . The system possesses the mixing property if (4.14) is valid.

Another definition of the mixing is the following: let  $A(t)$  and  $B(t)$  be two subdomains  $A \subset \Gamma$ ,  $B \subset \Gamma$  of a system that is ergodic in  $\Gamma$ . The system possesses the mixing property if

$$\lim_{t \rightarrow \infty} \text{Mes}(A(t + \tau) \cap B(\tau)) - \text{Mes } A \cdot \text{Mes } B = 0. \quad (4.15)$$

Again, according to the Liouville theorem,  $\text{Mes } A(t)$ ,  $\text{Mes } B(t)$  do not depend on time. Both definitions (4.14) and (4.15) are one-to-one equivalent (*Note 4.3*). Dynamics with mixing leads to a complication of the boundary shape of a phase space drop in the process of its time evolution (Fig. 4.1).

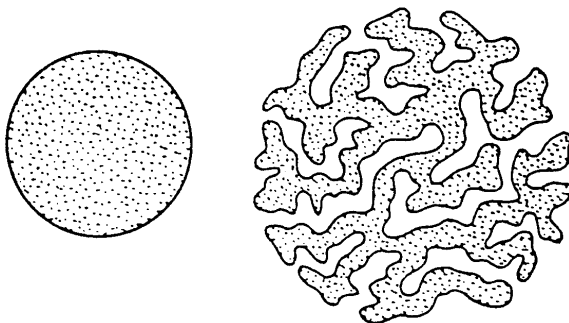


FIG. 4.1. Evolution of a domain in phase space in the case of mixing dynamics follows by a complication in its boundary shape.

Sometimes dynamical systems do not have mixing in a strong sense defined by (4.14),(4.15), but instead they have its weak equivalence. The *weak mixing* property means the existence of the limit:

$$\overline{\mathcal{R}^2(f, g; t)} = \lim_{t \rightarrow \infty} \frac{1}{t} \int_0^t d\tau \mathcal{R}^2[f(x(t + \tau)), g(x(\tau))] = 0. \quad (4.16)$$

Expression (4.16) permits the existence of large size and long-lasting fluctuations  $\delta \mathcal{R}^2$  with the only condition:

$$\lim_{t \rightarrow \infty} \frac{1}{t} \int_0^t |\delta \mathcal{R}^2(f, g; t)| = 0,$$

which means a fairly slow accumulation of these fluctuations. We will call them *persistent fluctuations*. They will be considered later.

Finally, let us write all definitions for the case when dynamical equations are given in a discrete form of a map:

$$x_{n+1} = \hat{T}x_n, \quad x_k \in \Gamma, \quad (\forall k) \quad (4.17)$$

with a time shift operator  $\hat{T}$ . Generally speaking,  $\hat{T} = \hat{T}(n)$  since the time intervals  $\Delta t_{n,n+1} = t_{n+1} - t_n > 0$  may not be equal. Then ergodicity means

$$\langle f(x) \rangle = \lim_{m \rightarrow \infty} \frac{1}{m} \sum_{n=0}^{m-1} f(\hat{T}^n x_n) = \overline{f(x_n)}, \quad (4.18)$$

mixing is

$$\mathcal{R}_n(f, g) = \langle f(\hat{T}^n x_0) g(x_0) \rangle - \langle f(x_0) \rangle \langle g(x_0) \rangle \quad (4.19)$$

and the weak mixing is

$$\overline{\mathcal{R}_n^2(f, g)} = \lim_{m \rightarrow \infty} \frac{1}{m} \sum_{n=0}^{m-1} \mathcal{R}_n^2(f, g). \quad (4.20)$$

Autocorrelation function is

$$\mathcal{R}(x, x; t) = \langle x(t; x_0) x_0 \rangle - \langle x \rangle^2 \quad (4.21)$$

and often is in use in physics. The mixing is a stronger property than ergodicity since the existence of mixing implies the ergodicity, but not vice versa.

One more definition is useful for analysis of dynamics: a dynamical system is *topologically transitive* if there exists an orbit that is dense in  $\Gamma$ . In other words, there exists an orbit that can approach any  $x \in \Gamma$  arbitrarily close. If A and B are two arbitrary small open sets, then the topological transitivity means that there is always an orbit that goes from A to B. It is worthwhile to mention that topological transitivity is a weaker property than ergodicity.

### 4.3 Local instability and Lyapunov exponents

Local analysis of the stability is an old and successful tool to study dynamical systems. The most relevant analyses to chaotic dynamics investigations were applied to the dynamics of a material point along geodesics of a surface with negative curvature (Hopf (1940)) and to the mixing property in a system with convex scatterers (Krylov (1979); Sinai (1963)).

Consider a system with finite dynamics, and two points as initial conditions for the trajectories exiting from these points. Let  $d(t)$  be a distance between the points (trajectories) at time  $t$  and  $d(0)$  is an infinitesimal value. Assume:

$$d(t) \sim d(0)e^{\nu t}, \quad \nu > 0. \quad (4.22)$$

We say that the system's dynamic in the phase space domain  $\Gamma$  has the *local instability* if the property (4.22) exists for  $d(0) \rightarrow 0$ ,  $t \rightarrow \infty$  (the order of limits is important) for any pair of initial conditions excluding, perhaps, a zero measure set of points. The increment of the local instability is

$$\nu = \lim_{d(0) \rightarrow 0} \lim_{t \rightarrow \infty} \frac{1}{t} \ln \left| \frac{d(t)}{d(0)} \right|. \quad (4.23)$$

In general,  $\nu$  is a function of the initial point.

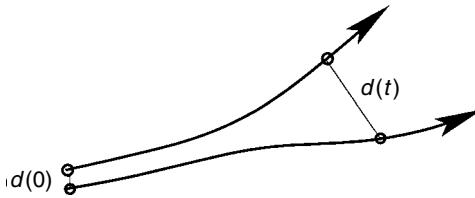


FIG. 4.2. Local instability of trajectories.

A more frequently used characteristic is *Lyapunov exponent*. Let us introduce it for discrete time equations (4.17). The Jacobian matrix  $\hat{M}$  of the map  $\hat{T}$  is

$$\hat{M} = D\hat{T}x_n = \left\| \frac{\partial x_{i;n+1}}{\partial x_{j;n}} \right\|, \quad (i, j = 1, \dots, 2N), \quad (4.24)$$

where  $N$  is the number of degrees of freedom. According to the Liouville theorem  $|\hat{M}| = 1$  for any  $n$ .

Consider the expression

$$\hat{M}_n = D_{\mathbf{v}}\hat{T}^n x,$$

where  $\mathbf{v}$  denotes a vector along which the derivative is taken. The numbers

$$\lambda(x, \mathbf{v}; n) = |D_{\mathbf{v}}\hat{T}^n x|^{1/n} \quad (4.25)$$

form an ‘ellipsoid’ of values  $\lambda$  with a centre at  $x$  and a fan of directions  $\mathbf{v}$ . The following values are the corresponding Lyapunov exponents, i.e.

$$\sigma_k(x) = \lim_{n \rightarrow \infty} \frac{1}{n} \ln |D_{\mathbf{v}_k}\hat{T}^n x|, \quad k = 1, \dots, 2N, \quad (4.26)$$

where  $\mathbf{v}_k$  defines orthogonal directions of maximal rates of dispersion of trajectories. They are well defined, due to the Oseledec (1968) theorem, for almost all  $x$ . The set  $\{\lambda_k(x)\}$  is called Lyapunov numbers at  $x$  and

$$\lambda_k(x) = \exp \sigma_k(x) \quad (4.27)$$

The *Lyapunov numbers*  $\lambda_j$  can be ordered with respect to their values:

$$\lambda_1 \leq \lambda_2 \leq \dots \leq \lambda_k \leq \dots \leq \lambda_{2N}, \quad (4.28)$$

separated by some  $\lambda_k$  and the condition  $\lambda_k \leq 1$ ,  $\lambda_{k+1} > 1$ . One can introduce  $N - k$  directions of stretching the distances between closed trajectories ( $\lambda_j > 1$ ,  $j > k$ ), and  $k$  directions of contracting or preserving the distances. Lyapunov

numbers  $\lambda_j$  depend on the point  $x$  since the matrix  $\hat{M}$  depends on  $x$ . If, for example,  $\hat{M}$  does not depend on  $x$  then one can write for a direction  $j$ :

$$d_j(n) = |\lambda_j|^n d_j(0) = d_j(0) \exp(\sigma_j n) \quad (4.29)$$

with

$$\sigma_j = \ln \lambda_j.$$

Numbers  $\sigma_j$  are Lyapunov exponents.

As it follows from (4.24), (4.29), the Lyapunov exponent is an increment of the growth of the distance between two close trajectories in some direction. Then we have a simple generalization of (4.27) to the continuous case and  $N = 1$ :

$$\begin{aligned} \sigma &= \lim_{t \rightarrow \infty} \frac{1}{t} \int_0^t dt' \ln \left| \frac{dx(t')}{dx(0)} \right| \\ &= \int_{\Gamma} dm(x_0) \ln \left| \frac{dx(t)}{dx(0)} \right|; \quad x_0 = x(0), \end{aligned} \quad (4.30)$$

where we use ergodic theorem, stationary probability measure  $dm(x_0)$ , and the property of the only value  $\sigma > 0$  since for  $N = 1$  we have  $\lambda_1 \lambda_2 = 1$ , or  $\sigma_1 + \sigma_2 = 0$ . We can interpret the Lyapunov exponent as a mean value of the local instability increment  $\nu$ , i.e.  $\sigma = \langle \nu \rangle$ , but we should remember that it is only for  $N = 1$  and that for  $N > 1$  a connection between  $\nu$  and  $\sigma$  is more complicated (*Note 4.4*).

The notion of the Lyapunov exponent is well defined, but it is hard to use for real Hamiltonian systems in real time. The reasons for that will be clear later. In this section we consider only the simplest examples which avoid ambiguities.

The following example is known as the Arnold cat map:

$$x_{n+1} = 2x_n + y_n \pmod{1}; \quad y_{n+1} = x_n + y_n \pmod{1}. \quad (4.31)$$

The phase space is a torus (square) and

$$\hat{T} = \begin{vmatrix} 2 & 1 \\ 1 & 1 \end{vmatrix}, \quad \hat{M} = \begin{vmatrix} 2 & 1 \\ 1 & 1 \end{vmatrix} = \text{const.} \quad (4.32)$$

Figure 4.3 shows the evolution of a dashed domain (in the original Arnold picture it was a cat cartoon) after one iteration. There is a direction of stretching the distances and their folding which leads to the mixing of the dashed domain uniformly inside the phase space as a square. Eigenvalues of  $\hat{M}$  are:

$$\lambda_{1,2} = \frac{1}{2}(3 \pm \sqrt{5}), \quad \lambda_1 > 1 > \lambda_2 \quad (4.33)$$

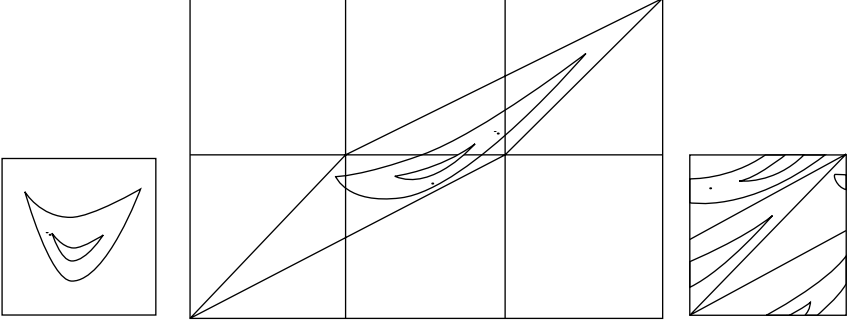


FIG. 4.3. A domain (dashed) after one iteration by the Arnold cat map (4.31).

and

$$\sigma_{1,2} = \ln \lambda_{1,2}, \quad \sigma_1 > 0, \quad \sigma_2 = -\sigma_1 < 0. \quad (4.34)$$

A more general map of the type (4.31) can be considered in the form:

$$\begin{aligned} (x_{n+1}, y_{n+1}) &= \hat{T}(x_n, y_n), \quad x, y \pmod{1}, \\ \hat{T} &= \left\| \begin{array}{cc} K+1 & 1 \\ K & 1 \end{array} \right\|, \quad \hat{M} = \left\| \begin{array}{cc} K+1 & 1 \\ K & 1 \end{array} \right\|. \end{aligned} \quad (4.35)$$

The eigenvalues of  $\hat{M}$  are

$$\lambda_{1,2} = \frac{1}{2}(2+K) \pm \sqrt{\frac{1}{4}(2+K)^2 - 1} \quad (4.36)$$

and  $\lambda_1 > 1$  for  $K > 0$  or for  $K < -4$ . Within the interval

$$-4 < K < 0 \quad (4.37)$$

we have  $|\lambda_{1,2}| = 1$  and  $\sigma_{1,2} = \ln |\lambda_{1,2}| = 0$ . For  $K \gg 1$

$$\lambda_1 \approx K, \quad \lambda_2 \approx \frac{1}{K}. \quad (4.38)$$

The result (4.38) clearly indicates the one-dimensional stretching along  $x$  and compressing along  $y$  with

$$\sigma_1 \approx \ln K > 0, \quad \sigma_2 \approx -\ln K < 0. \quad (4.39)$$

One can also consider the correlation function  $\mathcal{R}(f, g; n)$  introduced in (4.19). Let

$$f = e^{2\pi i x_n}, \quad g = e^{-2\pi i x_0}. \quad (4.40)$$



Then

$$\mathcal{R}_n \equiv \mathcal{R}(f, g; n) = \int_0^1 e^{2\pi i(x_n - x_0)} dm(x_0). \quad (4.41)$$

It is possible to estimate for large  $K \gg 1$  that

$$|\mathcal{R}_n| \sim e^{-n/\tau_c}, \quad \tau_c \sim \frac{1}{\sigma_1} \quad (4.42)$$

(see the Problem 4.2).

Using (4.38) we obtain for the characteristic time of decay of correlation

$$\tau_c = \frac{1}{\ln K}. \quad (4.43)$$

The map (4.35) can be rewritten in the form

$$\begin{aligned} y_{n+1} &= y_n + Kx_n, \quad (\text{mod } 1), \\ x_{n+1} &= x_n + y_{n+1}, \quad (\text{mod } 1). \end{aligned} \quad (4.44)$$

A generalization of (4.44) can be presented as

$$\begin{aligned} y_{n+1} &= y_n + Kf(x_n), \quad (\text{mod } 1), \\ x_{n+1} &= x_n + y_{n+1}, \quad (\text{mod } 1) \end{aligned} \quad (4.45)$$

and all results depend on the type of function  $f(x)$ ,  $|f(x)| \leq 1$ . The Jacobian matrix is

$$\hat{M}_n = \left\| \begin{pmatrix} 1 & Kf'(x_n) \\ 1 & 1 + Kf'(x_n) \end{pmatrix} \right\| \quad (4.46)$$

and it is not constant anymore. Particularly, drastic changes in results appear if there are points where  $f'(x) = 0$ . Different cases of (4.46) will be considered later.

#### 4.4 Hyperbolic systems

The *hyperbolic* or *Anosov-type system* is a special type of construction for which different kinds of ergodic properties mixing, correlation decay, etc., can be established fairly straightforwardly (Anosov (1963); Sinai (1966); Anosov and Sinai (1967)). For a simplicity, consider a two-dimensional map:

$$z_{n+1} = \hat{T}z_n, \quad z_n = (x_n, y_n), \quad x, y \in (0, 1) \quad (4.47)$$

and  $\hat{T}$  is area-preserving. For infinitesimal changes:

$$\delta z_{n+1} = \hat{M} \delta z_n, \quad \hat{M} = \left\| \frac{\partial z_{j;n+1}}{\partial z_{k;n}} \right\|, \quad |\hat{M}| = 1. \quad (4.48)$$

Vector  $\delta z_{n+1}$  is stretching if

$$\frac{|\delta z_{n+1}|^2}{|\delta z_n|^2} = \frac{|\hat{M} \delta z_n|^2}{|\delta z_n|^2} > 1 \quad (4.49)$$

and is contracting if

$$\frac{|\delta z_{n+1}|^2}{|\delta z_n|^2} = \frac{|\hat{M} \delta z_n|^2}{|\delta z_n|^2} < 1. \quad (4.50)$$

The system is of the hyperbolic type if:

- (a) domains of the contracting vectors  $\Gamma^-$  and of the stretching vectors  $\Gamma^+$  form full accessible space  $\Gamma = \Gamma^- \cup \Gamma^+$  at any step  $n$  and,
- (b) the property of vectors to belong either to  $\Gamma^+$  or to  $\Gamma^-$  is invariant at any step  $n$ .

Examples (4.31) and (4.44) belong to the hyperbolic systems. For these cases  $\hat{M}$  is constant and can be written as

$$\hat{M} = \left\| \begin{array}{cc} \lambda_1 & 0 \\ 0 & \lambda_2 \end{array} \right\| \quad (4.51)$$

in the corresponding basis. A basis does not depend on  $n$ . The boundary between  $\Gamma^-$  and  $\Gamma^+$  can be defined from the equation

$$\frac{|\hat{M} \delta z_n|^2}{|\delta z_n|^2} = 1 \quad (4.52)$$

or

$$|\delta x_n|^2 \lambda_1^2 + |\delta y_n|^2 \lambda_2^2 = |\delta x_n|^2 + |\delta y_n|^2. \quad (4.53)$$

From (4.53) we obtain the equation of the boundaries between  $\Gamma^-$  and  $\Gamma^+$ :

$$\delta x_n = \pm \left( \frac{1 - \lambda_2^2}{\lambda_1^2 - 1} \right)^{1/2} \delta y_n = \pm \frac{1}{\lambda_1} \delta y_n. \quad (4.54)$$

The equation (4.54) defines two straight lines and the corresponding cones  $\Gamma^-, \Gamma^+$  with a boundary that does not depend on  $n$ . In general, this situation is not the case and the boundaries can play a significant role in statistical properties of systems, as it will be discussed later.

## 4.5 Entropy of dynamical systems

### 4.5.1 Partitioning and coarse-graining

Consider a phase space  $\Gamma < \infty$  of the bounded dynamics of a system and partition  $\mathbf{P}(\xi)$  of  $\Gamma$  by a set of cells  $\xi = (\xi_1, \xi_2, \dots, \xi_N)$  that is assumed to be countable and cover full  $\Gamma$  without holes and intersections. A simple version of the partition  $\mathbf{P}(\xi)$  is in Fig. 4.4 where  $\Gamma$  is covered by a hypercubic lattice. The size of a cell  $\xi_j$  can be arbitrary small. Consider a set  $\xi_\ell$  of such cells that are crossed by a trajectory  $\ell$ . They cover a finite volume of phase space  $\Gamma_\ell$  and represent a real trajectory with some accuracy depending on the size of cells. The smaller the cells, the closer is  $\xi_\ell$  to the trajectory  $\ell$ . Replacement

$$\ell \rightarrow \xi_\ell \quad (4.55)$$

will be called *coarse-graining*.

Properties of  $\xi_\ell$  depend on the type of partitioning, size of cells, and on the type of trajectories (see Fig. 4.4). For example, periodic trajectory is covered by a number of cells  $N_\ell$  which is proportional to the length of the trajectory. For a finite segment of the trajectory during time interval  $t$  we have

$$N_\ell(t) \leq \text{const } t. \quad (4.56)$$

It is not the case for a mixing trajectory when  $N_\ell(t)$  grows faster than  $t$ . This new feature of the mixing dynamics can be characterized by the dynamical *entropy* if the number of cells grows exponentially with time.

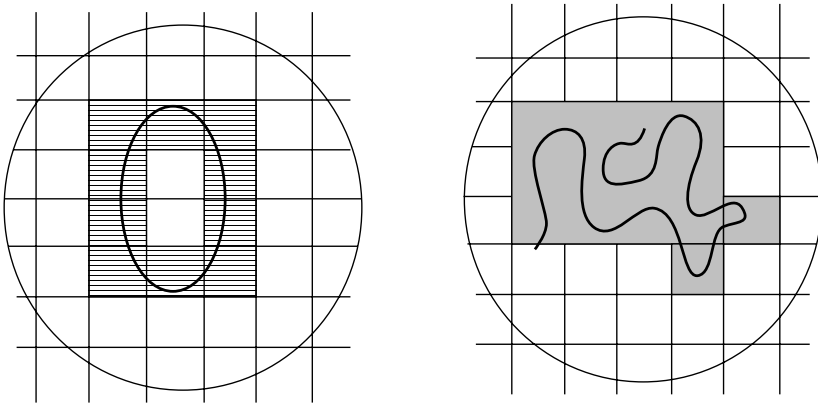


FIG. 4.4. Two cases of coarse-graining: Stable trajectory (left) of nonergodic dynamics and unstable trajectory (right) with mixing.

#### 4.5.2 Kolmogorov–Sinai (KS) entropy

Let us find a link between partitioning and time. Consider dynamics in phase space  $\Gamma$ , a point  $x_t \in \Gamma$  that represents a state of the system at time instant  $t$ , and let the dynamics be given by a map  $\hat{T}$ :

$$x_{n+1} = \hat{T}x_n, \quad (4.57)$$

which is discrete for a simplicity  $n \in \mathbb{N}$ . Let us fix a time  $n$  and partition  $\xi^{(n)} = (\xi_1^{(n)}, \xi_2^{(n)}, \dots)$ . Consider ‘dynamics’ of cells imposed by the same  $\hat{T}$ :

$$\hat{T}^{-1}\xi^{(n)} = \xi^{(n-1)} = (\xi_1^{(n-1)}, \xi_2^{(n-1)}, \dots) = (\hat{T}^{-1}\xi_1^{(n)}, \hat{T}^{-1}\xi_2^{(n)}, \dots) \quad (4.58)$$

and assume that  $\hat{T}$  is a stretching map, i.e. there exists at least one direction with positive Lyapunov exponent. For example,

$$x^{(n+1)} = \hat{T}x^{(n)} = 2x^{(n)}, \pmod{1}, \quad x \in (0, 1). \quad (4.59)$$

This is an area-preserving map stretching along  $x$  with coefficient 2. Phase volume  $\Gamma(\Delta x)$  of any interval  $\Delta x$  is constant, but the coarse-grained phase volume  $\bar{\Gamma}(\Delta x)$  will grow with time. Due to this, there exist different subdomains  $\Delta x_j^{(n-1)}$ ,  $j \in \mathbb{N}_j$  at time instant  $(n-1)$ , which are solutions of the equation

$$\hat{T}^{-1}\Delta x^{(n)} = \Delta x_j^{(n-1)}, \quad (j \in \mathbb{N}_j) \quad (4.60)$$

and  $\mathbb{N}_j \subset \mathbb{N}$ . This is reflected in Fig. 4.5 where  $j = 1, 2$  at time  $(n-1)$  and  $j = 1, 2, 3, 4$  at time  $(n-2)$  if we identify the cells  $\xi_k^{(m)}$  with the corresponding subdomains  $\Delta x_k^{(m)}$ .

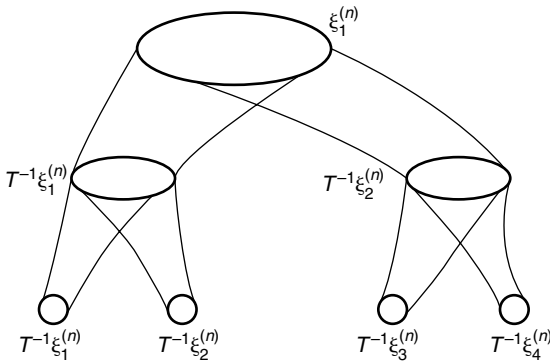


FIG. 4.5. ‘Dynamics’ of cells shows a proliferation of possible paths to arrive to the cell  $\xi_1^{(n)}$ .

Having, for example, information that at time  $(n)$  the trajectory is in  $\xi_1^{(n)}$ , means that the trajectory follows one of four possible paths beginning at time  $(n-2)$  at any of  $\xi_j^{(n-2)} = \hat{T}^{-2}\xi_j^{(n)}$ ,  $(j = 1, 2, 3, 4)$ . Let  $\boldsymbol{\xi} = \boldsymbol{\xi}^{(0)} = (\xi_1, \xi_2, \dots)$  be an initial condition at  $t = 0$  of a given partition  $\mathbf{P}(\boldsymbol{\xi})$ . Then

$$\ell(n) = \boldsymbol{\xi} \cap (\hat{T}^{-1}\boldsymbol{\xi}) \cap (\hat{T}^{-2}\boldsymbol{\xi}) \cap \dots \cap (\hat{T}^{-n}\boldsymbol{\xi}) = \boldsymbol{\xi} \cap \boldsymbol{\xi}^{(-1)} \cap \dots \cap \boldsymbol{\xi}^{(-n)} \quad (4.61)$$

defines a set of all possible paths during time interval  $n$  for any trajectory that appears in  $\boldsymbol{\xi}$  after  $(n)$  time steps. One can say that the full number of possible paths defines a level of indefiniteness of the coarse-grained dynamics.

Let  $\rho(\boldsymbol{\xi}^{(n)})$  be a measure of cells  $\boldsymbol{\xi}^{(n)}$  at time  $n$ . Evidently

$$\rho(\boldsymbol{\xi}^{(n)}) = \rho(\hat{T}\boldsymbol{\xi}^{(n)}) = \rho(\hat{T}^{-1}\boldsymbol{\xi}^{(n)}) \quad (4.62)$$

due to the area-preserving dynamics. For a full set of cells  $\xi_1^{(n)}, \xi_2^{(n)}, \dots$  let us define a sum

$$\hat{H}^{(n)}(\boldsymbol{\xi}) = - \sum_i \rho(\xi_i^{(n)}) \ln \rho(\xi_i^{(n)}) \quad (4.63)$$

and a sum along a path  $\ell$

$$\hat{H}(\boldsymbol{\xi}, \ell, n) = \hat{H}(\boldsymbol{\xi} \cap \hat{T}^{-1}\boldsymbol{\xi} \cap \dots \cap \hat{T}^{-n}\boldsymbol{\xi}). \quad (4.64)$$

After summation over all paths, we receive a function

$$\hat{H}(\boldsymbol{\xi}, n) = \sum_{\ell} \hat{H}(\boldsymbol{\xi}, \ell, n), \quad (4.65)$$

that shows proliferation of the number of paths with time  $n$ . The rate of this proliferation can be obtained as the limit

$$h(\boldsymbol{\xi}) = \lim_{n \rightarrow \infty} \frac{1}{n} \hat{H}(\boldsymbol{\xi}, n). \quad (4.66)$$

This expression depends on the partition and its cells  $\boldsymbol{\xi}$ . Finally

$$h_{\text{KS}} = \sup_{\boldsymbol{\xi}} h(\boldsymbol{\xi}) \quad (4.67)$$

is called *metric entropy*, or measure-theoretic entropy, or *Kolmogorov-Sinai entropy* (KS-entropy). The value  $h_{\text{KS}}$  is defined only by  $\hat{T}$  and it is non-zero if the number of possible paths grows exponentially with time. Otherwise,  $h_{\text{KS}} = 0$ . (Note 4.5).

As an example, consider the map (4.59) and the interval  $\Delta x^{(0)} = (0, 1)$ .  $\hat{T}^{-1}\Delta x^{(0)} = (0, 1/2)$  or  $(1/2, 1)$ , i.e. there are two possible paths. Evidently  $\hat{T}^{-n}\Delta x^{(0)}$  gives  $2^n$  possible paths. Consider partition  $\boldsymbol{\xi}^{(-n)}$  at the time  $n$

backward as  $2^n$  equals  $\xi_j^{(-n)}$ ,  $j \in (1, \dots, 2^n)$ . For a uniform distribution  $\rho(\xi_j^{(-n)}) = 2^{-n}$ ,  $\forall j$ . Then the expression (4.65) gives

$$\hat{H}(\boldsymbol{\xi}, n) = - \sum_{j=1}^{2^n} \frac{1}{2^n} \ln(2^{-n}) = n \ln 2 \quad (4.68)$$

and  $h_{\text{KS}} = \ln 2$ .

#### 4.5.3 Topological entropy

Another variant to characterize a proliferation of possible paths or trajectories due to the coarse-graining in phase volume is a so-called *topological entropy*. Consider a fairly large  $n$  and a partition  $\mathbf{P}(\boldsymbol{\xi}^{(n)})$  with fairly small cells  $\xi_j^{(n)}$  that densely cover full domain  $\Gamma$ . Let  $N(n, \boldsymbol{\xi}^{(n)})$  a number of cells not empty of segments of the trajectory (see Fig. 4.4). The larger  $n$  is, the larger  $N(n, \boldsymbol{\xi}^{(n)})$  is until full  $\Gamma$  will be covered. Nevertheless, it is always possible to make the partition so fine that not all  $\Gamma$  will be covered by the coarse-graining. The question is what is the rate of growth of  $N(n, \boldsymbol{\xi}^{(n)})$ .

Consider the quantity

$$h_{\text{top}}(\boldsymbol{\xi}) = \lim_{n \rightarrow \infty} \frac{1}{n} \ln N(n, \boldsymbol{\xi}^{(n)}) \quad (4.69)$$

and its upper limit

$$h_{\text{top}} = \sup_{\boldsymbol{\xi}} h_{\text{top}}(\boldsymbol{\xi}). \quad (4.70)$$

It is *topological entropy*. For the example (4.59)

$$h_{\text{top}} = \ln 2 = h_{\text{KS}}. \quad (4.71)$$

(Note 4.6).

#### 4.5.4 Physical interpretation

The analysis of this section is typical for statistical physics, and it permits to understand in a qualitative way the meaning of topological and KS entropies. The starting point is to consider three different types of phase volumes. Let a phase drop evolve with time under a mixing evolution operator  $\hat{T}$  and, after some time, the drop takes a complicated shape as in Fig. 4.1. Then  $\Gamma(t)$  is a real phase volume at time instant  $t$ ;  $\bar{\Gamma}(t)$  is a coarse-grained phase volume, and  $\hat{\Gamma}(t)$  is an enveloped phase volume. In the case of fairly uniform mixing

$$\hat{\Gamma}(t) \approx \bar{\Gamma}(t), \quad t \rightarrow \infty, \quad (4.72)$$

because all small bubbles disappear after coarse-graining, and large-size holes in  $\Gamma$  do not exist due to the uniformity of mixing. Condition (4.72) permits to estimate fairly simply  $h_{\text{top}}$ .

Let  $\Gamma_0$  be the volume of an initial phase space domain. According to the Liouville theorem  $\Gamma(t) = \Gamma_0$ , but for the coarse-graining phase volume  $\bar{\Gamma}(t)$  we have  $\bar{\Gamma}(t) \geq \Gamma_0$  since  $\bar{\Gamma}$  includes some empty parts (bubbles) of phase space. In the case that all points of  $\Gamma_0$ , except for some zero measure set, exhibit local instability, we can consider a simplified version when  $\hat{\Gamma}(t)$  grows exponentially, and the same is for  $\bar{\Gamma}(t)$  due to (4.72).

Consider a system with the following property: the limit

$$h = \lim_{\Gamma_0 \rightarrow 0} \lim_{t \rightarrow \infty} \frac{1}{t} \ln \bar{\Gamma}(t), \quad (4.73)$$

exists and does not depend on the coarse-graining procedure. Then  $h$  is the topological entropy. In this case, when the growth of  $\bar{\Gamma}(t)$  is due to the local instability with the only  $\nu = \sigma_1 > 0$ , we have

$$\bar{\Gamma}(t) = \Gamma_0 \exp \sigma_1 t = \Gamma_0 \exp(\ln \lambda_1 t) \quad (4.74)$$

and we have

$$h = \sigma_1 = \nu = \ln \lambda_1 = h_{\text{top}}. \quad (4.75)$$

Particularly for the example (4.59)  $h = \ln 2$ .

The entropy  $h$  has a simple physical meaning: since  $\ln \bar{\Gamma}(t)$  is the Boltzmann type entropy up to an additive constant, the topological entropy is the rate of the entropy growth per unit time (a step of the map).

Another definition considers an averaging of  $\ln \bar{\Gamma}$  over ensemble of initial conditions, i.e.

$$h^* = \lim_{\Gamma_0 \rightarrow 0} \lim_{t \rightarrow \infty} \frac{1}{t} \langle \ln \bar{\Gamma}(t) \rangle = h_{\text{KS}} \quad (4.76)$$

that makes the relation to the Boltzmann definition of entropy more evident. The difference between  $h$  and  $h^*$  or between  $h_{\text{top}}$  and  $h_{\text{KS}}$  is similar to the difference between microcanonical and canonical ensembles. In the case of uniform distribution

$$\rho(\xi_j^{(n)}) = \frac{\bar{\Gamma}(\xi_j^{(n)})}{\bar{\Gamma}(n)} = \frac{1}{N(n)} = \text{const} \quad (4.77)$$

(compare to the example (4.68)), where

$$\sum_1^{N(n)} \bar{\Gamma}(\xi_j^{(n)}) = \bar{\Gamma}(n) = N(n) \bar{\Gamma}(\xi_j^{(n)}). \quad (4.78)$$

Then

$$\langle \ln \bar{\Gamma}(n) \rangle = - \sum_{j=1}^{N(n)} \rho(\xi_j^{(n)}) \ln \rho(\xi_j^{(n)}) = \bar{\Gamma}(n) \sum_{j=1}^{N(n)} \frac{1}{\bar{\Gamma}(\xi_j^{(n)})} \ln N(n) = \ln N(n), \quad (4.79)$$

where we use (4.77). The result (4.79) is similar to the equivalence of the canonical and microcanonical ensembles in statistical physics. As it will be clear later, the situation is fairly often different in realistic models.

#### 4.5.5 Entropy and Lyapunov exponents

Since entropy, metric or topological, defines the rate of exponential growth of the coarse-grained phase volume, there is a possibility to find a connection of them with Lyapunov exponents.

Let a system have positive Lyapunov exponents  $\sigma_i^+$  in some direction  $\{i\} = \{i_1, i_2, \dots\}$ . Then, for constant  $\sigma_i^+$  the phase volume grows as  $\exp[(\sigma_{i_1}^+ + \sigma_{i_2}^+ + \dots)t]$  and

$$h_{\text{KS}} = \sum_i d_i \sigma_i^+ = \sum_i d_i \ln \lambda_i, \quad (4.80)$$

where the sum is over all directions  $i$  with  $\sigma_i > 0$  and  $d_i$  is a number of degeneracy of  $\sigma_i^+$ . This result for the area preserving maps is known as Pesin's formula (Pesin (1977)). In the general case the formula (4.80) should be rewritten as

$$h_{\text{KS}} = \sum_i \int \sigma_i^+(x) \delta_i(x) d\Gamma(x). \quad (4.81)$$

where  $\delta_i(x)$  is dimension of the phase space in the direction  $i$ , which can be fractional (Ledrappier and Young (1985)). This important generalization will be better understood later in the analysis of fractional kinetics.

### 4.6 Definition of chaotic dynamics

The word 'chaos' is not a uniquely defined scientific notion. In the most vague sense, chaotic dynamics are dynamics originated by regular dynamical equations with no stochastic coefficients, but at the same time, with solutions (trajectories) that are similar or indistinguishable from some stochastic processes. We also link the stochastic processes to a specific indefiniteness with respect to the information about the process, and the same should be for the dynamical equations with chaos. Such a definition is not constructive and has some indefiniteness. It has more from the 'feeling' than from the mathematical or physical background.



There are few definitions of the chaotic dynamics in the contemporary literature: there exists a domain in phase space where

- (a) a system with finite dynamics and at least one positive Lyapunov exponent  $\sigma > 0$  is chaotic;
- (b) a system with positive KS entropy is chaotic;
- (c) a system equivalent to the hyperbolic or Anosov system is chaotic.

The common part of all these definitions is the existence of local instability and exponential divergence of initially close trajectories. At the same time, all definitions are not exactly equivalent, especially if we consider different kinetic properties of dynamics. More discussions will appear later, after more realistic systems will be introduced.

#### 4.7 Chirikov resonance overlapping criteria

The resonance overlapping criteria of appearance of chaos was proposed in Chirikov (1959), and discussed for different applications (*Note 4.7*). Consider again an example from Section 3.5 where a resonance chain of islands was introduced for a non-linear one-degree of freedom system perturbed by a periodic force. The chain was defined by the resonance condition:

$$k_0\omega(I_0) = \ell_0\nu \quad (4.82)$$

with an appropriate pair of integers  $(k_0, \ell_0)$  and the resonant value of action  $I_0$ . The value

$$\frac{\Delta I_{\max}}{I_0} = \left( \frac{\epsilon V_0}{|\omega'|} \right)^{1/2} \frac{1}{I_0} \sim \left( \frac{\epsilon}{\alpha} \right)^{1/2}, \quad (4.83)$$

where  $\alpha$  is introduced in (3.41), defines the width of the resonance, i.e. the diameter of the separatrix loop along the action axis (see Fig. 3.3).

Let the neighbouring resonances be defined by the integers  $k_0, \ell_0 \pm 1$  and the action  $I_0 + \delta I$ . The value  $\delta I$  is called the *distance between resonances* along the action axis. The corresponding resonance condition is

$$k_0\omega(I + \delta I) = (\ell_0 \pm 1)\nu \quad (4.84)$$

(for other possibilities see Problem 4.3). Assuming that  $\delta I \ll I_0$  and using (4.82) we obtain:

$$\delta\omega = \omega'_0\delta I = \pm\nu, \quad \omega'_0 \equiv \frac{d\omega(I_0)}{dI_0}. \quad (4.85)$$

Chirikov has introduced a parameter

$$K_{ch} = \left| \frac{\Delta I}{\delta I} \right| = \left| \frac{\Delta\omega}{\delta\omega} \right|, \quad (4.86)$$

where  $\delta\omega$  is a frequency distance between resonances and

$$\Delta\omega = \omega'_0 \Delta I \quad (4.87)$$

is a frequency width of the  $(k_0, \ell_0)$  resonance. The Chirikov criteria of chaos is

$$K_{ch} \gtrsim 1 \quad (4.88)$$

or, using (4.84) and (4.85)

$$K_{ch} = (\epsilon\alpha)^{1/2} \frac{\omega_0}{\nu} \gtrsim 1. \quad (4.89)$$

This means the overlapping of resonances.

A non-trivial meaning of the condition (4.89) occurs from its structure. While  $|\Delta\omega|/\omega_0$  and  $|\delta\omega|/\omega_0$  are both small, their ratio can be large. Another meaning of the condition (4.88) is the absence of trajectories with locally bounded dynamics. This type of condition, an absence of trapped particles, was mentioned in Vedenov *et al.* (1961) for the so-called quasilinear theory of plasma.

The Chirikov criteria is very convenient for some simple practical estimates but should be applied cautiously in more formal problems due to the following reasons:

- (a) the set of resonances that should be considered for the overlapping is not defined from the criteria and it is necessary to guess the ‘correct’ set of them;
- (b) the domains of chaos exist even when  $K_{ch} \ll 1$ ;
- (c) the topology of chaos can be very different for  $K_{ch} \gtrsim 1$ , i.e. the structure of chaotic domains in phase space depends not only on the value of  $K_{ch}$  as it will be seen later.

## Notes

### Note 4.1

The basic information on ergodic theory with applications to dynamical systems can be found in Cornfeld *et al.* (1982). Discussion of different measures are in Sinai (1994); Cornfeld *et al.* (1982); Pesin (1997); Young (2002).

### Note 4.2

It is a general belief that typical physical systems are ergodic. Nevertheless, this notion should be used with some care since the ergodicity has a sense within ‘domains of ergodicity’ that are not defined. Fairly typical dynamics can reveal such a complicated topology of an infinite number of subdomains

$\Gamma_k$  that the notion of ergodicity can lose its usual sense, as it will be seen later. More discussions are in Section 22.6.

*Note 4.3*

In physical literature the mixing property is considered a necessary condition for the appearance of statistical properties and for kinetic description of dynamics. Some type of systems, as will be shown, have statistical behaviour without mixing. The importance of the mixing property and its relation to the local instability (see the next section) was discussed in detail in Krylov (1979).

*Note 4.4*

For more information on the Lyapunov exponents and their properties see Lichtenberg and Lieberman (1983); Ott (1993); Dorfman (1999).

*Note 4.5*

The definition of KS entropy appeared for the first time in Kolmogorov (1958) in an analogy to information entropy. The definition presented here follows Sinai (1959). See also Sinai (1994). For the most recent review paper see Young (2003).

*Note 4.6*

The topological entropy was introduced in Adler *et al.* (1965). An important discussion of different entropies can be found in Pesin (1997); Afraimovich and Sze-Bi Hsu (2003); Young (1995).

*Note 4.7*

See more in Zaslavsky and Chirikov (1972); Chirikov (1979); Zaslavsky (1970, 1985).

## Problems

More complicated problems are marked by (\*).

4.1 For the Arnold cat map (4.31) calculate the local instability increment  $\nu$  and compare it to the Lyapunov exponent  $\sigma$ .

4.2 Prove (4.42) using the induction method and assuming that  $dm(x_k) = dx_k$  for  $k \gg 1$ , i.e. assuming uniform distribution function for the probability density after a fairly large number of steps.

4.3 Other than (4.79), possibilities for the resonances correspond to different changes of integers  $(k_0, \ell_0)$  by 1, for example  $(k_0 \pm 1, \ell_0)$ ,  $(k_0 + 1, \ell_0 + 1)$ , etc. Find all possible resonance pairs of the integers  $(k, \ell)$  neighbouring to  $(k_0, \ell_0)$  and calculate the Chirikov criteria for them.

4.4\* Find the overlapping criteria for the resonances in the Problem 3.4.

## PHYSICAL MODELS OF CHAOS

All physical classical models are described by differential or integro-differential equations and the discrete time systems can be considered as simplified versions of these equations. A discrete form of the time evolution equations will be called *maps* and, generally speaking, they can be written in a form of iterations:

$$(\mathbf{p}_{n+1}, \mathbf{q}_{n+1}) = \hat{T}_n(\mathbf{p}_n, \mathbf{q}_n), \quad (5.1)$$

where the time-shift operator  $\hat{T}_n$  is  $(2N \times 2N)$  matrix that depends on  $n$ . An additional equation is necessary to define time instants of the application of operator  $\hat{T}_n$ :

$$t_{n+1} = g(t_n) \quad (5.2)$$

with an appropriate function  $g$ . It is important that the systems (5.1) and (5.2) describe physical phenomena adequately, and the absence of the second equation (5.2) may lead to an ambiguity or to a nonsense.

In this chapter we introduce the most typical physical models.

### 5.1 Mapping the dynamics

Let us start from an example with the *Zeno map*:

The Greek philosopher Zeno of Elea (*c.450 B.C.*) is credited with creating several famous paradoxes, one of which, the ‘Achilles paradox’, was described by Aristotle in the treatise *Physics*. The paradox concerns a race between the fleet-footed Achilles (the Greek hero of Homer’s *The Illiad*), and a slow-moving tortoise. The Achilles paradox postulates that as both start moving at the same time, Achilles can never catch the tortoise if the tortoise is given a head start. The Zeno map conveys this idea that Achilles can never catch the tortoise. It is a set of positions  $\{x_j\}$ , with Achilles initially at point  $x_0$ , and the tortoise at point  $x_1$ . When Achilles arrives at  $x_1$ , the tortoise achieves  $x_2$  and evidently  $x_2 - x_1 \ll x_1 - x_0$ . When Achilles arrives at  $x_2$ , the tortoise is at  $x_3$  and  $x_3 - x_2 \ll x_2 - x_1$ , and so on. There is always a finite distance between Achilles and the tortoise which are supposed to move with constant velocities. A solution for this paradox is in a special selection of the set of time instants  $t_j$  that generate the map  $\{x_0, x_1, \dots\}$ . This solution shows that no map of the form (5.1) can represent dynamics that is adequate to real trajectories or, simply, that adequately present

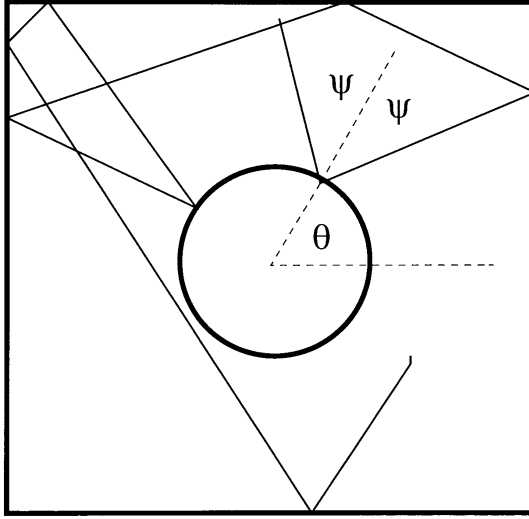


FIG. 5.1. Trajectory in the Sinai billiard model.

the trajectories in phase space. This solution cautions us in the choice of a map that should replace real trajectories.

Another example can be considered for the *Sinai billiard* model (Fig. 5.1): a convex scatterer (a circle for the sake of simplicity) in a square with elastic collisions between a point ball and the boundaries. The corresponding map can be naturally introduced, for example, as the connection between the coordinate  $\vartheta$  on the circle and velocity direction  $\psi$  at consequent collisions of the ball with the scatterer:

$$(\vartheta_{n+1}, \psi_{n+1}) = \hat{T}_n(\vartheta_n, \psi_n). \quad (5.3)$$

The results for the ergodicity, mixing, and kinetics depend significantly on equation (5.2) that defines the time intervals between the collisions.

The *Poincaré map* is most often used in physical applications. Consider a hyper-surface  $S$  in the phase space and the set of points  $(\mathbf{p}_n, \mathbf{q}_n)_S$  on  $S$  together with time instant  $t_n$ . The Poincaré map is the connection:

$$(\mathbf{p}_{n+1}, \mathbf{q}_{n+1})_S = \hat{T}(\mathbf{p}_n, \mathbf{q}_n)_S, \quad t_{n+1} = g_S(t_n) \quad (5.4)$$

(see Fig. 5.2).

For example, if  $N = 2$  and the dynamics is bounded, the area of location of trajectories is  $\mathbb{R}^3$  bounded by a hyper-surface of constant energy  $E$ :

$$E = H(p_1, q_1; p_2, q_2). \quad (5.5)$$

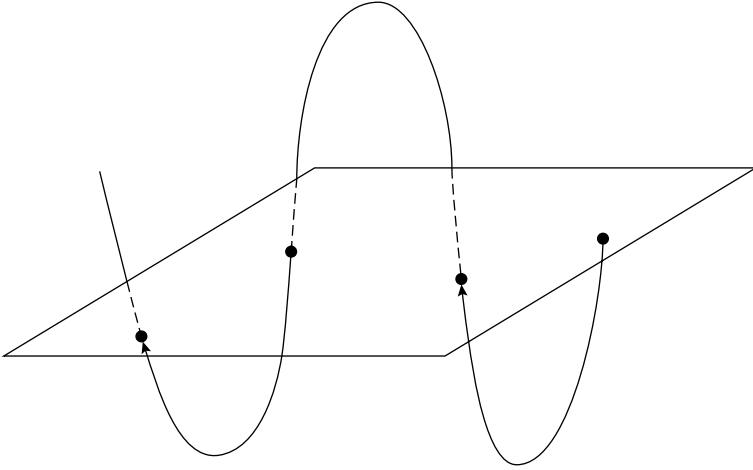


FIG. 5.2. Construction of the Poincaré map.

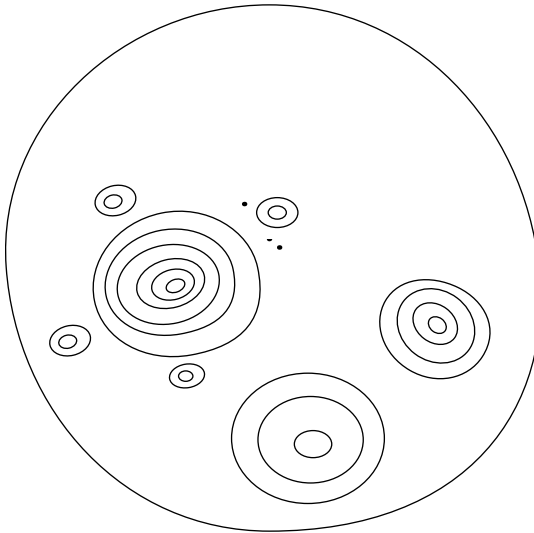


FIG. 5.3. Structure of phase space presented by the Poincaré map.

One can consider a plane, for example,  $q_2 = \text{const}$  and a trajectory intersection with this plane and condition  $p_2 > 0$  for the orientation. We will get circles in the case when trajectories wind the invariant tori, and the set of points  $(p_1, q_1)$  fills a domain densely when the trajectories are chaotic. A symbolic picture is presented in Fig. 5.3. The pattern can be different for different surfaces of

sections, and full information about the phase space topology can be obtained only by more detailed analysis of different Poincaré map sections (*Note 5.1*).

Figure 5.3 shows a large domain of chaotic dynamics called *stochastic sea and islands* filled by invariant KAM curves or tori. Inside the islands there can be narrow strips or layers filled by chaotic trajectories, called *stochastic layers*. We will see how complicated the phase space topology is when we consider specific examples.

## 5.2 Universal and standard map

Consider a Hamiltonian

$$H = H_0(p) + Kf(x) \sum_{n=-\infty}^{\infty} \delta\left(\frac{t}{T} - n\right) \quad (5.6)$$

in which perturbation is a periodic sequence of  $\delta$ -function type pulses (kicks) following with period  $T = 2\pi/\nu$ ,  $K$  is an amplitude of the pulses, and  $|f(x)| \leq 1$  is some function. The equations of motion, corresponding to (5.6), are

$$\begin{aligned} \dot{p} &= -Kf'(x) \sum_{n=-\infty}^{\infty} \delta\left(\frac{t}{T} - n\right), \\ \dot{x} &= H'_0(p) = \omega(p). \end{aligned} \quad (5.7)$$

Between any two consequent kicks there is a free motion

$$p = \text{const}, \quad x = \omega(p)t + \text{const}. \quad (5.8)$$

The solution on the left side of the  $n$ -th kick

$$p_n \equiv p(t_n - 0), \quad x_n \equiv x(t_n - 0), \quad t_n = nT \quad (5.9)$$

can be connected to the solution on the right side of the kick  $p(t_n + 0)$ ,  $x(t_n + 0)$  using equations (5.7) and the condition of continuity of  $x$ :

$$\begin{aligned} p(t_n + 0) - p(t_n - 0) &= -KTf'(x_n), \\ x(t_n + 0) &= x(t_n - 0). \end{aligned} \quad (5.10)$$

Using notations (5.9) and results (5.8) and (5.10) we can derive the iteration equation

$$\begin{aligned} p_{n+1} &= p_n - KTf'(x_n), \\ x_{n+1} &= x_n + \omega(p_{n+1})T. \end{aligned} \quad (5.11)$$

We will call (5.11) the *universal map*.

The obtained system, together with the condition  $t_n = nT$ , is equivalent to (5.7). In the case that  $f(x)$  is periodic with a period  $2\pi$ , any trajectory can be considered in the following four different types of phase space:

$$\begin{aligned} \mathbf{R}^2 : (-\infty < p < \infty; -\infty < x < \infty), \\ \mathbf{T}_1^2 : (-\pi < p < \pi; -\pi < x < \pi), \\ R_p^1 \times \mathbf{T}_x^1 : (-\infty < p < \infty; -\pi < x < \pi), \\ \mathbf{T}_p^1 \times R_x^1 : (-\pi < p < \pi; -\infty < x < \infty). \end{aligned} \quad (5.12)$$

Equations (5.11) define a Poincaré map for this specific case.

The properties of the map (5.11) depend drastically on the function  $f(x)$ . For example, if  $f'(x) = -x$  and  $\omega(p) = p$ , we have the Anosov type system (4.35). If there are points  $x^*$  with  $f'(x^*) = 0$ , then in the vicinity of these points we have invariant curves of the KAM type (see Problem 5.1). There is a special case for  $f(x) = -\cos x$  and  $\omega(p) = p$ , i.e.

$$p_{n+1} = p_n - K \sin x, \quad x_{n+1} = x_n + p_{n+1}. \quad (5.13)$$

The map (5.13) is known as the standard or Chirikov–Taylor map, or kicked rotator map (*Note 5.2*).

For small  $K \ll 1$  we can replace the difference equations (5.13) with the differential ones:

$$\dot{p} \approx p_{n+1} - p_n = -K \sin x, \quad \dot{x} \approx x_{n+1} - x_n = p \quad (5.14)$$

or

$$\ddot{x} + \omega_0^2 \sin x = 0, \quad \omega_0^2 = K. \quad (5.15)$$

This is the pendulum equation, and its solutions are presented in Fig. 5.4. Nevertheless Fig. 5.4 has additional small loops and stochastic layers (dark area magnified in part (b), which are due to the neglected terms of the original equations (5.13). To see all of these terms, we can use the identity:

$$\sum_{m=-\infty}^{\infty} \delta\left(\frac{t}{T} - m\right) = \sum_{m=-\infty}^{\infty} \cos\left(\frac{2\pi mt}{T}\right) \quad (5.16)$$

(see Problem 5.2). Applying (5.16), one can rewrite the Hamiltonian (5.6) in the form

$$H = \frac{1}{2}p^2 - K \cos x \sum_{m=-\infty}^{\infty} \cos mvt, \quad (5.17)$$

where a term with  $m = 0$  is responsible for the equation (5.15) while the other ones generate the higher order resonances and stochastic layers.



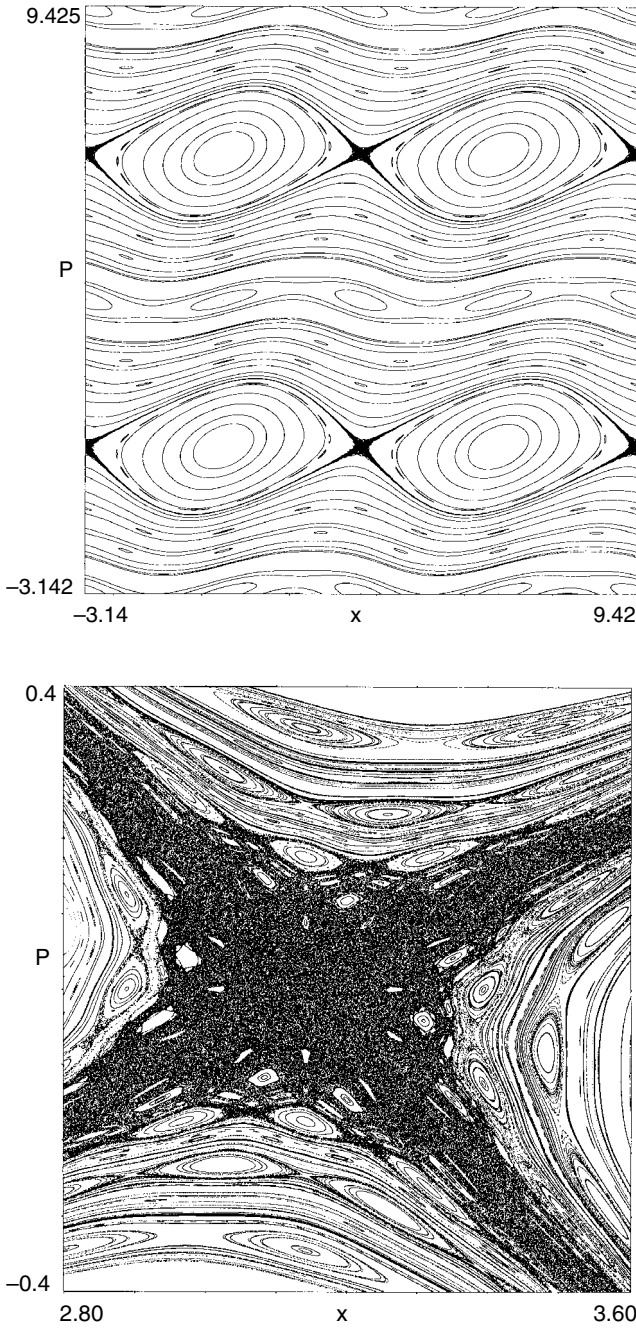


FIG. 5.4. Phase portrait of the standard map for  $K = 0.5$ : (a) part of the phase space  $2 \times 2$  periods; (b) magnification of an area of a stochastic layer at the edge of a separatrix loop.

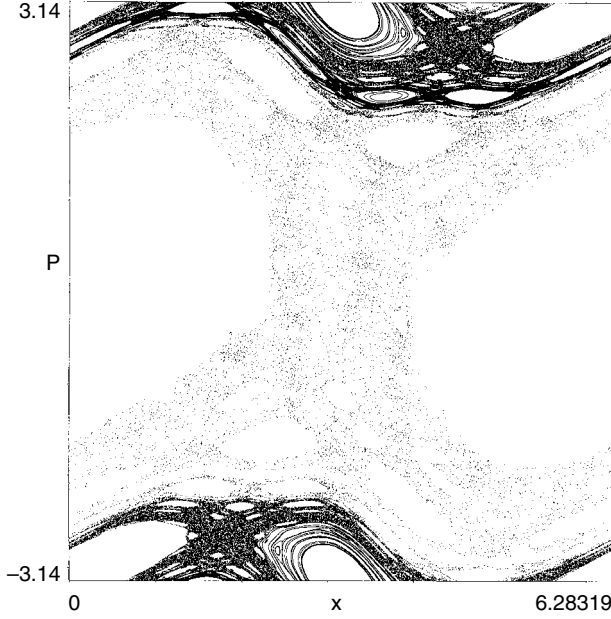


FIG. 5.5. Stochastic sea and islands for the standard map and  $K = 0.98 > K_c$ . Islands are filled by invariant curves.

Properties of stochastic layers will be studied in the next chapter. For small  $K$ , different stochastic layers are separated by invariant curves (Fig. 5.4). The breakup of these curves for  $K_c = 0.9716\dots$  calculated in Green (1979) and MacKay *et al.* (1984). The phase portrait for  $K > K_c$  is shown in Fig. 5.5 demonstrating a typical pattern of stochastic sea and islands.

A principal difference between the cases  $K < K_c$  and  $K > K_c$  is that an infinite diffusion along the  $p$ -direction is possible only for  $K > K_c$ .

Jacobian matrix of the universal map (5.11) is

$$\hat{M} = \begin{vmatrix} 1 & -Kf''(x) \\ \omega'(p) & 1 - K\omega'(p)f''(x) \end{vmatrix}, \quad (5.18)$$

where we put again  $T = 1$ , and its eigenvalues are

$$\lambda_{1,2} = \frac{2 + \tilde{K}}{2} \pm \left[ \frac{(2 + \tilde{K})^2}{4} - 1 \right]^{1/2}, \quad (5.19)$$

where

$$\tilde{K} = -K\omega'(p)f''(x), \quad (5.20)$$

and it consists of a product of the non-linearity  $\omega'$  and perturbation parameter  $K$ . Particularly, for the standard map (5.13):

$$\tilde{K} = -K \cos x. \quad (5.21)$$

Eigenvalues are real if  $\tilde{K} > 0$ , ( $\lambda_1 > 1$ ,  $\lambda_2 = 1/\lambda_1 < 1$ ) or  $\tilde{K} < -4$ , ( $|\lambda_2| > 1$ ,  $|\lambda_1| = |1/\lambda_2| < 1$ ). As it follows from (5.20) and (5.21), independently on the value of  $K$ , there are always intervals of  $x$  within which  $|\tilde{K}| \ll 1$  and islands of stability can appear. Using the first condition  $\tilde{K} > 0$  and comparing it to (5.20) and (5.11) we can write

$$K_c \equiv \max \left| \frac{dx_{n+1}}{dx_n} - 1 \right| \gtrsim 1 \quad (5.22)$$

as the qualitative condition that defines the occurrence of chaotic sea with unbounded diffusion along  $p$ .

The condition (5.22) will be called the *strong chaos* condition. As it is seen from Fig. 5.4, chaotic zones (chaotic layers) exist even for  $K < 1$  and, as it will be shown later, for any arbitrary small  $K$ . Between stochastic layers there are invariant curves that represent trajectories of regular dynamics. Condition (5.22) means also destruction of the invariant curves between stochastic layers. As it was already mentioned above, a theory of the critical value  $K_c$  was given by Greene (1979).

### 5.3 Web map (kicked oscillator)

The web map appears as a result of the consideration of particle motion in a constant magnetic field and an electrostatic wave packet propagating perpendicularly to the magnetic field (Zaslavsky *et al.* (1986)). The Hamiltonian of the system is

$$H = \frac{1}{2}(p^2 + \omega_0^2 x^2) - \frac{\omega_0 K}{T} \cos x \sum_{n=-\infty}^{\infty} \delta\left(\frac{t}{T} - n\right), \quad (5.23)$$

where  $\omega_0$  is the gyro-frequency and  $K$  is the dimensionless parameter proportional to the perturbation amplitude. The derivation of the map is similar to that for a standard map.

Consider the equation of motion that follows from (5.23):

$$\ddot{x} + \omega_0^2 x = -\frac{\omega_0 K}{T} \sin x \sum_{n=-\infty}^{\infty} \delta\left(\frac{t}{T} - n\right). \quad (5.24)$$

It describes a linear oscillator affected by a periodic set of kicks. The model (5.24) can be reduced to the standard map (5.13) in a singular limit:  $\omega_0 \rightarrow 0$ ,  $K \rightarrow \infty$ ,  $\omega_0 K = \text{const}$ . For any finite  $K$ , the results described below cannot be considered

in the limit  $\omega_0 = 0$ , and that makes the kicked-oscillator model independent of the kicked-rotator model. Let us define

$$x_n \equiv x(t_n - 0), \quad \dot{x}_n = v_n = \frac{p_n}{m} \equiv \dot{x}(t_n - 0) \quad (5.25)$$

with a discrete time  $t_n = nT$ . It follows from (5.4), by integration,

$$\begin{aligned} x(t_n + 0) &= x(t_n - 0), \\ \dot{x}(t_n + 0) &= \dot{x}(t_n - 0) - K\omega_0 \sin x_n. \end{aligned} \quad (5.26)$$

Between two adjacent kicks, the solution of (5.24) satisfies the free motion equation,

$$\ddot{x} + \omega_0^2 x = 0$$

that permits to express  $x_{n+1} = x(t_{n+1} - 0)$ ,  $\dot{x}_{n+1} = \dot{x}(t_{n+1} - 0)$  through  $x(t_n + 0)$ ,  $\dot{x}(t_n + 0)$ . After applying (5.26), we obtain the map

$$\begin{aligned} u_{n+1} &= (u_n + K \sin v_n) \cos \alpha + v_n \sin \alpha, \\ v_{n+1} &= -(u_n + K \sin v_n) \sin \alpha + v_n \cos \alpha \end{aligned} \quad (5.27)$$

(see Problem 5.4) where the following dimensionless variables are introduced:

$$u = \frac{\dot{x}}{\omega_0}, \quad v = -x, \quad \alpha = \omega_0 T. \quad (5.28)$$

The map (5.27) is called the web map for the reasons that will become clear soon.

Using the complex variable  $z = u + iv$ , we can rewrite the web map (5.27) as

$$z_{n+1} = \left( z_n + K \sin \frac{z - z^*}{2i} \right) e^{i\alpha}, \quad (5.29)$$

that is,

$$z_{n+1} = \hat{R}_\alpha (1 + \hat{S}(K)) z_n, \quad (5.30)$$

where  $\hat{R}_\alpha$  is the rotation transform by  $\alpha$  and  $\hat{S}(K)$  is the shear transform along  $\text{Im } z$  with intensity parameter  $K$ . We will also use a notation

$$\hat{T}_{W(\alpha)} \equiv \hat{R}_\alpha (1 + \hat{S}(K)). \quad (5.31)$$

The map  $\hat{T}_{W(\alpha)}$  possesses many different regimes that have not been studied in depth yet. The most interesting case, involving the web map (5.27), corresponds to the resonance between the sequence of kicks and the oscillator frequency

$\omega_0$ . To simplify this condition, consider

$$\alpha = \omega_0 T = \frac{2\pi}{q} \quad (5.32)$$

with an integer  $q$  and denote

$$\hat{T}_{W(q)} = \hat{R}_{2\pi/q}(1 + \hat{S}(K)). \quad (5.33)$$

Some simple examples of the resonance case (5.32) include

$$\begin{aligned} \hat{T}_{W(1)} : u_{n+1} &= u_n + K \sin v_n, & v_{n+1} &= v_n, \\ \hat{T}_{W(2)} : u_{n+1} &= -u_n - K \sin v_n, & v_{n+1} &= -v_n, \\ \hat{T}_{W(2)}^2 : u_{n+2} &= u_n + 2K \sin v_n, & v_{n+2} &= v_n, \end{aligned} \quad (5.34)$$

which are integrable and correspond to the operating regimes of the earliest cyclotrons. A more complicated case arises when  $q = 4$ :

$$\hat{T}_{W(4)} : u_{n+1} = v_n, \quad v_{n+1} = -u_n - K \sin v_n. \quad (5.35)$$

It is non-integrable and possesses chaotic trajectories (see Fig. 5.6).

One can meet in the literature the so-called Harper kicked oscillator model:

$$\hat{T}_H : \bar{u} = u + K \sin v, \quad \bar{v} = u - K \sin \bar{u}. \quad (5.36)$$

It is simple to show that

$$\left\| \begin{pmatrix} \bar{u} \\ \bar{v} \end{pmatrix} \right\| = \hat{T}_{W(4)}^2(u', v) \left\| \begin{pmatrix} -u' \\ -v \end{pmatrix} \right\| = \hat{T}_H \left\| \begin{pmatrix} u \\ v \end{pmatrix} \right\|, \quad (5.37)$$

where  $u' = u + \pi$ , i.e.  $\hat{T}_{W(4)}^2$  and  $\hat{T}_H$  are equivalent up to the axis reflection and a shift by  $\pi$  for one of the variables. This difference does not influence the phase space topology (see Problem 5.5).

The following comments about the web map distinguish it from the universal or standard map (5.11):

- (a)  $T_{W(q)}$  for  $q > 2$  has an unbounded net of stochastic layers called *stochastic web* in  $\mathbb{R}^2$  along both directions  $(u, v)$  or  $(p, x)$  for any arbitrary small  $K$  (see Chapter 6) contrary to the universal map or standard map. This property appears as a result of the degeneracy of the unperturbed Hamiltonian in (5.23) that can be written in the action-angle variable as:

$$\begin{aligned} H_0 &= \frac{1}{2}(p^2 + \omega_0^2 x^2) = \omega_0 I, \\ p &= (2\omega_0 I)^{1/2} \cos \vartheta, \quad x = \left( \frac{2I}{\omega_0} \right)^{1/2} \sin \vartheta, \end{aligned} \quad (5.38)$$

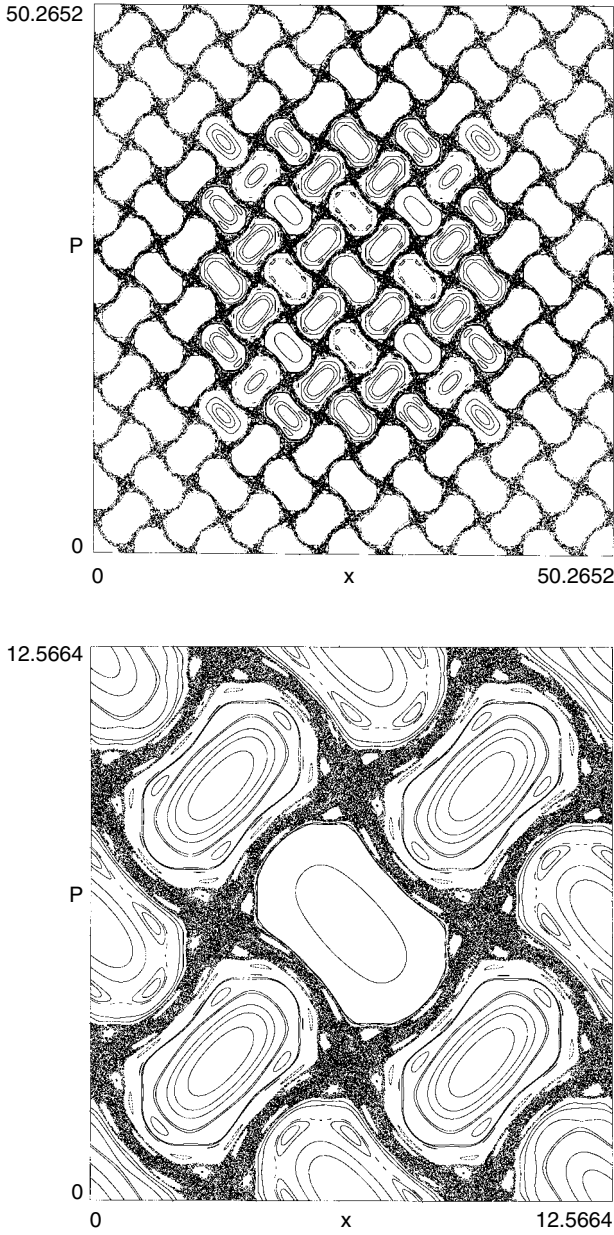


FIG. 5.6. Stochastic web and invariant curves for the four-fold symmetry web map  $\hat{T}_{W(4)}$  with  $q = 4$ ,  $K = 1.5$ : (a) an element of the web on the  $(u, v)$  plane and (b) magnification of the central part of the web.

i.e.

$$\omega(I) = \frac{dH_0}{dI} = \omega_0, \quad \frac{d\omega(I)}{dI} = \frac{d^2H_0}{dI^2} = 0 \quad (5.39)$$

(compare to (3.46)).

- (b) We cannot apply, at least straightforwardly, either the KAM theory due to the condition (3.46) of non-degeneracy, or the resonance overlapping criteria due to the condition (3.42) that requires the finiteness of the non-linearity  $\alpha \gg \epsilon > 0$ .
- (c) The standard map and the web map can be considered as two complementary cases that cover numerous physical situations. Many of them can be considered as a combination of both of these models (see Chapter 8).
- (d) The main theoretical interest to study the web map and its generalization has a threefold purpose: it is a system with or close to degeneracy; fast diffusion along the webs is an alternative to the slow Arnold diffusion (Arnold (1964)); it is a new method to study a symmetry of tiling the plane.

Different specific properties of the web map will be considered later (*Note 5.3*).

## 5.4 Kepler map

In this section we discuss a family of maps with variable time intervals between successive kicks. Such maps appear in dynamics in a gravitational field and they also are typical for many other problems. Consider a particle of the mass  $m$  moving in a vertical direction in the gravitational field and reflecting elastically by an oscillating plate (Fig. 5.7):

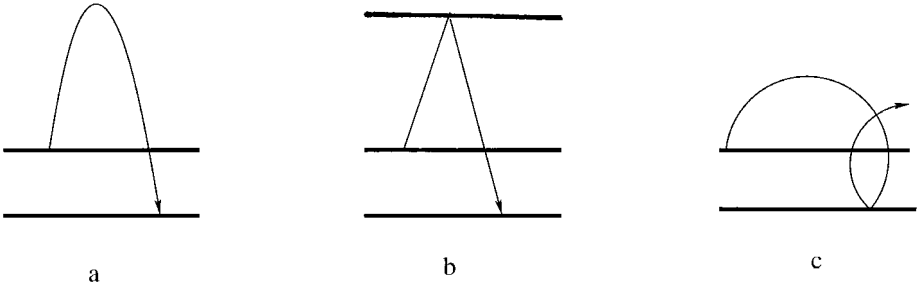


FIG. 5.7. A particle is jumping on the oscillating plate and returns due to: (a) gravitational field, (b) reflection from the upper plate, (c) a magnetic field.

A simplified map neglects the amplitude of the plate oscillations. Then:

$$\begin{aligned} v_{n+1} &= v_n + 2uf(\phi_n), \\ \phi_{n+1} &= \phi_n + \frac{2\nu|v_{n+1}|}{g}, \pmod{2\pi}, \end{aligned} \quad (5.40)$$

where  $\phi_n = \nu t_n$ ,  $t_n$  is a time instant of the plate-particle collision,  $f(\phi)$  is periodic function with  $|f(\phi)| \leq 1$  and frequency  $\nu$ , and  $u$  is an amplitude of the plate velocity. The function  $uf(\phi)$  determines the oscillations of the plate.

If there is no gravitational field but the particle returns due to reflection from an upper rest plate, at distance  $\ell$ , then (see Fig. 5.7(b)):

$$\begin{aligned} v_{n+1} &= v_n + 2uf(\phi_n), \\ \phi_{n+1} &= \phi_n + \frac{2\ell\nu}{|v_{n+1}|}, \pmod{2\pi}. \end{aligned} \quad (5.41)$$

Both models in different variants were considered with respect to the Fermi stochastic acceleration (*Note 5.4*).

One more modification of a similar model is a replacement of the gravitational field by a magnetic field (Fig. 5.7(c)). In this case one can write the coordinates of the skipping particle instead of its velocity (see more in Sagdeev *et al.* (1988) and references therein).

The Kepler map (Petrosky (1986) and Sagdeev and Zaslavsky (1987)) investigated the stochastic dynamics of comets from the Oort cloud, perturbed by Jupiter. A simplified version of the Kepler map has the following dimensionless form:

$$\begin{aligned} E_{n+1} &= E_n + \epsilon\sigma_n f(\phi_n), \\ \phi_{n+1} &= \phi_n + 2\pi(-2E_n)^{3/2}, \pmod{2\pi}, \end{aligned} \quad (5.42)$$

where  $E$  is the comet energy in the apocenter point,  $\phi$  is the comet phase (angle between the comet direction to its pericenter and to Jupiter),  $\epsilon$  is some constant,  $\sigma_n = \pm 1$  depending on the relative rotation directions of the comet orbit and Jupiter orbit, and  $f(\phi)$  is an integral of the Melnikov type (see Natenzon *et al.* (1990) for more details).

All equations of maps for different physical map problems (5.40)–(5.42) belong to the class of the universal map (5.11). Nevertheless, a difference for all of them will be apparent when studying the kinetics. For this part an additional information is necessary for the time interval between successive kicks. In all considered cases:

$$\Delta t_n = t_{n+1} - t_n = \frac{2\pi(\phi_{n+1} - \phi_n)}{\nu} \quad (5.43)$$



in contrast to the standard or web maps where  $\Delta t_n = \text{const} = T$  (compare to (5.2)).

All maps of this section were studied in detail (see, for example, Zaslavsky *et al.* (1991) and references therein), but this study is far from complete and there are different important questions that are still waiting for their resolutions. The reason for the difficulties is a complicated topology of phase space and non-uniformity of chaotic mixing. This situation will be studied later.

## Notes

### Note 5.1

For more information about maps see Sagdeev *et al.* (1988). The Sinai billiard was considered in numerous publications (Sinai (1961, 1970); Bunimovich *et al.* (1991); Young (1998a, 1998b)) and the model has inspired many works in the study of chaos. It was shown for the Sinai billiard that the correlation function depends on the type of the mapping construction (Bunimovich *et al.* (1991); Young (1998a)). For example, the map can be of the type (5.3) or  $(p, q)$  pair can be taken on a side of the square boundary, and the results are very different (Bunimovich *et al.* (1991); Chernov and Young (2000)). We will discuss the model more later as an example of appearance of fractional kinetics.

### Note 5.2

The standard map is also known as Chirikov–Taylor or Taylor–Chirikov map (Taylor (1969); Chirikov (1979)). Its discussion can be found in many textbooks because of the simplicity of its derivation. The map displays many features of the dynamics of real systems (see Lichtenberg and Lieberman (1983); Ott (1993); Sagdeev *et al.* (1988)).

### Note 5.3

More systematic discussion on the webs, their symmetry, and applications can be found in Zaslavsky *et al.* (1991). Physical problems with a coupled web map and a standard map were studied in Zaslavsky *et al.* (1989); Afanasiev *et al.* (1991); Neishtadt *et al.* (1991); Beloshapkin *et al.* (1994). For a generalization of the web map, see Dana and Amit (1995); Pekarsky and Rom-Kedar (1997).

### Note 5.4

The idea of a stochastic acceleration of particles was proposed by Fermi (1949) to explain the origin of highly energetic charged cosmic particles as a result of their encounters with randomly moving magnetic clouds. A simplified model to study the origin of chaotic (random) dynamics was introduced by Ulam (1961), but his own investigation of the problem did not show anything chaotic. A model of the (5.40) type was proposed in Zaslavsky and Chirikov (1964) and was investigated with analytical and numerical evidence and conditions

of the chaos occurrence. Different modifications appeared in Zaslavsky (1970, 1985).

### Problems

5.1 Find invariant curves near a point  $x^*$ ,  $f'(x^*) = 0$  for the map (5.11) expanding  $f(x)$  near  $x^*$ .

5.2 Prove the relation (5.16).

5.3 Find out the overlapping parameter  $K_c$  for the Hamiltonian (5.17). Use each term of the sum to calculate a width of different resonances.

5.4 Derive the equations (5.27).

5.5 Prove the connection (5.37).

5.6 Find the condition of strong chaos in (5.40) and provide its physical interpretation.

5.7 The same as in Problem 5.6. for the map (5.41).

5.8 The same as in Problem 5.6. for the map (5.42).

5.9 Explain the appearance of the term  $(-E)^{3/2}$  using the dimensionless Hamiltonian for the unperturbed Kepler problem in action-angle variables.

*This page intentionally left blank*

## 6

### SEPARATRIX CHAOS

In low dimensional Hamiltonian systems, the area near a separatrix is the most important domain to study the origin of chaos, since the dynamics near a saddle point is sensitive to small perturbations. The problem of the change of the dynamics near a separatrix under a periodic perturbation can be studied in fairly general way. Destruction of separatrices under perturbations leads to chaos, and that is why this problem is one of the most important ones in the analysis of dynamics.

#### 6.1 Description of models

Let us formulate a few different problems that have numerous physical applications:

(a) a perturbed pendulum with the Hamiltonian:

$$H = \frac{1}{2}p^2 - \omega_0^2 \cos x + \epsilon \omega_0^2 \cos(kx - \nu t), \quad (6.1)$$

where we put the mass  $m = 1$  for simplicity. This problem corresponds to a pendulum with rotating suspension point (Landau and Lifshits (1976)).

(b) a resonance interaction model:

$$\begin{aligned} H &= \frac{1}{2}p^2 - 2\omega_0^2 \cos\left(\frac{1}{2}\nu t\right) \cos x \\ &= \frac{1}{2}p^2 - \omega_0^2 \left[ \cos\left(x + \frac{1}{2}\nu t\right) + \cos\left(x - \frac{1}{2}\nu t\right) \right]. \end{aligned} \quad (6.2)$$

This problem has the same amplitude terms which correspond to two resonance chains separated by  $\nu$  in the frequency scale (see Sections 3.5 and 4.7).

(c) perturbed double-well dynamics:

$$H = \frac{1}{2}p^2 - \frac{1}{2}\omega_0^2 x^2 \left(1 - \frac{1}{2}x^2\right) + \epsilon V_0(x) \sin \nu t, \quad (6.3)$$

where  $V_0(x)$  is some smooth function.

We will see that an arbitrary small periodic perturbation destroys the separatrix and creates instead extremely complicated phase space topology with a

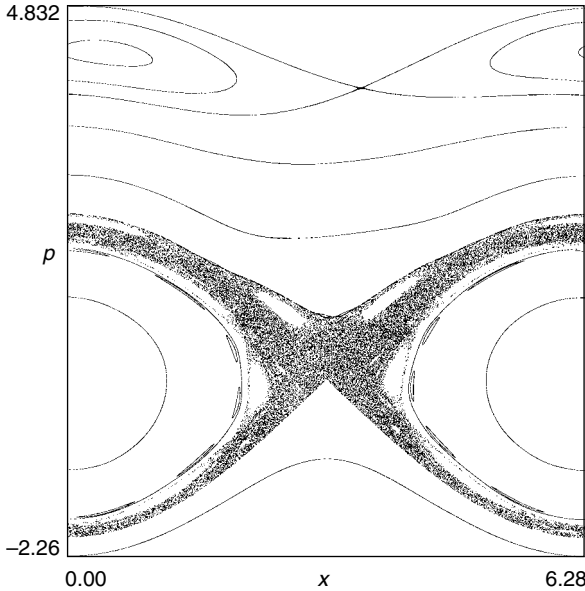


FIG. 6.1. A Poincaré map for the perturbed pendulum ( $\epsilon = 0.1$ ,  $\nu = 4.0$ ,  $k = 1$ ,  $\omega_0 = 1$ ) demonstrating the presence of a stochastic layer filled by KAM-curves and islands with possible other stochastic layers of higher order inside the islands.

domain of chaos, called the *stochastic layer* (or *ergodic layer*), and an infinite number of islands. All visualization of trajectories for the models (6.1)–(6.3) can be obtained by plotting the corresponding Poincaré map, i.e. points of trajectories plotted each time instant  $t_n = nT = 2\pi n/\nu$  ( $n \in \mathbb{N}$  are integers). Figure 6.1 provides an example of the stochastic layer for the pendulum model (6.1) (compare to Fig. 5.4).

Two other pictures in Fig. 6.2 for the same perturbed pendulum model are obtained for the parameters of the same order. Nevertheless, their difference is very strong and unpredictable from any qualitative type of analysis, including the overlapping criteria.

The difference of the phase space pattern (topology) is also important for the problem of kinetics and transport which, as we will see later, is sensitive to the island's topology. It is interesting that tiny islands persist in Fig. 6.2(b) and, despite the fairly dense plot of the trajectory points, we should expect an infinite set of small islands. The unsolved problem is: are there such values of  $(\epsilon, \nu)$  that islands disappear (together with invariant KAM-curves inside the islands)?

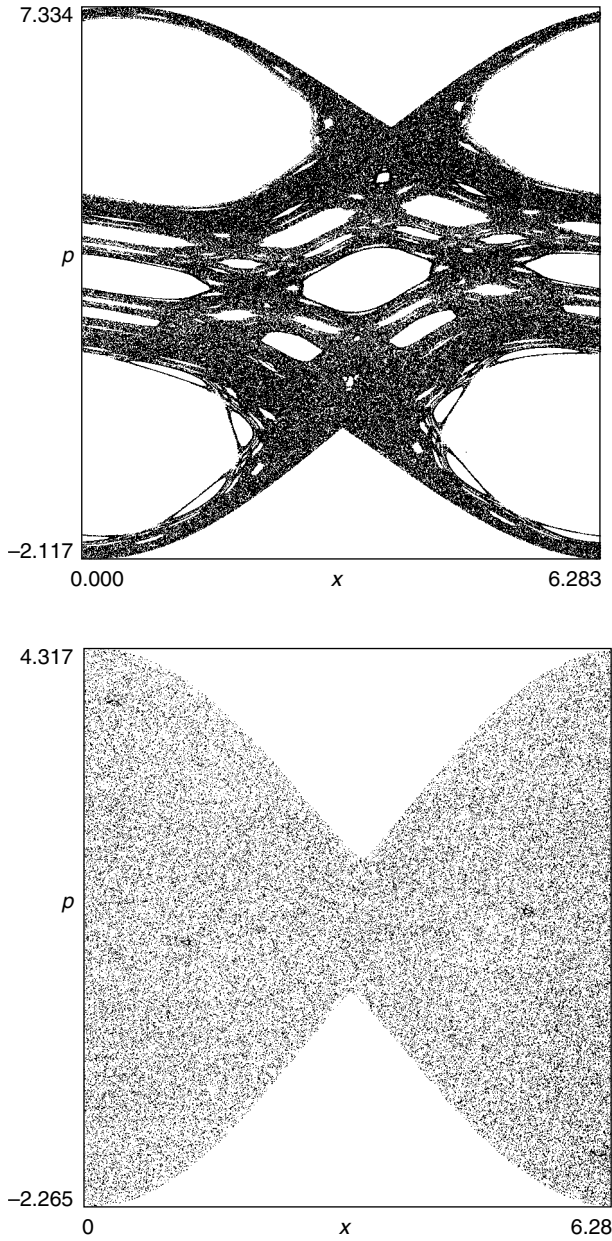


FIG. 6.2. Two different Poincaré section plots for the perturbed pendulum model with  $\omega_0 = k = 1$  and (top)  $\epsilon = 0.9$ ,  $\nu = 5.4$ , and (bottom)  $\epsilon = 1$ ,  $\nu = 2.07$ . There is a strong topological difference despite the same order of values of  $\epsilon, \nu$ .

## 6.2 Separatrix map

Consider a perturbed Hamiltonian in the form

$$H = H_0(p, x) + \epsilon V(x, t), \quad (6.4)$$

assuming that the unperturbed dynamics has a separatrix at some value

$$E_s = H_0(p_s, x_s) \quad (6.5)$$

of the unperturbed energy

$$E = H_0(p, x). \quad (6.6)$$

A general formula

$$\begin{aligned} \dot{E} &= \dot{H}_0(p, x) = [H_0, H] = \epsilon [H_0, V] \\ &= -\epsilon \frac{\partial H_0}{\partial p} \frac{\partial V}{\partial x} = -\epsilon p \frac{\partial V}{\partial x} \end{aligned} \quad (6.7)$$

is exact for the Hamiltonian (6.4). The change of the energy of the unperturbed system due to perturbation is

$$\Delta E(t', t'') = -\epsilon \int_{t'}^{t''} dt p \frac{\partial V}{\partial x}. \quad (6.8)$$

Particularly, for the perturbed pendulum (6.1) we have

$$\Delta E(t', t'') = \epsilon k \omega_0^2 \int_{t'}^{t''} dt \dot{x} \sin(kx - \nu t), \quad (6.9)$$

where we put  $p = \dot{x}$  for a unit mass particle. In the following we start from the pendulum model (6.1) and use either energy  $E$  or action  $I$  variables depending on the situation. The connection is given in Section 2.1:

$$\begin{aligned} E &= H_0(I), \quad E_s = \omega_0^2 = H_s, \\ I_s &= \frac{1}{\pi} 8\omega_0 E \left( \frac{\pi}{2}; 1 \right) = \frac{8}{\pi} \omega_0. \end{aligned} \quad (6.10)$$

We will be interested in the dynamics near the unperturbed separatrix, i.e.

$$|E - E_s| \ll E_s, \quad |I - I_s| \ll I_s. \quad (6.11)$$

The main idea for obtaining the separatrix map is based on a specific behaviour of the unperturbed velocity  $\dot{x} = v$  near the separatrix, shown in Fig. 2.3. As it follows from the results of Section 2.1, the width of a pulse in Fig. 2.3 is the width of solitons, i.e.  $\approx T_0 = 2\pi/\omega_0$ , and the interval between neighbour

pulses is of the order

$$T(h) = \frac{2}{\omega_0} \ln \frac{32}{h(E)}, \quad \omega(h) = \frac{\pi\omega_0}{\ln(32/h(E))}, \quad (6.12)$$

where

$$h(E) = \left| 1 - \frac{E}{E_s} \right| \ll 1. \quad (6.13)$$

This means that  $T \gg T_0$  for  $h(E) \rightarrow 0$  and the shape of pulses remains unchangeable with the exponential accuracy.

The performed analysis permits us to introduce the following map  $\hat{T}_S$ :

$$(E_{n+1}, \vartheta_{n+1}) = \hat{T}_S(E_n, \vartheta_n), \quad (6.14)$$

where the time instants set  $\{\tau_j\}$  of the mapping is taken at intervals  $T(E) = T(h)$ :

$$\{\tau_j\} = \{\tau_0, \tau_1 = \tau_0 + T(h_1), \tau_2 = \tau_1 + T(h_2), \dots\}. \quad (6.15)$$

The point  $\tau_0$  can be taken in the middle of two pulses. The corresponding sampling of points  $\tau_n$  and the energy values  $E_n$  (or  $h_n = h(E_n)$ ) are shown in Fig. 6.3.

Then the map (6.14) can be written in the form

$$\begin{aligned} h_{n+1} &= h_n + \Delta h_n, \\ \tau_{n+1} &= \tau_n + \frac{2\pi}{\omega(h_{n+1})}, \end{aligned} \quad (6.16)$$

where

$$\begin{aligned} \Delta h_n &= -\frac{\epsilon}{E_s} \int_{\tau_n^-}^{\tau_n^+} dt \dot{x} \frac{\partial V}{\partial x} \\ \tau_n^\pm &= \tau_n \pm \frac{T(h_n)}{\delta_n}. \end{aligned} \quad (6.17)$$

where  $\delta_n = 2$  or  $4$  depending on the cases (a) or (b) in Fig. 6.3. The expression (6.17) can be simplified since it should be taken over one pulse with a centre at  $t = \tau_n$ . The inequality  $T \gg T_0$  permits us to write (6.17) in the following form

$$\Delta h_n = -\frac{\epsilon}{E_s} \int_{\tau_n - \infty}^{\tau_n + \infty} dt \dot{x}_s \frac{\partial V}{\partial x_s} = \Delta h(\tau_n). \quad (6.18)$$

The map (6.16) together with (6.18) is not exactly of the universal type (5.11) and it will be called the *separatrix map*. It is written for energy-time variables and is area-preserving. It is worthwhile to mention that values  $(h_n, \tau_n)$  are taken in different time instants (see Fig. 6.3).



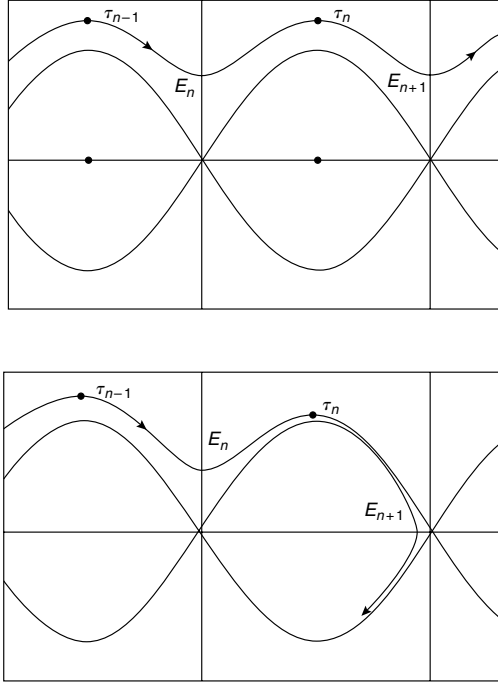


FIG. 6.3. Points of sampling for the separatrix map for two different cases.

Expression (6.18) depends on the sign of velocity  $\dot{x}$  with respect to the unperturbed saddle point. A specific analysis of the behavior of separatrices under perturbation leads to a phenomenon of *separatrix splitting*, discovered by Poincaré, and to appearance of very complicate structures of perturbed separatrices. They are known as homoclinic or heteroclinic structures that appear due to intersection of splitted separatrices (see Fig. 6.4).

The expression (6.18) is called the Melnikov (or sometimes Poincaré–Melnikov) integral (*Note 6.1*).

### 6.3 The stochastic layer

The *stochastic layer* is a domain of chaotic dynamics that replaces the perturbed and destroyed separatrix. There are other notions in use: *ergodic* or *chaotic layer*. From (6.16) and (6.18) we can write the Jacobian matrix as:

$$\hat{M}_n = \left\| \begin{array}{cc} 1 & \frac{d\Delta h_n}{d\tau_n} \\ \frac{-\pi}{\omega^2(h_n)} \frac{d\omega(h_n)}{dh_n} & 1 - \frac{\pi}{\omega^2(h_n)} \frac{d\omega(h_n)}{dh_n} \frac{d\Delta h_n}{d\tau_n} \end{array} \right\|. \quad (6.19)$$

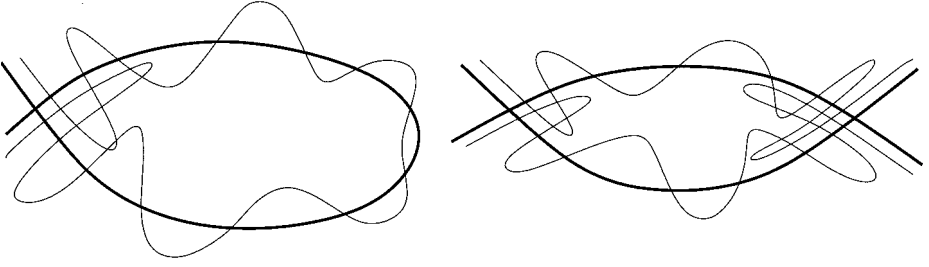


FIG. 6.4. Formation of homoclinic (left) and heteroclinic (right) structures.

Comparing this expression to (5.22) and the map (6.16) to (5.11), we can write the condition that defines the chaotic domain:

$$K_c = \max \frac{\pi}{\omega^2(h)} \left| \frac{d\omega(h)}{dh} \right| \left| \frac{d\Delta h}{d\tau} \right| > 1 \quad (6.20)$$

and the boundary of stochastic layer  $h_{s\ell}$  appears from the equation:

$$K_c = \max \frac{\pi}{\omega^2(h_{s\ell})} \left| \frac{d\omega(h_{s\ell})}{dh_{s\ell}} \right| \left| \frac{d\Delta h(\tau)}{d\tau} \right| = 1. \quad (6.21)$$

Let us calculate (6.21) for the perturbed pendulum model (6.1). We have

$$\begin{aligned} \dot{x}_s &= \frac{\pm 2\omega_0}{\cosh[\omega_0(t - t_n)]}, \\ x_s &= 4 \arctan \exp[\pm \omega_0(t - t_n)] - \pi, \end{aligned} \quad (6.22)$$

on the separatrix, where the time instant  $t_n$  is introduced as an initial condition. Near the separatrix we have also (6.10) and (6.12). This information is sufficient to calculate the Melnikov integral,  $\Delta h$ , in (6.18) and in the map (6.16). After substituting  $V = \cos(x_s - \nu(t - \tau_n))$  in (6.18) and omitting fairly simple calculations, it is found that

$$\begin{aligned} \Delta h_n &= \epsilon M_n \sin \phi_n, \\ M_n &= \frac{4\pi \left( \frac{\nu}{\omega_0} \right)^2 \exp \left( \sigma_n \frac{\pi \nu}{2\omega_0} \right)}{\sinh \frac{\pi \nu}{\omega_0}}, \\ \phi_n &\equiv \nu \tau_n \pmod{2\pi} \end{aligned} \quad (6.23)$$

with sign-function  $\sigma_n = \pm 1$  and

$$\sigma_{n+1} = \sigma_n \cdot \text{sign } h_n. \quad (6.24)$$

Using (6.23), the separatrix map for the perturbed pendulum can be presented in the following form:

$$\begin{aligned} h_{n+1} &= h_n + \epsilon M_n \sin \phi_n, \\ \phi_{n+1} &= \phi_n + \frac{\nu}{\omega_0} \ln \frac{32}{|h_{n+1}|}, \quad (\text{mod } 2\pi). \end{aligned} \quad (6.25)$$

The expression for  $M_n$  can be simplified in the case  $\nu \gg \omega_0$ :

$$\begin{aligned} M_n &= 8\pi \left( \frac{\nu}{\omega_0} \right)^2 \exp \left( -\frac{\pi\nu}{2\omega_0} \right), \quad \sigma_n > 0, \\ M_n &= 8\pi \left( \frac{\nu}{\omega_0} \right)^2 \exp \left( -\frac{3\pi\nu}{2\omega_0} \right), \quad \sigma_n < 0. \end{aligned} \quad (6.26)$$

When  $\sigma_n < 0$ , the value  $M_n$  is much smaller than that for  $\sigma_n > 0$  and it can therefore be ignored. Finally, the map (6.25), together with definitions (6.23) and (6.24), forms a separatrix map when  $\nu \gg \omega_0$ .

Combining the expressions (6.26), (6.21), (6.12), and (6.23), we obtain the half-width of the stochastic layer:

$$h_{s\ell} = 4\pi\epsilon \left( \frac{\nu}{\omega_0} \right)^3 \exp \left( -\frac{\pi}{2} \frac{\nu}{\omega_0} \right). \quad (6.27)$$

The result shows that the width is exponentially small with respect to the large parameter  $\nu/\omega_0$ . The general expression (6.23) for the Melnikov integral  $M_n$  can be used for an estimate when  $\nu \sim \omega_0$ . In this case:

$$h_{s\ell} \sim \epsilon, \quad (6.28)$$

which seems to be the largest width of the stochastic layer (*Note 6.2*).

To conclude this section, two comments need to be made:

(i) Consider a parameter

$$\delta_h = \frac{h_{s\ell}}{\max \Delta h} = \frac{h_{s\ell}}{\epsilon M} = \frac{\nu}{\omega_0}, \quad (6.29)$$

which is ratio of the stochastic layer width to the value of the Melnikov integral. For high frequency perturbation  $\delta_h \gg 1$  and the estimate of the domain of chaos strongly deviates from the value of the Melnikov integral.

(ii) A real parameter of expansion, in obtaining the value of  $h_{s\ell}$ , is the parameter of perturbation  $\epsilon$  if  $\nu \sim \omega_0$ . When  $\nu \gg \omega_0$ , the value of  $h_{s\ell}$  is exponentially

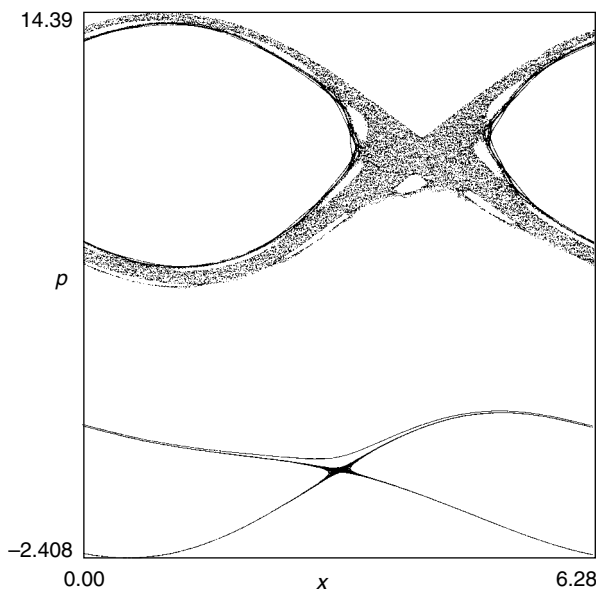


FIG. 6.5. Two stochastic layers for the perturbed pendulum model with large  $\epsilon = 5.1$ ,  $\nu = 10.4$  but small  $\bar{\epsilon}$ .

small (see (6.27)) and the real small parameter is

$$\bar{\epsilon} = \epsilon \left( \frac{\omega_0}{\nu} \right)^2 \ll 1, \quad (6.30)$$

which is due to the high frequency perturbation. Figure 6.5 illustrates a small width of stochastic layers for large  $\epsilon$  with a small  $\bar{\epsilon}$  (*Note 6.3*).

#### 6.4 The stochastic layer of the standard map

The standard map was introduced in Section 5.2 by the Hamiltonian

$$H = \frac{1}{2}p^2 - K \cos x \sum_{n=-\infty}^{\infty} \delta \left( \frac{t}{T} - n \right) = \frac{1}{2}p^2 - K \cos x \sum_{m=-\infty}^{\infty} \cos m\nu t. \quad (6.31)$$

Now we are interested in small perturbations:

$$K \ll 1. \quad (6.32)$$

Nevertheless, even with this simplification, (6.31) is still extremely complicated. This can be seen in Fig. 5.4 which demonstrates the phase portrait of system (6.31) for small  $K$ . It comprises different typical elements. Stochastic

layers replace the destroyed separatrices. Inside the layers, a family of nested invariant curves resides, which confines the point  $(0, 0; (\text{mod } 2\pi))$ . Outside the main stochastic layer, there are chains of separatrix loops with considerably thinner stochastic layers, which are not visible in Fig. 5.4(a), but they can be seen after magnification in Fig. 5.4(b). The chains correspond to non-linear resonances of different orders and invariant curves lie between them. Thus, the phase portrait resembles a sandwich composed of an infinite number of invariant curves alternated by stochastic layers. The stochastic layers do not merge for the values of  $K < K_c$  (see (5.22) and the following discussion).

There is a fairly simple way to observe the formation of stochastic layers for the standard map. To do so, consider the second form of the Hamiltonian (6.31) and keep only the terms with  $m = 0, \pm 1$ . Thus, we obtain

$$H \approx \frac{1}{2}p^2 - K \cos x - 2K \cos \nu t \cos x. \quad (6.33)$$

Equation (6.33) describes the perturbed pendulum model with a dimensionless pendulum frequency

$$\omega_0 = K^{1/2}. \quad (6.34)$$

It has the same amplitude as the main term in the Hamiltonian  $H$  and a perturbation frequency  $\nu$ , or its dimensionless form

$$\bar{\nu} = 2\pi \quad (6.35)$$

if we put the interval between kicks  $T = 1$ . Due to (6.32) and (6.34) we have  $\nu \gg \omega_0$  for small perturbations. This enables to use the formulas (6.23)–(6.27) for the width of the stochastic layer after some substitutions

$$\epsilon \rightarrow 2K, \quad \omega_0 \rightarrow K^{1/2}, \quad E_s = \omega_0^2 \rightarrow K, \quad \nu \rightarrow \bar{\nu} = 2\pi, \quad (6.36)$$

we obtain:

$$M_n \approx \frac{(4\pi)^3}{2K} \exp\left(\frac{-\pi^2}{K^{1/2}}\right) \equiv M \quad (6.37)$$

independently on the sign of  $\sigma_n$ . The corresponding separatrix map can be simplified due to the symmetry of the Hamiltonian (6.33) and  $M_n$ :

$$\begin{aligned} h_{n+1} &= h_n + 2KM \sin \phi_n, \\ \phi_{n+1} &= \phi_n + \left(\frac{2\pi}{K^{1/2}}\right) \ln\left(\frac{32}{h_{n+1}}\right), \quad (\text{mod } 2\pi) \end{aligned} \quad (6.38)$$

(see more details in Chirikov (1979)). In the same way as (6.27), we obtain a half-width of the stochastic layer:

$$h_{s\ell} = \frac{2(2\pi)^4}{K^{1/2}} \exp\left(\frac{-\pi^2}{K^{1/2}}\right). \quad (6.39)$$

Equation (6.39) defines an exponentially narrow stochastic layer for any small value of  $K$ .

Should the subsequent terms with  $m = \pm 2$  be retained in the sum (6.31), the resulting corrections to (6.39) will be exponentially small. This is because the effective frequency of perturbation due to these terms is  $\bar{\nu} = 4\pi$ . Thus, the definition of the exponential term in (6.39) is very accurate.

An important comment on the estimation (6.39) is that the coefficients for the main term,  $K \cos x$ , in (6.33) and the perturbation are of the same order, that is, the effective perturbation parameter is of the order one. Nevertheless, the smallness of the width of the stochastic layer is attributed to the exponential factor in (6.39), rather than to the amplitude, i.e. pre-exponential factor.

## 6.5 Hidden renormalization group near the separatrix

It would be too simplistic to remark that the perturbed motion near the separatrix is so complicated that we have not yet been able to create a more or less complete picture of the basic properties found inside the stochastic layer and in its vicinity. Surprisingly, some global properties of the layer's pattern can be obtained due to specific dynamics near a saddle point. This section describes the existence of a 'hidden' (non-evident from the Hamiltonian) renormalization transform. The occurrence of the transform, denoted as  $R_\epsilon$ , follows directly from a specific form of the separatrix map (6.25). Before deriving the transform  $R_\epsilon$ , let us provide a qualitative analysis of a general property of the motion near the separatrix (*Note 6.4*).

Consider again a periodically perturbed system

$$H = H_0(p, x) + \epsilon V(x, t) \quad (6.40)$$

with

$$V(x, t + T_\nu) = V(x, t), \quad T_\nu = \frac{2\pi}{\nu}. \quad (6.41)$$

If  $x = 0, p = 0$  is a saddle point of the unperturbed Hamiltonian  $H_0(p, x)$ , we can expand near the point

$$H_0(p, x) = \frac{1}{2}(p^2 - \omega_s^2 x^2) + \text{const} \quad (6.42)$$

with a constant  $\omega_s$  which defines the increment of instability. The dependence,  $x = x(t)$ , on an unperturbed trajectory near the saddle point can be obtained by a direct integration of equations of motion that follow from (6.42):

$$\begin{aligned} \omega_s t &= \omega_s \int^t \frac{dx}{\dot{x}} = \omega_s \int^t \frac{dx}{p} = \omega_s \int^t \frac{dx}{(2h + x^2)^{1/2}} \\ &= \ln |x + (2h + x^2)^{1/2}| + \text{const}, \end{aligned} \quad (6.43)$$

where, as in the previous section,

$$h = \frac{(H_0 - \omega_s^2)}{\omega_s^2} \quad (6.44)$$

is the dimensionless energy calculated from the separatrix value  $H_s = \omega_s^2$ .

Consider a renormalization of  $h$  and  $x$  in (6.43):

$$h \rightarrow \lambda_R h_\lambda, \quad x \rightarrow \lambda_R^{1/2} x_\lambda, \quad \lambda_R > 0, \quad (6.45)$$

where  $\lambda_R$  is a renormalization constant. The substitution of (6.45) into (6.43) leads to the time shift

$$\Delta t = \frac{1}{2\omega_s} \ln \lambda_R. \quad (6.46)$$

One can therefore conclude that in the case of a periodic dependence on the phase  $\omega_s t$ , the shift leads to the preservation of the equation of motion near the separatrix if  $\omega_s \Delta t$  is a multiple of  $\pi$ . Consequently, the phase space topology is preserved. This property is rigorously formulated and proven below. At this point, some general remarks are helpful:

- (i) The renormalization transform  $R_\epsilon$  derived below demonstrates the existence of scaling invariance with respect to the appropriate renormalization of the perturbation parameter  $\epsilon$ , that is, the renormalization constant  $\lambda_R$  depends on  $\epsilon$ .
- (ii) The invariance under the transform  $R_\epsilon$  appears as an approximate property of the topology of a part of phase space, which is in the vicinity of the saddle point.
- (iii) The  $R_\epsilon$ -transform can be applied to that part of phase space, which includes the stochastic layer and the nearest set of resonances lying outside.

Rewritten in a more general way than (6.42), the expansion of  $H_0(p, x)$  near a saddle point is

$$H_0 - E_s = \frac{1}{2}(A_p^2 p^2 - A_x^2 x^2) \equiv \omega_s a^+ a^- \quad (6.47)$$

where  $E_s = H_s = \omega_s^2$  is the energy at the saddle point and  $A_p, A_x$  are constants, and new amplitudes,

$$a^\pm = (2\omega_s)^{-1/2}(A_p p \pm A_x x) \quad (6.48)$$

and an imaginary ‘frequency’,

$$\omega_s = A_p A_x \quad (6.49)$$

are introduced. Hamiltonian (6.47) describes the hyperbolic motion with increment (decrement)  $\omega_s$ :

$$\dot{a}^\pm = \pm \frac{\partial H_0}{\partial a^\mp} = \pm \omega_s a^\pm, \quad (6.50)$$

that is,

$$a^\pm(t) = a^\pm(0) \exp(\pm \omega_s t). \quad (6.51)$$

The saddle point  $(0, 0)$  belongs to a singular curve, or separatrix. Consider the motion on a cylinder phase space  $\mathbb{R}_p \mathbf{C}_x$ . For fairly smooth Hamiltonians, the non-linear frequency near the separatrix can be written in a way that is similar to (6.12)

$$\omega(h) = \frac{A\omega_s}{\ln(B/h)}, \quad (6.52)$$

where  $A$  and  $B$  are some constants depending on the form of  $H_0(p, x)$ , and

$$h = \frac{|E - E_s|}{E_s}, \quad (6.53)$$

which is similar to (6.13) with energy  $E = H_0$ . In the example (6.12),  $\omega_s = \omega_0$ ,  $A = \pi$ ,  $B = 32$ .

The separatrix map (6.25) can be rewritten in a more general form as

$$\begin{aligned} h_{n+1} &= h_n + \epsilon M(n, \phi_n), \\ \phi_{n+1} &= \phi_n + \frac{\pi\nu}{\omega_s A} \ln \frac{B}{|h_{n+1}|}, \quad (\text{mod } 2\pi), \end{aligned} \quad (6.54)$$

where  $\epsilon M(n, \phi_n)$  is the Melnikov integral  $\Delta h(\phi_n)$  in (6.18),  $\phi_n = \nu\tau_n$ , and expression (6.52) has been used.

**Proposition (P1)** The separatrix map (6.54) is invariant under the transform

$$\begin{aligned} R_\epsilon : \quad \epsilon &\rightarrow \lambda_R \epsilon, \quad h \rightarrow \lambda_R h \\ \lambda_R &= \exp\left(\frac{2\omega_s A}{\nu}\right). \end{aligned} \quad (6.55)$$

It also follows from (6.55) that the invariance under the transform

$$R_\epsilon^m : \epsilon \rightarrow \lambda_R^m \epsilon, \quad h \rightarrow \lambda_R^m h, \quad m = \pm 1, \pm 2, \dots \quad (6.56)$$

with the same  $\lambda_R$  as in (6.55).

The statement (P1) follows from (6.54) if one takes into account that the phase  $\phi_{n+1}$  is defined in (6.54) up to a term  $2\pi m$  where  $m$  is an integer.



In other words, the renormalization transform  $R_\epsilon$  (6.55) preserves the phase space topology near the saddle point with the same level of accuracy with which the separatrix map (6.54) was obtained.

In order to formulate a similar invariancy to (P1) for the original Hamiltonian (6.40), let us recall that in the construction of the separatrix map (see Section 6.2) the time instants  $\tau_n$  correspond to the midway point between the two adjacent passages of a saddle point, say  $\tau_n^{(s)}$  and  $\tau_{n+1}^{(s)}$ . This means that

$$\tau_n = \tau_n^{(s)} + \frac{\pi}{2\omega(h_n)} \quad (6.57)$$

or, after multiplying by  $\nu$ ,

$$\phi_n = \phi_n^{(s)} + \frac{\pi\nu}{2\omega(h_n)}, \quad \phi_n^{(s)} = \nu\tau_n^{(s)}. \quad (6.58)$$

We also need to recall that the quantity  $h_n$  is taken precisely at the time instant  $\tau_n^{(s)}$  of the passage near the corresponding saddle point, that is,

$$h_n = h(\tau_n^{(s)}) \quad (6.59)$$

by definition. The substitution of (6.58) into (6.54) yields

$$\begin{aligned} h_{n+1} &= h_n + \epsilon M \left( n, \phi_n^{(s)} + \frac{\pi\nu}{2\omega(h_n)} \right), \\ \phi_{n+1}^{(s)} &= \phi_n^{(s)} + \frac{\pi\nu}{\omega_s A} \ln \frac{B}{|h_{n+1}|} + \frac{\pi\nu}{2\omega_s A} \ln \left| \frac{h_{n+1}}{h_n} \right|, \quad (\text{mod } 2\pi). \end{aligned} \quad (6.60)$$

The map (6.60) is called the shifted separatrix map (SSM). Its specific property is that both variables  $(h, \phi^{(s)})$  are taken at the same time instant.

Let us now formulate the invariant properties of the SSM.

**Proposition (P2)** The SSM (6.61) is invariant under the renormalization transform

$$\begin{aligned} R_\epsilon : \quad \epsilon &\rightarrow \lambda_R \epsilon, \quad h \rightarrow \lambda_R h, \quad \phi^{(s)} \rightarrow \phi^{(s)} + \pi, \\ \lambda_R &= \exp \left( \frac{2\omega_s A}{\nu} \right). \end{aligned} \quad (6.61)$$

The difference between (P2) and (P1) is that there is a phase shift of  $\phi^{(s)}$  by  $\pi$  for the case (6.61) where both variables  $(h, \phi^{(s)})$  are taken at the same time instant. The results, (6.61) can be applied directly to the Hamiltonian (6.40).

**Proposition (P3)** The phase portrait topology near the saddle point, obtained as a Poincaré map of the Hamiltonian (6.40), is persistent under the

renormalization transform

$$\begin{aligned}
 R_\epsilon : \quad & \epsilon \rightarrow \lambda_R \epsilon, \quad H_0 \rightarrow \lambda_R H_0, \quad t \rightarrow t + \frac{\pi}{\nu} \\
 & x \rightarrow \lambda_R^{1/2} x, \quad p \rightarrow \lambda_R^{1/2} p \\
 & \lambda_R = \exp\left(\frac{2\omega_s A}{\nu}\right).
 \end{aligned} \tag{6.62}$$

The proof for (P3) is based on the expansion (6.47) for  $H_0$  near the saddle point.

It follows from (P3) that the scaling transform

$$\begin{aligned}
 R_\epsilon^m : \quad & \epsilon \rightarrow \lambda_R^m \epsilon, \quad H_0 \rightarrow \lambda_R^m H_0, \quad t \rightarrow t + \frac{m\pi}{\nu} \\
 & x \rightarrow \lambda_R^{m/2} x, \quad p \rightarrow \lambda_R^{m/2} p, \quad m = \pm 1, \pm 2
 \end{aligned} \tag{6.63}$$

preserves the phase portrait near the saddle point with the same  $\lambda_R$  as in (6.62). Transform (6.63) is analogous to (6.56) and is valid up to some  $m < m_0$  when the accumulation of errors becomes significant.

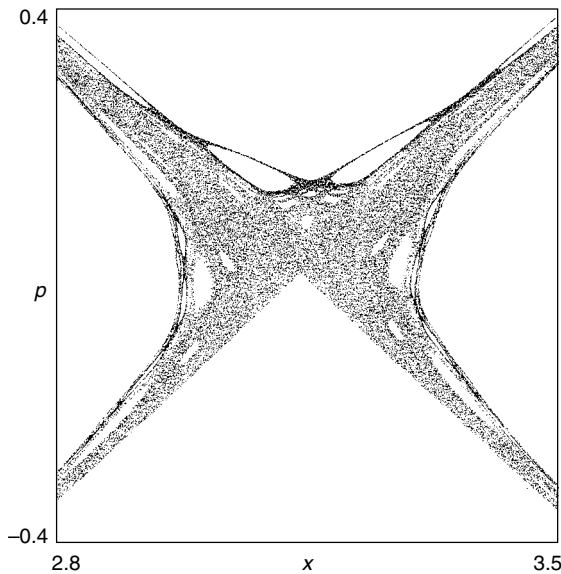


FIG. 6.6. Poincaré section of motion in the ergodic layer: (a) before the renormalization ( $\nu = 5.4$ ;  $\omega_0 = 1$ ;  $\epsilon = 0.01$ ); and (b) after the renormalization ( $\epsilon = 0.003124$ ;  $\lambda_R = 3.2011$ ).

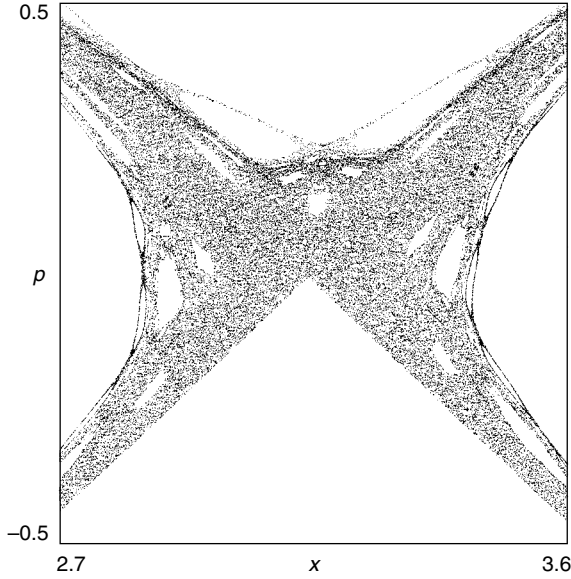
FIG. 6.6. (*Continued*).

Figure 6.6 illustrates the properties (P1) and (P3) for the perturbed pendulum model (6.61). In this model,  $\omega_s = \omega_0$ ,  $A = \pi$  and

$$\lambda_R = \exp\left(\frac{2\pi\omega_0}{\nu}\right). \quad (6.64)$$

In the numerical example in Fig. 6.6, we have  $\lambda_R = 3.2013$ . Hence the difference between the values of perturbation constant  $\epsilon$  and  $\epsilon/\lambda_R^2$  for the cases (a) and (b) is almost of one order.

There are two remarkable properties of the renormalization transform  $R_\epsilon$ : the existence of the *hidden renormalization* is not evident when looking at the Hamiltonian (and that is why we use the word ‘hidden’), and the renormalization parameter  $\lambda_R$  can be obtained directly from the Hamiltonian of the types (6.40) and (6.41) if the result (6.64) is known.

As another example, consider the Hamiltonian with a double-well potential

$$\begin{aligned} H_0 &= \frac{1}{2}p^2 - \frac{1}{2}\gamma^2 x^2 \left(1 - \frac{x^2}{2}\right), \\ \epsilon V &= \frac{1}{4}\epsilon x^4 \sin \nu t. \end{aligned} \quad (6.65)$$

For this case  $\lambda_R$  is of the same type as in (6.64):

$$\lambda_R = \exp\left(\frac{2\pi\gamma}{\nu}\right). \quad (6.66)$$

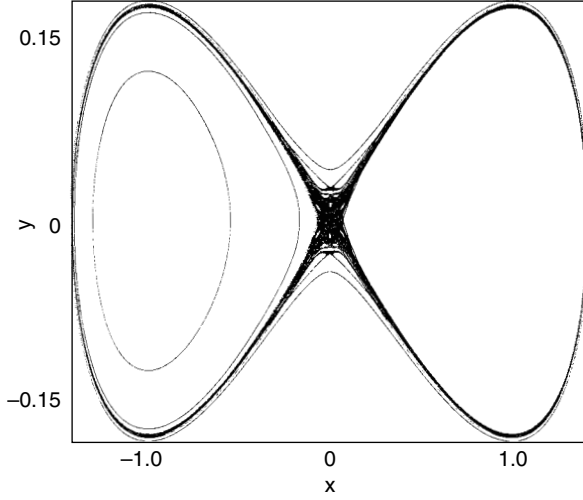


FIG. 6.7. Stochastic layer for a double-well potential:  $\epsilon = 8.3 \times 10^{-5}$ ,  $a = 1$ ,  $\alpha = 0.25$  and  $\beta = 1$ .

Furthermore, for the numerical example in Fig. 6.7, we have  $\gamma/\nu = 0.25$ ;  $\lambda_R = 4.81$ . Figure 6.8 reveals a strong coincidence in the topology near the saddle point for both the original and renormalized phase portraits. This type of renormalization  $R_\epsilon$  does not exist for the standard map due to a lack of constants that can be renormalized.

## 6.6 Renormalization of resonances

The transform  $R_\epsilon$  can be applied to the stochastic layer as well as to the resonances lying beyond it, though not too far from the separatrix.

A resonance condition can be written for the phase equation (6.54) as

$$\phi_{n+q} = \phi_n + 2\pi s, \quad (6.67)$$

where  $s$  is an integer. By definition, (6.67) corresponds to the  $(q, s)$ -order resonance. When the phase equation (6.54) is iterated  $q$  times, it yields

$$\phi_{n+q} = \phi_n + \frac{\pi\nu}{\omega_s A} \sum_{j=1}^q \ln \frac{B}{|h_{n+j}(q, s)|}. \quad (6.68)$$

Let us make a formal transform

$$h = \frac{h'}{\lambda_R} \quad (6.69)$$

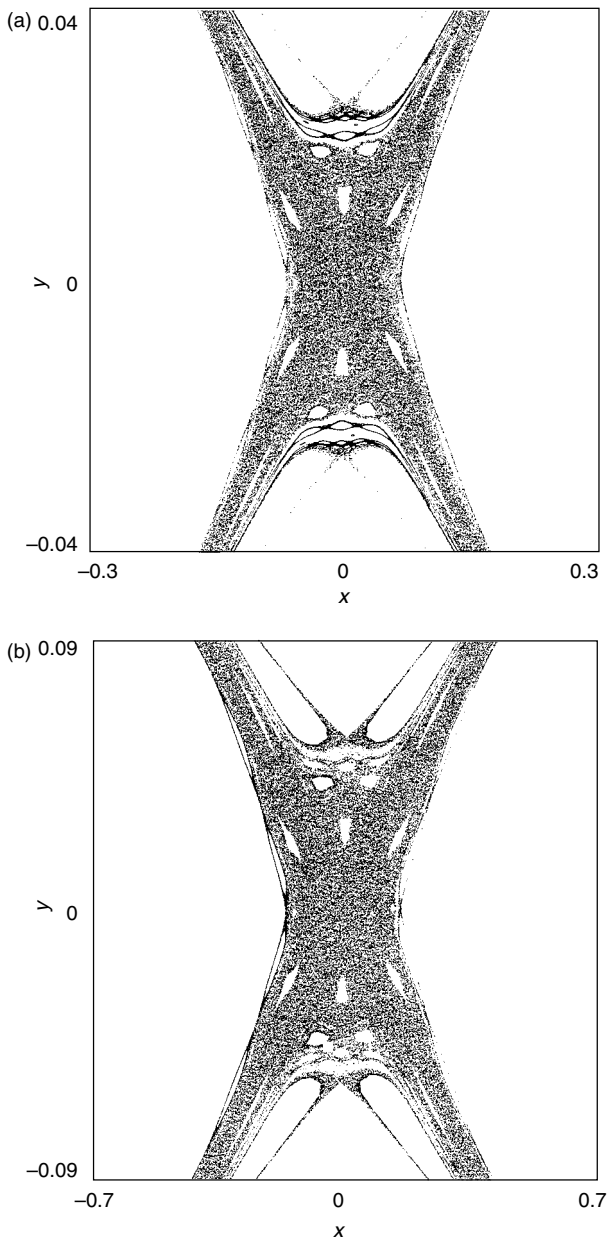


FIG. 6.8. The vicinity of the saddle point for the same model as presented in Fig. 6.7: (a) before the renormalization (see parameters in Fig. 6.7); and (b) after the renormalization with  $\lambda_R = 4.81$  and the phase shifted by  $\pi$ .

and apply it to (6.68):

$$\phi_{n+q} = \phi_n + \frac{\pi\nu}{\omega_s A} \sum_{j=1}^q \ln \frac{B}{|h'_{n+j}|} + \frac{\pi\nu}{\omega_s A} q \ln \lambda_R, \quad (\text{mod } 2\pi). \quad (6.70)$$

From (6.70), we obtain a condition that the resonances of the separatrix map (6.54) are invariant under the transform (6.69)

$$\frac{\pi\nu}{\omega_s A} q \ln \lambda_R = 2\pi s' \quad (6.71)$$

with an integer  $s'$ . This gives

$$\lambda_R(q, s') = \exp \left( \frac{2s'}{q} \frac{\omega_s A}{\nu} \right). \quad (6.72)$$

In particular, for the perturbed pendulum (6.61),  $A = \pi$  and  $\omega_s = \omega_0$ , and instead of (6.72) we have

$$\lambda_R(q, s') = \exp \left( 2\pi \frac{s'}{q} \frac{\omega_0}{\nu} \right). \quad (6.73)$$

In the case when  $s' = q$ , we have the same renormalization constant as (6.55) and (6.61) as well as the transformation of the resonance family (6.67) into a family

$$\phi_{n+q} = \phi_q + 2\pi s'', \quad s'' = s + s'. \quad (6.74)$$

Condition (6.74) should be used together with (6.70) to determine the resonance energies  $h' = h'(q, s'')$ . The result can be formulated as follows:

**Proposition (P4)** When the condition (6.67) defines a resonance family of order  $(q, s)$ , and (6.68) defines the corresponding resonance values of energy  $h = h(q, s)$ , it leads to the existence of a family (6.72) of renormalization constants,  $\lambda_R = \lambda_R(q, s')$ , which transforms the resonance of order  $(q, s)$  into  $(q, s'')$  with energy  $h' = h'(q, s'')$ , that satisfies (6.74).

This renormalization of resonances near the separatrix is also hidden, i.e., it is not obvious from the initial Hamiltonian.

## 6.7 Hidden renormalization for coupled oscillators

A more complicated situation appears for two coupled degrees of freedom. Nevertheless, due to the specific behaviour near the saddle point, the *hidden renormalization group* still exists.

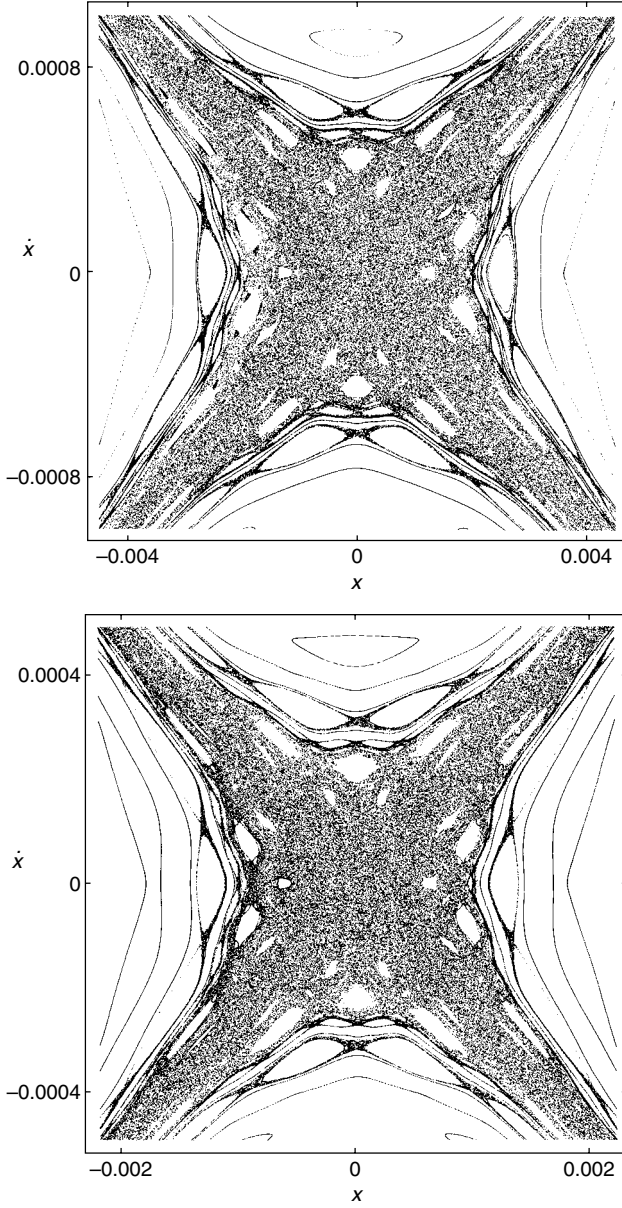


FIG. 6.9. Poincaré section for the Hamiltonian (6.75) with  $\hat{\delta} = 0.0625$ ,  $a = 1$ ,  $\gamma = 1$ ,  $\hat{\alpha} = 0.4$ ,  $E = 0.5$ ,  $\vartheta = 0$ , for two values of perturbation. Top:  $(x, \dot{x})$  plane with  $\hat{\beta} = 10^{-4}$ . Bottom:  $(x, \dot{x})$  plane with  $\hat{\beta} = 2.377 \times 10^{-5}$ , spatial dimensions scaled by  $\lambda_R^{1/2} = 0.4875$ .  $\dot{y} = 0$ ,  $\ddot{y} > 0$ .

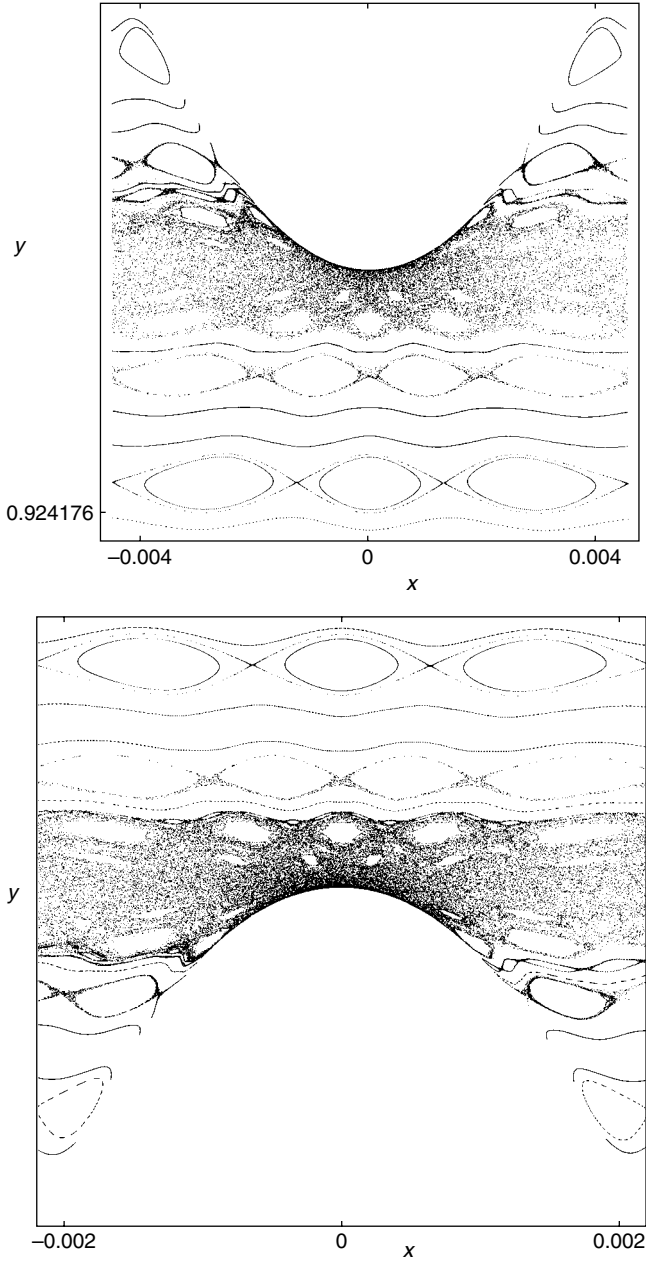


FIG. 6.10. The same data as in Fig. 6.9, but  $(x, y)$  plane. Top:  $\hat{\beta} = 10^{-4}$ . Bottom:  $\hat{\beta} = 2.377 \times 10^{-5}$ ,  $x$  scaled by  $\lambda_R^{1/2} = 0.4875$  and  $y$  scaled by  $\lambda_R = 0.2337$ .  $\dot{y} = 0$ ,  $\ddot{y} > 0$ .



Consider a Hamiltonian with 2 degrees of freedom:

$$H = \frac{1}{2}(\dot{x}^2 + \dot{y}^2) - \frac{1}{2}\hat{\delta}x^2 \left(1 - \frac{x^2}{2a^2}\right) + \frac{1}{2} \left( \hat{\gamma}y^2 + \frac{1}{2}\hat{\alpha}y^4 \right) + \frac{1}{2}\hat{\beta}x^2y^2, \quad \hat{\gamma}, \hat{\alpha} > 0. \quad (6.75)$$

Such Hamiltonian appears in the classical dynamics of homogeneous Yang–Mills field. The saddle point for  $\hat{\beta} = 0$  exists at  $x = 0$ . Then the renormalization  $R_\epsilon$  has the following definition (Kuznetsov and Zaslavsky (1997)):

$$\begin{aligned} R_\epsilon : \epsilon &\rightarrow \lambda_R \epsilon, \quad \hat{\delta} \rightarrow \hat{\delta} + (\lambda_R - 1)\hat{\beta}\langle y_0^2 \rangle, \\ a^2 &\rightarrow a^2 \left[ 1 + \frac{(\lambda_R - 1)\hat{\beta}\langle y_0^2 \rangle}{\hat{\delta}} \right], \quad \hat{\beta} = \epsilon \hat{\delta} \hat{\gamma} / E, H = E \\ x &\rightarrow \lambda_R^{1/2} x, \quad \dot{x} \rightarrow \lambda_R^{1/2} \dot{x}, \quad \vartheta \rightarrow \vartheta + \pi, \quad y \rightarrow -y \\ \lambda_R &= \exp \left[ \frac{2\pi(\hat{\delta} - \hat{\beta}\langle y_0^2 \rangle)^{1/2}}{\nu} \right], \end{aligned} \quad (6.76)$$

where

$$\langle y_0^2 \rangle = \left( \frac{1}{T_y} \right) \int_0^{T_y} y_0^2(t) dt \quad (6.77)$$

with  $y_0(t)$  as an unperturbed motion with period  $T_y$ . The corresponding demonstration is given in Figs. 6.9 and 6.10. The calculations were performed with symplectic integrator of fifth order, and they demonstrated the high coincidence of the topological structures in both planes of projections.

## Notes

### Note 6.1

The story of the Melnikov theory (Melnikov (1963)) from the ‘physical point of view’ is the following. The paper appeared in 1963 and attracted the attention of physicists working on the problem of stable magnetic surfaces in such toroidal devices as tokamak and stellarator designated for fusion. The main message from the paper was the destruction of unperturbed separatrices and their replacement by a complicated pattern now known as the homo(hetero)-clinic structure (see Fig. 6.4). Although the Anosov systems, the models with positive KS entropy, and the resonance overlapping criteria already were presented in the literature with respect to chaotic (stochastic) dynamics, there were no statements anywhere, including the original (Melnikov, 1963) publication, that the homo(hetero)-clinic structure meant chaos. A few years later

the problem of stability of magnetic surfaces became a research project of the Institute of Nuclear Physics in Novosibirsk and a first appearance of chaos (stochasticity) of magnetic field lines was a subject of the paper (Rosenbluth *et al.* (1966)). Immediately after that, Roald Sagdeev proposed to extend this result expecting the overlapping of resonances near the separatrix as a universal phenomenon. This work was performed in Filonenko *et al.* (1967) with first estimates of the width of stochastic layer and simulation that showed the presence of a positive Lyapunov exponent (local instability). Soon after these results the separatrix map was derived in Zaslavsky and Filonenko (1968) and a formal approach was formulated for the estimate of the stochastic layer width in the non-adiabatic case including an estimate of the exponentially small width. There were further developments of these results in Chirikov (1979); Zaslavsky *et al.* (1991); Afanasiev *et al.* (1990), along with some rigorous results in Lazutkin *et al.* (1989); Rom-Kedar (1994, 1995); Treschev (1996, 1997, 2002).

#### Note 6.2

Both estimations for the stochastic layer width, the exponentially small (6.27) and of the order  $\epsilon$  (6.28), were obtained in Zaslavsky and Filonenko (1968). They were re-derived in a number of subsequent publications: Chirikov (1979); Zaslavsky (1985); Lazutkin *et al.* (1980); Treschev (1996). In the latter two references, more power methods were used (see also Treschev (1997)), which improved the tools of obtaining the pre-exponential numerical constant in (6.27). A more sophisticated case is the adiabatic perturbation with  $\nu \gg \omega_0$ . Special methods were developed in Neishtadt (1975); Cary *et al.* (1986); Neishtadt *et al.* (1997). The form of the separatrix map with  $M_n$  as a function of  $n$  was proposed in Rom-Kedar (1995). For some recent results see Luo (2004) and for experimental observations see Evans *et al.* (2002).

#### Note 6.3

The appearance of a factor  $(\omega_0/\nu)^2 \ll 1$  is typical for high frequency perturbations (Landau and Lifshits (1976)). Its discussion for the stochastic layer can be found in Zaslavsky (1994c).

#### Note 6.4

The hidden renormalization transform was found in Zaslavsky and Abdullaev (1995) and then was generalized and applied to different systems in Abdullaev and Zaslavsky (1996) and Abdullaev and Spatschek (1999), and particularly for two degrees of freedom (Kuznetsov and Zaslavsky (1997)) and for homoclinic tangles in Kuznetsov and Zaslavsky (2002). The figures in this section are taken from Kuznetsov and Zaslavsky (1997).

## Problems

More complicated problems are marked by (\*).

6.1 Prove that (6.16) is an area preserving map using (6.18).

6.2 Find the separatrix map for a model of resonance interaction with the Hamiltonian (6.2).

6.3\* For the model (6.2) find a width of the stochastic layer (use results of Problem 6.2).

6.4 Find a renormalization constant  $\lambda_R$  for the model (6.2) (use results of Problem 6.2).

## WEAK CHAOS AND SYMMETRY

Chaotic dynamics *per se* means a strong instability of trajectories and their exponential separation from each other. Nevertheless, the area occupied by chaotic trajectories can be very small, even exponentially small, comparing to the whole phase space. An example of this situation appears when stochastic layers are narrow. Considering higher dimension phase space, one can imagine it being filled by different bounded domains of regular integrable dynamics, which are separated by thin channels of stochastic motion. We call this situation *weak chaos*. The channels of chaotic motion can form a web that penetrates phase space. We call it the *stochastic web*. The first example of the stochastic web was proposed by Arnold (1964). The Arnold web universally exists for  $N > 2$ .

Typically in Hamiltonian systems stochastic webs replace the separatrices destroyed due to interaction of different degrees of freedom. A non-trivial result of the existence of stochastic webs is that the phase space partitioned by the webs will carry a symmetry imposed by the web symmetry. This is a situation of the dynamical origin of symmetry.

### 7.1 Stochastic webs

Consider again a system that is close to an integrable system, with the Hamiltonian

$$H = H_0(I) + \epsilon V(I, \vartheta), \quad (7.1)$$

where  $I = (I_1, \dots, I_N)$  and  $\vartheta = (\vartheta_1, \dots, \vartheta_N)$  are the  $N$ -dimensional vectors of action and angle, respectively, and  $\epsilon$  is a small parameter of perturbation. For  $\epsilon = 0$ , the system is described by its Hamiltonian  $H_0$  and possesses  $N$  commuting first integrals of motion (actions). The motion is performed along an  $N$ -dimensional torus defined by specific values of  $I$ . In the set of the tori, some are singular and correspond to separatrices or hypersurfaces with self-intersections. In two-dimensional phase space, separatrices are special trajectories that pass through saddle points. The set of separatrices can form a connected net in the phase space (see Fig. 7.1) where a particle can move. In fact, the likelihood of a particle moving along a separatrix is minimal since the time taken to reach a saddle point is infinite and particles are not able to pass through any saddle (see Problems 7.1 and 7.2). Inside the meshes of the net, dynamics is finite. This leads to a conclusion that the general type of integrable motion is partitioned by

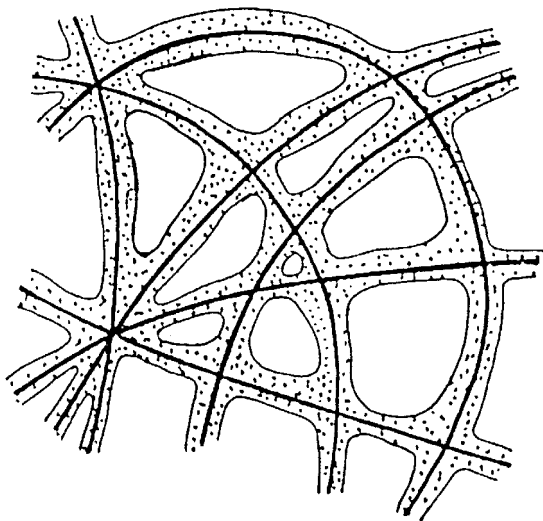


FIG. 7.1. Stochastic web formation.

a net of separatrices in an integrable case, in addition to the Liouville–Arnold theorem on integrability.

The influence of a small perturbation in (7.1) does not significantly change the motion inside the meshes of the net. However, it causes a crucial destruction of the separatrices and their replacement by stochastic layers. A connected net of channels of finite width along which an effective particle transport can be performed is therefore created. The set of channels is called a *stochastic web* presented in Fig. 7.1.

Different kinds of finite or infinite stochastic webs are possible, including those with or without symmetry. It is convenient to introduce a notion of the *web skeleton* since the width of the web tends to zero if  $\epsilon \rightarrow 0$ . It can happen that the skeleton of the web does not coincide with the separatrices net for  $\epsilon = 0$ , and the web can only occur when there is a finite perturbation. Such a case takes place for the periodically kicked oscillator introduced in Section 5.3:

$$H = \frac{1}{2}(\dot{x}^2 + \omega_0^2 x^2) - \frac{\omega_0}{T} K \cos x \sum_{m=-\infty}^{\infty} \delta\left(\frac{t}{T} - n\right), \quad (7.2)$$

where the oscillator mass is equal to one. The unperturbed part of the Hamiltonian corresponds to a free oscillator motion,

$$H_0 = \frac{1}{2}(\dot{x}^2 + \omega_0^2 x^2) \quad (7.3)$$

with a degenerate rotational symmetry and without any separatrices and saddle points. The perturbation has an amplitude  $K$  and a translational symmetry along  $x$ :  $x \rightarrow x + 2\pi m$  with integer  $m$ . As it was demonstrated in Section 5.3, for  $K \neq 0$ , stochastic webs occur if the resonant condition

$$\alpha = \omega_0 T = \frac{2\pi}{q} \quad (7.4)$$

is valid, where  $q$  is an integer. Although this is not the only case of the existence of stochastic webs, condition (7.4) will be used for the sake of simplicity.

Our general comments to the web problem are:

- (i) The existence of stochastic webs is an important physical phenomenon since infinite particle transport is performed along the channels of the web.
- (ii) The skeleton of the web tiles the phase plane (or partitions the volume) and imposes a dynamical origin of symmetry groups.

For example, the Arnold diffusion occurs for the number of degrees of freedom  $N > 2$ . It requires the non-degeneracy condition

$$\left| \frac{\partial^2 H_0}{\partial I_j \partial I_k} \right| \neq 0. \quad (7.5)$$

The diffusion rate is very low. Stochastic webs, that occur in the model (7.2), correspond to the case when (7.5) is not valid and  $N < 2$ . The diffusion rate along the channels of the web is much faster than in the case of Arnold diffusion. Many other possibilities also exist for higher dimensions ( $N > 2$ ). Some of them will be considered in this chapter (*Note 7.1*).

## 7.2 Stochastic webs with quasi-crystalline symmetry

The stochastic webs considered below occur when the condition of non-degeneracy (7.5) is violated. Rewrite the Hamiltonian (7.2) using the more convenient variables (5.28)  $u = \dot{x}/\omega_0$  and  $v = -x$ , and renormalize  $H$  by a constant

$$H = \frac{\alpha}{2}(u^2 + v^2) - K \cos v \sum_{n=-\infty}^{\infty} \delta(\tau - n). \quad (7.6)$$

The equations of motion are

$$\dot{u} = \frac{\partial H}{\partial v}, \quad \dot{v} = -\frac{\partial H}{\partial u}, \quad (7.7)$$

where the dot denotes a derivative with respect to the dimensionless time  $\tau = t/T$ . The equations of motion (7.7) can be partially integrated (as it was

done in Section 5.3) in order to replace them by the discrete map (5.27):

$$\hat{T}_{W(\alpha)} : \begin{aligned} u_{n+1} &= (u_n + K \sin v_n) \cos \alpha + v_n \sin \alpha, \\ v_{n+1} &= -(u_n + K \sin v_n) \sin \alpha + v_n \cos \alpha. \end{aligned} \quad (7.8)$$

In this section we consider the resonance case (7.4) which defines the web map

$$\hat{T}_{W(q)} : \begin{aligned} u_{n+1} &= (u_n + K \sin v_n) \cos \frac{2\pi}{q} + v_n \sin \frac{2\pi}{q}, \\ v_{n+1} &= -(u_n + K \sin v_n) \sin \frac{2\pi}{q} + v_n \cos \frac{2\pi}{q}. \end{aligned} \quad (7.9)$$

The map  $\hat{T}_{W(\alpha)}$  in  $u, v \in (-\pi, \pi)$  has a central elliptic fix point  $(0, 0)$ . The eigenvalues,  $\lambda_\alpha$ , of the tangent matrix,  $\hat{M}_\alpha$  at this point satisfy the equation

$$\lambda_\alpha^2 - 2Tr\hat{M}_\alpha \cdot \lambda_\alpha + 1 = 0, \quad (7.10)$$

where  $Tr\hat{M}_\alpha$  refers to the sum of diagonal elements of  $\hat{M}_\alpha$ . The solution of (7.10) leads to a condition

$$K > 2 \left| \cotan \left( \frac{\alpha}{2} \right) \right| \equiv K_\alpha^{(0)} \quad (7.11)$$

when the origin  $(0, 0)$  becomes unstable and the elliptic point is transformed to the hyperbolic one.

In Section 5.3 we demonstrated a few cases of the stochastic web with a crystalline symmetry, that is, when  $q = 3, 4, 6$  and belongs to the set

$$\{q_c\} \equiv \{1, 2, 3, 4, 6\}. \quad (7.12)$$

The set  $\{q_c\}$  corresponds to the cases when rotational and translational symmetries coexist on the plane  $(u, v)$ . The cases  $q = 1, 2$  are trivial and their corresponding motion is therefore regular. Figure 5.6 shows the stochastic web with the crystal-type symmetry of order 4. Figure 7.2 corresponds to  $q = 3$  and 6. Some of their properties are formulated as follows:

- (i) Crystal-type stochastic webs exist for arbitrarily small  $K$ . The size of the meshes do not change since  $K \rightarrow 0$  (up to the higher order terms in  $K$ , and it disappears when  $K = 0$ ). Proof of this statement is in Section 7.4.
- (ii) Diffusion coefficient along the webs is proportional to  $K^2$  unless an anomalous transport takes place. This statement is proven in Chapter 14.

A stochastic web still exists for  $q \neq \{q_c\}$  if  $1 > K > K_c$ , where  $K_c$  is a small critical value. Examples of the corresponding webs for  $q = 5$  are shown in Fig. 7.3 and for  $q = 7$  and 8 in Fig. 7.4. In all these figures, the webs are infinite and their finite sizes correspond to a finite computing time. All the webs have the quasi-crystal type symmetry which will be explained in the next section. It can be

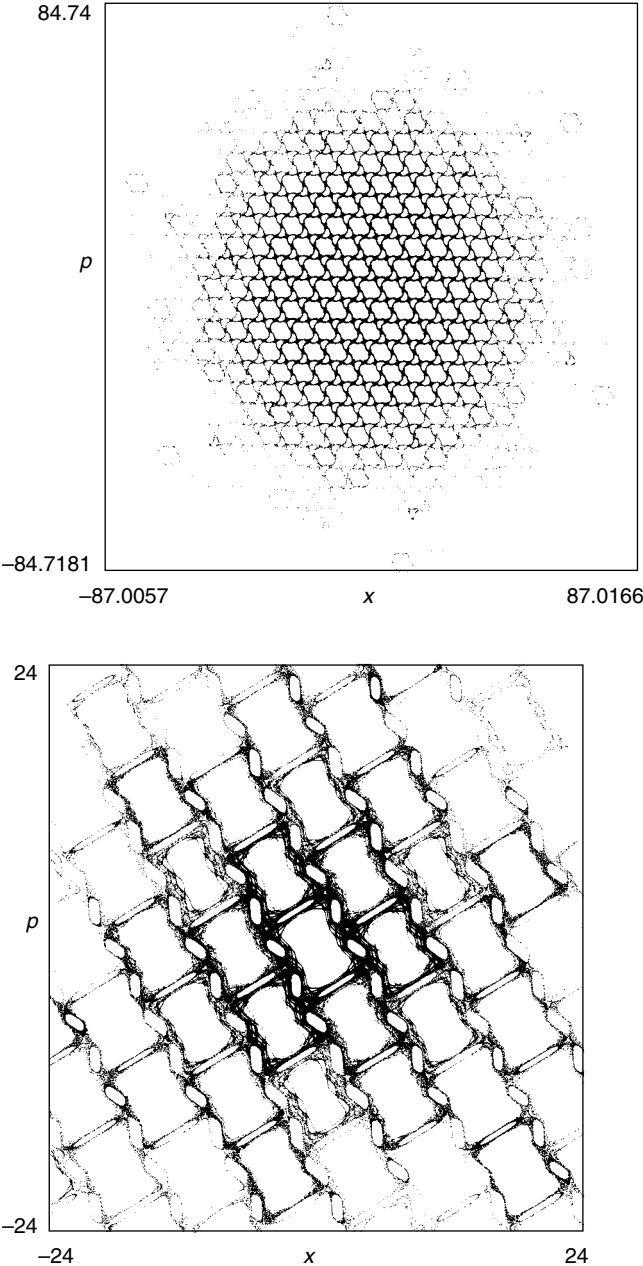


FIG. 7.2. Stochastic webs with crystal symmetries  $q = 3, 6$ : (top)  $q = 6$ ,  $K = 1.2$ ; (bottom)  $q = 3$ ,  $K = 1.7$ .



conjectured that  $K_c = 0$ , i.e. unlimited stochastic webs of the quasi-crystal type exist for arbitrarily small  $K > 0$ . Characteristic sizes of their meshes increase as  $K$  decreases. This point will be discussed more in Section 7.4 (*Note 7.2*).

### 7.3 Stochastic web skeleton

A Hamiltonian in the form of (7.6) with the resonance condition (7.4) is time-dependent. Nevertheless, the maps of the trajectories shown in Figs. 7.2–7.4 and others reveal the existence of invariant structures. To obtain an effective Hamiltonian,  $H_q(u, v)$ , which describes the structures, let us introduce polar

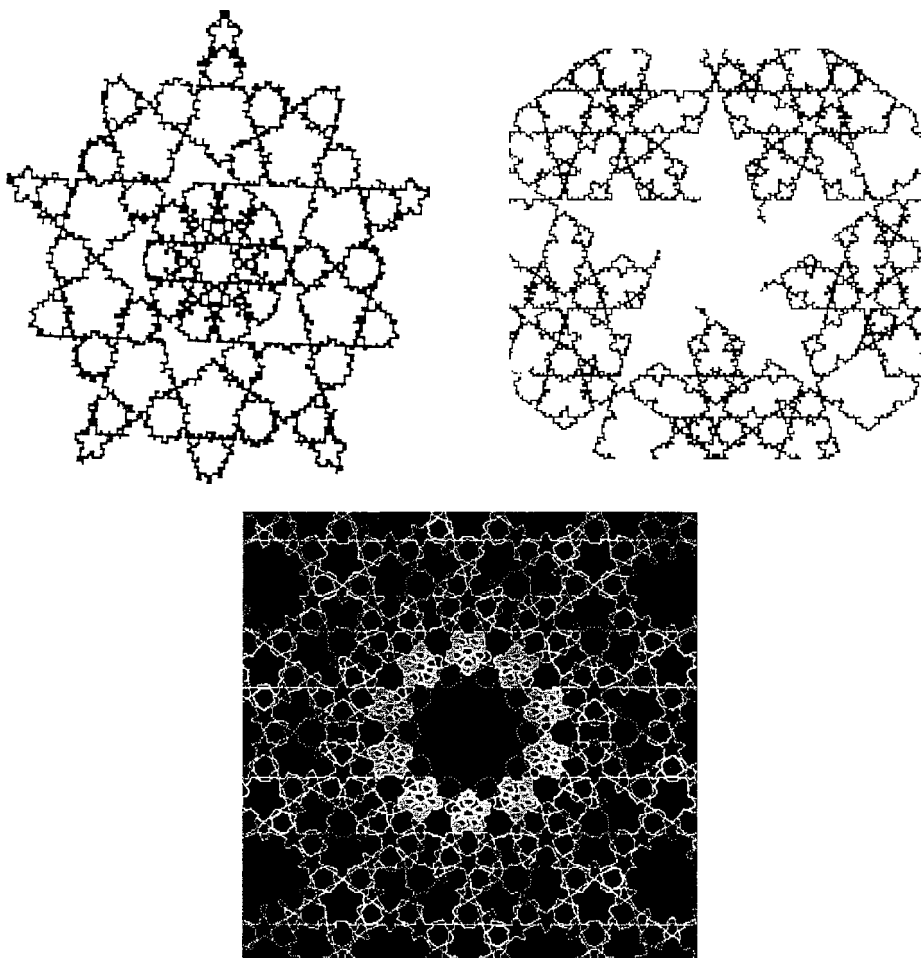


FIG. 7.3. Three different samples of the five-fold symmetric stochastic web.

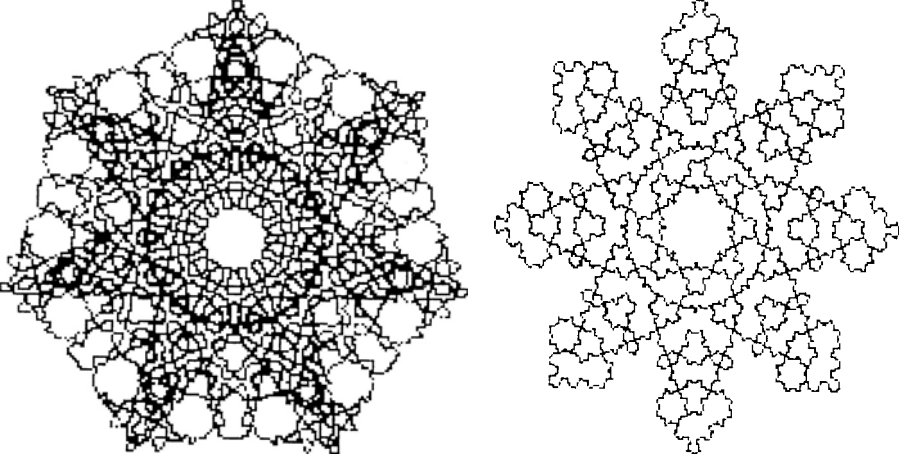


FIG. 7.4. Stochastic webs of the (a) seven-fold and (b) eight-fold symmetries.

coordinates  $(\rho, \phi)$ :

$$u = \rho \sin \phi, \quad v = -\rho \cos \phi \quad (7.13)$$

and generating function

$$F = (\phi - \alpha\tau)I, \quad I = \frac{1}{2}\rho^2 \quad (7.14)$$

that corresponds to the transformation to a coordinate system rotating with a frequency  $\alpha$  and new angle  $\hat{\phi}$  (in the following we write simply  $\phi$ ). In new variables, the new Hamiltonian becomes

$$\tilde{H} = H + \frac{\partial F}{\partial \tau} = -K \cos[\rho \cos(\phi - \alpha\tau)] \sum_{n=-\infty}^{\infty} \delta(\tau - n), \quad (7.15)$$

where the first term of the Hamiltonian (7.6), which represents linear oscillations, disappears. This is a typical feature of the transformation into a rotating frame of reference.

Consider the following identity

$$\sum_{n=-\infty}^{\infty} \delta(\tau - n) = \sum_{j=1}^q \sum_{m=-\infty}^{\infty} \delta(\tau - (mq + j)), \quad (7.16)$$

where we use the representation for a sum of  $\delta$ -functions:

$$\sum_{m=-\infty}^{\infty} \delta(\tau - j - mq) = \frac{1}{q} \sum_{m=-\infty}^{\infty} \exp\left(2\pi i m \frac{\tau - j}{q}\right). \quad (7.17)$$

Substitution of (7.16) and (7.17) into (7.15) and a regrouping of terms yields

$$\begin{aligned}\tilde{H} &= H_q + V_q, \\ H_q &= -\frac{1}{q}K \sum_{j=1}^q \cos \xi_j, \\ V_q &= -\frac{2}{q}K \sum_{j=1}^q \cos \xi_j \sum_{m=1}^q \cos \left( \frac{2\pi m}{q}(\tau - j) \right),\end{aligned}\tag{7.18}$$

where

$$\xi_j = -\rho \sin \left( \phi + \frac{2\pi}{q}j \right) = v \cos \left( \frac{2\pi}{q}j \right) - u \sin \left( \frac{2\pi}{q}j \right).\tag{7.19}$$

Expression (7.19) can also be written in a compact form

$$\xi_j = \boldsymbol{\rho} \cdot \mathbf{e}_j, \quad (j = 1, \dots, q)\tag{7.20}$$

using a unit vector definition

$$\mathbf{e}_j = \left[ \cos \left( \frac{2\pi j}{q} \right), -\sin \left( \frac{2\pi j}{q} \right) \right], \quad (j = 1, \dots, q)\tag{7.21}$$

and

$$\boldsymbol{\rho} = (v, u).\tag{7.22}$$

Equation (7.21) defines a regular star formed by  $q$  unit vectors  $\mathbf{e}_j$  and (7.20) defines the projection of the star unit vectors onto a two-dimensional plane.

Expressions (7.18)–(7.22) define the stationary Hamiltonian

$$H_q \equiv H_q(u, v) = -\frac{1}{2}\Omega_q \sum_{j=1}^q \cos(\boldsymbol{\rho} \cdot \mathbf{e}_j), \quad \Omega_q \equiv \frac{2K}{q}\tag{7.23}$$

which we call the *skeleton Hamiltonian*. The rest of  $\tilde{H}$  is  $V_q$ , which defines the non-stationary part of the Hamiltonian  $\tilde{H}$ . The expression  $H_q = H_q(u, v)$  defines a surface and the isolines of a constant energy,

$$E = -\frac{1}{2}\Omega_q \sum_{j=1}^q \cos(\boldsymbol{\rho} \cdot \mathbf{e}_j).\tag{7.24}$$

The isolines are invariant curves that tile the plane  $(u, v)$  with a symmetry called  $q$ -symmetry. For example, if  $q = 4$ ,

$$H_4 = -\Omega_4(\cos u + \cos v)\tag{7.25}$$

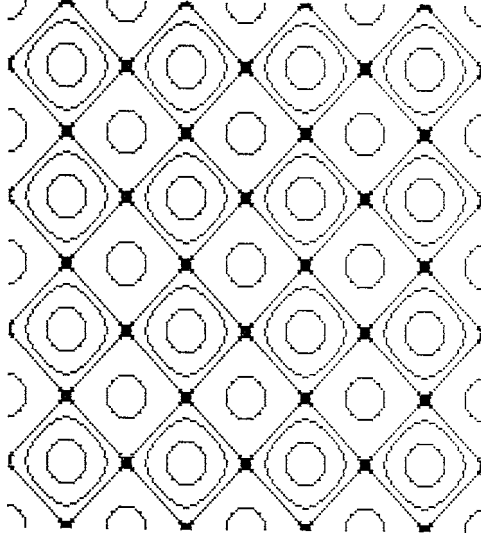


FIG. 7.5. Isolines of the four-fold symmetric skeleton Hamiltonian.

and the corresponding isolines are shown in Fig. 7.5. The values of  $E > 0$  define sections of humps on the surface of  $E = H_4(u, v)$ , the values of  $E = H_4(u, v) < 0$  define sections of wells, and the value  $E = H_4(u, v) = E_s = 0$  defines an infinite net of separatrices that tile the plane with the four-fold symmetry. This net is the skeleton of the stochastic web for  $q = 4$ .

Similarly, one can obtain expressions when  $q = 3$  and 6:

$$H_6 = 2H_3 = -\frac{1}{2}\Omega_6 \left[ \cos v + \cos \left( \frac{1}{2}v + \frac{\sqrt{3}}{2}u \right) + \cos \left( \frac{1}{2}v - \frac{\sqrt{3}}{2}u \right) \right]. \quad (7.26)$$

The structure of isolines is shown in Fig. 7.6. The net of separatrices can be obtained from the equation

$$E = E_s = \frac{1}{2}\Omega_6 = H_6(v_s, u_s) \quad (7.27)$$

and all solutions are

$$\begin{aligned} v_s &= \pi(2n_1 + 1), & v_s &= \sqrt{3}u_s + 2\pi(2n_2 + 1), \\ v_s &= -\sqrt{3}u_s + 2\pi(2n_3 + 1), & (n_{1,2,3} &= 0, \pm 1, \dots). \end{aligned} \quad (7.28)$$

The net of separatrices at the skeleton of the stochastic web forms the so-called kagome lattice with hexagonal symmetry.

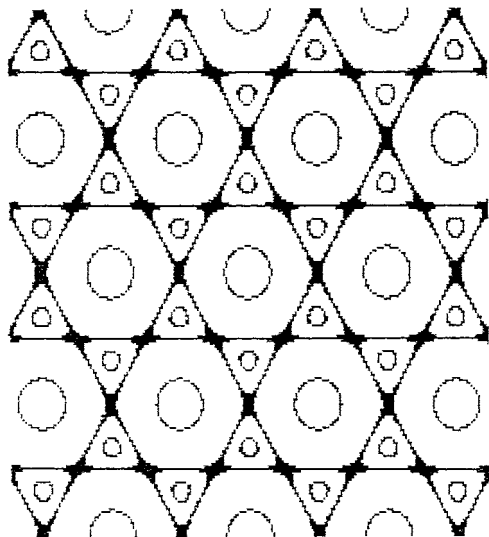


FIG. 7.6. Isolines for the three(six)-fold symmetric skeleton Hamiltonian.

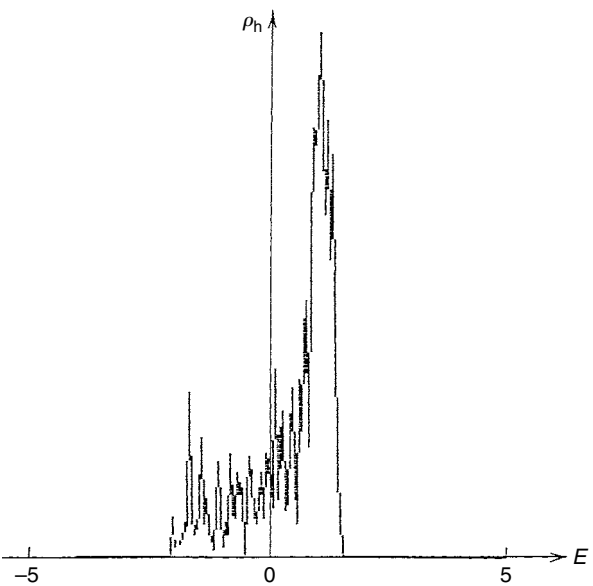


FIG. 7.7. Distribution of saddles for  $H_5$ .

Here are some general features of skeletons for the crystalline symmetry ( $q = 3, 4, 6$ ):

- (i-c) All saddle points of the Hamiltonian  $H_q(u, v)$  have the same value of energy  $E_s$  (see Figs. 7.5, 7.6).
- (ii-c) All separatrices are isolines of the same energy surface  $H_q(u_s, v_s) = E_s$ .
- (ii-c) Skeletons are unbounded and they tile the plane with the corresponding square or hexagonal symmetry.

In the case of  $q \neq \{q_c\}$ , the saddle points of the Hamiltonian  $H_q(u, v)$  do not belong to some unique value of energy anymore. They are distributed in a complicated manner although some values of energy do exist where a higher concentration of saddle points is found. For example, when  $q = 5$ , the maximum number of saddle points corresponds to  $E_m \approx -\frac{1}{2}\Omega_5$  (see Fig. 7.7). In fact, not much is known about the distribution of saddles and elliptic points for the values of  $q \neq \{q_c\}$  (Note 7.3).

Consider, for example, all isolines for the values of energy  $E$  taken in a layer  $E \in (E_m - \Delta E, E_m + \Delta E)$ . They form a ‘thick’ line structure. The corresponding pattern is shown in Fig. 7.8(a) and is related to the so-called quasi-crystal symmetry of the fifth order. The Hamiltonian  $H_q$  in (7.23) is a general expression which generates quasi-crystal symmetry of isolines. The examples of isolines for  $q = 7, 8$ , and  $12$  are shown in Figs. 7.8(b)–(d). They are obtained in the same way as for  $q = 5$ . Here are some features of the Hamiltonian  $H_q(u, v)$  for  $q \notin \{q_c\}$ :

- (i-cq) Some constant energy plane  $H_q = E$  consists of separatrices that form webs, but all of the webs are of finite sizes. There is no connected net that tiles the entire plane in the same sense as it was for  $q \in \{q_c\}$ . In other words, a connected infinite net with a finite size of meshes does not exist when  $q \notin \{q_c\}$ .
- (ii-cq) Consider a thin layer  $(E, E + \Delta E)$  of the width  $\Delta E$ . Any two saddle points are connected if their corresponding energies are  $E \in (E, E + \Delta E)$ . A net, connected through the layer  $\Delta E$ , exists for a finite  $\Delta E \geq \Delta E_c$ , and it is the way of formation of a skeleton of the stochastic web with  $q$ -fold symmetry. In other words, a connected ‘thick’ net with the thickness  $\Delta E_c$  exists. An example of ‘thick isolines’ for  $q = 5$  is shown in Fig. 7.9. The connected net is easily visualized and it forms a specific grid. Distances between parallel lines correspond to the so-called one-dimensional quasi-crystal (see Fig. 7.10) (Note 7.4).
- (ii-cq) It is assumed that the property (ii-cq) can be strengthened by a conjecture:  $\Delta E_c = 0$ , i.e. any finite thickness,  $\Delta E > 0$ , of the energy layer induces an infinitely connected net with a finite size for its meshes. The smaller  $\Delta E$  is, the larger the meshes.

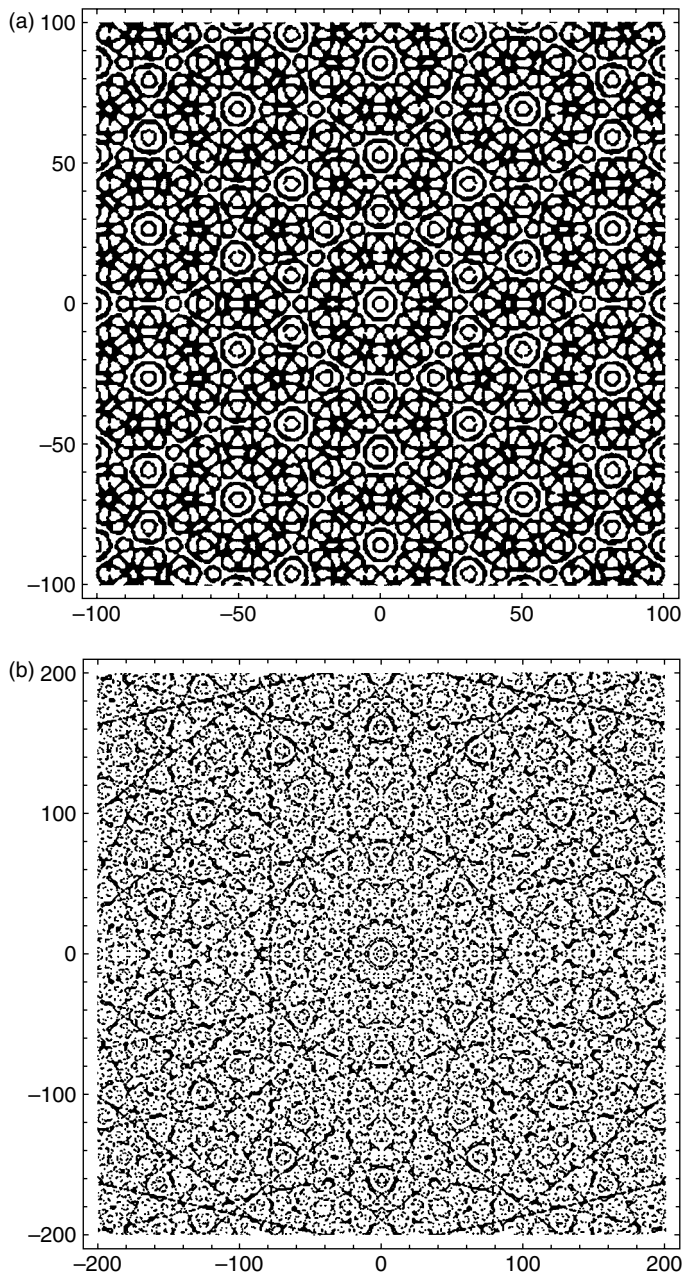


FIG. 7.8. Isolines of the skeleton Hamiltonian for different quasi-crystal type symmetries: (a)  $q = 5$ ; (b)  $q = 7$ ; (c)  $q = 8$ ; and (d)  $q = 12$ .

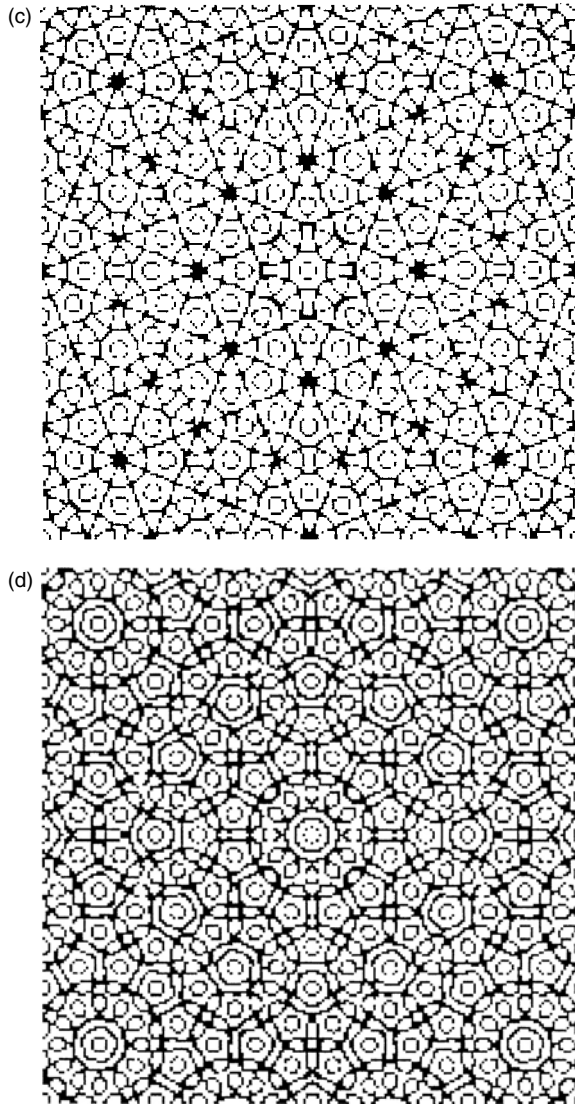


FIG. 7.8. (*Continued*).

- (iv-cq) The Hamiltonian  $H_q$  has  $q$ -fold rotational symmetry for even  $q$  and  $2q$ -fold rotational symmetry for odd  $q$ . The symmetry of  $H_q$  does not coincide with the symmetry of the original Hamiltonian  $H$  because of the averaging procedure. Up to the corresponding correction, the symmetries of  $H_q$  are sub-symmetries of  $H$  for small  $K$ , and the symmetry properties of  $H_q$  can be used to describe real trajectories of the original Hamiltonian  $H(x, \dot{x}, t)$ .



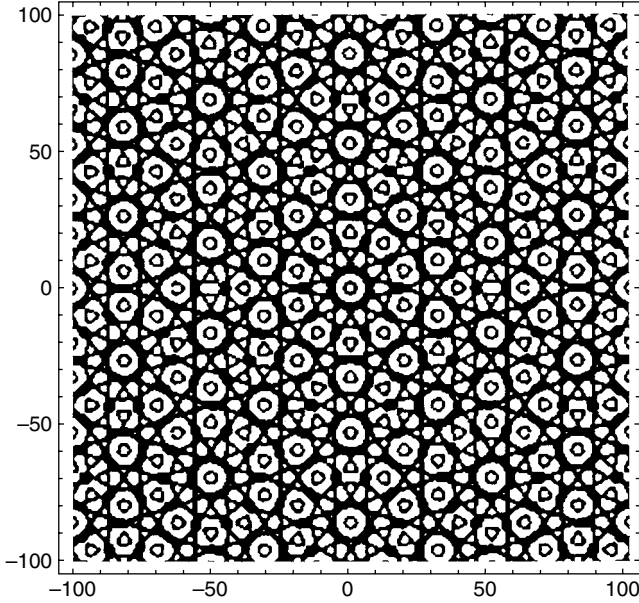


FIG. 7.9. ‘Thick isolines’ for  $q = 5$  in the energy layer  $E \in (0, 2)$  forms an infinite web.

(v-cq) Hamiltonian  $H_q$  defines an integrable system but there is no description of its solutions which follows from the equation (compare to (7.7)):

$$\dot{u} = \frac{\partial H_q}{\partial v}, \quad \dot{v} = -\frac{\partial H_q}{\partial u}. \quad (7.29)$$

From all properties described above, one can deduce the existence of a dynamical generator of symmetry. It means that the Hamiltonian  $H(u, v, t)$  in (7.6) is associated with a specific composition of orbits and singular points in phase space (phase plane) which partitions or tiles the space with approximate  $q$ -fold symmetry (better known as quasi-symmetry). The accuracy of the quasi-symmetry can be enhanced by applying the averaging procedure to obtain a skeleton Hamiltonian,  $H_q$ , in (7.23). The smaller the parameter  $K$  in (7.6), the closer the generalized quasi-symmetry is to a symmetry (*Note 7.5*).

#### 7.4 Symmetries and their dynamical generation

This section demonstrates how we can obtain non-trivial symmetries from dynamics. It also shows how symmetries can be modified by applying methods of dynamics. In considering how the five-fold symmetry can arise in dynamics, we use the Hamiltonian (7.6) for  $q = 5$ , and the map  $\hat{T}_{W(5)}$  from (7.9). This constitutes the first step. In the second step, the averaged Hamiltonian  $\hat{H}_{q=5}$  in

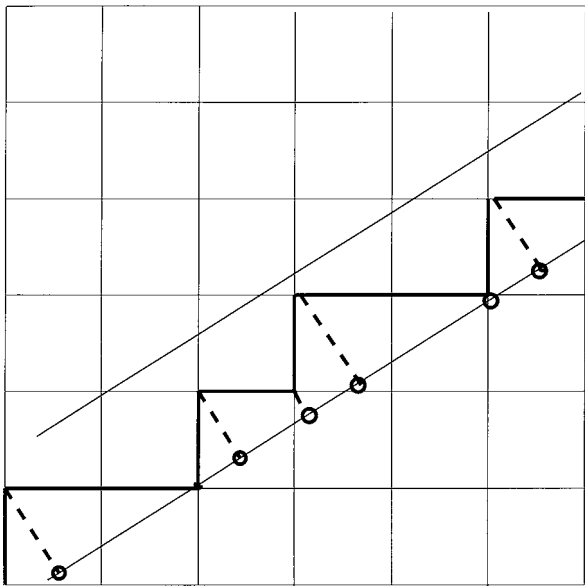


FIG. 7.10. A one-dimensional quasi-crystal is a sequence of black points obtained as a projection from a strip of a square lattice. The slope of the strip is  $1/\tau_0$ ,  $\tau_0 = 2\cos(\pi/5)$ , and the distances between the black points follow the Fibonacci sequence (see *Note 7.4*).

(7.23) is obtained. In the third step, both the maximum saddle point distribution as a function of energy, and the corresponding value  $E_{\max}$  are derived. In the fourth step, the ‘thick isolines’ portrait which belongs to the finite energy layer,  $(E_{\max} - \Delta E/2, E_{\max} + \Delta E/2)$ , with an appropriate small  $\Delta E$  is found. In the fifth step, using the thick isolines portrait (see Fig. 7.8(a)) as a stencil and, applying algorithm to connect different points on the stencil, a tiling is created. As an example, Fig. 7.11 demonstrates the famous Penrose tiling by connecting the centers of small five-stars with centers of small pentagons. A deliberate attempt was made to show a slightly asymmetrical tiling by using two kinds of rhombuses to illustrate different possibilities. A more sophisticated seven-fold symmetric tiling with three kinds of rhombuses is shown in Fig. 7.12. Figure 7.8(b) has been used as a seven-fold symmetric stencil to produce the tiling in Fig. 7.13. This tiling (Zaslavsky *et al.* (1991)) uses only 3 different tiles as rombi with angles  $(\pi/7, 6\pi/7)$ ,  $(2\pi/7, 5\pi/7)$ , and  $(3\pi/7, 4\pi/7)$  (*Note 7.6*).

The above comments suggest a new and unique opportunity of investigating a complex symmetry such as the quasi-crystalline symmetry by using methods of Hamiltonian dynamics. Let us demonstrate the relationship between symmetry

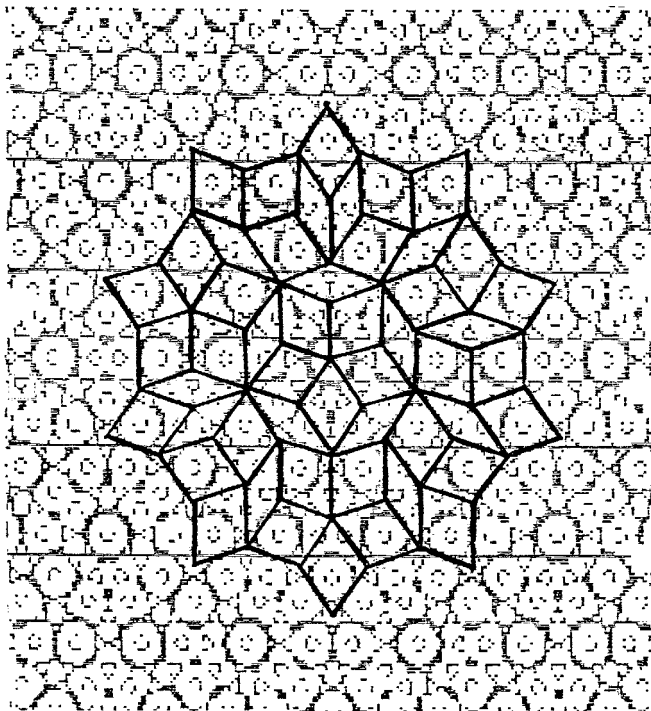


FIG. 7.11. Formation of the Penrose tiling using Fig. 7.9 as a stencil.

breaking and bifurcation in a dynamic system, for  $q = 3$ . The invariant curves of the map  $\hat{T}_{W(3)}$  form a tiling of the hexagonal type if  $K < K_\alpha^{(0)}$  with  $\alpha = 2\pi/3$ , where  $K_\alpha^{(0)}$  is defined in (7.11). The tiling is shown in Fig. 7.13(a). From the same map  $\hat{T}_{W(3)}$ , one can obtain a tiling of the brickwall type (Fig. 7.13(b)) if  $K > K_\alpha^{(0)}$ . The value  $K > K_\alpha^{(0)}$  corresponds to the value of  $K$  where the elliptic points at the centre of the hexagons lose their stability. For  $q = 3$  or  $\alpha = 2\pi/3$ ,  $K_\alpha^{(0)} = 2/\sqrt{3} = 1.1547\dots$ . If certain ‘fine’ details of the figure are ignored, the hexagons are modified to become close to rectangles and there is a corresponding change in the symmetry of the stochastic web which occupies very narrow regions between the rectangles, if  $K > K_\alpha^{(0)}$ . An example of a web with the brickwall symmetry is shown in Fig. 7.13(b).

The examples described in this section enable us to formulate the following statement: the web map  $\hat{T}_{W(q)}$  is considered as a dynamic generator for tiling a plane which has either a symmetry of an arbitrary order  $q$  of the crystalline type when  $q \in \{q_c\}$ , or of the quasi-crystalline type when  $q \notin \{q_c\}$ . As a method of tiling, we can first obtain a web skeleton and then perform a desirable algorithm

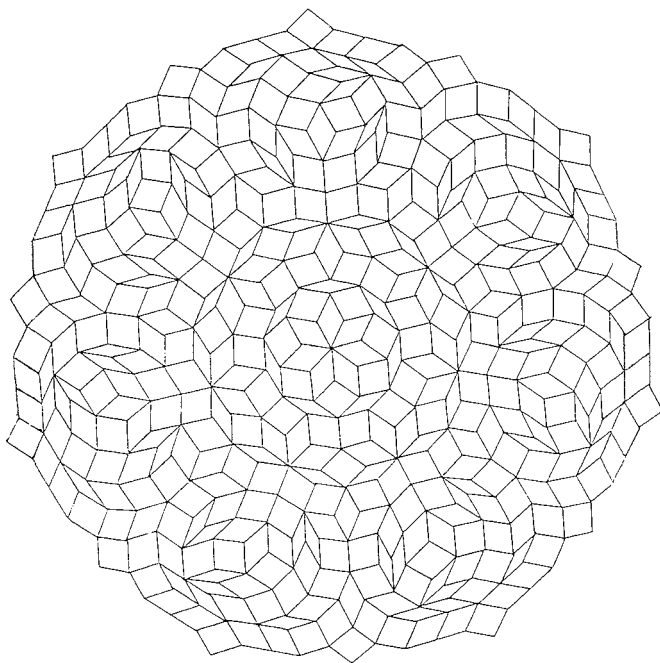


FIG. 7.12. Seven-fold symmetric tiling using three types of rhombuses.

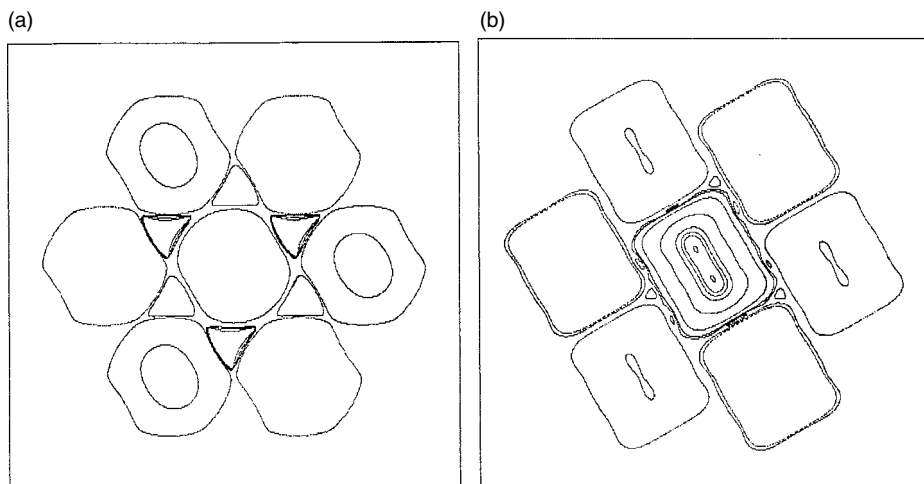


FIG. 7.13. Invariant curves for  $q = 3$  form hexagonal tiling when (a)  $K = 0.5$  and (b) brickwall tiling when  $K = 1.3$ .

for the tiling (this method was described above). Another method uses the phase portrait of the system directly and it can be simplified by removing some of small details or smoothing some special orbits. It should be noted that part of the phase portrait lying inside a cell of the web may have a completely different symmetry from that of the web itself and, in particular, it may not have any special symmetry. Inside the central cell of the web, there are various stochastic layers which are separated from one another and from the stochastic web by invariant curves.

We can also say that a 2D-tiling with a  $q$ -fold symmetry is the result of a decoration of the phase portrait. The *decoration* refers to a rule to select and/or alter some elements of the phase portrait. A *decoration of the skeleton* in Fig. 7.11 ( $q = 5$ ) results in its conversion into the Penrose tiling.

### 7.5 Width of the stochastic web

To calculate the width of the stochastic web, the representation (7.18) for the Hamiltonian  $\tilde{H}$  in the rotating frame of reference is used. The case of  $q = 4$  provides a good illustration of the application of the method described in Section 6.3.

Using (7.18), we obtain

$$\begin{aligned}\tilde{H} &\approx H_4 + V_4, \\ H_4 &= -\Omega_4(\cos u + \cos v), \\ V_4 &= -2\Omega_4(\cos v - \cos u) \cos \pi\tau\end{aligned}\tag{7.30}$$

by neglecting the other terms in  $V_4$  which are proportional to  $\cos(m\pi\tau)$  with  $m > 1$ . Their small correction will become apparent at the end of the calculations. Due to the degeneracy of the unperturbed Hamiltonian (7.3), there is no small parameter in the perturbation  $V_4$  in (7.30) and the influence of the perturbation is small via a different mechanism (as it was, for example, in Section 6.4).

For the unperturbed Hamiltonian  $H_4$ , defined in (7.23), the energy value on the separatrices is  $H_4 = 0$  and the corresponding separatrices are defined by the equations

$$v_s = \pm(u_s + \pi) + 2\pi m, \quad (m = 0, \pm 1, \dots).\tag{7.31}$$

From the equation of motion (7.29) we derive

$$\dot{u} = \Omega_4 \sin v, \quad \dot{v} = -\Omega_4 \sin u.\tag{7.32}$$

On the separatrices

$$\dot{u}_s = \mp \Omega_4 \sin u_s, \quad \dot{v}_s = \pm \Omega_4 \sin v_s\tag{7.33}$$

or

$$\begin{aligned}\tan\left(\frac{u_s}{2}\right) &= e^{\mp\Omega_4(\tau-\tau_n)}, \\ \tan\left(\frac{v_s}{2}\right) &= e^{\pm\Omega_4(\tau-\tau_n)},\end{aligned}\tag{7.34}$$

where  $\tau_n$  is the point of reference in time. Other than (7.34), another form of solution is

$$\sin u_s = -\sin v_s = -\frac{1}{\cosh[\Omega_4(\tau - \tau_n)]}.\tag{7.35}$$

Adopting the same scheme used in Sections 6.2 and 6.3, (7.31) yields

$$\dot{H}_4 = 4\Omega_4^2 \sin u \cdot \sin v \cdot \cos \pi \tau.\tag{7.36}$$

Replacing  $u, v$  on the right-hand side with  $u_s, v_s$  and substituting (7.35) in (7.36) as well as performing the integration, one obtains a change in the energy due to the perturbation of particle motion in the vicinity of the separatrix:

$$\Delta H_4 = -4\Omega_4^2 \int_{\tau_n-\infty}^{\tau_n+\infty} d\tau \frac{\cos \pi \tau}{\cosh^2 \Omega_4(\tau - \tau_n)} = -4\pi^2 \frac{\cos \pi \tau_n}{\sinh(\pi^2/2\Omega_4)}.\tag{7.37}$$

Since  $\Omega_4 = K/2 \ll 1$ , this expression takes the form of

$$\Delta H_4 = -8\pi^2 \cos \pi \tau_n \exp\left(-\frac{\pi^2}{K}\right).\tag{7.38}$$

The period of oscillations in the vicinity of the separatrix is

$$T(H_4) = \frac{4}{\Omega_4} \ln\left(\frac{8\Omega_4}{|H_4|}\right) = \frac{8}{K} \ln\left(\frac{4K}{|H_4|}\right).\tag{7.39}$$

The time needed to pass near the separatrix is equivalent to one-quarter of the period, that is,

$$\tau_{n+1} - \tau_n \approx \frac{T(H_4)}{4} = \frac{1}{\Omega_4} \ln\left(\frac{8\Omega_4}{|H_4|}\right) = \frac{2}{K} \ln\left(\frac{4K}{|H_4|}\right).\tag{7.40}$$

Setting  $H_4$  to be equal to  $H_4^{(n+1)}$ , and taking the expression (7.37) into account, we obtain the separatrix map in the form

$$\begin{aligned}H_4^{(n+1)} &= H_4^{(n)} - 8\pi^2 \exp\left(-\frac{\pi^2}{K}\right) \cos \pi \tau_n, \\ \tau_{n+1} &= \tau_n + \frac{2}{K} \ln\left(\frac{4K}{|H_4^{(n+1)}|}\right).\end{aligned}\tag{7.41}$$

This procedure was described in Sections 6.2 and 6.3. Using the same procedure, we obtain a boundary of the stochastic layer from the condition

$$\max \left| \frac{\delta\tau_{n+1}}{\delta\tau_n} - 1 \right| > 1. \quad (7.42)$$

Hence, the border  $H_s$  of the stochastic layer is

$$H_s = \frac{16\pi^3}{K} \exp\left(-\frac{\pi^2}{K}\right). \quad (7.43)$$

This result was obtained in Afanas'ev *et al.* (1990).

The quantity  $2H_s$  defines a width of the stochastic layer. Since all separatrices are connected, forming a single network, the quantity  $2H_s$  is also the width of the stochastic web. It is exponentially small since  $K \ll 1$ . The neglected terms, arising from  $V_4$  in (7.18), give a correction of the order  $\exp(-2\pi^2/K)$  which is too small compared to (7.43).

The same considerations can be applied in the case of an arbitrary value of  $q$ . The width of the stochastic web can be estimated as

$$H_s \sim \exp\left(-\frac{\text{const}}{K}\right), \quad (7.44)$$

where the value of const increases somewhat with the growth of  $q$ . However, for all  $q \notin \{q_c\}$ , there is a peculiarity which needs to be discussed.

It was mentioned in Section 7.3 that all hyperbolic points belong to the same energy level  $E$  for  $q \in \{q_c\}$ . In the case of  $q \notin \{q_c\}$ , this property is absent. Saddles and separatrices are distributed among different energy levels and there is no single infinite net of unperturbed separatrices for any value of the energy. An example of isolines for  $H_5$  is presented in Fig. 7.14 for  $q = 5$ . The figure shows saddles forming a pattern resembling a family of parallel straight lines (a). However, in Fig. 7.14(b), it can be seen that near the value  $E_m = -\Omega_5/2$  (see Fig. 7.7), the separatrix loops approach each other very closely. Nevertheless, the intersections of the loops are located on different planes of constant energy. The gaps between some separatrices can be so small that even a small perturbation can create narrow stochastic layers which overlap these gaps. This is how a single stochastic web net is formed. In the case of quasi-symmetry, the mechanism for the web formation is quite different from that for the crystal symmetry since there is no single separatrix for the web-skeleton Hamiltonian  $H_q$ .

Concluding this section we should mention that topological properties of the phase plane are defined by a set of singular points and curves. These properties can be imposed by an unperturbed Hamiltonian and a perturbation. The symmetry of the Poincaré map is the result of a complex interplay between the symmetries of the unperturbed Hamiltonian and the perturbation.

Thin filaments (channels) of chaotic dynamics, called the stochastic web, form a net with a symmetry or quasi-symmetry. The web map of the type discussed

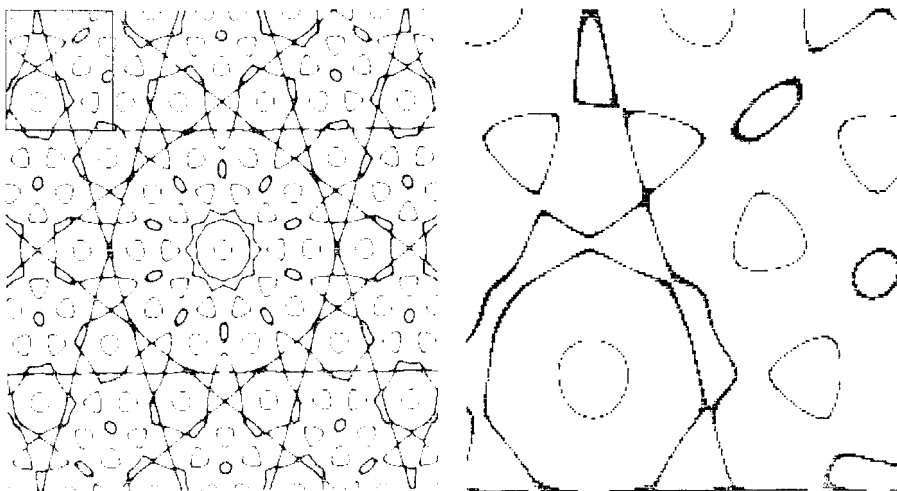


FIG. 7.14. Example of isolines for  $H_5$ : (left) the ‘thick lines’ belong to the range of energy  $E \in (0.8, 1.2)$ ; (right) an enlarged image of isolines from the marked square in (left) with  $E \in (0.9, 1.1)$ .

in Section 5.3 generates the web that tiles the phase space with a symmetry of the quasi-crystal type. The tiling can be characterized by a web skeleton. Thus, the web map is a generator of the  $q$ -fold symmetric tiling of an arbitrary order  $q$ .

It is significant that the connected net with  $q$ -fold symmetry appears as a structure of finite-width channels in phase plane. However, the width of the channels is exponentially small.

## 7.6 Symmetry in art and nature

### 7.6.1 *Symmetry and chaos*

This chapter would not be complete without a discussion of symmetry in art and nature. Symmetry in nature has captivated human consciousness from the ancient times. It has since become a challenge to science to determine how and why natural symmetry occurs. It is significant that the fundamental methods used by contemporary physicists are now the symmetry-based approaches that investigate the basic laws of dynamics and the interaction of particles. It would be an oversimplification to say that symmetry is a mere reflection of ‘harmony in nature’. The symmetries can be considered as the unique or only possible way for natural laws to self-organize, for instance as it is reflected in the fundamental equations of motion. This view of symmetry, that of it being the result of specific features of natural forces, was introduced and discussed by Johannes Kepler (1619). Kepler also attempted to find a five-fold symmetric tiling of a plane.



What is puzzling and paradoxical, however, is the fact that the knowledge of five-fold symmetric tiling had already existed, possibly as far back as the twelfth century in Iran (Makovsky (1992)). Yet this knowledge remained unknown to scientists well up until modern times, and the publication of the Penrose tiling (Penrose (1974)) was considered as a discovery. This discovery, of course, encouraged the hope for the existence of quasi-crystals of five-fold symmetry. Schehtman *et al.* (1984) were able to get, in fact, real quasi-crystals.

Symmetry does not exclude chaos, and *vice versa*. While some variables have a symmetry, others can be of chaotic changes. A trivial example is the Newton equation for the periodically perturbed pendulum. It is area-preserving and symmetric with respect to time shift by the period of perturbation. To speak in more detail about the symmetry of dynamics, it is convenient to include some elements of the dynamics that are invariant with respect to the system evolution, or, simply, which do not depend on time. These are stationary points and separatrices. One can say that a set of elliptic and hyperbolic points is a 'carrier' of symmetry in phase space. Invariance of these points has been used to obtain a symmetric tiling of the phase plane by chaotic attractors (*Note 7.7*).

The role of chaos is still vague, and we should go further to understand more. The following problem was posed by Weyl (1952): can we find a dynamical generator of different kinds of symmetries? This is a more specific formulation of the attempts of Kepler. Can, for example, we find a dynamical generator (within Hamiltonian equations), i.e. a kind of force, that drives a particle exactly along a square lattice? There is a precise answer: 'No.' Trajectories along the lattice are separatrices and an infinite time is necessary to overcome even one side of the lattice. This situation can be reckoned with if we take into account that any small periodic perturbation splits the separatrices, and then replaces them by a thin stochastic web, as in Fig. 7.1. Particle dynamics along the web is random and has a finite speed. This means that one trajectory with an initial condition within the web tiles the infinite plane following the channels of the web. This tiling does not have exact symmetry because of the finite and non-uniform width of the web. Nevertheless, the deviations from the exact symmetric tiling can be arbitrary small. We call this type of tiling *quasi-symmetric*, i.e. a stochastic web tiles the plane with a *quasi-symmetry*. In other words, the web map  $W(q)$  can be considered as a generator of  $q$ -fold symmetry since the corresponding stochastic web tiles the plane with  $q$ -fold quasi-symmetry. Let us remember that the tiling created by the only trajectory can be performed because of chaotic dynamics within the stochastic web, and this can be considered as a unique demonstration of the coexistence of chaos and symmetry and even of *chaos-assisted symmetric tiling*.

### 7.6.2 Ornamental patterns

The history of mosaics can be traced back some 4,000 years with the use of terracotta stones for stenciling of mostly simple patterns. Ancient tilings, or

ornamental patterns were used as architectural decorations in the Byzantine Empire and Rome, and later and most intensively in oriental art. The main condition of decorative ornamental art is: (1) to make a stencil that is unbounded and has a finite number of elements (tiles), and (2) to decorate the tiles. The first problem is purely mathematical or geometrical, and it appears in contemporary design art, such as wallpaper, that should satisfy any size of walls, with no seams or jumps in the patterning. It happens that three-, four-, and six-fold symmetries globally dominated in ancient patterns, while the five-fold symmetry tiling appeared probably in Iran during the twelfth century (Markovicky (1992)), and later moving to other places such as Alhambra Palace in Granada (Spain), Seville (Spain), Jerusalem, and other places. Figures 7.15–7.17, obtained by the author, show different variants of the five-fold symmetric ornaments in the architecture. More about different tilings can be found in Grunbaum and Schepard (1987) and for oriental ornaments in Critchlow (1999).

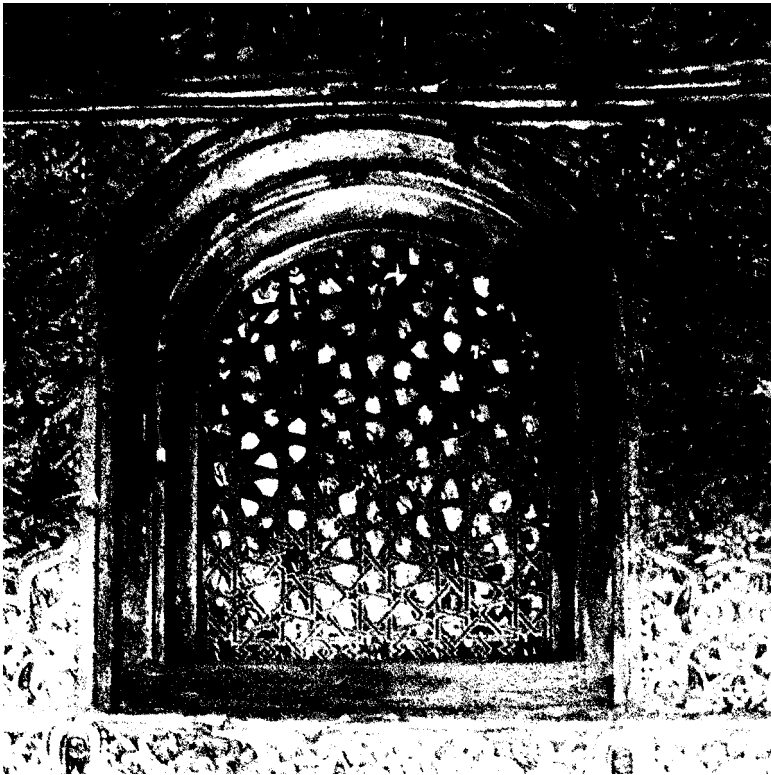


FIG. 7.15. Ornamental window in the Mirador de Lindaraja (Alhambra Palace, c. sixteenth century).

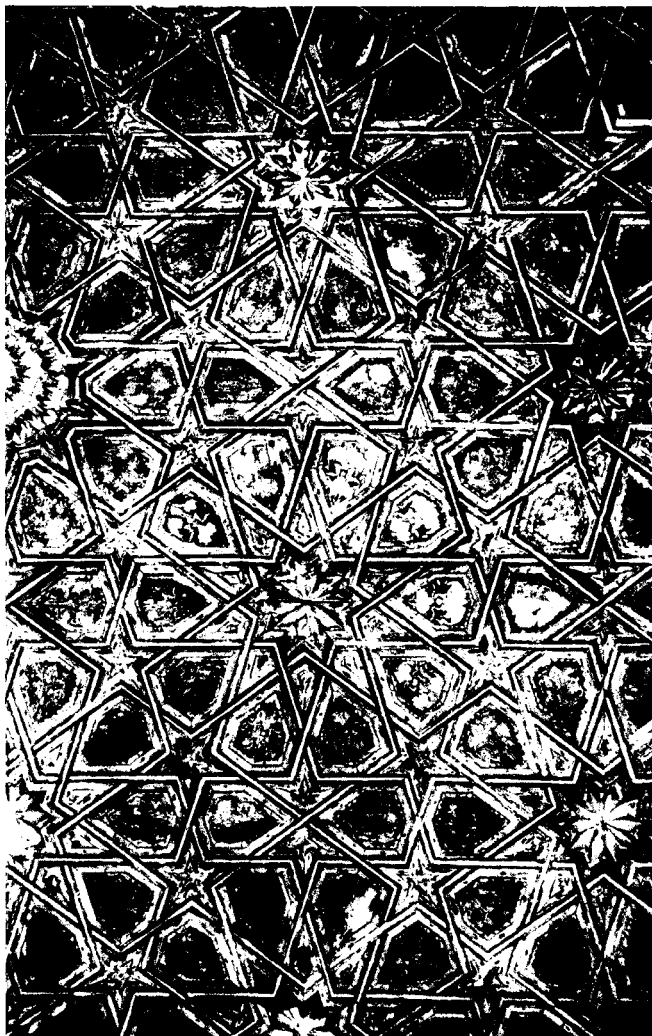


FIG. 7.16. Ceiling in the Pilato House (Seville, *c.* fifteenth century).

### 7.6.3 *Patterns in nature*

Patterns with five-fold symmetry, or with a five-fold axis of symmetry, can be found often in nature. Living organisms such as echinoderms (starfish, brittle star, sea urchin, feather star, sea cucumber, and sand dollars) have an axis symmetry of the fifth order. Plants, such as sunflowers or pine cones, have

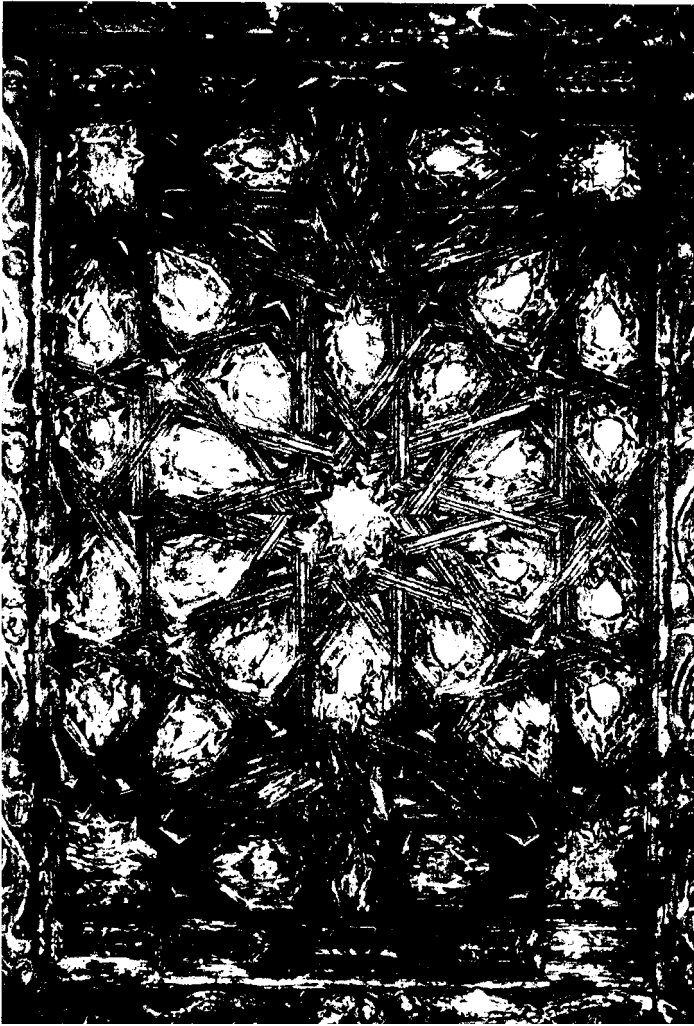


FIG. 7.17. A door in the Los Reales Alcázares (Seville, *c.* sixteenth century).

a spiral structure (called ‘phyllotaxis’ or plant spirals) of seeds that correspond to the Fibonacci series. Sections of DNA have a decagonal structure.

Why is it that we meet with pentagonal order in living nature, yet we do not meet with triangular, or square-shaped plants or creatures? One interesting hypothesis has been expressed by Belov (1976): because the pentagonal structure is resistant to its crystallization. An important comment was also given

by Schrödinger (1944): not as much information can be written on the periodic structure. At the same time, the molecules responsible for life should have a fixed, but not periodic (crystalline) order. In this way Schrödinger arrives at the notion of *aperiodic crystals* as an ordered structure that can carry a fairly large amount of information.

In a set of experiments (Douady and Couder (1992, 1996)), the dynamical situations that can lead to phyllotactical patterns were modelled. In another set of experiments (Gollub (1995)), two-dimensional quasi-crystal patterns were obtained in the capillar wave dynamics. These brief comments indicate a deep link of quasicrystal type symmetry in physical and biological phenomena (Note 7.8).

## Notes

### Note 7.1

The Arnold diffusion, introduced in Arnold (1964), is the subject of numerous investigations and applications (Chirikov (1979); Lichtenberg and Lieberman (1983); Nekhoroshev (1997)). Contemporary results and their discussion can be found in Delshams *et al.* (2003). Recently the Arnold diffusion has received a new fundamental aspect of a great interest. As was mentioned in Arnold *et al.* (1993), the Arnold diffusion may guarantee the metrical transitivity of Hamiltonian dynamics for  $N > 2$ .

### Note 7.2

For further reading on stochastic webs, see Zaslavsky *et al.* (1991). Different properties of stochastic webs were considered in Lowenstein (1991, 1992, 1994a, 1994b); Pekarsky and Rom-Kedar (1997); Dana (1995); Dana and Amit (1995). The symmetries of the webs were studied in Arnold (1988); Lowenstein (1992, 1993); Lamb (1993); Lamb and Quispel (1994).

### Note 7.3

More information on the distribution of elliptic and hyperbolic points can be found in Zaslavsky *et al.* (1991) and Lowenstein (1991, 1994b). Particularly, the distribution of saddles is important for a problem of percolation in a quasi-symmetric potential (Chaikovsky and Zaslavsky (1991); Isichenko (1992)). An interesting result was obtained in Chernikov and Rogalsky (1994): the fractal dimension of a long (possibly infinite) curve for  $H_q$  for large enough  $q$  (for example  $q > 32$ ) coincides with the fractal dimension of a percolated trajectory. The percolated trajectory is any infinite curve that crosses the infinite domain with the random potential  $V(u, v)$  and energy level  $E = V(u, v) \gtrsim E_c$ , where  $E_c$  corresponds to the percolation threshold.

For the Hamiltonian  $H_q, q \notin \{q_c\}$  the existence of infinite curves has not been proven yet. See more discussion on this problem in the book Arnold *et al.* (2003).

*Note 7.4*

The one-dimensional analogue of the quasi-crystal with a five-fold symmetry is simply a one-dimensional ‘grid’ of points with coordinates

$$x_n = n + \beta_1 + \frac{1}{\tau_0} \left[ \frac{n}{\tau_0} + \beta_2 \right],$$

where  $n$  is an integer,  $\beta_1$  and  $\beta_2$  are any constants,  $[a]$  is the integer part of  $a$ , and  $\tau_0$  is the golden mean:

$$\tau_0 = \frac{1 + \sqrt{5}}{2} = 2 \cos \left( \frac{\pi}{5} \right).$$

This grid is related to the so-called Ammann lattice. Information on the Ammann lattice can be found in Grunbaum and Shepard (1987). It is easy to find this grid in Fig. 7.9. A one-dimensional grid is rotated 5 times by  $2\pi/5$ . The points  $x_n$  form the Fibonacci sequence. See more in Seneshal (1995).

*Note 7.5*

The problem of dynamical generation of symmetries was formulated by A. Weyl (1952). The web-map can be considered as a generator for the crystal and quasi-crystal symmetries in a two-dimensional case.

*Note 7.6*

For more information on the Penrose tiling see Penrose (1974); Senechal (1995); Zaslavsky *et al.* (1991).

*Note 7.7*

There exists rich literature on obtaining different structures with crystallographic symmetry by using chaotic attractors (Field and Golubitsky (1992); Dumont and Reiter (2000); Dumont *et al.* (2001)). For the  $q$ -fold symmetry generation, see Zaslavsky *et al.* (1991). For more on the Penrose tiling, see Gardner (1977).

*Note 7.8*

For more discussions of patterns in nature, see Ball (1999), and for a different appearance of the five-fold symmetry, see Hargittai (1992). On the appearance of the five-fold symmetry in architecture and art, see Zaslavsky *et al.* (1991).

**Problems**

More complicated problems are marked by (\*).

7.1\* The  $m$ -tuple saddle point 0 is shown in Fig. P7.1. Consider  $m = 4$ .

- (a) Write down a model Hamiltonian that describes the dynamics in the vicinity of 0.
- (b) Consider a particle dynamics with energy  $E$  such that  $|E - E_0| \ll E_0$  where  $E_0$  is the energy on a separatrix. Find the solution  $q(t), p(t)$ .

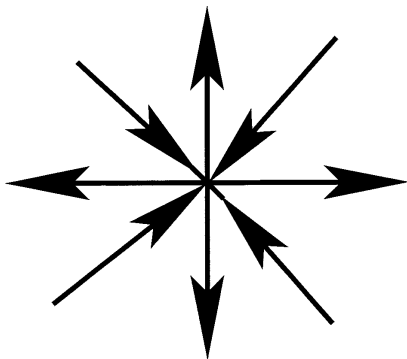


FIG. P7.1. Example of the  $m$ -tuple saddle point with  $m = 4$ .

(c) Find a time that is necessary to reach the turning point, that is close to 0, from a distant point if the particle has energy  $E$  and  $|E - E_0| \ll E_0$ .

7.2 Describe the dynamics on the separatrix near the  $m$ -tuple point.

7.3 Prove that rotational and translational symmetries on the plane coexist only when the rotational angle is  $2\pi/q$ ,  $q \in \{q_c\}$  (see (7.12)).

## BEYOND THE KAM-THEORY

In Chapter 3 we discussed different approaches based on the idea that a fairly strong non-linearity can stabilize the perturbed dynamics. KAM-theory is perhaps the most important example of this situation. As was mentioned, the main two parameters that characterize the evolution of the system under a perturbation are dimensionless perturbation parameter  $\epsilon$  and the non-linearity parameter  $\alpha$ . We saw in the previous chapter that in the case of degeneracy, that is,  $\alpha = 0$ , qualitatively different dynamics can appear and the corresponding physical situation becomes different. In fact, any kind of condition like  $\epsilon \rightarrow 0$  or  $\alpha \rightarrow 0$  sometimes is physically senseless since the ratio of small but finite  $\epsilon$  and  $\alpha$  can be of importance for the understanding different possible processes. This will be the subject of this chapter, where the case of vanishing non-linearity will be studied. Let us recall that the important condition of the applicability of the KAM-theory is just the opposite: a finite non-linearity and vanishing perturbation (*Note 8.1*).

### 8.1 Small non-linearity

This section continues with a consideration of 1 1/2 degrees of freedom systems, that is, a time-periodic perturbation in a system with one degree of freedom. The results can be extended to systems with two degrees of freedom. The KAM-theory guarantees the persistence of invariant tori (curves) within the limit of a small enough perturbation

$$\epsilon \rightarrow 0 \tag{8.1}$$

provided the non-degeneracy condition

$$\left| \frac{\partial^2 H_0(I)}{\partial I_k \partial I_\ell} \right| \neq 0. \tag{8.2}$$

The system to be considered is described by the Hamiltonian

$$H = H_0(I) + \epsilon V(I, \vartheta, t), \tag{8.3}$$

where  $I, \vartheta$  are action-angle (phase), and  $\epsilon$  is the dimensionless parameter of the perturbation. The form of the Hamiltonian (8.3) shows that its unperturbed



part,  $H_0$ , describes an integrable system. The non-degeneracy condition (8.2) takes the form

$$\frac{d^2 H_0(I)}{dI^2} = \frac{d\omega(I)}{dI} \neq 0, \quad (8.4)$$

where the non-linear frequency

$$\omega(I) = \frac{dH_0(I)}{dI} \quad (8.5)$$

is introduced for the unperturbed motion. Condition (8.4) therefore concludes that the unperturbed system should be non-linear for the results of the KAM-theory to be applicable.

From the physical point of view, condition (8.1) means that  $\epsilon$  should be fairly small, or  $\epsilon < \epsilon_0$ . However, condition (8.2) has no meaning since it does not indicate a critical value,  $\alpha_0$ , for the dimensionless non-linear parameter

$$\alpha = \left| \frac{d\omega}{dI} \right| \frac{I}{\omega}, \quad (\omega \neq 0), \quad (8.6)$$

such that fairly small  $\alpha < \alpha_0$  should be considered as a violation of the condition (8.2). It would be more acceptable to write the condition of validity of the KAM-theory as

$$\epsilon < C\alpha^\delta, \quad (\epsilon, \alpha \rightarrow 0) \quad (8.7)$$

with some  $\delta > 0$  and constant  $C$  independent (or slightly dependent) on  $\alpha$ . A situation which differs from that in the KAM-theory occurs when the inequality (8.7) is not valid.

This problem can be described more specifically by using the typical models of perturbed pendulum and perturbed oscillator with the Hamiltonians

$$H = \frac{1}{2}\dot{x}^2 - \omega_0^2 \cos x + \epsilon \frac{\omega_0^2}{k^2} \cos(kx - \nu t) \quad (8.8)$$

for the perturbed pendulum and

$$H = \frac{1}{2}\dot{x}^2 + \frac{1}{2}\omega_0^2 x^2 + \epsilon \frac{\omega_0^2}{k^2} \cos(kx - \nu t) \quad (8.9)$$

for the perturbed oscillator; their corresponding equations of motion are, respectively,

$$\ddot{x} + \omega_0^2 \sin x = \epsilon \frac{\omega_0^2}{k} \sin(kx - \nu t) \quad (8.10)$$

and

$$\ddot{x} + \omega_0^2 x = \epsilon \frac{\omega_0^2}{k} \sin(kx - \nu t). \quad (8.11)$$

The effect of the perturbation for a linear oscillator is the strongest in the resonant case

$$\nu = n_0 \omega_0, \quad (8.12)$$

which has an integer  $n_0$ . Unless another condition is mentioned, this assumption is used below. The amplitude of a linear oscillator grows linearly with time until it is stopped by the non-linearity. The latter is induced by the same perturbation.

It is evident that system (8.8) (but not (8.9)) satisfies the condition of non-degeneracy in (8.4). At the same time, the expansion

$$\cos x = 1 - \frac{x^2}{2} + \frac{x^4}{24} \cdots \quad (8.13)$$

endows (8.8) with the same Hamiltonian as (8.9) when the non-linear term  $x^4$  can be neglected. This gives rise to the following questions: how small should  $\epsilon$  be to be able to apply the KAM-theory in (8.8)? And how should one consider (8.9) which is a non-KAM-case? The answers will be formulated in the following sections.

## 8.2 Web-Tori

Let us introduce the polar coordinates for the perturbed oscillator (8.9) and (8.11)

$$x = \rho \sin \phi; \quad \dot{x} = \omega_0 \rho \cos \phi. \quad (8.14)$$

The following expansion,

$$\cos(kx - \nu t) = \cos(k\rho \sin \phi - \nu t) = \sum_m J_m(k\rho) \cos(m\phi - \nu t) \quad (8.15)$$

is also used, where  $J_m$  is the Bessel function. With the new variables the Hamiltonian (8.9) becomes

$$H = \frac{1}{2} \omega_0^2 \rho^2 + \frac{1}{k^2} \epsilon \omega_0^2 \sum_m J_m(k\rho) \cos(m\phi - \nu t) \quad (8.16)$$

or with a singled out term with  $m = n_0$ :

$$H = \frac{1}{2} \omega_0^2 \rho^2 + \frac{1}{k^2} \epsilon \omega_0^2 J_{n_0}(k\rho) \cos(n_0\phi - \nu t) + \frac{1}{k^2} \epsilon \omega_0^2 \sum_{m \neq n_0} J_m(k\rho) \cos(m\phi - \nu t). \quad (8.17)$$

Let us introduce new action-angle variables:

$$I = \frac{\omega_0 \rho^2}{2n_0}, \quad \theta = n_0 \phi - \nu t. \quad (8.18)$$

A new Hamiltonian is then written as

$$\tilde{H} = H - \nu I, \quad (8.19)$$

where  $H$  is expressed as a function of  $(I, \theta)$ . A direct calculation ensures that the equations

$$\dot{I} = -\frac{\partial \tilde{H}}{\partial \theta}, \quad \dot{\theta} = \frac{\partial \tilde{H}}{\partial I} \quad (8.20)$$

are equivalent to the equation of motion (8.11). Substitution of (8.18) in (8.17) and (8.19) yields

$$\begin{aligned} \tilde{H} = & (n_0 \omega_0 - \nu)I + \frac{1}{k^2} \epsilon \omega_0^2 J_{n_0}(k\rho) \cos \theta + \frac{1}{k^2} \epsilon \omega_0^2 \sum_{m \neq n_0} J_m(k\rho) \\ & \times \cos \left[ \frac{m}{n_0} \theta - \left( 1 - \frac{m}{n_0} \right) \nu t \right], \end{aligned} \quad (8.21)$$

where  $\rho$  is introduced to obtain a more compact notation. According to (8.18),  $\rho$  is

$$\rho = \left( \frac{2n_0 I}{\omega_0} \right)^{1/2}. \quad (8.22)$$

Thus, the expression  $\tilde{H} = \tilde{H}(I, \theta; t)$  is the Hamiltonian with respect to the new canonical variables  $(I, \theta)$ . It can also be written as

$$\tilde{H} = \tilde{H}_0(I, \theta) + \tilde{V}(I, \theta; t), \quad (8.23)$$

where in accordance with (8.21),

$$\begin{aligned} \tilde{H}_0(I, \theta) = & (n_0 \omega_0 - \nu)I + \frac{1}{k^2} \epsilon \omega_0^2 J_{n_0}(k\rho) \cos \theta, \\ \tilde{V}(I, \theta; t) = & \frac{1}{k^2} \epsilon \omega_0^2 \sum_{m \neq n_0} J_m(k\rho) \cos \left[ \frac{m}{n_0} \theta - \left( 1 - \frac{m}{n_0} \right) \nu t \right] \end{aligned} \quad (8.24)$$

and expression (8.22) is used for  $\rho$ .

Turning now to the resonance case (8.12), the expression (8.24) for the Hamiltonian part  $\tilde{H}_0$  takes the following form:

$$\tilde{H}_0 = \frac{1}{k^2} \epsilon \omega_0^2 J_{n_0}(k\rho) \cos \theta = \frac{1}{k^2} \epsilon \omega_0^2 J_{n_0} \left[ k \left( \frac{2n_0 I}{\omega_0} \right)^{1/2} \right] \cos \theta. \quad (8.25)$$

In performing a preliminary analysis of the dynamic system that emerges in a resonance case, it is noted that the two terms in the Hamiltonian (8.23),  $\tilde{H}_0$  and  $\tilde{V}$ , are proportional to  $\epsilon$ . Hence, the stationary part of the Hamiltonian, which is time-independent, is affected by the time-dependent part which is considered as a perturbation. The fully transformed Hamiltonian  $\tilde{H}$  vanishes at  $\epsilon \rightarrow 0$ . This is a new feature of the problem which has not yet been discussed and that shows that *the limit  $\epsilon \rightarrow 0$  cannot be performed*.

It is possible to consider  $\tilde{H}_0(I, \theta)$  as an unperturbed part of the Hamiltonian  $\tilde{H}$  and  $\tilde{V}(I, \theta, t)$  as a perturbation. The phase portrait for the Hamiltonian (8.25), presented in Fig. 8.1, corresponds to  $(x, \dot{x})$  plane if a time instant is fixed. Separatrices form a net on the plane  $(x, \dot{x})$  in the form of a spider-web with the number of rays  $2n_0$  and the rotational symmetry at an angle  $\alpha = \pi/n_0$ .

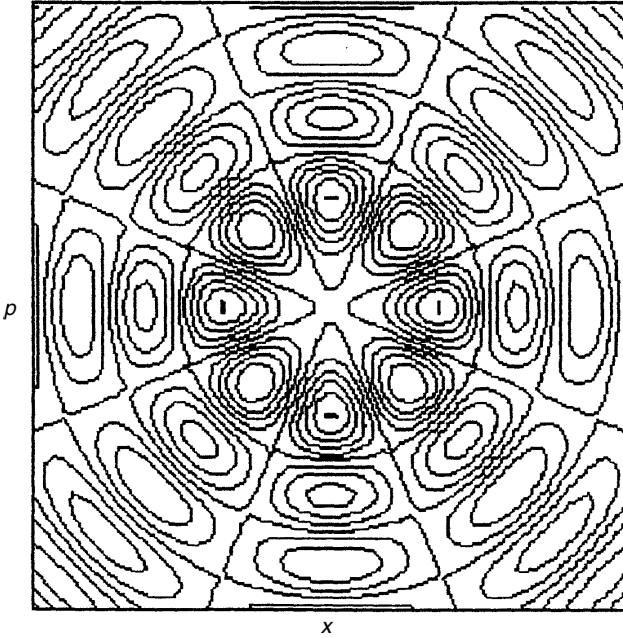


FIG. 8.1. Phase portrait of a system with the separatrix net in the form of a web ( $n_0 = 4$ ).

The singular points of the system can be found from the following equations:

$$\frac{\partial \tilde{H}_0}{\partial I} = 0, \quad \frac{\partial \tilde{H}_0}{\partial \theta} = 0. \quad (8.26)$$

For  $\tilde{H}_0$  (8.25) we obtain a set of hyperbolic points  $(\rho_h, \theta_h)$

$$J_{n_0}(k\rho_h) = 0, \quad \theta_h = \pm \frac{\pi}{2} \quad (8.27)$$

and a set of elliptic points  $(\rho_e, \theta_e)$

$$J'_{n_0}(k\rho_e) = 0, \quad \theta_e = 0, \pi. \quad (8.28)$$

A family of separatrices is formed by  $2n_0$  rays and circumferences with the radii  $\rho_h^{(s)}$  crossing the rays at points which are solutions to the equations (8.27). Inside the cells of the web, motion occurs along closed orbits around elliptic points located at the centres of the cells.

There is a principal difference between the motion described by the Hamiltonian (8.25) and the motion of a non-linear pendulum. In the former, the web of separatrices covers the entire space with a regular set of finite meshes, and the particle motion along the web can occur in a radial direction. In the latter, however, any motion in the radial direction is ruled out. This is a typical feature for non-linear cases where the non-degeneracy condition (8.2) or (8.4) holds.

However, the radial motion is only possible along separatrices in the unperturbed case. In the vicinity of hyperbolic points, the radial motion is frozen. Hence there is no progress along the radius for the Hamiltonian  $\tilde{H}_0$  (8.25) unless the perturbation  $\tilde{V}$  in (8.24) is taken into account. As a result, the separatrices in the unperturbed form would disappear and be replaced by channels of finite width and with stochastic dynamics along them. Before discussing this phenomenon in greater detail, consider a structure of the unperturbed web-tori (*Note 8.2*). For the sake of simplicity, consider the regions which are sufficiently far from the centre of the web, that is, with

$$k\rho \gg 1. \quad (8.29)$$

The asymptotics of Bessel function are

$$J_n(k\rho) \sim \left(\frac{2}{\pi k\rho}\right)^{1/2} \cos\left(k\rho - \frac{1}{2}\pi n - \frac{1}{4}\pi\right). \quad (8.30)$$

A cell in the web is singled out for a description of the family of unperturbed trajectories found inside it (Fig. 8.2). Let  $\rho_0$  be an elliptic point in the centre of

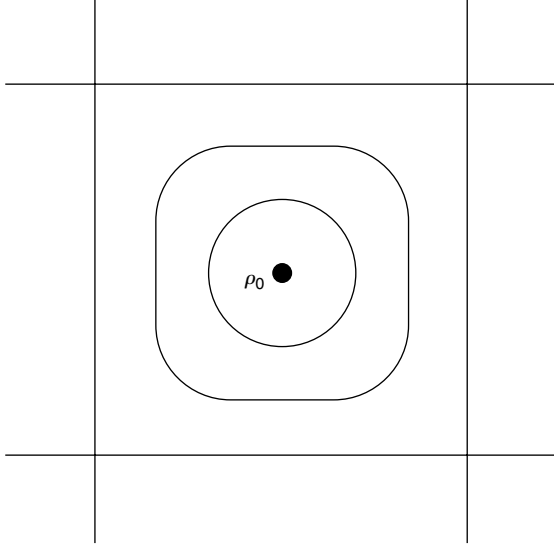


FIG. 8.2. A cell of the web.

the cell, then, according to (8.28) and (8.30), there are two possibilities:

$$k\rho_0 - \frac{1}{2}\pi n_0 - \frac{1}{4}\pi = 0, \quad k\rho_0 - \frac{1}{2}\pi n_0 - \frac{1}{4}\pi = \pi. \quad (8.31)$$

Using the expression (8.30) and the condition (8.31), the Hamiltonian (8.25) can be rewritten as

$$\tilde{H}_0 = -\sigma\epsilon \frac{\omega_0^2}{k^2} \left( \frac{2}{\pi k \rho_0} \right)^{1/2} \cos k\tilde{\rho} \cos \theta, \quad \sigma = \pm 1, \quad (8.32)$$

where  $\tilde{\rho} = \rho - \rho_0$ . Different signs correspond to different directions of rotations around the elliptic point as well as to different coordinates of the elliptic points.

The analysis of trajectories determined by the Hamiltonian (8.32) shows that the size of the separatrix cell is of the order  $2\pi/k$ . Therefore,  $\max \Delta\rho = 2\pi/k$  and according to inequality (8.29),

$$|\tilde{\rho}| = |\rho - \rho_0| \ll \rho_0. \quad (8.33)$$

From the definition of action (8.18) it follows

$$I = \frac{1}{2n_0} \omega_0 \rho^2 \approx \frac{1}{2n_0} \omega_0 \rho_0^2 + \frac{\omega_0 \rho_0}{n_0} \tilde{\rho}. \quad (8.34)$$

A change of the variable

$$\tilde{I} = I - \frac{1}{2n_0}\omega_0\rho_0^2 = \frac{\omega_0\rho_0}{n_0}\tilde{\rho} \quad (8.35)$$

is canonical (shifted by a constant). Within the same approximation and, as in the case of the Hamiltonian  $\tilde{H}$ , the pair of variables  $(\tilde{\rho}, \theta)$  is canonical. Thus, Hamiltonian equations of motion have the following form:

$$\dot{\tilde{\rho}} = -\frac{n_0}{\rho_0\omega_0} \frac{\partial \tilde{H}_0}{\partial \theta}, \quad \dot{\theta} = \frac{n_0}{\rho_0\omega_0} \frac{\partial \tilde{H}_0}{\partial \tilde{\rho}}. \quad (8.36)$$

In fact, they coincide with those derived from (8.20) under condition (8.33).

After denoting

$$\omega_w = -\sigma \left(\frac{2}{\pi}\right)^{1/2} \frac{\epsilon n_0 \omega_0}{(k\rho_0)^{3/2}} \quad (8.37)$$

and defining a new Hamiltonian,

$$H_w = \omega_w \cos \xi \cos \theta, \quad (8.38)$$

where  $\xi = k\tilde{\rho}$ , the equations

$$\dot{\xi} = \frac{\partial H_w}{\partial \theta}, \quad \dot{\theta} = -\frac{\partial H_w}{\partial \xi} \quad (8.39)$$

are equivalent to (8.36). The Hamiltonian  $H_w$  can be called Hamiltonian of the web-tori (see *Note 8.1*) and  $\omega_w$  is frequency of small oscillations.

Rewriting (8.39) in an explicit form:

$$\dot{\xi} = -\omega_w \cos \xi \sin \theta, \quad \dot{\theta} = \omega_w \sin \xi \cos \theta, \quad (8.40)$$

using (8.38), and integrating (8.40), we obtain

$$\sin \theta = \kappa \operatorname{sn}(\omega_w(t - t_0); \kappa), \quad (8.41)$$

where  $\operatorname{sn}$  is the Jacobian elliptic function,  $t_0$  is a time instant at which  $\theta = 0$ , and  $\kappa$  is the modulus of the elliptic function

$$\kappa = \left(1 - \frac{H_w^2}{\omega_w^2}\right)^{1/2}. \quad (8.42)$$

Using solution (8.41) and expressions (8.38) and (8.42), we derive

$$\sin \xi = \kappa \frac{\operatorname{cn}(\omega_w(t - t_0); \kappa)}{\operatorname{dn}(\omega_w(t - t_0); \kappa)}. \quad (8.43)$$

Both solutions (8.41) and (8.43) are periodic functions of time. The period of non-linear oscillations is

$$T(H_w) = \frac{1}{|\omega_w|} 4K(\kappa), \quad (8.44)$$

where  $K(\kappa)$  is a full elliptic integral of the first kind. When  $\kappa \rightarrow 1$ ,

$$T_w = \frac{2\pi}{|\omega_w|}, \quad (8.45)$$

that is, the frequency of small oscillations coincides with frequency (8.37). Near the separatrix,  $\kappa \rightarrow 0$  and it follows from (8.44) that

$$\begin{aligned} T(H_w) &= \frac{4}{|\omega_w|} \ln \frac{4}{(1 - \kappa^2)^{1/2}} = \frac{4}{|\omega_w|} \ln \frac{4|\omega_w|}{|H_w|} \\ &= \left(\frac{\pi}{2}\right)^{1/2} \frac{4}{\epsilon n_0 \omega_0} (k \rho_0)^{3/2} \ln \left[ 4\epsilon \frac{\omega_0^2}{k^2} \left( \frac{2}{\pi k \rho_0} \right)^{1/2} \frac{1}{|\tilde{H}_0|} \right]. \end{aligned} \quad (8.46)$$

On the separatrices,  $H_w = 0$ . From (8.38), it follows that four separatrices in Fig. 8.2 are defined by equations:

$$\cos \xi = 0, \quad \xi = \pm \frac{\pi}{2} \quad (8.47)$$

and

$$\cos \theta = 0, \quad \theta = \pm \frac{\pi}{2}. \quad (8.48)$$

They correspond to four sides of the square (under the approximation  $\tilde{\rho} \ll \rho_0$ ) in Fig. 8.2. Solution for the case (8.47) is

$$\sin \theta = \pm \tanh[2|\omega_w|(t - t_0)], \quad \xi = \pm \frac{\pi}{2}. \quad (8.49)$$

It corresponds to two horizontal separatrices. For the case (8.48) of two vertical separatrices, the solution is

$$\sin \xi = \mp \tanh[2|\omega_w|(t - t_0)], \quad \theta = \mp \frac{\pi}{2}. \quad (8.50)$$

Closed trajectories defined by the Hamiltonian (8.32) and (8.38) become cross-sections of the invariant tori if we add a ‘time’ variable to phase space  $(I, \theta)$  (see also *Note 8.1*) in a usual way (that is, by taking into account the perturbation  $V$  which is periodic in time). The invariant tori lying inside a web are referred to as *web-tori* and they differ from the KAM-tori in the way how their period  $T_w$  depends  $\epsilon$ . In the case of KAM-tori,  $T \sim 1/\epsilon^{1/2}$  while for the web-tori  $T_w \sim 1/\epsilon$ .



Another important difference between KAM-tori and web-tori is the angle at which their separatrices cross. It can be arbitrarily small for KAM-tori while it is a constant for the web-tori [ $\pi/2$  in the case of (8.38)], depending on the web's structure.

We can state that in the case of the web-tori, the degeneracy condition

$$\frac{d^2 H_0(I)}{dI^2} = 0 \quad (8.51)$$

allows radial infinite diffusion while the conditions (8.4) do not allow it in the KAM-case and  $1\ 1/2$  degrees of freedom.

### 8.3 Width of the stochastic web

For the perturbed oscillator model (8.9), the Hamiltonian was rewritten as (8.24) which transforms into

$$H_{n_0}(\tilde{I}, \theta) = \epsilon \frac{\omega_0^2}{k^2} J_{n_0}(k\tilde{\rho}) \cos \theta + \epsilon \frac{\omega_0^2}{k^2} \sum_{m \neq n_0} J_m(k\tilde{\rho}) \cos \left[ \frac{m}{n_0} \theta - \left( 1 - \frac{m}{n_0} \right) \nu t \right] \quad (8.52)$$

for the resonance (8.12) with

$$\tilde{\rho} = \left( \frac{2n_0 \tilde{I}}{\omega_0} \right)^{1/2} \quad (8.53)$$

[see (8.22)]. Unperturbed motion is defined by the first term in (8.52) which corresponds to the Hamiltonian (8.25). Its phase plane is covered by a web-like net of separatrices (Fig. 8.1). The second term in (8.52) defines a perturbation

$$V_{n_0} = \epsilon \frac{\omega_0^2}{k^2} \sum_{m \neq n_0} J_m \left[ k \left( \frac{2n_0 \tilde{I}}{\omega_0} \right)^{1/2} \right] \cos \left[ \frac{m}{n_0} \theta - \left( 1 - \frac{m}{n_0} \right) \nu t \right], \quad (8.54)$$

whose presence destroys the separatrices and replaces them with stochastic layers. The width of the stochastic layers can be obtained using the same scheme described in Chapter 6.

To simplify estimations, we use the inequality (8.29) in the form

$$k\rho_0 = k \left( \frac{2n_0 \tilde{I}}{\omega_0} \right)^{1/2} \gg 1 \quad (8.55)$$

and retain two terms with  $m = n_0 \pm 1$  in the sum (8.54). It gives

$$V_{n_0} \approx 2\epsilon \frac{\omega_0^2}{k^2} \left( \frac{2}{\pi k \rho_0} \right)^{1/2} \sigma \sin k \tilde{\rho} \sin \theta \sin \left[ \frac{1}{n_0} (\theta + \nu t) \right] \quad (8.56)$$

for the perturbation (8.54) where the sign function,  $\sigma$ , indicates similarity to (8.32), a type of the considered cell. Thus, the entire problem is described by the following Hamiltonian:

$$H_{n_0} = \sigma \epsilon \frac{\omega_0^2}{k^2} \left( \frac{2}{\pi k \rho_0} \right)^{1/2} \left\{ -\cos k \tilde{\rho} \cos \theta + 2 \sin k \tilde{\rho} \sin \theta \sin \left[ \frac{1}{n_0} (\theta + \nu t) \right] \right\}. \quad (8.57)$$

Calculations are omitted and the final results can be obtained in a similar way as those in Chapter 6. For the Melnikov integral (6.18) we have

$$\Delta H_{n_0} = 2\pi^2 \frac{\omega_0^2}{k^2} \exp \left\{ -\frac{1}{\epsilon} \left( \frac{\pi}{2} \right)^{5/2} (k \rho_0)^{1/2} \right\} \sin \phi_0, \quad (8.58)$$

where  $\phi_0$  is a phase that depends on an initial time instant. The corresponding width of the stochastic web is

$$\Delta H_s = 2^{1/2} \pi^{7/2} \frac{1}{\epsilon} (k \rho_0)^{1/2} \frac{\omega_0^2}{k^2} \exp \left\{ -\frac{1}{\epsilon} \left( \frac{\pi}{2} \right)^{5/2} (k \rho_0)^{1/2} \right\}. \quad (8.59)$$

Expression (8.59) indicates that the width of the web decreases quickly as the radius  $\rho_0$  grows, that is, the width of the web for fairly distant cells is exponentially small due to two large parameters in the exponent:  $1/\epsilon$  and  $k \rho_0$  (*Note 8.3*).

#### 8.4 Transition from KAM-Tori to Web-Tori

Compare now equations for the perturbed pendulum and oscillator, (8.10) and (8.11), respectively, using the expansion (8.13). Hamiltonian (8.24) for the perturbed oscillator can be rewritten as:

$$\begin{aligned} H = & (n_0 \omega_0 - \nu) I - \frac{n_0^2}{6} I^2 \sin^4 \theta + \epsilon \frac{\omega_0^2}{k^2} J_{n_0}(k \rho) \cos \theta + \epsilon \frac{\omega_0^2}{k^2} \sum_{m \neq n_0} J_m(k \rho) \\ & \times \cos \left[ \frac{m}{n_0} \theta - \left( 1 - \frac{m}{n_0} \right) \nu t \right]. \end{aligned} \quad (8.60)$$

For the purpose of estimation:

1. Consider only the part which includes the first three terms and keep as a perturbation only the term with  $m = n_0 \pm 1$  in the sum.

2. Ignore the non-resonant detuning arising from the first term in  $H$ , that is, put  $n_0\omega_0 = \nu$ .
3. Replace  $\sin^4 \phi$  by its average value  $3/8$ .

Elliptic and hyperbolic points of the unperturbed Hamiltonian satisfy (8.26). Non-trivial solutions exist for these equations if

$$\frac{n_0^2}{8} I < \epsilon \frac{\omega_0^2}{k^2} \frac{dJ_{n_0}(k\rho)}{dI}, \quad (8.61)$$

which means that non-linearity is smaller than perturbation. The ‘effective’ perturbation parameter is

$$\bar{\epsilon} = \frac{\epsilon \omega_0^2}{k^2} \quad (8.62)$$

and the condition (8.61) becomes

$$\bar{\epsilon} k^4 > \frac{\omega_0^2 \xi^3}{16 J'_{n_0}(\xi)}, \quad (8.63)$$

where  $\xi = k\rho$  is a dimensionless parameter required for the determination of a stationary point radius. The criterion for its existence is given by (8.63), where  $\xi$  is proportional to  $I^{1/2}$  and it characterizes a level of non-linearity. The expression (8.63) has a perturbation parameter on its left-hand side and a non-linearity on its right-hand side.

Consider now the unperturbed, i.e. time-independent, Hamiltonian in (8.60) for the case of exact resonance  $n_0\omega_0 = \nu$ :

$$H_0 = -\frac{1}{6} n_0^2 I^2 \sin^4 \theta + \bar{\epsilon} J_{n_0}(\xi) \cos \theta. \quad (8.64)$$

The equations for elliptic and saddle points are

$$\frac{\partial H_0}{\partial I} = 0, \quad \frac{\partial H_0}{\partial \theta} = 0. \quad (8.65)$$

The exact equations (8.65), without averaging  $\sin^4 \theta$ , can modify slightly the const multiplier in (8.63), but we will ignore this difference as not essential.

If condition (8.63) is valid, non-trivial solutions of (8.65) exist. A bounded stochastic web is implanted in the separatrix loop of the perturbed pendulum. Numerical examples of this phenomenon are presented in Fig. 8.3. Figure 8.3(a) shows the separatrix loop of the perturbed pendulum with a thin stochastic layer instead of the destroyed separatrix. At the same time, fragments

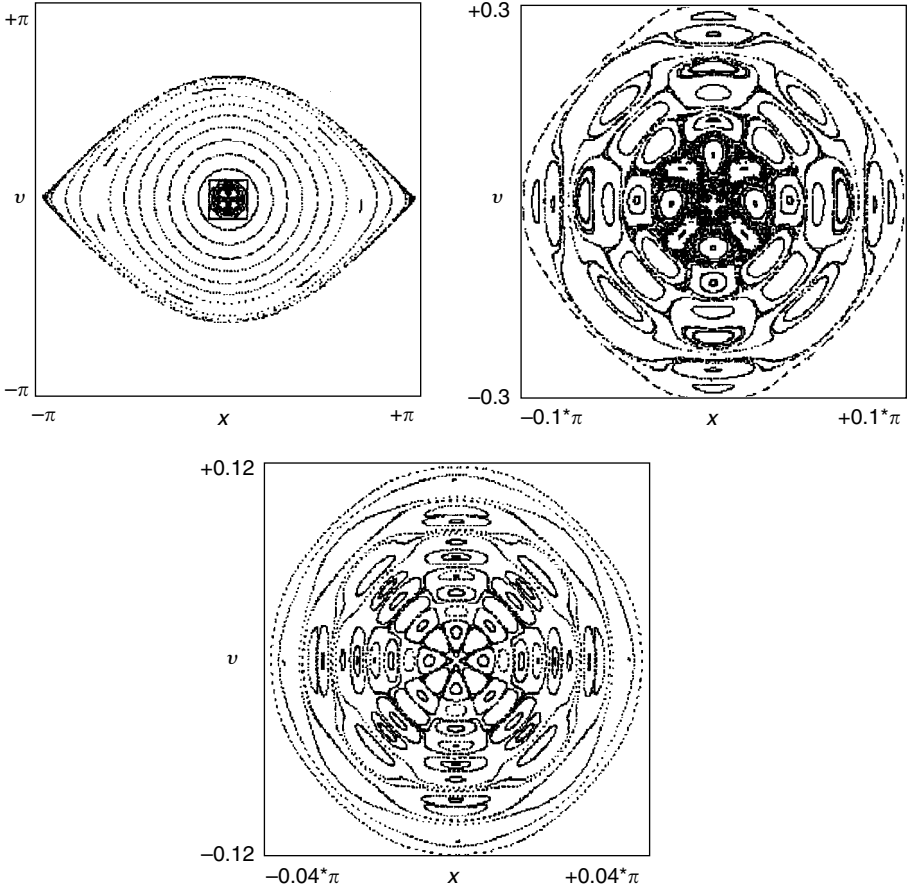


FIG. 8.3. Implantation of a part of the web in the separatrix loop of the perturbed pendulum problem with  $\omega_0 = 1$ ,  $\nu = 4$ ,  $k = 75$  and  $\epsilon/k = 3/200$ : (a) separatrix loop with implemented web; (b) magnification of the central part of (a); (c) the same as (b) but with  $k = 300$  and  $\epsilon/k = 1/400$ .

of the web-tori with a stochastic web between them, instead of the regular KAM-tori, are implanted around the central elliptic point. The corresponding web-structure is magnified in Figs. 8.3(b) and (c).

It follows from (8.63) that for an appropriate vicinity of the resonance condition and arbitrarily small perturbation  $\bar{\epsilon} \rightarrow 0$ , it is possible to find  $k$  such that the KAM-tori structure does not exist in the vicinity of the origin.

A deviation from exact resonance  $\delta\omega = \nu - n\omega_0 \neq 0$  can be considered in the same way as small non-linearity (*Note 8.4*).

## Notes

### Note 8.1

The material of this chapter follows the publications of Chernikov *et al.* (1987, 1988). See also Zaslavsky *et al.* (1991).

### Note 8.2

We deliberately use the notion of tori or web-tori even though the Poincaré map consists of invariant curves and not tori. When we allow for the motion along  $z$ , as, for example, happens for a charged particle dynamics in a constant magnetic field, the closed curves inside the cells of the web represent sections of the corresponding invariant tori. Also, a time axis can be used instead of the  $z$  axis.

### Note 8.3

The width  $\Delta H_s$  for the stochastic web was obtained in Fukuyama *et al.* (1977). See also Zaslavsky *et al.* (1991).

### Note 8.4

The described web structure and transition between web-tori and KAM-tori follow Chernikov *et al.* (1987, 1988). The phenomenon of radial transport arising from the stochastic web has various applications in plasma physics (Lichtenberg and Liberman (1992); Horton and Ichikawa (1996)).

## Problems

More complicated problems are marked by (\*).

8.1 Consider an electron dynamics in a constant magnetic field  $\mathcal{B}$  oriented along the  $z$ -axis and in the electrostatic wave field  $\mathcal{E} = \mathcal{E}_0 \cos(kx - \nu t)$  directed along the  $x$ -axis. Find the equation of motion, compare them to (8.9), and find  $\omega_0$ .

8.2 Derive formulas (8.41) and (8.42) using properties of elliptic functions.

8.3 Find asymptotics of solutions (8.41) and (8.42) for  $\kappa \rightarrow 1$  and explain the result.

8.4 Find the Melnikov integral (8.58).

8.5\* Write the separatrix map for the web defined by the Hamiltonian (8.52) and calculate the Melnikov integral (8.58).

8.6 Estimate a width  $\Delta H_s$  of the stochastic web (see (8.59)).

## PHASE SPACE OF CHAOS

The phase space of an idealized system with chaotic dynamics is uniformly filled by almost all trajectories. This reveals both ergodicity and mixing independently on the initial conditions up to zero measure exclusions. The Arnold cat area-preserving map

$$x_{n+1} = 2x_n + y_n, \quad y_{n+1} = x_n + y_n, \quad (x, y \bmod 1) \quad (9.1)$$

is an example of such a system. Physical reality is so different from the case (9.1) that there is still a lack of understanding of different properties of chaotic trajectories. For example, there are no answers to several questions, such as:

- (i) Is the measure of chaotic orbits finite (non-zero)?
- (ii) How many different measures (or distribution functions) exist in the domain of chaotic motion?
- (iii) What is the connection between the character of mixing and the phase space topology?

The major difficulty stems from the existence of infinite number of elliptic points and islands with invariant stable curves that fill the islands. This property is guaranteed by the KAM-theory and it was demonstrated in Figs. 5.4 and 5.5. The presence of islands makes the chaotic motion non-ergodic. Initially, it was believed that, after excluding the islands set, the remaining domain would consist of the ergodic motion with ‘normal’ (chaotic) properties such as for the system (9.1). Unfortunately, we have to admit that:

- (a) A measure of the remaining domain after the island set has been extracted is unknown, and one cannot exclude a possibility that this measure may be zero.
- (b) Behaviour of trajectories around the boundaries of islands is ‘sticky’ to the boundaries and the stickiness depends on a type of islands and on some parameters. Therefore, singular zones exist formed by the boundary layers of the islands.

### 9.1 Topological non-universality of chaos

Despite the complicated situation of our insufficient understanding of the chaotic dynamics, some general features and scenarios can be introduced with a reasonable level of certainty. It seems that the destruction of separatrices and

the creation of stochastic layers is the typical seed of chaos in low-dimensional Hamiltonian systems. Locations and connection of the separatrices in the phase space form a net that can be considered as a *topological skeleton of chaos*. A common difficulty in finding the skeleton arises because, in an attempt to ease the problems of doing so, we prefer to consider small perturbations of systems close to the integrable ones. That means that sometimes unperturbed systems do not have any separatrices. Also, the separatrices sometimes occur after the effect of a perturbation has taken place and, more precisely, they reveal themselves in the destroyed form of thin stochastic layers. Examples of this phenomenon include the kicked rotator and oscillator. Both display two different scenarios: the standard map has thin layers strongly separated from each other in  $p$ -direction, while the web-map has a stochastic web that covers the entire phase space in both directions like a connected net (see Fig. 5.4(a)). In both cases, the thickness of stochastic layers and the perturbation parameter  $\epsilon$  tends to zero without any changes in their skeleton topology. However, there are situations where the skeleton topology depends significantly on  $\epsilon$  when  $\epsilon \rightarrow 0$ .

Consider what happens when  $\epsilon$  increases. For the standard map (5.13), the parameter  $K$  is equivalent to the parameter  $\epsilon$ , and for  $K > K_c = 0.9716\dots$ , the stochastic layers merge (as in Fig. 9.1), creating a connected domain of chaotic motion that covers the entire phase plane and permits the unbounded

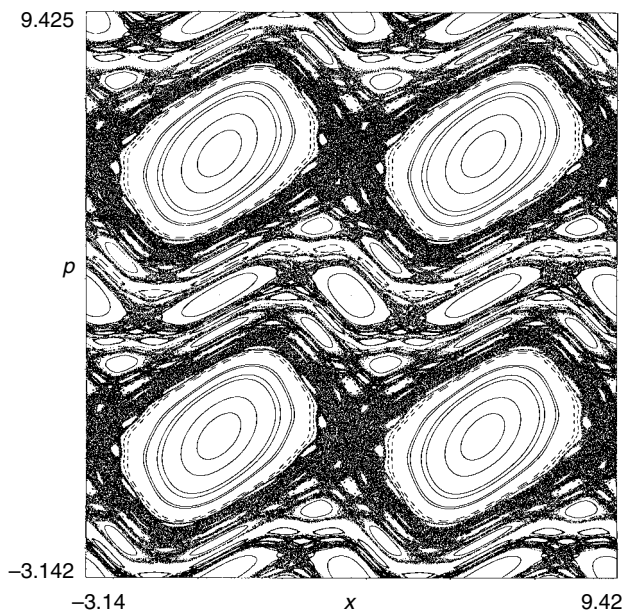


FIG. 9.1. Stochastic sea and islands for the standard map with overlapping resonances ( $K = 1$ ).

propagation of particles in  $p$ -direction. When  $K$  continues to increase, the visible size of the islands decreases and only the largest of them can be found in the ‘stochastic sea’. In fact, the islands play an extremely complicated bifurcation game, such as splitting, appearing, and disappearing. Some of the properties of the islands are discussed in Section 9.4.

The transition of the separated stochastic layers to the stochastic sea, described for the standard map, does not exist for the web map (5.27) or (5.35). This is because the meshes of the stochastic web cover the entire phase plane. The islands for the value of  $K = 3.15$  (Fig. 9.2(a)), are sufficiently small and we can say that they are embedded in the stochastic sea. The distribution of the points of a trajectory in the stochastic sea looks fairly uniform if we exclude the area of the islands. Nevertheless, the boundary of some islands has a dark area, indicating that it is a more frequently visited area due to the phenomenon of stickiness that will be discussed in Section 9.3. In Fig. 9.2(b) we present a magnified view of a tiny island from Fig. 9.2(a). Its area is smaller than that of a large island in Fig. 9.2(a) by more than two orders. At the same time, the influence of tiny islands on the process of diffusion is much stronger as will be shown later. This reveals how deceptive an oversimplified consideration of

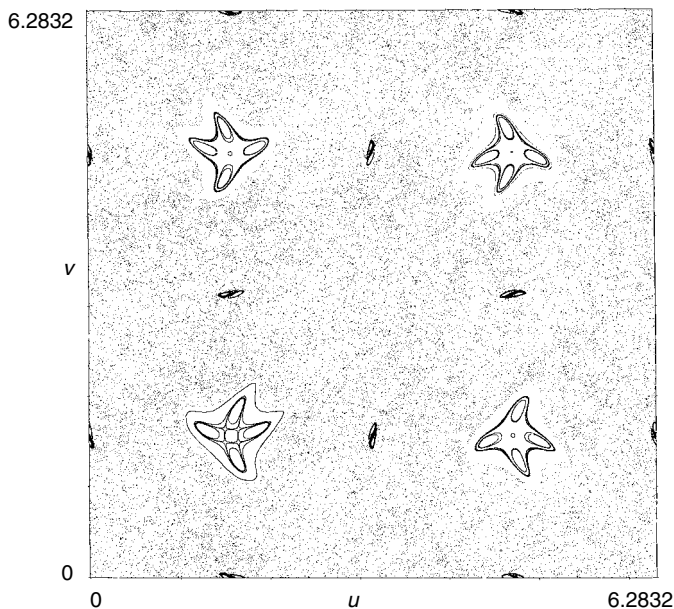
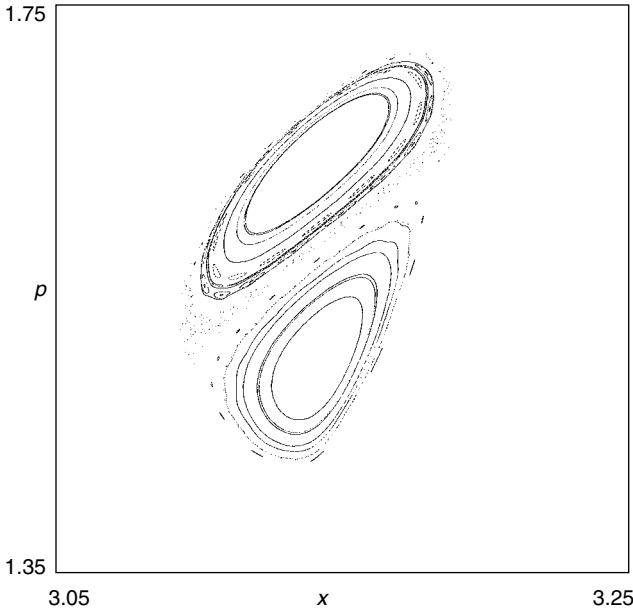


FIG. 9.2. Phase portrait for the web-map with  $q = 4$  and  $K = 3.15$ : (a) stochastic sea and islands; and (b) magnification of some small island in (a) which corresponds to the accelerator mode (Section 9.3).



FIG. 9.2. (*Continued*).

chaotic dynamics can be. The significant difference in the roles of the islands is due to their different properties, which are considered in Section 9.4.

## 9.2 Examples with billiards

Two more examples emphasize a non-trivial role of the non-ergodicity in phase space.

The first example is related to the Sinai billiard of the so-called infinite horizon type. A typical picture of its trajectory is given in Fig. 9.3. Any trajectory has an infinite number of arbitrarily long parts that correspond to a particle that bounces almost vertically (or horizontally), as shown in Fig. 9.3(a). In the periodically continued billiard, that is, for the corresponding Lorentz gas (Fig. 9.4), the long bounces correspond to long ‘flights’ without any scattering. The Poincaré map for a particle trajectory can be introduced in different ways. Let us use a coordinate  $x$ , when the trajectory hits the lower horizontal side, and velocity  $v_x$  at the same time instant. The corresponding phase portrait in Fig. 9.3(b) does not have islands. The motion is ergodic up to some zero-measure area. The distribution of points for the Poincaré section seems constant. One can see four scars of zero-measure which are due to the stagnation of the trajectory near the singular zones that correspond to infinite bounces without scattering (infinite flights). Two of the scars are related to horizontal and vertical bounces, and two others are related to oblique motion. In fact, an infinite number of

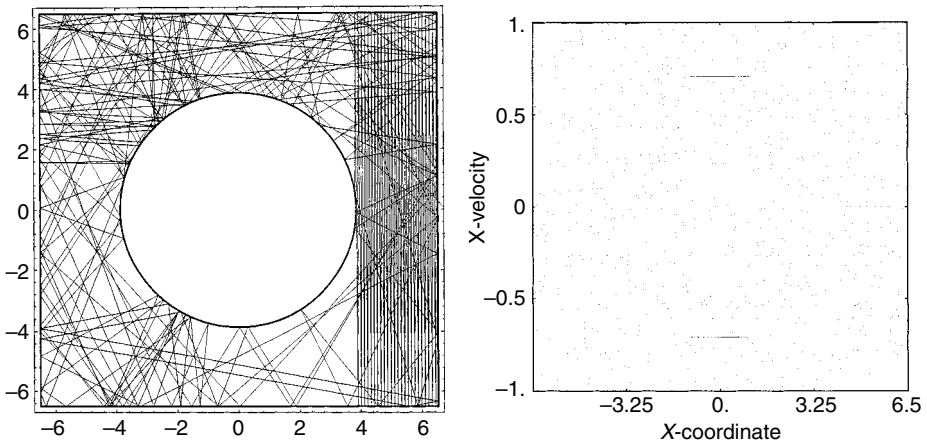


FIG. 9.3. Sinai billiard: (left) trajectory of a bouncing particle with a long-lasting non-dispersive part; (right) Poincaré section for the same trajectory unveils ‘scars’ that correspond to the flights.

such scars exist in the phase space of the billiard. The zero-measure domains of non-ergodicity strongly influence all kinetics and long-term characteristics of the motion, as will be shown in Chapter 22.

The second example is related to the so-called Bunimovich, or stadium, billiard (Fig. 9.5) for which dynamics is chaotic and there are no islands. Nevertheless, the situation is similar to the Sinai billiard, and zero-measure domains strongly influence kinetics and other statistical features of the system.

### 9.3 Accelerator mode islands

An island with an adjoining boundary layer is called a singular zone. Dynamics in the entire phase space is influenced by the presence of these islands. Nevertheless a local structure of islands and their vicinity may be sufficient in predicting large-scale asymptotics. In other words, there exists a possibility of finding a connection between the local properties of a singular zone and large-scale properties such as kinetics and transport. This gives rise to an interest in the origin, structure, and transformations of islands. At present, there is no complete classification of types of islands. However, there are few types of islands that are known to influence the kinetics.

Islands imbedded in the area of stochastic motion correspond to some resonances between unperturbed motion and perturbations. As the perturbation parameter changes, the topology of the islands also change and different bifurcations follow one after another. In Sections 3.4, 3.5, and 4.7 we considered *resonance islands*. They exist around the elliptic points due to KAM-theory. Some islands can occur from the parabolic points as a result of bifurcation. They

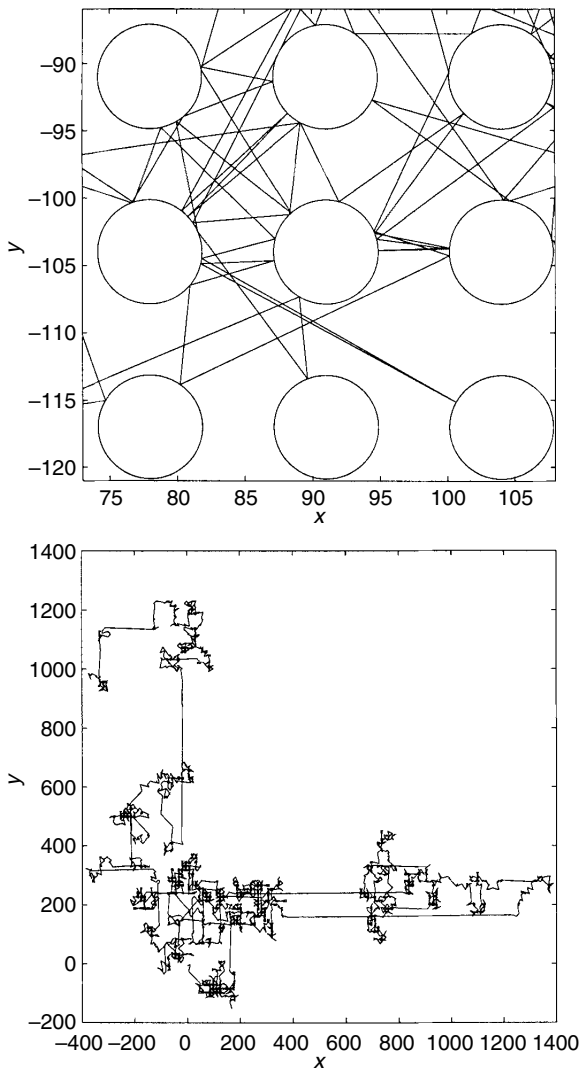


FIG. 9.4. So-called Lorentz gas is a model of point particles scattered by a double-periodic lattice of similar objects (top). This figure is obtained by a double-periodic continuation of Sinai billiard. A larger part of the same trajectory is shown at the bottom. The free flights of a particle correspond to the bouncing parts of the particle's trajectory in the Sinai billiard.

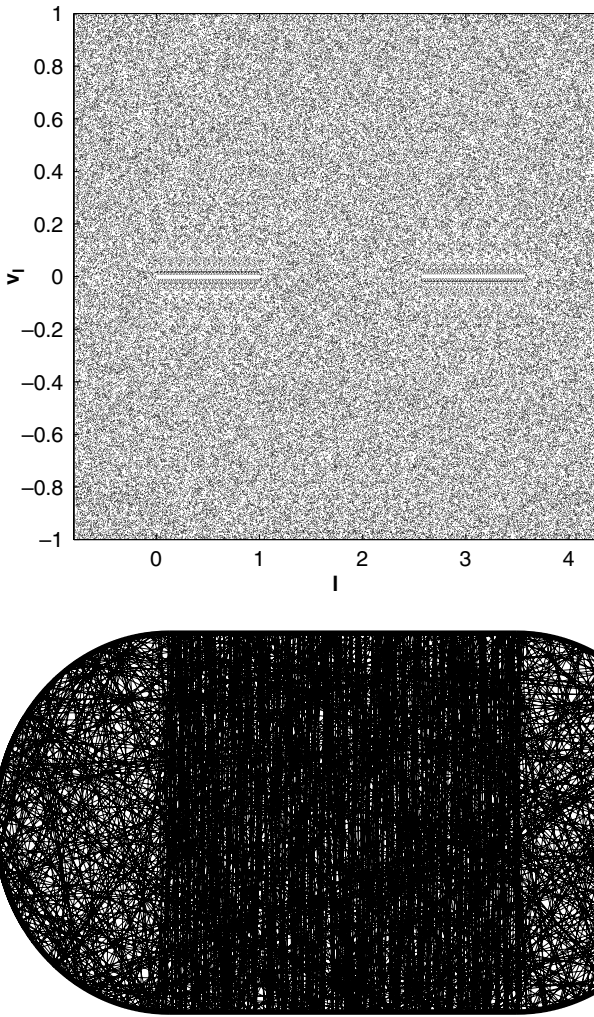


FIG. 9.5. Bunimovich (stadium) billiard (bottom), and Poincaré section of a trajectory (top) show scars and bounces similar to the Sinai billiard.

are called tangle islands (Rom-Kedar and Zaslavsky (1999)). In this section we will be interested in catching a birth (or death) of the so-called *accelerator mode* islands at some critical values of the perturbation parameter  $K$  (Note 9.1).

Consider the standard map (5.13)

$$p_{n+1} = p_n + K \sin x_n, \quad x_{n+1} = x_n + p_{n+1}, \quad (\text{mod } 2\pi) \quad (9.2)$$

in the fundamental domain ( $0 \leq p \leq 2\pi$ ,  $0 \leq x \leq 2\pi$ ), which can be periodically continued in  $x$  and  $p$  directions as shown in Fig. 5.4(a). An attempt can be made to find a solution that corresponds to a ballistic motion along  $x$ - or along both the  $x$ - and  $p$ -directions. For example, let

$$p_0^{(a)} = 2\pi m, \quad K \sin x_0^{(a)} = 2\pi \ell, \quad (\ell \geq 1), \quad (9.3)$$

where  $m, \ell$  are integers. Then

$$p_n^{(a)} = 2\pi \ell \cdot n + p_0^{(a)} \quad (9.4)$$

is known as the accelerator mode. This is because the momentum  $p$  grows linearly with time  $t$  (number of iterations  $n$ ) and, correspondingly,  $x$  grows as  $t^2$ .

The values (9.3) and (9.4) can be stirred slightly without destroying the existence of the accelerator mode. To find a domain of the stability of the accelerator mode, consider the tangent matrix to (9.2)

$$M' = \begin{vmatrix} 1 & K \cos x \\ 1 & 1 + K \cos x \end{vmatrix} \quad (9.5)$$

and find its eigenvalues  $\lambda$ . From the equation

$$\lambda^2 - 2\lambda \left( 1 + \frac{1}{2} K \cos x \right) + 1 = 0 \quad (9.6)$$

one derives

$$\lambda = 1 + \frac{1}{2} K \cos x \pm \left[ \left( 1 + \frac{1}{2} K \cos x \right)^2 - 1 \right]^{1/2} \quad (9.7)$$

and the stability condition is

$$0 > K \cos x > -4. \quad (9.8)$$

Combining (9.8) and (9.3), the stability domain for the accelerator mode is obtained:

$$2\pi \ell < K < [4 + (2\pi \ell)^2]^{1/2}. \quad (9.9)$$

For example, when  $\ell = 1$  the critical value is  $K_c = 2\pi$  such that for  $K < K_c$ , the accelerator mode is unstable, and the domain of stability appears in phase space only for  $K > K_c$ . An example of such an island is given in Fig. 9.6. Its phase portrait is presented on the torus:  $(x, p) \in (0, 2\pi; -\pi, \pi)$ . Invariant closed curves inside the island correspond to the accelerator mode trajectories in the infinite phase space. Any initial condition outside the island will correspond to a chaotic trajectory. Similar islands of stability of accelerator modes can be obtained for

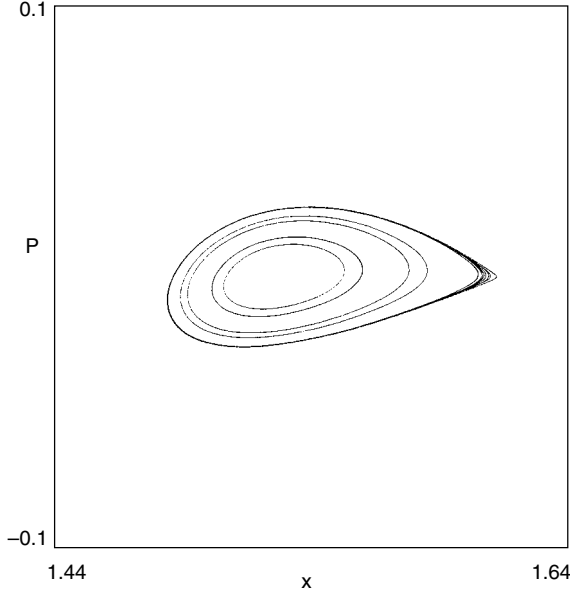


FIG. 9.6. Birth of an accelerator mode island for the standard map ( $K = 6.2890$ ).

any  $\ell$  with a corresponding threshold  $K_c = 2\pi\ell$  and the condition  $K > K_c$ . The larger  $\ell$  is, the smaller the area of stability and the size of the island are.

In writing a Hamiltonian for the invariant curves inside the island,  $K_c = 2\pi$  is retained for the sake of simplicity,  $K = 2\pi + \Delta K$ ;  $x = \pi/2 + \Delta x$  and  $p = \Delta p$ , where

$$\Delta K = K - K_c = K - 2\pi, \quad (9.10)$$

$$\Delta x = x - x^{(a)}, \quad \Delta p = p - p^{(a)}, \quad (\text{mod } 2\pi) \quad (9.11)$$

and  $x^{(a)}$ ,  $p^{(a)}$  belong to the accelerated trajectories (9.3) and (9.4) taken on the torus. This means that a trajectory  $(x, p)$  is in the vicinity of the trajectory with initial points  $(x_0^{(a)}, p_0^{(a)}) = (\pi/2, 0)$ . For the terms up to the second order in  $\Delta x$ ,  $\Delta p$  and the first order in  $\Delta K$ , the equations can be derived from (9.2):

$$\Delta \dot{p} = -\Delta K + \pi(\Delta x)^2, \quad \Delta \dot{x} = \Delta p, \quad (9.12)$$

where

$$\Delta \dot{p} \approx p_{n+1} - \Delta p_n, \quad \Delta \dot{x} \approx \Delta x_{n+1} - \Delta x_n \quad (9.13)$$

are replaced and the dot refers to the derivative with respect to dimensionless time  $t/T$ . Equations (9.12) are of the Hamiltonian type with a canonical pair of

variables  $(\Delta p, \Delta x)$ :

$$\begin{aligned} H^{(a)} &= \frac{1}{2}(\Delta p)^2 + \Delta K \cdot \Delta x - \frac{\pi}{3}(\Delta x)^3, \\ \Delta \dot{p} &= -\frac{\partial H^{(a)}}{\partial \Delta x}, \quad \Delta \dot{x} = \frac{\partial H^{(a)}}{\partial \Delta p}. \end{aligned} \quad (9.14)$$

It can be easily concluded from (9.14) that the island collapses at  $\Delta K = 0$ , that is, at  $K = K_c$ , and it does not exist if  $\Delta K < 0$ , that is,  $K < K_c$ . The structure of the Hamiltonian (9.14) is important since it defines a rescaling possibility in the form

$$\begin{aligned} \Delta x &\rightarrow \xi(\Delta K)^{1/2}, \quad \Delta p \rightarrow \eta \cdot (\Delta K)^{3/4} \\ H^{(a)}(\Delta x, \Delta p) &\rightarrow H^{(a)}(\xi, \eta) \cdot (\Delta K)^{3/2}, \end{aligned} \quad (9.15)$$

where  $(\xi, \eta)$  are rescaled variables. This case is further discussed in Chapter 12 with respect to the dynamical traps.

A similar example exists for the web map  $\hat{T}_{W(4)}$  in (5.35):

$$u_{n+1} = v_n, \quad v_{n+1} = -u_n - K \sin v_n. \quad (9.16)$$

For instance, the conditions

$$K_c = 2\pi, \quad u_0 = \frac{\pi}{2}, \quad v_0 = \frac{\pi}{2} \quad (9.17)$$

define the accelerator mode trajectory

$$u_{n+4}^{(a)} = u_n^{(a)} + 4\pi, \quad v_{n+4}^{(a)} = v_n^{(a)} - 4\pi. \quad (9.18)$$

As in (9.11), let us introduce the deviations of the parameter  $K$  from the value  $K_c = 2\pi$  and the coordinates  $(u, v)$  from the initial trajectory (9.18):

$$\Delta u_{n+4} = u_{n+4} - u_{n+4}^{(a)}, \quad \Delta v_{n+4} = v_{n+4} - v_{n+4}^{(a)}, \quad \Delta K = K - K_c. \quad (9.19)$$

The absence of the superscript ‘ $a$ ’ indicates an arbitrary trajectory (9.16) with parameter  $K$  and the initial conditions that are close to (9.17) respectively. After iteration of (9.16) four times and expanding it up to the second order terms in  $\Delta u, \Delta v$  and first order terms in  $\Delta K$ , it yields

$$\begin{aligned} \Delta u_{n+4} &= \Delta u_n - 2\Delta K + 2\pi(\Delta v_n)^2, \\ \Delta v_{n+4} &= \Delta v_n - 2\Delta K + 2\pi(\Delta u_{n+4})^2 \end{aligned} \quad (9.20)$$

or simply,

$$\begin{aligned}\Delta\dot{u} &= \frac{1}{2}\Delta K - \frac{1}{2}\pi(\Delta v)^2, \\ \Delta\dot{v} &= \frac{1}{2}\Delta K - \frac{1}{2}\pi(\Delta u)^2,\end{aligned}\tag{9.21}$$

where the dot indicates a time derivative that appears after a replacement similar to (9.13):

$$\begin{aligned}\frac{1}{4}(\Delta u_{n+4} - \Delta u_n) &\approx \Delta\dot{u}_n, \\ \frac{1}{4}(\Delta v_{n+4} - \Delta v_n) &\approx \Delta\dot{v}_n.\end{aligned}\tag{9.22}$$

The system (9.21) can be written in the Hamiltonian form

$$\Delta\dot{u} = \frac{\partial H^{(a)}}{\partial \Delta v}, \quad \Delta\dot{v} = -\frac{\partial H^{(a)}}{\partial \Delta u}\tag{9.23}$$

with

$$H^{(a)} = \frac{1}{2}\Delta K(\Delta v - \Delta u) - \frac{\pi}{6}[(\Delta v)^3 - (\Delta u)^3].\tag{9.24}$$

Isolines for the Hamiltonian (9.24) and separatrices are presented in Fig. 9.7(a). The corresponding trajectories for the map (9.16) and  $K = 6.28318531$ , which are very close to  $K_c = 2\pi$ , are given in Fig. 9.7(b). A coincidence is observed in the topology of the patterns. The double-island structure occurs only when

$$K_{\max} - K_c > \Delta K = K - K_c > 0\tag{9.25}$$

with some value of  $K_{\max}$  (see Problem 9.5). When the islands collapse to zero, the topology of the isolines, imposed by the Hamiltonian  $H^{(a)}$  in (9.24), persists. The Hamiltonian of the accelerator mode island satisfies a rescaling transformation

$$\begin{aligned}\Delta u &\rightarrow \xi(\Delta K)^{1/2}, \quad \Delta v \rightarrow \eta(\Delta K)^{1/2}, \\ H^{(a)}(\Delta u, \Delta v) &\rightarrow (\Delta K)^{3/2}H^{(a)}(\xi, \eta),\end{aligned}\tag{9.26}$$

which is similar to (9.15) for the accelerator mode of the standard map. Nevertheless, like the phase space topologies, the Hamiltonians (9.24) and (9.15) are different (*Note 9.2*).



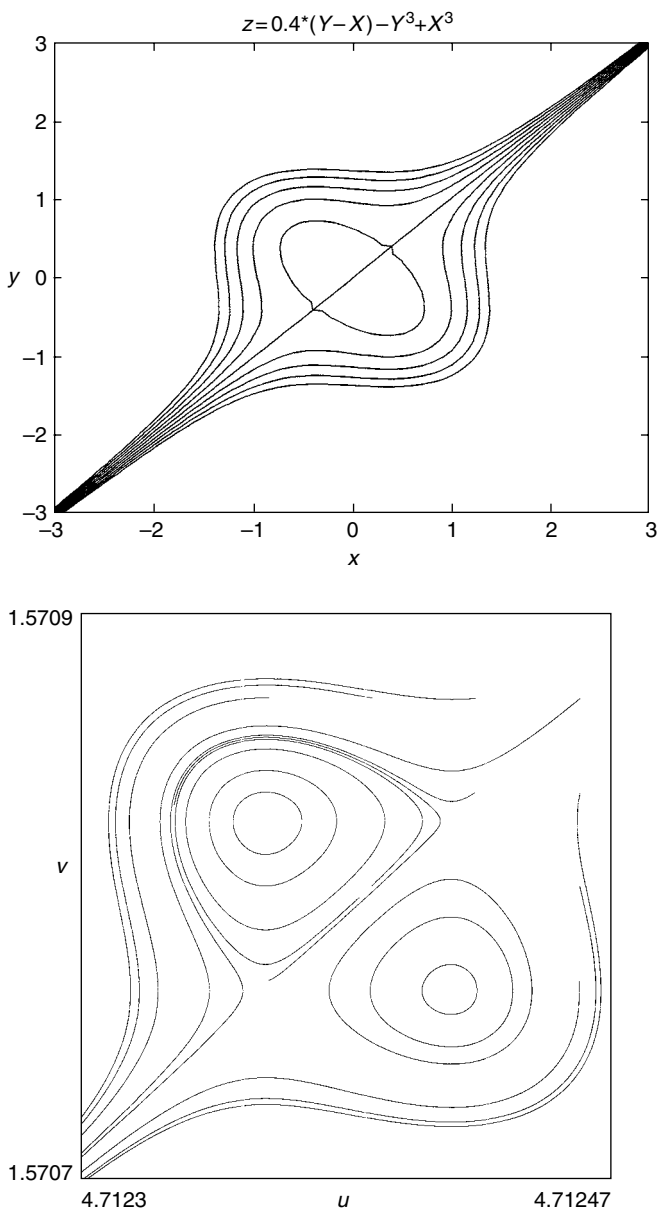


FIG. 9.7. Borning (collapsing) pair of islands for the four-fold symmetry web map: (a) isolines of the model Hamiltonian; and (b) phase portrait ( $q = 4$ ,  $K = 6.28318531$ ) obtained from the original map (9.16).

### 9.4 Ballistic mode islands

In the previous section we considered islands with such trajectories inside the islands that corresponded to the constant acceleration dynamics. In this section, another case will be considered that corresponds to the trajectories with a constant velocity. This is the so-called *ballistic mode* or *ballistic trajectories*.

As an example, consider the separatrix map

$$\begin{aligned} h_{n+1} &= h_n + \epsilon K_n \sin \phi_n \\ \phi_{n+1} &= \phi_n + \nu \ln \left( \frac{32}{|h_{n+1}|} \right), \pmod{2\pi} \end{aligned} \quad (9.27)$$

with

$$\begin{aligned} M_n &= \begin{cases} M = 8\pi\nu^2 \exp\left(-\frac{\pi\nu}{2}\right), & \sigma_n = 1, \\ 0, & \sigma_n = -1, \end{cases} \\ \sigma_{n+1} &= \sigma_n \operatorname{sign} h_{n+1} \end{aligned} \quad (9.28)$$

for a model equation of the perturbed pendulum

$$\ddot{x} + \sin x = \epsilon \sin(x - \nu t). \quad (9.29)$$

The equations (9.27) and (9.28) are equivalent to (6.25) and (6.26) if we put  $\omega_0 = 1$  and neglect  $M_n$  for  $\sigma_n = 1$  due to its smallness. The basic ballistic trajectory is

$$\sigma_0 = 1, \quad h_0^* = \frac{\epsilon^* M^*}{2}, \quad \phi_0 = \frac{3\pi}{2} \quad (9.30)$$

with an additional condition

$$\epsilon^* M^* = 64 \exp\left(-\frac{\pi}{2\nu^*}(2m+1)\right), \quad m = 0, 1, \dots \quad (9.31)$$

Since  $M = M(\nu)$ , equation (9.31) defines  $\epsilon^* = \epsilon^*(\nu)$  and we have only one free parameter  $\nu$ .

Let us define new variables

$$\begin{aligned} \Delta\psi_k &= \Delta\phi_k + \frac{\nu}{h^*} \Delta h_k, \quad \Delta h_k = h_k - h_k^*, \quad \Delta\phi_k = \phi_k - \phi_k^*, \\ \delta &= \frac{\Delta\epsilon}{\epsilon^*} = \frac{(\epsilon - \epsilon^*)}{\epsilon^*}. \end{aligned} \quad (9.32)$$

Then

$$\begin{aligned} h_4^* &= h_0^*, \quad \phi_4^* = \phi_0^* + (4m+2)\pi = \phi_0, \pmod{2\pi}, \\ \sigma_4^* &= \sigma_0 \end{aligned} \quad (9.33)$$

up to the terms of the order of  $\delta^2$ ,  $\delta\Delta h_h$ ,  $\delta\Delta\psi_k$ ,  $(\Delta\psi_k)^2$ ,  $\delta\psi_k\Delta h_k, \dots$ , and the dynamics is ballistic with averaging over four steps. The effective Hamiltonian for trajectories within the ballistic island is

$$H^{(\text{bal})} = h^*(\Delta\psi)^2 + 4\nu \frac{\epsilon - \epsilon^*}{\epsilon^*} \Delta h - \frac{2}{3} \frac{\nu^2}{h^{*2}} (\Delta h)^3 \quad (9.34)$$

and it defines the Hamiltonian equations

$$\begin{aligned} \Delta\dot{\psi} &= -4\nu\delta + 2 \frac{\nu^2}{(h^*)^2} (\Delta h)^2 = -\frac{\partial H^{(\text{bal})}}{\partial \Delta h}, \\ \delta\dot{h} &= 2h^* \Delta\psi = \frac{\partial H^{(\text{bal})}}{\partial \Delta\psi}, \end{aligned} \quad (9.35)$$

where the dot corresponds to the derivative with respect to  $\tau = t/4$ . The ballistic island exists for  $\delta > 0$ , that is,  $\epsilon > \epsilon^*$ , in the domain

$$0 \leq \Delta h \leq \left( \frac{6\delta(h^*)^2}{\nu^2} \right)^{1/2} = 16(3\pi\Delta\epsilon)^{1/2} \exp \left\{ -\frac{\pi}{4} \left( \frac{2m+1}{\nu} + \nu \right) \right\} \quad (9.36)$$

(Note 9.3).

## 9.5 Cantori

The notion of *cantorus* has been coined by Persival (1974, 1979) for a specific singular object in phase space, which is a product of a cantor-type circle  $\mathbf{S}_c^1$  and  $\mathbb{R}$  or  $\mathbf{S}_c^1$  and  $\mathbf{T}^{N-1}$ .

Let us start from a definition of rotational number  $\hat{\nu}$  (see Arnold, 1992). Consider again the standard map on the torus as an example:

$$p_{n+1} = p_n + K \sin x_n, \quad x_{n+1} = x_n + p_{n+1}, \quad (p, x) \in \mathbf{T}^2 \quad (9.37)$$

and, for simplicity, put  $T = 1$ .

For  $K = 0$

$$p_n = p_0, \quad x_n = x_0 + np_0, \quad (\text{mod } 2\pi). \quad (9.38)$$

Trajectories defined by (9.38) reduce to a finite set of points if  $p_0/2\pi$  is rational, and densely cover the torus if  $p_n/2\pi$  is irrational. The expression

$$\nu = \lim_{m \rightarrow \infty} \frac{1}{m} \sum_{n=1}^m (x_n - x_{n-1}) = \lim_{m \rightarrow \infty} \frac{1}{m} (x_m - x_0) = \lim_{m \rightarrow \infty} \frac{x_m}{m}, \quad (9.39)$$

defines a mean rotation frequency along  $x$ , that is,  $\nu/2\pi$  is a number of revolutions along  $x$ . For the case (9.38) it is  $\nu = p_0$ . In the general case of  $p_0$ , we can

present  $\nu/2\pi$  as a continued fraction

$$\hat{\nu} \equiv \frac{\nu}{2\pi} = \frac{1}{a_1 + \frac{1}{a_2 + \dots}} = [a_1, a_2, \dots]. \quad (9.40)$$

Any  $n$ -th approximation of  $\hat{\nu}$

$$\hat{\nu}_n = [a_1, a_2, \dots, a_n] \quad (9.41)$$

corresponds to a periodic curve since  $\hat{\nu}_n$  is a rational number. The existence of periodic invariant curves is evident for the map (9.38) but it is not so clear for the standard map with  $K > 1$ .

Equations (9.37) can be rewritten in the form

$$x_{n+1} - 2x_n + x_{n-1} = K \sin x_n. \quad (9.42)$$

Since any solution of (9.42) is located on  $\mathbf{T}^2$ , one can expect that solutions should be periodic along  $x$  direction with the period  $2\pi$ , that is, with  $\hat{\nu} = 1$  or with  $\hat{\nu} = m \in \mathbf{N}$ . It was shown in different publications that there also exist solutions with arbitrary irrational  $\hat{\nu}$ . Such solutions can be written in the form

$$x_n = 2\pi(n\hat{\nu} + \hat{\nu}_0) + f(n\hat{\nu} + \hat{\nu}_0) \quad (9.43)$$

where  $\hat{\nu}_0$  is arbitrary constant,  $0 < \hat{\nu}_0 < 1$ , and  $f(\xi)$  is periodic in  $\xi$  with a period  $T_\nu = 1/\hat{\nu} = 2\pi/\nu$ .

The following properties of the rotational number are important in finding the solution (9.43):

- (i) The limit (9.39) exists for the equation (9.42) with arbitrary  $K$ .
- (ii) If there exists a gap of the interval  $x \in (0, 2\pi)$  free of points of the solution (9.43), than all images of the gap obtained by iterations (9.37) do not have any intersections. For  $K > K_c = 0.9716$  any trajectory periodic with an irrational  $\hat{\nu}$  has a cantor type closure on the circle  $x \in (0, 2\pi)$ . This is a cantor-circle or the cantor  $\mathbf{S}_c^1$ . In a similar way we can introduce cantor  $\mathbf{T}_c^2 = \mathbf{T}^1 \cdot \mathbf{S}_c^1$  (Note 9.4).

The cantori are invariant, unstable, and dense. They are embedded in the stochastic sea and they make a kind of *dynamical barrier* for particle diffusion. Diffusion along the  $p$ -direction is possible due to the gaps in the cantori (which are the larger) the bigger  $K - K_c$  is, and the farther the cantori are from the border of an island. The role of the cantori is very important if we are interested in the phenomenon of anomalous transport. Nevertheless, work with cantori is difficult and constructive tools have not been found yet (see also Hanson *et al.* (1985); MacKay *et al.* (1984); Reichl (1992)). Due to specific structure of the cantori, particle trajectories stick to the cantori borders making the particle transport non-Gaussian (see Fig. 9.8).

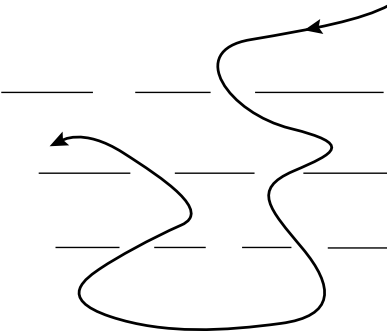


FIG. 9.8. Particle passing through cantori gaps.

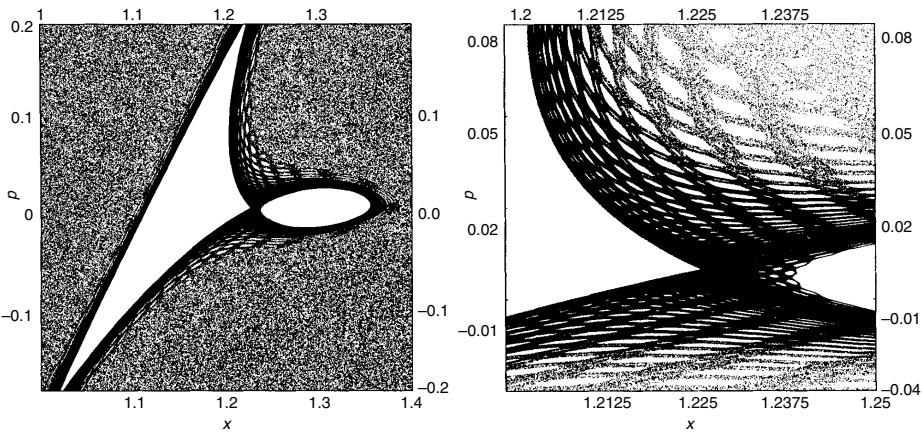


FIG. 9.9. A ‘net trap’ for the standard map with  $K = 6.9009$  after  $10^9$  iterations: (left) an island that is close to the bifurcation value of  $K$ ; (right) magnification of the vicinity of the island.

9.6 Sticky domains and escapes

There is no classification of sticky domains, or of their description and theory. Only a few of them can be described in a phenomenological way. In Fig. 9.9 (see Zaslavsky (2002a)) we show an example of a singular zone for the standard map, which appears for a specific value of  $K$  near the value of a bifurcation. The bifurcation corresponds to a separation of three islands from the central island. The figure shows the points that belong only to the trajectory, and the dark area means that this trajectory spends a longer time there.

A phenomenological description of a singular zone can be done by introducing a probabilistic description of the stickiness. Let  $P_{\text{esc}}(t; A)dt$  be a probability to escape a domain  $A$  during the interval  $(t, t+dt)$ . Then  $P_{\text{esc}}(t; A)$  is normalized as

$$\int_0^\infty P_{\text{esc}}(t; A)dt = 1. \quad (9.44)$$

We can distinguish two limit cases for  $P_{\text{esc}}(t; A)$ : the exponential law

$$P_{\text{esc}} = h_{\text{esc}} \exp(-h_{\text{esc}}t) \quad (9.45)$$

and the power law

$$P_{\text{esc}} \sim \frac{\text{const}}{t^{\gamma_{\text{esc}}}}, \quad (t \rightarrow \infty) \quad (9.46)$$

with some escape rate  $h_{\text{esc}}$  and escape exponent  $\gamma_{\text{esc}}$ . We provide different estimates in Chapter 12.

## Notes

### Note 9.1

For a description of the resonance islands, see Meiss (1986, 1992). A description of the accelerator mode islands can be found in Lichtenberg and Liberman (1983); Ichikawa *et al.* (1987). A description of an accelerator mode island for the standard map, and its appearance from a parabolic point is in Karney (1983). See also Rom-Kedar and Zaslavsky (1999) and references therein.

### Note 9.2

The structure of the accelerator mode island for the web map with four-fold symmetry was obtained in Zaslavsky and Niyazov (1997) and Zaslavsky *et al.* (1997).

### Note 9.3

The Hamiltonian (9.34) and the domain (9.36) for ballistic island were obtained in Rom-Kedar and Zaslavsky (1999). The ballistic trajectory (9.31) for the separatrix map was considered in Iomin *et al.* (1998).

### Note 9.4

The discovery of solutions of the (9.43) type with irrational rotation numbers  $\hat{\nu}$  is in Percival (1974, 1979) and Aubry (1983). Persival proposed this solution as a consequence of special variational principle, giving them a name ‘cantori’. Many properties of cantori were described by J. Mather (Mather (1982)). S. Aubry has arrived at the cantori by considering some problem of the condensed matter physics and the commensurate-incommensurate phase transition in a chain of coupled atoms. The critical value  $K_c$  is the same as that obtained by J. Greene for the destruction of the last invariant curve.

## Problems

More complicated problems are marked by (\*).

9.1 Find a size of the accelerator mode island for the standard map and arbitrary  $l$ .

9.2 The same as in Problem 9.1. for the web map of four-fold symmetry.

9.3 Derive the equations (9.18).

9.4 Find a trajectory of the accelerator mode for the four-fold symmetry web map (9.16) and initial conditions  $K_c = 2\pi$ ,  $u_0 = 3\pi/2$ ,  $v_0 = \pi/2$ .

9.5 Find  $K_{\max}$  in (9.25) and estimate the size of the domain of the corresponding accelerator mode island.

9.6 Prove the relations (9.33) applying the separatrix map (9.27) and (9.28) four times and neglecting the small terms indicated after (9.33).

9.7\* Using the notations (9.32), show that

$$\begin{aligned}\Delta\psi_4 &\approx \Delta\psi_0 - 4\nu\delta + 2\nu^3(h^*)^{-2}(\Delta h_0)^2, \\ \Delta h_4 &\approx \Delta h_0 + 2h^*\Delta\psi_4\end{aligned}$$

(see Rom-Kedar and Zaslavsky (1999)).

PART 2

FRACTALITY OF CHAOS



*This page intentionally left blank*

## FRACTALS AND CHAOS

The structures generated by chaotic dynamics in the phase space are so complex that they cannot be described in a conventional way. One is therefore reduced to dealing with objects that are unusual, ‘wild’, and ‘strange’. There is a possibility to use the notion of fractal objects in chaotic dynamics but, as will be seen below, even this proves insufficient in describing chaos. There are a few reasons for this:

- (i) Any trajectory is a solution of the equations of motion. This means that the *fractality*, i.e. fractal features, of trajectories cannot be introduced *a priori* but, instead, they should be ‘derived’ from the first principles, i.e. from the Hamiltonian of the system. Extremely complicated phase space topology prevents an easy way of describing the fractality of dynamical systems.
- (ii) Any trajectory describes the system evolution in phase space and time. Evidently, fractal features in space and in time are different for a generic case.
- (iii) For a practical reason, it is important not just to describe the fractality, but to describe the system evolution, i.e. kinetics, transport, etc., and one can expect that to be a *non-stationary fractality*.

In this and the following chapters, we present different approaches to the fractal features of chaotic dynamics (*Note 10.1*).

### 10.1 Fractal dynamics

The main feature of a fractal object is its self-similarity. A brief discussion of the definition of fractal properties of dynamical systems starts from a set of elements  $\{u_j\}$  distributed in the phase space. One can imagine a set of points on the Poincaré map in the phase space. Then  $\{u_j\}$  is a set of functions of the coordinates  $r_j$  with the subscript  $j$  indicating the iteration number of the map. There are many different ways to characterize distribution of the points of a map in phase space. A normal physical approach is to introduce a distribution function,  $F(r_j, p_j; t)$  in the phase space. This function should be coarse-grained, or smoothed, in some way to simplify the description of the dynamics by reducing the information on the trajectories. Nevertheless, even a typical coarse-graining of the distribution function does not remove some underlying ‘wild’ structures of the space, which form a support for chaotic trajectories. A brief glance at Fig. 5.4 warns that the object of consideration, the phase space of chaos, is highly complex and can be analysed, in part, via its fractal properties.

Let us start with some definitions. Consider a set of elements, say points, embedded in an arbitrary dimension space confining these elements. Cover the elements by using a set of balls with the same diameter  $\epsilon$  and consider only the minimal set of balls,  $N_\epsilon$ . There are two ways to proceed:

(i) **Box dimension.** Consider a limit

$$d_C = \lim_{\epsilon \rightarrow 0} \frac{\ln N_\epsilon}{\ln(1/\epsilon)}. \quad (10.1)$$

$d_C$  is called box dimension because of the relation

$$\epsilon^{d_C} \cdot N_\epsilon \sim \text{const} \quad (10.2)$$

in the limit  $\epsilon \rightarrow 0$ , that is,  $d_C$  is an ‘effective’ dimension of small boxes that cover the set of points. More accurately, one can say that there are two limits, upper  $\bar{d}_C$  and lower  $\underline{d}_C$ . For typical systems,  $\bar{d}_C = \underline{d}_C = d_C$  but there do exist exotic examples when it is not the case (Pesin, 1988).

(ii) **Hausdorff dimension.** Consider a sum

$$S(\epsilon, d) = \inf \sum_j \epsilon_j^d, \quad (10.3)$$

where  $j$  labels a ball and *inf* means that summation is performed over a minimal set of balls with diameter  $\epsilon_j$ , which is assumed to be in some interval  $\epsilon_j \in (\epsilon, \epsilon + \delta\epsilon)$ . For  $\epsilon \rightarrow 0$ , the number of terms in (10.3) tends to infinity. Since  $S(\epsilon, d)$  is a monotonic function of  $\epsilon$ , the limit exists. Moreover, there exists a critical value  $d_H$  such that

$$S(d) = \lim_{\epsilon \rightarrow 0} S(\epsilon, d) = \begin{cases} \infty, & d < d_H, \\ \text{const} > 0, & d = d_H, \\ 0, & d > d_H, \end{cases} \quad (10.4)$$

where  $d_H$  is some number called the *Hausdorff dimension*. For more details see Pesin (1988) and Afraimovich and Hsu (2003).

If all  $\epsilon_j$  are the same, the expression (10.3) yields

$$S(d_H) = \lim_{\epsilon \rightarrow 0} N(\epsilon) \epsilon^{d_H} \quad (10.5)$$

and  $d_C$  will coincide with  $d_H$ . In fact, there are some exceptions which will not be discussed here.

An example of a fractal object is shown in Fig. 10.1 where the proliferation of balls continues until infinity. This type of object is called the *Sierpinski carpet*. Let

$$S_{n+1} = \lambda_S S_n, \quad (10.6)$$

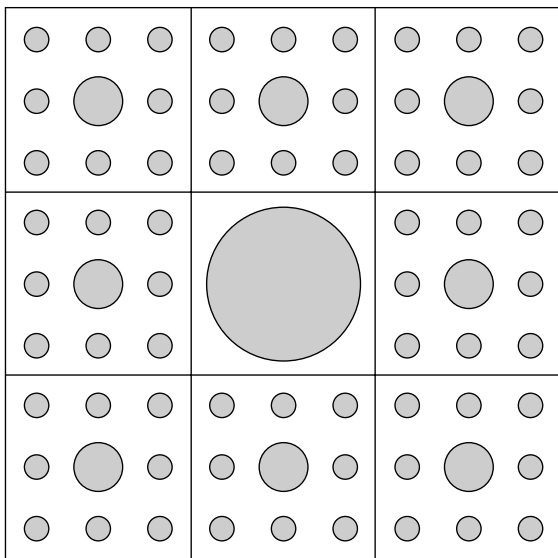


FIG. 10.1. Sierpinski carpet as a fractal object. Only 3 generations are shown. All smaller disks should appear in a similar way.

where  $S_n$  is the area of a circle of the  $n$ -th generation and  $\lambda_S < 1$  is a constant, each generation gives birth to  $q$  circles ( $q = 8$  in Fig. 10.1). Thus, for the  $n$ -th generation

$$N_n = q^n, \quad S_n = \lambda_S^n \quad (10.7)$$

and

$$d_C = d_H = \lim_{n \rightarrow \infty} \frac{\ln q^n}{|\ln \lambda_S^{n/2}|} = \frac{\ln q}{|\ln \lambda_S^{1/2}|}. \quad (10.8)$$

Since  $q = 8$  and  $\lambda_S \leq 1/9$ , one has  $d_H \leq \ln 8 / \ln 3 < 2$ .

## 10.2 Generalized fractal dimension

As will be seen later, different scaling properties of dynamical systems can be formulated in a similar way as (10.4). However, they do not have a specific relation with dimensions. This means that the characteristic exponents of the self-similarity can be negative or complex. Such a situation can be described by a dimension-like characteristic introduced in Caratheodory (1914) and generalized in Pesin (1988); (see also Pesin (1997)). Here it is called a generalized fractal dimension or *Caratheodory-Pesin dimension*.

Let  $u_j$  be an element of phase space,  $\{u_j\}$  be a partition of phase space, and  $\xi(u_j)$  and  $\eta(u_j)$  are some ‘good’ functions defined on the partition element  $u_j$ . One can select the elements of the partition in any convenient shapes so that its effective diameter satisfies the condition  $\text{diam } u_j \leq \epsilon$ . Consider a limit of the minimal sum,

$$S(\xi, \eta; d; \{u_j\}) = \lim_{\epsilon \rightarrow \infty} \inf \sum_j \xi(u_j) \eta^d(u_j), \quad (10.9)$$

where the infimum of the sum refers to a cover of the set of points with coordinates  $r_j$  by using a minimal number of the partition elements  $u_j = u_j(\tau, \epsilon)$ . We can introduce a constant  $d_g$  similar to  $d_H$  in (10.4), for which the sum  $0 < S(\xi, \eta; d_g; \{u_i\}) < \infty$  exists. The number  $d_g$  is the *generalized fractal dimension*. The following examples illustrate the use of  $d_g$  in different situations:

1.  $\xi = 1$ ,  $\eta(u_j) = \epsilon_j$ . This gives the Hausdorff dimension [see (10.3)].
2.  $\xi = 1$ ,  $\eta(u_j) = \eta(\epsilon_j)$ . This yields the Carathéodory dimension.

More sophisticated examples will be considered in Chapter 12.

Definition (10.9) and the existence of the limit provide a broad view on the notion of fractal dimension that can be related to some non-geometrical characteristics of an object. An example in the next section confirms this statement.

### 10.3 Renormalization group and generalized fractal dimension

Consider an object,  $\mathcal{A}_0$ , and its consecutive transformations:

$$\mathcal{A}_1 = \hat{T}\mathcal{A}_0, \quad \mathcal{A}_n = \hat{T}\mathcal{A}_{n-1} = \cdots = \hat{T}^n \mathcal{A}_0. \quad (10.10)$$

For example,  $\mathcal{A}_j$  may be a domain of phase space and  $\hat{T}$  is either a time-shift operator at interval  $T$  or any another transformation of the domain  $\mathcal{A}_j$ . Let  $\mathcal{A}_j = \mathcal{A}_j(r)$  and  $r$  be a characteristic diameter of  $\mathcal{A}_j$ . Consider also the transformation of  $r$  by a factor  $\lambda$ :

$$\hat{S}\mathcal{A}_j(r) = \mathcal{A}_j(\lambda r). \quad (10.11)$$

Let  $V(\mathcal{A}_n)$  be a function defined for the domains  $\mathcal{A}_j$ . For example,  $V(\mathcal{A}_n)$  may be a volume of  $\mathcal{A}_n$ . Consider the transform

$$\hat{R} = \hat{S}\hat{T} \quad (10.12)$$

and assume that there exists a self-similarity of volume  $V$

$$V(\hat{R}\mathcal{A}_n) = \lambda^{d_R} V(\mathcal{A}_n), \quad (10.13)$$

where  $d_R$  is an exponent that characterizes the self-similarity of  $\{\mathcal{A}_j\}$  under the renormalization transform  $\hat{R}$ . In general, condition (10.13) is valid only in the limit

$$d_R = \lim_{n \rightarrow \infty} \frac{\ln[V(\hat{S}\mathcal{A}_{n+1})/V(\mathcal{A}_n)]}{\ln \lambda} = \lim_{n \rightarrow \infty} \frac{\ln[V(\hat{R}\mathcal{A}_n)/V(\mathcal{A}_n)]}{\ln \lambda}, \quad (10.14)$$

where we use the definitions (10.10) to (10.12). If the sequence  $\{\mathcal{A}_0, \mathcal{A}_1, \dots\}$  has a fixed point  $\mathcal{A}^*$ , it follows from (10.14) that

$$d_R = \frac{\ln[V(\hat{S}\mathcal{A}^*)/V(\mathcal{A}^*)]}{\ln \lambda} \quad (10.15)$$

or the equivalent equation

$$V(\hat{S}\mathcal{A}^*) = \lambda^{d_R} V(\mathcal{A}^*) \quad (10.16)$$

can be used to define  $\mathcal{A}^*$  and  $d_R$ .

One can see that the definition of  $d_R$  coincides with that of  $d_C$  in (10.1). Indeed, as a result of (10.11)

$$V(\hat{S}\mathcal{A}^*(r)) = V(\mathcal{A}^*(\lambda r)) \quad (10.17)$$

and we should take into account the fact that  $V(\mathcal{A}^*)$  in (10.15) does not depend on  $\lambda$  while  $V(\hat{S}\mathcal{A}^*(r))$  does. It follows from (10.15)

$$d_R = \lim_{\lambda \rightarrow \infty} \frac{\ln V(\mathcal{A}^*(\lambda r))}{\ln \lambda} = d_C. \quad (10.18)$$

If  $r$  is not a diameter and  $V$  is not a volume, then the definition of (10.15) for  $d_R$  has the same structure as (10.9). To show it, rewrite (10.9) as

$$S(\eta, d; \{u_j\}) \sim N(u_j) \cdot \eta^d(u_j) \sim \text{const} \quad (10.19)$$

The condition for the existence of a limit when  $N \rightarrow \infty$ ,  $\eta \rightarrow 0$  yields

$$d = d_g = \lim_{N \rightarrow \infty} \frac{\ln N(u_j)}{\ln(1/\eta(u_j))} = d_R, \quad (10.20)$$

which is the same formula for (10.18). The crucial reason for considering  $d_R$  as a particular case of  $d_g$  is due to the existence of both the Renormalization Group and the fixed point (see also Suzuki (1983)).

### 10.4 Multifractal spectra

A situation may occur when the set of objects  $\{u_j(r_j)\}$  and the behaviour in the vicinity of  $r_j$ , cannot be described using the same self-similarity exponent,  $d_g = d_R$  and more of such exponents are needed to do so. To be more specific, consider partition of the space by using a set of elements,  $\{u_j\}$ , and let:

$$\ell_j \equiv \text{diam } u_j \leq \epsilon. \quad (10.21)$$

Assume that for a fairly small  $\epsilon$  the probability of finding a particle in the cell  $u_j$  is

$$P_j = \text{const} \cdot \ell_j^{\gamma_j}, \quad (10.22)$$

where  $\gamma_j$  is a characteristic exponent defined locally for the  $j$ -th cell. Let us construct a generating sum:

$$Z_\ell(q) = \sum_j P_j^q = \text{const} \sum_j \ell_j^{\gamma_j q}. \quad (10.23)$$

On the right-hand side, the summation over  $j$  runs throughout the entire set  $\{u_j\}$ . The aim is to rewrite the sum (10.23) in a way that takes into account the existence of different cells with the same value  $\gamma$ . If  $\Delta N(\gamma)$  be a number of cells with the same value  $\gamma$ , then instead of (10.23), we have

$$Z_\ell(q) = \text{const} \sum_\gamma \Delta N(\gamma) \ell^{q\gamma}, \quad (10.24)$$

where a desired change of variables from  $j$  to  $\gamma$  is performed. Expression (10.24) indicates a new situation called *multifractality* since the system has many different scaling exponents  $\gamma$ . The same property as in (10.22) can be applied to  $\Delta N(\gamma)$ , that is,

$$\Delta N(\gamma) = \ell^{-f(\gamma)}, \quad (10.25)$$

where a new important exponent,  $f(\gamma)$ , is introduced. It is called a *dimension spectral function* which is the quantitative characteristic of the multifractality (*Note 10.2*).

The calculations that follow are very formal. Substitute (10.25) into (10.24):

$$Z_\ell(q) = \text{const} \sum_\gamma \ell^{q\gamma - f(\gamma)}. \quad (10.26)$$

There are two ways to proceed. First, one can apply the same consideration as in (10.9) where the generalized dimension was introduced. Second, which is more typical in physical consideration, is to replace the sum (10.26) by integration. The expression

$$\Delta N(\gamma) \rightarrow dN(\gamma) = \rho(\gamma) \ell^{-f(\gamma)} d\gamma \quad (10.27)$$

is used instead of (10.25). Here  $\rho(\gamma)$  is a density function which does not depend on  $\ell$  or depends slowly. Hence

$$Z_\ell(q) = \int d\gamma \rho(\gamma) \exp \left\{ - \left( \ln \frac{1}{\ell} \right) [q\gamma - f(\gamma)] \right\}, \quad (10.28)$$

where the const in (10.26) is included in the definition of  $\rho(\gamma)$ . Consider a limit

$$Z(q) = \lim_{\ell \rightarrow 0} Z_\ell(q). \quad (10.29)$$

Without any special comments, we can put

$$\kappa \equiv \ln \frac{1}{\ell} \quad (10.30)$$

and consider a limit  $\kappa \rightarrow \infty$  instead of  $\ell \rightarrow 0$ . After applying the steepest-descent method, we arrive at

$$Z(q) \sim \exp\{-\kappa[q\gamma_0 - f(\gamma_0)]\}, \quad (\kappa \rightarrow \infty), \quad (10.31)$$

where the saddle-point,  $\gamma_0$ , satisfies the equation

$$\frac{df(\gamma_0)}{d\gamma_0} = q. \quad (10.32)$$

The final expression, (10.31), can also be rewritten as

$$Z(q) = \exp(-\kappa \mathcal{D}(q)), \quad (\kappa \rightarrow \infty), \quad (10.33)$$

where

$$\mathcal{D}(q) = \gamma_0 q - f(\gamma_0) \quad (10.34)$$

and  $\gamma_0 = \gamma_0(q)$ . The new variable,  $\mathcal{D}(q)$ , is a new dimension type characteristic of the system.  $\mathcal{D}(q)$  and  $f(\gamma_0)$  form a Legendre transform pair.

It is also convenient to introduce the so-called *Rényi dimension*  $D_q$ ,

$$\mathcal{D}(q) = (q-1)D_q \quad (10.35)$$

(see Rényi (1970)), and consider its meaning for different values of  $q$ . For  $q = 0$  we have

$$D_q = -\mathcal{D}(q) \quad (10.36)$$

and (10.33) yields

$$Z(0) = e^{\kappa D_0} = \frac{1}{\ell^{D_0}} = N(\ell), \quad (\kappa \rightarrow \infty, \ell \rightarrow 0), \quad (10.37)$$

which is similar to (10.2). Hence  $D_0$  is the same as  $d_C$ , that is, the box dimension.



To obtain  $D_1$ , consider the definition (10.23)

$$Z_\ell(1 + \delta_q) = \sum_j P_j^{1+\delta_q} = 1 + \delta_q \sum_j P_j \ln P_j, \quad (10.38)$$

where  $\delta_q = q - 1 \ll 1$ . From (10.33) and (10.35), we have

$$Z_\ell(1 + \delta_q) = \ell^{\delta_q \cdot D_q}. \quad (10.39)$$

A comparison of (10.38) and (10.39) gives

$$D_1 = \lim_{q \rightarrow 1} \frac{\mathcal{D}(q)}{1 - q} = \lim_{\ell \rightarrow 0} \frac{[-\sum_j P_j \ln P_j]}{\ln(1/\ell)} = \lim_{\ell \rightarrow 0} \frac{\ln N(\ell)}{\ln(1/\ell)}, \quad (10.40)$$

where  $P_j = 1/N(\ell)$  with the number of cells  $N(\ell)$ . (Compare this to (10.1) and (10.2)). The quantity

$$S_{\text{inf}}(\ell) = -\sum_j P_j \ln P_j = \ln N(\ell) \quad (10.41)$$

is also known as *information entropy*. It follows from (10.40) that

$$N(\ell) \sim \ell^{-D_1} \quad (10.42)$$

and in correspondence to (10.37),

$$D_1 = D_0. \quad (10.43)$$

One more dimension,  $D_2$ , is of a special interest since it defines the Grassberger-Hentschel-Procaccia *correlation dimension* (Note 10.3). Consider the pair correlation function between points  $r_j$  and  $r_k$ :

$$C_{\text{cor}}(\ell) = \frac{1}{N_\ell^2} \sum_{j,k} \theta(\ell - |r_j - r_k|), \quad (10.44)$$

where

$$\theta(\xi) = \begin{cases} 1, & \xi \geq 0, \\ 0, & \xi < 0. \end{cases}$$

It follows from (10.44) that  $C_{\text{cor}}(0) \equiv C_{\text{cor}}$  is obtained when  $r_j$  and  $r_k$  belong to the same cell. If  $P_j$  is the probability for a particle to exist in the  $j$ -th cell, then the probability of two particles existing in the same cell is simply  $P_j^2$  and

$$C_{\text{cor}} = \sum_j P_j^2 = Z_\ell(2) \sim \ell^{D_2} \quad (10.45)$$

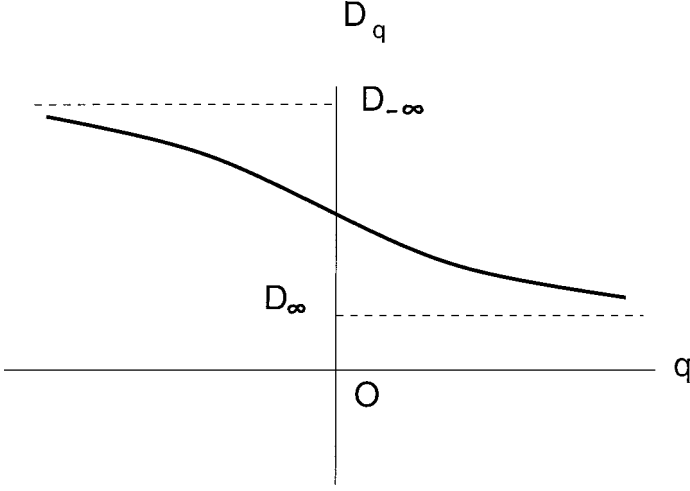


FIG. 10.2. Typical behaviour of the fractal dimension  $D_q$ .

based on the definition (10.23). Hence

$$D_2 = \lim_{\ell \rightarrow 0} \frac{\ln C_{\text{cor}}(\ell)}{\ln \ell}. \quad (10.46)$$

For the limit cases  $q = \pm\infty$ , it follows from the definition (10.23)

$$\begin{aligned} Z_\ell(q \rightarrow \infty) &\sim P_{\text{max}}^q \sim \ell^{\gamma_{\text{min}} q} \sim \ell^{q D_\infty}, \\ Z_\ell(q \rightarrow -\infty) &\sim P_{\text{min}}^q \sim \ell^{\gamma_{\text{max}} q} \sim \ell^{q D_{-\infty}}. \end{aligned} \quad (10.47)$$

Therefore,

$$D_\infty = \gamma_{\text{min}}, \quad D_{-\infty} = \gamma_{\text{max}}. \quad (10.48)$$

A typical behaviour of the dimension  $D_q$  as a function of  $q$  and, correspondingly, of the spectral function  $f(\gamma)$  is shown in Fig. 10.2.

### 10.5 Thermodynamic interpretation

Some of the results of the previous section can be interpreted using ‘thermodynamic language’. The sum  $Z_\ell(q)$  in (10.26) can be considered as a statistical sum

$$Z_\ell(q) = \text{const} \sum_{\gamma} \ell^{\gamma \ell - f(\gamma)} = \text{const} \sum_{\gamma} \exp\{-\kappa Q(q, \gamma)\} \sim \exp\{-\kappa \hat{Q}(q, \gamma_0)\}, \quad (10.49)$$

where

$$Q(q, \gamma) = q\gamma - f(\gamma) \quad (10.50)$$

is an analogue to a Hamiltonian multiplied by inverse ‘temperature’, and

$$\hat{Q}(q, \gamma_0) = q\gamma_0 - f(\gamma_0) \quad (10.51)$$

is an analogue to a free energy, that is,

$$\hat{Q}(q, \gamma_0) = - \lim_{\kappa \rightarrow \infty} \frac{\partial \ln Z_\kappa(q)}{\partial \kappa}, \quad (10.52)$$

where we have replaced the notation  $Z_\ell(q) \rightarrow Z_\kappa(q)$ . The value  $\gamma_0$  is defined by the expression

$$q = \frac{df(\gamma_0)}{d\gamma_0}, \quad (10.53)$$

that is, by the condition of extremum of  $Q(q, \gamma)$ . The transition from a sum to the final result in (10.49) is equivalent to the steepest descent method that becomes evident if we replace the sum by an integral and consider the limit  $\kappa \rightarrow \infty$ .

The thermodynamic limit corresponds to  $\kappa \rightarrow \infty$ , and  $\kappa$  can be considered as an effective number of particles. Then  $\hat{Q}(q, \gamma_0)$  is proportional to the free energy  $\mathcal{F}$  per particle and (10.50) can be interpreted as

$$\hat{Q} = \frac{1}{\hat{t}} \mathcal{F}(q) = \frac{1}{\hat{t}} \mathcal{F}(q, \gamma_0(q)) = \frac{1}{\hat{t}} \mathcal{U} - S \quad (10.54)$$

with ‘internal energy’ per particle

$$\mathcal{U} = \gamma_0(q) = \left. \frac{dQ(q, \gamma)}{d\gamma} \right|_{\gamma=\gamma_0} \quad (10.55)$$

‘entropy’ per particle

$$S = f(\gamma_0) \quad (10.56)$$

and  $\hat{t}$  as a temperature

$$\frac{1}{\hat{t}} = q = \frac{df(\gamma_0)}{d\gamma_0} = \frac{dS(\gamma_0)}{d\gamma_0} = \frac{dS}{d\mathcal{U}}. \quad (10.57)$$

Using all these definitions, it is possible to define a ‘pressure’

$$\mathcal{P} = - \frac{\partial(\kappa \mathcal{F})}{\partial \kappa} = -\mathcal{F}, \quad (10.58)$$

where the role of a volume is played by  $\kappa$ . Using (10.54) and (10.52), we arrive at

$$\mathcal{P} = -\hat{t}\hat{Q} = \hat{t} \lim_{\kappa \rightarrow \infty} \frac{\partial \ln Z_\kappa(q)}{\partial \kappa} = \hat{t}\hat{\mathcal{P}}. \quad (10.59)$$

$\mathcal{P}$  is called *topological pressure* (Note 10.4).

## 10.6 Complex dimension and log-periodicity

Consider again the sum (10.9) and assume that it is finite and non-zero for some  $d = d_g$ . Applications of the sum to dynamics, as we will see later, impose a necessity to expand the domain of definition of  $d$  to complex space and keep  $S(\xi, \eta; d; \{u_j\})$  in real space. If  $d_g$  is the dimension related to the problem then

$$d_{cg}^{(m)} = d_g + 2\pi im, \quad (m = 0, \pm 1, \dots) \quad (10.60)$$

is also a solution for the problem since it does not change  $S(\xi, \eta; d; \{u_j\})$ , where  $d_{cg}^{(m)}$  is complex generalized dimension that depends on the arbitrary integer  $m$ .

Consider any physical characteristic  $\mathcal{M}(\{u_j\}, d_{cg}^{(m)})$  of a system and assume the existence of an expansion

$$\mathcal{M}(\{u_j\}) = \sum_{m=-\infty}^{\infty} C^{(m)} \mathcal{M}(\{u_j\}, d_{cg}^{(m)}) \quad (10.61)$$

with some coefficients  $C^{(m)}$ . The expansion (10.61) is typical for multifractals, and for real  $\mathcal{M}(\{u_j\})$  we have

$$C^{(-m)} = (C^{(m)})^*. \quad (10.62)$$

Let, for example,  $\xi = 1$  in the sum (10.9),  $\eta \rightarrow \infty$  but there exist  $\eta_{\max}(u_j)$ . Then we can write in the real space

$$S \sim \eta_{\max}^{d_g}. \quad (10.63)$$

Generalization of this expression for the complex dimensions (10.60) is similar to (10.61):

$$\begin{aligned} S &\sim \sum_{m=-\infty}^{\infty} S^{(m)}(\eta_{\max}) d_{cg}^{(m)} \\ &= \sum_{m=-\infty}^{\infty} S^{(m)}(\eta_{\max}) d_{cg}^{(0)} (\eta_{\max})^{2\pi im} \\ &= S^{(0)}(\eta_{\max}) d_{cg}^{(0)} \left\{ 1 + 2 \sum_{m=1}^{\infty} \left| \frac{S^{(m)}}{S^{(0)}} \right| \cos(2\pi m \ln \eta_{\max} + \phi_S^{(m)}) \right\}, \end{aligned} \quad (10.64)$$

where we use

$$S^{(m)} = |S^{(m)}| e^{i\phi_S^{(m)}} \quad (10.65)$$

and

$$S^{(-m)} = (S^{(m)})^* \quad (10.66)$$

similarly to (10.62).

The complexity of the generalized dimension leads to a periodic term, comparing (10.64) to (10.63), with respect to  $\ln \eta_{\max}$  instead of  $\eta_{\max}$  as a variable. This phenomenon will be called *log-periodicity* and it will be implicated later for the studying of anomalous transport.

## Notes

### Note 10.1

The notion of ‘fractals’ was coined by B. Mandelbrot (1982) who also showed a widespread appearance of fractal structures in nature, and who discussed possible applications of the fractals in turbulence, economics, etc. Fractals as a mathematical object, i.e. a set of points that has specific properties, may be attributed first to F. Hausdorff (1919) and A. Besicovitch (1929, 1934), and were then developed in many important publications: L. Richardson (1961), A. Renyi (1957), C. Caratheodory (1914), *et al.* For specific applications of fractals to dynamical systems and random processes, see Pesin (1997); Kadanoff (1981, 1993); Grassberger and Procaccia (1984); Halsey *et al.* (1986); Hentschel and Procaccia (1983); Afraimovich and Hsu (2003) and reviews in Montroll and Shlesinger (1984); Paladin and Vulpiani (1987); Zaslavsky (2002b).

### Note 10.2

Fractal and multi-fractal analysis of dynamical systems with chaotic motion became a routine method after the publication of a series of pioneering works: Hentschel and Procaccia (1983); Frisch and Parisi (1985); Jensen *et al.* (1985); Halsey *et al.* (1986). The rigorous consideration provided in Pesin (1997) confirmed the basic physical concepts. For a review of different topics related to fractals and multi-fractals, see Paladin and Vulpiani (1987).

### Note 10.3

See Grassberger *et al.* (1983) for the original publication and Pesin and Weiss (1997) for the discussions and rigorous results. The correlation dimension is very convenient for different practical estimations.

### Note 10.4

The analogy to the thermodynamics for the sum  $Z_\ell(q)$  looks like a kind of a formal toy. Nevertheless, there are some similarities in the construction of statistical mechanics-thermodynamics transition and expression for multi-fractal sums that are similar to statistical sums. In addition to this, the steepest

descent method should be used in (10.49) and the extremum condition (10.53) leads to the corresponding Legendre form (10.51). For more discussion see Dorfman (1999) and Ott (1993).

## Problems

More complicated problems are marked by (\*).

10.1 Find the box dimension for the *Sierpinski carpet* in the Fig. P10.1.

10.2\* The *Koch island* is obtained from a square by replacing each side with a broken line (see Fig. P10.2). Find the box dimension of the Koch island.

10.3\* Find the box dimension of the set of loops of the *Moran* construction in Fig. P10.3 (see Afraimovich and Sze-Bi Msu (2003)).

10.4 Prove that  $d_C = d_H$  for the Sierpinski carpet in Fig. P10.1.

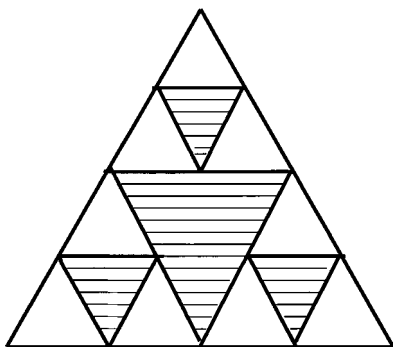


FIG. P10.1. Formation of the Sierpinski carpet. The white area is empty.

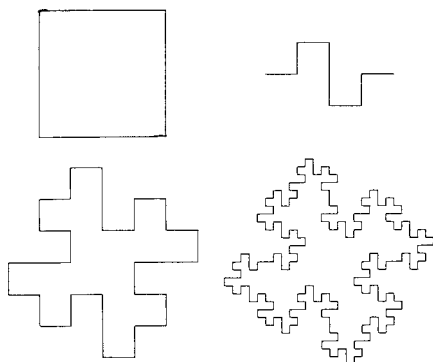


FIG. P10.2. Formation of the Koch island.

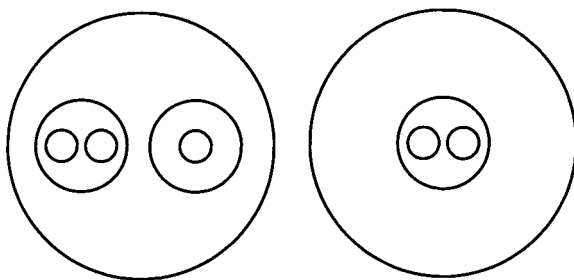


FIG. P10.3. Formation of the Moran construction.

*This page intentionally left blank*

## POINCARÉ RECURRENCES

Poincaré recurrences, or simply *recurrences*, are one of the most important notions for kinetic theory and dynamical analysis of random-like motion. For a long time after the famous discussion between Boltzmann and Zermelo recurrences did not play any serious constructive role in the study of dynamical systems. The situation has drastically changed in recent decades after developing new tools for time series analysis and for kinetic description of non-linear systems with chaotic dynamics. The application of properties of the recurrences will be seen throughout the rest of the book, and more specific discussion will be continued in Chapter 12 (*Note 11.1*).

### 11.1 Poincaré theorem on recurrences

Consider a domain  $A$  in the phase space of a Hamiltonian system with finite dynamics (see Fig. 11.1), and points  $x^{(0)} \in A$  as an initial condition for trajectories that start in  $A$ . Then the trajectories return back to  $A$  after some time repeatedly and infinitely many times, except for some of them with a set of initial points of zero measure.

A proof of this theorem is based only on the Liouville theorem on the preservation of phase volume.

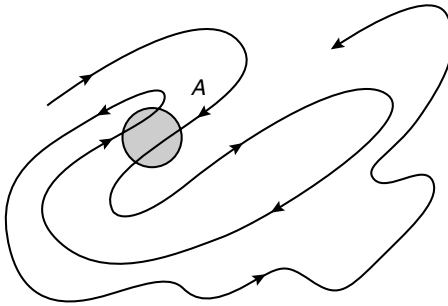


FIG. 11.1. Poincaré recurrences to the domain  $A$ .



Let  $B_0 \subseteq A$  be a set of points that never return to  $A$ . Then there exists a time  $t_1$  such that  $B_1 = \hat{T}(t_1)B_0$  and  $A \cap B_1 = \emptyset$ . Otherwise there are points in  $B_1$  that do not exit  $A$ . There should be a time  $t_2 > t_1$  such that for  $B_2 = \hat{T}(t_2)B_0 = \hat{T}(t_2 - t_1)\hat{B}_1$  we have  $B_1 \cap B_2 = \emptyset$ . Otherwise there are points in  $B_1$  that do not return to  $A$  and do not exit from  $B_1$  and, consequently,  $B_1$  is a sink in contradiction to the Liouville theorem. In a similar way, we can indicate an infinite sequence  $t_1 < t_2 < t_3, \dots$  and the corresponding set of images  $B_k = \hat{T}(t_k)B_0$  of  $B_0$  such that  $B_j \cap B_k = \emptyset$ , for all  $(j, k)$ . Due to the same Liouville theorem  $\Gamma(B_j) = \Gamma(B_0)$  for all  $j$ , that is in the process of dynamics of trajectories with initial points in  $B_0$ , they cover the phase volume

$$\Gamma_B = \sum_{j=0}^{\infty} \Gamma(B_j) = \Gamma(B_0) \cdot \infty. \quad (11.1)$$

It follows from (11.1) that either  $\Gamma_B = \infty$ , which contradicts the finiteness of the dynamics, or  $\Gamma(B) = 0$ . This proves the theorem.

Applying the same theorem after any return to  $A$ , we conclude that any trajectory, up to zero measure exclusions, returns infinitely many times to  $A$ . A time interval between two adjacent returns will be called the *Poincaré cycle*, or simply a cycle (for a periodic dynamics) and a *quasi-cycle* (for an aperiodic case).

A weakness of this theorem is, as was first pointed out by Boltzmann, that there is no information about the time of recurrences, i.e. a length of the quasi-cycles. Some information about this appears in the next section.

## 11.2 Recurrence time distributions and Kac lemma

For non-periodic dynamics, Poincaré cycles can be characterized by their distribution function  $P_{\text{rec}}(t; A)$  such that

$$d\mathcal{P}_{\text{rec}}(t; A) = P_{\text{rec}}(t; A)dt \quad (11.2)$$

is a probability to have recurrence times to the domain  $A$  within an interval  $(t, t + dt)$ . This function can be normalized in the following way:

$$\lim_{\Gamma(A) \rightarrow 0} \frac{1}{\Gamma(A)} \int_0^{\infty} P_{\text{rec}}(t; A)dt = 1 \quad (11.3)$$

assuming that the limit

$$P_{\text{rec}}(t) = \lim_{\Gamma(A) \rightarrow 0} \frac{1}{\Gamma(A)} P_{\text{rec}}(t; A) \quad (11.4)$$

exists as a Lebesgue measure of the set of recurrence times  $\{t_j\}$ . Then the mean recurrence time  $\tau_{\text{rec}}$  can be introduced as

$$\tau_{\text{rec}} = \int_0^\infty t P_{\text{rec}}(t) dt, \quad (11.5)$$

that is, the first moment of  $P_{\text{rec}}(t)$ . The mean recurrence time was first introduced by Smoluchowski for discrete dynamics

$$\tau_{\text{rec}}(A) = \frac{\sum_{k=1}^\infty k t_0 P_{\text{rec}}(k t_0; A)}{\sum_{k=1}^\infty P_{\text{rec}}(k t_0; A)}, \quad (11.6)$$

where  $t_0$  is a time interval for discrete dynamics (time between consequent steps of a map) and  $P_{\text{rec}}(k t_0)$  is a probability to return first time back to a domain after  $k$  steps (Smoluchowski (1912, 1913, 1915)).

The most important result for the  $\tau_{\text{rec}}$  was obtained by Kac and known as *Kac lemma* (Note 11.2). For the simplicity, we consider it here for discrete maps. Let  $A$  be a domain of the phase space  $\Gamma$  of the system with bounded dynamics and  $x^{(0)} \in A$  are all points of  $A$  considered at time instant  $t_0 = 0$  as initial conditions for trajectories started dynamics in  $A$ . All trajectories, excluding some of them of zero measure, return back to  $A$  after some time (number of steps of the map  $\hat{T}$ ). Let  $E^{(0)}(n) \subset A$  be a set of those points  $x^{(0)}(n) \in E^{(0)}(n)$  that return first time to  $A$  after  $n$  steps. Evidently

$$A = \cup_{k=1}^\infty E^{(0)}(k). \quad (11.7)$$

Consider a set of points

$$E^{(1)}(n) = \hat{T} E^{(0)}(n), \quad n > 1. \quad (11.8)$$

They occupy a domain disjoint with  $E^{(0)}$  and out of  $A$ . Otherwise, they will include points that have a first return time equal to one (see Fig. 11.2). The same can be applied to

$$E^{(k)}(n) = \hat{T}^k E^{(0)}(n), \quad k = 1, 2, \dots, n-1. \quad (11.9)$$

The set of points

$$E(n) = \cup_{k=0}^{n-1} E^{(k)}(n) = \cup_{k=0}^{n-1} \hat{T}^k E^{(0)}(n) \quad (11.10)$$

consists of all those points of  $\Gamma$  that have the recurrence time  $n$  since all  $E^{(k)}(n)$  are disjoint. Some of these points are in  $A$  but others are on their way to  $A$ .

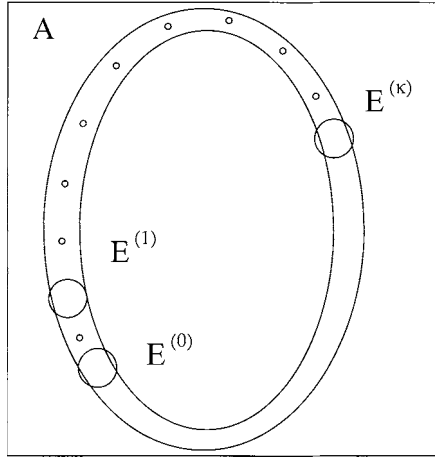


FIG. 11.2. A sketch of recurrences to the domain  $A$ .

All following steps are very formal. From (11.10) we have

$$\sum_{n=0}^{\infty} E(n) = \sum_{n=1}^{\infty} \sum_{k=0}^{n-1} \hat{T}^k E^{(0)}(n) \quad (11.11)$$

and

$$\rho \left( \sum_{n=0}^{\infty} E(n) \right) = \sum_{n=0}^{\infty} \rho(E(n)) = \sum_{n=0}^{\infty} \sum_{k=0}^{n-1} \rho(\hat{T}^k E^{(0)}(n)), \quad (11.12)$$

where  $\rho(E(n))$  is a measure of the set  $E(n)$ .

For the left-hand side we have simply

$$\sum_{n=0}^{\infty} \rho(E(n)) = \Gamma \quad (11.13)$$

and for the right-hand side we have

$$\rho(\hat{T}^k E^{(0)}(n)) = \rho(E^{(0)}(n)) \quad (11.14)$$

due to the Liouville theorem. Then applying (11.13) and (11.14) to (11.12), we have

$$\Gamma = \sum_{n=1}^{\infty} n \rho(E^{(0)}(n)). \quad (11.15)$$

From (11.7) we have, similarly to (11.13):

$$\Gamma(A) = \rho \left( \bigcup_{k=1}^{\infty} E^{(0)}(k) \right) = \sum_{k=1}^{\infty} \rho(E^{(0)}(k)). \quad (11.16)$$

The ratio of (11.15) and (11.16) gives

$$\tau_{\text{rec}}(A) = t_0 \frac{\Gamma}{\Gamma(A)} < \infty \quad (11.17)$$

due to the Smoluchowski formula (11.6). Similar results exist for (11.17) for the continuous time case.

The result (11.17) can be easily understood if we assume a uniform mixing of trajectories in the finite phase space  $\Gamma$ . Then the time to come back to  $A$  from a whole domain out of  $A$  is proportional to  $[\Gamma - \Gamma(A)]/\Gamma(A) \approx \Gamma/\Gamma(A)$  since  $\Gamma(A)$  is small compared to  $\Gamma$ .

The expression (11.5) for the continuous time case provides the mean recurrence time normalized per unit phase volume. The extension of the Kac lemma for the continuous case (Kac, 1958) gives also

$$\tau_{\text{rec}} < \infty \quad (11.18)$$

or the asymptotics

$$P_{\text{rec}}(t) \leq \frac{1}{t^\gamma}, \quad \gamma > 2, \quad t \rightarrow \infty. \quad (11.19)$$

in the case of a power law recurrences distribution. In this case  $\gamma$  is called *recurrence exponent*. Formula (11.19) gives the condition for a fairly fast decay of the recurrence time probability density when  $t \rightarrow \infty$ .

### 11.3 Distribution of recurrences in uniform mixing

Mixing of trajectories in phase space for the Anosov-type systems will be called *uniform mixing* because of the absence in phase space of singular zone domains with zero Lyapunov exponents. The phase space is full of unstable periodic orbits (cycles). A trajectory that starts in a vicinity of any point of the cycle will disperse exponentially from the cycle.

Consider a small domain  $A$  and a point  $0 \in A$ . After some time the corresponding trajectory returns the first time to  $A$  (see Fig. 11.3). A part  $00'$  of the trajectory is a quasi-cycle. Since an exponential growth of the distance between two initially close trajectories, we can write

$$\delta x(t) \sim \delta x(0) \exp(\sigma t), \quad (11.20)$$

where  $\sigma > 0$  is the largest Lyapunov exponent. If  $\delta x(t) \sim \overline{00'} \lesssim \text{diam } A$ , then

$$\delta x(0) < \text{diam } A \cdot \exp(-\sigma t), \quad (11.21)$$

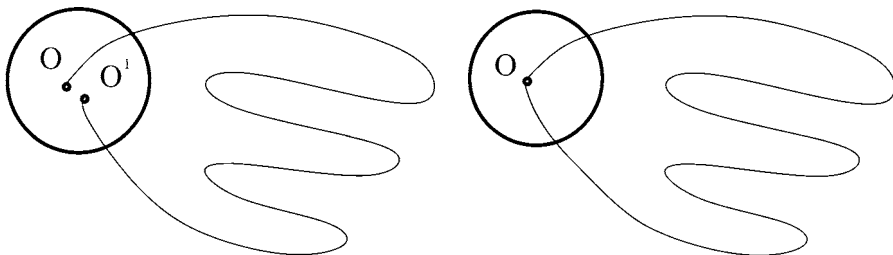


FIG. 11.3. Poincaré cycle or quasi-cycle (left) and just a cycle (right) for a system with uniform mixing.

i.e. by an exponentially small perturbation of the initial condition one can transform a quasi-cycle into a cycle. A formal expression of this fact is given by the Bowen theorem (Bowen (1972)) formulated below.

Let  $C_{\Delta\Gamma}$  be a closed orbit  $C$  that crosses a small volume  $\Delta\Gamma(A)$ , and let  $x(C_{\Delta\Gamma})$  be a coordinate on the orbit  $C_{\Delta\Gamma}$ . Different closed orbits, i.e. cycles, will be distinguished by their periods  $T$  only;  $C_{\Delta\Gamma} = C_{\Delta\Gamma}(T)$ . Denote by  $\rho(x)$  a stationary distribution density in phase space, and  $\rho_C(x)$  the density at points  $x(C_{\Delta\Gamma})$ . Define

$$\rho_0(\Delta\Gamma, T)\Delta\Gamma = \sum_{C \in C_{\Delta\Gamma}(T)} 1, \quad (11.22)$$

where summation is over all cycles of the period  $T \in (T, T + \Delta T)$  and

$$\Delta T = \frac{dT}{d\Gamma} \Delta\Gamma. \quad (11.23)$$

The value (11.22) is the number of such cycles.

Then for systems of the Anosov type and any integrable function  $g(x)$  the following is correct (Bowen (1972)):

$$\langle g(x) \rangle = \int g(x)\rho(x)dx = \lim_{T \rightarrow \infty} \frac{1}{\rho_0(\Delta\Gamma, T)\Delta\Gamma} \sum_{C \in C_{\Delta\Gamma}(T)} \int_{x \in C_{\Delta\Gamma}(T)} g(x)\rho_C(x)dx. \quad (11.24)$$

The formula (11.24) states that the ensemble average is equal to the average over a periodic orbit with an asymptotically large period. The result is an analogue of the ergodic theorem for periodic orbits. Due to the uniform mixing any unstable periodic orbit fills uniformly phase space similarly to non-periodic orbits. This leads to:

**Conjecture** For uniformly mixing systems, distribution of periods of unstable periodic orbits  $\rho_C(T)$  coincides asymptotically with the distribution of Poincaré

recurrences, that is,

$$\lim_{T \rightarrow \infty} [\rho_C(T) - P_{\text{rec}}(T)] = 0 \quad (11.25)$$

and it provides a way to estimate the recurrences distribution. It is also assumed that both,  $\rho_C(T)$  and  $P_{\text{rec}}(T)$ , are coarse-grained distributions.

The following result belongs to Margulis (1969, 1970)—the number of unstable periodic orbits with a period  $T$  for good mixing systems is:

$$N_C(T) \sim \exp(hT), \quad T \rightarrow \infty \quad (11.26)$$

and a probability density to find a periodic orbit with the period  $T \in (T, T + dT)$  is

$$\rho_C(T) = h \exp(-hT) = \frac{1}{\langle T \rangle} \exp\left(-\frac{T}{\langle T \rangle}\right), \quad T \rightarrow \infty, \quad (11.27)$$

where

$$\langle T \rangle = \frac{1}{h} = \tau_{\text{rec}} \quad (11.28)$$

is the mean period of orbits or the mean recurrence time. Here is an example of direct calculation of  $N_C(T)$ .

Consider a map

$$x_{n+1} = \hat{T}x_n = Kx_n, \pmod{1} \quad (11.29)$$

with  $K = 2$  (see Fig. 11.4). This map belongs to the Anosov-type system and  $h = \ln K$ , that is,  $h > 0$  for  $K > 1$  (*Note 11.3*).

The number of solutions of the equations

$$\hat{T}x = x, \quad \hat{T}^2x = x, \dots \quad (11.30)$$

permits the estimation of the number of periodic orbits with periods  $1, 2, \dots$  correspondingly. The result is

$$N_C(n) = 2^{n-1} = \exp[(n-1) \ln 2] \sim \exp(n \ln 2), \quad n \rightarrow \infty \quad (11.31)$$

conforming the result (11.26) for integer  $n \gg 1$ .

It is possible to extend for a general case of uniformly mixing dynamical systems, that

$$P_{\text{rec}}(t)dt \sim \text{const} \frac{dt}{N_C(t)} \quad (11.32)$$

with  $N_C(t)$  as a number of periodic orbits with the periods within interval  $(t, t + dt)$  (*Note 11.4*).

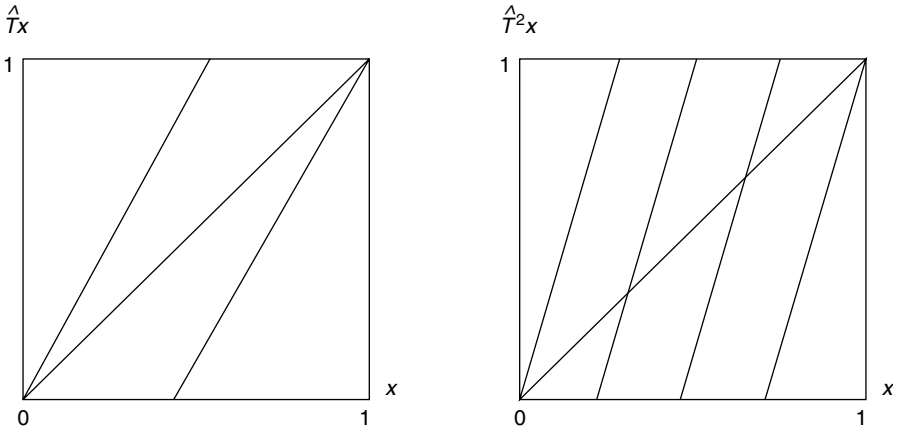


FIG. 11.4. A plot of  $\hat{T}x = 2x, (\text{mod } 1)$  and  $\hat{T}^2x = 2(2x), \text{mod } 1$ .

#### 11.4 More asymptotics on recurrences

Some cases of chaotic dynamics permit a fairly simple estimate for the distribution of periodic orbits  $\rho_C(t)$  and recurrences (quasi-cycles)  $P_{\text{rec}}(t)$ . Consider a small domain  $A$  of the phase volume  $\Delta\Gamma_0 \ll \Gamma_\infty$ , where  $\Gamma_\infty$  is the phase volume of the bounded dynamics. Considering evolution of the phase volume  $\Delta\Gamma_0$ , it is convenient to introduce the coarse-grained volume  $\overline{\Delta\Gamma}_t$  which depends on time. In the case of uniform mixing we have

$$\overline{\Delta\Gamma}_t \sim \Delta\Gamma_0 \exp(ht) \quad (11.33)$$

with

$$h = \sum_{\sigma_j > 0} \sigma_j, \quad (11.34)$$

where  $\sigma_j$  are positive Lyapunov exponents and summation is over all of them. Expression (11.33) simply shows the exponential growth of the enveloping volume of the initial domain  $A$ . Uniformity of mixing inside  $\overline{\Delta\Gamma}_t$  imposes the estimate of the number of periodic orbit  $N_C(t)$  with a period  $\leq t$ :

$$N_C(t) \sim \frac{\overline{\Delta\Gamma}_t}{\Delta\Gamma_0}, \quad (11.35)$$

where the elementary cell of the coarse-graining is equal to  $\Delta\Gamma_0$ .

We can use a standard physical estimate prescribing the probability of an event to be equal to the normalized phase volume occupied by the event, that

is, a probability to return to  $\Delta\Gamma_0$  from  $\overline{\Delta\Gamma_t}$  during time  $\geq t$

$$P_{\text{rec}}(0, t) = 1 - \int_0^t P_{\text{rec}}(t) dt \sim 1 - \frac{1}{N_C(t)} = 1 - \exp(-ht) \quad (11.36)$$

with a boundary condition

$$P_{\text{rec}}(0, 0) = 0, \quad P_{\text{rec}}(0, \infty) = 1. \quad (11.37)$$

Differentiation of (11.36) gives a probability density  $P_{\text{rec}}(t)$  of the returns normalized to the unit phase volume

$$P_{\text{rec}}(t) \sim h \exp(-ht) \quad (11.38)$$

in correspondence to (11.27) and (11.25).

Let  $\Psi(t; \Delta\Gamma_0)$  be a *survival probability* for the considered initial domain  $\Delta\Gamma_0$ , that is, a probability not to escape from  $\Delta\Gamma_0$  during the time interval  $(0, t)$ . Then

$$P_e(t; \Delta\Gamma_0) = 1 - \Psi(t; \Delta\Gamma_0) = \int_0^t \psi(t'; \Delta\Gamma_0) dt' = 1 - \int_t^\infty \psi(t'; \Delta\Gamma_0) dt', \quad (11.39)$$

where  $P_e(t; \Delta\Gamma_0)$  is a probability to escape from  $\Delta\Gamma_0$  during the time interval  $(0, t)$  and  $\psi(t, \Delta\Gamma_0)$  is a probability density to escape at a time instant  $t$  within the interval  $(t, t + \Delta t)$ .

We have an evident inequality

$$P_{\text{rec}}(0, t) \leq \Psi(t; \Delta\Gamma_0) \quad (11.40)$$

since the number of return events cannot exceed the number of escapes. This gives asymptotically

$$P_{\text{rec}}(t; \Delta\Gamma_0) \sim \psi(t; \Delta\Gamma_0), \quad t \rightarrow \infty \quad (11.41)$$

or for the case (11.38)

$$\psi(t; \Delta\Gamma_0) \sim h \exp(-ht), \quad t \rightarrow \infty \quad (11.42)$$

that is, a probability to escape from a domain at a fairly large time is exponentially small. It follows from (11.41) and (11.42) that  $1/h$  is a mean time of staying in the domain  $\Delta\Gamma_0$ , normalized per unit area of the phase space.

Applying the Kac lemma (11.18), definitions (11.39), and the asymptotics (11.41), we obtain for the mean *trapping time*

$$\tau_{\text{tr}} = \int_0^\infty t \psi(t; \Delta\Gamma_0) dt < \infty, \quad (11.43)$$



which means that the mean time is finite for a trajectory to be trapped in some domain. Due to (11.40), we have inequalities

$$\tau_{\text{tr}} \leq \tau_{\text{rec}} < \infty \quad (11.44)$$

that appear as a consequence of the phase volume preserved dynamics.

As has been mentioned before and will be seen later, typical Hamiltonian systems do not have uniform mixing, and recurrences and escapes should be considered in more detail including specific structures of singular zones.

Let  $\{t_j^-\}$  be a set of time instants when a trajectory leaves  $A$ , and let  $\{t_j^+\}$  be the set of time instants when a trajectory enters  $A$  as in Fig. 11.1. The set

$$\{\tau_j^{(\text{rec})}\}_A = \{t_j^- - t_{j-1}^-\}_A, \quad (j = 1, 2, \dots) \quad (11.45)$$

is the set of recurrences. We call  $\{\tau_j^{(\text{rec})}\}$  the recurrence time at  $j$ -step, or the  $j$ -th quasi-cycle. There are some other characteristics related to the recurrences.

Exit (escape) times can be introduced as a time interval between the adjacent entrances to  $A$  and exits from  $A$ :

$$\{\tau_j^{(\text{esc})}\}_A = \{t_j^- - t_j^+\}_A. \quad (11.46)$$

Similarly, one can introduce time intervals  $\{\tau_j^{(\text{ext})}\}$  that a trajectory spends outside of  $A$  during one cycle:

$$\{\tau_j^{(\text{ext})}\}_A = \{t_j^+ - t_{j-1}^-\}_A. \quad (11.47)$$

There is an evident connection:

$$\tau_j^{(\text{rec})} = \tau_j^{(\text{esc})} + \tau_j^{(\text{ext})}. \quad (11.48)$$

The set of recurrence times  $\{\tau_j^{(\text{rec})}\}$  forms a specific mapping of trajectories. The sequence  $\{\tau_j^{(\text{rec})}\}$  can have fractal or multifractal features. These properties of recurrences will be considered in Chapter 12. Similarly, one can consider the mapping for  $\{\tau_j^{(\text{esc})}\}$  and  $\{\tau_j^{(\text{ext})}\}$ .

The set of intervals  $\{\tau_j^{(\text{esc})}\}_A$  in (11.46) does not play a significant role in the case of uniform mixing, especially when  $\Gamma(A) \rightarrow 0$ , but it is not the case when there are singular zones. The distributions of escape time and recurrences time may depend on how the domain  $A$  is selected, how a singular zone intersects  $A$ , and which zone is included into  $A$  when there are more than one singular zones.

It is important to stress that all the introduced functions  $\psi, \Psi, P_e$ , and quantity  $t_{\text{tr}}$  are local characteristics of motion, that is, they are defined for an infinitesimal domain  $\Delta\Gamma_0$  and can depend on the shape and location of  $\Delta\Gamma_0$ . In other words,  $\psi, \Psi, P_e$ , and  $t_{\text{tr}}$  depend only on the properties of the system's trajectories inside the  $\Delta\Gamma_0$ . The reverse situation is one where the distribution of Poincaré cycles  $P_{\text{rec}}(\tau)$  depends on full, infinitely long trajectories and does not depend on  $\Delta\Gamma_0$  for sufficiently small  $\Delta\Gamma_0$ . This means that  $P_{\text{rec}}(\tau)$  is a global characteristic of the system. Nevertheless, a connection between  $P_{\text{rec}}(\tau)$  and  $P_e(\tau; \Delta\Gamma_0)$  can be established for some special cases, when there is no uniform mixing.

When  $\psi(t; \Delta\Gamma_0)$  possesses the asymptotic property

$$\psi(t; \Delta\Gamma_0) \sim t^{-\gamma_{\text{esc}}}, \quad t \rightarrow \infty, \quad (11.49)$$

one derives from the definition (11.39)

$$\Psi(t; \Delta\Gamma_0) \sim t^{1-\gamma_{\text{esc}}}, \quad t \rightarrow \infty \quad (11.50)$$

and from (11.43)

$$t_{\text{tr}}(\Delta\Gamma_0) \sim \int_{\text{const}}^{\infty} t^{1-\gamma_{\text{esc}}} d\tau = \begin{cases} \langle \tau \rangle < \infty, & \gamma_{\text{esc}} > 2, \\ \lim_{t \rightarrow \infty} \ln t = \infty, & \gamma_{\text{esc}} = 2, \\ \infty & \gamma_{\text{esc}} < 2. \end{cases} \quad (11.51)$$

It follows from (11.51) that the mean trapping time is finite only for  $\gamma_{\text{esc}} > 2$ , while for  $\gamma_{\text{esc}} \leq 2$  the mean trapping time is infinite and the domain  $\Delta\Gamma_0$  works like a real trap in the sense of the time average.

In the case of the exponential (Poissonian) distribution of escapes (11.42), there is a finite characteristic time of escape,  $1/h$ , but in the case (11.49) such time does not exist. This gives a possibility of the definition of a *sticky domain* as a domain of subexponential (polynomial) time-dependence of the probability density of escapes. It can be many different sticky domains  $\Delta\Gamma_s$  and the corresponding distributions  $\psi(t; \Delta\Gamma_s)$  and  $\Psi(t; \Delta\Gamma_s)$ . All of them are giving their specific contributions to the general multifractal structure of the escapes and recurrences that will be discussed in the next chapter.

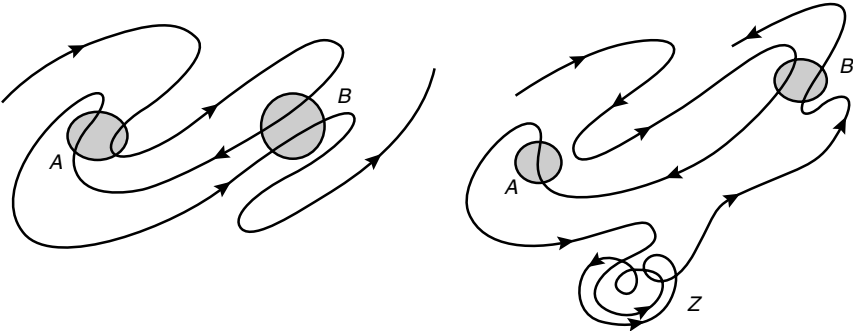


FIG. 11.5. Targeting without (left) and with (right) a singular zone  $Z$ .  
A trajectory escapes the domain  $A$  and first enters the domain  $B$ .

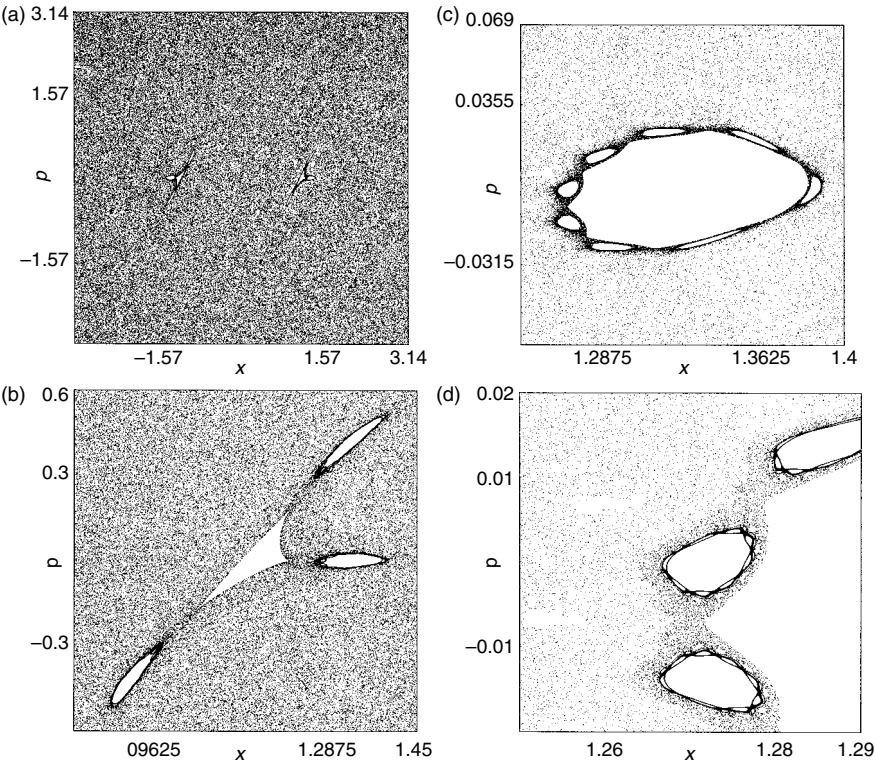


FIG. 11.6. Hierarchy of sticky islands  $2 - 3 - 8 - 8 - 8 \dots$  for the standard map for  $K = K^* = 6.908745$ . A set of consequent zooms.

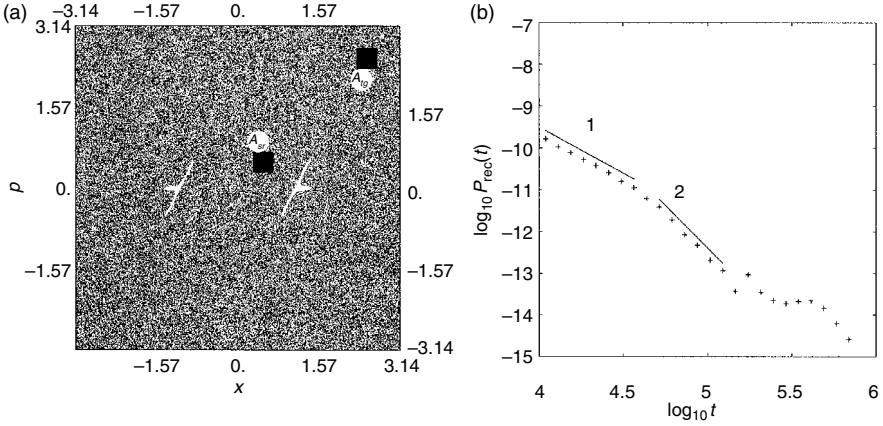


FIG. 11.7. Targeting for the case in Fig. 11.6. Left: location of the starting domain  $A_{st}$  and the targeting domain  $A_{tg}$  (both in black squares); right: distribution of  $P_{rec}(t)$ . Slope 1 is  $-2.19$ ; slope 2 is  $-4.09$ . The data obtained after averaging over  $3.22 \times 10^9$  initial conditions  $P_{targ}(t)$  cannot be distinguished from  $P_{rec}(t)$ .

In an oversimplified form for the case of non-uniform mixing, we can expect the asymptotic

$$P_{rec}(t; \Delta\Gamma) \sim \sum_k \frac{C_k}{t^{\gamma_k}}, \quad t \rightarrow \infty. \quad (11.52)$$

The expression (11.52) means that as  $t \rightarrow \infty$ , different ‘windows’  $(t_k^-, t_k^+)$  of *intermediate recurrence asymptotics* will appear with the recurrence exponent  $\gamma_k$ , and finally will be for sufficiently large  $t$

$$P_{rec}(t; \Delta\Gamma) \sim \frac{C_{min}}{t^{\gamma_{min}}}. \quad (11.53)$$

We also can expect that

$$\gamma_{min} = \min \gamma_{esc}, \quad (11.54)$$

where  $\min \gamma_{esc}$  is related to the singular zone with the  $\max \tau_{esc}$ .

To illustrate this way of consideration of recurrences, consider *trajectory targeting*, that is, distribution of time intervals that takes a trajectory to exit from a domain  $A$  and to first enter a domain  $B$  (see Fig. 11.5).

The corresponding statistics can be collected from one trajectory or from a large number of trajectories. In its process of wandering, a trajectory arrives to  $B$  fairly fast due to a strong mixing process. Nevertheless, there is small but

finite probability of the trajectory being trapped for a long time in  $Z$ . Just such events are responsible for the distribution of  $P_{\text{rec}}(t)$  and  $P_{\text{targ}}(t)$  for  $t \rightarrow \infty$ . The corresponding  $P_{\text{rec}}(t)$  was obtained for the standard map with a value of  $K = K^* = 6.908745$  for which there is strong stickiness (see Fig. 11.6 from Zaslavsky *et al.* (1997)). The plots of  $P_{\text{rec}}(t)$  (see Fig. 11.7 from Zaslavsky and Edelman (2000)) and  $P_{\text{targ}}(t)$  are indistinguishable.

## Notes

### Note 11.1

The description and discussion of the *Zermelo paradox* can be found in Zaslavsky (1985, 1999). It will also appear in Chapter 22.

### Note 11.2

For the original proof of the Kac lemma in discrete and continuous dynamics, see Kac (1958). There were some other simplified proofs of the similar result in Cornfeld *et al.* (1982) and Meiss (1997).

### Note 11.3

More information and references about the map (11.29) can be found in Zaslavsky (1985).

### Note 11.4

For more information on the periodic orbits, see Dorfman (1999) and Ott (1993).

## Problems

More complicated problems are marked by (\*).

11.1 Derive the number of periodic orbits  $N_c(T)$  for the map (11.29) with integer  $K$ .

11.2\* The same as in Problem 11.1, but for any  $K \gg 1$ .

11.3 Estimate the number of periodic orbits for the cat-map.

11.4 Estimate the number of periodic orbits for the Anosov type map (4.35) with  $K \gg 1$ .

11.5\* Estimate the number of periodic orbits for the standard map on the torus and  $K \gg 1$ , assuming that phases  $X$  are distributed uniformly.

## DYNAMICAL TRAPS

In this chapter, dynamical traps will be considered in more detail. When the mixing process in phase space is uniform, escape of a trajectory from the selected small domain follows the Poissonian law and, consequently, there exists a characteristic time of the escape (see Sections 11.3 and 11.4). Typical Hamiltonian systems do not have uniform mixing and the escapes from a domain, recurrences, and targetings may not have a characteristic time. Moreover, Hamiltonian dynamics does not involve trajectories that are trapped forever, i.e. the notion of trapping should be accurately defined. In fact, we should speak about the *quasi-trap* rather than about the *absolute trap*, and use a description of the specific way of a particle that crosses the domain with some stickiness (Fig. 12.1).

As it will be seen, the nature of quasi-traps can be very versatile, strongly depending on the system parameters. We can state that understanding of the properties of the quasi-trap is an unavoidable part of the understanding of global properties of any dynamical system (*Note 12.1*).

### 12.1 Definition of the dynamical trap

Consider a small domain  $A$  in phase space and a large number of trajectories  $N_A$  that start at  $A$ . Let  $\Delta N(t, A)$  be a number of trajectories that exit  $A$  at time within the interval  $(t, t + dt)$ . Then the probability density to exit from  $A$  at  $t$  is

$$\psi(t; A) = \lim_{\Delta\Gamma \rightarrow 0} \lim_{N_A \rightarrow \infty} \frac{1}{\Delta\Gamma} \frac{\Delta N(t, A)}{N_A}, \quad (12.1)$$

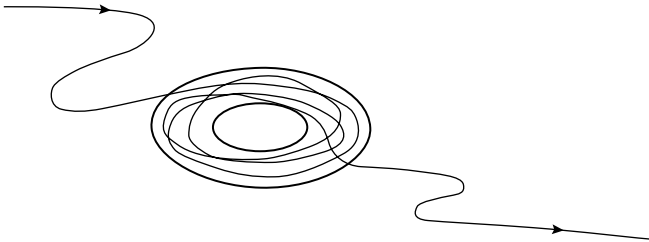


FIG. 12.1. A sketch of an orbit that gets stuck in a quasi-trap.

where  $\Delta\Gamma = \Gamma(A)$  and the normalization condition

$$\int_0^\infty \Delta N(t, A) dt = N_A \cdot \Delta\Gamma \quad (12.2)$$

leads to

$$\int_0^\infty \psi(t; A) dt = 1. \quad (12.3)$$

The phase space of a dynamical system will be called uniform with respect to the exit distribution if  $\psi(t; A)$  does not depend on  $A$ . Let  $A_s$  be a domain such that  $\psi(t; A_s)$  has subexponential asymptotics for  $t \rightarrow \infty$ , that is,

$$\psi(t; A_s) \sim C(t)/t^{\gamma_{\text{sec}}}, \quad (t \rightarrow \infty) \quad (12.4)$$

with a slow varying function  $C(t)$ . The moments of  $\psi(t; A_s)$  are

$$\tau_{\text{esc}}^{(m)} = \int_0^\infty t^m \psi(t; A_s) dt. \quad (12.5)$$

Then, due to (12.4), there exists some  $m_0$  such that

$$\tau_{\text{esc}}^{(m)} = \infty, \quad m \geq m_0 > 1, \quad (12.6)$$

where the condition  $m_0 > 1$  is a collorary from the Kac lemma.

**Definition** A domain  $A$  is a quasi-trap or, simply, dynamical trap if there exists a finite  $m_0$  that satisfies (12.6).

Since

$$P_{\text{rec}}(t) \sim \psi(t; A_s), \quad t \rightarrow \infty \quad (12.7)$$

it follows that the system has a singular zone  $A_s$  which is a dynamical trap if and only if there exists such  $m_0$  that

$$\tau_{\text{esc}}^{(m)} = \int_0^\infty t^m P_{\text{rec}}(t) dt = \infty, \quad m \geq m_0 > 1; \quad \tau_{\text{esc}} = \tau_{\text{esc}}^{(1)} < \infty. \quad (12.8)$$

Two examples below demonstrate the definitions. In Fig. 9.3 we showed the *Sinai billiard* (with infinite horizon) and a sample trajectory with long lasting bounces. The Poincaré map of the same trajectory displays ‘scars’ that correspond to the unreachable part of the phase space. The set  $S_{\text{sc}}$  of scars corresponds to the infinitely bouncing trajectories and has zero measure. Any domain  $A_s : A_s \cap S_{\text{cr}} \neq \emptyset$  is singular. Some qualitative estimates show that for the Sinai billiard in Fig. 9.3

$$P_{\text{rec}}(t) \sim 1/t^3, \quad \gamma_{\text{rec}} = 3 \quad (12.9)$$

(Note 12.2).

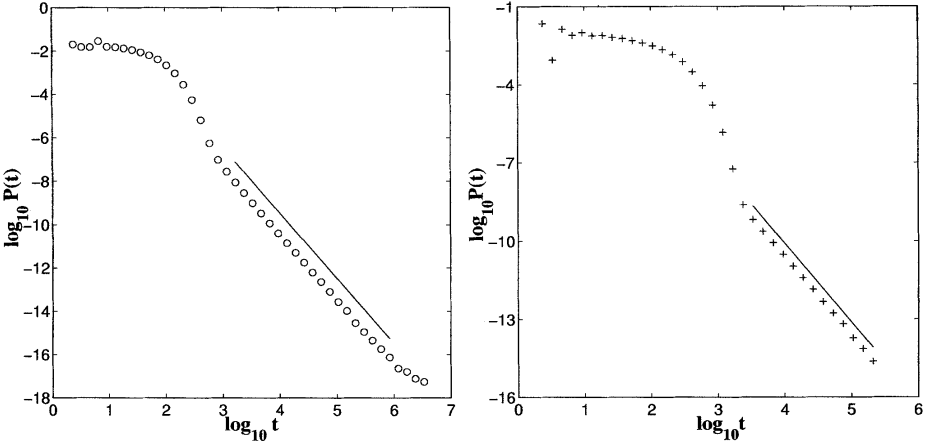


FIG. 12.2. Distributions of the Poincaré recurrences for the Sinai billiard (left) and Bunimovich billiard (right).

A similar pattern appears for the *Bunimovich billiard* (*stadium billiard*) with the same distribution of recurrences (12.9). Numerically obtained distributions of the recurrences (Zaslavsky and Edelman, 1997, 2004) are similar (see Fig. 12.2).

The function  $P_{\text{rec}}(t)$  has two parts:

$$P_{\text{rec}}(t) \approx \begin{cases} \exp(-ht), & t < t^*, \\ \frac{1}{t^3}, & t > t^* \end{cases} \quad (12.10)$$

with some crossover value  $t^*$  that depends on the geometry and location of the domain  $A$ . There are two conclusions from this result. Firstly, the distribution of the recurrences has two characteristic time scales: mixing time  $1/h$  and the crossover time  $t^*$  of the transition from the exponential law of the recurrences distribution to the power law. Secondly, there exists a dynamical trap with  $m_0 = 2$ .

Another important comment on the situation with both examples is a strong change of statistical properties of the dynamically chaotic system due to the *non-ergodicity of dynamics* with an excluded volume of zero measure.

## 12.2 Hierarchical-islands trap (HIT)

Consider a set of domains embedded into each other:  $A_0 \supset A_1 \supset \dots \supset A_n \supset \dots$ , and their differences  $A_0 - A_1$ ,  $A_1 - A_2, \dots, A_n - A_{n+1}$ ,  $\dots$ , such that  $\Delta A_n = A_n - A_{n+1} \equiv \Gamma(A_n - A_{n+1})$  is the phase volume of  $A_n - A_{n+1}$ . Let us introduce a characteristic residence time  $T_n$  that a trajectory spends in  $\Gamma_n$  during the time interval between the first arrival to  $\Delta A_n$  and the first following departure from  $\Delta A_n$  (see Fig. 12.3).



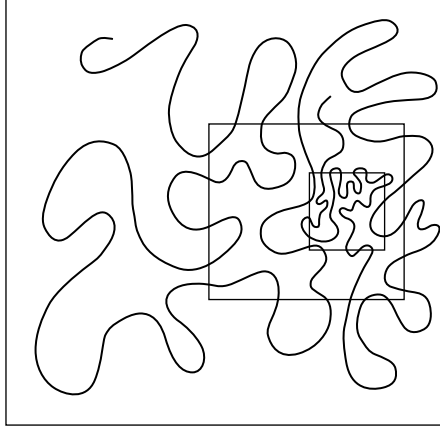


FIG. 12.3. A model of the hierarchical-islands trap.

The *hierarchical islands trap* (HIT) is defined by the following scaling properties:

$$\begin{aligned}\Gamma_{n+1} &= \lambda_\Gamma \Gamma_n, & (\lambda_\Gamma < 1), \\ T_{n+1} &= \lambda_T T_n, & (\lambda_T > 1).\end{aligned}\tag{12.11}$$

Let us point out that, contrary to systems with uniform mixing and with residence time proportional to the phase volume of a considered domain, the conditions  $\lambda_T > 1$ ,  $\lambda_\Gamma < 1$  are exactly the opposite ones: the smaller the domain  $\Delta A_n$  is, the longer the trajectories stay there. Conditions (12.11) reflect not only the presence of a singular zone, but also its self-similar structure.

An exact self-similarity that follows from (12.11) is

$$T_n = \lambda_T^n T_0, \quad \Gamma_n = \lambda_\Gamma^n \Gamma_0,\tag{12.12}$$

a kind of an idealization, and it can appear only for special values of a control parameter, say  $K^*$ , obtained with very high accuracy. More typical is the situation when the scaling parameters in (12.11) depend on  $n$ , i.e. instead of (12.12) we have:

$$\Gamma_n = \bar{\lambda}_\Gamma^n \Gamma_0, \quad T_n = \bar{\lambda}_T^n T_0, \quad (n \rightarrow \infty),\tag{12.13}$$

where  $\bar{\lambda}_\Gamma$  and  $\bar{\lambda}_T$  are some effective values defined by the equations

$$\begin{aligned} \ln \bar{\lambda}_\Gamma &= \frac{1}{n} \sum_{j=1}^n \ln \lambda_\Gamma(j) < 0, \quad (n \rightarrow \infty), \\ \ln \bar{\lambda}_T &= \frac{1}{n} \sum_{j=1}^n \ln \lambda_T(j) > 0, \quad (n \rightarrow \infty) \end{aligned} \quad (12.14)$$

with scaling constants  $\lambda_\Gamma(j)$ ,  $\lambda_T(j)$  on  $j$ -th step.

Figures 11.6 and 12.4 are demonstrations of HIT for the standard map and web map with the sequences of islands  $2 - 3 - 8 - 8 - 8 \dots$  and  $2 - 8 - 8 - \dots$  (times four) correspondingly. The values  $\Gamma_n$  correspond to the area inside an island of the  $n$ -th generation, and  $T_n$  is a period of rotation of the last invariant

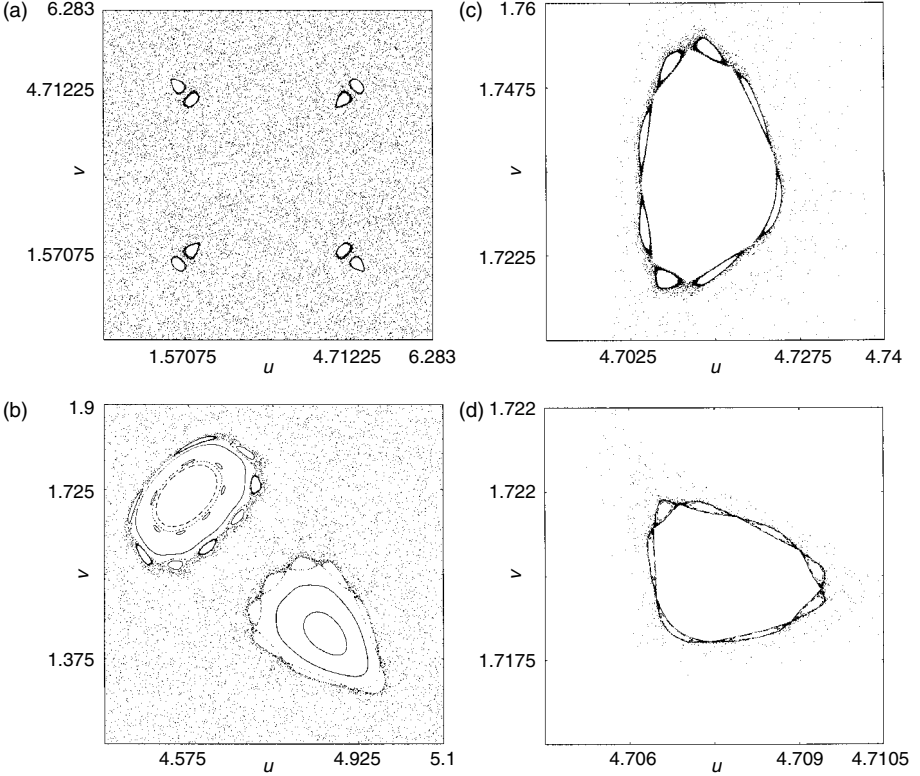


FIG. 12.4. Hierarchical-islands trap for the web map with  $K^* = 6.349972$ . A set of consequent zooms.

curve inside the island. The borders of the islands are sticky and that is why they are dark in the figures (*Note 12.3*).

For the standard and web maps  $K$  is the only control parameter. The set  $\{K^*\}$ , for which there exist an HIT, is infinite and each value  $K_j^*$  has its own ‘word’  $(n_1, \dots, n_m)_j$  that shows a sequence  $n_k$  of islands-around-islands. Repeating of this sequence reflects a hierarchical structure similar to what we find for fractals or multifractals. In contrary to geometrical fractals, the HIT also carries an adjoint fractal structure of the time sequence that a trajectory spends visiting different objects of the geometric fractal. Better understanding of this phenomenon needs a notion of the fractal time that will be considered in the next section.

One more general property of the HIT should be mentioned. The stickiness of the boundary layers of the islands can be characterized in some formal way. We can introduce a topological structure  $G$  of all sticky borders that can be hit by the same trajectory. Let us call  $d_{\Gamma_n} = \Gamma_n^{1/2}$  a diameter of an island that belongs to the  $n$ -th generation. Then  $G\{d_{\Gamma_n}, T_n, W_{n,n\pm 1}\}$  includes geometric factors  $d_{\Gamma_n}$  for all islands of the  $n$ -th generation, the approximate time that a trajectory spends near an island’s boundary  $T_n$ , and a probability of transition  $W_{n,n\pm 1}$  from one level of the island’s generation to an island of a nearest generation. Transitions to the non-nearest generations are neglected. Such structure is called a *sticky set* (Afraimovich and Zaslavsky, 1998).

A remarkable feature of the HIT and the corresponding sticky set is the existence of a universal relation between space-time properties of the structure. It follows from (12.12) that

$$n = \frac{\ln(T_n/T_0)}{\ln \lambda_T} \quad (12.15)$$

and

$$\frac{\Gamma_n}{\Gamma_0} = \exp(-n |\ln \lambda_\Gamma|) = \left(\frac{T_n}{T_0}\right)^{-\mu_\Gamma}, \quad (12.16)$$

where

$$\mu_\Gamma = \frac{|\ln \lambda_\Gamma|}{\ln \lambda_T}. \quad (12.17)$$

From the definition of the diameters we have

$$d_{n+1} \equiv d_{\Gamma_{n+1}} = \lambda_\Gamma^{1/2} d_{\Gamma_n} = \lambda_\Gamma^{1/2} d_n \quad (12.18)$$

and similarly to (12.16)

$$\left(\frac{d_n}{d_0}\right)^2 = \left(\frac{T_0}{T_n}\right)^{\mu_\Gamma}. \quad (12.19)$$

This expression will be used later in the analysis of particle transport. Meanwhile, let us comment that the parameter  $\mu_\Gamma$  characterizes some non-trivial properties of the sticky set by connecting its time and space scaling parameters.

### 12.3 Renormalization for the exit time distribution

It was mentioned above that the exit time probability distribution depends on the location of the domain  $\Delta\Gamma$ . If, for example,  $\Delta\Gamma$  is taken in the domain  $\Delta\Gamma_s$  of a singular zone around an island, then due to (12.7)

$$\psi(t; \Delta\Gamma_s) \sim P_{\text{rec}}(t), \quad (t \rightarrow \infty), \quad (12.20)$$

where  $P_{\text{rec}}(t)$  does not depend on  $\Delta\Gamma_s$ . Equation (12.20) has two advantages:

1. It presents a possibility of finding the asymptotics for the distribution function of recurrences  $P_{\text{rec}}(t)$  using the local information of singular zone properties.
2. Due to the space-time similarity of the domain  $\Delta\Gamma_s$ , as discussed in detail in Section 12.2, it enables the application of renormalization methods to  $\psi(t; \Delta\Gamma_s)$ .

Assuming a singular zone  $\Delta\Gamma_s$  is an annulus surrounding the main island and there are  $q$  islands of the first generation in the annulus ( $q = 6$  in Fig. 12.5), we can divide the annulus into  $q$  equal parts each containing a sub-island of the next generation and perform the same type of partitioning for each segment as it is shown in Fig. 12.5.

This process can be continued to infinity. Recall that the self-similarity properties for the islands in the vicinity of the boundary layers (annuluses) area

$$S_{k+1} = \lambda_S S_k, \quad \lambda_S < 1, \quad (12.21)$$

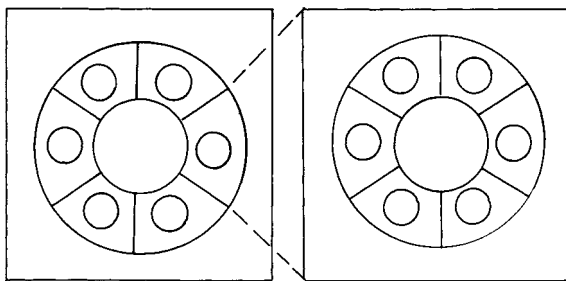


FIG. 12.5. A model of the singular zone near the island boundary: (a) boundary layer as an annulus and its partition; and (b) self-similar rescaling.

where  $S_k$  are areas of the islands, and for periods of rotation around the islands very close to the island boundary,

$$T_{k+1} = \lambda_T T_k, \quad \lambda_T > 1 \quad (12.22)$$

as mentioned in Section 12.2. The two equations (12.21) and (12.22) are based on the existence of a set  $\{K_j^*\}$  of the control parameter  $K$ , for which they are valid, and  $\lambda_S = \lambda_S(K_j^*)$ ,  $\lambda_T = \lambda_T(K_j^*)$ . In the following we omit the dependence on  $K_j^*$  and assume that the  $\lambda_S, \lambda_T$  are taken for a special value  $K^*$  that is specified by the structure of the singular zone and by the value of  $q$ . Evidently

$$\lambda_S = \lambda_d^2 = \lambda_\Gamma, \quad q = \lambda_T. \quad (12.23)$$

The numerical observations in Fig. 12.6 show that the escape probability from a singular zone of the HIT type is a self-similar function of  $t$  (Zaslavsky *et al.* (1997)). To apply a renormalization transform, let us introduce a set of

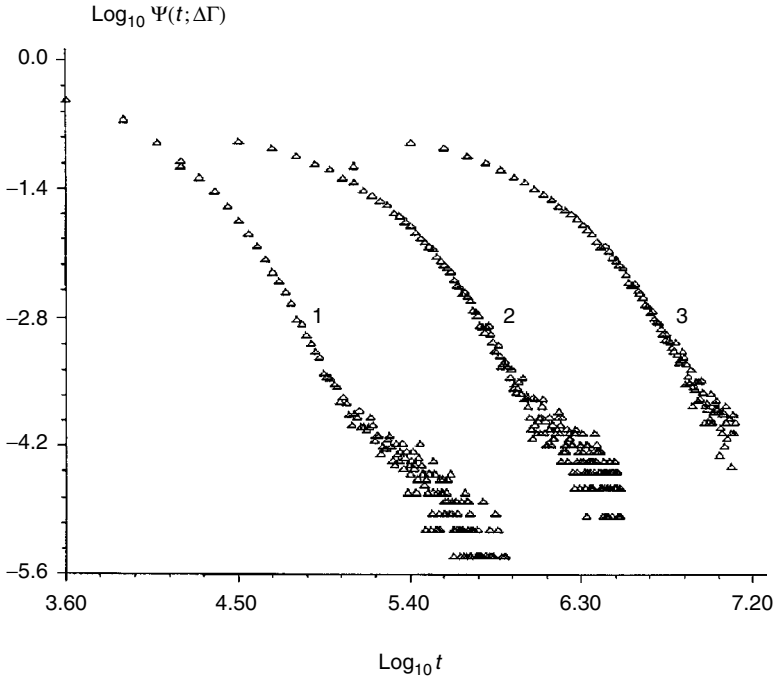


FIG. 12.6. Exit time distributions for domains taken in the boundary layers for the first, second, and third generations (curves 1, 2, and 3, respectively) obtained after averaging over  $9 \times 10^4$  trajectories for the four-fold symmetric web map.

instants

$$\{t_k\} = \{T_0, T_1 = \lambda_T T_0, \dots, T_k = \lambda_T^k T_0, \dots\}. \quad (12.24)$$

and the corresponding set of intervals

$$\{\delta t_k\} = \{\hat{t} - t_k\} = \{\hat{t} - T_0 \lambda_T^k\}, \quad (12.25)$$

where  $\hat{t}$  means that  $t$  is taken in the vicinity of the instants  $t_k$ , that is,

$$t_k < \hat{t} \ll t_{k+1}. \quad (12.26)$$

For the survival probability we can write the renormalization equation in the form

$$\begin{aligned} \Psi(\delta t_{k+1}; \Delta \Gamma_{k+1}) \Delta \Gamma_{k+1} &= \lambda_T \Psi\left(\frac{1}{\lambda_T} \delta t_{k+1}; \Delta \Gamma_k\right) \Delta \Gamma_k \\ &= \lambda_T \Psi(\delta t_k; \Delta \Gamma_k) \Delta \Gamma_k, \quad (t \rightarrow \infty) \end{aligned} \quad (12.27)$$

which differs from a usual form of the renormalization equation by the factors  $\Delta \Gamma_j$ . We also use the relation

$$\delta t_{k+1} = \hat{t} - t_{k+1} = \lambda_T (\hat{t} - t_k) \quad (12.28)$$

(see definition (12.25)). The appearance of  $\Delta \Gamma_j$  can be interpreted as a conservation of the normalized number of escaping trajectories for the islands of different generations (compare to (12.1)).

The following steps are very formal. For the asymptotics (12.4) we have

$$\Psi(\delta t_{k+1}; \Delta \Gamma_{k+1}) \sim \frac{C_1}{(\hat{t} - t_{k+1})^{\gamma_{\text{esc}} - 1}} \quad (12.29)$$

and from (12.27) it follows the condition

$$\frac{\lambda_T}{\lambda_\Gamma} \frac{1}{\lambda_T^{\gamma_{\text{esc}} - 1}} = 1 \quad (12.30)$$

up to the slow varying in time terms. Finally, (12.30) gives

$$\gamma_{\text{esc}} = 2 + \frac{|\ln \lambda_\Gamma|}{\ln \lambda_T} = 2 + \mu_\Gamma, \quad (12.31)$$

where  $\mu_\Gamma$  is the same as in (12.17). For  $t \rightarrow \infty$  and the only singular zone, we have also

$$\gamma_{\text{rec}} = \gamma_{\text{esc}} = 2 + \mu_\Gamma \quad (12.32)$$

as an additional important information on the hierarchical-islands trap. From (12.23) it follows that

$$\mu \equiv \frac{|\ln \lambda_S|}{\ln \lambda_T} = \mu_\Gamma \quad (12.33)$$

and

$$\gamma_{\text{rec}} = 2 + \mu = 2 + \frac{|\ln \lambda_S|}{\ln \lambda_T}. \quad (12.34)$$

Parameter  $\mu$  is known as the transport exponent due to reasons that will appear later. Figure 12.6 demonstrates the self-similarity of the HIT. Three almost identical curves are shifted by a value of  $\ln \lambda_T \approx 2.2$  as should occur from the renormalization equation (12.27).

The hierarchical structures in phase space and self-similarity of time that trajectories spend in the structures make a solid basis for an origin of fractal time. This will be considered in detail in Chapter 13.

## 12.4 Stochastic layer trap

The HIT, described above, is an example of a well-structured part of the phase space where the dynamics can be described in a fairly predictable way. Opposite to this case is the almost unpredictable and not well understood case when a trajectory can be trapped in a stochastic layer without any well-described structure for an arbitrary long time. We call this structure the *stochastic layer trap* (Note 12.4).

The main features of the stochastic layer trap can be understood from Fig. 12.7. Let an island with one elliptic point be embedded into the stochastic sea. After a change of the control parameter, a bifurcation appears that creates two additional elliptic and hyperbolic points. The separatrices are destroyed (split) by the perturbation and they are replaced by an exponentially narrow stochastic layer. As we continue to change the control parameter, the width of the stochastic layer becomes larger. An important feature of the pattern in Fig. 12.7 is that the stochastic layer is separated from the stochastic sea. By a small change of the control parameter, we can achieve a merge of the stochastic layer to the stochastic sea as can be seen on the bottom of Fig. 12.7. An intersection area of the merge can be arbitrarily small and therefore a probability of crossing the border can be arbitrarily small. The domain of the former stochastic layer is a trap, and a trajectory that enters the trap can spend an astronomical time there.

An example for the standard map is given in Fig. 12.8. While part (a) of Fig. 12.8 does not show a big difference from part (a) of Fig. 11.6, the sequence of resonances that is resolved in Fig. 12.8 is 1-3-7-9-10 and after that we see in part (d) of Fig. 12.8 a different situation. The dark strip in (c) and (d) of Fig. 12.8 corresponds to a trajectory trapped for an extremely long time near a high order islands-chain. The simulations show the escape from the strip after

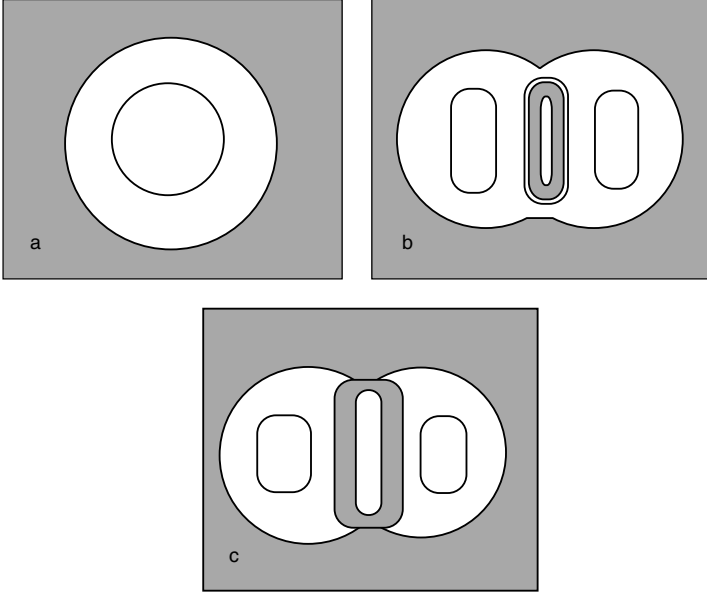


FIG. 12.7. Appearance of the stochastic layer trap as a result of a bifurcation.

$10^6$ – $10^7$  iterations. This means that we need trajectories with at least two more orders (i.e.  $N \sim 10^8$ – $10^9$ ) to find an escape exponent  $\gamma_{\text{esc}}(A)$  for the part  $A$  of phase space that corresponds to the stochastic layer (dark strip area) in Fig. 12.8. A simple estimate can help to find a time of pure ballistic dynamics due to the trapping. Let

$$\langle p^{2m} \rangle \sim \langle p^{2m} \rangle_{\text{anom}} + \langle p^{2m} \rangle_{\text{ball}}, \quad (12.35)$$

where the first term corresponds to the trajectories and their parts that participate in the so-called anomalous diffusion that will be considered later, and the second term corresponds to the ballistic trajectories. Rewriting (12.35) as

$$\langle p^{2m} \rangle \sim N t^{\mu(m)} + \delta N \cdot t^{2m} \quad (12.36)$$

with  $\delta N$  as a number of ballistic trajectories, and  $N$  as a number of the others, we have a condition when the second term suppresses the non-ballistic diffusion:

$$t^{2m-\mu(m)} \gtrsim \frac{N}{\delta N} \sim N \quad (12.37)$$

or

$$(2 - \mu(1))m \gtrsim \frac{\ln N}{\ln t}. \quad (12.38)$$



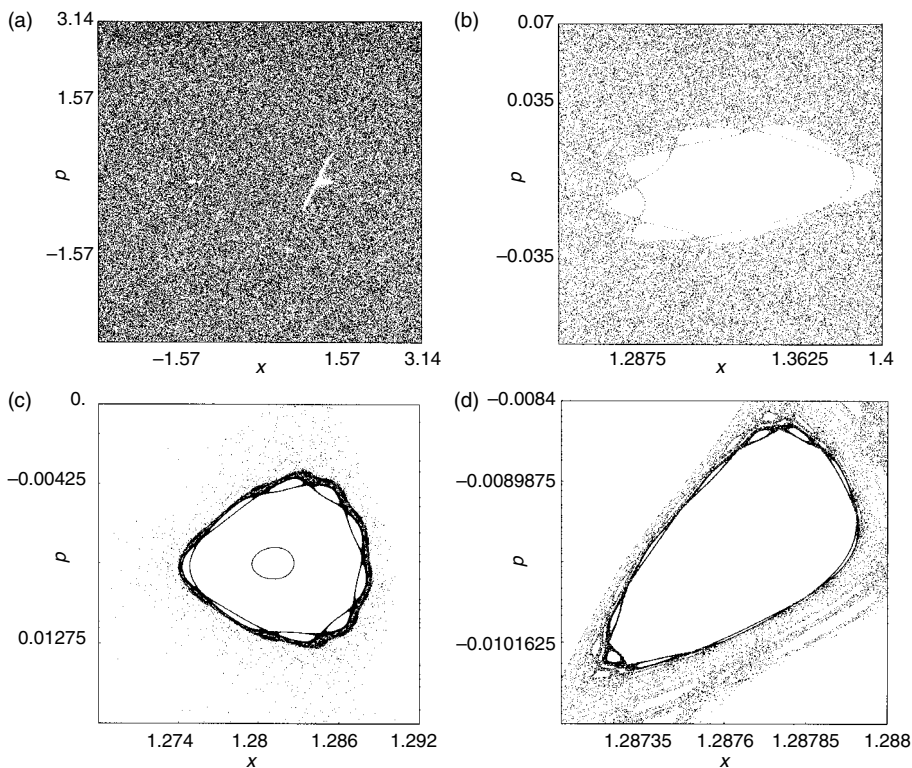


FIG. 12.8. Stochastic layer trap for the standard map with  $K = 6.9115$ .

For  $t \sim 10^7$ ,  $N \sim 10^6$ , and  $\mu(m) \sim 1.5m$ , we obtain  $m \gtrsim 2$ , i.e. even one long-trapped trajectory with the ballistic dynamics can influence the values of high moments. Similar situations were described in (Afanasiev *et al.* (1991)) where we called a bundle of the long-staying together trajectories as *stochastic jets* (Note 12.5).

## Notes

### Note 12.1

The material of this section related to the traps is based on the publications Zaslavsky *et al.* (1997); Zaslavsky and Edelman (1997); Zaslavsky (1995, 2002a). See also a review paper (Zaslavsky (2002b)).

*Note 12.2*

There are many publications related to the Sinai and Bunimovich billiards and to the estimate (12.9) confirmed numerically (Bunimovich and Sinai (1973, 1981); Machta and Zwanzig (1983); Zacherl *et al.* (1986)). The results in Figs. 9.3, 9.5, and 12.2 are from Zaslavsky and Edelman (1997, 2004). Some rigorous results on the Sinai billiard can be found in Young (1998) and Chernov and Young (2000).

*Note 12.3*

Hierarchical-islands traps were defined in Zaslavsky (1995), and observations of them are found in Zaslavsky and Niyazov (1997); Zaslavsky *et al.* (1997); Benkadda *et al.* (1997); White *et al.* (1998); Kassibrakis *et al.* (1998) for both the standard and web maps. For advection see Zaslavsky *et al.* (1993) and Kuznetsov and Zaslavsky (1998, 2000).

*Note 12.4*

The stochastic layer trap was discussed in Petrovichev *et al.* (1990) for the problem of particle advection in Beltrami flow and in Rakhlin (2000) for the problem of electron dynamics in the magnetic field and periodic lattice. Some recent publications are Aurell *et al.* (1997) and Zaslavsky (2002a). There is not yet a quantitative description of this trap.

*Note 12.5*

For stochastic (chaotic) jets, see more in Leoncini and Zaslavsky (2002).

*This page intentionally left blank*

## FRACTAL TIME

*Fractal time* can be considered as one of the most important concepts in the description of fractal properties of chaotic dynamics. One can consider any time series as a set of samples  $\{t_j\}$  imbedded into one-dimensional space and determine the box or Hausdorff dimension of the set. The notion of fractal time was coined in Berger and Mandelbrot (1963) to characterize transmission in telephone networks. Some time later the notion of fractal time was linked to the intrinsic structure of the set  $\{t_j\}$  and the so-called *Bernoulli scaling* and *Weierstrass random walk* (Montroll and Shlesinger (1984); Shlesinger and Hughes (1981); Shlesinger (1988)). This new concept of the origin of fractal time appears to be crucial for dynamical systems resembling the situation with hierarchical island traps and other structures in phase space. Depending on the choice of the set  $\{t_j\}$ , one can consider structural properties of different physical nature and develop a new kind of analysis of dynamical systems (*Note 13.1*).

### 13.1 Fractal time

A quick way to introduce the notion of fractal time is to consider a set of events ordered in time and to apply a notion of fractal dimension to the set of time instants  $\{t_j\}$ . However, this method is too formal and not representative enough. In previous sections, it was shown that for chaotic trajectories the distribution of exit times and Poincaré recurrences possess the self-similarity property in large time asymptotics, and that corresponding power-like tails were described in Chapters 11 and 12. It was also mentioned that a power-like tail in the time events distribution leads to the divergence in moments.

The idea of considering the random processes of infinite moments is historically related to the so-called St Petersburg Paradox of Nicolas Bernoulli. It is based on a special scaling known as the ‘Bernoulli scaling’ (*Note 13.2*). When the time events  $\{\tau_j\}$  are scaled as

$$\{\tau_j\} = \{\tau, b\tau, b^2\tau, \dots\} \quad (13.1)$$

the probability of having an event  $\tau_j = b^j\tau$  is scaled as

$$p_j(\tau) = c^j p(b^j\tau) \quad (13.2)$$

with some scale parameters  $b, c$ . Expressions (13.1) and (13.2) can be interpreted as follows: there are different ways to escape from the domain  $\Delta\Gamma$  and each  $j$ -th

way is described by the probability density  $p_j(\tau)$ . Hence the probability density of escaping in time  $t \geq \tau$  is

$$\psi(\tau) = \sum_{j=0}^{\infty} p_j(\tau) = \sum_{j=0}^{\infty} c^j p(b^j \tau) \quad (13.3)$$

with the normalization condition

$$\int_0^{\infty} \psi(\tau) d\tau = 1. \quad (13.4)$$

In the St Petersburg Paradox, Bernoulli had considered the tossing of a coin. The  $j$ -th event is a set of  $j$  unsuccessful tail flips until the first head appears. The corresponding probability is  $p_j = (1/2)^{j+1}$ . The winning award was  $d^j$  so that the mean winning is

$$\langle d \rangle = \sum_{j=1}^{\infty} d^j p_j = \frac{1}{2} \sum_{j=1}^{\infty} (d/2)^j, \quad (13.5)$$

which diverges if  $d \geq 2$ . Similarly, it is possible that  $\langle d \rangle < \infty$  but  $\langle d^2 \rangle = \infty$  if  $d \geq 2^{1/2}$ , etc.

Fractal properties of the exit time distribution can be demonstrated using a model for (13.3) considered by Shlesinger and Hughes (1981):

$$\psi(t) = \frac{1-a}{a} \sum_{j=1}^{\infty} (ab)^j \exp(-b^j t), \quad a, b < 1, \quad (13.6)$$

that has a fairly simple physical interpretation. If  $\psi(t)$  is a probability density to escape from a domain at time  $t$ , then the survival probability for the time  $t$  is

$$\Psi(t) = \int_t^{\infty} dt' \psi(t') = \frac{1-a}{a} \sum_{k=1}^{\infty} a^k \exp(-b^k t) \quad (13.7)$$

with the natural normalization condition

$$\Psi(0) = 1. \quad (13.8)$$

The parameter  $b$  defines a scale of the survival time, and  $a^k < 1$  can be considered as a probability to have the survival time scale  $b^k$ , that is, the survival probability  $\Psi(t)$  is a sum of the survival with all possible time scales.

Performing a Laplace transform of (13.6) we obtain

$$\psi(s) = \int_0^{\infty} e^{-st} \psi(t) dt = \frac{1-a}{a} \sum_{k=1}^{\infty} \frac{a^k}{s + b^k} \quad (13.9)$$

with a rescaling identity

$$\psi(s) = a\psi\left(\frac{s}{b}\right) + \frac{1-a}{a} \frac{ab}{b+s}. \quad (13.10)$$

The solution of the homogeneous part of the equation

$$\psi^*(s) = a\psi^*\left(\frac{s}{b}\right) \quad (13.11)$$

is the only one that can be a singular one. Equation (13.10) is a typical equation of the *renormalization group*, and it will be considered in detail in Section 15.5. Here we just mention that

$$\psi^*(s) = s^{\beta'} K(s), \quad (13.12)$$

where  $K(s)$  is a slow varying function of  $s$  and

$$\beta' = \frac{\ln a}{\ln b}. \quad (13.13)$$

Inverse transform of (13.12) gives the asymptotics

$$\psi^*(t) \sim \frac{1}{t^{1+\beta'}}, \quad (t \rightarrow \infty), \quad (13.14)$$

that is,

$$\gamma_{\text{esc}} = 1 + \beta' = 1 + \frac{\ln a}{\ln b}. \quad (13.15)$$

The importance of the result (13.14) is in expressing of the escape exponent  $\gamma_{\text{esc}}$  through the structure parameters  $a$  and  $b$  that define the process of the escape from the domain.

Particularly,

$$\tau_{\text{esc}} = \int_0^\infty t\psi(t)dt = -\left.\frac{\partial\psi^*}{\partial s}\right|_{s=0} = \begin{cases} \infty, & \beta' \leq 1, \\ < \infty, & \beta' > 1, \end{cases} \quad (13.16)$$

i.e. mean time of escape is finite for  $\gamma_{\text{esc}} > 2$ . This conclusion does not contradict the Kac lemma for Hamiltonian dynamics, and it shows the finite  $\tau_{\text{esc}}$  with  $\gamma_{\text{esc}} > 2$ .

But according to the Kac lemma, other results are impossible in Hamiltonian bounded dynamics, i.e.  $\beta' < 1$  is impossible and the described model cannot be a model of fractal time in Hamiltonian dynamics. We are very close to the model of the hierarchical island trap for a scaling, similar to the Bernoulli one, and in the next section we demonstrate a more general approach.

### 13.2 Fractal and multifractal recurrences

For Hamiltonian systems with chaotic dynamics, the motion is not ergodic in the full phase space and one needs to subtract a (multi-) fractal set of islands to obtain a domain with ergodic chaotic trajectories. The islands form a singular part of the phase space. The behaviour of the trajectories near an island boundary layer was discussed in Chapters 9 and 12. It was shown that for some values of the control parameter, the set of islands is a fractal object which imposes a power-wise distribution of different time-dependent characteristics in large time asymptotics. More specifically, the boundary of the island is sticky, with that of the sub-islands being more sticky and so forth. Consequently, the fractal space-time properties of the trajectories should be examined. We encounter a new situation in which: (i) fractal properties exist simultaneously in space and time; and (ii) the multiplicity of the sets of resonances that generate islands corresponds to a multifractal construction of the trajectories rather than to a fractal one.

This section describes the multifractal time and the corresponding spectral function of dimensions. In general for chaotic dynamics the fractal time cannot be introduced without a consideration of the space structure. For that reason, space-time coupling is non-trivial and the same is true of the spectral function of the fractal dimensions. One needs to extend the methods described in Section 10.4 in such a way that they permit a consideration of the phase space and time instants of the events related to a chaotic trajectory as a (multi-) fractal object. As an event, one can again take the particle trajectory that enters a cell, which is a part of the annulus in Fig. 12.5, and spends some time there before escaping from the cell. This process was described in Section 12.3. Also, for some values of the control parameter  $K$  in the standard map and web map, the self-similarities of the islands' area and the periods of their last invariant curves were demonstrated in Section 12.3. However, a more general way of considering the hierarchical structures is needed.

Using space-time partitioning, which was introduced in Fig. 12.5 and resembles the Sierpinski carpet (Fig. 10.1), the central square is assumed to be an island of zero-generation. The island is then surrounded by an annulus which represents the boundary island layer. It consists of  $g_1$  ( $g_1 = 8$  in Fig. 12.4) sub-islands of the first generation (smaller islands in Fig. 12.4). We can partition the annulus by  $g_1$  domains in the same manner as in Fig. 12.5 so that each of them includes exactly one island of the first generation. Each of the first generation island is then surrounded by an annulus of the second generation. The process is repeated, after which the segments are squared. On the  $n$ -th step, the structure is described by a 'word':

$$w_n = w(g_1, g_2, \dots, g_n). \quad (13.17)$$

The full number of islands on the  $n$ -th step is

$$N_n = g_1 \dots g_n \quad (13.18)$$

and any island from the  $n$ -th generation can be labeled as

$$u_i^{(n)} = u(i_1, i_2, \dots, i_n), \quad 1 \leq i_j \leq g_n, \quad \forall n. \quad (13.19)$$

Let us introduce a time that a particle spends in the boundary layer of an island. This time,

$$T_i^{(n)} = T(u_i^{(n)}) \quad (13.20)$$

carries all information on the  $n$ -th generation islands (13.17)–(13.19). By introducing a *residence time* for each island boundary layer, a new situation arises, compared to the plain Sierpinski carpet or a plain fractal situation because of the non-triviality of space-time coupling. In fact, an additional parameter responsible for the temporal behaviour is attached to a simple geometric construction similar to the Cantor-set.

A simplified situation corresponds to the exact self-similarity of the construction described above, that is,

$$\begin{aligned} S_i^{(n)} &= S^{(n)} = \lambda_S^n \cdot S^{(0)}, & (\forall i), \\ T_i^{(n)} &= T^{(n)} = \lambda_T^n \cdot T^{(0)}, & (\forall i), \end{aligned} \quad (13.21)$$

where  $S_i^{(n)}$  is the area of an island,  $u_i^{(n)}$ ,  $T_i^{(n)}$  are introduced in (13.20), and the sign  $\forall i$  is related to the same generation. The expressions (13.21) correspond to equal areas and *residence times* for all islands of the same generation. Two scaling parameters,  $\lambda_S$  and  $\lambda_T$ , represent the existence of the exact self-similarity in space and time respectively. Such a situation was described in Section 12.2 for the standard map and web map with

$$\lambda_S < 1, \quad \lambda_T > 1. \quad (13.22)$$

In addition to (13.22) there is a self-similarity in the islands' proliferation, that is,

$$g_n = \lambda_g g_0, \quad \lambda_g \geq 3 \forall n. \quad (13.23)$$

It follows from (13.18) and (13.23) that

$$N_n = \lambda_g^n g_0 = \lambda_g^n \quad (13.24)$$

if it begins with a single island ( $g_0 = 1$ ). It is useful to introduce a *residence frequency*,

$$\omega_i^{(n)} = \frac{1}{T_i^{(n)}} \quad (13.25)$$

with the self-similarity property

$$\omega_i^{(n)} = \omega^{(n)} = \lambda_T^{-n} \omega^{(0)} = \frac{\lambda_T^{-n}}{T^{(0)}} \quad (13.26)$$



for all  $i$  of the same generation. Consider the partition which corresponds to conditions (13.17)–(13.20) with a simplification (13.23), and for which the  $n$ -th level corresponds to that of the islands' hierarchy. This means that each space bin has an area  $S_i^{(n)}$  and a co-joint residence time  $T_i^{(n)}$  (both are defined in (13.21)) whose values do not depend on  $i$  within the same generation. The elementary probability of spending time  $T_i^{(n)}$  in the domain  $S_i^{(n)}$  can be presented in a simple form as

$$P_i^{(n)} \equiv P_{i_1, i_2, \dots, i_n} = C_n \omega_i^{(n)} S_i^{(n)}, \quad 1 \leq i_j \leq g_n, \quad \forall n, \quad (13.27)$$

where  $C_n$  is a normalization constant. Calling  $P_i^{(n)}$  an elementary bin-probability and using (13.21), (13.22) and (13.25), one can rewrite (13.27) as

$$P_i^{(n)} = C_n \left( \frac{\lambda_S}{\lambda_T} \right)^n, \quad (\forall i). \quad (13.28)$$

Having expression (13.28), one can consider different sums and partition functions. For example, in the sum

$$\begin{aligned} Z^{(n)} &= \sum_{i_1, \dots, i_n} P_i^{(n)} = C_n \sum_{i_1, \dots, i_n} \omega_i^{(n)} S_i^{(n)} = C_n \sum_{i_1, \dots, i_n} \exp[-n(|\ln \lambda_S| + \ln \lambda_T)] \\ &= \sum_{i_1, \dots, i_n} \exp[-n(|\ln \lambda_S| + \ln \lambda_T) + n\mathcal{F}_n] = 1, \end{aligned} \quad (13.29)$$

where the 'free energy' density

$$\mathcal{F}_n = \frac{1}{n} \ln C_n \quad (13.30)$$

is introduced, and the number of terms in (13.29) follows from (13.24). Therefore, in the limit  $n \rightarrow \infty$ , one obtains

$$\lim_{n \rightarrow \infty} \mathcal{F}_n = \mathcal{F} = |\ln \lambda_S| + \ln \lambda_T - \ln \lambda_g. \quad (13.31)$$

A more precise formulation of the result (13.31) is that the sum in (13.29) diverges if  $\mathcal{F}_n > \mathcal{F}$ , converges to zero if  $\mathcal{F}_n < \mathcal{F}$ , and converges to one if  $\mathcal{F}_n = \mathcal{F}$ .

In the case when the proliferation of islands does not follow a simple rule (13.23) and we should consider (13.18), it is necessary to apply the steepest descent method to (13.29) and consider an equation

$$|\ln \lambda_S| + \ln \lambda_T = \frac{d}{dn}(n\mathcal{F}_n) = \frac{1}{C_n} \frac{dC_n}{dn}. \quad (13.32)$$

It defines an extremum value  $n^*$  and the corresponding value for free energy  $\mathcal{F}_{n^*}$ . The value

$$\mathcal{F}_{n^*} = \lim_{n \rightarrow \infty} \frac{1}{n} \sum_{k=1}^n \ln g_k + |\ln \lambda_S| + \ln \lambda_T = \frac{1}{n^*} \ln C_{n^*} \quad (13.33)$$

replaces (13.31), and the value  $n^*$  provides an effective cut-off of the hierarchy of islands. In this case the infinite number of the islands proliferation effectively does not exist.

The goal of these manipulations is to describe a method of partitioning and a way of operating using a corresponding sum, such as  $Z^{(n)}$ , in the case when a bin of the partition should be defined by its phase space location or volume, and by the residence time. On the basis of this information, we can introduce a multifractal spectrum for the recurrence time set.

### 13.3 Multifractal space-time and its dimension spectrum

It was mentioned already that chaotic dynamical systems with rich sets of islands have a multifractal rather than fractal space-time structure. This section introduces a spectral function of dimensions which is analogous to Section 10.4.

Following a method common in statistical mechanics, let us introduce a partition function in the form of

$$Z^{(n)}\{\lambda_T, \lambda_S; q\} = \sum_{i_1, i_2, \dots, i_n} (\omega_i^{(n)} S_i^{(n)})^{\gamma q}. \quad (13.34)$$

Here the space-time partitioning probability  $\omega_i^{(n)} S_i^{(n)}$  to stay in a cell  $i$  is similar to (13.27), and  $\gamma$  is a parameter of the bins. Considering a multi-scaling situation, it is assumed that the real elementary probability of occupying a bin has the same scaling dependence as (13.27) up to a power of  $\gamma$ , and that there are different values of  $\gamma$  in the sum. With the exponent  $q$ , one can consider different moments of the elementary bin probability. In particular, for  $q = 0$ , the sum simply defines a number of bins. Replace summation by integration in (13.34)

$$Z^{(n)}\{\lambda_T, \lambda_S; q\} = \int d\gamma \rho(\gamma) [\omega^{(n)} S^{(n)}]^{-f(\gamma) + \gamma q}, \quad (13.35)$$

where we introduce a density of the space-time bins

$$dN^{(n)}(\gamma) = d\gamma \rho(\gamma) [\omega^{(n)} S^{(n)}]^{-f(\gamma)}. \quad (13.36)$$

The function  $f(\gamma)$  is a spectral function of the space-time dimension-like characteristics, or simply, dimensions. The distribution density  $\rho(\gamma)$  is a slow function of  $\gamma$ . To be more accurate, it is also assumed that the bin-probability  $\omega^{(n)} S^{(n)}$  depends on  $\gamma$ . This is because for different island-sets, the bins have different structures.

Consider again a simplified situation when (13.21) and (13.26) are valid. Then (13.35) is transformed into

$$Z^{(n)}\{\lambda_T, \lambda_S; q\} = \int d\gamma \rho(\gamma) \exp\{-n[\gamma q - f(\gamma)](|\ln \lambda_S| + \ln \lambda_T)\}, \quad (13.37)$$

where  $\lambda_S$  and  $\lambda_T$  are slow functions of  $\gamma$ . For  $n \rightarrow \infty$ , the standard steepest descent procedure yields

$$Z^{(n)}\{\lambda_T, \lambda_S; q\} \sim \exp\{-n[\gamma_0 q - f(\gamma_0)](|\ln \lambda_S| + \ln \lambda_T)\}, \quad (13.38)$$

where  $\gamma_0 = \gamma_0(q, \lambda_S, \lambda_T)$  satisfies the equation

$$q = f'(\gamma_0). \quad (13.39)$$

On the other hand, recall that for  $q = 0$ , expression (13.34) defines  $Z^{(n)}\{\lambda_T, \lambda_S; 0\}$  as the number of bins. For the one-scale situation, this number can be derived from (13.24) as  $\lambda_g^n$ . In the multifractal case, a power of  $\lambda_g^n$  can be written by introducing a generalized dimension,  $D_q$ , which was done in Section 10.4:

$$Z^{(n)}\{\lambda_S, \lambda_T; q\} \sim \lambda_g^{-n(q-1)D_q} \sim \exp\{-n \ln \lambda_g \cdot (q-1)D_q\}. \quad (13.40)$$

The scaling parameter  $\lambda_g$  defines a coefficient of the proliferation of space-time bins and one can therefore consider

$$\lambda_g = \lambda_g(\lambda_T, \lambda_S), \quad (13.41)$$

that is, we consider dynamical systems with only two independent scaling parameters. This restriction is not important and, if necessary, it can be very easily lifted.

A comparison of (13.40) and (13.38) gives

$$(q-1)D_q \cdot \ln \lambda_g = [\gamma_0 q - f(\gamma_0)](\ln \lambda_T + |\ln \lambda_S|). \quad (13.42)$$

In some limit cases,  $\lambda_g$  in (13.41) should satisfy the following conditions:

$$\lambda_g = \begin{cases} |\lambda_S|, & \text{if } \lambda_T = 1, \\ \lambda_T, & \text{if } \lambda_S = 1. \end{cases} \quad (13.43)$$

Then we arrive at the standard situation of one-parametric scaling. For a general situation  $\lambda_g, \lambda_T, \lambda_S \neq 1$ , and (13.42) is rewritten in its final form as

$$(q-1)D_q = \frac{\ln \lambda_T}{\ln \lambda_g} (1 + \mu) [\gamma_0 q - f(\gamma_0)], \quad (13.44)$$

where the parameter

$$\mu = \frac{|\ln \lambda_S|}{\ln \lambda_T} \quad (13.45)$$

was introduced in (12.35).

It follows from (13.44) that for  $q = 0$ ,

$$D_0 = \frac{\ln \lambda_T}{\ln \lambda_g} (1 + \mu) \cdot f(\gamma_0). \quad (13.46)$$

This means that now there is no simple connection between the dimension  $D_0$  and the spectral function. The regular formula

$$D_0 = f(\gamma_0) \quad (13.47)$$

appears only in the case of (13.43) when a multi-fractal structure exists only in space or in time. For  $q = 1$ , the use of (13.39) and (13.44) yields

$$D_1 = \gamma_0(1) \cdot \frac{\ln \lambda_T}{\ln \lambda_g} (1 + \mu), \quad (13.48)$$

where the value  $\gamma_0(1) = \gamma_0(q = 1)$  can be obtained from (13.39):

$$f'(\gamma_0(q = 1)) = 1.$$

In (13.42), the generalized dimension  $D_q$  was expressed through the spectral function  $f(\gamma)$  (which was the case in Section 10.4). Nevertheless, the formulas (13.42), (13.44), (13.46), and (13.48) show that a knowledge of the spectral function is not sufficient to describe a typical dynamical system, and additional information on the structure of the system in space and time is therefore necessary. A simplification can be made in cases where  $\lambda_g, \lambda_S$  and  $\lambda_T$  are known for some special values of the control parameter.

### 13.4 Critical exponent for the Poincaré recurrences

This section examines the partitioning introduced in Section 13.2 (see Fig. 12.5) and recurrences or escapes from the boundary island layer of the  $n$ -th generation. The corresponding ‘number of states’ (13.27) normalized to the unit probability for a bin to be occupied by a particle, can be written as

$$Z_r^{(n)} = \sum_{i_1, \dots, i_n} \frac{1}{S_i^{(n)} \omega_i^{(n)}} = \sum_{i_1, \dots, i_n} \left( \frac{\lambda_T}{\lambda_S} \right)^n. \quad (13.49)$$

Instead of (13.49), we can consider a more general expression:

$$Z_r^{(n)}(q) = \sum_{i_1, \dots, i_n} \frac{1}{S_i^{(n)} [\omega_i^{(n)}]^q} = \sum_{i_1, \dots, i_n} \frac{\lambda_T^{nq}}{\lambda_S^n} \quad (13.50)$$

and the corresponding ‘grand sum’:

$$Z_r(q) = \sum_{n_0}^{\infty} Z_r^{(n)}(q), \quad (13.51)$$

where  $n_0$  is the number that corresponds to the order of a resonance at the beginning of the ‘word’ in (13.17).

Using (13.24) we obtain the following estimate

$$Z_r(q) \sim \sum_{n_0}^{\infty} \exp\{n(q \ln \lambda_T + |\ln \lambda_S| + \ln \lambda_g)\}. \quad (13.52)$$

The expression can be simplified if  $\lambda_g = \lambda_T$ , that is, the proliferation coefficient for the number of islands coincides with the scaling of periods. Hence

$$Z_r(q) \sim \sum_{n_0}^{\infty} \exp\{n[(q+1) \ln \lambda_T + |\ln \lambda_S|]\}. \quad (13.53)$$

This expression is finite if

$$q \leq q_c = -\frac{(|\ln \lambda_S| + \ln \lambda_T)}{\ln \lambda_T} = -(1 + \mu). \quad (13.54)$$

The result obtained has a remarkable interpretation.

Consider a powerwise probability density for the recurrences

$$P_{\text{rec}}(t) \sim \frac{1}{t^{\gamma_{\text{rec}}}}, \quad (t \rightarrow \infty) \quad (13.55)$$

and the corresponding integral probability

$$P_{\text{rec}}^{\text{int}}(t) = \int_t^{\infty} dt' P(t') \sim \frac{1}{t^{\gamma_{\text{rec}}-1}}, \quad (t \rightarrow \infty) \quad (13.56)$$

to have recurrence after time larger than  $t$ .

From another side, we can consider the sum (13.51) as having the same probability as (13.56) defined on the fractal time support

$$T_i^{(n)} = \frac{1}{\omega_i^{(n)}}, \quad \forall i, \quad n \in [n_0, \infty). \quad (13.57)$$

Then the permitted power of  $T_i$  is  $q \leq q_c < 0$ . Due to the negative value of  $q_c$ , the time asymptotics for  $Z_r(q)$  and  $t \rightarrow \infty$  is defined by the  $Z_r(q_c)$ , that is,

$$Z_r(T) \sim \frac{1}{T^{|q_c|}}, \quad (t \rightarrow \infty), \quad (13.58)$$

where ‘ $i$ ’ and ‘ $n$ ’ are omitted. If  $Z_r(T)$  and  $P_{\text{rec}}^{\text{int}}(t)$  have the same meanings in  $t \rightarrow \infty$ , then

$$\gamma_{\text{rec}} - 1 = |q_c| \quad (13.59)$$

and, after comparing (13.59) and (13.54), it follows a connection

$$\gamma_{\text{rec}} = 2 + \mu = 2 + \frac{|\ln \lambda_S|}{\ln \lambda_T}. \quad (13.60)$$

This result was obtained before from a consideration of the hierarchical islands trap in Section 12.3. In Chapter 16 we will see how this expression appears in the anomalous transport problem for which  $\mu$  is the so-called transport exponent. The expression (13.60) provides the connection between recurrence and transport exponents.

## Notes

### *Note 13.1*

For the notion of fractal time in dynamical systems, see Zaslavsky (1984, 1987); Afraimovich (1997); Afraimovich and Zaslavsky (1997); and the review Zaslavsky (2002b).

### *Note 13.2*

The notion of the Bernoulli scaling was introduced by M. Shlesinger. For more information on the St Petersburg Paradox and Bernoulli scaling, see Montroll and Shlesinger (1984).

## Problems

*13.1* Derive (13.10) from (13.7) and (13.9).

*This page intentionally left blank*

PART 3

CHAOTIC KINETICS



*This page intentionally left blank*

## GENERAL PRINCIPLES OF KINETICS

The first detailed approach to the kinetic description of many particle systems appeared in the famous works of Boltzmann (1872, 1895, 1898). The main idea of the derivation of a kinetic equation is to describe a complex system dynamics using a reduced number of variables. For example, a complete description of a dynamical system can be done with a Liouville equation:

$$\frac{\partial F}{\partial t} + \dot{\boldsymbol{\vartheta}} \cdot \frac{\partial F}{\partial \boldsymbol{\vartheta}} + \dot{\mathbf{I}} \cdot \frac{\partial F}{\partial \mathbf{I}} = 0, \quad (14.1)$$

where  $\mathbf{I} \in \mathbb{R}^N$ ,  $\boldsymbol{\vartheta} \in \mathbb{R}^N$ ,  $F = F(\mathbf{I}, \boldsymbol{\vartheta}, t)$  is the density distribution function in phase space, and  $(\mathbf{I}, \boldsymbol{\vartheta})$  satisfy the Hamiltonian equations. There are two typical reductions of variables:

- (i) averaging over fast variables, phase  $\boldsymbol{\vartheta}$ , and the corresponding transition

$$F = F(\mathbf{I}, \boldsymbol{\vartheta}, t) \rightarrow F(\mathbf{I}, t) \quad (14.2)$$

- (ii) transition from  $N$ -degrees of freedom to one degree of freedom

$$F(\mathbf{I}, t) \rightarrow F(I, t), \quad I \in \mathbb{R}. \quad (14.3)$$

All approaches and methods exploit a randomness of the dynamics in explicit or implicit form and due to the fact all kinetic equations acquire a remarkable feature, *irreversibility*, and they satisfy the so-called  $H$ -theorem that also has been discovered by Boltzmann (*Note 14.1*).

Dynamical chaos gives rise to a new vision of the basic principles of kinetics. The main feature of a new wave in kinetic theories is that the random element of the dynamics can be found directly from the Hamiltonian equation of motion, in contrast to introducing randomness as an assumption. New models of the kinetic theory are sometimes very different from the previously known types of kinetic equations, and this will be the subject of the following chapters (*Note 14.2*).

### 14.1 Time scales

All approximate methods of the derivation of kinetics require a differentiation of time-scales. Here are presented the most typical ones.

The collision time  $\tau_{\text{coll}}$  characterizes the duration of a ‘collision’ of a particle with external object or field. Typically this time shows how long a perturbation

acts on the particle. As a result of this action, there is a change of variables  $\Delta I, \Delta \vartheta$ . The value  $\Delta t_{\text{coll}}$  is the time interval between two adjacent collisions. A ‘good’ situation is when

$$\tau_{\text{coll}} \ll \Delta t_{\text{coll}}, \quad (14.4)$$

which means that particle dynamics can be considered as unperturbed, that is, free, between any two adjacent collisions. The introduction of the notion of ‘collision time’ is meaningful only in the case (14.4). It also permits to introduce a map

$$(I_{n+1}, \vartheta_{n+1}) = \hat{T}_n(I_n, \vartheta_n) \quad (14.5)$$

or in a more specific form

$$\begin{aligned} I_{n+1} &= I_n + f_1(I_n, \vartheta_n), \\ \vartheta_{n+1} &= \vartheta_n + \omega_n \Delta t_n + f_2(I_n, T_n), \end{aligned} \quad (14.6)$$

where  $f_1, f_2$  are some functions related to the perturbation,  $\omega_n$  is frequency, and  $\Delta t_n$  is a time interval between  $n$ -th and  $(n+1)$ -th collisions. For example, in the standard map

$$f_2 = f_1 = K \sin \vartheta_n, \quad \Delta t_n = \text{const} = T, \quad \omega_n = \frac{I_n}{T} \quad (14.7)$$

and the condition (14.4) is automatically valid since  $\tau_{\text{coll}} = 0$ .

As a result of perturbation, one can expect the occurrence of chaotic dynamics that has at least two time-scales. The first one is a time  $\tau_c$  of the decay of phase correlations. In the good mixing or Anosov-type systems it is of the order

$$\tau_c \sim \frac{\Delta t}{h} \sim \frac{\Delta t}{\sigma}, \quad (14.8)$$

where  $h$  is KS-entropy and  $\sigma$  is a dimensionless Lyapunov exponent. For some cases of the standard map and  $K \gg 1$

$$\tau_c = \frac{2T}{\ln K}, \quad (14.9)$$

that is, less than a time  $\Delta t = T$  between collisions. The second time, due to chaos, describes a slow evolution of the action variable  $I_n$ . Typically, this time  $\tau_d$  satisfies the condition

$$\tau_d \gg \tau_c \quad (14.10)$$

and is known as *diffusion time*.

How these time scales work will be demonstrated using some simple examples, but our main emphasis is that for typical Hamiltonian dynamics the described

scheme is very insufficient due to the presence of singular zones, dynamical traps, etc. Just these deviations from regular (or normal) kinetics make it necessary to extend the class of possible equations to the so-called fractal kinetic equations (*Note 14.3*).

## 14.2 Fokker–Planck–Kolmogorov (FPK) equation

The FPK equation was obtained by Fokker (1914), Smolukhowski (1915), Einstein (1905), and Planck (1917). Landau (1937) and Kolmogorov (1938) derived the kinetic equation using a special scheme and conditions that are important for understanding some basic principles of kinetics (*Note 14.4*). Let  $W(x, t; x', t')$  be a probability density of having a particle at the position  $x$  at time  $t$  if the particle was at the position  $x'$  at time  $t' \leq t$ . A chain equation of the Markov-type process can be written for  $W(x, t; x', t')$ :

$$W(x_3, t_3; x_1, t_1) = \int dx_2 W(x_3, t_3; x_2, t_2) W(x_2, t_2; x_1, t_1), \quad (14.11)$$

which has a simple meaning that the transition  $(x_1, t_1) \rightarrow (x_3, t_3)$  can go through all possible states  $(x_2, t_2)$ .

A typical assumption for  $W$  is its time uniformity, i.e.:

$$W(x, t; x', t') = W(x, x'; t - t'). \quad (14.12)$$

Consider the evolution of  $W(x, x'; t - t')$  during an infinitesimal time  $\Delta t = t' - t$  and use the expansion

$$W(x, x_0; t + \Delta t) = W(x, x_0; t) + \frac{\partial W(x, x_0; t)}{\partial t} \Delta t + \dots \quad (14.13)$$

Equation (14.13) is valid providing the limit:

$$\lim_{\Delta t \rightarrow 0} \frac{1}{\Delta t} \{W(x, x_0; t + \Delta t) - W(x, x_0; t)\} = \frac{\partial W(x, x_0; t)}{\partial t} \quad (14.14)$$

has a sense. The existence of the limit (14.14) for  $\Delta t \rightarrow 0$  imposes specific physical constraints that will be discussed in Section 14.4.

Let us now introduce a new notation:

$$P(x, t) \equiv W(x, x_0; t), \quad (14.15)$$

where the initial coordinate  $x_0$  is omitted. With the help of Eqs. (14.11)–(14.13), we can transform (14.14) into:

$$\frac{\partial P(x, t)}{\partial t} = \lim_{\Delta t \rightarrow 0} \frac{1}{\Delta t} \left\{ \int dy W(x, y; \Delta t) P(y, t) - P(x, t) \right\}. \quad (14.16)$$

The first important feature in the derivation of the kinetic equation is the introduction of two distribution functions  $P(x, t)$  and  $W(x, y; \Delta t)$  instead of the one  $W(x, t; x', t')$ . The function  $P(x, t)$  will be used for  $t \rightarrow \infty$  or, more accurately, for  $t$  which satisfies the condition

$$t \gg \tau_{\text{coll}}, \quad (14.17)$$

where  $\tau_{\text{coll}}$  is not defined yet. In this situation  $W(x, x_0; t)$  does not depend on the initial condition  $x_0$  and this explains the notation (14.15). Contrary to  $P(x, t)$ ,  $W(x, y; \Delta t)$  defines the transition during very short time  $\Delta t \rightarrow 0$ . For  $\Delta t = 0$  it should be no transition at all if the velocity is finite, i.e.:

$$\lim_{\Delta t \rightarrow 0} W(x, y; \Delta t) = \delta(x - y). \quad (14.18)$$

Following this restriction we can use the expansion over  $\delta$ -function and its derivatives (Zaslavsky 1994a; Zaslavsky 1994b), i.e.:

$$W(x, y; \Delta t) = \delta(x - y) + A(y; \Delta t)\delta'(x - y) + \frac{1}{2}B(y; \Delta t)\delta''(x - y), \quad (14.19)$$

where  $A(y; \Delta t)$  and  $B(y; \Delta t)$  are some functions. The prime denotes a derivative with respect to the argument, and we consider the expansion up to the second order only.

Distribution  $W(x, y; \Delta t)$  is called *transfer probability* and it satisfies two normalization conditions:

$$\int W(x, y; \Delta t) dx = 1 \quad (14.20)$$

and

$$\int W(x, y; \Delta t) dy = 1. \quad (14.21)$$

The coefficients  $A(x; \Delta t)$  and  $B(x; \Delta t)$  have a fairly simple meaning. They can be expressed as moments of  $W(x, y; \Delta t)$ :

$$\begin{aligned} A(y; \Delta t) &= \int dx (y - x) W(x, y; \Delta t) \equiv \langle\langle \Delta y \rangle\rangle, \\ B(y; \Delta t) &= \int dx (y - x)^2 W(x, y; \Delta t) \equiv \langle\langle (\Delta y)^2 \rangle\rangle. \end{aligned} \quad (14.22)$$

In a similar way, coefficients for the higher orders of the expansion of  $W(x, y; \Delta t)$  can be expressed through the higher moments of  $W$ .

Integration of (14.19) over  $x$  does not provide any additional information due to (14.20), but integrating over  $y$  and using (14.21) gives:

$$A(y; \Delta t) = \frac{1}{2} \frac{\partial B(y; \Delta t)}{\partial y} \quad (14.23)$$

or applying the notations (14.22),

$$\langle\langle\Delta y\rangle\rangle = \frac{1}{2} \frac{\partial}{\partial y} \langle\langle(\Delta y)^2\rangle\rangle. \quad (14.24)$$

Expressions (14.23) and (14.24) were first obtained in Landau (1937) as a result of the *microscopic reversibility*, or detailed balance principle. In Landau (1937), dynamical Hamiltonian equations were used for (14.24), while here we use the expansion (14.19) and ‘reversible’ normalization (14.21). The final step is an assumption that we name the following existing limits *Kolmogorov conditions*:

$$\begin{aligned} \lim_{\Delta t \rightarrow 0} \frac{1}{\Delta t} \langle\langle\Delta x\rangle\rangle &\equiv \mathcal{A}(x), \\ \lim_{\Delta t \rightarrow 0} \frac{1}{\Delta t} \langle\langle(\Delta x)^2\rangle\rangle &\equiv \mathcal{B}(x), \\ \lim_{\Delta t \rightarrow 0} \frac{1}{\Delta t} \langle\langle(\Delta x)^m\rangle\rangle &= 0, \quad (m > 2). \end{aligned} \quad (14.25)$$

It is due to the Kolmogorov conditions that irreversibility appears at the final equation. Now it is just formal steps. Substituting (14.19), (14.22), and (14.24) into (14.16) gives

$$\frac{\partial P(x, t)}{\partial t} = -\frac{\partial}{\partial x} (\mathcal{A}P(x, t)) + \frac{1}{2} \frac{\partial^2}{\partial x^2} (\mathcal{B}P(x, t)), \quad (14.26)$$

which is the equation derived by Kolmogorov and which is called the Fokker–Planck–Kolmogorov (FPK) equation. It is a diffusion-type equation and it is irreversible. After using the relations (14.23) and (14.24) we get the diffusion equation (14.26) in the final form:

$$\frac{\partial P(x, t)}{\partial t} = \frac{1}{2} \frac{\partial}{\partial x} \mathcal{D} \frac{\partial P(x, t)}{\partial x} \quad (14.27)$$

with a *diffusion coefficient*

$$\mathcal{D} = \mathcal{B} = \lim_{\Delta t \rightarrow 0} \frac{\langle\langle(\Delta x)^2\rangle\rangle}{\Delta t}. \quad (14.28)$$

Equation (14.27) has a divergent form that corresponds to the conservation law of the number of particles:

$$\frac{\partial P}{\partial t} = \frac{\partial J}{\partial x} \quad (14.29)$$

with the particle flux

$$J = \frac{1}{2} \mathcal{D} \frac{\partial P}{\partial x}. \quad (14.30)$$

In the following section we will see how a similar scheme can be applied to derive the fractional kinetic equation.

An additional condition follows from (14.24) and notations (14.25) and (14.28)

$$\mathcal{A}(x) = \frac{1}{2} \frac{\partial \mathcal{B}(x)}{\partial x} = \frac{1}{2} \frac{\partial \mathcal{D}}{\partial x}, \quad (14.31)$$

which explains a physical meaning of  $\mathcal{A}(x)$  as a convective part of the particle flux. This part of the flux and  $\mathcal{A}(x)$  are zero if  $\mathcal{D} = \text{const}$  (*Note 14.5*).

### 14.3 Detailed balance principle

The divergent form (14.27) of the FPK equation is a particular case of (14.26). This form appears due to some symmetry of the moments that follows from (14.23) or (14.24). In its turn, (14.23) is a result of the expansion (14.19) with symmetry conditions (14.20) and (14.21) for the transitional probability. Such condition of symmetry is known as the *detailed balance principle*, and its connection to the divergent form of the kinetic equation was shown by Landau (1937). Landau also has shown in the same paper a simple way to derive (14.24) based on the uniformity of the phase distribution.

Let the Hamiltonian of a system be  $H = H(I, \vartheta; t)$  and let us calculate a change of action  $I$  during a small time interval  $\Delta t$  up to the terms of the order  $(\Delta t)^2$ . It follows:

$$\begin{aligned} \Delta I &= I(t + \Delta t) - I(t) = \dot{I} \Delta t + \frac{1}{2} \ddot{I} (\Delta t)^2 \\ &= -\frac{\partial H}{\partial \vartheta} \Delta t - \frac{1}{2} \left\{ \frac{\partial}{\partial \vartheta} \frac{\partial H}{\partial t} + \frac{\partial^2 H}{\partial \vartheta^2} \frac{\partial H}{\partial I} - \frac{\partial^2 H}{\partial I \partial \vartheta} \frac{\partial H}{\partial \vartheta} \right\} (\Delta t)^2, \end{aligned} \quad (14.32)$$

where the Hamiltonian equations

$$\dot{I} = -\frac{\partial H}{\partial \vartheta}, \quad \dot{\vartheta} = \frac{\partial H}{\partial I}, \quad (14.33)$$

have been used and the operator has been applied

$$\frac{d}{dt} = \frac{\partial}{\partial t} + \dot{I} \frac{\partial}{\partial I} + \dot{\vartheta} \frac{\partial}{\partial \vartheta}. \quad (14.34)$$

Finally, (14.32) transfers into

$$\Delta I = -\frac{\partial H}{\partial \vartheta} \Delta t - \frac{1}{2} \frac{\partial}{\partial \vartheta} \left[ \frac{\partial H}{\partial t} - \dot{I} \vartheta \right] (\Delta t)^2 + \frac{1}{2} \frac{\partial}{\partial I} (\dot{I})^2 (\Delta t)^2. \quad (14.35)$$

We are interested in the coarse-grained, that is, phase averaged, observables. The phase averaging means

$$\langle\langle \cdots \rangle\rangle = \frac{1}{2\pi} \int_0^{2\pi} d\vartheta \cdots \quad (14.36)$$

that is, any expression that can be presented as  $\vartheta$ -derivative of some function vanishes after applying (14.36). Thus, up to  $(\Delta t)^2$ ,

$$\begin{aligned} \langle\langle \Delta I \rangle\rangle &= \frac{1}{2} \frac{\partial}{\partial I} \langle\langle \dot{I}^2 \rangle\rangle (\Delta t)^2, \\ \langle\langle (\Delta I)^2 \rangle\rangle &= \langle\langle \dot{I}^2 \rangle\rangle (\Delta t)^2. \end{aligned} \quad (14.37)$$

It follows from (14.15) that

$$\langle\langle \Delta I \rangle\rangle = \frac{1}{2} \frac{\partial}{\partial I} \langle\langle (\Delta I)^2 \rangle\rangle \quad (14.38)$$

be known as a consequence of the *detailed balance* principle, that is, that the probabilities of some transition from a state  $A$  to  $B$  are the same as for the transition from  $B$  to  $A$ . The expression (14.38) is similar to the expression (14.24) derived directly from the symmetry of definitions (14.22).

Here we have also to comment that in the proposed qualitative derivation of (14.38) phase averaging that leads to (14.38) is not supported by any microscopic consideration and the way to do it is fairly lengthy. It is also important to mention that  $\langle\langle \Delta I \rangle\rangle$  and  $\langle\langle (\Delta I)^2 \rangle\rangle$  are of the same order of magnitude.

#### 14.4 Solutions and normal transport

There are numerous sources related to the solutions of the FPK equation (14.27) for different initial and boundary conditions (see for example Weiss (1994); Risken (1989)). Our goal here is just to mention a few simple properties of the FPK equation which are important for the future.

Let us simplify the case considering  $\mathcal{D} = \text{const}$ ,  $x \in (-\infty, \infty)$ , and the initial condition for a particle to be at  $x = 0$ . Then

$$P(x, t) = (2\pi \mathcal{D} t)^{-1/2} \exp\left(-\frac{x^2}{2\mathcal{D} t}\right), \quad (14.39)$$

known as a Gaussian distribution. Its odd moments are zero, the second moment is

$$\langle x^2 \rangle = \mathcal{D} t \quad (14.40)$$

and the higher moments are

$$\langle x^{2m} \rangle = \mathcal{D}_m t^m, \quad (m = 1, 2, \dots), \quad (14.41)$$



where  $\mathcal{D}_{m=1} = \mathcal{D}$  and  $\mathcal{D}_{m>1}$  can be easily expressed through  $\mathcal{D}$  but they do not depend on  $t$ . (See Problems 14.1–14.3.) There are two properties that we will refer to in the following section: all moments of  $P(x, t)$  are finite, as a result of the exponential decay of  $P$  for  $x \rightarrow \infty$ , and the distribution  $P(x, t)$  is invariant under the renormalization

$$\hat{R}(a) : x' = ax, \quad t' = a^2 t \quad (14.42)$$

with arbitrary  $a$ , that is, the renormalization group  $\hat{R}(a)$  is continuous. Evolution of moments  $\langle x^m \rangle$  with time will be called *transport*. Dependence (14.40) and (14.41) will be called *normal transport*.

Another type of the distribution function is the so-called moving Gaussian packet

$$P(x, t) = (2\pi\mathcal{D}t)^{-1/2} \exp \left[ -\frac{(x - ct)^2}{2\mathcal{D}t} \right] \quad (14.43)$$

with a velocity  $c$ . The distribution (14.43) satisfies the equation

$$\frac{\partial P}{\partial t} + c \frac{\partial P}{\partial x} = \frac{1}{2} \mathcal{D} \frac{\partial^2 P}{\partial x^2} \quad (14.44)$$

for which the condition (14.23) or (14.31) fails. They can be restored if we consider the moments  $\langle (x - ct)^m \rangle$ . It follows from (14.43) that

$$\langle x \rangle = ct \quad (14.45)$$

and

$$\langle (x - \langle x \rangle)^2 \rangle = \mathcal{D}t \quad (14.46)$$

similarly to (14.40).

## 14.5 Growth of entropy

Consider the magnitude

$$\mathcal{S}_B = -\langle \ln P(x, t) \rangle = - \int_{-\infty}^{\infty} dx P(x, t) \ln P(x, t) \quad (14.47)$$

known as Boltzmann's entropy, and calculate its time evolution

$$\dot{\mathcal{S}}_B = -\frac{d}{dt} \langle \ln P(x, t) \rangle = - \int_{-\infty}^{\infty} dx \frac{\partial P(x, t)}{\partial t} - \int_{-\infty}^{\infty} dx \frac{\partial P(x, t)}{\partial t} \ln P(x, t). \quad (14.48)$$

The first term in the right-hand side is zero due to the normalization condition

$$\int_{-\infty}^{\infty} dx \frac{\partial P(x, t)}{\partial t} = \frac{d}{dt} \int_{-\infty}^{\infty} dx P(x, t) = 0. \quad (14.49)$$

The second term in (14.48) can be modified by using (14.27):

$$\begin{aligned} \int_{-\infty}^{\infty} dx \frac{\partial P(x, t)}{\partial t} \ln P(x, t) &= \frac{1}{2} \int_{-\infty}^{\infty} dx \ln P(x, t) \frac{\partial}{\partial x} \left\{ \mathcal{D} \frac{\partial P(x, t)}{\partial x} \right\} \\ &= -\frac{1}{2} \int_{-\infty}^{\infty} dx \frac{\mathcal{D}}{P(x, t)} \left[ \frac{\partial P(x, t)}{\partial x} \right]^2. \end{aligned} \quad (14.50)$$

From the definition (14.28)  $\mathcal{D} > 0$ . Since  $P(x, t) > 0$  we conclude

$$\frac{d\mathcal{S}_B}{dt} = -\frac{d}{dt} \langle \ln P(x, t) \rangle \geq 0. \quad (14.51)$$

The magnitude  $\mathcal{S}_B$  defined in (14.47) is called *entropy*, and the result (14.51) represents the so-called *H*-theorem of Boltzmann applied to the FPK equation (Note 14.6).

The *H*-theorem is a specific signature of kinetic equations. We can consider the existence of the property (14.51) as an indication of a ‘normal form’ of the kinetic equations. At the equilibrium  $\mathcal{S}_B$  reaches its maximum and  $\dot{\mathcal{S}}_B = 0$ .

The description of dynamic systems with chaotic trajectories needs more sophisticated types of kinetics for which the divergent form does not exist and/or the inequality (14.51) may not be valid. All these topics will be discussed in the forthcoming chapters (see also Problem 14.4).

## 14.6 Kolmogorov conditions and conflict with dynamics

A perfect mathematical scheme often has constraints which limit its application to real phenomena. Constraints related to the Kolmogorov conditions (14.25) are very important for all problems related to the anomalous transport that will be discussed in the forthcoming chapter. Consider the limit  $\delta t \rightarrow 0$  and an infinitesimal displacement  $\delta x$  along a particle trajectory that corresponds to this limit. Then  $\delta x / \delta t \rightarrow v$  where  $v$  is the particle velocity, and the conditions (14.25) with the notation (14.28) gives

$$\frac{(\delta x)^2}{\delta t} = v^2 \delta t = \mathcal{D} = \text{const}. \quad (14.52)$$

This means that  $v$  should be infinite in the limit  $\delta t \rightarrow 0$ , which makes no physical sense.

Another manifestation of the conflict can be obtained directly from the solution (14.39) to the FPK equation. This solution satisfies the initial condition

$$P(x, 0) = \delta(x), \quad (14.53)$$

that is, a particle is at the origin at  $t = 0$ . For any finite time  $t$  solution (14.39) or (14.43) has non-zero probability of the particle to be at any arbitrary distant point  $x$ , which means the same: the existence of infinite velocities to propagate from  $x = 0$  to  $x \rightarrow \infty$  during an arbitrary small time interval  $t$ . A formal acceptance of this result appeals to the exponentially small input from the propagation with infinite velocities. A physical approach to the obstacle in using the FPK equation is to abandon the limit  $\Delta t \rightarrow 0$  in (14.25), to introduce  $\min \Delta t$ , and to consider a limit

$$\frac{t}{\min \Delta t} \rightarrow \infty. \quad (14.54)$$

A more serious question is how to use (14.54) and how the FPK equation can be applied to real dynamics. Let us demonstrate the answer using the standard map (5.13) as an example.

As was mentioned in Section 5.2, the map (5.13) corresponds to a periodically kicked particle dynamics, that is,  $\min \Delta t = 1$  in dimensionless variables. For  $K \gg 1$  one can consider variable  $x$  to be random with almost uniform distribution in the interval  $(0, 2\pi)$  (*Note 14.7*). Then

$$\begin{aligned} \langle \langle \sin x \rangle \rangle &= 0, & \langle \langle \sin^2 x \rangle \rangle &= \frac{1}{2} \\ \Delta p_n \equiv p_{n+1} - p_n, & \quad \langle \langle \Delta p_n \rangle \rangle = 0, & \quad \langle \langle (\Delta p_n)^2 \rangle \rangle &= \frac{K^2}{2}, \end{aligned} \quad (14.55)$$

where double brackets  $\langle \langle \dots \rangle \rangle$  means averaging over  $x$ , and one can write the corresponding FPK equation with respect to the slowly varying momentum  $p$ :

$$\frac{\partial P(p, t)}{\partial t} = \frac{1}{2} \mathcal{D}(K) \frac{\partial^2 P(p, t)}{\partial p^2} \quad (14.56)$$

with

$$\mathcal{D}(K) = \frac{K^2}{2}. \quad (14.57)$$

Equation (14.56) provides the normal transport. Particularly

$$\langle p^2 \rangle = \frac{1}{2} K^2 t. \quad (14.58)$$

More sophisticated analysis gives for  $\mathcal{D}(K)$  an oscillating behaviour

$$\mathcal{D}(K) = K^2 \left( \frac{1}{2} - J_2(K) \right) \quad (14.59)$$

with  $J_2(K)$  as the Bessel function. Due to the presence of the Bessel function, the diffusion coefficient  $\mathcal{D}(K)$  oscillates as a function of  $K$ . The oscillations were observed numerically in Chirikov (1979). Their theory is known as the

*Rechester–White diffusion.* It keeps the same equation (14.56), and changes only  $\mathcal{D}(K)$ . (See Rechester and White (1980); Rechester *et al.* (1981)). More serious changes to the diffusional equation will be discussed in Chapter 16. Our main goal here is to show how the described conflict can be eliminated using truncated distributions.

## 14.7 Truncated distributions

A general scheme to perform a simulation of the problem of diffusion and transport for given dynamical equations is to select a set of initial points in phase space  $\{x_0, p_0, t = 0\}$  and let them move until a large time  $t$ . Then for different time instants  $t_1, t_2, \dots, t$  one can collect points into bins located in phase space and create a distribution function  $P(x, p, t_j)$  or its projections  $P(x, t_j)$ ,  $P(p, t_j)$ . All these distributions are always truncated by some values  $x_{\max}$ , and  $p_{\max}$  because velocities of trajectories for all initial conditions are bounded during the finite time interval  $(0, t)$ . For a fairly large  $t$  we can split, for example,  $P(p, t)$  into two parts:

$$P(p, t) = P_{\text{core}}(p, t) + P_{\text{tail}}(p, t) \quad (14.60)$$

and calculate the corresponding moments

$$\langle p^m \rangle = \langle p^m \rangle_{\text{core}} + \langle p^m \rangle_{\text{tail}}. \quad (14.61)$$

Let us estimate the second term in (14.61).

Assume that  $p^*$  is the point of splitting of  $P(p, t)$  into the core and tail parts. Then

$$\langle p^m \rangle_{\text{tail}} = \int_{p^*}^{p_{\max}} dp p^m P(p, t) < (p_{\max})^m P(p^*, t). \quad (14.62)$$

For the Gaussian distribution  $P(p^*, t)$  is exponentially small and we can neglect  $\langle p^m \rangle_{\text{tail}}$  independently on  $m$ . This resolves the paradox with the Kolmogorov conditions for the solutions of Gaussian type. The situation is different if for large values of  $p$  the distribution function behaves algebraically, that is,

$$P(p, t) \sim \frac{c(t)}{p^{\delta_p}}, \quad (p \rightarrow \infty). \quad (14.63)$$

All moments  $\langle p^m \rangle$  diverge for  $m \geq \delta_p - 1$  and estimate (14.62) should be replaced by

$$\langle p^m \rangle_{\text{tail}} = \frac{c(t)}{m - \delta_p + 1} p_{\max}^{m - \delta_p + 1} \rightarrow \infty, \quad (p_{\max} \rightarrow \infty). \quad (14.64)$$

Expression (14.64) shows that for the truncated distribution with an algebraic asymptotics, the time evolution of fairly large moments is defined through the

largest value of momentum that a particle can obtain during its dynamics. The result imposes some constraints on how large can  $m$  be for the given model with its  $\delta_p$  and for a selected observation time  $t$ . Opposite to the Gaussian case, we can neglect  $\langle p^m \rangle_{\text{core}}$  in (14.61).

A similar statement exists for the coordinate distribution function  $P(x, t)$  if its behaviour is algebraic for large  $x > 0$ , that is,

$$P(x, t) \sim \frac{c(t)}{x^{\delta_x}}, \quad (x \rightarrow \infty). \quad (14.65)$$

This consideration will be important when we consider anomalous transport in Chapter 16.

The distribution defined as

$$P(p, t) = \begin{cases} P^{(\text{tr})}(p, t), & 0 < p \leq p_{\text{max}}, \\ 0, & p > p_{\text{max}} \end{cases} \quad (14.66)$$

will be called *truncated distribution*, and the corresponding moments will be called *truncated moments*. Any kind of simulations of the direct dynamics deal only with the truncated distributions and moments.

Finally, we arrive at the following important constraints which are necessary for a realistic analysis of the dynamics:

$$\delta t \geq \delta t_{\text{min}}, \quad (x, p) \leq (x_{\text{max}}, p_{\text{max}}) \quad (14.67)$$

which means the infinitesimal time is bounded from below and the phase space variables are bounded from above. Other consequences of the truncation can be found in Ivanov *et al.* (2001).

## Notes

### Note 14.1

There exist plenty of books and papers that provide excellent presentations of the origin and improvement of the contemporary kinetic theory: from the original works of Boltzmann (1872, 1895, 1898); Ehrenfest and Ehrenfest (1911); Smolukhowski (1915); and Einstein (1905), to more sophisticated methods in Kac (1958) and Prigogine (1962). (See also the review and other references in Liboff (1998)). The transition (14.2) is known as the *random phase approximation*, and the transition (14.3) is known as the *one-particle approximation*. For more discussions, see Zaslavsky (1985).

### Note 14.2

Using the properties of dynamical equations to derive a kinetic equation was first performed by Boltzmann (1872, 1895). The theory of chaotic dynamics was formally involved into kinetic theory by Zaslavsky and Sagdeev (1967)

(see also in books Zaslavsky (1985); Sagdeev *et al.* (1988); Dorfman (1999); and Lichtenberg and Lieberman (1983)).

*Note 14.3*

For the review of fractional kinetics and the anomalous transport in Hamiltonian dynamics, see Zaslavsky (2002b).

*Note 14.4*

For the review of derivation, properties, and applications of the FPK equation, see Chandrasekhar (1943) and more recently Liboff (1998).

*Note 14.5*

The way to derive (14.27) is slightly different from what has been used in the original works of Kolmogorov and Landau, due to the use of expansion (14.19) over  $\delta$ -function and its derivatives.

*Note 14.6*

Boltzmann considered the expression

$$H = \langle \ln P \rangle = -S \leq 0$$

which explained the origin of the name of the  $H$ -theorem ( $H$  in Boltzmann's original work should not be confused with the Hamiltonian).

*Note 14.7*

In fact, in the vicinity of some arbitrary large values of  $K$  there are strong localized deviations from the uniformity. They will be considered in detail later. These deviations lead to the anomalous transport described by an equation that significantly differs from the FPK equation.

## Problems

More complicated problems are marked by (\*).

*14.1* Derive the solution (14.39) for (14.27) with  $\mathcal{D} = \text{const}$ ,  $P(x, t = 0) = \delta(x)$ ,  $x \in (-\infty, +\infty)$ .

*14.2\** Find an expression for the probability  $P(x_0, t_0 = 0; x_0, t)$  of the first return to a point  $x_0$  after time  $t$  (see Risken (1989)).

*14.3* Find a recurrent formula for the higher moments coefficients  $\mathcal{D}_m$  in (14.41).

*14.4\** Consider  $\dot{\mathcal{S}}_B$  with the definition of  $\mathcal{S}_B$  in (14.47), and the distribution function  $P(x, t)$  which satisfies (14.26). Find a condition of the validity of a monotonic entropy growth.

*This page intentionally left blank*

## LÉVY PROCESS, LÉVY FLIGHTS, AND WEIERSTRASS RANDOM WALK

Considering random processes one can model different situations with different levels of the dependence of events at different time instants, with different levels of memory and correlation between the events, and so on. This kind of an axiomatic approach to the kinetics of dynamical systems is hardly acceptable unless the intrinsic dynamical features will be involved into the random process model in an explicit way. From the very beginning of the investigation of chaos, there were observations of an intermittent character of the time behaviour of chaotic trajectories. It became clear that the models of Gaussian type process and normal diffusion were not always valid and there were many typical situations when simplified models of independent or weakly dependent random events must be abandoned (*Note 15.1*).

Different careful observations of Hamiltonian systems with chaotic dynamics impose the necessity of extending the tools to explain how the dynamics should be described and what kind of approximations fit better. The Gaussian distribution links to the so-called *large number law* are well-known: the sum of independent random variables is distributed in the same way as any of them. The uniqueness of the Gaussian distribution was reconsidered by Lévy (1937) who had formulated a new approach that can also be applied to distributions with infinite second moment. There is a nice description of the history of Lévy's discovery, as well as its relation to other probabilistic theories and to the St Petersburg paradox of Daniel Bernoulli in Montroll and Shlesinger (1984). It happened that the Lévy distribution and Lévy processes had a strong impact on different areas of scientific analysis including not only the probability theory, but also physics, economics, financial mathematics, geophysics, dynamical systems, and so on. Mandelbrot (1982) has indicated numerous applications of the Lévy distributions and coined a notion of *Lévy flights*.

It became clear that the ideas related to the Lévy processes can be important in the analysis of chaotic dynamics after some modification is applied. In this chapter, brief information about the Lévy processes will be introduced with an emphasis on which features of the process can be or cannot be used for the dynamically chaotic trajectories (*Note 15.2*).



### 15.1 Lévy distribution

Let  $P(x)$  be a normalized distribution of a random variable  $x$ , i.e.

$$\int_{-\infty}^{\infty} P(x) dx = 1 \quad (15.1)$$

with a characteristic function

$$P(q) = \int_{-\infty}^{\infty} dx e^{iqx} P(x). \quad (15.2)$$

Consider two different random variables  $x_1$  and  $x_2$  and their linear combination

$$cx_3 = c_1x_1 + c_2x_2, \quad c, c_1, c_2 > 0. \quad (15.3)$$

The law is called stable if all  $x_1, x_2, x_3$  are distributed due to the same function  $P(x_j)$ . Gaussian distribution

$$P_G(x) = (2\pi\sigma_d)^{-1/2} \exp\left(-\frac{x^2}{2\sigma_d}\right) \quad (15.4)$$

is an example of the stable distribution with a finite second moment

$$\sigma_d = \langle x^2 \rangle \quad (15.5)$$

(compare to (14.39)). Another class of solutions was found by Lévy (1937).

Let us write the equation

$$P(x_3)dx_3 = P(x_1)P(x_2)\delta\left(x_3 - \frac{c_1}{c}x_1 - \frac{c_2}{c}x_2\right)dx_1dx_2, \quad (15.6)$$

where the condition (15.3) has been used. Following the definition (15.2), one can write the equation for characteristic function

$$P(cq) = P(c_1q)P(c_2q) \quad (15.7)$$

or

$$\ln P(cq) = \ln P(c_1q) + \ln P(c_2q). \quad (15.8)$$

Equations (15.7) and (15.8) are functional ones with an evident solution

$$\ln P_\alpha(cq) = (cq)^\alpha = c^\alpha e^{-i\frac{\pi}{2}\alpha(1-\text{sign } q)}|q|^\alpha \quad (15.9)$$

and condition

$$\left(\frac{c_1}{c}\right)^\alpha + \left(\frac{c_2}{c}\right)^\alpha = 1 \quad (15.10)$$

which consists of an arbitrary parameter  $\alpha$ .

The distribution  $P_\alpha(x)$  with the characteristic function

$$P_\alpha(q) = \exp(-c|q|^\alpha) \quad (15.11)$$

is known as *Lévy distribution* with the *Lévy index*  $\alpha$ . For  $\alpha = 2$  we arrive at the Gaussian distribution  $P_G(x)$ . An important condition introduced by Lévy is

$$0 < \alpha \leq 2 \quad (15.12)$$

which guarantees positiveness of

$$P_\alpha(x) = \int dq e^{iqx} P_\alpha(q). \quad (15.13)$$

The case  $\alpha = 1$  is known as Cauchy distribution

$$P_1(x) = \frac{c}{\pi} \frac{1}{x^2 + c^2}. \quad (15.14)$$

An important case is the asymptotic of large  $|x|$

$$P_\alpha(x) \sim \frac{1}{\pi} \alpha c \Gamma(\alpha) \sin \frac{\pi\alpha}{2} \frac{1}{|x|^{\alpha+1}}, \quad (0 < \alpha < 2) \quad (15.15)$$

(*Note 15.3*). It shows that the moments of  $P_\alpha(x)$

$$\langle x^m \rangle = \int_{-\infty}^{\infty} dx x^m P_\alpha(x) \quad (15.16)$$

diverge for

$$m \geq \alpha, \quad (15.17)$$

that is,  $\langle x^2 \rangle = \infty$  and that is why the large number law does not work for the considered situation.

## 15.2 Lévy process

There are many different ways to introduce the Lévy process, i.e. a time-dependent process that at an infinitesimal time has the Lévy distribution of the process variable (Lévy (1937); Gnedenko and Kolmogorov (1959); Feller (1957); Uchaikin and Zolotarev (1999); Montroll and Shlesinger (1984)). Here we use a simplified version for the infinitely divisible processes described below.

Consider the transition probability density  $P(x_0, t_0; x_N, t_N)$  that satisfies the chain equation

$$\begin{aligned} P(x_0, t_0; x_N, t_N) &= \int dx_1 \dots dx_{N-1} P(x_0, t_0; x_1, t_1) \\ &\times P(x_1, t_1; x_2, t_2) \dots P(x_{N-1}, t_{N-1}; x_N, t_N) \end{aligned} \quad (15.18)$$

and put

$$t_{j+1} - t_j = \Delta t, \quad (\forall j); \quad t_N - t_0 = N\Delta t. \quad (15.19)$$

Assume that the process is uniform in time and space, i.e.

$$P(x_j, t_j; x_{j+1}, t_{j+1}) = P(x_{j+1} - x_j; t_{j+1} - t_j) = P(x_{j+1} - x_j; \Delta t). \quad (15.20)$$

Then (15.18) transforms into

$$P(x_N - x_0; N\Delta t) = \int dy_1 \dots dy_N P(y_1, \Delta t) \dots P(y_N; \Delta t), \quad (15.21)$$

where  $y_j = x_j - x_{j-1}$ ;  $j \geq 1$ .

By introducing the characteristic functions

$$\begin{aligned} P(q) &= \int dy_j e^{iqy_j} P(y_j; \Delta t), \quad (j \neq N), \quad (\forall j), \\ P_N(q) &= \int dy^{(N)} e^{iqy^{(N)}} P(y^{(N)}; N\Delta t), \quad y^{(N)} = \sum_1^N y_j = y_N - y_0, \end{aligned} \quad (15.22)$$

we obtain from (15.21)

$$P_N(q) = [P(q)]^N \quad (15.23)$$

(see Problem 15.1). Following the concept of stable distributions and using the expression (15.7), let us consider  $P(q)$  as a function of two parameters  $\alpha$  and  $c$  that will be defined later. Namely, change the notation

$$P(q) \rightarrow P_\alpha(q; \Delta c); \quad P_N(q) \rightarrow P_\alpha(q; c_N), \quad (15.24)$$

where  $\Delta c$  or  $c_N$  should replace  $c$  in (15.11). These equations are consistent if

$$c_N = N\Delta c = N\Delta t \cdot \frac{\Delta c}{\Delta t} \equiv cN\Delta t = ct \quad (15.25)$$

and (15.23) with notations (15.24) takes the form

$$P_\alpha(q; ct) = \exp(-cN\Delta t|q|^\alpha) \quad (15.26)$$

with  $t = N\Delta t$  and  $t_0 = 0$ . In the limit  $\Delta t \rightarrow 0$ ,  $N \rightarrow \infty$ ,  $N\Delta t = t$ , and  $c = \Delta c/\Delta t$  we arrive to the *characteristic function* of the *Lévy process*:

$$P_\alpha(q, t) = \exp(-ct|q|^\alpha). \quad (15.27)$$

The original Lévy process can be written as the inverse Fourier transform of (15.27)

$$P_\alpha(x, t) = \int dq e^{iqx - ct|q|^\alpha} \quad (15.28)$$

with the asymptotics for  $|x| \rightarrow \infty$  similar to (15.15)

$$P_\alpha(x, t) \sim \frac{1}{\pi} \alpha c \Gamma(\alpha) \sin \frac{\pi\alpha}{2} \cdot \frac{t}{|x|^{\alpha+1}}. \quad (15.29)$$

From (15.28) we have for the moment of order  $m$  (not necessarily integer)

$$\langle |x|^m \rangle = \infty, \quad m \geq \alpha \quad (15.30)$$

and, since  $\alpha < 2$ ,

$$\langle x^2 \rangle = \infty \quad (15.31)$$

for any  $t$ , in contrary to the Gaussian process.

There are different generalizations of Lévy distributions and Lévy processes that can be useful in applications. Mainly, they are related to the anisotropy of the distributions. For example

$$P_\alpha(q, \xi, c) = \exp \left\{ -c|q|^\alpha \left[ 1 + i\xi \operatorname{sign} q \cdot \tan \left( \frac{\pi\alpha}{2} \right) \right] \right\}, \quad \alpha \neq 1; \quad 0 < \alpha < 2 \quad (15.32)$$

with

$$\xi = \frac{c^+ - c^-}{c^+ + c^-}, \quad c = a_\alpha(c^+ + c^-), \quad (15.33)$$

where  $a_\alpha$  is a constant defined by the normalization condition and for  $\alpha = 1$ ,  $\tan(\pi\alpha/2)$  should be replaced by  $(\pi/2) \ln |q|$  (Note 15.4). Distribution (15.32) provides the asymptotics

$$P_\alpha(x, \xi, c) \sim \frac{c^\pm}{|x|^{\alpha+1}}. \quad (15.34)$$

Streaming distribution

$$P_\alpha(x, t) \sim \frac{\text{const}}{|x - vt|^{\alpha+1}} \quad (15.35)$$

was considered in Montroll and Shlesinger (1984). Another important generalization, the so-called Lévy walks (Shlesinger *et al.* (1987)) will be considered in Chapter 18.

### 15.3 Poincaré recurrences and Feller's theorems

In this section we describe some results formulated in Feller (1949). They show a connection between the Lévy processes and Poincaré recurrences. Although these results are not related directly to dynamical systems, the Poincaré recurrences distribution plays an important role in kinetics as we will see in following chapters. From that point, Feller's theorems are 'half-way' to the dynamics.

Consider a small domain  $A$  and recurrences to  $A$ . The recurrence time is the time interval between two subsequent crossings of the boundary of  $A$  by a trajectory of the particle on its way out of  $A$ . In bounded Hamiltonian dynamics the sequence of recurrence times  $\{t_j\} \equiv t_1, t_2, \dots, t_n, \dots$  is infinite for non-periodic orbits. It is assumed that  $t_j$  are mutually independent and they belong to the same class of events with all identical probability distribution function

$$P_{\text{rec}}(\tau) = \text{Prob}\{t_k = \tau\}, \quad (\forall k), \quad (15.36)$$

i.e. independent on  $k$ . The integrated probability of recurrences is

$$P_{\text{rec}}^{\text{int}}(t) = \int_0^t d\tau P_{\text{rec}}(\tau) \quad (15.37)$$

and

$$\Phi_S(t) = 1 - P_{\text{rec}}^{\text{int}}(t) = \int_t^\infty d\tau P_{\text{rec}}(\tau) \quad (15.38)$$

has a meaning of a probability that the recurrence time is  $\geq t$ , that is, the survival probability (probability to survive time  $t$  in  $A$ ).

Feller (1949) introduced two additional characteristics of the recurrences chain: sum of  $n$  recurrence times

$$S_n = t_1 + \dots + t_n \quad (15.39)$$

and number of the recurrences  $N_t$  during time interval  $(0, t)$ . An evident connection between them is

$$\text{Prob}\{N_t \geq n\} = \text{Prob}\{S_n \leq t\}. \quad (15.40)$$

Due to the Kac lemma the mean recurrence time  $\tau_{\text{rec}}$  is finite. Then under the conditions of independence of  $t_j$  and finiteness of  $\tau_{\text{rec}}$ , two following theorems are valid (Feller (1949)):

1. If  $\sigma_0^2 < \infty$  then for every fixed  $\xi$

$$\begin{aligned} \text{Prob}\{S_n - n\tau_{\text{rec}} \leq n^{1/2}\sigma_0\xi\} &\rightarrow \Phi(\xi) = (2\pi)^{-1/2} \int_{-\infty}^{\xi} dy \exp\left(-\frac{y^2}{2}\right), \\ \text{Prob}\left\{N_t \geq \frac{t}{\tau_{\text{rec}}} - t^{1/2} \frac{\sigma_0\xi}{\tau_{\text{rec}}^{3/2}}\right\} &\rightarrow \Phi(\xi), \end{aligned} \quad (15.41)$$

where

$$\sigma_0^2 = \langle (t_k - \langle t_k \rangle)^2 \rangle = \langle (t_k - \tau_{\text{rec}})^2 \rangle \quad (15.42)$$

and the connection from (15.40) has been used

$$n\tau_{\text{rec}} + n^{1/2}\sigma_0\xi = t. \quad (15.43)$$

A simple meaning of this theorem is that fluctuations of the recurrence time from its mean value  $\tau_{\text{rec}}$  are distributed due to the Gaussian law.

2. Let  $\Phi_S(t)$  in (15.38) has the asymptotics

$$\Phi_S(t) = \frac{1}{t^\alpha} h(t), \quad 0 < \alpha < 2 \quad (15.44)$$

with

$$\lim_{x \rightarrow \infty} \frac{h(cx)}{h(x)} = 1.$$

Then for  $1 < \alpha < 2$

$$\text{Prob} \left\{ N_t \geq \frac{t}{\tau_{\text{rec}}} - \frac{b_t}{\tau_{\text{rec}}^{(1+\alpha)/\alpha}} \xi \right\} \rightarrow P_\alpha(\xi), \quad (15.45)$$

that is, to the Lévy distribution with  $P_\alpha(\xi)$  from (15.15) and  $b_t$  to be obtained from the equation

$$\Phi_S(b_t) \sim \frac{1}{t^{1/\alpha}}. \quad (15.46)$$

Distribution (15.45) is *the only possible non-normal distribution for  $N_t$  and  $1 < \alpha < 2$* .

The last statement of the Feller's theorem does not leave us any possibility to escape the Lévy distribution for physical problems since the conditions of the theorem are fairly broad. We do not put the case  $0 < \alpha < 1$  since it is forbidden due to the Kac lemma. Indeed, comparing (11.19), (15.38), and (15.44) we obtain  $\alpha = \gamma - 1$  and the condition  $\gamma > 2$  means  $\alpha > 1$ .

The presented theorems extend our information about a universality of distribution of the recurrence time fluctuations as random variables: for a finite dispersion  $\sigma_0^2$  they are distributed due to the Gaussian law, and for an infinite dispersion due to the Lévy law. Although the Gaussian or Lévy distributions can sometimes be a good approximation, the chaotic Hamiltonian dynamics show much more complicated processes.

## 15.4 Lévy flights and conflict with dynamics

The analysis of Chapters 11–13 shows that the distribution of Poincaré recurrences provides fairly detailed information about trajectories in phase space. In the previous section, a fairly strong statement imposes an alternative kind of

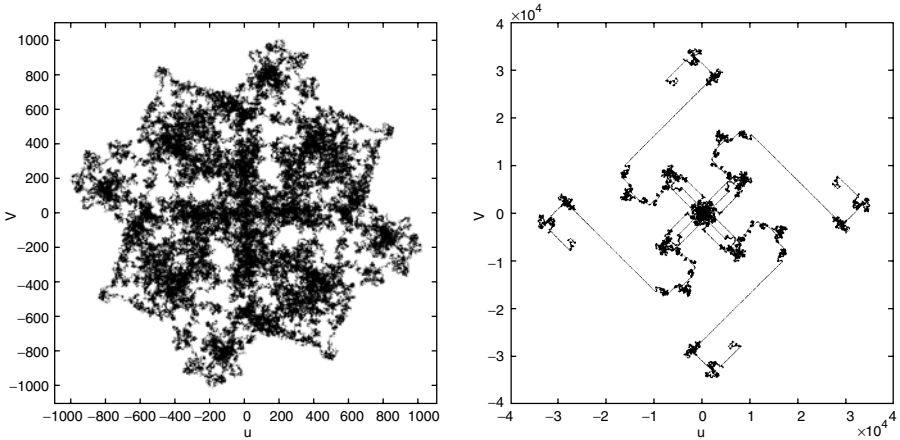


FIG. 15.1. Two samples of trajectories for the web map: trajectory without flights (left) for  $K = 5.001$ ; and trajectory with flights (right) for  $K = 6.349972$ .

time behaviour of independent events linked them to either Gaussian or Lévy type processes. What is the actual type of the process that is related to real dynamical systems?

Let us first provide a few demonstrations of trajectories of different types.

Figure 15.1 (Zaslavsky and Niyaziv (1997)) shows two different kinds of trajectories for the web map (5.35). They correspond to slightly different values of the control parameter  $K$ .

The qualitative difference is more drastic. On the left figure the trajectory makes a more or less uniform random walk in phase space, while on the right figure the trajectory exhibits ‘flights’ of a length of  $10^3$  or more. Similar quasi-regular pieces exist for the standard map, billiards, etc. These deviations from the uniform distribution of trajectories in phase space lead to a non-Gaussian diffusion with power-like asymptotical distribution of the displacements of trajectories.

Intermittency can be of different kind and, depending on that, different flights can appear. The example in Fig. 15.2 shows parabolic shape pieces of trajectories in phase space. They appear near a constant value of acceleration, that is, near the accelerator mode trajectory.

Another example is related to the ‘*Cassini billiard*’ which is a square table with the Cassini oval shape of the scatterer inside the square:

$$(x^2 + y^2)^2 - 2c^2(x^2 - y^2) - (a^4 - c^4) = 0,$$

where  $a, c$  are parameters of the oval.

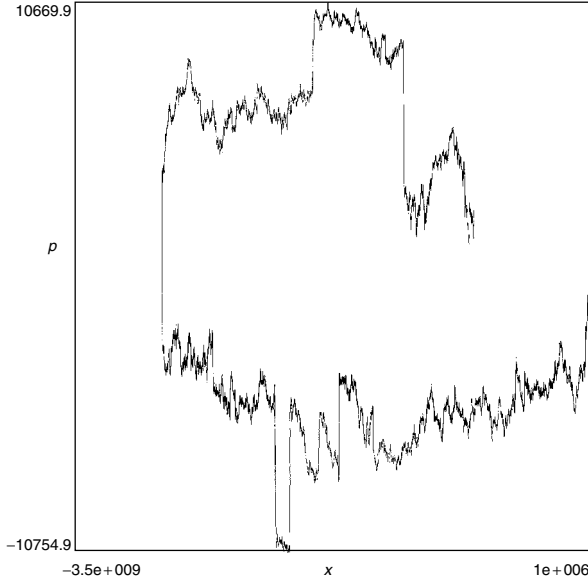


FIG. 15.2. Parabolic flights for the standard map  $K = 6.908745$ .

In Fig. 15.3 we can see stickiness in phase space (dark strips in part (a)) and flights in part (b) (*Note 15.5*). Magnifications of the phase space area near a sticky island are shown in Fig. 15.4. A sequence of zooms display a sequence of islands-around-islands  $4 - 8 - 4 - 8 - \dots$ . Two parameters can characterize the hierarchical dynamical trap related to the sticky area near the island's boundary:  $\Delta S_k$ -area of an island of  $k$ -th generation,  $T_k$ -period of the last invariant curve in an island of  $k$ -th generation. All these parameters are presented in Table 15.1. This also includes the initial two islands (in Fig. 15.3 we show only one of two central islands).

Table 15.1 also displays the values of proliferation coefficient  $q_k$  for the  $k$ -th generation, and the area

$$\delta S_k = q_k \Delta S_k \quad (15.47)$$

of all islands of  $k$ -th generation. In accordance with Section 12.2, two scaling parameters can be introduced in order to describe a self-similarity of the islands' hierarchy:

$$\begin{aligned} \lambda_S^{(k)} &= \frac{\delta S_k}{\delta S_{k-1}}, \\ \lambda_T^{(k)} &= \frac{T_k}{T_{k-1}} \end{aligned} \quad (15.48)$$



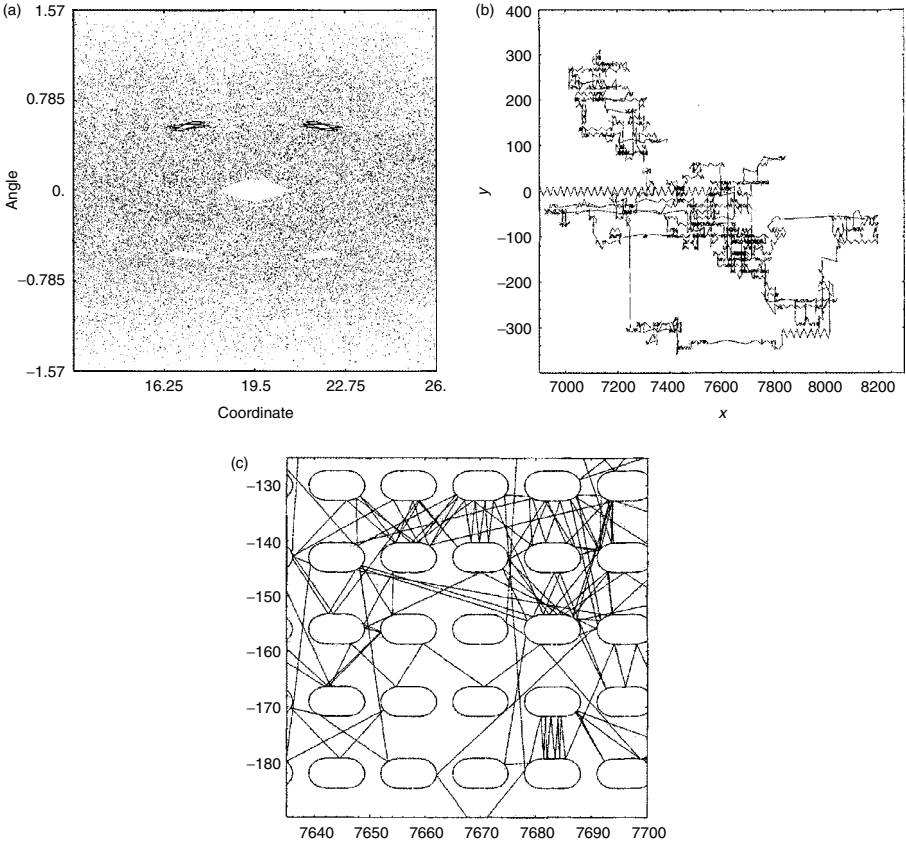


FIG. 15.3. One trajectory of the Cassini billiard: (a) Poincaré section in the phase space  $(x, \cos^{-1} v_x)$  on the torus; (b) the same trajectory in the coordinate space  $(x, y)$  of the corresponding Lorentz-type gas, i.e. a periodically continued set of scatterers in  $(x, y)$  directions; (c) magnification of the same as in (b) trajectory in  $(x, y)$  space. Parameters are  $a = 4.030952$ ;  $c = 3$ .

and the constant value  $q_k = q$  ( $\forall k \geq 1$ ) means the existence of constant (approximately) values of scaling parameters

$$\lambda_S^{(k)} = \lambda_S, \quad \lambda_T^{(k)} = \lambda_T, \quad (\forall k \geq 1). \quad (15.49)$$

In the case in Figs. 15.3 and 15.4 for the Cassini billiard we are faced with a new situation. It has two values of  $\lambda_S^{(1,2)}$  and  $\lambda_T^{(1,2)}$  which are found in Table 15.1:

$$\begin{aligned} \lambda_T^{(1)} &\sim 7.4, & \lambda_T^{(2)} &\sim 4.2, \\ \lambda_S^{(1)} &\sim 0.017, & \lambda_S^{(2)} &\sim 0.21, \end{aligned} \quad (15.50)$$

TABLE 15.1 Parameters  $\Delta S_k$ ,  $T_k$  of the island's hierarchy in the sequence  $4 - 8 - 4 - 8 - \dots$ .

$k$	$q_k$	$T_k$	$T_k/T_{k-1}$	$\Delta S_k$	$\Delta S_k/\Delta S_{k-1}$	$\delta S_k$	$\delta S_k/\delta S_{k-1}$
0	2	16.36	—	$1.47 \times 10^{-2}$	—	$2.94 \times 10^{-2}$	
1	4	118	7.21	$3.96 \times 10^{-3}$	$2.69 \times 10^{-2}$	$3.17 \times 10^{-2}$	1.08
2	8	508.9	4.31	$8.53 \times 10^{-6}$	$2.15 \times 10^{-3}$	$5.46 \times 10^{-4}$	0.017
3	4	3910	7.69	$4.4 \times 10^{-7}$	$5.2 \times 10^{-2}$	$1.1 \times 10^{-4}$	0.21
4	8	15 740	4.02	$0.96 \times 10^{-10}$	$2.2 \times 10^{-3}$	$2.0 \times 10^{-6}$	0.018

where the mean values are taken and  $\delta S_1/\delta S_0$  is skipped since it does not correspond to the set ( $q_0 \neq 8$ ). These values of the scaling parameters can be used to analyse the Poincaré recurrences distribution function in kinetics which will be discussed in Chapter 16. In particular, one can expect that there can be more than one exponent that characterizes different distributions.

There are different observations that the recurrences distribution can be of the algebraic type (13.54) with  $\gamma_{\text{rec}} \geq 3$  or  $\alpha \geq 2$  if we apply the notations of the Feller's theorems with a corresponding Lévy index (*Note 15.6*).

One can expect more different deviations from (15.45) if we recall that the condition of independency of the recurrence times  $\{t_j\}$  in Section 15.2 is a kind of approximation in dynamical systems with chaos. Typically, there are correlations between the neighbouring steps of Poincaré maps that are important for kinetics. Subsequently, there is a possibility of deviations from the Lévy distribution and Lévy process, and a more general approach is necessary. In other words, Lévy's idea of distributions with infinite moments can be valid for a fairly broad set of cases, but it does not mean that the infiniteness of the moments of distribution functions imposes the Lévy process. This also means there is a necessity to define a *flight* in some general way as to be able to provide a practical use of the notion in physical and mathematical senses.

In a very qualitative way, we can think about a phase space domain of motion  $\Gamma$  as strongly nonuniform area with small subdomains  $\delta\Gamma_k$ ,

$$\sum_k \delta\Gamma_k \ll \Gamma, \quad (15.51)$$

such that the finite time positive Lyapunov exponents

$$\max \sigma_k \ll \sigma, \quad (15.52)$$

where  $\sigma$  is the Lyapunov exponent of the domain  $\Gamma \setminus \sum_k \delta\Gamma_k$ . Correspondingly, a piece of trajectory that passes a domain  $\delta\Gamma_k$  will be called a *flight*. There are different flights of the same trajectory due to it passing through different subdomains of vanishing Lyapunov exponent  $\delta\Gamma_k$  and through the same subdomain

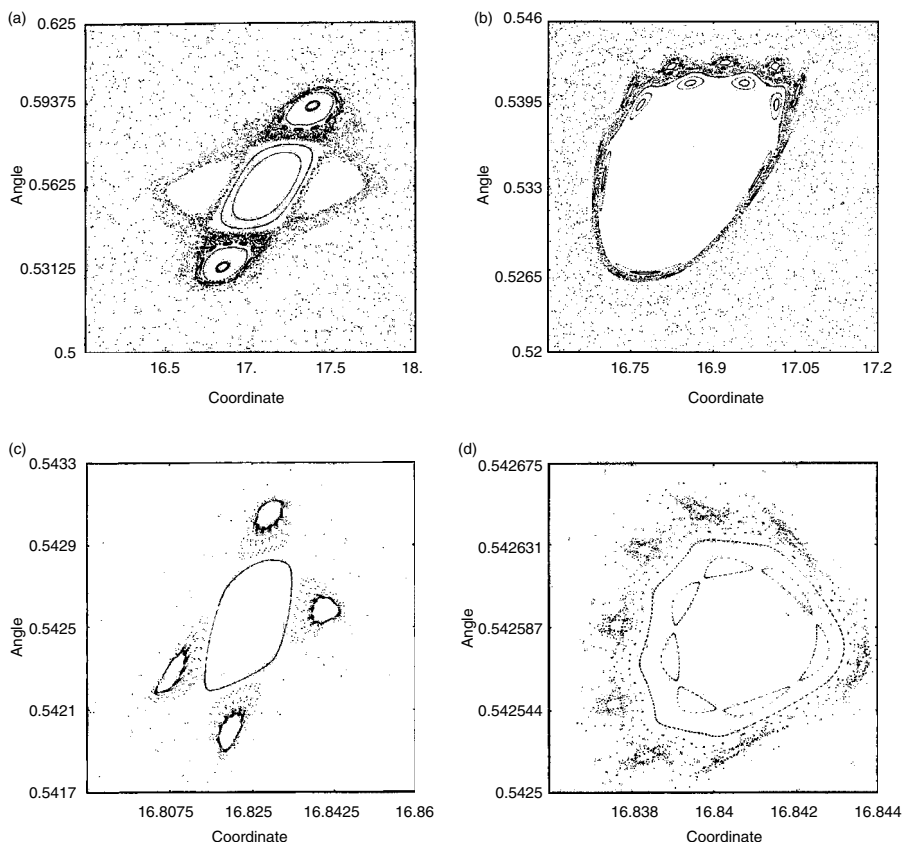


FIG. 15.4. An island and its vicinity for the Cassini billiard with  $a = 4.030952$  and  $c = 3$ : (a) Poincaré plot of the initial island taken from Fig. 15.3(a); (b) magnification of the bottom island from (a); (c) magnification of the top left island from (b); and (d) magnification of the right island from (c).

at different time instants. A more accurate definition will be given in Chapter 21 through the notion of  $\epsilon$ -separation of trajectories.

## 15.5 Weirstrass random walks (WRW)

The Weirstrass random walks (WRW) is perhaps the most appropriate model to understand simultaneously the origin of flights, their relation to the renormalization group equation, and the connection of the dynamics with HIT to the random processes with Bernoulli scaling. Having been coined by Shlesinger *et al.*, the WRW prepares a specific basis to understand the origin of fractional kinetics, fractal time, etc. (*Note 15.7*).

Consider a random walk on a one-dimensional periodic ‘lattice’ with a spacing equal to one and a probability  $p_j$  to make a step of the length  $a_j$ . Then probability density to make a step of the length  $\ell$  is

$$P(\ell) = \frac{1}{2} \sum_{j=1}^{\infty} p_j [\delta(\ell - a_j) + \delta(\ell + a_j)], \quad (15.53)$$

if the random walk is symmetric, and

$$\int_{-\infty}^{\infty} d\ell P(\ell) = 1. \quad (15.54)$$

The crucial idea of the WRW is to consider only scaling type steps and corresponding probabilities, that is,

$$a_j = a^j, \quad p_j = C p^j \quad (15.55)$$

with the normalization constant  $C$

$$C = 1 - p. \quad (15.56)$$

Now  $P(\ell)$  appears in the form

$$P(\ell) = \frac{1}{2} (1 - p) \sum_{j=0}^{\infty} p^j [\delta(\ell - a^j) + \delta(\ell + a^j)]. \quad (15.57)$$

Using (15.57), we have for the second moment

$$\langle \ell^2 \rangle = \int_{-\infty}^{\infty} \ell^2 P(\ell) d\ell = (1 - p) \sum_{j=0}^{\infty} (a^2 p)^j, \quad (15.58)$$

which diverges if  $a^2 p \geq 1$ . The characteristic function of  $P(\ell)$  is

$$P(k) = \int_{-\infty}^{\infty} d\ell e^{ik\ell} P(\ell) = (1 - p) \sum_{j=0}^{\infty} p^j \cos(ka^j), \quad (15.59)$$

which is the Weierstrass function and it explains the origin of the name WRW.

The function  $P(k)$  satisfies the evident functional equation

$$P(k) = p P(ka) + (1 - p) \cos k. \quad (15.60)$$

The solution of (15.60) can be presented as a sum

$$P(k) = P_s(k) + P_r(k) \quad (15.61)$$

of regular (holomorphic)  $P_r(k)$  and singular  $P_s(k)$  parts. The singular part  $P_s(k)$  satisfies the renormalization equation

$$P_s(k) = p P_s(ak) \quad (15.62)$$

and its solution has a singular behaviour at  $k = 0$ .

The equation (15.60) is similar to the *renormalization group equation* (RGE) of the phase transition theory

$$F(g) = \ell^{-d} F(g') + G(g) \quad (15.63)$$

for free energy  $F$ , interaction constant  $g$ , renormalized interaction constant  $g' = g'(g)$ , regular part  $G$  of the free energy, renormalization length  $\ell$ , and the system's dimension  $d$ . Nevertheless, (15.60) is simpler since its original explicit form (15.59) permits us to find  $P(k)$  explicitly.

A qualitative analysis of the expression for  $P(k)$  is based on the assumption that the form of the singular part  $P_s(k)$  has the following behaviour near  $k = 0$

$$P_s(k) = |k|^\mu Q(k) \quad (15.64)$$

with some exponent  $\mu$  and nonsingular function  $Q(k)$ . That is sufficient to conclude that  $0 < \mu < 2$  since the regular part of (15.59) has only even powers of  $k$ , and that  $Q(k)$  should be periodic in  $\ln k$  with a period  $\ln a$  that follows from (15.62). After substitution of (15.64) in (15.62) we also obtain

$$\mu = \frac{|\ln p|}{\ln a}. \quad (15.65)$$

Let us recall that the Mellin transform  $f_M(k)$  of a function  $f(x)$  is defined as

$$f_M(s) = \int_0^\infty dk f(k) k^{s-1} \quad (15.66)$$

and the corresponding inverse equation is

$$f(k) = \int_{c-i\infty}^{c+i\infty} ds f_M(s) k^{-s} \quad (15.67)$$

(see Oberhettinger (1974)). Application of the Mellin transform to  $f(k) = \cos(a^n k)$  gives

$$f_M(s) = \int_0^\infty dk \cos(a^n k) k^{s-1} = a^{-ns} \int_0^\infty d\xi \cos \xi \cdot \xi^{s-1}. \quad (15.68)$$

Substitution of (15.68) into (15.67) and (15.60) gives

$$\begin{aligned} P(k) &= \frac{1-p}{2\pi i} \sum_{j=0}^{\infty} p^j \int_{c-i\infty}^{c+i\infty} ds \frac{\Gamma(s) \cos(\pi s/2)}{a^{sj} |k|^s} \\ &= \frac{1-p}{2\pi i} \int_{c-i\infty}^{c+i\infty} ds \frac{\Gamma(s) |k|^{-s} \cos(\pi s/2)}{1-p/a^s} \end{aligned} \quad (15.69)$$

(see *Note 15.7* for references). The numerator has poles at  $s = 0, -2, \dots$ , and the denominator has poles at

$$s_j = \frac{\ln p}{\ln a} \pm \frac{2\pi i j}{\ln a} = -\mu \pm \frac{2\pi i j}{\ln a}. \quad (15.70)$$

The final result from (12.69) and (12.70) is obtained by application of the residues over all poles:

$$P(k) = 1 + |k|^\mu Q(k) + p \sum_{n=1}^{\infty} \frac{(-1)^n k^{2n}}{(2n)!(1 - pa^{2n})},$$

$$Q(k) = \frac{p}{\ln a} \sum_{n=-\infty}^{\infty} \Gamma(s_n) \cos\left(\frac{\pi s_n}{2}\right) \exp\left(\frac{-2\pi i n \ln |k|}{\ln a}\right)$$

in full correspondence with (15.64) and (15.61).

The concluding remarks from the obtained result are fairly spectacular:

- (i) The random walk model corresponds to the Bernoulli scaling and, at the same time, the model shows singularity (15.64) and infinite second moment;
- (ii) The equation for the characteristic function (15.60) is similar to the renormalization group equation of the phase transition theory;
- (iii) The singular part of the distribution function  $Q(k)$  in (15.71) possesses slow oscillation with respect to  $\ln k$ , but not  $k$ . This is the so-called *log-periodicity* which will be one of the most important signatures of kinetics in chaotic systems (*Note 15.8*).

## Notes

### *Note 15.1*

The deviations from the ‘Gaussianity’ were mainly observed in numerical simulations although, from the very beginning, they were attributed to the presence of islands and cantori (Karney (1983); Chirikov and Shepelyansky (1984); Beloshapkin and Zaslavsky (1983); Geisel (1984); Ichikawa *et al.* (1987); Aizawa *et al.* (1989); Horita *et al.* (1990); and Zaslavsky *et al.* (1991)).

### *Note 15.2*

Important theorems on the Lévy and Lévy-type distributions can be found in Gnedenko and Kolmogorov (1949); Feller (1949); Zolotarev (1986, 1997); Uchaikin and Zolotarev (1999); and Uchaikin (2003). Contemporary applications of the Lévy processes were analysed in Montroll and Shlesinger (1984); Bouchaud and Georges (1990); Geisel *et al.* (1987a, 1987b); and Geisel (1995). For applications to the chaotic dynamics, see Afanasiev *et al.* (1991); Zaslavsky (1992, 1994a,b); and Shlesinger *et al.* (1993, 1995a).

*Note 15.3*

See more on Lévy distribution in Lévy (1937); Feller (1949, 1957); Uchaikin and Zolotarev (1999).

*Note 15.4*

Different generalizations of the Lévy processes can be found in Uchaikin and Zolotarev (1999) and Uchaikin (2000). See also some example in Yanovsky *et al.* (2000).

*Note 15.5*

The results of simulation in Figs. 15.3 and 15.4 and in Table 15.1 are from Zaslavsky and Edelman (1997).

*Note 15.6*

These observations were obtained by simulation (see, for example, in Zaslavsky and Niyazov (1997); Zaslavsky *et al.* (1997); Rakhlin (2000); Leoncini and Zaslavsky (2002)). Another example, the Sinai billiard (Sinai (1963)) with infinite horizon, seems to have  $\gamma = 3$  and  $\alpha > 2$  up to a logarithmic factor that follows from a qualitative analysis and simulations (Bunimovich and Sinai (1973); Geisel *et al.* (1987b); Zacherl *et al.* (1986); Machta (1983); Machta and Zwanzig (1983); Zaslavsky and Edelman (1997)).

*Note 15.7*

The first paper on the WRW appeared in Shlesinger *et al.* (1981). This section follows the original work and the following publications in Hughes *et al.* (1981); Hughes *et al.* (1982); Shlesinger (1988); and Montroll and Shlesinger (1984). The connection to the RGE for the free energy was made in Shlesinger and Hughes (1981). The paper Hughes *et al.* (1982) showed that in higher dimensions the WRW leads to a lacunary series of spherical Bessel function for the generating function, which are cosines in the one-dimensional case. For the discussions of the WRW and dynamics, see Zaslavsky (2002b).

*Note 15.8*

The *log-periodicity* of the singular part  $P_s(k)$  through the function  $Q(k)$  with respect to  $k$  was well known in the RG theory of phase transitions (Niemeijer and van Leeuwen (1976)) but it did not play such an essential role as it did in the dynamical systems theory (Benkadda *et al.* (1999); Zaslavsky (2000a, 2002b)). For other applications of the log-periodicity see Sornette (1998).

## Problems

More complicated problems are marked by (\*).

15.1 Prove (15.23) using the chain property (15.21).

15.2\* Prove asymptotics (15.34) using the steepest descent method.

15.3 Derive the equation (15.69) replacing summation and integration.

## FRACTIONAL KINETIC EQUATION (FKE)

Any kind of kinetic equation is an approximate way to describe an ensemble of trajectories or particles, while neglecting some details of dynamics. All this means that, depending upon the information about the system we would like to preserve, the type and specific structure of the kinetic equation depends on our choice of the reduced space of variables and on the level of coarse-graining of trajectories.

The origin of the *fractional kinetic equation* (FKE), or simply *fractional kinetics* (FK) is two-fold. First, it is based on the existence of singular zones in phase space that create a set of sticky domains. We can map the dynamics considering only parts of trajectories in sticky domains and neglecting the parts of trajectories of their transition from one sticky domain to another one. In such a way we define a new support of the reduced part of phase space. Second, the new support based on a set of sticky domains is of a fractal or multifractal structure, generally speaking, in time and in phase space (or configuration space) simultaneously. These properties of dynamics require a new approach to kinetics when the scaling features of the dynamics dominate others and, moreover, do not have a universal pattern as in the case of Gaussian processes, but instead, are specified by the phase space topology and the corresponding characteristics of singular zones.

This chapter consists of a specific approach to the kinetic description of Hamiltonian chaotic dynamics. The derived equation is called the Fractional Fokker–Planck–Kolmogorov (FFPK) equation, or simply FKE (*Note 16.1*).

Some elements of *fractional calculus* proved to be useful for FFPK and we put the necessary definitions and useful formulas in Appendices C and D (*Note 16.2*).

### 16.1 Derivation of FKE

A derivation of the FFPK consists of two steps: a formal phenomenological derivation of the equation and an establishment of the relations between the critical exponents. At the first step we follow a similar scheme as introduced by Kolmogorov for the FPK equation, with some modification (see Section 14.2). We use the same notation as in Section 14.2:

$$W(x, x_0; t, t_0) = W(x, x_0; t - t_0) = W(x, x_0; t) \equiv P(x, t) \quad (16.1)$$



for the transition probability (14.11) with time uniformity (14.12), and the notation (14.15) for a convenience.

Let us start from a general expression for kinetic equations and let  $\hat{\Delta}_t P(x, t)$  be a generalized infinitesimal shift of  $P(x, t)$  along  $t$  by  $\Delta t$ . In a ‘regular’ case of the smooth variable  $t$  we have simply

$$\hat{\Delta}_t P(x, t) = P(x, t + \Delta t) - P(x, t) = \frac{\partial P(x, t)}{\partial t} \Delta t + O(\Delta t^2), \quad t > 0. \quad (16.2)$$

In the case of fractal time with fractal exponent  $\beta$  we have

$$\hat{\Delta}_t^\beta P(x, t) = \frac{\partial^\beta P(x, t)}{\partial t^\beta} (\Delta t)^\beta + O((\Delta t)^{\beta_1}), \quad 0 < \beta \leq 1, \quad \beta_1 > \beta, \quad t > 0, \quad (16.3)$$

where the fractional derivative of order  $\beta$  has been introduced (see its definition in Appendix C). The explicit form of the shift difference operator  $\hat{\Delta}_t^\beta$  is given in Appendix D. The main feature of (16.3) is that in the limit  $\Delta t \rightarrow 0$  the right-hand side is proportional to  $(\Delta t)^\beta$  and it shows a singular behaviour.

Let us now introduce an infinitesimal change of  $P(x, t)$  due to transitions from other states  $P(x', t)$  during the same time interval  $\Delta t$ . Since  $\Delta t \rightarrow 0$ , these transitions are local and they can be performed only from the points  $x'$  in the vicinity of  $x$ , assuming the absence of infinite velocities. A local structure of the phase space near a point  $x$  can be characterized by the fractal dimension  $\alpha$ , and the corresponding changes  $\hat{\Delta}_x^\alpha P(x, t)$  can be presented in a form similar to (14.16):

$$\hat{\Delta}_x^\alpha P(x, t) = \int dy W(x, y; \Delta t) P(y, t) - P(x, t) + O((\Delta t)^{\beta_2}), \quad \beta_2 > \beta. \quad (16.4)$$

Since  $P(x, t)dx$  can be interpreted as a number of particles at time  $t$  in the volume  $dx$ , the conservation of particles can be expressed as a balance equation

$$\hat{\Delta}_t^\beta P(x, t) = \hat{\Delta}_x^\alpha P(x, t) + O((\Delta t)^{\beta_3}), \quad \beta_3 = \min(\beta_1, \beta_2) \quad (16.5)$$

or

$$\lim_{\Delta t \rightarrow 0} \frac{1}{(\Delta t)^\beta} \hat{\Delta}_t^\beta P(x, t) = \lim_{\Delta t \rightarrow 0} \frac{1}{(\Delta t)^\beta} \hat{\Delta}_x^\alpha P(x, t). \quad (16.6)$$

This expression is a formal representation of the FKE and its development depends on how the right-hand side will be calculated. Substituting (16.3)

and (16.4) into (16.6), we obtain

$$\frac{\partial^\beta P(x, t)}{\partial t^\beta} = \lim_{\Delta t \rightarrow 0} \frac{1}{(\Delta t)^\beta} \left\{ \int dy W(x, y; \Delta t) P(y, t) - P(x, t) \right\}, \quad 0 < \beta \leq 1. \quad (16.7)$$

This equation is still exact and no assumption has been done about the properties of  $W(x, y; \Delta t)$ .

Let us assume now the existence of the expansion, similar to (14.19), in the limit  $\Delta t \rightarrow 0$ :

$$W(x, y; \Delta t) = \delta(x - y) + A(y; \Delta t) \delta^{(\alpha)}(x - y) + B(y; \Delta t) \delta^{(\alpha_1)}(x - y), \quad (0 < \alpha < \alpha_1 \leq 2) \quad (16.8)$$

with appropriate fractal dimension characteristics  $\alpha$  and  $\alpha_1$ . Beginning from (16.8), the approach to the kinetic equation becomes approximate. The approximation is in taking a finite number of terms in (16.8) and, what is more important, in assuming of the coefficients  $A(y; \Delta t)$ ,  $B(y; \Delta t)$  independent on  $P(x, t)$ . Since the transition probability  $W(x, y; \Delta t)$  represents the local features of the dynamics ( $|x - y| \rightarrow 0$ ) and  $P(x, t)$  represents strongly non-local features ( $x, t \rightarrow \infty$ ), a physical nature of the assumption is independence of local transitions from the large time behaviour. At that point it is necessary to mention that the local-non-local independence hypothesis is the same for the FPK equation in Section 14.2 and here for the fractal space-time case. But the major difference is in the way the splitting of local-non-local distribution appears: for the FPK equation there exists a finite time  $t^*$  such that for  $t > t^*$  one can assume an independence of  $W(x, y; \Delta t)$  from the distribution  $P(x, t)$ , and there is no such  $t^*$  for fractional kinetic case as it will be clear later.

It is still possible to write the definition of the coefficient  $B(y; \Delta t)$  through a moment of  $W$ :

$$\langle\langle |\Delta x|^{\alpha_1} \rangle\rangle \equiv \int dx |x - y|^{\alpha_1} W(x, y; \Delta t) = \Gamma(1 + \alpha_1) B(y; \Delta t), \quad (16.9)$$

which is similar to (14.22), but the coefficient  $A(y; t)$  does not have so simple an interpretation for the general case unless  $B = 0$ , or  $\alpha_1 = \alpha + 1$ .

By integrating (16.8) over  $y$  we obtain a relation

$$\frac{\partial^\alpha \mathcal{A}(x)}{\partial (-x)^\alpha} + \frac{\partial^{\alpha_1} \mathcal{B}(x)}{\partial (-x)^{\alpha_1}} = 0, \quad (16.10)$$

where

$$\begin{aligned}\mathcal{A}(x) &= \lim_{\Delta t \rightarrow 0} \frac{A(x, \Delta t)}{(\Delta t)^\beta}, \\ \mathcal{B}(x) &= \lim_{\Delta t \rightarrow 0} \frac{B(y; \Delta t)}{(\Delta t)^\beta} = \frac{1}{\Gamma(1 + \alpha_1)} \lim_{\Delta t \rightarrow 0} \frac{\langle\langle |\Delta x|^{\alpha_1} \rangle\rangle}{(\Delta t)^\beta}\end{aligned}\quad (16.11)$$

similar to (14.25). Equation (16.10) is a generalization of (14.23) for the detailed balance principle. Existence of the limits (16.11) when  $\Delta t \rightarrow 0$  is instead of the Kolmogorov conditions (16.25). Fractional values of  $\alpha, \alpha_1$ , and  $\beta$  represent a new type of the fractal properties of coarse-grained dynamics.

An important particular case is  $\alpha_1 = \alpha + 1$ , and (16.10) transforms into

$$\frac{\partial^\alpha}{\partial(-x)^\alpha} \left[ \mathcal{A}(x) - \frac{\partial \mathcal{B}(x)}{\partial x} \right] = 0 \quad (16.12)$$

equivalent to (14.31), up to a constant in the notations, with

$$\begin{aligned}\mathcal{B}(x) &= \frac{1}{\Gamma(2 + \alpha)} \lim_{\Delta t \rightarrow 0} \frac{\langle\langle |\Delta x|^{\alpha+1} \rangle\rangle}{(\Delta t)^\beta}, \\ \mathcal{A}(x) &= \frac{1}{\Gamma(1 + \alpha)} \lim_{\Delta t \rightarrow 0} \frac{\langle\langle |\Delta x|^\alpha \rangle\rangle}{(\Delta t)^\beta}.\end{aligned}\quad (16.13)$$

The generalization of the Landau formulas (14.23) and (14.24) is:

$$\Delta t \rightarrow 0: \quad \frac{\langle\langle |\Delta x|^\alpha \rangle\rangle}{(\Delta t)^\beta} = \frac{\Gamma(1 + \alpha)}{\Gamma(2 + \alpha)} \frac{\partial}{\partial x} \frac{\langle\langle |\Delta x|^{\alpha+1} \rangle\rangle}{(\Delta t)^\beta}. \quad (16.14)$$

The existence of the limits (16.13) can be considered as a generalized Kolmogorov condition (compare to (14.25)).

The FKE can be derived from (16.7) rewritten as:

$$\frac{\partial^\beta P(x, t)}{\partial t^\beta} = \lim_{\Delta t \rightarrow 0} \frac{1}{(\Delta t)^\beta} \left\{ \int dy [W(x, y; t + \Delta t) - \delta(x - y)] P(y, t) \right\}. \quad (16.15)$$

Using the expansion (16.8) and definitions (16.11), we obtain

$$\frac{\partial^\beta P(x, t)}{\partial t^\beta} = \frac{\partial^\alpha}{\partial(-x)^\alpha} (\mathcal{A}(x) P(x, y)) + \frac{\partial^{\alpha_1}}{\partial(-x)^{\alpha_1}} (\mathcal{B}(x) P(x, y)). \quad (16.16)$$

This equation will be called the Fractional Fokker–Planck–Kolmogorov equation (FFPK). It can be simplified in the case  $\alpha_1 = \alpha + 1$

$$\frac{\partial^\beta P}{\partial t^\beta} = - \frac{\partial^\alpha}{\partial(-x)^\alpha} \left( \mathcal{B} \frac{\partial P}{\partial x} \right), \quad (16.17)$$

which transfers into regular diffusion equation for  $\alpha = 1$  and  $\mathcal{B} = \frac{1}{2} \mathcal{D}$ .

Fractional derivatives are well defined in a specified direction (see the Appendix C), and there is no simple replacement  $x \rightarrow -x$  or  $t \rightarrow -t$ . That is why a more general operator should be considered for the processes in  $x \in (-\infty, \infty)$ . For example, instead of the derivative of order  $\alpha$  one can consider:

$$\hat{L}_x^{(\alpha)} = \frac{\mathcal{A}^+ \partial^\alpha}{\partial x^\alpha} + \frac{\mathcal{A}^- \partial^\alpha}{\partial (-x)^\alpha}. \quad (16.18)$$

For a symmetric case one can use Riesz derivative

$$\frac{\partial^\alpha}{\partial |x|^\alpha} = -\frac{1}{2 \cos(\pi\alpha/2)} \left[ \frac{\partial^\alpha}{\partial x^\alpha} + \frac{\partial^\alpha}{\partial (-x)^\alpha} \right], \quad (\alpha \neq 1). \quad (16.19)$$

The corresponding FKE (16.16) takes the form (Saichev and Zaslavsky (1997))

$$\frac{\partial^\beta P}{\partial t^\beta} = \frac{\partial^\alpha}{\partial |x|^\alpha} (\mathcal{A}P) + \frac{\partial^{\alpha_1}}{\partial |x|^{\alpha_1}} (\mathcal{B}P), \quad 0 < \alpha < \alpha_1 \leq 2. \quad (16.20)$$

In the case when the term with  $\mathcal{B}$  can be neglected, we have a simplified version of FKE

$$\frac{\partial^\beta P}{\partial t^\beta} = \frac{\partial^\alpha}{\partial |x|^\alpha} (\mathcal{A}P). \quad (16.21)$$

In the case  $\beta = 1$ ,  $\alpha = 2$  it is a normal diffusion equation. For  $0 < \beta < 1$ ,  $\alpha = 2$

$$\frac{\partial^\beta P}{\partial t^\beta} = \frac{\partial^2}{\partial x^2} (\mathcal{A}P), \quad (\beta < 1) \quad (16.22)$$

is called the equation of fractional Brownian motion (Mandelbrot and Van Ness (1968); Montroll and Shlesinger (1984)). For  $\beta = 1$  and  $1 < \alpha < 2$  the FKE corresponds to the Lévy process (see Section 15.2):

$$\frac{\partial P}{\partial t} = \frac{\partial^\alpha}{\partial |x|^\alpha} (\mathcal{A}P), \quad (1 < \alpha < 2) \quad (16.23)$$

(Note 16.3).

Parameters  $\beta, \alpha, \alpha_1$  will be called the *critical exponents*. They are subjected to be evaluated from the dynamics.

## 16.2 Conditions for the FKE

Any type of the FKE and its generalization can be considered as an independent mathematical problem. If we want to stay close to specific applications of the FKE to dynamical systems, restrictions related to the physical nature and the origin of the FKE should be imposed. Before considering solutions to the FKE, let us make a few comments about some constraints. Other conditions will be

presented later.

(a) *Interval condition.* We should define interval of consideration in space-time. Speaking about the space, we have in mind phase space (coordinate-momentum) and the variable  $x$  can represent any or both of them. The infinite intervals assume a possibility to have infinite moments of  $P(x, t)$  while finite intervals  $(x_{\min}, x_{\max})$ ,  $(t_{\min}, t_{\max})$ , that will be called *space* and *time windows*, lead to the finite moments since  $P(x, t)$  is integrable.

(b) *Positiveness.* Solution  $P(x, t)$  has the meaning of probability, and it should be positively defined, i.e.

$$P(x, t) \geq 0 \quad (16.24)$$

in the domain of consideration. For the infinite space-time domains condition (16.24) leads to restrictions on the possible values of critical exponents. Particularly we have the condition  $0 < \alpha \leq 2$  for the Lévy processes ( $\beta = 1$ ) or the condition:

$$0 < \beta \leq 1, \quad 0 < \alpha \leq 2 \quad (16.25)$$

(Saichev and Zaslavsky (1997)) for (16.21) with  $\mathcal{A} = \text{const}$ . A rigorous consideration of the  $P(x, t)$  positiveness for both fractal values of  $(\alpha, \beta)$  does not exist yet. Examples of the violation of (16.25) will be shown later.

(c) *Intermediate asymptotics.* It can be that dynamics imposes different asymptotics for different space-time windows. An example of two different asymptotics for particles advection in convective flow can be found in (Young *et al.* (1989)). Other examples will be indicated later. For such cases it should be different pairs  $(\alpha_j, \beta_j)$  for different windows. Particularly, we should mention a multifractal situation when there are few different singular zones that impose different critical exponents for the FKE.

(d) *Definition of fractional integro-differentiation.* This definition is not unique (Samko *et al.* (1987)). We use the Riemann–Liouville form (see Appendix C) while sometimes other definitions may be more convenient. In fact, the structure of the FKE together with a type of the fractional derivative depends on the specific physical problem and the corresponding boundary and initial condition. More accurately, one can say that the distribution  $P(x, t)$  is defined not only by the boundary-initial conditions but also by the type of derivatives used in FKE. A similar situation exists with Fourier or Laplace transforms. Any of them can be used if we know how to select a contour of integration in the complex plane to satisfy the boundary-initial conditions.

### 16.3 Evolution of moments (transport)

Let  $P(x, t)$  be a solution for the FKE. The moments

$$\langle |x|^\delta \rangle = \int dx |x|^\delta P(x, t) \quad (16.26)$$

are the macroscopic observables. Their dependence on time defines the *transport*, i.e. the macroscopic evolution of the system.

It is easy to obtain the time-dependence of some moments if  $\mathcal{A} = \text{const}$  in (16.21). Let us multiply the equation by  $|x|^\alpha$  and integrate it over  $x$ . Then

$$\begin{aligned} \frac{\partial^\beta \langle |x|^\alpha \rangle}{\partial t^\beta} &= \mathcal{A} \int dx |x|^\alpha \frac{\partial P(x, t)}{\partial |x|^\alpha} \\ &= \mathcal{A} \int dx P(x, t) \frac{\partial^\alpha}{\partial |x|^\alpha} |x|^\alpha = \mathcal{A} \Gamma(1 + \alpha), \end{aligned} \quad (16.27)$$

where we use the formulas from the Appendix C. After integrating (16.27) over  $t^\beta$  (or differentiation with respect to  $t^{-\beta}$ ) we obtain

$$\langle |x|^\alpha \rangle = \mathcal{A} \frac{\Gamma(1 + \alpha)}{\Gamma(1 + \beta)} t^\beta. \quad (16.28)$$

For the case of the self-similarity of the solution for FKE, which we will discuss more in Section 18.1, one may expect

$$\langle |x| \rangle \sim t^{\beta/\alpha} = t^{\mu/2}, \quad (16.29)$$

where we introduce the *transport exponent*

$$\mu \equiv \frac{2\beta}{\alpha}. \quad (16.30)$$

The meaning of the transport exponent is very simple: in the case that the second moment exists, i.e.  $\langle x^2 \rangle < \infty$  and it is meaningful, we can write

$$\langle x^2 \rangle \sim t^\mu, \quad (16.31)$$

that is, for the normal diffusion it should be  $\mu = 1$ . The case

$$\mu = \frac{2\beta}{\alpha} > 1 \quad (16.32)$$

will be called *superdiffusion*, and the case

$$\mu = \frac{2\beta}{\alpha} < 1 \quad (16.33)$$

will be called *subdiffusion*.

It will be shown in the next chapter that the moments with  $\delta > \alpha$  diverge. Nevertheless, there are some constraints on the application of the FKE to real dynamics, which we discuss in the following section.

### 16.4 Conflict with dynamics

Limitations for application of the FKE to dynamical systems can be compared to the limitations for diffusional process described in Section 14.6. Consider analogues (16.13) and (16.14) to the Kolmogorov condition (14.25):

$$\frac{(\delta x)^\alpha}{(\delta t)^\beta} = v^\alpha (\delta t)^{\alpha-\beta} = \mathcal{A} = \text{const}, \quad (\delta t \rightarrow 0). \quad (16.34)$$

At the same time,

$$\alpha - \beta = \alpha \left(1 - \frac{\beta}{\alpha}\right) = \alpha \left(1 - \frac{\mu}{2}\right) > 0 \quad (16.35)$$

since  $\mu < 2$ . This means that in the limit  $\delta t \rightarrow 0$  should be  $v \rightarrow \infty$ , and we arrive at the same conflict as in the normal diffusion case, that is, to the existence of infinite velocity in dynamics, which has no physical sense. A resolution of this conflict is similar to the case of normal diffusion: there exists  $\delta t_{\min}$  such that for  $\delta t < \delta t_{\min}$  the FKE cannot be applied.

More serious constraints are imposed by the condition of positiveness of  $P_{\alpha,\beta}(x, t)$ , i.e.  $\beta < 1$ ,  $0 < \alpha < 2$ . Some simulations show, as we will see later, the values of  $\alpha > 2$ . A theory of the FKE is not developed yet for  $\beta > 1$  and  $\alpha > 2$ .

We also need to consider truncated distribution function

$$P_{\alpha,\beta}(x, t) = \begin{cases} P_{\alpha,\beta}^{(\text{tr})}(x, t), & 0 < x \leq x_{\max}, \\ 0, & x > x_{\max} \end{cases} \quad (16.36)$$

(compare to (14.66)) and truncated moments

$$\langle |x|^m \rangle_{\text{tr}} = \int dx P_{\alpha,\beta}^{(\text{tr})}(x, t) < \infty \quad (16.37)$$

in order to avoid infinite velocities in the solutions, forbidden by the dynamics. All these comments will be necessary when real experimental or simulation data are compared to the theory. As it follows in the case of self-similarity

$$\langle |x|^m \rangle_{\text{tr}} \sim t^{m\mu/2} \quad (16.38)$$

and all truncated moments are finite, although there is a restriction on the value of  $m$  which depends on  $t_{\max}$  (see the discussion in Section 14.7). Particularly

$$\langle |x|^2 \rangle_{\text{tr}} \sim t^\mu \quad (16.39)$$

introducing the transport exponent  $\mu$  instead of (16.29).

For  $\beta = 1$  we have the Lévy process with  $\mu = 2/\alpha < 2$  since the second and higher moments ( $\mu \geq 2$ ) diverge. The Lévy condition  $\alpha < 2$  means that

$$1 < \mu < 2 \quad (16.40)$$

or that the permitted values of  $\alpha$  are

$$1 < \alpha < 2 \quad (16.41)$$

and it is not clear from the dynamics why the values of  $0 < \alpha < 1$  are not achievable. For the interval (16.40)  $\mu > 1$ , that is, the transport is superdiffusive, and it is not clear from the dynamics if subdiffusive transport with  $\mu < 1$  is forbidden or not. The value  $\mu = 2$  corresponds to the pure ballistic case. This will be discussed more later (*Note 16.4*).

All simulation data in the book will only be truncated moments and truncated distribution functions, although it will not be indicated explicitly.

## 16.5 Dynamical origin of critical exponents

In this section we demonstrate two examples of how the critical exponents can be obtained from the dynamical consideration of a model. More examples and speculations will be proposed in Chapter 17. These two examples are related to the web map and standard map (*Note 16.5*).

First, let us demonstrate the presence of the superdiffusion for the two maps. Figure 16.1 shows the behaviour of the second moment:

$$\mathcal{D} = \lim_{n \rightarrow \infty} \frac{1}{n} \langle R_n^2 \rangle = \lim_{n \rightarrow \infty} \frac{1}{n} \langle u_n^2 + v_n^2 \rangle$$

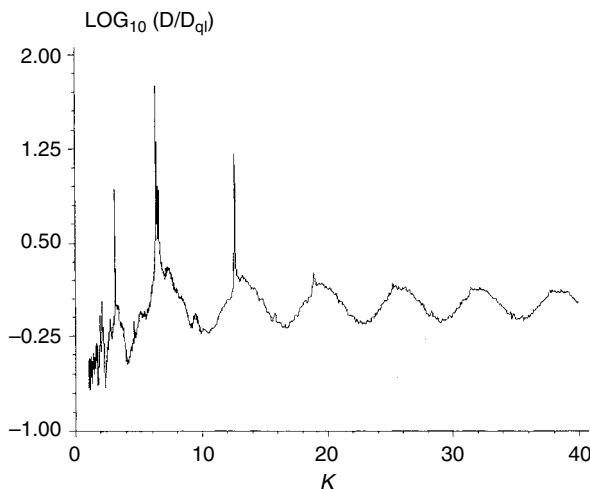


FIG. 16.1. Diffusion coefficient  $\mathcal{D}$  from the simulation of the web map vs.  $K$ , normalized over the value  $\mathcal{D}_{q\ell} = K^2/2$  that corresponds to the normal diffusion (so-called quasi-linear approximation).



for the web map. In the case of a normal diffusion  $\mathcal{D} = \text{const} = \mathcal{D}_{q\ell} = K^2/2$ . In the superdiffusive case

$$\langle R^2 \rangle = \langle u^2 + v^2 \rangle \sim t^\mu \quad (16.42)$$

with  $\mu > 1$ , that is,  $\langle R^2 \rangle/t \rightarrow \infty$  as  $t \rightarrow \infty$ . Sharp peaks in Fig. 16.1 indicate the phenomenon of superdiffusion near special values of  $K$ . The larger  $t$  is, the sharper and higher are the peaks.

A set  $\{K^{(j)}\}$  of the special values of  $K$  corresponds to the occurrence of accelerator mode islands of different resonance order (see Section 9.2), and there are intervals  $\Delta K$  where the set of  $K^{(j)} \in \Delta K$  is as dense as rationals. This property means that the topology of phase space is sensitive to the changes of control parameter  $K$  and, particularly, we arrive to the important conclusion of the dependence

$$\mu = \mu(K), \quad (16.43)$$

which is non-analytical (*Note 16.6*).

A similar example exists for the standard map (Fig. 16.2) for which the regular diffusion is governed by the equation

$$\frac{\partial F(p, t)}{\partial t} = \frac{1}{2} \mathcal{D} \frac{\partial^2 F(p, t)}{\partial p^2} \quad (16.44)$$

with  $\mathcal{D} = \mathcal{D}_{q\ell} = K^2/2$ . It follows from (16.44) that

$$\langle p^2 \rangle = \mathcal{D}t, \quad (16.45)$$

that is,  $\langle p^2 \rangle/\mathcal{D}t = \text{const}$ . In fact, simulations show the superdiffusion

$$\langle p^2 \rangle = \text{const} \cdot t^{\mu_p}, \quad \mu_p > 1 \quad (16.46)$$

with  $\mu_p = \mu_p(K)$  for some values of  $K$ . Figure 16.2 displays the values  $\langle p^2 \rangle/t$  that have sharp peaks due to  $\mu_p > 1$ . For the normal diffusion  $2\mathcal{D}/K^2 = 1$ . The larger the time, the larger the peaks. They also appear due to the accelerator mode islands (*Note 16.7*):

These two examples show that there should be many different pairs  $(\alpha, \beta)$  of critical exponents depending on the value of  $K$ . The way to observe the fractional kinetics can be formulated in the following scheme of assumptions:

- (i) The value of the control parameter, say  $K$ , would be selected to have  $t \rightarrow \infty$  domination of the only pair  $(\alpha, \beta)$  and the corresponding fractal structure of phase space and flights.
- (ii) Having only one scaling for time, say  $\lambda_T$ , and for space or phase space, say  $\lambda_\ell$ , we link

$$\beta = \frac{1}{\ln \lambda_T}, \quad \alpha = \frac{1}{\ln \lambda_\ell}, \quad (16.47)$$

that is,

$$\mu = \frac{2\beta}{\alpha} = \frac{2\ln \lambda_\ell}{\ln \lambda_T}. \tag{16.48}$$

- (ii) The scaling constants  $\lambda_T, \lambda_\ell$  can be obtained from any characteristics of space-time dynamics. For example,  $\lambda_T$  can be obtained from the scaling property of the Poincaré recurrences, or from the scaling of periods of islands-around-islands, and  $\lambda_\ell$  can be obtained from the scaling parameter  $\lambda_S$  of the areas of islands-around-islands.

Let us show an example for the web map (Zaslavsky and Niyazov (1997)). Table 16.1 shows parameters of islands for a special value of  $K = 6.34972$  that corresponds to the islands’ hierarchy and the corresponding HIT 1–8–8–8–... (see Section 12.2 and Fig. 12.4). The table is similar to Table 15.1:

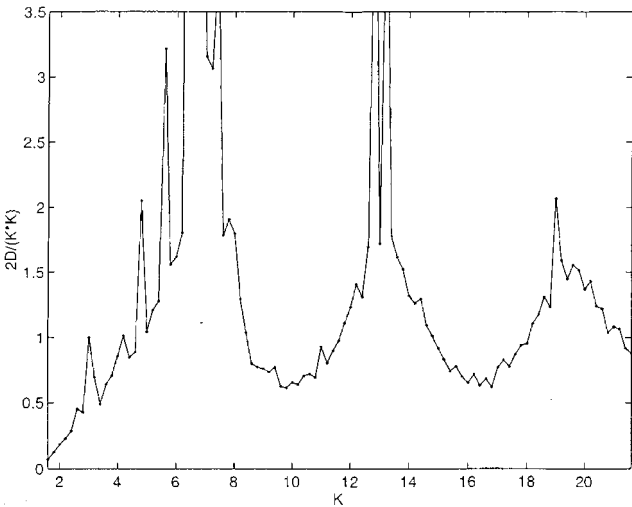


FIG. 16.2. Second moment  $\langle p^2 \rangle/t$  dependence on  $K$  for the standard map.

TABLE 16.1 Parameters of self-similarity for the web map with  $K = 6.349972$ .

$k$	$q_k$	$T_k$	$T_k/T_{k-1}$	$\Delta S_k$	$\Delta S_k/\Delta S_{k-1}$	$\delta S_k$	$\delta S_k/\delta S_{k-1}$
0	1	16.4	...	0.436	...	0.436	...
1	8	131.8	<b>8.04</b>	$5.24 \times 10^{-3}$	<b><math>1.20 \times 10^{-2}</math></b>	$4.19 \times 10^{-2}$	<b>0.0961</b>
2	8	1049	<b>7.96</b>	$5.30 \times 10^{-5}$	<b><math>1.01 \times 10^{-2}</math></b>	$3.39 \times 10^{-3}$	<b>0.0809</b>
3	8	8420	<b>8.02</b>	$5.32 \times 10^{-7}$	<b><math>1.00 \times 10^{-2}</math></b>	$2.72 \times 10^{-4}$	<b>0.0802</b>

Here the notations are the same as in Chapter 13, that is,  $q_k$  is a constant of proliferation of islands

$$q_n = \lambda_q = \text{const.}, \quad n > 0 \quad (16.49)$$

and for the considered case  $\lambda_q = 8$ ;

$$\delta S_n = q_n \Delta S_n \quad (16.50)$$

(compare to (15.47)) and

$$\begin{aligned} \lambda_S &= \frac{\delta S_k}{\delta S_{k-1}} \approx \text{const} < 1, \\ \lambda_T &= \frac{T_k}{T_{k-1}} \approx \text{const} > 1. \end{aligned} \quad (16.51)$$

The values of  $\lambda_T, \lambda_S$  are evident from Table 16.1.

When a trajectory sticks near the boundaries of islands that are of the  $k$ -th generation, it rotates almost regularly in narrow annuluses around the islands. Let  $\ell_k$  be the full length of the corresponding piece of trajectory, that is,  $\ell_k$  is the length of a flight that corresponds to the stickiness to the islands of the  $k$ -th generation. Self-similarity of flights means

$$\ell_{k+1} = \lambda_\ell \ell_k. \quad (16.52)$$

The particle flux due to the flight of the  $k$ -th generation is

$$\mathcal{N}_k = \text{const} \cdot \ell_k d_k = \text{const} \cdot \ell_k \delta S_k^{1/2}, \quad (16.53)$$

where  $d_k$  is a diameter of the  $k$ -th generation island. When the particles (trajectories) switch their flights from being around the islands of  $k$ -th generation to being around the islands of a nearest generation, say  $k \pm 1$ , there should be preservation of the flux due to the Liouville theorem, that is,

$$\mathcal{N}_k = \text{const} \cdot \ell_k \delta S_k^{1/2} \approx \text{const} \quad (16.54)$$

or

$$\ell_0 \cdot \delta S_0^{1/2} \lambda_\ell^k \lambda_S^{k/2} \approx \text{const}. \quad (16.55)$$

It follows that

$$\lambda_\ell \approx \frac{1}{\lambda_S^{1/2}}. \quad (16.56)$$

Substitution of (16.56) to (16.48) gives the transport exponent as

$$\mu = \frac{|\ln \lambda_S|}{\ln \lambda_T} \quad (16.57)$$

and the corresponding FFPK equation

$$\frac{\partial^\beta P(\ell, t)}{\partial t^\beta} = \mathcal{A} \frac{\partial^\alpha P(\ell, t)}{\partial \ell^\alpha} \quad (16.58)$$

for the distribution function  $P(\ell, t)$  of the flight length  $\ell$  and time. The corresponding transport equation reads

$$\langle \ell^\alpha \rangle = \text{const} \cdot t^\beta. \quad (16.59)$$

The formula (16.57) shows how the dynamical features of trajectories, i.e. the scaling constant  $\lambda_S, \lambda_T$ , define the transport features—the fractal space-time exponents  $(\alpha, \beta)$  and the transport exponent  $\mu$ . All these conclusions can be compared to experiments or to simulations that will be discussed in the following section.

The final formulas (16.57) or (16.48) can be compared to (13.45) and (13.60) for the Poincaré recurrences exponent. We have an important connection for the case when the phase space topology provides a hierarchical set of sticky islands:

$$\gamma_{\text{rec}} = 2 + \mu = 2 + \frac{|\ln \lambda_S|}{\ln \lambda_T} = 2 \left( 1 + \frac{\ln \lambda_\ell}{\ln \lambda_T} \right). \quad (16.60)$$

Performing collection of data we can obtain the exponents (16.47) for the flight length and their time scaling and calculate the exponent for recurrences  $\gamma_{\text{rec}}$  or the transport exponent  $\mu$ , and vice versa. All these characteristics are now linked. Particularly for the web map with the data given in Table 16.1, the phase space with a clear stickiness topology is in Fig. 12.4, a sample of trajectory is in Fig. 15.1, right, and the value of  $\mu$  from Table 16.1 is  $\mu \approx 1.21$ , while the directly obtained value  $\mu \approx 1.26$  with a good agreement (*Note 16.8*).

## 16.6 Principles of simulations

Comparison of any kind of theoretical prediction to the experimental or simulation data for fractal objects is very non-trivial, and here we discuss some major principles of the simulation performance. The reason for that is a specific kind of the randomness of trajectories when the Lyapunov exponent is small in singular zones of the phase space.

(a) *Non-universality*. It is always desirable in physics to have some universal constants for the most important phenomena. The only universal behaviour is the normal, or Gaussian, transport. Anomalous transport is not universal and the same is true of critical exponents  $\alpha, \beta$ , and  $\mu$ . Nevertheless, there are classes of universality which will be discussed later. It is always necessary to select a value of the control parameter  $K$  that defines a type of stickiness, dynamical trap, or singular zone.

(b) *Representativity of the ensemble of initial data*. The phase space and mixing is non-uniform in the case of stickiness of trajectories and presence of singular zones. To have a correct averaging  $\langle \dots \rangle$  over trajectories, their initial

conditions should be taken uniformly at the most uniform part of phase space to avoid influence of a fine structure of singular zones.

(c) *Non-ergodicity*. A specific value of the control parameter  $K^*$  defines a type of the singular zone in phase space. We assume that  $K^*$  is selected in such a way that the only singular zone dominates the transport. Nevertheless, the value of  $K^*$  can be selected only approximately and, due to that, for  $t > t^*$  some other singular zones can influence the transport. Since the time of simulation is bounded from above and there is no finite time of relaxation to the uniform mixing, a long time of simulation does not provide a good approximation to the transport exponent, related to  $K^*$ , i.e. the value  $\mu = \mu(K^*)$ . The selection of large number of initial conditions rather than long time of observation can improve the situation.

(d) *Values of critical exponents*. It seems that a pure fractal situation with accurate values of critical exponents is a fairly rare phenomenon for at least two reasons: multiplicity of the islands' topology of phase space and log-periodicity discussed already in Section 10.6. A correct way is to introduce a spectral function for the critical exponents similar to the spectral function of multifractals (see in Zaslavsky (2000b)). Nevertheless, by a convenient choice of  $K^*$  one can create a situation close enough to the monofractality.

## Notes

### Note 16.1

The idea of exploiting fractional calculus and presenting kinetics in a form of an equation with fractional integro-differentiation is not new. For example, some variants of FK were used in Mandelbrot and Van Ness (1968) for signals; Young *et al.* (1989) for kinetics of advected particles; Hanson *et al.* (1985) for kinetics through cantori for the standard map; Nigmatullin (1986) for the porous media; Douglas *et al.* (1986, 1987) in macromolecules (see also a review paper by Douglas (2000)). For more recent publications, see Isichenko (1992) and Milovanov (2001) for the problem of percolation; Hilfer (1993, 1995a,b) for evolution and thermodynamics; West and Grigolini (2000) for time series. The material of this chapter is based on the results in Zaslavsky (1992, 1994a, 1994b), where FKE was derived with fractional derivatives in space and in time for the dynamics with singularities.

### Note 16.2

For details on fractional calculus, see Gelfand and Shilov (1964); Samko *et al.* (1987); Miller and Ross (1993); Podlubny (1999); West *et al.* (2003). Different review articles and applications are collected in Hilfer (2000).

### Note 16.3

There are different forms for the FKE that generalize forms (16.20)–(16.23): anisotropic equations were considered in Yanovsky *et al.* (2000); Meerschaert *et al.* (2001); equations with directional fractality in Weitzner

and Zaslavsky (2001); Meerschaert *et al.* (2001); non-linear fractional equations (Biler *et al.* (1998); Barkai (2001); Schertzer *et al.* (2001)). Some of these equations will be considered later.

We should mention that the investigation of the type and properties of the FKE is at its beginning stage and a number of important questions are not answered yet. Some of these questions will be discussed in the following sections.

#### Note 16.4

The conclusion on the absence of subdiffusion in Hamiltonian dynamics occurs after some assumption of applicability of the Lévy type process and the Kac lemma. Subdiffusion can appear along some axis while the whole random walk corresponds to the superdiffusion. We cannot exclude a possibility of the ‘absolute’ subdiffusion (in all directions) due to violation of some specific conditions of the lemma, for example, the absence of non-singular distributions.

#### Note 16.5

For the details of simulations, see Zaslavsky *et al.* (1997); Zaslavsky and Niyazov (1997); and Benkadda *et al.* (1997). More data and speculations around them will be shown later.

#### Note 16.6

This conjecture was proposed in Chernikov *et al.* (1990) after considering advection in a hexagonal variant of the so-called ABC-flow (see Section 23.1). The dependence of the type  $\mu = \mu(K)$  was presented from simulation, and its singular dependence on  $K$  was linked to bifurcations and changes of the phase space topology.

#### Note 16.7

Peaks in diffusion for the standard map were noted in Ichikawa *et al.* (1987). Similar results with more details were also reported in Benkadda *et al.* (1997) and Zaslavsky *et al.* (1997).

#### Note 16.8

The data are given from Zaslavsky and Niyasov (1997). The directly obtained value  $\mu$  means calculation of moments  $\langle R^{2m} \rangle$  with  $m = 1/2, 1, 2, \dots$ . We discuss them in Chapter 17. There are other simulations for different values of control parameters and different problems (Benkadda *et al.* (1997); Zaslavsky *et al.* (1997); White *et al.* (1998); Carreras *et al.* (1999); Carreras *et al.* (2001); Kuznetsov and Zaslavsky (1998, 2000); Leoncini *et al.* (2001); and others).

## Problems

More complicated problems are marked by (\*).

16.1 Starting from (16.58), calculate the constant in (16.59).

*This page intentionally left blank*

## RENORMALIZATION GROUP OF KINETICS (RGK)

In the previous chapters we discussed in detail how the dynamics forms a specific topology of phase space, which leads to self-similar patterns in time and phase space. The existence of scaling properties in the space-time behaviour makes it possible to apply the renormalization group approach which we call *Renormalization Group of Kinetics* (RGK).

An important feature of the RGK is the coupling of space-time scalings. This coupling has a dynamical origin and it imposes the necessity of a deep understanding of the dynamical singularities in order to find the links between spatial and temporal behaviour of trajectories (*Note 17.1*).

### 17.1 Space-time scalings

In Section 16.1 the kinetic equation was considered as a kind of balance equation between a change in the number of particles in a unit volume during a small time interval  $\Delta t$ , and the corresponding change due to particle dynamics into and out of the volume. This concept will be continued further in this section in a more general way.

Let  $\ell$  be a space variable and  $t$  be the time variable so that  $P(\ell, t)$  is a density distribution along the dynamical trajectories. Consider an infinitesimal change of  $P(\ell, t)$  in time, i.e.

$$\delta_t P(\ell, t) = \hat{\Delta}_t^\beta P(\ell, t), \quad (17.1)$$

where the shift operator  $\hat{\Delta}_t^\beta$  is defined in (16.3) and in Appendix C. The corresponding to  $\Delta t$  infinitesimal change in space is

$$\delta_\ell P(\ell, t) = \sum_{\Delta \ell} \hat{\Delta}_\ell^\alpha P(\ell, t), \quad (17.2)$$

where the sum is performed over all possible paths of the displacement  $\Delta \ell$  in the phase space during the same time interval  $\Delta t$ . Fractal properties of the chaotic trajectories can be applied directly to (17.1) and (17.2)

$$\begin{aligned} \delta_t P &= (\Delta t)^\beta \frac{\partial^\beta P}{\partial t^\beta}, \\ \delta_\ell P &= \sum_{\Delta \ell} \frac{\partial^\alpha}{\partial \ell^\alpha} (|\Delta \ell|^\alpha \mathcal{A}' P), \end{aligned} \quad (17.3)$$



where  $\alpha, \beta$  are critical exponents that characterize the fractal structures of space-time,  $\ell$  is assumed to be positive (length of a flight), and  $\mathcal{A}'$  is a function of  $\ell$  and other phase space variables additional to  $\ell$ .

A typical kinetic equation appears as a balance equation

$$\delta_t P = \overline{\delta_\ell P}, \quad (17.4)$$

where the bar means averaging over all possible paths and additional to  $\ell$  variables. Using a notation

$$\mathcal{A} \equiv \sum_{\Delta \ell} \frac{|\Delta \ell|^\alpha}{(\Delta t)^\beta} \mathcal{A}' \quad (17.5)$$

we arrive from (17.4) to

$$\frac{\partial^\beta P}{\partial t^\beta} = \frac{\partial^\alpha}{\partial \ell^\alpha} (\mathcal{A}P), \quad (17.6)$$

i.e. to a simplified version of the FKE (16.23) with  $\ell = |x|$ .

The RGK can be introduced starting from the dynamics. Let the dynamics possess the rescaling properties

$$\hat{R}_K : \Delta \ell \rightarrow \lambda_\ell \Delta \ell, \quad \Delta t \rightarrow \lambda_T \Delta t, \quad (17.7)$$

which one may accept in a broad sense, i.e. the rescaling exists after some averaging or coarse-graining, in restricted time-space domains, etc. (*Note 17.2*). The basic feature of the RGK is that the balance equation (17.4) is invariant under the renormalization transform (17.7), i.e.

$$\hat{R}_K \delta_t P = \hat{R}_K \overline{\delta_\ell P}, \quad (17.8)$$

which means that

$$\frac{\partial^\beta P}{\partial t^\beta} = \frac{\lambda_\ell^\alpha}{\lambda_T^\beta} \frac{\partial^\alpha}{\partial \ell^\alpha} (\mathcal{A}P). \quad (17.9)$$

Starting from some minimal values  $\Delta t, \Delta \ell$ , one can apply  $\hat{R}_K$  arbitrary number  $n$  times. This transforms (17.9) into

$$\frac{\partial^\beta P}{\partial t^\beta} = \left( \frac{\lambda_\ell^\alpha}{\lambda_T^\beta} \right)^n \frac{\partial^\alpha}{\partial \ell^\alpha} (\mathcal{A}P). \quad (17.10)$$

The kinetic equation (17.6) ‘survives’ under the action of  $\hat{R}_K$  if the limit  $n \rightarrow \infty$  has a sense, i.e. if there exists a limit

$$\lim_{n \rightarrow \infty} \left( \frac{\lambda_\ell^\alpha}{\lambda_T^\beta} \right)^n = 1, \quad (17.11)$$

which leads to the fixed point solution

$$\frac{\beta}{\alpha} = \frac{\ln \lambda_\ell}{\ln \lambda_T} \equiv \frac{\mu}{2}. \quad (17.12)$$

The equation (17.12) shows an important connection between the exponents  $(\alpha, \beta)$  and scaling constants  $(\lambda_\ell, \lambda_T)$ . This result can be expanded to a more fundamental property if we consider the moment equation for (17.6), i.e.

$$\langle \ell^\alpha \rangle = \mathcal{D}_{\alpha\beta} t^\beta \quad (17.13)$$

(compare to (16.28)) with

$$\mathcal{D}_{\alpha\beta} = \frac{\Gamma(1+\alpha)}{\Gamma(1+\beta)} \mathcal{A}. \quad (17.14)$$

Comparing (17.12) to (16.30) we obtain the result that  $\mu$  is the transport exponent

$$\mu = \frac{2 \ln \lambda_\ell}{\ln \lambda_T}, \quad (17.15)$$

which is now expressed through the scaling parameters  $(\lambda_\ell, \lambda_T)$ .

The obtained result is consistent with the conjecture (16.47) on the relationship between  $(\alpha, \beta)$  and  $(\lambda_\ell, \lambda_T)$ .

## 17.2 Log-periodicity

The phenomenon of log-periodicity was considered already in Section 10.6. It occurs as a result of the existence of discrete renormalization. The non-uniform mixing in phase space leads to some scaling properties for trajectories with fixed parameters of the scale transform  $\lambda_\ell, \lambda_T$  in (17.7). Similar log-periodicity can be found for the transport properties governed by the FKE.

The existence of FKE is based on the formal existence of the limit

$$\lim_{\Delta t \rightarrow 0} \overline{\mathcal{A}' |\Delta \ell|^\alpha / (\Delta t)^\beta} = \text{const}, \quad (17.16)$$

which is equivalent to the Kolmogorov condition for the FPK equation

$$\lim_{\Delta t \rightarrow 0} \overline{(\Delta \ell)^2 / \Delta t} = \text{const}. \quad (17.17)$$

The essential difference, in addition to the difference of the exponents, appears when we impose invariance of the FKE under the RG-transform  $\hat{R}_K$ . Indeed, the Gaussian distribution is invariant under the transform

$$\hat{R}_G : \Delta \ell \rightarrow \lambda^{1/2} \Delta \ell, \quad \Delta t \rightarrow \lambda \Delta t \quad (17.18)$$

with arbitrary value of  $\lambda$ . That means that the Gaussian renormalization  $\hat{R}_G$  is continuous, while the  $\hat{R}_K$  in (17.7) is discrete with fixed values of  $\lambda_\ell$  and  $\lambda_T$ .

The FKE (17.6) is linear and a sum of its solutions is also a solution. Particularly, the fixed-point equation (17.11) has an infinite number of solutions. For example,

$$\beta_k = \frac{\alpha \ln \lambda_\ell}{\ln \lambda_T} + \frac{2\pi i k}{\ln \lambda_T} = \frac{1}{2}\alpha\mu + \frac{2\pi i k}{\ln \lambda_T}, \quad (k = 0, \pm 1, \dots) \quad (17.19)$$

satisfies (17.11) and the expression (17.12) gives a particular solution only for  $k = 0$ . Using (17.19), we can rewrite the moment equation (17.13) in the form of the superposition

$$\langle \ell^\alpha \rangle = \sum_{k=0}^{\infty} \mathcal{D}_{\alpha\beta}^{(k)} t^{\beta_k} = \mathcal{D}_{\alpha\beta}^{(0)} t^\beta \left\{ 1 + 2 \sum_{k=1}^{\infty} \left( \frac{\mathcal{D}_{\alpha\beta}^{(k)}}{\mathcal{D}_{\alpha\beta}^{(0)}} \right) \cdot \cos \left( \frac{2\pi k}{\ln \lambda_T} \ln t \right) \right\}, \quad (17.20)$$

where new coefficients  $\mathcal{D}_{\alpha\beta}^{(k)}$  ( $k > 0$ ) are unknown and typically are small. The term in brackets is periodic with respect to  $\ln t$  and the period is

$$T_{\log} = \ln \lambda_T. \quad (17.21)$$

Figure 17.1 provides an example of log-periodicity for the web map of the four-fold symmetry. More examples appear in the forthcoming sections.

For the cases when the initial kinetic equation has a discrete renormalization invariance in an explicit form the coefficients  $\mathcal{D}_{\alpha\beta}^{(k)}$  can be explicitly calculated (Hanson *et al.* (1985); Montroll and Shlesinger (1984); see also Section 15.5 on WRW). Another comment is related to the limit  $\Delta t \rightarrow 0$  in (17.16). When the RG is discrete, there are cut-off values of  $\min \Delta \ell \equiv \Delta \ell_0$  and  $\min \Delta t \equiv \Delta t_0$ , and all other permitted values of  $\Delta \ell, \Delta t$  are greater or much greater of  $\Delta \ell_0, \Delta t_0$ . A physical meaning of this was given in Section 12.2. Some other applications of the log-periodicity can be found in Shlesinger and West (1991).

A few important conclusions follow from the obtained result (17.20):

- (a) Until now, knowledge of the transport exponent  $\mu$  did not permit us to obtain  $\alpha$  and  $\beta$ , but only their ratio (see (17.12)). Observing log-periodicity and its period (17.21), one can obtain  $\beta$  for some simplified situations as

$$\beta = \frac{1}{T_{\log}}. \quad (17.22)$$

- (b) It can happen that the amplitudes  $\mathcal{D}_{\alpha\beta}^{(k)}$  have a ‘noisy’ character and the term in brackets of (17.20) vanishes after averaging. Then the only exponent  $\mu$  defines the transport. In general case *there is no monofractality* for the anomalous transport.

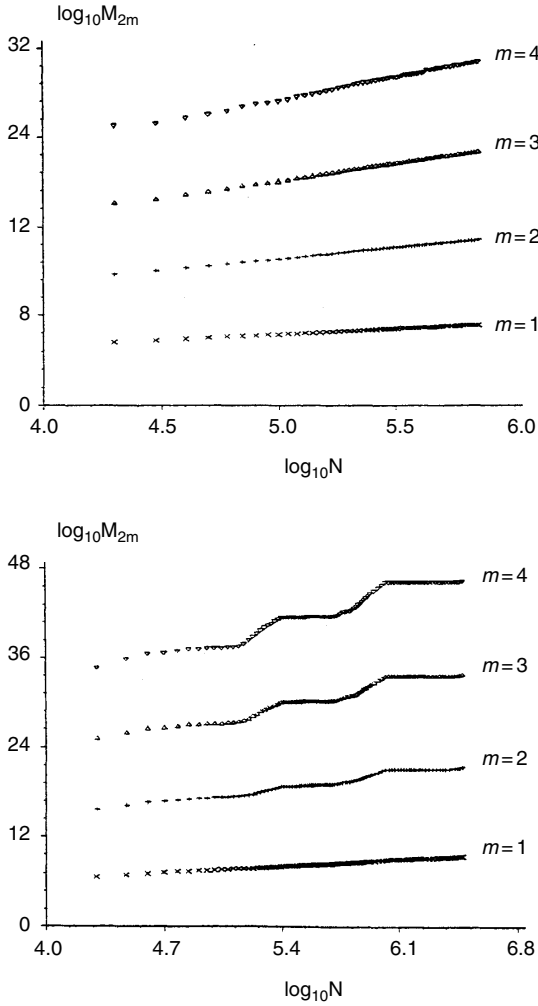


FIG. 17.1. Log-log plots of the even moments  $M_{2m} = \langle R^{2m} \rangle$  of the trajectories displacement  $R$  vs. number of iterations (time)  $N$  for the web map with four-fold symmetry where  $K = 6.25$ , top, with normal diffusion, and  $K = 6.349972$ , bottom, with superdiffusion.

### 17.3 Duality of the dynamics and the origin of multi-fractality

Power-like behaviour of different distributions and their moments vs. time creates a very specific physical situation that is worthwhile to discuss separately. We are often interested in the asymptotics  $t \rightarrow \infty$ , but if distributions do not have

a finite time cut-off, we should go to more and more fine structures of the phase space. Such property of the dynamics will be called *duality*, and  $(\xi_t, \eta_0)$  will be called *dual observables* if properties of  $\xi_t \rightarrow \infty$  ( $t \rightarrow \infty$ ) are defined by the invariant local characteristic  $\eta_0 \rightarrow 0$ . As an example, consider the stickiness of the islands' boundaries.

Depending on the control parameter of the considered maps, it can happen that each island is surrounded by a set of  $q_1$  islands of a first generation, and each island of the first generation is surrounded by  $q_2$  islands of the second generation, and so on. In this way, a hierarchical set of sticky zones attached to the islands emerges in phase space. The smaller the sticky island of the  $n$ -th generation, characterized by its area  $S_n$ , the longer the trajectory stays in the boundary layer and the longer the flight length  $\ell_n$ . We will say that the duality property exists for the magnitudes  $(\ell, S)$ , which means that the limits

$$\ell \rightarrow \infty, \quad S \rightarrow 0 \tag{17.23}$$

are equivalent and we omit the subscript  $n$ . More precisely, for the cases considered in Chapter 16, it was shown that

$$\ell S^{1/2} \sim \text{const}, \quad (\ell \rightarrow \infty, S \rightarrow 0). \tag{17.24}$$

One may also introduce a period  $T_n$  of the last invariant curve in an island of the  $n$ -th generation and write down another duality connection

$$T \text{ dual } S^{-1/2} \text{ dual } \ell \tag{17.25}$$

but  $T$  is not dual to  $\ell$ .

Consider a Poincaré map of a low-dimensional Hamiltonian system with chaotic dynamics. The points of the map fill the stochastic sea evading islands. At least this feature of the chaotic dynamics makes the distribution function of the points of a strongly non-uniform trajectory. Singular domains can be related to the well-known homoclinic structure (Fig. 17.2) near an unperturbed saddle point or, to a more complicated structure such as a sticky domain. A common conjecture is that these structures impose large time-space asymptotics. This property can be described on the basis of the duality of dynamics.

Considering a homoclinic structure like in Fig. 17.2, we understand that the presented complexity of the picture is only the first few steps of the iteration process, and that the more steps to be performed, the more complicated the pattern will be and the smaller the meshes. It is very natural to describe a homoclinic structure by its (multi)-fractal characteristics which can be obtained from the local properties of the pattern, i.e. sizes of the meshes  $\Delta x_j \rightarrow 0$ . We need this limit in order to calculate fractal dimensions. One may assume that fractal or multifractal properties of a homoclinic structure strongly depend on the control parameter, say  $K$ , for the web map. But it is not a complete picture and the existence of a hierarchy of sticky islands brings an additional source of the fractality,

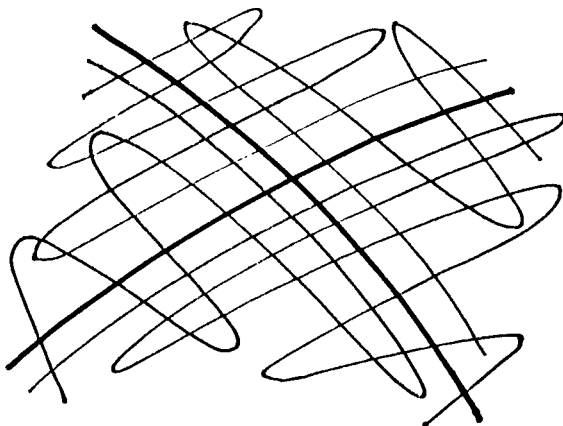


FIG. 17.2. Sketch of a homoclinic structure endowing the islands' hierarchy.

which also sensitively depends on the control parameter, and which also is local as the sizes of islands tend to zero. Just the latter property and its duality should specify the multifractal feature of fractional kinetics. Unfortunately not too much is known yet in this direction (*Note 17.3*).

## 17.4 Multifractal kinetics

In Section 10.4 we considered a description of multifractal objects using the spectral function of dimensions. Another very specific multifractal property i.e. log-periodicity, was described in Section 17.3 for the FKE. In this section we show how to combine both of the multifractal features in order to provide a more realistic description of the kinetics and transport.

Let us write a natural generalization of the moment equation (17.13). Assume for simplicity that for a large time interval taken near a much larger time instant  $t$ , transport is defined by different values of  $\beta$  so that (17.6) is

$$\frac{\partial^\beta F(\ell, t; \beta)}{\partial t^\beta} = \mathcal{A}(\beta) \frac{\partial^\alpha F(\ell, t; \beta)}{\partial \ell^\alpha}, \quad (17.26)$$

where we assume that  $\mathcal{A}$  does not depend on  $\ell$ . The normalization condition is

$$\int_{\ell_{\min}}^{\infty} \int d\beta \rho(\beta) F(\ell, t; \beta) = 1, \quad (17.27)$$

where  $\rho(\beta)$  is a weighting function of different values of  $\beta$ , and  $\ell_{\min}$  is a lower boundary of the flight's length. The integration over  $\beta$  can be replaced by the summation when the set of  $\beta$  is discrete. Then the moment equation (17.13)

should be modified as

$$\langle \ell^{m\alpha} \rangle = \int_{\ell_{\min}}^{\infty} d\ell \int d\beta \rho(\beta) \mathcal{A}^{(m)}(\beta) t^{m\beta} F(\ell, t; \beta), \quad (17.28)$$

where we have introduced some power  $m$ .

Now let us discretize integration over  $\ell$  using, as a support, the hierarchy of islands with characteristic scales in time

$$T_{\beta}^{(n)} = \lambda_T^n(\beta) T_{\beta}, \quad \lambda_T(\beta) > 1 \quad (17.29)$$

and in length

$$\ell_{\beta}^{(n)} = \lambda_{\ell}^n(\beta) \ell_{\beta}, \quad \lambda_{\ell}(\beta) > 1. \quad (17.30)$$

Here  $T_{\beta}$  and  $\ell_{\beta}$  are related respectively to the last invariant curve period and length of a flight for the main island in the island's hierarchy, and we drop the superscript (0) in  $T_{\beta}^{(0)}$  and  $\ell_{\beta}^{(0)}$  for simplicity. In the same way,  $T_{\beta}^{(n)}$  and  $\ell_{\beta}^{(n)}$  are related to an island of the  $n$ -th generation. Scaling constants  $\lambda_T(\beta)$  and  $\lambda_{\ell}(\beta)$  are intrinsic characteristics of the island's hierarchical set. The discretized version of (17.28) means the replacements

$$\ell \rightarrow \ell_{\beta}^{(n)}, \quad t \rightarrow T_{\beta}^{(n)} \equiv t_{\beta}^{(n)}. \quad (17.31)$$

The second limit in (17.31) defines also a type of asymptotic expression that will be obtained as a final result below.

The transformation (5.7) influences also  $\rho(\beta)$ . Indeed, following on from Section 10.4, let us introduce a spectral function of dimensions  $f(\beta)$  as

$$\rho(\beta) = \rho_0(\Delta x)^{f(\beta)}, \quad (17.32)$$

where  $\Delta x$  is a linear size of a small domain of the phase space partition (see also Afraimovich and Zaslavsky, 1997). Recalling that the partition is induced by the island's hierarchy, we can replace  $\Delta x \rightarrow S^{1/2}$  or, using the duality (17.24) and (17.25), we arrive at

$$\rho(\beta) = \rho_0 t^{-f(\beta)} \rightarrow \rho_0 (t_{\beta}^{(n)})^{-f(\beta)}. \quad (17.33)$$

The normalization condition (17.27) permits us to replace the integration over  $d\ell$  in (17.28) by a function  $C(\beta)$  which depends insignificantly on  $\beta$ . Substituting (17.33) into (17.28) we obtain

$$\langle \ell^{m\alpha} \rangle = \int d\beta C(\beta) t^{m\beta - f(\beta)}. \quad (17.34)$$

Since  $t \rightarrow \infty$  (see (17.31) and (17.29)) we can apply a steepest descent method and consider a maximum of the function

$$\Phi(\beta) = m\beta - f(\beta), \quad (17.35)$$

that is, the point  $\beta_s$  such that

$$\frac{d\Phi(\beta_s)}{d\beta_s} = 0, \quad \frac{d^2\Phi(\beta_s)}{d\beta_s^2} < 0, \quad (17.36)$$

which gives

$$f'(\beta_s) = m, \quad f''(\beta_s) > 0. \quad (17.37)$$

Until now the expressions (17.34)–(17.37) look similar to the known ones from Section 10.4. Nevertheless, there exists a strong difference from the results of Section 10.4 when we consider the origin of the problem and the limit  $t \rightarrow \infty$ .

The exponents  $\alpha, \beta$  appear from a dynamical model as a result of the stickiness of trajectories to the island's hierarchies. As we show in Section 17.2, the exponent  $\beta$  can be complex due to an invariance of the kinetics with respect to a discrete Renormalization Group Kinetics (RGK). The 'permitted' complex values of  $\{\beta\}$  are:

$$\{\beta\} \equiv \beta_j = \beta + \frac{2\pi i j}{\ln \lambda_T}, \quad (j = 0, \pm 1, \dots), \quad (17.38)$$

where  $\beta$  is a real part of  $\beta_j$ .

Assume that the local multifractal properties of the singular part of phase space are defined by the only spectral function  $f(\beta)$ . For the multifractal situation we should replace (17.38) by

$$\beta_j = \beta + \frac{2\pi i j}{\ln \lambda_T(\beta)}, \quad (17.39)$$

where we replace  $\lambda_T \rightarrow \lambda_T(\beta)$  in contrary to (17.38). The expression (17.34) should be replaced by

$$\langle \ell^{m\alpha} \rangle = \sum_{j=-\infty}^{\infty} \int d\beta C_j(\beta) t^{m\beta_j - f(\beta)}, \quad (17.40)$$

where we have replaced  $C(\beta)$  in (17.34) by  $C_j(\beta)$  which may be different for different values of  $j$ .

In the limit  $t \rightarrow \infty$  we can apply the steepest descent method for integrating over the parameter  $\beta$  in (6.3). Instead of (17.35), we now have the equation

$$\Phi_j(\beta) = m\beta_j - f(\beta) = m \left[ \beta + 2\pi i \frac{j}{\ln \lambda_T(\beta)} \right] - f(\beta), \quad (17.41)$$



which is defined on the complex plane. Instead of (17.36), we have the equation for the extremum point of  $\Phi_j(\beta)$ :

$$\Phi'_j(\beta) \equiv \frac{d\Phi_j(\beta)}{d\beta} = 0, \quad (\forall j) \quad (17.42)$$

or the complex root  $\beta_s$  of (17.42)

$$\beta_s = \bar{\beta}_s + i\bar{\bar{\beta}}_s \quad (17.43)$$

satisfies the equation

$$m = \frac{f'(\beta_s)}{1 - 2\pi i j \lambda'_T / \lambda_T [\ln \lambda_T(\beta_s)]^2}, \quad (17.44)$$

where  $\bar{\beta}_s, \bar{\bar{\beta}}_s$  are real. Both of the parameters  $\bar{\beta}_s, \bar{\bar{\beta}}_s$  depend on  $m$ , which is typical for the multifractal theory, and on  $j$ , which is a result of the complexification of the problem. Indeed, (17.44) does not have in general real solutions unless  $\lambda'_T(\beta_s) = 0$ .

To see how the imaginary part in (17.43) influences the transport, assume that  $\bar{\bar{\beta}}_s$  is small compared to  $\bar{\beta}_s$ . Then, in the first approximation, we obtain from (17.44)

$$m = f'(\bar{\beta}_s), \quad (17.45)$$

that is, the equation for the real part of the exponent  $\bar{\beta}_s$  coincides with (17.37).

In the same approximation, expanding  $f(\beta_s)$  over small  $\bar{\bar{\beta}}_s$ , we have

$$\bar{\bar{\beta}}_s = -\frac{2\pi j \lambda'_T f'(\bar{\beta}_s)}{f''(\bar{\beta}_s) \lambda_T [\ln \lambda_T(\bar{\beta}_s)]^2}. \quad (17.46)$$

This term grows with  $j$ , and the formula (17.46) can be used only for the first terms in the sum (17.40). Since the sum (17.40) is performed over positive and negative  $j$ , the signs of  $\lambda'_T(\beta_s)$ ,  $f''(\bar{\beta}_s)$  are of no importance.

Equation (17.44) provides a solution for  $\beta_s = \beta_s(m, j)$ ,  $\bar{\beta}_s = \bar{\beta}_s(m, j)$ ,  $\bar{\bar{\beta}}_s = \bar{\bar{\beta}}_s(m, j)$ . For not too large  $j$  we may use (17.45) and (17.46), that is,

$$\begin{aligned} \bar{\beta}_s(m) &= [f']^{-1}(m) \equiv \beta^{(0)}(m), \\ \bar{\bar{\beta}}_s(m, j) &= -\frac{2\pi j \lambda'_T(\beta^{(0)}(m)) f'(\bar{\beta}_s)}{f''(\beta^{(0)}(m)) \lambda_T [\ln \lambda_T(\beta^{(0)}(m))]^2}. \end{aligned} \quad (17.47)$$

Result (17.47) shows that the real part of  $\beta$  at the extreme point does not depend on  $j$  (for not too large  $j$ ) and that the imaginary part of  $\beta$  is linearly proportional to  $j$ . Both of them are functions of  $m$ . Nevertheless, we have to point out that for large  $j$ , terms  $\bar{\bar{\beta}}_s(m, j)$  can be fairly large.

Finally, (17.40) transforms into

$$\langle \ell^{m\alpha} \rangle \sim \sum_{j=-\infty}^{\infty} C_j(\beta_s) t^{m\beta_{j,s} - f(\beta_s)}, \quad (17.48)$$

where  $\beta_{j,s}$  is the complex solution of (17.44)

$$\beta_{j,s} = \beta_s + \frac{2\pi i j}{\ln \lambda_T(\beta_s)} \quad (17.49)$$

(compare to (17.38)).

When  $\bar{\beta}_s \ll \beta_s$ , we have a simplification

$$\langle \ell^{m\alpha} \rangle \sim 2 \sum_{j=1}^{\infty} C_j(\bar{\beta}_s) t^{m\bar{\beta}_s - f(\bar{\beta}_s)} \cos \left\{ 2\pi j \frac{\ln t}{\ln \lambda_T(\bar{\beta}_s)} \left[ 1 + \frac{\lambda'_T(\bar{\beta}_s)}{f''(\bar{\beta}_s) \lambda_T(\bar{\beta}_s)} \right] \right\}. \quad (17.50)$$

In the absence of multifractality ( $\bar{\beta}_s = \beta$ ,  $f(\beta) \equiv 0$ ) the expression (17.50) yields the known result up to the moment the multiplier  $m$  shows the self-similarity

$$\langle \ell^{m\alpha} \rangle = t^{m\alpha\mu/2} 2 \sum_{j=-\infty}^{\infty} C_j \cos \left( 2\pi j \frac{\ln t}{\ln \lambda_T} \right), \quad (17.51)$$

where we put the transport exponent  $\mu = 2\beta/\alpha$ . Equation (17.51) coincides with (17.20).

For a general situation described by (17.50), we meet again log-periodicity with a period

$$T_\ell = \frac{\ln \lambda_T(\bar{\beta}_s)}{1 + (\lambda'_T(\bar{\beta}_s)/f''(\bar{\beta}_s) \ln \lambda_T(\bar{\beta}_s))}, \quad (17.52)$$

where  $\bar{\beta}_s$  is a solution for (17.45) and it depends on  $m$  (see (17.47)). The larger  $m$  is, the stronger the dependence of the log-periodic oscillations on  $m$  will be.

We may assume that the log-periodicity and its intermittent character are due to the multifractality of the singular domains of phase space, and it is not only a property of chaotic dynamical systems, but is also a feature that can be observed in different turbulent data. Let us mention in this respect, small ‘waving’ observed in particle dispersion in 2D turbulence (Paret and Tabeling (1997)), and dependence of the waving on the moment number in Boffetta *et al.* (2000). To observe the phenomenon of the intermittent log-periodicity in turbulence, more accurate measurements or simulations are necessary for higher moments. An important comment is that some averaging procedures can nullify or reduce the effect of waving. Indeed, until now we consider  $C_j(\bar{\beta}_s)$  to be real.

In fact,  $C_j(\bar{\beta}_s)$  is complex and the complex ones will be coefficient  $C_j$ . Due to this, a phase shift

$$\Delta\phi_j = \tan^{-1} \left( \frac{\text{Im } C_j}{\text{Re } C_j} \right) \quad (17.53)$$

should appear in the argument of cosine in (17.49). If the averaging procedure for data includes also averaging over  $\Delta\phi_j$ , the effect of log-periodicity can disappear. This may happen, for example, when data are collected from topologically non-equivalent realizations.

## Notes

### Note 17.1

The renormalization group is a powerful tool to study physical phenomena with scaling properties (see for example Kadanoff (1981, 1993, 2000); Greene *et al.* (1981); MacKay (1983); Hentschel and Procaccia (1983); Jensen *et al.* (1985)). Initially, the method of the renormalization group proved to be efficient in field theory and statistical physics and later they were applied to dynamics and chaos. The Gaussian process can be considered as the first and trivial example of a possible application of the renormalization group theory in the kinetics, and crucial achievements were obtained for kinetics near a phase transition point (Wilson and Kogut (1974); Hohenberg and Halperin (1977)). Chaotic dynamics near the cantori exhibits scaling properties and the corresponding kinetic equation was derived by Hanson *et al.* (1985) (see also MacKay *et al.* (1984)). The material of this section follows Zaslavsky (1984a, 1984b, 2000a) and Benkadda *et al.* (1999).

### Note 17.2

In typical renormalization group theory applied in statistical physics this is the most difficult part of the computations requiring the use of the diagrams technique. Here, in dynamics, this part of the work is receiving a special value of the control parameter  $K^*$ , for which the property (17.7) is valid, simultaneously with determination of the scaling constants  $\lambda_T, \lambda_S, \lambda_\ell$ . We have partly discussed this issue in Chapters 11 through 13. There will be more examples later.

### Note 17.3

For the islands related to the accelerator and ballistic modes within the homoclinic structure, see Rom-Kedar and Zaslavsky (1999). For more about homoclinic structure and its self-similarity, see Rom-Kedar *et al.* (1990) and Rom-Kedar (1994).

## FRACTIONAL KINETIC EQUATION: SOLUTIONS AND MODIFICATIONS

This section presents mainly technical material on how to operate with the fractional kinetic equation. We provide only some preliminary information addressing details in special literature (see the book by Podlubny (1999) and references therein). There are three different approaches to the solutions of FKE: series, Fourier–Laplace transform, and separation of variables. We consider a simplified form of them with respect to some simple models (*Note 18.1*).

### 18.1 Solutions to FKE (series)

In this section we consider FKE in the form

$$\frac{\partial^\beta}{\partial t^\beta} P(x, t) = \frac{\partial^\alpha}{\partial |x|^\alpha} P(x, t) + S(x, t), \quad (18.1)$$

where  $S(x, t)$  is a source. For the source we use the standard form

$$S(x, t) = \delta(x)\delta(t) \quad (18.2)$$

or a time distributed point source

$$\begin{aligned} S(x, t) &= S_0(t)\delta(x), \\ S_0(t) &= \frac{t^{-\beta}}{\Gamma(1-\beta)} = \frac{\partial^\beta}{\partial t^\beta} \hat{1} \rightarrow_{\beta \rightarrow 1} \delta(t), \end{aligned} \quad (18.3)$$

which will be explained later and where

$$\hat{1} = \begin{cases} 1, & t > 0, \\ 0, & t < 0. \end{cases}$$

Consider a Fourier transform with respect to  $x$

$$P(q, t) = \int_{-\infty}^{\infty} dx e^{iqx} P(x, t) \quad (18.4)$$

and similarly for the source (18.4)

$$S(q, t) = \int_{-\infty}^{\infty} dx e^{iqx} S(x, t) = S_0(t). \quad (18.5)$$

Equation (18.2) transforms into

$$\frac{\partial^\beta}{\partial t^\beta} P(q, t) + |q|^\alpha P(q, t) = S_0(t), \quad (t > 0). \quad (18.6)$$

For the case (18.5), the solution for (18.6) can be written in the form

$$P(q, t) = \sum_{m=0}^{\infty} \frac{(-1)^m}{\Gamma(m\beta + 1)} (|q|^\alpha t^\beta)^m = E_\beta(-|q|^\alpha t^\beta), \quad (t > 0), \quad (18.7)$$

where

$$E_\beta(z) = \sum_{m=0}^{\infty} \frac{z^m}{\Gamma(m\beta + 1)} \quad (18.8)$$

is the Mittag-Leffler function of order  $\beta$  (see Appendix D).

Using the inverse transform

$$P(x, t) = \int_{-\infty}^{\infty} dq e^{-iqx} P(q, t) \quad (18.9)$$

we can write the solution in the series form

$$P(x, t) = \frac{1}{\pi|y|} \frac{1}{t^{\mu/2}} \sum_{m=0}^{\infty} \frac{(-1)^m}{|y|^{m\alpha}} \frac{\Gamma(m\alpha + 1)}{\Gamma(m\beta + 1)} \cos \left[ \frac{\pi}{2} (m\alpha + 1) \right], \quad (18.10)$$

where

$$y = \frac{x}{t^{\mu/2}} \quad (18.11)$$

and  $\mu$  is the same as in (16.30). The asymptotics of (18.10) are

$$P(x, t) \sim \frac{1}{\pi} \frac{t^\beta}{|x|^{\alpha+1}} \frac{\Gamma(1 + \alpha)}{\Gamma(1 + \beta)} \sin \frac{\pi\alpha}{2} \quad (18.12)$$

under the condition

$$|x|^2 \gg t^\mu. \quad (18.13)$$

The expression (18.12) coincides for  $\beta = 1$  with the Lévy process distribution  $P_\alpha(x, t)$  in (15.29). We can conclude from (18.12) that the moments

$$\langle |x|^\delta \rangle < \infty \quad \text{if } 0 < \delta < \alpha \leq 2. \quad (18.14)$$

The series (18.10) also shows that the solution can be considered in a self-similar form

$$P(x, t) = t^{-\mu/2} P \left( \frac{|x|}{t^{\mu/2}} \right), \quad (18.15)$$

which we will discuss later. For  $\alpha = 2$ ,  $\beta \leq 1$  all moments  $\langle x^m \rangle$  are finite.

## 18.2 Solutions to FKE (separation of variables)

This section, having more technical details, provides an important physical interpretation of the FKE (Saichev and Zaslavsky (1997)).

Consider Laplace in time and Fourier in space transforms of  $P(x, t)$ :

$$P(q, u) = \int_0^\infty dt \int_{-\infty}^\infty dx e^{-ut+iqx} P(x, t) \quad (18.16)$$

with the inverse formula

$$P(x, t) = \frac{1}{2\pi i} \int_{c-i\infty}^{c+i\infty} du \int_{-\infty}^\infty dq e^{ut-iqx} P(u, q). \quad (18.17)$$

Application of (18.16) to the FKE (18.1) with the source (18.2) gives

$$P_{\alpha,\beta}(q, u) = \frac{1}{(u^\beta + |q|^\alpha)} \quad (18.18)$$

(see Appendix C for integral transforms of fractional derivatives). This result can be rewritten in the form

$$P_{\alpha,\beta}(q, u) = \int_0^\infty ds \exp[-s(u^\beta + |q|^\alpha)] = \int_0^\infty ds Q_\beta(u, s) W_\alpha(q, s) \quad (18.19)$$

with

$$Q_\beta(u, s) = e^{-su^\beta}, \quad W_\alpha(q, s) = e^{-s|q|^\alpha}, \quad (18.20)$$

where  $Q_\beta(u, s)$  and  $W_\alpha(q, s)$  can be interpreted as corresponding Lévy-type characteristic functions with a parameter  $s$ , and (18.19) is a separation of variables formula for the characteristic function  $P_{\alpha,\beta}(q, u)$  of the solution.

Let us apply now the inverse transform (18.17) and use the presentation (18.19):

$$P_{\alpha,\beta}(x, t) = \int_0^\infty ds Q_\beta(t, s) W_\alpha(x, s) \quad (18.21)$$

with

$$\begin{aligned} Q_\beta(t, s) &= \frac{1}{2\pi i} \int_{c-i\infty}^{c+i\infty} du e^{ut} Q_\beta(u, s) = \frac{1}{2\pi i} \int_{c-i\infty}^{c+i\infty} du \exp(ut - su^\beta), \\ W_\alpha(x, s) &= \int_{-\infty}^\infty dq e^{-iqx} W_\alpha(q, s) = \int_{-\infty}^\infty dq \exp(-iqx - s|q|^\alpha). \end{aligned} \quad (18.22)$$

The result (18.21) completes the separation of variables and presents the solution through a superposition of Lévy processes along  $x$  and  $t$ . A similar presentation can be developed for the more complicated source (18.3) (see Problem 18.1).

### 18.3 Continuous time random walk (CTRW)

This is a *probabilistic model*. We use the notion ‘probabilistic models’ to underline the fact that the main axiomatic approach to the final kinetic equation is based on a construction of random wandering process rather than on the construction of a model for dynamic trajectories without *a priori* probabilistic elements. The most popular and widely used is the *continuous time random walk* (CTRW) model introduced in (Montroll and Weiss (1965)) and developed in a number of succeeding publications (Weiss (1984); Montroll and Shlesinger (1984)) (*Note 18.2*).

CTRW theory operates with two kinds of probabilities related to the random walk of a particle: the probability density to find a particle at the position  $x$  after executing  $j$  steps  $P_j(x)$ , and the probability density to find a particle at  $x$  at time  $t$ ,  $P(x, t)$ . The corresponding random walk equation assumes independence of changes at each step together with a uniformity of the probability distributions of time and distance intervals between consequent steps. Under these conditions we have for  $P_j(x)$

$$P_{j+1}(x) = \int_{-\infty}^{\infty} dx' W(x - x') P_j(x') \quad (18.23)$$

with  $W(x)$  as a transitional probability, and

$$P(x, t) = \int_0^t d\tau \phi(t - \tau) Q(x, \tau) \quad (18.24)$$

with  $\phi(t)$  as a probability density to stay in the achieved position  $x$  for a time  $t$ , and  $Q(x, t)$  as a probability to find a particle in  $x$  at  $t$  immediately after a step has been taken.

The probability  $\phi(t)$  can be expressed through the probability density  $\psi(t)$  to have an interval  $t$  between two consequent steps:

$$\phi(t) = \int_t^{\infty} dt' \psi(t'). \quad (18.25)$$

Let  $\psi_j(t)$  be the probability density to make the  $j$ -th step at a time instant  $t$ . Then

$$\psi_{j+1}(t) = \int_0^t d\tau \psi(t - \tau) \psi_j(\tau), \quad \psi_1(t) \equiv \psi(t). \quad (18.26)$$

The following obvious equation

$$Q(x, t) = \sum_{j=1}^{\infty} \psi_j(t) P_j(x) \quad (18.27)$$

establishes the connection between discrete steps random walk and continues the waiting time at different steps.

It is convenient to use Fourier transforms of  $P_j(x)$  and  $W(x)$ :

$$\begin{aligned} P_j(q) &= \frac{1}{(2\pi)} \int_{-\infty}^{\infty} dx e^{iqx} P_j(x), \\ W_j(q) &= \frac{1}{(2\pi)} \int_{-\infty}^{\infty} dx e^{iqx} W(x), \end{aligned} \quad (18.28)$$

which for simplicity are written in one-dimensional case. From (18.23) and (18.28) we obtain

$$P_j(q) = W(q)P_{j-1}(q) = [W(q)]^j \quad (18.29)$$

with an initial condition  $P_0(q) = 1$ , that is, the particle is initially at the origin. Thus, from (18.29)

$$P_j(x) = \int_{-\infty}^{\infty} dx e^{-iqx} [W(q)]^j. \quad (18.30)$$

Consider a Laplace transform of  $\psi_j(t)$ ,  $\psi(t)$  and  $Q(x, t)$ :

$$\begin{aligned} \psi_j(u) &= \int_0^{\infty} dt e^{-ut} \psi_j(t), \\ \psi(u) &= \int_0^{\infty} dt e^{-ut} \psi(t), \\ Q(x, u) &= \int_0^{\infty} dt e^{-ut} Q(x, t). \end{aligned} \quad (18.31)$$

Then it follows from (18.26) and (18.31)

$$\psi_j(u) = \psi(u)\psi_{j-1}(u) = [\psi(u)]^j. \quad (18.32)$$

After combining (18.24) and (18.31) with (18.27) we obtain

$$Q(x, u) = \int_{-\infty}^{\infty} dx \frac{e^{-iqx}}{1 - W(q)\psi(u)}. \quad (18.33)$$

Finally, using the connection (18.25) in the form

$$\phi(u) = \frac{[1 - \psi(u)]}{u} \quad (18.34)$$

and applying it and (18.33) to (18.34) we arrive at the solution:

$$P(x, t) = \frac{1}{2\pi} \frac{1}{2\pi i} \int_{-i\infty}^{c+i\infty} du \frac{1}{u} [1 - \psi(u)] e^{ut} \int_{-\infty}^{\infty} dq \frac{e^{-iqx}}{1 - \psi(u)W(q)}, \quad (18.35)$$



which is known as the *Montroll-Weiss equation*. The final result has been expressed through the two basic probabilities:  $W(x)$  for the length of a step, and  $\psi(t)$  for the time interval between the consequent steps (*Note 18.3*).

The main applications of the Montroll-Weiss equation are related to the limits  $t \rightarrow \infty$ ,  $x \rightarrow \infty$  and corresponding approximations with two transition probability functions  $\psi(u)$  and  $W(q)$  which form a considerable model of the random walk process. By choosing  $\psi(u)$  and  $W(q)$  one can create a model that presumably should fit the physical situation. Equation (18.35) is just a formal presentation of the solutions that can be very different depending on the model functions  $W(q)$  and  $\psi(u)$ . Let us rewrite (18.35) in the form

$$[1 - \psi(u)W(q)]P(q, u) = \frac{1}{u}[1 - \psi(u)] \quad (18.36)$$

and consider some cases for  $\psi(u)$  and  $W(q)$ . For example we can assume that

$$\psi(u) = 1 + t_0 u, \quad W(q) = 1 - ix_0 q + \frac{1}{2} \sigma q^2 \quad (18.37)$$

considering the limits  $u \rightarrow 0$ ,  $q \rightarrow 0$  equivalent to the limits  $t \rightarrow \infty$ ,  $x \rightarrow \infty$ , and introducing constants  $t_0$ ,  $x_0$ , and  $\sigma$ . Then, up to the higher orders terms, (18.36) becomes

$$\left( t_0 u - ix_0 q + \frac{1}{2} \sigma q^2 \right) P(q, u) = t_0, \quad (18.38)$$

which is equivalent to the diffusion equation

$$t_0 \frac{\partial P(x, t)}{\partial t} + x_0 \frac{\partial P(x, t)}{\partial x} = \frac{1}{2} \sigma \frac{\partial^2 P(x, t)}{\partial x^2} + t_0 \delta(x) \delta(t). \quad (18.39)$$

It is also assumed that  $t_0$ ,  $\sigma \neq 0$ .

Consider now the case

$$W(q) = 1 - |q|^\alpha, \quad \psi(u) = 1 - u^\beta, \quad (u, q \rightarrow 0), \quad (18.40)$$

where constants are included into the definition of  $q$  and  $u$ . Substitution of (18.40) into (18.36) gives

$$(u^\beta + |q|^\alpha)P(q, u) = u^{\beta-1}, \quad (18.41)$$

where we neglect the product  $u^\beta |q|^\alpha$ , or

$$P(q, u) = \frac{u^{\beta-1}}{u^\beta + |q|^\alpha} \quad (18.42)$$

and

$$P(x, t) = \frac{1}{2\pi} \frac{1}{2\pi i} \int_{c-i\infty}^{c+i\infty} du \int_{-\infty}^{\infty} dq \frac{u^{\beta-1}}{u^{\beta} + |q|^{\alpha}}. \quad (18.43)$$

The last expression can be used to obtain the moments  $\langle |x|^{\delta} \rangle$ . By replacing the variables we can obtain

$$\langle |x| \rangle = \text{const } t^{\beta/\alpha} = \text{const} \cdot t^{\mu/2} \quad (18.44)$$

(Afanasiev *et al.* (1991)). This result coincides with (16.29) for the FKE. In fact, it is a consequence of (18.41) that coincides with (18.1) if the source will be taken in the form (18.3). To prove this, let us use the formulas of the Laplace–Fourier transforms of the derivatives (see Appendix C):

$$\begin{aligned} \frac{d^{\alpha}}{d|x|^{\alpha}} g(x) &\xrightarrow{(F)} -|q|^{\alpha} g(q), \\ \frac{d^{\beta}}{dt^{\beta}} g(t) &\xrightarrow{(L)} u^{\beta} g(u), \\ \frac{d^{\beta}}{dt^{\beta}} \hat{1} &\xrightarrow{(L)} u^{\beta-1}, \end{aligned} \quad (18.45)$$

where  $(F)$  and  $(L)$  indicate Fourier and Laplace transforms. Applying (18.45) and (18.3) to (18.41), we arrive at

$$\frac{\partial^{\beta} P(x, t)}{\partial t^{\beta}} = \frac{\partial^{\alpha} P(x, t)}{\partial |x|^{\alpha}} + \frac{t^{-\beta}}{\Gamma(1-\beta)} \delta(x), \quad (18.46)$$

which coincides with the FKE (16.21) when the source is taken in the special form (18.3) and  $\mathcal{A} = \text{const}$ . This result establishes the connection between the FKE and CTRW as well as differences since the equations are obtained in different approximations and different initial assumptions. For example the equation (18.36) or (18.35) is fairly general and does not use approximations  $q \rightarrow 0$ ,  $u \rightarrow 0$  while the transition to FKE does. At the same time, in the limit  $q \rightarrow 0$ ,  $u \rightarrow 0$ , (18.35) has a special type of the source (18.3) while the FKE does not specify the source. In addition, the FKE in the form (18.46) or (18.42) can be valid not only in the limit  $q \rightarrow 0$ ,  $u \rightarrow 0$  but for fairly small time-space scales as we will see for dynamical systems.

## 18.4 Lévy walks and other generalizations of CTRW

There are few generalizations that enhance possible applications of the CTRW theory: the Lévy walk (Shlesinger *et al.* (1987)), the relativistic model of CTRW (Shlesinger *et al.* (1995b)), multiplicative random walks (Shlesinger and Klafter (1989)), and others. Here we would like to stop briefly on the Lévy walk which was introduced in (Shlesinger *et al.* (1987)) in order to avoid infinite moments

of the displacement  $x$ . In the same scheme of derivation of the CTRW, let us introduce a probability density  $\psi(x, t)$  to make a jump of the length  $x$  in a time  $t$ :

$$\psi(x, t) = \psi(t | x)W(x), \quad (18.47)$$

where  $W(x)$  has the same meaning as in (18.23) and  $\psi(x|t)$  is a conditional probability. It is also possible to write

$$\psi(x, t) = W(x | t)\psi(t) \quad (18.48)$$

with  $\psi(t)$  the same as in (18.25) and  $W(x | t)$  as a conditional probability.

As a simple demonstration, consider an expression

$$\psi(t | x) = \delta\left(t - \frac{x}{V(x)}\right), \quad (18.49)$$

where  $V(x)$  is a velocity as a function of the displacement  $x$ . This form appeared in Shlesinger and Klafter (1989) to show that for the Kolmogorov scaling  $V(x) \sim x^{1/3}$  and for  $W(x) \sim |x|^{1+\beta}$  one can find for the mean square displacement  $x(t)$ :

$$\langle x^2(t) \rangle = \begin{cases} t^3, & \beta \leq \frac{1}{3}, \\ t^{2+(3/2)(1-\beta)}, & \frac{1}{3} \leq \beta \leq \frac{1}{2}, \\ t, & \beta \geq \frac{1}{2}. \end{cases} \quad (18.50)$$

The idea of the Lévy walk is to couple space-time memory by using expressions (18.47)–(18.49) and to obtain, in this way, the finite second moment of the displacement at time instant  $t$  while the distribution of all possible displacements  $W(x)$  has infinite second moment.

One additional type of generalization of the CTRW can be useful for applications. This is related to the master equation. It was proposed in Kenkre *et al.* (1973) (see also Montroll and Shlesinger (1984)) to write the master equation in the form

$$\frac{\partial P(x, t)}{\partial t} = \int_0^t d\tau \phi(t - \tau) \left\{ \sum_{x'} W(x - x') P(x', t) - P(x, \tau) \right\} \quad (18.51)$$

with an appropriate transition probability  $W(x)$  and a delay probability function  $\phi(t - \tau)$ .

A generalized fractional Kolmogorov–Feller equation was proposed in Saichev and Zaslavsky (1997):

$$\frac{\partial^\beta P(x, t)}{\partial t^\beta} = \int_{-\infty}^{\infty} dy W(y) [P(x - y; t) - P(x, t)], \quad (18.52)$$

which is similar to (18.51). The fractional derivative with respect to  $t$  is written in an explicit form, while a fractional derivative with respect to  $x$  can appear from  $W(y)$ .

### 18.5 Conflict with dynamics

The CTRW or Montroll–Weiss equations are governed by two arbitrary probabilistic functions  $W(x)$  and  $\psi(t)$ , and there are high resources for applications when these probabilities appear from known processes. Chaotic dynamics in its contemporary stage does not provide information about  $W(x)$  and  $\psi(t)$  except for maybe some special solutions. In lieu of this comment, one should be very careful in applying the CTRW to experimental and simulation data. The best example is related to the basic assumption for the derivation of the CTRW equation: the independence of steps in the random walk which definitely is not the case for the standard map, web map, and all other more complicated models of chaos. A similar comment can be made for the Lévy walk. The dynamic equations and, for example, the standard map do not impose the relation of the (18.47)–(18.49) type and the observations of many other dynamical models show an absence of the strong coupling of type (18.49) (*Note 18.4*).

### 18.6 Subdiffusion and superdiffusion

While the diffusion equation has a fixed form, the form of fractional kinetics is not prescribed and there exists a possibility of numerous fractional formats depending on physical situations. For example, numerous variants of kinetics can appear if we modify the expansions (16.3) and (16.8), or make special selections of the basic spectral functions  $\psi(u)$ ,  $W(q)$  in (18.35) for the CTRW.

As an example, instead of (18.37) consider

$$\begin{aligned} \frac{1}{\psi(u)} &= 1 + u^\beta, \quad u \rightarrow 0, \quad (0 < \beta \leq 1), \\ W(q) &= 1 - ix_0q + \frac{1}{2}\sigma q^2. \end{aligned} \tag{18.53}$$

Then  $P(q, u)$  satisfies the equation

$$\left( u^\beta - ix_0q + \frac{1}{2}\sigma q^2 \right) P(q, u) = u^{\beta-1} \tag{18.54}$$

or in  $(x, t)$  variables

$$\frac{\partial^\beta P(x, t)}{\partial t^\beta} + x_0 \frac{\partial P(x, t)}{\partial x} = \frac{1}{2}\sigma \frac{\partial^2 P(x, t)}{\partial x^2} + \frac{t^{-\beta}}{\Gamma(1-\beta)} \delta(x); \quad (0 < \beta \leq 1). \tag{18.55}$$

This equation that corresponds to the fractal Brownian motion (Mandelbrot and Van Ness (1968)) can be generalized to the three-dimensional random walk:

$$\frac{\partial^\beta P(\mathbf{r}, t)}{\partial t^\beta} + \mathbf{v} \cdot \nabla P(\mathbf{r}, t) = \mathcal{D} \Delta P(\mathbf{r}, t) + \frac{t^{-\beta}}{\Gamma(1-\beta)} \delta(\mathbf{r}), \quad (0 < \beta \leq 1) \quad (18.56)$$

(Compte (1997); Uchaikin (2000); Weitzner and Zaslavsky (2001)).

As it was mentioned in Section 18.1 for the case (18.55), all moments  $\langle x^m \rangle$  are finite. The function  $\psi(u)$  in (18.53) is a characteristics of delays or traps with a probability density to stay time  $t$  before the escape

$$\psi(t) \sim \frac{1}{t^{1+\beta}}, \quad t \rightarrow \infty. \quad (18.57)$$

This probability has an infinite mean time of escape

$$t_{\text{esc}} \equiv \langle t \rangle = \int_0^\infty t \psi(t) dt \quad (18.58)$$

for  $\beta < 1$ , imposing infinite recurrence time. Such a situation should not appear in Hamiltonian dynamics. At the same time, equation (18.55) provides

$$\langle x^2 \rangle = \frac{\sigma}{\Gamma(1+\beta)} t^\beta, \quad (0 < \beta \leq 1) \quad (18.59)$$

that correspond to the subdiffusion (Saichev and Zaslavsky (1997)). The Hamiltonian phase space is at least two-dimensional, and the subdiffusion along one variable and superdiffusion or diffusion along the other one are not forbidden (*Note 18.5*).

In FK the second moments  $\langle \xi^2 \rangle$  of some physical variable  $\xi$  can be infinite as they are for the Lévy processes. In a fairly general situation we can use the expression (16.29)

$$\langle |\xi| \rangle \sim t^{\beta/\alpha} = t^{\mu/2}, \quad (18.60)$$

where we replace  $x$  by an abstract  $\xi$ . The transport exponent  $\mu$  (see (16.30)) is defined in a way that  $\mu > 1$  corresponds to the superdiffusion. This definition assumes self-similarity or for the truncated moments,

$$\langle \xi^2 \rangle_{\text{tr}} \sim t^\mu \quad (18.61)$$

(compare to (16.39)). Dynamical systems, even fairly simple at first glance, display a rich set of different possibilities: the value of  $\mu$  can be very close to one, but the dynamics can be too far from the Gaussian process, self-similarity can be valid in some restrictive way and can not be applied for all moments, etc.

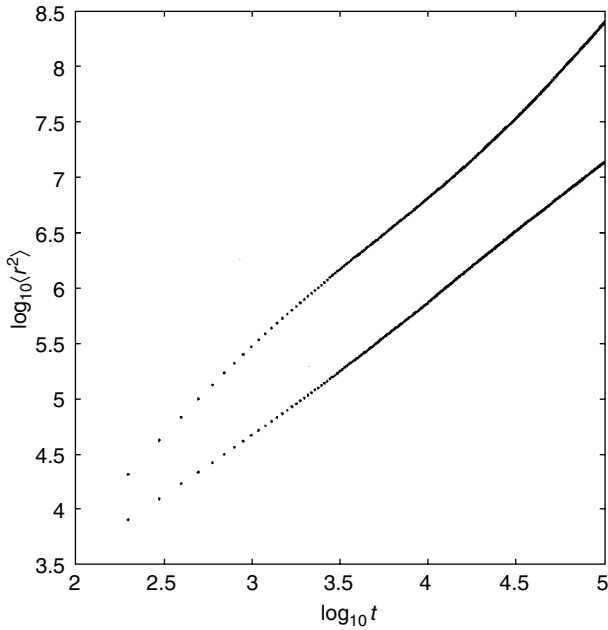


FIG. 18.1. Example of different transport exponents for different directions of the diffusion for the web map:  $\mu = 1.25$  along the  $u$ -direction and  $\mu = 1.50$  along the diagonal direction (upper line).

We will meet these examples in the following sections (see also Sections 24.2 and 24.3).

A simplified version of superdiffusion can be introduced directly as (16.23) or (16.28)

$$\frac{\partial P(\xi, t)}{\partial t} = \mathcal{A} \frac{\partial^\alpha P(\xi, t)}{\partial |\xi|^\alpha} \quad (18.62)$$

or

$$\langle |\xi|^\alpha \rangle = \Gamma(1 + \alpha) \mathcal{A} t, \quad (18.63)$$

where we put  $\mathcal{A} = \text{const}$ ,  $\beta = 1$ , and replace  $x$  by  $\xi$ . Expression (18.63) implies in the case of self-similarity

$$\mu = \frac{2}{\alpha} > 1, \quad (18.64)$$

since  $\alpha < 2$ . A similar result comes from (18.12) if we put  $\beta = 1$ .

We should comment that the superdiffusion can also exist for  $\beta < 1$ .

An interesting situation appears in the case when there are few different directions of diffusion. In Hamiltonian dynamics there are at least two directions: along the coordinate and along the momentum. In such a case

$$\langle |\xi_{\mathbf{e}^{(0)}}| \rangle \sim \mathcal{D}_{\mathbf{e}^{(0)}} t^{\mu(\mathbf{e}^{(0)})/2}, \quad (18.65)$$

that is, the transport exponent  $\mu$  depends on the direction of transport, given by the unit vector  $\mathbf{e}^{(0)}$ . In this way the FK imposes a new type of the anisotropy which reveals not only in the diffusion constant  $\mathcal{D}_{\mathbf{e}^{(0)}}$  but also in the transport exponent  $\mu(\mathbf{e}^{(0)})$ . An example of such anisotropy is given in Fig. 18.1. It follows from the Kac lemma that at least one direction should be superdiffusive. Generalization of the FK for the anisotropic case can be performed in different ways.

The simplest form is to use the Riesz fractional derivative for the fractional Laplace operator

$$(-\Delta)^{\alpha/2} \xrightarrow{F} |\mathbf{k}|^{\alpha} \quad (18.66)$$

defined through its Fourier transform. Explicit expression for the fractional Laplacian is more complicated (see Appendix D). Using expression (18.66) one can write down the generalized FKE

$$\frac{\partial^{\beta} P(\mathbf{r}, t)}{\partial t^{\beta}} = \mathcal{D}_{\alpha\beta} (-\Delta)^{\alpha/2} P(\mathbf{r}, t). \quad (18.67)$$

Different asymptotic solutions for (18.67) are given in (Zolotarev *et al.* (1999); Weitzner and Zaslavsky (2001)) (*Note 18.6*).

## Notes

### *Note 18.1*

Sections 18.1 and 18.2 follow the paper of Saichev and Zaslavsky (1997). Some additional material can be found in Weitzner and Zaslavsky (2001, 2003); Saichev and Woyczynski (1997); Afanasiev *et al.* (1991); Fogedby (1994); Meerschaert *et al.* (2001).

### *Note 18.2*

See also Uchaikin (2000); Metzler and Klafter (2000).

### *Note 18.3*

There are numerous investigations of the Montroll–Weiss equation. See Weiss (1984); Montroll and Shlesinger (1984); Afanasiev *et al.* (1991); Metzler and Klafter (2000); Uchaikin (2000), and references therein.

### *Note 18.4*

See for example Kuznetsov and Zaslavsky (2000) for simulations for advected particles in the 3-vortex flow.

*Note 18.5*

It seems that this type of subdiffusion was observed in Afanasiev *et al.* (1991); Schwägel and Krug (1991); Benenti *et al.* (2001).

*Note 18.6*

Anisotropic cases of the anomalous transport were also considered in Chernikov *et al.* (1990); Petrovichev *et al.* (1990); Meershaert and Scheffler (2000); Yanovsky *et al.* (2000).

**Problems**

More complicated problems are marked by (\*).

18.1\* Prove the equation (see (18.3)):

$$\lim_{\beta \rightarrow 1} \frac{\partial^\beta}{\partial t^\beta} \hat{1} = \delta(t),$$

where  $\hat{1} = 1(t > 0)$  or  $0(t < 0)$ .

18.2 Using the method of separation of variables (see 18.2) write the final expression for the solution (18.1) with the source (18.3).

18.3 Derive the expressions (18.50).



*This page intentionally left blank*

## PSEUDOCHAOS

Integrable systems in a compact phase space have a full set of integrals of motion and simple periodic or quasi-periodic dynamics. Systems with chaotic dynamics have a positive Lyapunov exponent and uniform mixing in phase space. There are different ways to fill the gap between integrability and chaoticity. This will be a theme of discussion in Chapter 22. Here we consider some examples of systems with zero Lyapunov exponent but, at the same time, with random dynamics which can be described by a distribution function (physical measure) that satisfies, under some conditions, a fractional kinetic equation. This type of systems has, or may have, non-ergodicity and weak mixing in phase space. We call the corresponding dynamics *pseudochaos* (*Note 19.1*).

The interest in these types of systems is three-fold: they are an interesting mathematical object for a general theory of dynamical systems; they have different interesting applications, and, which may be the most important, they can be considered as good approximations to study the fine properties of kinetics of typical chaotic systems possessing stickiness.

### 19.1 Billiards in polygons

Billiards with a fixed plane table can be considered as a Hamiltonian system with two degrees of freedom. The table can have polygonal obstacles or slits inside. A ball is considered as a moving point with unit mass and the collisions with hard boundaries are elastic. Such collisions preserve the value of velocity and rotates the velocity vector (*Note 19.2*). A *rational polygon* has  $\pi$ -rational angles between sides. An *irrational billiard* is a polygon with at least one angle that is not  $\pi$ -rational. Examples of polygonal billiards are given in Fig. 19.1. For some cases billiard trajectories can be considered in the *lifted space* (periodically continued in two directions) or *semi-lifted space* (periodically continued in one direction). Examples are given in Figs. 19.2 and 19.3. The cases in Fig. 19.2 will be called *generalized Lorentz gas* (GLG).

Here are some important properties of polygonal billiards (for details see a survey in Gutkin, 1996, 2003, and references therein).

Dynamics in a typical polygonal billiard is ergodic in a specific sense. Omitting details, one can define a ‘space’ of polygons and a subset of those ones for which typical trajectories are ergodic. The theorem (Kerckhoff *et al.* (1986))

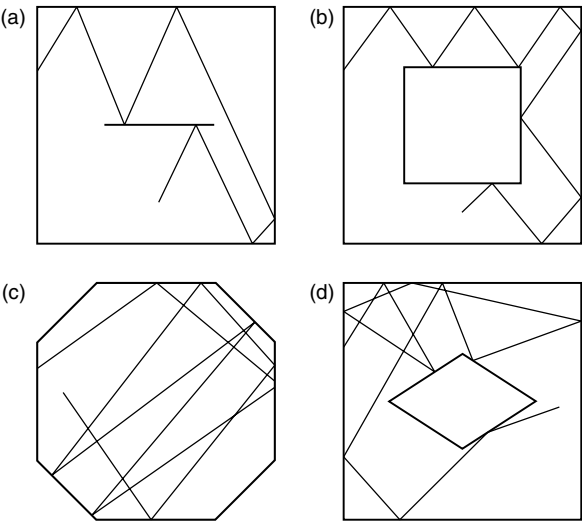


FIG. 19.1. Examples of polygonal billiards.

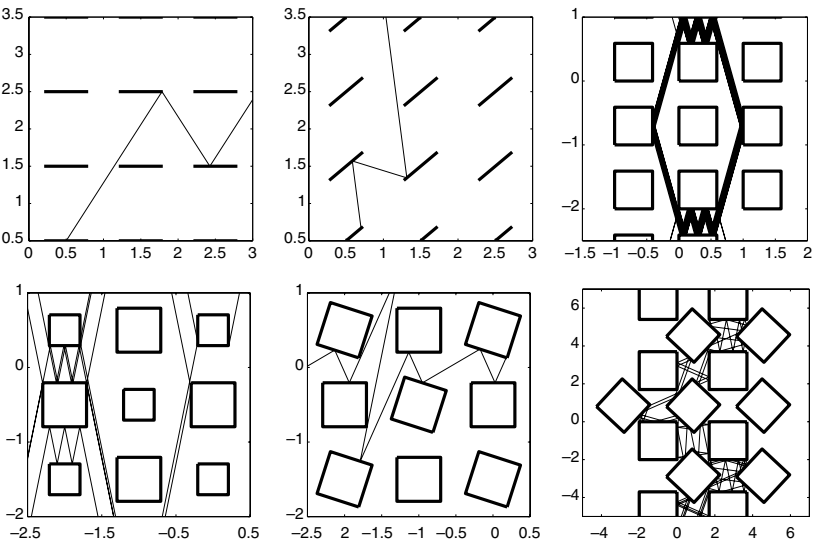


FIG. 19.2. Periodically continued billiard tables form a generalized Lorentz gas (GLG).

claims that the subset of billiards with the following properties is dense in the corresponding space of polygons:

- (1P) The Lyapunov exponent is zero and so is the KS-entropy due to Pesin's theorem.

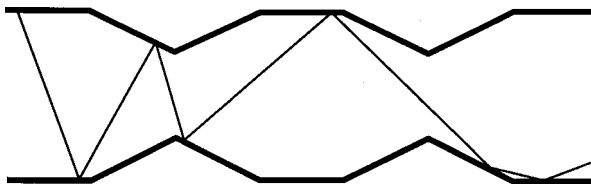


FIG. 19.3. Ray propagation in a wave guide can be considered, sometimes, as a billiard model with a piece-wise periodic non-uniformity.

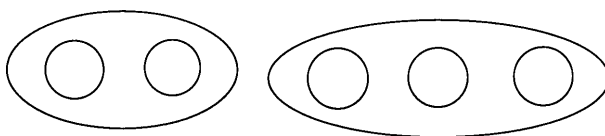


FIG. 19.4. Surfaces with  $g = 2$  (left) and  $g = 3$  (right).

- (2P) For any rational polygon and any trajectory of a ball where the dynamics is not mixing, it is probably that the dynamics of a ball is weakly mixing.
- (3P) After a proper definition (see the next chapters) the dynamics of the polygonal billiards has a *polynomial complexity*.
- (4P) The following property is important for interpretation of some results and for their applications. Let  $\hat{P}$  be a rational polygon with angles  $\pi m_i/n_i$ , ( $i = 1, \dots, p$ ) and integers  $m_i, n_i$  are co-prime. The billiard flow is isomorphic to the geodesics flow on an oriented invariant surface  $\hat{S}$  with a topology determined by the only integer  $g(\hat{S}) \geq 1$ , which is a topological genus

$$g(\hat{S}) = 1 + \frac{1}{2}N \sum_{i=1}^p \frac{m_i - 1}{n_i}, \quad (19.1)$$

where  $N$  is the least common denominator of  $\{n_i\}$ . Two examples of surfaces are given in Fig. 19.4, and the left one corresponds to the square billiard with a slit in Fig. 19.1(a).

Applying results of Kozlov (1983, 1996), we can conclude that the billiard for which  $g(\hat{S}) > 1$  is non-integrable. Sometimes they are called *pseudointegrable billiards*.

A possible way to study dynamics in billiards is to construct a corresponding *interval exchange transform* (Zorich (1997)). Consider a trajectory in the GLG in Fig. 19.2(a). Trajectories can be written as a map of an interval (slit) into

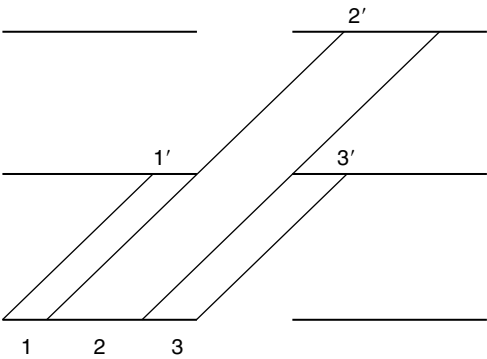


FIG. 19.5. Mapping the interval into itself as a way to present the dynamics in the billiard square-with-slit:  $(1, 2, 3) \rightarrow (3', 2', 1')$

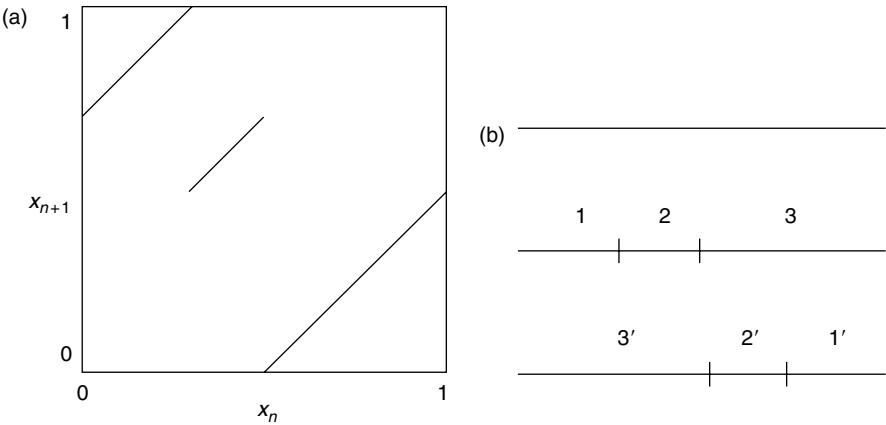


FIG. 19.6. The same mapping as in Fig. 19.5 shows the breaking of the unit interval into 3 pieces (a) and their permutation (b). The signature  $(x_{n+1}^-, x_n^+)$  is omitted.

itself. Let  $x^\pm \in (0, 1)$  be a coordinate on the bar (slit) where a trajectory hit the bar and ‘+’ is for its upper side and ‘−’ is for its lower side. Figure 19.5 shows a transform of intervals from  $x_n^+$  to  $x_{n+1}^-$ . Another presentation of the same transform is in Fig. 19.6 where we omit the signatures.

As it is seen from Fig. 19.6, each step of the map  $\hat{T}^{(\pm)}$  or  $\hat{T}^{(\mp)}$  consists of adding two breaking points and permutation of the corresponding 3 sub-intervals. Let  $\ell_j(n)$  be the  $j$ -th sub-interval of the initial interval  $L$ . Then at the  $n$ -th step

$$L(n) = \cup_{j=1}^{2n+1} \ell_j(n). \tag{19.2}$$

There are no gaps between  $\ell_j(n)$  and no overlapping of  $\ell_j(n)$ . Let us submit each sub-interval by its signature  $s_j(n)$ . Then the dynamics can be written as in the transform

$$\{\ell_j(n+1), s_j(n+1)\}_{j=1}^{2n+3} = \hat{T}_n^{(s_n)}\{\ell_j(n), s_j(n)\}_{j=1}^{2n+1}. \quad (19.3)$$

An important part is missed in (19.3). From Fig. 19.5 we see that different sub-intervals have different lengths and times between two consequent steps of the transform. To have a correct description of trajectories, their ensembles, and kinetics, each sub-interval  $\ell_j(n)$  should be assigned by an additional equation that maps the time intervals  $\Delta t_j(n)$ . This makes the problem of dynamics of balls in billiards different from the interval exchange transforms.

### 19.2 Continued fractions and scalings of trajectories

In this and the following section we consider the square-with-slit billiard (Fig. 19.1(a)) and its double periodic continuation (GLG in Fig. 19.2(a)) on the  $(x, y)$ -plane. Let  $\vartheta$  be a pitch angle of a trajectory. Rational/irrational trajectories have corresponding rational/irrational  $\tan \vartheta$ . Elementary rational trajectories are periodic in a square, and irrational ones are aperiodic. Since there is no change of velocity along  $x$ , the coordinate  $x$  in infinite space (GLG) is proportional to time  $t$ . The diffusion process can appear only along  $y$ . A sample of irrational trajectory is given in Fig. 19.7. It shows almost the same pieces repeating in different scales. This sample represents qualitatively the presence of self-similarity of irrational trajectories in space-time (*Note 19.3*).

To make a statistical type prediction it is necessary to construct an ensemble of initial conditions and to consider a distribution function of the observables and the moments as functions of time. The main focus will be on the density function  $F(y, t)$  of displacements  $y(t)$  and on the distribution of the recurrences  $P(t)$  with the normalization conditions

$$\begin{aligned} \int_{-\infty}^{\infty} F(y, t) dy &= 1, \\ \int_0^{\infty} P(y, t) dy &= 1. \end{aligned} \quad (19.4)$$

As an ensemble, it is possible to select a large number of initial conditions  $\{\vartheta_0^{(i)}, y_0\}$  with different values of  $\{\vartheta_0^{(i)}\}$  in a small interval  $\Delta\vartheta$ :  $\vartheta_0^{(i)} \in (\vartheta_0, \vartheta_0 + \Delta\vartheta)$ . The motivation for such a construction is the following: it seems that for the considered system with the Lyapunov exponent  $\sigma_L = 0$  the limit for time average observables does not exist. For example:

$$\bar{y} = \lim_{T \rightarrow \infty} \bar{y}_T = \lim_{T \rightarrow \infty} \frac{1}{T} \int_0^T y(t) dt \quad (19.5)$$

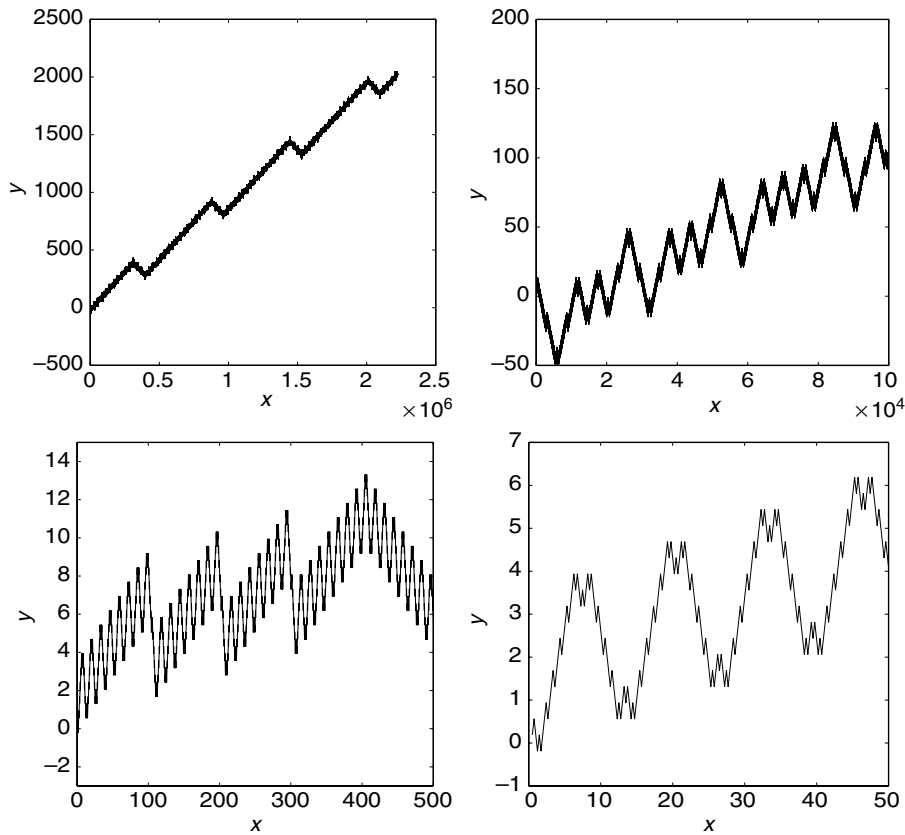


FIG. 19.7. A sample of irrational trajectory presented in different space-time scales.

does not exist and due to that the ergodic theorem fails. We discuss this more in Chapter 22. In Fig. 19.8 we show four examples of  $\bar{y}_T$  with very large values of  $T = 10^{11}$ . Either the limit does not exist or it can only be achieved in a non-realistic time. This leads us to consider only ensemble-averaged observables. For any observable  $g(x, y)$  we define

$$\langle g(x, y) \rangle = \frac{1}{N} \sum_{i=1}^N g(x_0^{(i)}, y_0^{(i)}, \vartheta_0^{(i)}), y(x_0^{(i)}, y_0^{(i)}, \vartheta_0^{(i)})),$$
$$\vartheta_0^{(i)} \neq \vartheta_0^{(k)}, \quad (\forall i, k; i \neq k) \tag{19.6}$$

i.e. the ensemble of initial coordinates must include a large number  $N$  of different angles  $\vartheta_0^{(i)}$ . The meaning of the last condition will be clear soon.

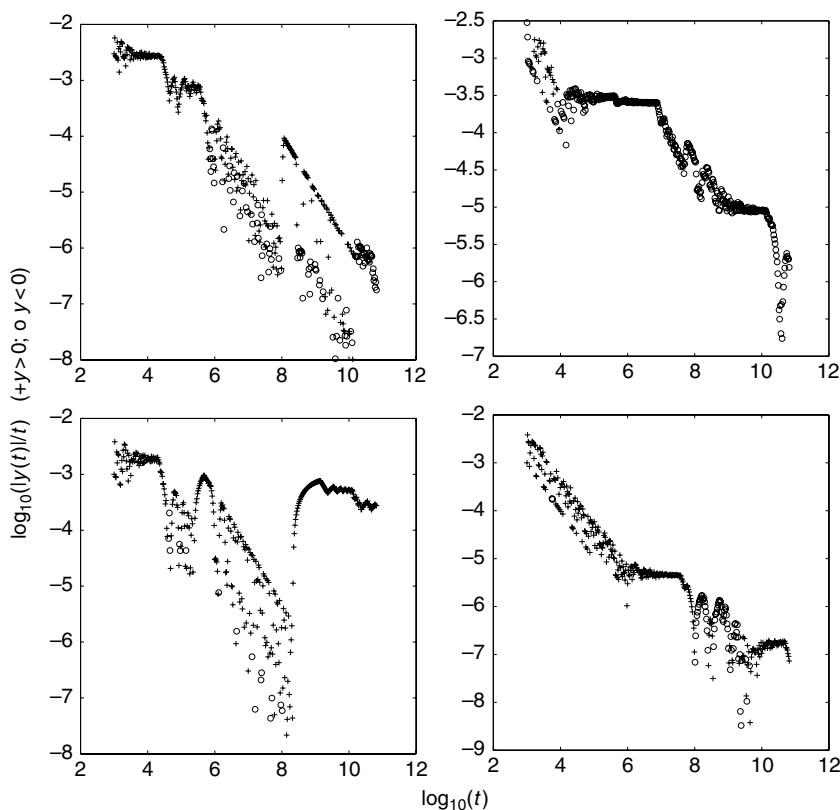


FIG. 19.8. Four examples of time-averaged coordinates of displacement along  $y$  vs. time for the square-with-slit billiard.

Let us recall that continued fraction  $\xi \in (0, 1)$  can be presented in the form

$$\xi = 1/(a_1 + 1/(a_2 + \dots)) = [a_1, a_2, \dots] \quad (19.7)$$

(Note 19.4). For example,  $\tan \vartheta$  can be presented as

$$\tan \vartheta = a_0 + [a_1, a_2, \dots]. \quad (19.8)$$

The sequence  $[a_1, a_2, \dots]$  is infinite if  $\xi$  is irrational. A finite convergent, or approximate, of  $\xi$  can be written in the form

$$\xi_n \equiv [a_1, \dots, a_n] = \frac{p_n}{q_n} \quad (19.9)$$



with co-prime  $p_n, q_n$  and with recurrent equations

$$\begin{aligned} p_k &= a_k p_{k-1} + p_{k-2}, \\ q_k &= a_k q_{k-1} + q_{k-2}, \quad k = 1, 2, \dots \end{aligned} \quad (19.10)$$

and  $p_0 = 0, p_{-1} = 1, q_0 = 1, q_{-1} = 0$ .

There are two important results that will be used: the first is related to the sequence  $\{a_j\}$ ,

$$\lim_{n \rightarrow \infty} (a_1 \dots a_n)^{1/n} = \prod_{k=1}^{\infty} \left( 1 + \frac{1}{k^2 + 2k} \right)^{\ln k / \ln 2} = 2.685 \dots \quad (19.11)$$

and the second one is related to the sequence  $\{q_j\}$ ,

$$\lim_{n \rightarrow \infty} \left( \frac{1}{n} \ln(q_n) \right) = \frac{\pi^2}{12} \ln 2 = 1.186 \dots \quad (19.12)$$

Equations (19.11) and (19.12) indicate the existence of scalings,

$$\prod_1^n a_k \sim \lambda_a^n g_a(n), \quad (n \rightarrow \infty) \quad (19.13)$$

$$q_n \sim \lambda_q^n g_q(n), \quad (n \rightarrow \infty),$$

where  $\lambda_a, \lambda_q$  are two scaling parameters, and  $g_a(n), g_q(n)$  are sub-exponentially varying functions such that

$$\lim_{n \rightarrow \infty} \frac{1}{n} \ln g_{a,q}(n) = 0. \quad (19.14)$$

The result (19.13) for  $q_n$  has an immediate application for the dynamics of a particle in the considered billiard. Indeed, rational trajectory is periodic, as was mentioned before. Moreover, if  $\tan \vartheta = p/q$  with co-prime  $(p, q)$ , then trajectories are periodic along the coordinate  $x$  with the period  $T = q$ . Taking an ensemble of initial values  $\{\vartheta_0^{(j)}\}$  with irrational  $\tan \vartheta_0^{(j)}$  and considering them as an ensemble of rational approximants of  $p^{(j)}/q^{(j)}$ , we arrive at an ensemble of trajectories with different periods  $T^{(j)}$  as first approximations. That means that the ensemble of irrational trajectories should display different quasi-periodic segments with periods that scale in the same way as  $q_n$  for large  $n$ , i.e.

$$T_n \sim \lambda_T^n g_T(n) \quad (19.15)$$

with sub-exponential dependence of  $g_T(n)$  and  $\lambda_T$  as a scaling parameter,

$$\ln \lambda_T = \ln \lambda_q = \frac{\pi^2}{12 \ln 2} = 1.186 \dots \quad (19.16)$$

as it follows from (19.12) and (19.13).

As an example, we provide the numerical data in Fig. 19.9 for the first 19 points of  $q_n$  with  $n \in (1, 19)$  obtained with the quadruple precision for the value  $\tan \vartheta = 4.153087\dots$  A plot of their values in Fig. 19.9 gives

$$\ln \lambda_q = 1.17 \pm 0.08 \quad (19.17)$$

in good agreement with (19.16). The quasi-periods  $T_n$  correspond to those that can be obtained from the denominators  $q_n$ .

It is remarkable that the universal constant (19.12) linked to the properties of continued fractions enters as a universal feature of the quasi-periods of the weak-mixing billiard trajectories. We show in the following how the value of  $\ln \lambda_T$  appears in the kinetics.

Let us call a quasi-periodic segment of a trajectory a ‘flight’. The expression (19.16) shows a time scaling of flights and hierarchical structures of different flights in time. Corresponding hierarchical structures should exist for the lengths  $\ell_n$  of the flights along  $y$ . Nevertheless, there is an ambiguity of the flight lengths  $\ell_n$  since trajectories can have different coordinate oscillations for the same time duration of flights. To find a corresponding scaling parameter  $\lambda_y$ , we assume that

$$\ln \lambda_y = \overline{\ln \lambda_{\text{den}}}, \quad (19.18)$$

where  $\lambda_{\text{den}}$  means a scaling parameter of different possible denominators of the rational convergent of  $\xi$ , obtained at the same hierarchical level along a trajectory, and the bar means averaging over such possibilities. For example, at the

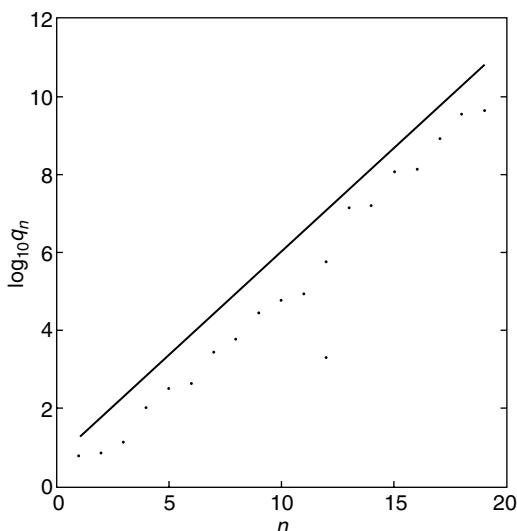


FIG. 19.9. Values of the denominators  $q_n$  of the  $n$ -th approximations for  $\tan \vartheta = 4.153087\dots$

hierarchical level  $n$ ,  $\xi_n$  has  $q_n$  as the minimal denominator and  $a_1 \dots a_n$  as the maximal denominator since

$$(a_1 \dots a_n)^{1/n} \geq (q_n)^{1/n}, \quad n \rightarrow \infty. \quad (19.19)$$

Applying (19.11) and (19.13) we obtain

$$\min \lambda_{\text{den}} = \lambda_T, \quad \max \lambda_{\text{den}} = \lambda_a. \quad (19.20)$$

The simplest estimate is

$$\ln \lambda_y = \overline{\ln \lambda_{\text{den}}} \approx \frac{1}{2} (\ln \lambda_T + \ln \lambda_a) \approx 1.087 \dots \quad (19.21)$$

The obtained information can be applied to construct the kinetic evolution of an ensemble of trajectories.

### 19.3 Fractional kinetics of irrational trajectories

Let us recall that a simplified version of the FKE can be written in the form

$$\frac{\partial^\beta F(y, t)}{\partial t^\beta} = \mathcal{D} \frac{\partial^\alpha F(y, t)}{\partial |y|^\alpha}, \quad (19.22)$$

where we assume a symmetry with respect  $y \rightarrow -y$ ,  $\mathcal{D}$  is a diffusion constant, and  $(\alpha, \beta)$  would be obtained from the dynamics. This equation suggests a solution in the form

$$F(|y|, t) \sim t^{-\mu/2} F_0 \left( \frac{|y|}{t^{\mu/2}} \right) \quad (19.23)$$

with

$$\mu = \frac{2\beta}{\alpha} \quad (19.24)$$

and the moment

$$\langle |y|^\alpha \rangle = \text{const} \cdot t^\beta \quad (19.25)$$

(see Section 18.1).

In the case of self-similarity for the truncated distribution function, we can write

$$\langle |y|^{2m} \rangle_{\text{tr}} = \text{const} \cdot t^{\mu(m)} \quad (19.26)$$

with

$$\mu(1) = \frac{2\beta}{\alpha} = \mu. \quad (19.27)$$

And in the multi-exponent  $\beta$  case

$$\langle |y|^\alpha \rangle = \sum_{k=-\infty}^{\infty} C_k t^{\beta_k} \quad (19.28)$$

with coefficients  $C_k$  that should be defined by initial and boundary conditions (see Section 17.4).

In the considered case the self-similarity of the dynamics is defined by invariance under renormalization transform

$$\hat{R} : t \rightarrow \lambda_T t, \quad y \rightarrow \lambda_y y \quad (19.29)$$

with values of  $\ln \lambda_T$  and  $\ln \lambda_y$  from (19.16) and (19.21). From the fix-point condition (17.11)

$$\lim_{n \rightarrow \infty} \left( \frac{\lambda_y^\alpha}{\lambda_T^\beta} \right) = 1 \quad (19.30)$$

and  $\alpha = \text{const}$  we have a solution for  $\beta$ :

$$\beta_k = \frac{1}{2} \alpha \mu + \frac{2\pi i k}{\ln \lambda_T}, \quad (k = 0, 1, 2, \dots) \quad (19.31)$$

and (19.28) can be rewritten as

$$\langle |y|^\alpha \rangle^{2/\alpha} = t^\mu \sum_{k=0}^{\infty} \mathcal{D}_k \cos \left( 2\pi k \frac{\ln t}{\ln \lambda_T} + \psi_k \right) \quad (19.32)$$

with

$$\mu = \frac{2 \ln \lambda_y}{\ln \lambda_T} \quad (19.33)$$

and new coefficients  $\mathcal{D}_k$  and phases  $\psi_k$  instead of  $C_k$  (compare to (17.20)). We can substitute the value of  $\lambda_T$  from (19.16) and  $\lambda_y$  from (19.17) into (19.33) and get

$$\mu = 1.8. \quad (19.34)$$

The new expression (19.32) shows modulated self-similarity with log-periodicity and a period

$$T_{\log} = \ln \lambda_T. \quad (19.35)$$

All these results can be compared with simulations (see *Note 19.3*). In Fig. 19.10 there is a plot of the tails of non-normalized distribution function  $N(|y|, t) = \text{const} \cdot F(|y|, t)$ , taken in different time instants. It has a power law dependence and self-similar shift in time. The transport exponent  $\mu$  can be

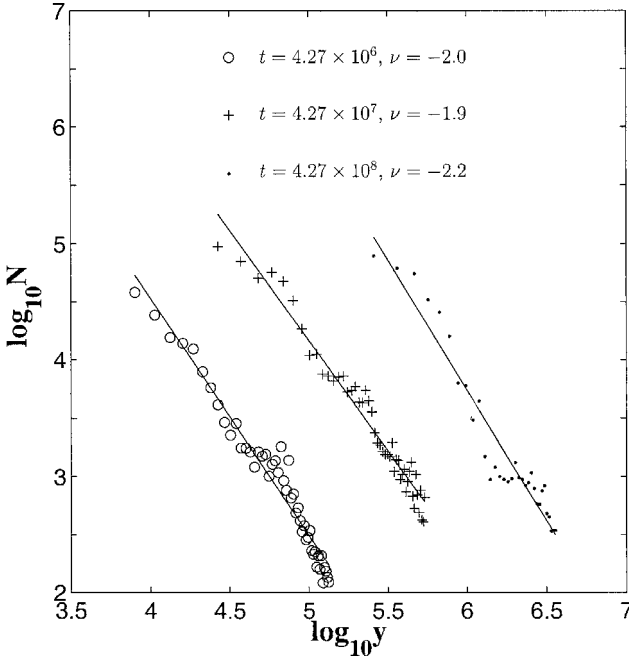


FIG. 19.10. Non-normalized distribution function (number of events  $N$ ) vs. vertical displacement  $|y|$  for three different time instants (the bar length 0.59; the square side is 1;  $68 \times 48$  trajectories near the  $\vartheta = \tan^{-1} 4.153087\dots$ ).

obtained with fairly high accuracy from Fig. 19.11. It gives  $\mu = 1.76 \pm 0.10$  in a good agreement with the theoretical value (19.34).

Consideration of log-periodicity needs a more delicate approach since  $\mathcal{D}_k$  and  $\psi_k$  in (19.32) are unknown and the phases  $\psi_k$  can be, in general, random to some extent. Consider a spectral function

$$\Psi(r) = \int_{-\infty}^{\infty} d\tau \Psi(\tau) \exp(2\pi i \tau r) \quad (19.36)$$

with

$$\Psi(\tau) = \langle |y| \rangle - \text{const} \cdot t, \quad \tau = \log_{10} t. \quad (19.37)$$

Then the ‘width’ of the spectral power  $|\Psi(r)|^2$  is defined as

$$r_{\max} \sim \frac{1}{T_{\log}}, \quad (19.38)$$

which gives  $r_{\max} \sim 2$  in decimal base of (19.16). Figure 19.12 displays just the same value.

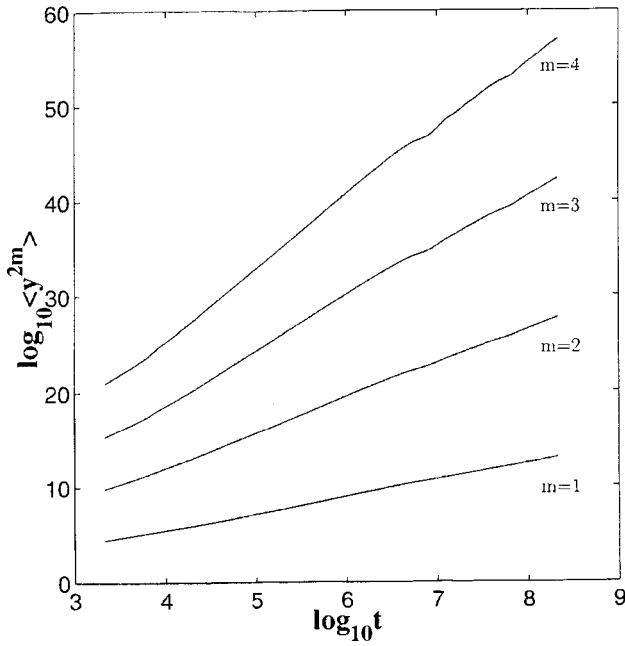


FIG. 19.11. Truncated moments vs. time for the same conditions as in Fig. 19.10.

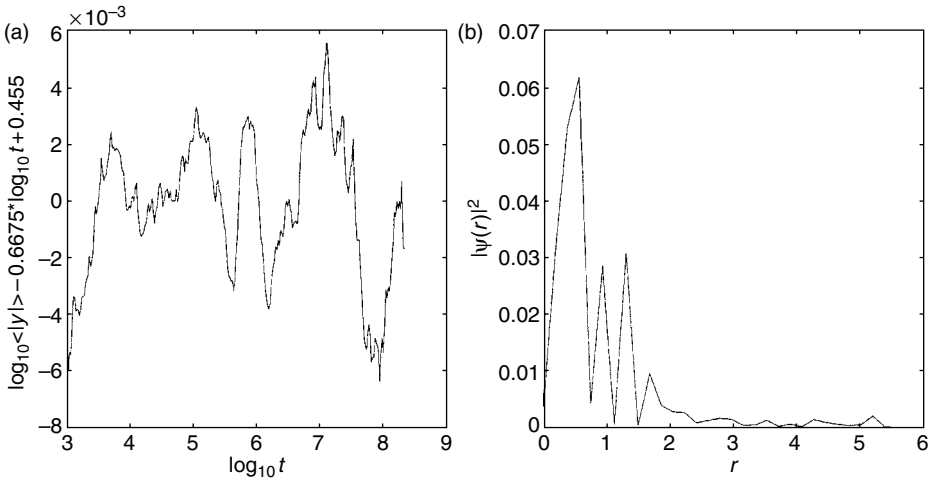


FIG. 19.12. Log-periodic oscillations of the moment  $\langle y \rangle$  in (19.25) and their Fourier spectrum power in (b). The result is obtained after simulation of 51,200 trajectories.

Distribution of the Poincaré recurrences  $P_A(t)$  can be considered for trajectories in a unit cell, i.e. in a square-with-slit, and for a similar ensemble of initial conditions as was defined to study diffusion. An interval  $A$  on the slit can be taken as a domain to return. Simulations show that, independently on  $A$  and on the geometry of the billiard (the length of the slit), the distribution is

$$P(t) = \frac{\text{const}}{t^\gamma} \quad (19.39)$$

with

$$\gamma = 2.75 \pm 0.1 \quad (19.40)$$

(see Fig. 19.13).

The result (19.40) can be written as

$$\gamma = \mu + 1 \quad (19.41)$$

and interpreted qualitatively in the following way.

Consider a domain  $A$  in phase space with a phase volume  $\Gamma_0$  and let the domain  $A$  be filled with particles that escape from  $A$  after some time. Hamiltonian dynamics preserves the phase volume  $\Gamma_0$  but the enveloped (coarse-grained) volume  $\Gamma_t$  grows with time, increasing the number of possible states

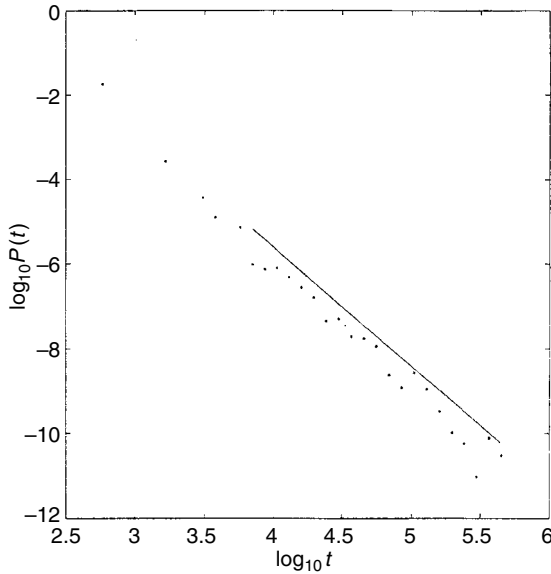


FIG. 19.13. Distribution of Poincaré recurrences for 576 trajectories with time  $10^7$ .

that can be occupied by particles from  $\Gamma_0$ . Let  $t_0$  be a characteristic time during which a particle from  $\Gamma_t$  returns for the first time to  $A$ . Typically,  $t_0 = \langle t \rangle_{\text{rec}}$ , i.e. mean recurrence time. We consider  $t \gg t_0$ . For simplicity, let us take such  $t$  that  $t/t_0 = n_t$ . Then the normalized effective volume occupied by particles (trajectories) with first return to  $A$  is

$$\frac{n_t \Gamma_t}{\Gamma_0} = \left( \frac{t}{t_0} \right) \left( \frac{\Gamma_t}{\Gamma_0} \right). \quad (19.42)$$

Expression (19.42) is the normalized phase space volume of a cylinder of the length  $t$  and base ‘area’  $\Gamma_t$ . An integrated probability of a particle with first return at time  $t$  after the exit from  $A$  at time  $t = 0$  is

$$P_{\text{int}}(t) \sim \frac{\Gamma_0}{n_t \Gamma_t} = \frac{\Gamma_0 t_0}{t \Gamma_t}. \quad (19.43)$$

The next step is the estimation of  $\Gamma_t$  for a two-dimensional phase space,

$$\Gamma_t \sim y p_y \sim \frac{y^2}{t} \quad (19.44)$$

and we arrive at

$$P_{\text{int}}(t) \sim \frac{\text{const}}{y^2}. \quad (19.45)$$

Let us replace  $y^2 \rightarrow \langle y^2 \rangle_{\text{tr}} \sim t^\mu$  and compare (19.45) to (19.39). Then (19.45)  $P_{\text{int}} \sim t^{-\mu}$  while from (19.39)  $P_{\text{int}} \sim t^{-\gamma+1}$ . This gives (19.41). For the case of self-similar islands hierarchy we have (see Section 16.5):

$$\Gamma_t^{-1} \sim \Gamma_S \sim S_t \sim \frac{1}{t^2}, \quad (19.46)$$

where  $\Gamma_S$  is the phase volume of a corresponding island with area  $S_t$ . The smaller the island, the larger the trapping time to the sticky border of the island. Substitution of (19.46) to (19.43) and comparison to (19.39) gives

$$\gamma = \mu + 2, \quad (19.47)$$



where we use

$$\langle t^2 \rangle_{\text{tr}} \sim t^\mu \quad (19.48)$$

for the truncated second moment of the flight length (*Note 19.5*).

All presented results for a square-with-slit billiard can be applied to the square-in-square billiard in Figs. 19.1(b) and 19.2(b) due to the symmetry of the dynamics. Data of simulations in Fig. 19.14 confirm this statement in full, particularly obtained for  $\gamma \approx 2.7$  and for  $\mu \approx 1.7$ . In Fig. 19.14(c) we show the

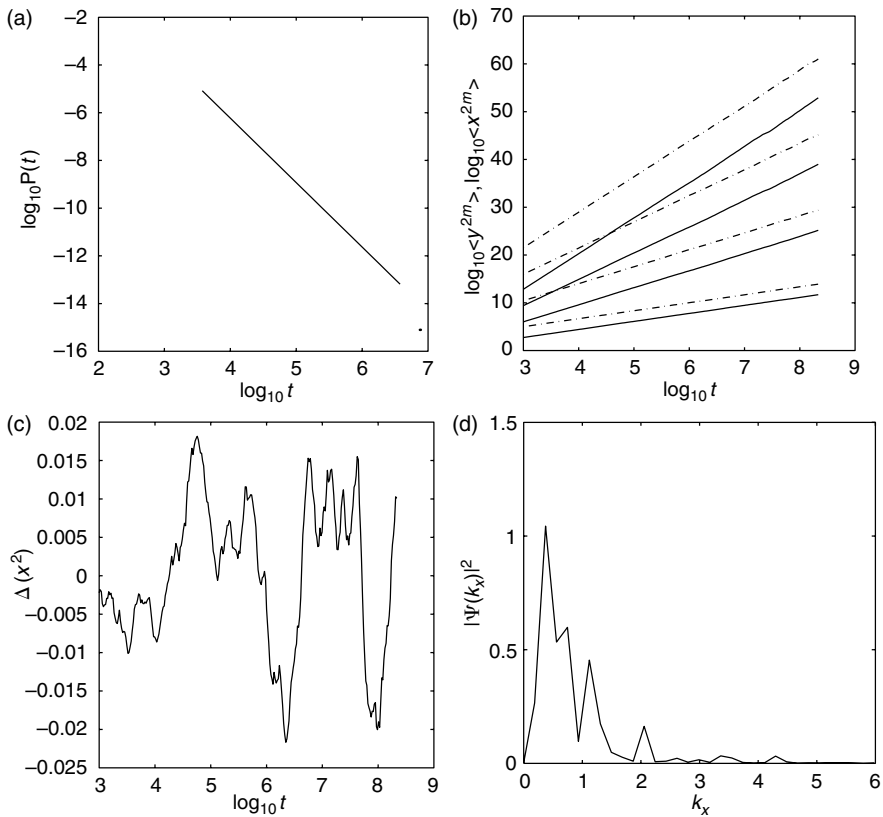


FIG. 19.14. Statistical properties of the square-in-square billiard: (a) density distribution function of the recurrences  $P(t)$ ; (b) moments of  $x$  (full lines) and  $y$  (dash lines) for  $m = 1, 2, 3, 4$  starting from the bottom; (c) fluctuations of the second moment of  $x$  vs. time; and (d) their Fourier spectrum. The data are obtained for 4,048 trajectories during the time  $10^8$  for each.

amplitudes of the 2d moment log-periodic oscillations

$$\Delta(x^2) = \langle x^2 \rangle_{\text{tr}} - \text{const} \cdot t^\mu \quad (19.49)$$

and its Fourier transform is

$$\Psi(k_x) = \int dt \, e^{2\pi i k_x \tau} \Delta(x^2), \quad \tau = \log_{10} t \quad (19.50)$$

(compare to (19.36) and (19.37)). Figure 19.14(d) displays the power spectrum of oscillations and its cut at  $k_x \sim 2$ .

## 19.4 More examples of pseudochaos

In this section we provide three examples of pseudochaotic dynamics based on simulations (*Note 19.6*). In spite of the lack of a theory for these examples, all of them have a good scientific or applied reason to warrant the attention.

### 19.4.1 Rhombic billiard

This type of billiard is shown in Fig. 19.1(c),(d), and Fig. 19.3 (*Note 19.7*). In the following examples below we consider only irrational rhombuses.

In Fig. 19.15 we present a sample trajectory which shows trappings and very slow escape from the trapping domains. This feature of the trajectories can be especially well observed from the Poincaré section: each point corresponds to a trajectory crossing of the interval  $\ell$ :  $y = 1$ ,  $x \in (0, 1)$ . There is an extremely slow process of mixing along the velocity  $v_\ell$  and the filling of the phase space is performed mainly along  $x$  for some special values of  $v_\ell$ .

The specific feature of the phase portrait in Fig. 19.15(b) is that the values of  $v_\ell$ , where the trajectory sticks for a long time, correspond to rational approximants of a fraction that corresponds to the tangent of pitch-angle of the trajectory. A no less interesting property of the rhombic billiard is that its Poincaré recurrences distribution is of the powerwise form (19.39) with

$$\gamma \gtrsim 2, \quad (19.51)$$

i.e. the recurrence exponent is close to the minimal value permitted by the Kac lemma. This type of billiard should provide the strongest fluctuations compared to other systems with  $\gamma > 2$ .

### 19.4.2 More billiards

The billiards in Fig. 19.1(e) and (f) can be related to some kind of material with *granular structure*. The case (e) has *infinite horizon*, i.e. there is a possibility of infinitely long segments of trajectories with free motion, while the case (f) corresponds to the *finite horizon* where free motion without scattering is bounded. The general structure of trajectories is difficult to describe. Their samples are given

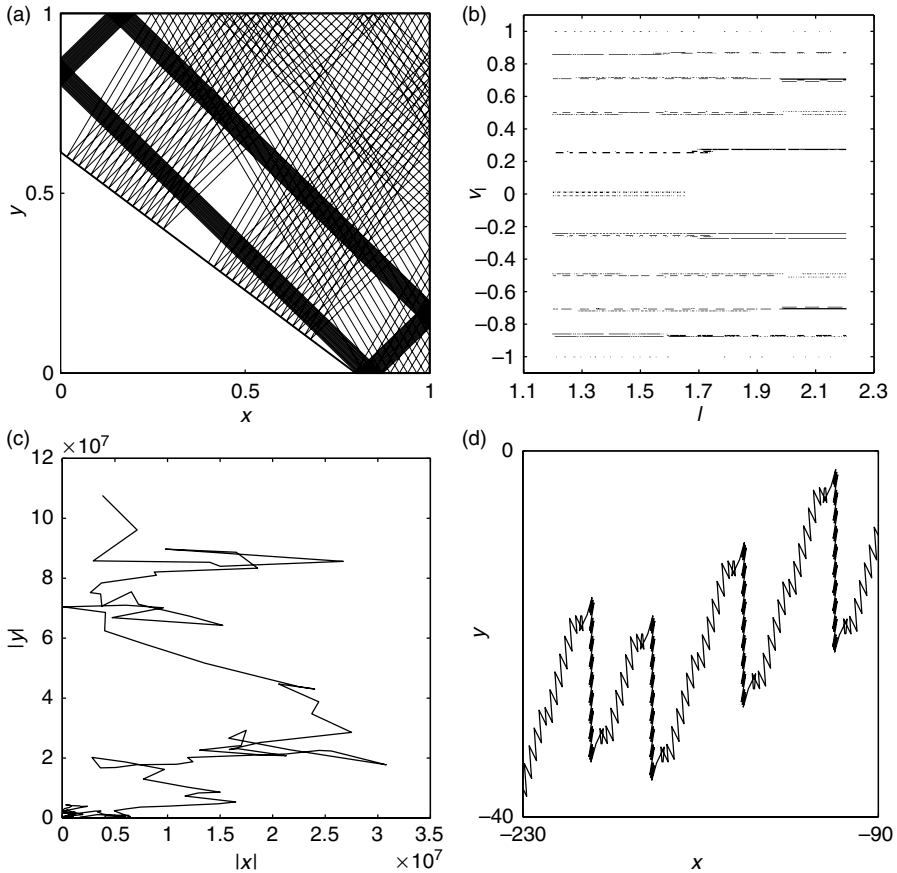


FIG. 19.15. Rhombic billiard with the  $x$ -diagonal = 1.6 and  $y$ -diagonal = 1.2290472: (a) a sample trajectory in a square with  $\frac{1}{4}$  part of the rhombics shows slow evolution; (b) phase plane  $\ell, v_\ell$  ( $\ell$  is the upper side of the square in (a)) shows slow evolution in the angle (i.e. along  $v_\ell$ ); (c) a sample trajectory in large scale (generalized Lorenz gas of rhombuses); and (d) its zoom.

in Fig. 19.16(a) and (b). Nevertheless, this billiard has fairly good statistical description of the dynamics of particles inside the billiard.

In Fig. 19.16 we present two types of statistical properties of trajectories for the finite horizon billiard in Fig. 19.1(f).

The moments of the coordinate displacements are

$$\langle x^{2m} \rangle \approx t^{\mu_x(m)}, \quad \langle y^{2m} \rangle \approx t^{\mu_y(m)} \quad (19.52)$$

with  $\mu_x(m) = \mu_y(m) \equiv \mu(m) \approx m\mu(1) \approx 1.5m$ . Considering one cell of the lattice (similarly to the billiards in Fig. 19.1), one can obtain a distribution

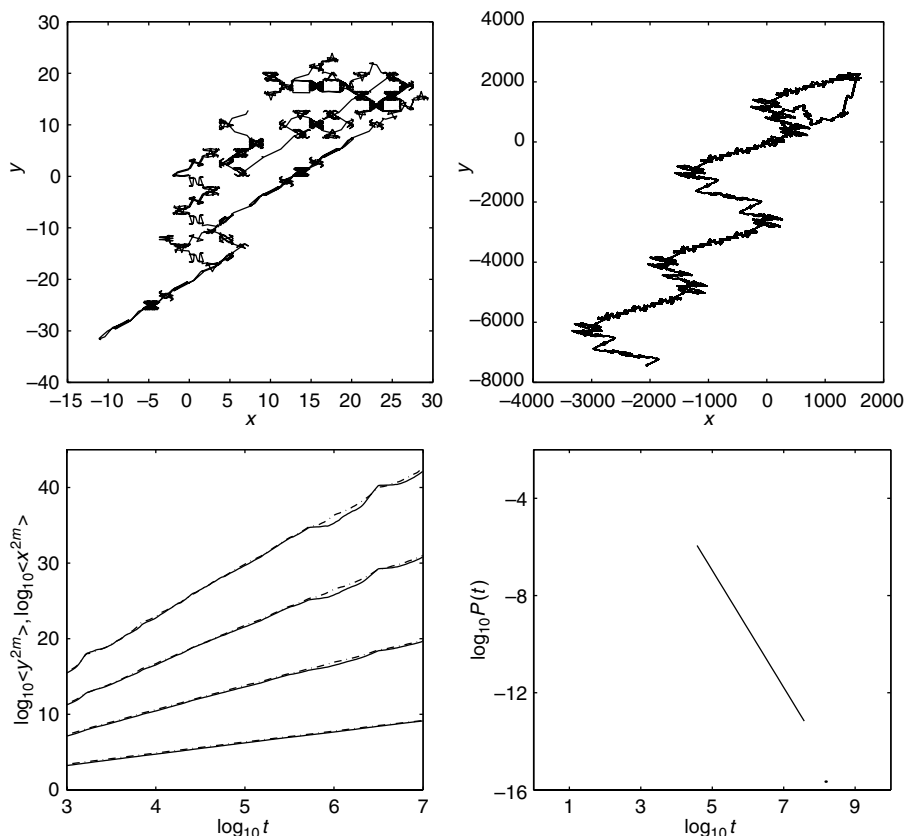


FIG. 19.16. A trajectory for small (left top) and large (right top) time intervals for the square scatterers billiard with finite horizon; moments vs. time (left bottom, full line for  $x$ , point-dash line for  $y$ ); and the Poincaré recurrences vs. time (right bottom).

function of Poincaré recurrences. The simulation gives for the recurrence exponent  $\gamma \approx 2.4$  in a good agreement with the relation (19.41) within the accuracy of computations. Similar values of  $\mu(1) \approx 1.5$  were obtained for the billiard with the infinite horizon (Fig. 19.2(e)) with the recurrence exponent  $\gamma \approx 2.5$ .

A more sophisticated case of billiards appears with the billiard with an edge of a fractal shape. Such types of billiards were considered in (Sapoval *et al.* (1991)) with respect to the sound propagation in a porous media. In Fig. 19.17 we provide a sample trajectory with few zooms. The shape of the billiard border corresponds to the Koch curve of the 3<sup>rd</sup> generation and to the propagation of the wave along  $x$ . There are evident quasi-traps for trajectories, which influence the transport features of the model, presented in Fig. 19.2(e). The results are

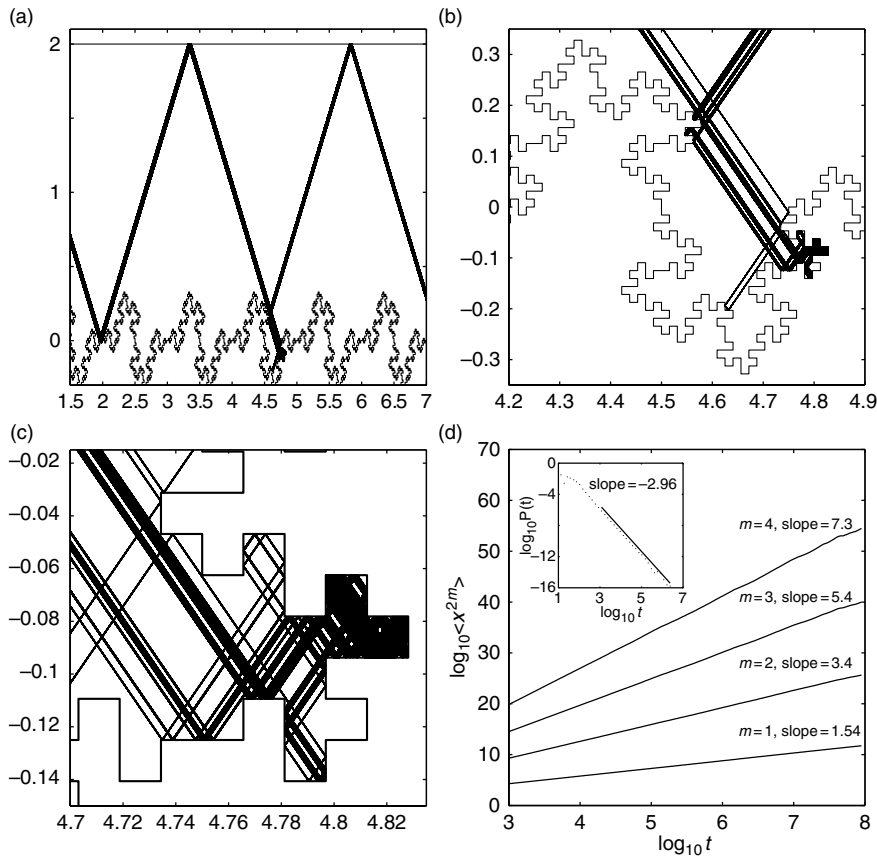


FIG. 19.17. A sample of a trajectory with two zooms for a billiard with a 3<sup>rd</sup> generation Koch fractal boundary, and the moments vs. time for the boundary as a 1<sup>st</sup> generation Koch fractal. Insertion shows the Poincaré recurrences distribution vs. time for 3276 trajectories.

different from the ones obtained for the cases in Fig. 19.1(a) and (b) even if the border is of the Koch curve shape of the 1<sup>st</sup> generation. Namely,  $\mu(1) = 1.54$  while  $\gamma = 2.96$ . Despite the fact that formula (19.41) does not work, both cases demonstrate anomalous transport, self-similar scaling of the moments, and a power law for the Poincaré recurrences.

19.4.3 Saw-tooth web map

The last example is related to the maps with discontinuities. Such maps appear in the description of overflow in digital filters and in some problems of round-off (Note 19.8). Here we present an example related to the web map of the four-fold symmetry:

$$u_{n+1} = v_n, \quad v_{n+1} = -u_n - Kf(v_n) \pmod{1} \tag{19.53}$$

with  $K$  as a parameter and

$$f(v) = \{v_n\}, \quad (19.54)$$

where the brackets  $\{\dots\}$  mean the fractional part. This is the saw-tooth shape of  $f(v)$ . It is simple to show that the Lyapunov exponent is zero for

$$|K| \leq 2 \quad (19.55)$$

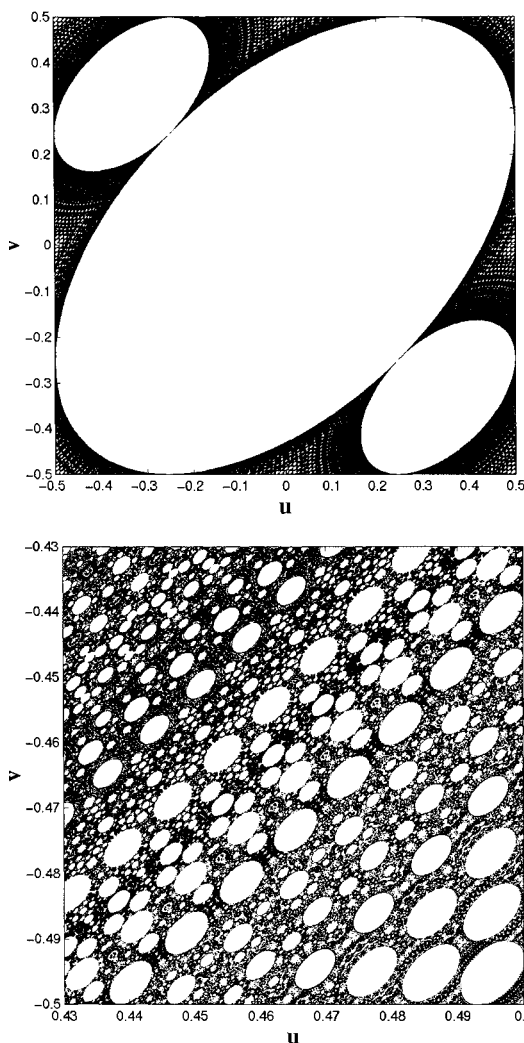


FIG. 19.18. A sample of riddling trajectory for the saw-tooth web map and three consequent zooms clockwise ( $k = -1.0192\dots$ ).

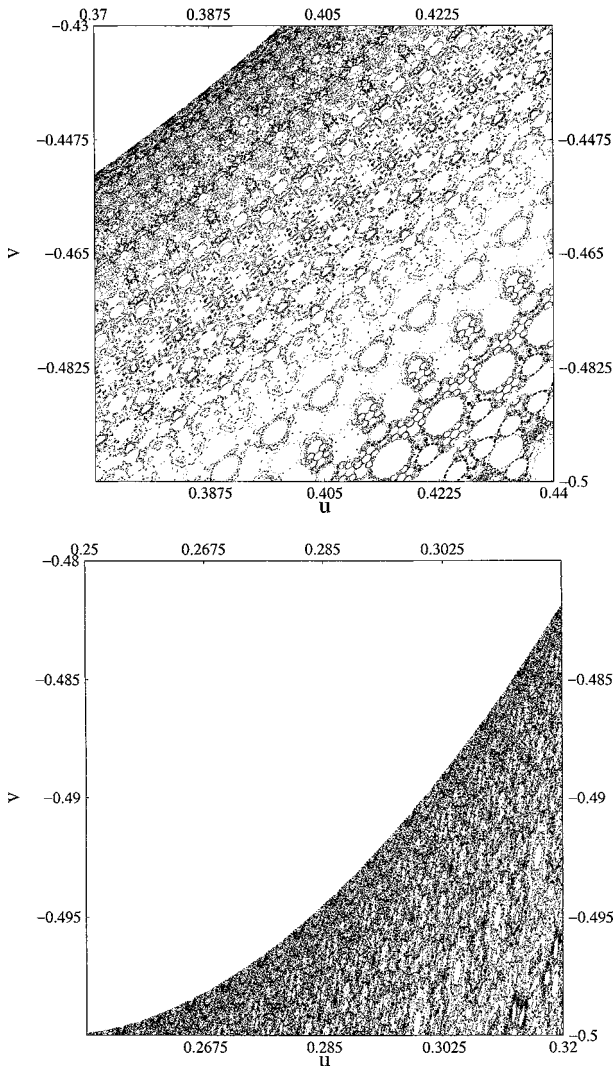


FIG. 19.18. (*Continued*)

and positive for  $|K| > 2$ . A sample of a trajectory is presented in Fig. 19.18. Such a behaviour is called *riddling*. General properties of the riddling trajectories are not well-known, although for some round-off models the scaling properties are established exactly (see *Note 19.8*). The transport properties may depend sensitively on the values of  $K$ . One can assume that there are special values

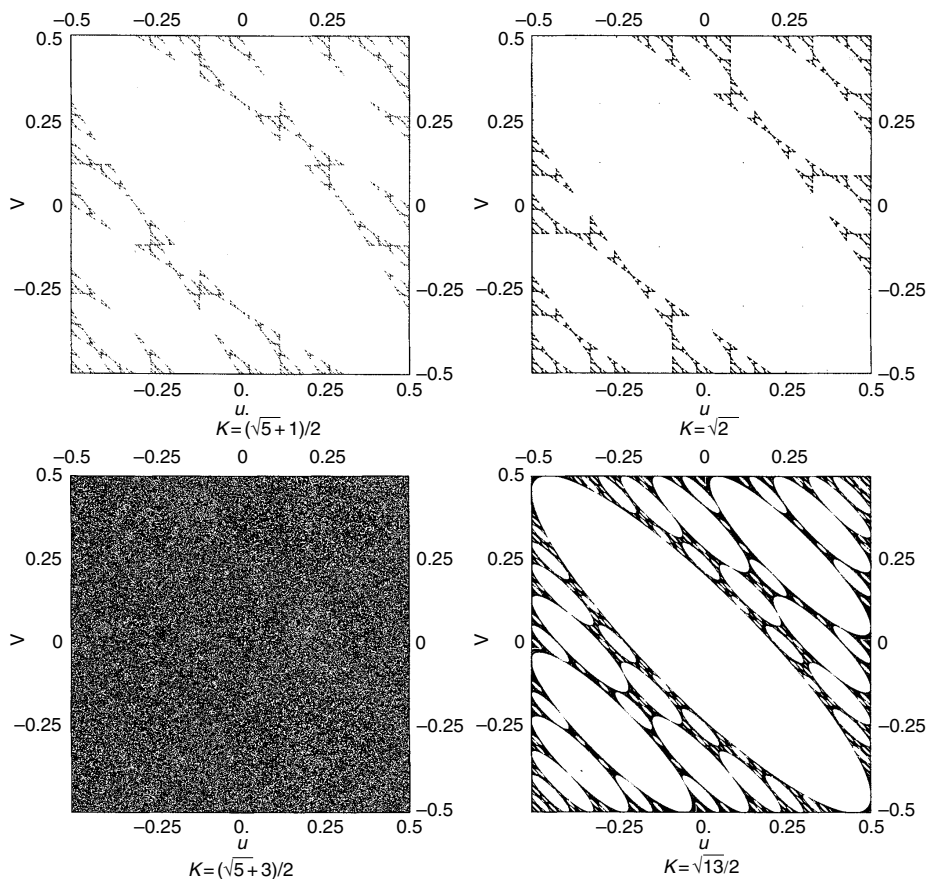


FIG. 19.19. Special cases for a four-fold symmetry web map: the top plates consist of periodic orbits only; the bottom plates correspond to unbounded orbits.

of  $K$  that impose only finite (periodic) trajectories (see Fig. 19.18). Particular arithmetic properties of the parameter  $K$  seem to be an essential element of the transport features of the model.

## Notes

### Note 19.1

Sometimes in the literature such systems are called pseudointegrable. Systems with a zero Lyapunov exponent and pseudochaos have fairly vast area of



applicability and practical or theoretical interest. Let us mention some of them: interval exchange transformation (Katok (1980); Zorich (1997)); polygonal billiards (Katok (1980); Gutkin (1986, 1996); Galperin and Zemlyakov (1990)); media with fractal boundaries (Sapoval *et al.* (1991)); sound propagation in a non-uniform media (Zaslavsky and Abdullaev (1997)); magnetic field lines behaviour in toroidal plasma (Zaslavsky and Edelman (2001); Carreras *et al.* (2003)); overflows in filters (Chua and Lin (1998)); dynamics of errors in a roundoff problem (Lowenstein and Vivaldi (1998)); as a model to study some properties of stastistical systems (Artuzo *et al.* (1997, 2000)).

*Note 19.2*

A good introduction to billiards can be found in Galperin and Zemlyakov (1990).

*Note 19.3*

The material of this section is from Zaslavsky and Edelman (2001, 2003).

*Note 19.4*

For the properties of continued fractions see Khinchin (1964) and Cornfeld *et al.* (1982).

*Note 19.5*

Neither (19.41) nor (19.47) have a rigorous proof with conditions of applicability of these expressions. Nevertheless, there are many examples of different Hamiltonian systems where these results have occurred. See examples in the review Zaslavsky (2002b).

*Note 19.6*

All examples are from Zaslavsky and Edelman (2003) and Lyubomudrov *et al.* (2003).

*Note 19.7*

Some related models were considered in Artuso *et al.* (1997, 2000); Casati and Prosen (1999); Lepri *et al.* (2000).

*Note 19.8*

For the problem of filter overflowing, see Chua and Lin (1988); Adler *et al.* (2001); Ashwin (1997); Davies (1995). For the round-off problem and error dynamics, see Lowenstein and Vivaldi (1998, 2000) and Kouptsov *et al.* (2002). Although in all these cases the equations are different, they probably are related to the same type of phenomenon.

## Problems

More complicated problems are marked by (\*).

19.1\* Show that the equivalent surface for the billiard square-in-square (Fig. 19.1(b)) has genus 5, and provide a sketch of the surface (Richens and Berry (1981)).

19.2 Write in analytical form the map for the billiard in Fig. 19.5 as  $x_{n+1}^+ = \hat{T}^\pm x_n^-$  and  $x_{n+2}^+ = \hat{T}^{(++)} x_n^+$  using the parameter  $k = \tan \vartheta$ , where  $\vartheta$  is the angle between a trajectory and the bar, and the geometric parameter of the billiard.

19.3 Prove that the Lyapunov exponent is zero for the map (19.53) if  $|K| \leq 2$ .

19.4 Consider the saw-tooth variant of the standard map

$$p_{n+1} = p_n + Kf(x_n), \quad x_{n+1} = x_n + p_{n+1} \quad (x, p \bmod 1)$$

and  $f(x) = \{x\}$ . Prove that the Lyapunov exponent is zero for  $-4 < K < 0$ .

*This page intentionally left blank*

PART 4

APPLICATIONS

*This page intentionally left blank*

## COMPLEXITY AND ENTROPY OF DYNAMICS

This chapter is devoted to the extension of notions of entropy and complexity of Hamiltonian dynamics that can be chaotic or pseudochaotic. We have partly set out this discussion in Section 4.5, but for strongly intermittent motions of Hamiltonian systems, we need more specific details of trajectories to perform the entropy analysis. The notion of complexity has a rigorous meaning and it presents a quantity that characterizes systems and that can be measured. In an oversimplified way, one can say that the less predictable a system is, the larger the complexity that should be assigned to the system. The original version of the complexity of dynamics was closely linked to the system's instability and entropy (Kolmogorov and Tikhomirov (1959), Tikhomirov (1963), Bowen (1973)). A typical situation of the chaotic dynamics could be associated with a positive Kolmogorov–Sinai entropy, or be similar to the Anosov-type systems (Sections 4.5 and 4.6). This type of randomness and complexity of the systems can be characterized by the exponential divergence of trajectories in phase space.

As long as the investigation of chaotic dynamics reveals new and more detailed pictures of chaos, the simplified version of the complexity cannot be applied to typical systems. Let us recall that typical Hamiltonians do not possess ergodicity, the boundary of islands in phase space makes the dynamics singular in their vicinity, and even zero measure phase space domains in the Sinai billiard are responsible for the anomalous kinetics (*Note 20.1*).

We saw numerous examples of Hamiltonian systems, referred as the chaotic ones, that *do not have* exponential dispersion of trajectories for arbitrary lengthy time intervals. These pieces of trajectories, called flights, appear with a probability that is not exponentially small and they define the asymptotics of the distribution function.

The behaviour of systems with zero Lyapunov exponents, considered in Chapter 19, definitely has some level of complexity and some value of entropy in a physical sense, but the regular notion of the Kolmogorov–Sinai entropy and the standard definitions of complexity being applied to such systems do not give much information about them. The most appropriate thing to say about such systems is that the proliferation of an indefiniteness has an algebraic dependence on time rather than the exponential one. Moreover, some systems behave in a mixed way: partly with an exponential growth of their enveloping (coarse-grained) phases volume and partly with its algebraic growth with time.

All the above mentioned facts lead to a necessity to introduce a new notion of complexity and entropy and this is the goal of this chapter, following Afraimovich and Zaslavsky (2003).

### 20.1 Complexity in phase space

Consider a dynamical system on the  $n$ -dimensional torus  $\mathbf{T}^n$  and let the dynamics of a particle be defined by an evolution operator

$$\hat{T}(t): (p(t), q(t)) = \hat{T}(p(0), q(0)), \quad (20.1)$$

which preserves the measure  $\Gamma(p, q) = \text{const}$  (phase volume), and  $p, q \in \mathbf{T}^n$  are generalized momentum and coordinate. What kind of dynamics should be considered as a simple one and what as a complex one? We do not assume that there is one definition of complexity which particularly depends on how this notion will be applied to the dynamics.

A more or less usual definition of the complexity depends on how trajectories are mixed in phase space due to the dynamics (20.1). The stronger the mixing, the more complex the dynamics. One can immediately comment on some weak features of this type of approach dealing with global phase space and global mixing. The process of mixing can be non-uniform in time and can have different local rates in space. We call these features of mixing in space-time non-uniformities. Concerning the space, we have in mind the full phase space or the part where the dynamics is ergodic.

The former comment leads us to need to define the complexity, which could embrace non-uniformity of space-time dynamic processes represented by trajectories.

Space-time non-uniformity suggests that the vicinities of any trajectory considered at different points  $(p_j, q_j; t_j)$  with  $p_j = p(t_j)$ ,  $q_j = q(t_j)$  may have very different dynamics of trajectories (see Fig. 20.1). A strong ‘inconvenience’ of this conclusion becomes clear if we assume the ‘vicinity’ as an infinitesimal ball of a radius  $\epsilon \rightarrow 0$  around a point  $(p_j, q_j; t_j)$ ; it is difficult, if not impossible, to

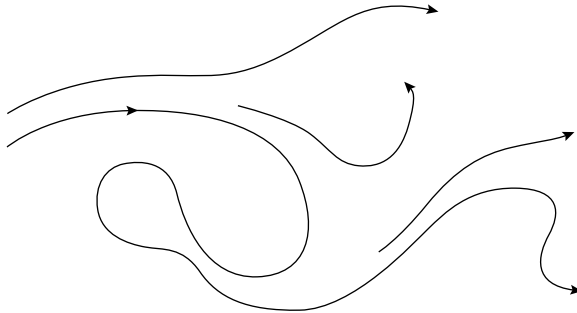


FIG. 20.1. Dispersion of trajectories in phase space.

describe a trajectory with finite-time behaviour on the basis of the information about the trajectory from an infinitesimal domain of phase space. The necessary data should arrive from finite pieces of trajectories which make a possible definition of complexity to be *space-time non-local*. We should be ready to have a situation with an exponential divergence of trajectories at some small parts of the phase space, and to have a sub-exponential divergence in other parts (Note 20.2).

## 20.2 Symbolic and topological complexities

It is convenient to start from a notion of *symbolic complexity*. Let us consider a set of symbols  $x_1, x_2, \dots$  and a set of ‘words’  $\{x\} = \{x_k, x_{k+1}, \dots, x_{k+n-1}\}$ . This word starts from  $x_k$  and has a length  $n$ . Each word can be finite or infinite, and all words  $\{x\} \in X$  belong to a space  $X$  of different admissible words. The following question is a kind of a problem of predictability: given a fixed word  $\{x^0\}$  of some length  $n_0$ , how many admissible words of the length  $n > n_0$  exist in  $X$ ? The exact answer can be given only if all necessary information is presented, that is, if  $\{x^0\}$  is specified and all elements of the space  $X$  are identified. It is more interesting to answer the question for typical systems and with a typical initial condition, for example: how many admissible words of the length  $n \gg n_0$  are in  $X$  and how does this number  $C(n_0, n)$  depend on  $n_0$  and  $n$ ?

Questioning in such a way, we introduce an element of the unknowable or indefiniteness in the answer, since only the number of words is asked for and information about the structure of the words is neglected. It is clear that the answer depends on how the admissible set of words  $X$  is prepared. One can assume the existence of systems for which there is the exponential law

$$C(n_0, n) \sim \exp(hn), \quad n \rightarrow \infty \quad (20.2)$$

or sub-exponential law

$$C(n_0, n) \sim n^\gamma, \quad \gamma > 0, \quad n \rightarrow \infty \quad (20.3)$$

independently on  $n_0$ .

**Example 1** Let the ‘alphabet’ of possible values of  $x$  have two symbols  $(x_1, x_2)$  and all words are possible. Then the number  $C(n_0, n)$  is (20.2) with  $h = \ln 2$ .

**Example 2** Consider a map  $\hat{T}x : x_{n+1} = x_n + \omega, \text{ mod } 1, x \in (0, 1)$  which is a shift by irrational  $\omega \in (0, 1)$ . After the first application of  $\hat{T}$  the interval  $(0, 1)$  will be broken into two sub-intervals  $(0, 1 - \omega)$  and  $(1 - \omega, 1)$  such that within each sub-interval the dependence  $\hat{T}x$  on  $x$  is smooth. Each application of  $\hat{T}$  adds one more sub-interval, i.e. after  $n$  steps the number of sub-intervals is  $n + 1$ . Let us consider an arbitrary point  $x \in (0, 1)$  and let us find the admissible sub-intervals for the point  $\hat{T}^{-n}x$ . The number of possible (admissible) intervals is  $C(n_0 = 1, n) = n + 1$ , i.e.  $\gamma = 1$  in (20.3).



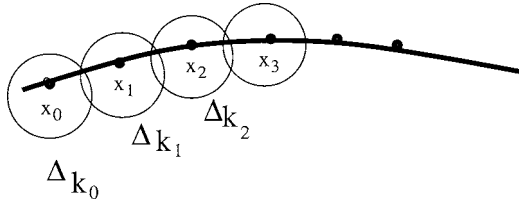


FIG. 20.2. Covering the trajectory  $\{x_0, x_1, \dots, x_n, \dots\}$  by a set of balls  $\{\Delta\}$ .

The number  $C(n_0, n)$  is called *symbolic complexity*. The more unpredictable the system, the larger  $C(n_0, n)$  is, as a function of time  $n$ , i.e. the larger the proliferation of the number of possible states the larger the indefiniteness.

Transition to dynamical systems is fairly natural. Let the words represent a state of a dynamical system, and let admissible space be the phase space, and any sequence

$$\{x_0, x_1, \dots, x_n, \dots\} = \{x_0, \hat{T}x_0, \dots, \hat{T}^n x_0, \dots\} \quad (20.4)$$

shows itinerary, or trajectory, of the system. An important element of the consideration is a *finite cover* by a set of balls  $\{\Delta\} = \{\Delta_{k_1}, \Delta_{k_2}, \dots\}$ , that is a ball of the diameter  $\Delta_i$  such that  $x_{k_i} \in \Delta_{k_i}$  (see Fig. 20.2), and the full trajectory is covered by this set of balls. Replacing the real trajectories by the ‘covered trajectories’ creates an indefiniteness, or a *coarse-graining*, even if at least one point of the trajectory is covered.

Let all balls that cover a full trajectory have the same diameter  $\delta$ , and let  $m_\delta(n)$  be a minimal number of a set of the balls that covers the trajectory. This set will be called a *minimal cover set*. Depending on the type of dynamics, different numbers of trajectories of the time length  $n$  can have minimal cover sets  $\Delta^{(k)}(x_0^k, n)$  such that all initial conditions  $x_0^{(k)} \in \Delta_0$ , i.e. belonging to the same initial ball, and that

$$\Delta^{(k_1)}(x_0^{(k_1)}, n) \cap \Delta^{(k_2)}(x_0^{(k_2)}, n) = 0, \quad \forall k_1 \neq k_2 \quad (20.5)$$

i.e. all different minimally covered trajectories do not intersect each other at time  $n$  (see Fig. 20.3). The maximal number of such trajectories  $C(\Delta, n)$  is called *topological complexity*. It depends on time  $n$  and on the coverage set  $\{\Delta\}$ . For chaotic dynamics

$$C(\Delta, n) \sim \exp(h_{\text{top}} n), \quad (20.6)$$

where  $h_{\text{top}}$  is topological entropy, provided that  $\{\Delta\}$  is correctly chosen. The larger  $n$  is, the smaller the diameter of  $\Delta_k$  can be (Note 20.3).

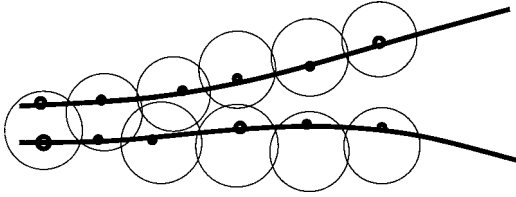


FIG. 20.3. A sketch of two different minimal covered sets that correspond to two different trajectories starting at the same ball.

It will be seen later that it is more convenient and more constructive to use a notion of  $(\epsilon, n)$ -separation (Note 20.4). This notion will be the most important in this chapter. Let  $x(t)$  be a point of the phase space  $M$  at time instant  $t$ . Then the function

$$d(x(t); y(t)) = \text{dist}(\hat{T}^t x_0, \hat{T}^t y_0) \quad (20.7)$$

defines a distance between two trajectories

$$x(t) = \hat{T}^t x_0, \quad y(t) = \hat{T}^t y_0, \quad x_0, y_0 \in M \quad (20.8)$$

with initial conditions  $x_0, y_0$  and the same time evolution operator  $\hat{T}^t$  at time  $t$ . For a discrete time  $t = n$  should be a corresponding replacement in (20.8). Any segment of a trajectory of the temporal length  $n$  can be written as

$$\ell_n(x) = \cup_{k=0}^{n-1} \hat{T}^k x. \quad (20.9)$$

Two segments  $\ell_n(x), \ell_n(y)$  are said to be  $(\epsilon, n)$ -separated if there exists  $k$ , such that

$$d(\hat{T}^k x, \hat{T}^k y) < \epsilon; \quad 0 \leq k \leq n-1, \quad \text{and} \quad d(\hat{T}^n x, \hat{T}^n y) \geq \epsilon. \quad (20.10)$$

Consider a set  $A \subset M$  of initial conditions  $x \in A$  and the corresponding bunch of trajectories started at  $x \in A$ . After time  $n$  we have a set of segments, and some of them are mutually  $\epsilon$ -separated. The magnitude

$$C_{\epsilon, n} = \max\{\# \text{ segments of mutually } (\epsilon, n) - \text{separated}\} \quad (20.11)$$

is said to be  $(\epsilon, n)$ -complexity of the set  $A$ . The value  $\ln C_{\epsilon, n}(A)$  is called  $(\epsilon, n)$ -capacity of the set  $A$ .

It is easy to understand a meaning of the definition (20.11). Assume that initially  $\text{diam } A < \epsilon$ , that is, an arbitrary selected point  $x^* \in A$  at  $t = 0$  may belong to any of  $C_{\epsilon, n}(A)$  orbits at time  $\tau \in [0, t]$ , i.e. the number  $C_{\epsilon, n}$  characterizes the level of indefiniteness of an arbitrarily taken initial point to belong to some trajectory  $(\epsilon, n)$ -separated from all others in (20.11).

### 20.3 Topological and metric entropies

In this section topological and metric entropies (see Section 4.5) will be considered in their link to the complexity.

From the physical point of view, the complexity  $C_{\epsilon,n}(A)$  gives a number of possible  $\epsilon$ -different states that can represent any selected point  $x^* \in A$  after time  $t = n$ . The system that exhibits instability has a growing value  $C_{\epsilon,n}(A)$  as a function of  $n$ . The value

$$h_{\text{top}}(A) = \lim_{\epsilon \rightarrow 0} \overline{\lim}_{n \rightarrow \infty} \frac{1}{n} C_{\epsilon,n}(A) \quad (20.12)$$

is called the *topological entropy*, where the bar means the upper limit. It was shown in Bowen (1973) that for the Anosov type systems

$$h_{\text{top}} = h_{\text{KS}}, \quad (20.13)$$

i.e. the topological entropy coincides with the Kolmogorov–Sinai entropy for a compact set  $A$  of initial points.

The above definition of entropy depends on the set  $A$ . Let us consider many different subsets  $A_k$ :  $A = \cup_{k=1}^{N(A)} A_k$ , and define  $C_{\epsilon,n}(A_k)$  in a similar way to (20.11). Let us also partition the phase space domain  $M$  by a fixed set of subdomains of the diameter  $\epsilon$ . The number of the subdomains is fixed, i.e. it is

$$\mathcal{N}(M, \epsilon) = \frac{\Gamma(M)}{\epsilon^b}, \quad (20.14)$$

where  $b$  is the box dimension of the set  $A$ , and the box dimensions of all subsets  $A_k$  is assumed to be the same. Define the following *metric entropy*

$$h_\rho = - \lim_{\epsilon \rightarrow 0} \lim_{n \rightarrow \infty} \frac{1}{n} \sum_{j=1}^{\mathcal{N}(M, \epsilon)} \rho_j(n) \ln \rho_j(n), \quad (20.15)$$

where  $\rho_j$  is density function, i.e. the normalized number of trajectories, initially at  $A$ , distributed in the set of cells of the volume  $\epsilon^b$  of the partition of  $M$ . It is clear that in the limit  $\epsilon \rightarrow 0$ ,  $\rho_j$  tends to a natural measure of the system. It follows that for chaotic systems

$$h_\rho = h_{\text{KS}} \quad (20.16)$$

and, moreover, for typical chaotic systems

$$h_\rho = h_{\text{top}} \quad (20.17)$$

on the set of typical points with respect to the measure. The last equality is an analogue of the equivalence of canonical and micro-canonical ensembles in statistical physics.

To get more details on the introduced definitions, let us consider a one dimensional system with uniform mixing dynamics on the interval  $[0, \ell]$ ,  $x \in [0, \ell]$  and with an exponential divergence of trajectories. Let  $\delta x_0$  be the initial distance at  $t = 0$  between two trajectories and  $\delta x_t = \epsilon$  be the distance at time  $t$ . Then

$$\epsilon = \delta x_0 \exp ht, \quad (20.18)$$

that is, for  $\tau \geq t$  two trajectories are  $\epsilon$ -separated. The number of such trajectories is

$$C_{\epsilon,t}(A) = \frac{\ell_A}{\delta x_0} = \frac{\ell_A}{\epsilon} e^{ht}, \quad (20.19)$$

where  $\ell_A$  is the length of a small initial interval  $A$ . For  $\tau > t$  the complexity grows exponentially. The properties (20.11)–(20.13) follow directly from (20.19). If the set  $A$  has the box-dimension  $b$ , then (20.18) should be replaced by

$$\left( \frac{\epsilon}{\delta x_0} \right)^b = e^{ht} \quad (20.20)$$

and correspondingly, instead of (20.19),

$$C_{\epsilon,t}(A) = \left( \frac{\ell_A}{\delta x_0} \right)^b = \left( \frac{\ell_A}{\epsilon} \right)^b e^{ht}. \quad (20.21)$$

For more general situations we may assume

$$C_{\epsilon,t}(A) = \left( \frac{\ell_A}{\epsilon} \right)^b e^{ht} \bar{C}(\epsilon, t), \quad (20.22)$$

where  $\bar{C}(\epsilon, t)$  is a slow varying function of  $\ln \epsilon$  and  $t$  compared to the main multipliers. It also can be written

$$b = \lim_{n \rightarrow \infty} \lim_{\epsilon \rightarrow 0} \frac{1}{n} \frac{\ln C_{\epsilon,n}(A)}{\ln(1/\epsilon)} \quad (20.23)$$

(Takens, (1983)).

The expression (20.22) shows in an explicit way how the topological complexity depends on the time interval  $t$ , accuracy  $\epsilon$ , and dimension  $b$  to determine the location of trajectories and the domain  $A$  of a set of initial conditions. The dependence on  $A$  can be eliminated from (20.19) or (20.21) by choosing a normalized complexity  $C_{\epsilon,t}$  per unit volume,

$$C_{\epsilon,t} = \frac{C_{\epsilon,t}(A)}{\ell_A^b}, \quad (20.24)$$

which is possible due to the uniformity of mixing in the considered dynamical system. This interpretation can be continued using the phase space partitioning in a more formal way.

Let again  $M$  be the phase space,  $\Gamma = \Gamma(M)$  its phase volume,  $\Gamma_0$  be the phase volume of a set of initial conditions  $A_0 \subset M$  at time  $t_0 = 0$ , and consider their evolution  $A_t$  up to time  $t$ . Let  $\bar{\Gamma}_t$  be a minimal enveloping  $A_t$  convex phase volume. Then for systems with exponential divergence of trajectories

$$\bar{\Gamma}_t = \Gamma_0 e^{ht}. \quad (20.25)$$

To find how many different states can occupy the volume  $\bar{\Gamma}_t$ , one should define an ‘elementary’ minimal volume of one state, i.e.  $\epsilon^b$ . Then

$$\max_A \left\{ \# \text{ states in } \bar{\Gamma}_t = \left( \frac{\Gamma_0}{\epsilon^b} \right) e^{ht} \right\}, \quad (20.26)$$

where the maximum is considered with respect to different sets  $A$  in  $\Gamma_0$ .

Expressions (20.19) and (20.20) permit an important physical interpretation. Hamiltonian chaotic dynamics preserves the phase volume, i.e.  $\Gamma_0 = \Gamma(A_t)$ . The enveloped or coarse-grained phase volume  $\bar{\Gamma}_t$  grows approximately as (20.25). The number of states in  $\bar{\Gamma}_t$  depends on the definition of a state in the enveloped phase volume. Let one state occupy an elementary volume  $\Delta\Gamma$ , then the number of states that occupy the volume  $\bar{\Gamma}_t$  is simply

$$\mathcal{N}(t; \Delta\Gamma) = \frac{\bar{\Gamma}_t}{\Delta\Gamma} = \left( \frac{\Gamma_0}{\Delta\Gamma} \right) \exp(ht) \leq \frac{\Gamma(M)}{\Delta\Gamma}. \quad (20.27)$$

Let us emphasize that this interpretation stops working when  $t > (1/h) \times \log(\Gamma(M)/\Gamma_0)$ . Now instead of the  $\epsilon$ -separated trajectories we can introduce  $\Delta\Gamma$ -separated ones, associated to a partitioning of  $\Gamma(M)$  into elementary cells. Two trajectories will be  $\Delta\Gamma$ -separated over the time interval  $t$  if they do not stay at the same cell during  $t$ . If the volume of an elementary cell is  $\Delta\Gamma = \epsilon^b$ , then

$$\mathcal{N}(t, \Delta\Gamma) \equiv \mathcal{N}(t, \epsilon) = \left( \frac{\Gamma_0}{\epsilon^b} \right) \exp(ht) \quad (20.28)$$

and we arrive at the connection

$$C_{\epsilon,t}(A_0) = \text{const } \mathcal{N}(t, \epsilon). \quad (20.29)$$

We also can introduce the entropy  $S(t, \Delta\Gamma)$  for the  $\Delta\Gamma$ -separated states, i.e.

$$S(t, \Delta\Gamma) \equiv \ln \mathcal{N}(t, \Delta\Gamma) = \ln C_{\epsilon,t}(A_0) + \text{const} \quad (20.30)$$

with a condition for the states-separation

$$\Delta\Gamma = \epsilon^b. \quad (20.31)$$

It is essential that the entropy  $S(t, \Delta\Gamma)$  is defined relatively to a definition of the elementary phase volume  $\Delta\Gamma$  which depends on the system and the type of the evolution process. Non-universality of the entropy  $S(t, \Delta\Gamma)$  will be more evident in the next sections where the algebraic complexity will be considered. Here we would like to mention that partitioning of phase space depends on the level of information we want to ignore in the description of dynamics, and on the level of information we would like to keep about system trajectories.

In the case of uniform mixing, the initial set  $A_0$  uniformly spreads over  $\mathcal{N}(t, \Delta\Gamma)$  cells. Thus a probability density  $\rho_j$  to occupy a cell  $\Delta\Gamma_j$  is simply

$$\rho_j(t) = \frac{\Delta\Gamma_j}{\bar{\Gamma}_t} = \frac{1}{\mathcal{N}(t, \Delta\Gamma)}, \quad \forall j, \quad (20.32)$$

where we use (20.27). Substitution of (20.32) to (20.15) gives

$$\begin{aligned} h_\rho &= - \lim_{\Delta\Gamma \rightarrow 0} \lim_{t \rightarrow \infty} \frac{1}{t} \sum_{j=1}^{\mathcal{N}(t, \Delta\Gamma)} \mathcal{N}^{-1}(t, \Delta\Gamma) \ln \mathcal{N}^{-1}(t, \Delta\Gamma) \\ &= \lim_{\Delta\Gamma \rightarrow 0} \lim_{t \rightarrow \infty} \frac{1}{t} \ln \mathcal{N}(t, \Delta\Gamma) \\ &= \lim_{\Delta\Gamma \rightarrow 0} \lim_{t \rightarrow \infty} \frac{1}{t} \ln C_{\Delta\Gamma, t}(A_0) = h_{\text{top}} \end{aligned} \quad (20.33)$$

(compare to (20.12)) where we replace  $\epsilon$ -separation for  $C_{\epsilon, t}(A_0)$  by  $\Delta\Gamma$ -separation  $C_{\Delta\Gamma, t}(A_0)$ . In fact, there is some difference for  $\Delta\Gamma$ - or  $\epsilon$ -separations in a non-one-dimensional case, which is not so important unless systems with non-uniform mixing are considered. Moreover, expression (20.33) just proved this statement.

## 20.4 Conflict with dynamics

All definitions and considerations of the previous sections of this chapter were based on the exponential growth complexity or, what is the same, the exponential uniform dispersion of trajectories. Real Hamiltonian dynamics does not possess uniformity. There are singular zones of different types where the Lyapunov exponent is close to zero. As a result, for a time that can be astronomically large and not achievable in any practice, the corresponding segments of trajectories have only polynomial dispersion in time. The formal expressions (20.22) for  $C_{\epsilon, t}(A)$  or (20.28) for  $\mathcal{N}(t, \Delta\Gamma)$  are the same up to a constant (compare to (20.29)) and both definitions have the same limitation for the bounded Hamiltonian dynamics:

$$C_{\epsilon, t}(A) \leq \frac{\Gamma(M)}{\epsilon^b}, \quad \mathcal{N}(t; \Delta\Gamma) \leq \frac{\Gamma(M)}{\Delta\Gamma}. \quad (20.34)$$

The constraints (20.34) do not depend on time and thus it follows the existence of

$$t_{\max} = t_c(\epsilon) \quad \text{or} \quad t_{\max} = t_N(\Delta\Gamma), \quad (20.35)$$

such that trajectories or their segments, being non-separated during the  $t_{\max}$ , will be non-distinguishable. This property of the definitions (20.22) and (20.28) eliminates a significant part of the dynamics with non-uniform mixing in phase space.

All above definitions of entropy use limits  $n \rightarrow \infty$  or  $t \rightarrow \infty$ . These limits exclude a significant information for systems with weak mixing or strongly intermittent dynamics. This comment makes a necessity of different approaches to the problem of complexity (see more discussions in Afraimovich and Zaslavsky (2003)).

## Notes

### *Note 20.1*

Attempts to find adequate complexity and entropy definitions for realistic chaotic dynamics were the subject of many publications and reviews: Grassberger and Procaccia (1984); Abel *et al.* (2000); Badii and Politi (1999); Boffetta *et al.* (2002). The basic idea of these developments is to involve a finite time of the system's unstable evolution into a definition of the complexity or entropy.

### *Note 20.2*

The importance of observing a trajectory with some precision  $\epsilon$  during a finite time  $t$  was discussed in Grassberger and Procaccia (1983, 1984) and Procaccia (1985). They also consider fluctuations of the Lyapunov exponents obtained from a finite time observation. These works also presented a space-time partitioning as a way of obtaining correlation properties of trajectories. The analysis here will be extended, comparing it to Grassberger and Procaccia (1984) and Procaccia (1985), in two directions: it will be applied to Hamiltonian dynamical systems that may have a sub-exponential divergence of trajectories at some phase space domains, and it will use some results on the Poincaré recurrences.

### *Note 20.3*

Symbolic complexity was considered in Hedlund and Morse (1938), and then developed by Kolmogorov and Tikhomirov (1959). See also Tikhomirov (1963) and Brudno (1983).

### *Note 20.4*

The idea of  $\epsilon$ -separation of curves during time  $t$ , or discrete time  $n$ , was introduced first in Kolmogorov and Tikhomirov (1959) and then developed by Bowen (1973). There were some related works on the so-called  $(\epsilon, \tau)$ -entropy and complexity in Shannon (1960), Cohen and Procaccia (1985). See also review (Gaspard and Wang (1993)).

## Problems

*20.1* Prove the result of Example 1 in Section 20.2.

## COMPLEXITY AND ENTROPY FUNCTIONS

The goal of this chapter is to introduce a new definition of a complexity function rather than just complexity in order to be able to characterize a system with at least two different time scales of ‘complex’ dynamics: one time scale can characterize an exponential dispersion of trajectories while the second time scale is related to the power-wise dispersion. It is worthwhile to mention from the very beginning important differences from the definitions of the previous chapter:

- (i) instead of the complexity as a number, there will be a complexity function of two variables, time and length, along the trajectory;
- (ii) time and length variables will be continuous;
- (iii) the new complexity function notion can be applied to systems with zero Lyapunov exponents.

Some other features will be mentioned along the way. The definition of the entropy function follows automatically from the definition of the complexity function (*Note 21.1*).

### 21.1 Definitions of complexity function

As before, we deal with Hamiltonian dynamics of systems in a phase space  $M$  endowed with a distance  $dist$  and discrete or continuous time  $t$ . The dynamical system  $\hat{T}^t: M \rightarrow M$  defines a distance  $dist(\hat{T}^t x, \hat{T}^t y)$  between two trajectories at time  $t$  that were initially at points  $x, y \in M$ . One can also introduce a natural length  $\ell^t = \ell(x, \hat{T}^t x) = \ell(x, x^t)$  along the trajectory initially at  $x$ . We will need the following definition:

Two trajectories with initial points  $x, y \in A$  will be  $(\epsilon, t)$ -indistinguishable if

$$d_\tau(x, y) = dist(\hat{T}^\tau x, \hat{T}^\tau y) < \epsilon, \quad 0 \leq \tau < t. \quad (21.1)$$

A notion of complexity is based on the verification of divergence of trajectories from fixed several ones. We start with a definition of local complexity.

Consider a small domain  $A \subset M$  with diameters  $\delta_A, \delta_M$  where  $\delta_A \ll \delta_M$ , and fix some number  $\epsilon$

$$\delta_A \ll \epsilon \ll \delta_M. \quad (21.2)$$



Let us pick a point  $x_0 \in A$  and call the corresponding trajectory the basic one or *the reference trajectory*. A set  $Q_N = \{x_k \in A\}_{k=1}^N$  is said to be locally  $(\epsilon, t)$ -separated if:

- (i) For every  $x_k$  there is  $0 \leq \tau_k \leq t$  such that

$$\text{dist}(x_k(\tau_k), x_0(\tau_k)) \geq \epsilon \quad (21.3)$$

and

$$\text{dist}(x_k(\tau), x_0(\tau)) < \epsilon, \quad 0 \leq \tau < \tau_k \quad (21.4)$$

- (ii) for every pair  $(k, k')$ ,  $1 \leq k, k' \leq N$ ,

$$\text{dist}(x_k(\tau_k), x_{k'}(\tau_{k'})) \geq \epsilon, \quad 0 \leq \tau_k, \tau_{k'} \leq t. \quad (21.5)$$

Time  $\tau_k$  in (21.3) can be considered as the ‘first arrival’ to the  $\epsilon$ -separation.

If (21.5) is not valid, then a pair of trajectories corresponding to the pair  $(k, k')$  is  $\epsilon$ -indistinguishable, and it should be treated as one trajectory during the time  $t$ .

**Definition 1** The number

$$C(\epsilon, t, x_0, A) = \max\{N \mid Q_N \text{ is locally } (\epsilon, t)\text{-separated}\} \quad (21.6)$$

is called the *local complexity function* of  $t$ .

A set  $Q_N$  is called  $(\epsilon, t)$ -optimal if it is locally  $(\epsilon, t)$ -separated and  $N = C(\epsilon, t; x_0, A)$ .

It is simple to see that

$$C(\epsilon, t; x_0, A) \leq \frac{\Gamma(M)}{\epsilon^b} = \mathcal{N} \quad (21.7)$$

and

$$C(\epsilon, t'; x_0, A) \geq C(\epsilon, t; x_0, A) \quad \text{if } t' \geq t. \quad (21.8)$$

So, if we are interested in the separation of a bunch  $Q_N$  of  $N$  trajectories with initial points  $x_j \in Q_N$ ,  $j = 1, \dots, N$ , and their evolution  $x_j(t) = \hat{T}^t(x_j)$ , then after time  $t$  we find out that there are  $N_0 = N_0(\epsilon, t, Q_N)$   $\epsilon$ -separated (from the basic one) trajectories—denote this set by  $Q_{N_0}$ —and  $N - N_0$  indistinguishable (from the basic one) trajectories (see Fig. 21.1).

If  $Q_{N_0}$  is locally separated then we obtain an estimate,

$$N_0(\epsilon, t, Q_N) \leq C(\epsilon, t; x_0, A). \quad (21.9)$$

If, in addition,  $Q_{N_0}$  is  $(\epsilon, t)$ -optimal, then

$$N_0(\epsilon, t, Q_N) = C(\epsilon, t; x_0, A) \leq \mathcal{N} \quad (21.10)$$

(compare to (20.34)).

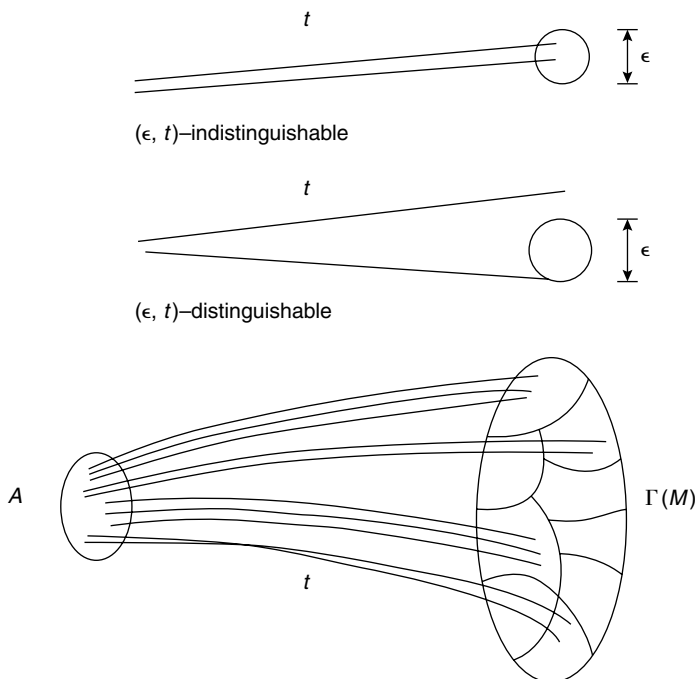


FIG. 21.1. Example of the evolution of 10 trajectories from the set  $A$  of the size  $\delta \ll \epsilon$  during time  $t$ . The optimal (maximal) number of  $(\epsilon, t)$ -separated trajectories  $\mathcal{N} = 9$ . The diameter of all nine domains of  $\Gamma(M)$  is  $\epsilon$ . The initial bunch  $Q_N$  has 10 trajectories with  $N_0 = C(\epsilon, t; x_0, A) = 4$  of the  $(\epsilon, t)$ -separated ones. The two top examples show the process of evolution that makes a pair of trajectories (in)distinguishable.

In Definition 1 we consider  $(\epsilon, t)$ -separation of the set  $A$  of trajectories that are close to the basic one started at  $x_0$ . That is why the complexity  $C(\epsilon, t; x_0, A)$  is called local. Now we can consider a set  $B$  of basic trajectories with initial points  $x_0^{(m)} \in B$ . For each  $x_0^{(m)}$ , we can attach a set  $\{A^{(m)}\}$  of trajectories with initial conditions  $x_k^{(m)}$  in the vicinity of  $x_0^{(m)}$ . For the sake of definiteness, assume that

$$\text{dist}(x_0^{(m)}, x_0^{(m')}) > 2\epsilon, \quad m \neq m', \quad (21.11)$$

so that any two trajectories from the vicinities of different basic trajectories are disjoint at least by  $\epsilon$  and thus  $(\epsilon, t)$ -separated.

Each basic trajectory generates the corresponding local complexity function  $C(\epsilon, t; x_0^{(m)}, \{A^{(m)}\})$ . The set  $B$  of initial points of basic trajectories will be called *B-ensemble*.

**Definition 2** The number

$$C(\epsilon, t; B, \{A\}) = \sum_m C(\epsilon, t; x_0^{(m)}, \{A^{(m)}\}) \quad (21.12)$$

is called the *complexity function of the B-ensemble*. The  $B$ -ensemble is specified by the  $B$ -set of  $x_0^{(m)}$  and initial conditions  $x_k^{(m)} \in A^{(m)}$  around each  $x_0^{(m)}$  within domain  $\delta_A^{(m)} \ll \epsilon$  (compare to (21.2)).

While the construction of sets  $A^{(m)}$  can be done fairly uniformly due to its small size, the choice of  $B$ -ensemble is free and makes it flexible depending on the problem to be solved.

The complexity functions  $C(\epsilon, t; x_0, A)$  and  $C(\epsilon, t; B, \{A_k\})$  show a level of time-proliferation of  $\epsilon$ -separated trajectories from the initial set of a large number of indistinguishable points.

If we are interested in the only typical (for some measure) orbits we may adjust the definitions above to this situation by assuming that  $B$ -set always consists of typical points  $x_0^{(k)}$  of this measure.

## 21.2 Probability of $\epsilon$ -divergence

One of the main points we are interested in is the behaviour of complexity functions in a neighborhood of a sticky set (Afraimovich and Zaslavsky (1998)). It is well-known that a typical trajectory in a chaotic sea behaves in an intermittent way: after relatively short chaotic burst it is attracted to a sticky set for a long time, then comes back to the mixing part of the chaotic sea, and so on. If our consideration is restricted to a neighborhood of one (or several) basic orbit(s), then fast separated pieces of orbits correspond to a mixing type of behaviour and their initial points are situated much ‘further’ from the sticky set than initial points of slow-separated pieces of orbits. By using this observation, we may eliminate fast-separated points (see the next section), i.e. we may choose initial points in  $B$ -set which practically belong to the sticky set. In other words, we may, in principle, calculate local or non-local complexity of a measure concentrated on the sticky set.

More rigorously, assume that an invariant measure  $\rho$  is given. Then in Definition 1 we consider only sets  $Q_N = \{x_j\}_{j=1}^N$  such that

- (i)  $Q_N$  is locally  $(\epsilon, t)$ -separated;
- (ii)  $x_j$  are the points belonging to the set on which the measure  $\rho$  is concentrated (or in a real situation, as close as it is possible). The maximal number of

elements in such sets,  $Q_N$ , will be called the *local  $(\epsilon, t)$ -complexity of measure  $\rho$* . We denote it by  $C_\rho(\epsilon, t; x_0, A)$ .

Similarly if in Definition 2 we consider only sets  $Q_N$  containing  $\rho$ -typical (or, in reality, the closest set to them), then we obtain the  *$(\epsilon, t)$ -complexity of measure  $\rho$* ,  $C_\rho(\epsilon, t; B, \{A\})$ .

It is useful to introduce the following quantity

$$P_\rho(\epsilon, t; \Delta t, x_0) = \frac{1}{N} [C_\rho(\epsilon, t + \Delta t; x_0, A) - C_\rho(\epsilon, t; x_0, A)] \approx p_\rho(\epsilon, t; x_0) \Delta t, \quad (21.13)$$

where  $N = C_\rho(\epsilon, t; x_0, A)$ . This quantity gives a probability to diverge by distance  $\epsilon$  from the basic orbits during the time interval  $[\tau, \tau + \Delta t]$ , and  $p_\rho(\epsilon, t; x_0)$  is the corresponding probability density function. We call them  *$\epsilon$ -divergence probability* and  *$\epsilon$ -divergence probability density*.

Similarly,

$$P_\rho(\epsilon, t; \Delta t, B) = \frac{1}{N} [C_\rho(\epsilon, t + \Delta t, B, \{A\}) - C_\rho(\epsilon, t; B, \{A\})] \approx p_\rho(\epsilon, t, B) \Delta t \quad (21.14)$$

gives the probability to diverge from basic orbits going through the  $B$ -ensemble during the time interval  $[\tau, \tau + \Delta t]$ , and  $p_\rho(\epsilon, t, B)$  is the corresponding probability density function.

### 21.3 Calculation of local complexity function

In this section we would like to show that the above introduced definitions of complexity or  $\epsilon$ -divergence probabilities are constructive and fairly simple for their utilization.

From now, we will choose initial points  $x_j$  in  $A$  in such a way that the distances between  $x_j$  and the basic point  $x_0$  are the same for all  $j$ , and we denote it by  $\delta$ . Moreover, for the sake of simplicity we omit the argument  $A$  in  $C(\epsilon, t; x_0, A)$  and  $\{A\}$  in  $C(\epsilon, t; B, \{A\})$ . So  $C(\epsilon, t; x_0) = C(\epsilon, t; x_0, A)$  and  $C(\epsilon, t, B) = C(\epsilon, t; B, \{A\})$ .

As usual in numerical simulations we will assume that randomly chosen points  $x_0, x_0^{(k)}$  are typical with respect to some measure  $\rho$  we are interested in.

The values of  $N_0$  in (21.9) and (21.10), and in (21.13) and (21.14) depend on the choice of  $\delta, \epsilon, x_0$  (or  $B$ ).

The smaller  $\delta$  is, the longer  $t$  should be considered to be until the maximal values of  $C(\epsilon, t, B)$  or  $C(\epsilon, t; x_0)$  will be achieved. This makes the limit  $\delta \rightarrow 0$  fairly simple. Understanding a way to work with the parameter  $\epsilon$  is more complicated. Consider one trajectory  $x^t$  that starts at  $x$  and has a natural length  $\ell = \ell(x, x^t)$ . Let  $t$  be fairly large and select a set of points  $x_k$  along a trajectory and, approximately, almost uniformly distributed. We can operate with points

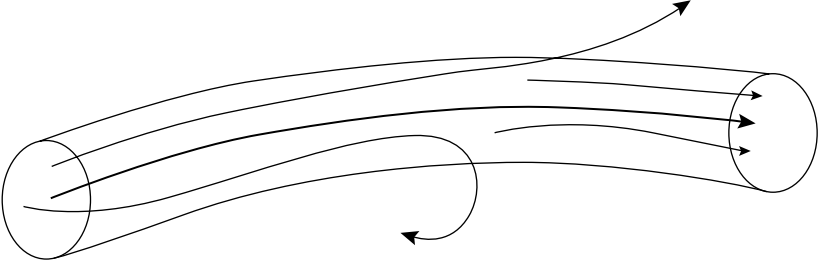


FIG. 21.2. A sketch of  $\epsilon$ -separation from the basic (thick) trajectory.

$x_k$  in the same way as with the basic points  $x_0^{(k)}$  in (21.12). As a result, we obtain the quantity

$$\bar{C}(\epsilon, t; x_k) = N_0(\epsilon, t; x_k) \leq \frac{\Gamma(A)}{e^b} = \mathcal{N}, \quad (21.15)$$

where points  $x_k$  belong to the same trajectory. That means that while  $C(\epsilon, t; x)$  characterizes the  $\epsilon$ -divergence from  $x$  during  $t$ ,  $\bar{C}(\epsilon, t; x_k)$  characterizes the  $\epsilon$ -divergence from  $x_k$ : points  $x$  are taken in different places of the phase space and points  $x_k$  are taken along the only trajectory. It is natural to believe that for an appropriately typical set of  $x \in M$  and of  $x_k \in \ell(x, x^t)$  and fairly large  $t$ , the equality

$$C(\epsilon, t; x) = \bar{C}(\epsilon, t; x), \quad t \rightarrow \infty \quad (21.16)$$

holds where subscripts  $k$  are omitted. This equality can be treated as an analog of the ergodic theorem.

A corresponding simulation for  $\bar{C}(\epsilon, t; x)$  was performed in Leoncini and Zaslavsky (2002) for a system of tracer dynamics in the field of point vortices. The basic trajectory was created by a tracer, and a few ‘host tracers’ were considered within a small distance  $\sim \delta$  from the basic trajectory. Each time a host tracer moved a distance  $\epsilon$  from the basic one, it was removed and replaced by a new host tracer at a distance  $\delta$  from the basic one (Fig. 21.2).

The scheme of calculation of  $\bar{C}(\epsilon, t; x)$  is similar to one used for calculation of the Lyapunov exponents, except for the following details:

- (a) The value of  $\epsilon$  is much less than the distance typically used to evaluate the Lyapunov exponents.
- (b) Trajectories of some tracers are  $\epsilon$ -separated after a very long time. Only these trajectories correspond to events of our main interest, i.e. to the intermittent segments of trajectories, and their statistics should be collected.
- (c) The scheme of obtaining of  $\bar{C}(\epsilon, t; x)$  simultaneously provides two different distributions: ‘probability’  $\bar{C}(\epsilon, t; x)/\mathcal{N}$  to have  $\epsilon$ -separation at time  $t$ , and

$\bar{C}(\epsilon; \ell^t, x)/\mathcal{N}$  as a ‘probability’ to have  $\epsilon$ -separation after the travel over natural length  $\ell^t$  along the trajectory. Both of these probabilities cannot be obtained by a simple transformation of variables  $t = t(\ell)$  since the trajectories can be of a fractal type, and the variables may not be transformable. This necessitates us to use more general distribution than  $\bar{C}(\epsilon; \ell^t, x)$  or  $\bar{C}(\epsilon, t, x)$ , which will be done in the following section.

## 21.4 Flight complexity function

One more important comment is that the existence of indistinguishable orbits for a time  $t$  can be studied as an exit time distribution from the  $\epsilon$ -vicinity of the basic orbit. This section will formalize this statement and extend the complexity function notion for getting more information. To do this we need a formal definition of flights considered in the previous chapters.

Consider a small domain  $A \subset M$ , a typical point  $x \in A$  and a typical close point  $y \in A$  at  $\delta$ -distance from  $x$ . The  $\epsilon$ -separation of the pair  $(x, y)$ ,  $\epsilon \gg \delta$  occurs at some time  $t$  and distance  $s = \ell^t = \ell(x, x^t)$ . Here we omitted  $\epsilon$  as an argument of  $\ell$ . Furthermore, let us remark that the distance  $s$  depends on the choice of the pair  $(x, y)$ .

The distance  $s$  of the  $(\epsilon, t)$ -separation is said to be the *length of a flight*, i.e. a length of the path that two nearby trajectories are flying together and not distinguishable. A set of flights, i.e. the set of  $(\epsilon, t)$ -indistinguishable trajectories will be called *jets* of duration  $t$  and length  $s$ . It is also assumed that if  $N_J \gg 1$  is the initial number of trajectories with  $x_0^{(k)} \in A$ ,  $1 \leq k \leq N_J$ , then at time  $t$  and at distance  $s$  the change in the number of trajectories in the jet due to  $\epsilon$ -separation is  $\Delta N_J \ll N_J$ . The following generalization of the notion of complexity will include  $s$  as a distance of  $\epsilon$ -separation and as independent to the  $t$  variable. Such a procedure permits us to consider fractal features of space and time independently. The corresponding adjustment can be made to definitions 1 and 2.

Let us treat  $x$  as the basic point and consider the set  $Q_N = \{x_k\}_{k=1}^N$  of points  $\delta$ -close to  $x$ . This set is called locally  $(\epsilon, t, s)$ -separated if it is locally  $(\epsilon, t)$ -separated (see (21.3)–(21.5)) and moreover  $s_k < s$  where  $s_k = \ell(x, x^{\tau_k})$ .

**Definition 3** The number

$$C(\epsilon, t, s, x) = \max\{N \mid Q_N \text{ is locally } (\epsilon, t, s)\text{-separated}\} \quad (21.17)$$

is called the local  $(\epsilon, t, s)$ -complexity. As a function of  $t$ ,  $s$ , it is called the *local flight complexity function*.

Similarly to the definition of  $C(\epsilon, t, B)$  in (21.12), we can consider a collection of flights and their lengths and time intervals from different domains  $A^{(m)} : B = \cup_m A^{(m)}$ . As a result we have the local *flight complexity function* of

the ensemble  $B$

$$C(\epsilon, t, s; B) = \sum_m C(\epsilon, t, s; x_0^{(m)}, \{A^{(m)}\}), \quad (21.18)$$

where  $x_0^{(m)} \in B$  are basic points.

As in Section 21.1 we may choose  $N^{(m)}$  initial points in  $A^{(m)}$  for any  $m$ , select the maximal  $(\epsilon, t, s)$ -separated subset consisting of  $N_0^{(m)}(\epsilon, t, s)$  points and form the sum

$$\sum_m N_0^{(m)}(\epsilon, t, s) \leq C(\epsilon, t, s, B). \quad (21.19)$$

The sum is equal to the flight complexity function if initial points form an optimal set.

We can extend the definition (21.18) further by considering the  $B$ -ensemble that fills all  $M$ . Then:

**Definition 4** The number

$$C(\epsilon, t, s) = \max\{N \mid Q_N \text{ is } (\epsilon, t, s)\text{-separated}\} \quad (21.20)$$

is called the *flight complexity*. As a function of  $t, s$ , it is called the *flight complexity function*.

This quantity has a simple meaning: let us take a large enough number  $\mathcal{N}_\delta$  of  $\delta$ -close pairs within  $M$  with a fairly typical distribution of the initial conditions  $x_k \in M$ ,  $k = 1, \dots, \mathcal{N}_\delta$ .  $C(\epsilon; t, s)$  is the number of trajectories that are mutually  $\epsilon$ -separated ( $\epsilon \gg \delta$ ) during time  $t$  at distance  $s$ . Therefore  $C(\epsilon, t + \Delta t, s + \Delta s) - C(\epsilon, t, s)$  is the number of trajectories that are  $\epsilon$ -separated during time  $t \in (t, t + \Delta t)$  at distance  $s \in (s, s + \Delta s)$ .

One can introduce the function,

$$p(\epsilon, t; s) \cong \frac{1}{N} \frac{1}{\Delta t} \frac{1}{\Delta s} [C(\epsilon, t + \Delta t, s + \Delta s) - C(\epsilon, t, s)], \quad (21.21)$$

where  $N = C(\epsilon, t, s)$ . It is called the *flight probability density*.

The main goal of the new definitions is to connect the notion of complexity with the space-time local instability properties of systems. The necessity of such a notion appears due to the specific features of Hamiltonian systems to have chaotic dynamics strongly non-uniform in phase space and strongly intermittent in time, and particularly due to the existence of dynamical traps.

Let us consider again a small domain  $A$  and pick some  $N$  trajectories in  $A$  with a characteristic distance  $\delta$  between them. Due to the instability these  $N$  trajectories will fill at time  $t$  an enveloped phase volume  $\Gamma_{\text{env}}(t; A, \delta) > \Gamma(0, A, \delta)$ , because of the larger distance between trajectories. After coarse-graining of  $\Gamma_{\text{env}}(t; A, \delta)$  we arrive at  $\bar{\Gamma}(t, A) \sim \Gamma_{\text{env}}(t; A, \delta)$  but without empty space

(‘bubbles’) presented in  $\Gamma_{\text{env}}(t; A, \delta)$ . This is a typical physical situation of growth of the coarse-grained phase volume and the problem is reduced to the estimate of the growth rate. The presence of dynamical traps makes the growth of  $\bar{\Gamma}(t, A)$  sensitively dependent on all its parameters  $t$ ,  $A$ , and  $\delta$  or, in other words, expanding of  $\bar{\Gamma}$  depends on the initial coordinate and observational time. For example, if  $A$  is taken in the chaotic sea,  $\bar{\Gamma} \sim \exp(ht)$  but if  $A$  is taken inside a dynamical trap,  $\bar{\Gamma} \sim t^{\mu_{\Gamma}}$ .

The flight probability density (21.21) can now be considered as a distribution function of having displacement  $s$  at a time instant  $t$  and the corresponding entropy can be easily introduced (see the next section).

One more useful connection appears from the expression

$$P_{\text{tr}}(\epsilon, t; A) = \frac{1}{\Gamma(A)} \int_0^t dt p(\epsilon, t; A) \quad (21.22)$$

that is a probability to be trapped in a tube of the diameter  $\epsilon$  supported by the domain  $A$  during time  $t$ .

Respectively,

$$P_{\text{esc}}(\epsilon, t; A) = 1 - P_{\text{tr}}(\epsilon, t; A) \quad (21.23)$$

is a probability to exit from the tube during some time  $> t$ , and for  $t \rightarrow \infty$  and  $P_{\text{esc}} \sim 1/t^{1+\beta}$  we arrive at

$$P_{\text{rec}}(t) \sim \frac{1}{t^\gamma} \quad (21.24)$$

of the probability density to return to any small domain  $\mathcal{A}$  with

$$\gamma = \min \beta(A) + 1 \quad (21.25)$$

and no dependence of  $\gamma$  on  $A$ . Due to the Kac lemma  $\gamma > 2$  for the bounded Hamiltonian dynamics, and

$$\min \beta > 1. \quad (21.26)$$

In this chapter we considered the case of continuous time. But all ideas, definitions, and results can be applied to the case of discrete time. One can choose different analogs of the length of the piece of an orbit, for example in an Euclidean space one may consider the length of union of segments joining consecutive points of the orbit. The main ideas are independent of the choice of the definition of the lengths.

## 21.5 Entropy function

The function  $C(\epsilon, t, s)$  characterizes local  $\epsilon$ -divergence of trajectories and it can be considered as a new characteristic of the dynamics. Its main role is to describe



the evolution of a typical pair of orbits taken apart a small distance  $\delta$ . Let us show how the  $(\epsilon, t, s)$ -complexity works.

Following a general physical approach let us define

$$S(\epsilon, t, s) = \ln C(\epsilon, t, s) \quad (21.27)$$

as the  $(\epsilon, t, s)$ -entropy function of the dynamics since  $C(\epsilon, t, s)$  is a number of  $(\epsilon, t, s)$ -separated states. Qualitatively speaking, due to (21.15) the number of separated states cannot be more than  $\mathcal{N}$ , that is, for the ergodic dynamics

$$S(\epsilon, t, s) \leq \ln \mathcal{N}. \quad (21.28)$$

Due to a mixing property in phase spaces or, more specifically, due to an instability and separation of any initially close orbits, one can expect the growth of  $S(\epsilon, t, s)$  with time until the  $\max S = \ln \mathcal{N}$  is reached. The definition (21.27) permits us to estimate from  $C(\epsilon, t, s)$  some fine properties of the evolution of  $S(\epsilon, t, s)$  as a function of time  $t$  and the length of separation  $s$ .

For the case of the Anosov-type systems,

$$s = s(t) = \text{const} \cdot s(0)e^{ht}, \quad s(0) = \delta. \quad (21.29)$$

Then

$$C(\epsilon; t, s) = C(\epsilon, t) = \text{const} \left( \frac{\delta}{\epsilon} \right)^b e^{ht} \quad (21.30)$$

and (21.30) coincides with (20.21) up to a non-important constant. Similarly

$$S(\epsilon, t, s) = S(\epsilon, t) = \ln C(\epsilon, t) = b \ln \frac{1}{\epsilon} + ht + \text{const}, \quad (21.31)$$

that is,

$$S(\epsilon, t, s) \rightarrow ht, \quad t \rightarrow \infty \quad (21.32)$$

and we arrive to the standard expression.

We can rewrite the results (21.30) and (21.31) in the form

$$\begin{aligned} h &= \frac{\partial S(\epsilon, t)}{\partial t} = \frac{\partial \ln C(\epsilon, t)}{\partial t} = \text{const}, \\ b &= \frac{\partial S(\epsilon, t)}{\partial \ln(1/\epsilon)} = \frac{\partial \ln C(\epsilon, t)}{\partial \ln(1/\epsilon)} = \text{const}. \end{aligned} \quad (21.33)$$

The formula (21.33) expresses another view on the system invariants  $h$  and  $b$ , which will be discussed more at the end of this chapter. Here we just need to mention that  $h$  and  $b$  are expressed as specific partial derivatives of the entropy function. We may conclude that being given complexity function or entropy

function instead of complexity or entropy, we can obtain the entropy rate  $h$  and box dimension  $b$  without limits  $t \rightarrow \infty$  or  $\epsilon \rightarrow 0$  as it was in the definitions (20.12) or (20.2).

In the opposite case of integrable system, it is possible to show that

$$C(\epsilon, t) = \text{const} \cdot t \quad (21.34)$$

and correspondingly

$$S(\epsilon, t) = \ln t + \text{const} \quad (21.35)$$

(see Problem 21.2). It follows from (21.35) that

$$\frac{\partial S(\epsilon, t)}{\partial t} \rightarrow 0, \quad (t \rightarrow \infty), \quad (21.36)$$

but

$$\frac{\partial S(\epsilon, t)}{\partial \ln t} = 1, \quad (21.37)$$

i.e. information that can be obtained from the complexity or entropy function depends on a right choice of variables (*Note 21.2*).

## 21.6 Polynomial and mixed complexities and anomalous transport

Complexity defined in (21.30) grows exponentially with time reflecting an existence of a positive Lyapunov exponent and exponential divergence of trajectories in phase space. This is not the case for zero Lyapunov exponent systems and for diffusional type processes. To consider large scale processes such as the diffusion for systems of that kind, let us use the partition function  $\mathcal{N}(t, \Delta\Gamma)$ ,

$$\mathcal{N}(t, \Delta\Gamma) = \text{const} \cdot C(\epsilon, t). \quad (21.38)$$

In numerous cases the process of mixing in phase space and the corresponding separation of trajectories has algebraic dependence on time. Particularly, it is related to the dynamics with the fractal time and the diffusional type of processes. For this case, the complexity is polynomial in time and

$$\mathcal{N}(t, \Delta\Gamma) = \text{const} \cdot \left(\frac{t}{t_0}\right)^\beta = \text{const} \cdot C(\epsilon, t) \quad (21.39)$$

with some exponent  $\beta$  and characteristic time scale  $t_0 \ll t$ . As in (21.37), the entropy growth rate can be defined in the  $\ln t$  scale

$$\frac{\partial S(\epsilon, t)}{\partial \ln t} = \frac{\partial \ln C(\epsilon, t)}{\partial \ln t} = \beta \quad (21.40)$$

and the exponent  $\beta$  characterizes the corresponding rate of the entropy growth. As appeared in previous chapters, chaotic dynamics of real Hamiltonian systems

may not display, in general, exponential growth of the complexity, and the number  $\mathcal{N}$  of  $\epsilon$ -separated orbits grows asymptotically as polynomial in time and length of separation  $s = \ell(x, x^t)$ . In this case the complexity can be written as

$$C(\epsilon, t, s) = \left(\frac{s_0}{s}\right)^\alpha \left(\frac{t}{t_0}\right)^\beta g(\epsilon, s, t), \quad (21.41)$$

where  $s_0, t_0$  are characteristic scales of length and time,  $\alpha, \beta > 0$ , and  $g(\epsilon, t, s)$  is a slow varying function. We will be interested in the asymptotics

$$\frac{s}{s_0} \rightarrow \infty, \quad \frac{t}{t_0} \rightarrow \infty. \quad (21.42)$$

The conditions (21.42) correspond to the increasing of the number of  $\epsilon$ -separated states with the growth of time and the decreasing of this number with the growth of the separation distance. For example  $\alpha = 1$  and  $\beta = 1/2$  correspond to the normal one-dimensional diffusion, while other powers appear for the anomalous diffusion.

Following the definition (21.27) let us introduce the entropy function:

$$S(\epsilon, t, s) = \ln C(\epsilon, t, s) = -\alpha \ln \left(\frac{s}{s_0}\right) + \beta \ln \left(\frac{t}{t_0}\right) + \ln g(\epsilon, t, s). \quad (21.43)$$

This expression will be analysed in the next section.

Here we would like to mention that the complexity in the form (21.41) suggests that the corresponding partition function

$$\mathcal{N}(\epsilon, t, s) = \text{const} \cdot C(\epsilon, t, s) = \text{const} \cdot \left(\frac{t^\beta}{s^\alpha}\right) g(\epsilon, t, s) \quad (21.44)$$

has a self-similar dependence on  $(t, s)$  in the limit (21.42), and consequently for its moment we have

$$\langle s^\alpha \rangle = \mathcal{D} \cdot t^\beta \quad (21.45)$$

with  $\mathcal{D}$  that may depend slowly on  $t$ . Equation (21.45) describes the anomalous diffusion with the transport exponent

$$\mu = \frac{2\beta}{\alpha} \quad (21.46)$$

that can be obtained from

$$(\langle s^\alpha \rangle)^{2/\alpha} \sim t^\mu. \quad (21.47)$$

Parameters  $\alpha, \beta$ , and  $\mu$  can be considered as new dynamical invariants intimately linked to the  $(\epsilon, t, s)$ -complexity, that is, the complexity function and the corresponding entropy.

Dependence of the complexity function on two variables  $s$  and  $t$  makes it possible to have ‘mixed’ complexities of the following types:

$$\begin{aligned} C^{(1)}(\epsilon, t, s) &= \left(\frac{s_0}{s}\right)^\alpha e^{ht} g^{(1)}(\epsilon, t, s), \\ C^{(2)}(\epsilon, t, s) &= e^{sw} \left(\frac{t}{t_0}\right)^\beta g^{(2)}(\epsilon, t, s), \end{aligned} \quad (21.48)$$

i.e. algebraic in one variable and exponential in the second one. The case  $C^{(1)}(\epsilon, t, s)$  shows exponential divergence in time and a fractal length structure with a box dimension  $\alpha$ . The case  $C^{(2)}(\epsilon, t, s)$  does not have yet analogy or physical interpretation.

Similar definitions can be done for the entropy function:

$$\begin{aligned} S^{(1)}(\epsilon, t, s) &= \ln C^{(1)}(\epsilon, t, s), \\ S^{(2)}(\epsilon, t, s) &= \ln C^{(2)}(\epsilon, t, s). \end{aligned} \quad (21.49)$$

On the basis of all definitions of entropy we can make an important remark about its extensivity. Typically, the extensivity is considered in statistical physics with respect to the coordinate variable. Dynamical systems analysis provides an extensivity with respect to the number of degrees of freedom, or with respect to time. Here we would like to mention that instead of  $t, s$  there can be  $\ln t$  or  $\ln s$ , or their different combinations. For example, in the case of  $C^{(1)}$  the entropy  $S^{(1)}$  is additive in the space of variables  $(\ln s, t)$  while in the case (21.41) the entropy is additive in the space  $(\ln t, \ln s)$ .

Our final remark for this chapter is that  $(\epsilon, t, s)$  dependence of the complexity function is considered for a system with evolution and it may happen very typically, with are two time intervals: at the beginning, the evolution of complexity is exponential and after a fairly long time it becomes algebraic. A similar pattern occurs for the Sinai billiard where a distribution of the Poincaré recurrences follows exponential law for the beginning and then decays as  $\sim 1/t^3$ .

## 21.7 Travelling waves and Riemann invariants of entropy and complexity

In this section we provide a more general and more formal view on the critical exponents of kinetics, if they exist. Let us recall that the basic principle of statistical physics is to define an ensemble of equivalent in some sense or of equal probability states. The microcanonical ensemble is a nice example of this principle. The famous Boltzmann formula for entropy,  $S = \kappa \ln W$ , makes use of the similar principle of the equivalency of  $W$  states. A possibility to have a fairly simple presentation for the complexity or entropy functions reflects similar features that we formalize below.

Consider new variables,

$$\xi = \ln \left( \frac{s}{s_0} \right), \quad \eta = \ln \left( \frac{t}{t_0} \right) \quad (21.50)$$

and rewrite (21.41) as

$$S(\epsilon, t, s) = (-\alpha\xi + \beta\eta) + \ln g(\epsilon, \xi, \eta), \quad (21.51)$$

where  $g$  is a slow function of  $\xi, \eta$ . Neglecting the derivatives of  $g$ , we can conclude from (21.51) that the entropy is constant along the traveling wavefront, with coordinates

$$\xi = \left( \frac{\beta}{\alpha} \right) \eta \equiv c\eta, \quad (21.52)$$

where  $c$  is the wave speed. Due to (21.46)

$$\mu = 2c \quad (21.53)$$

and the transport exponent can be interpreted as the double speed of the travelling wave of the entropy or complexity functions. This property appears as a result of a non-trivial coupling between time and phase space of dynamical systems. Indeed, any kind of randomness which is assumed for kinetics in a stochastic field differs from the randomness of chaotic dynamics since the randomization of trajectories occurs as a result of non-linearity and dynamical instability.

The structure of the entropy function (21.51) or complexity function (21.41) is invariant, with respect to the renormalization of  $\xi$  and  $\eta$ , namely

$$s \rightarrow \lambda_s s, \quad t \rightarrow \lambda_t t, \quad (21.54)$$

if we neglect variations of  $g(\epsilon; \xi, \eta)$ , and if  $\lambda_s, \lambda_t$  satisfy the equation

$$\frac{\mu}{2} = c = \frac{\beta}{\alpha} = \frac{\ln \lambda_s}{\ln \lambda_t}. \quad (21.55)$$

Equation (21.55) shows a connection between parameters  $\alpha, \beta$  of the dynamical origin, transport exponent  $\mu$ , and velocity  $c$  of the travelling wave of the complexity. The parameter  $c$  also defines a direction in  $(t, s)$  coordinates of the travelling wave propagation or, in other words, *directional complexity and directional entropy rate*. For different dynamical models scaling parameters  $\lambda_s, \lambda_t$  were defined in the previous chapters.

In fact,  $(\alpha, \beta)$  or  $(\lambda_s, \lambda_t)$  are not constants, and wave propagation can be different in different directions. This situation is an analog to multifractal space-time structure. For any direction with ‘velocity’  $c$  in  $(\xi, \eta)$  space, there is a corresponding curve in  $(s, t)$  space and an isoline of the section of the

surface  $S(t, s)$  by a plane  $S(t, s) = \text{const}$ . The fractional exponents  $(\alpha, \beta)$  of the complexity space-time dependence are receiving a new meaning as characteristics of the entropy/complexity functions

$$\frac{\partial S}{\partial \xi} = \frac{\partial \ln C}{\partial \xi} = -\alpha, \quad \frac{\partial S}{\partial \eta} = \frac{\partial \ln C}{\partial \eta} = \beta, \quad (21.56)$$

along which the travelling waves have a constant velocity. In this way we have a generalization of the usual notion of entropy for a finite system. This analogy can be advanced further by comparing waves of complexity/entropy to simple waves in fluid dynamics. Then the velocity  $c$  is the Riemann invariant and so is  $\mu$ .

We arrive to an interesting conclusion: the transport exponent  $\mu$  can be interpreted as a *Riemann invariant* of the complexity (entropy) *simple wave* in the  $(\ln t, \ln s)$ -space. This interpretation can be developed further to a possibility of anisotropic phase space with different values of  $\mu$  in different directions, and even to anisotropy in the extended space that includes phase space and time. Correspondingly, we will have different Riemann invariants in different directions. Indeed, the cases (21.41) and (21.43) of the self-similar behavior of the complexity function shows explicitly that the entropy can be written in the form

$$S(\epsilon; t, s) \cong S(\xi - c\eta) \quad (21.57)$$

up to a slow varying function  $g$ . The expression (21.57) permits us to consider joint space-time variables as a two-dimensional space  $(\xi, \eta)$  where entropy propagates along a line in the direction with tangent  $c$ . As was mentioned, Riemann invariants can be different in different directions, and we have introduced corresponding velocities  $c_{\mathbf{e}}$  where  $\mathbf{e}$  is a unit vector along some direction:

$$S(\epsilon, t, s) = S(\epsilon_{\mathbf{e}} - c_{\mathbf{e}}\eta_{\mathbf{e}}), \quad (21.58)$$

where  $\xi_{\mathbf{e}}, \eta_{\mathbf{e}}$  are linear combinations of  $\xi, \eta$ . In this way a mixing of phase space and time variables appears to explicitly define directional entropy and complexity functions.

Together with directional complexity and entropy, we have strongly anisotropic transport with a transport exponent  $\mu_{\mathbf{e}}$  which is different for different directions (*Note 21.3*).

## Notes

### *Note 21.1*

The definitions and applications of this chapter follow Afraimovich and Zaslavsky (2003).

### *Note 21.2*

It is necessary to mention that the term in (21.34) or (21.35), that depends on  $t$  due to a regular shear-type flow in phase space, is of the universal type and can be always excluded by a corresponding renormalization. After that, only a

real phase space mixing or weak mixing will give an input into the complexity. Even if we coarse-grain the free shear-type flow, the coarse-grained initial ensemble  $A$  with  $\bar{\Gamma}(A) \ll \Gamma_M$  will always satisfy this condition  $\bar{\Gamma}(A) \ll \Gamma_M$  and will never fill full phase space with an arbitrary dense net of trajectories.

*Note 21.3*

Directional complexity was introduced for cellular automata by Milnor (1988) and then developed for dynamical systems in Afraimovich *et al.* (2002).

## Problems

More complicated problems are marked by (\*).

*21.1\** Derive the formula (21.30) considering large  $t$ .

*21.2* Consider the following integrable system given by the map

$$r_{n+1} = r_n; \quad \vartheta_{n+1} = \vartheta_n + r_n, \quad (\text{mod } 2\pi).$$

Find the complexity and entropy functions for the system. Find the constants in (21.34), (21.35) (see also Afraimovich and Zaslavsky (2003)).

*21.3* Find the complexity and entropy functions for the Arnold cat map.

## CHAOS AND FOUNDATION OF STATISTICAL MECHANICS

This is a chapter dedicated to a very special topic of theoretical physics and statistical mechanics: the role of chaos in the foundation of laws of statistical mechanics. Any kind of a physical object, particle, or field can be described by the corresponding equations, Newton equation, Maxwell equations, etc. These equations are reversible in time and fully deterministic, i.e. there exists a unique solution (trajectory) at any time instant  $t > 0$  if some initial conditions are given at  $t = 0$ . How, when, and why can an ensemble of a large number of such objects be described in a statistical or probabilistic way, with time irreversible equations, growth of entropy, relaxation to the equilibrium, and other features of the kinetics? The question implies two sides of the problem: one formal and one real.

The first, formal approach, is related to a rigorously formulated scheme of derivation of some irreversible kinetic equation from the reversible dynamic equations. Typically, such a scheme includes a hypothesis on the existence of a random element in the dynamical equations or in trajectory properties, or an equivalent condition of the randomness. An example includes the hypothesis on the collision (Stosszahlansatz) of Boltzmann (1872) or random phase approximation. The second, natural approach, is related rather to the observation than to the equations: a gas located in some part of a vessel expands uniformly over full vessel, but we will never see the gas return back to the initial domain in full or almost in full. Why this happens questions the theory and the answer should be based on the first principles.

The story of the foundation of statistical mechanics can be started from the publication of Boltzmann's H-theorem (1872), and the discussion about the origin of the laws of statistical mechanics and the origin of randomness looks still very topical. Understanding of the phenomenon of chaos does not provide sufficient information to make clear everything related to the world of statistical physics and probability. Nevertheless, as follows from this chapter, we can succeed in understanding part of the problem of the origin and a type of the probabilistic features due to dynamics of systems with a few degrees (*Note 22.1*).

### 22.1 Zermelo's and Loschmidt's paradoxes

#### 22.1.1 *Historical comments*

In 1872 Boltzmann published a paper 'Further Investigation of Heat Equilibrium between Gas Molecules', where he had proved the existence of a non-increasing



function  $H(t)$  that characterized the evolution of a system of large number of colliding molecules in their approach to the equilibrium state. This result became known as the *H-theorem* of Boltzmann (*Note 22.2*). The expression

$$H = \langle \ln f(p, q) \rangle_{\Gamma} = -S \quad (22.1)$$

was simply the minus entropy  $S$  and the H-theorem declares the monotonic (non-decreasing) change of entropy.

In 1895 L. Boltzmann published the fundamental work ‘Lectures on Gas Theory’, Part 1 (Boltzmann (1895)) where the monotonic evolution of systems toward the equilibrium first obtained in (Boltzmann (1872)) was proclaimed in a more consequential, full, and generalized way. The H-theorem met two serious objections: from a mathematician E. Zermelo (Zermelo (1896)) and from Boltzmann’s friend and teacher J. Loschmidt. Today their objections are known as the paradox of Zermelo and the paradox of Loschmidt. In the following years there was an intensive discussion between Boltzmann from one side and Zermelo, Loschmidt, and other scientists on the other. Boltzmann committed suicide in 1906, and in many publications it was seen as a reaction to a combination of the hostile attacks on his results, sensitivity, and a lack of understanding and support from his friends and colleagues. Shortly after Boltzmann’s death, his kinetic theory and H-theorem were accepted and recognized, especially after the publication of the paper of (Ehrenfest (1911)) and Perrin’s experiments on Brownian motion.

Some idea of the difficulties that Boltzmann experienced during that time can be gained from the Foreword to Part 2 of the ‘Kinetic Theory of Gases’ (Boltzmann (1898)):

‘In my opinion it would be a great tragedy for science if the theory of gases were temporarily thrown into oblivion because of a momentary hostile attitude toward it, as was for example with the wave theory because of Newton’s authority. I am conscious of being only an individual struggling weakly against the stream of time. But it still remains in my power to contribute in such a way that, when the theory of gases is again revived, not too much will have to be rediscovered.’

### 22.1.2 *Paradox of recurrence*

The paradox was formulated in (Zermelo (1896)) and based on the Poincaré theorem of recurrences. A gas of particles in a volume can be considered as a compact Hamiltonian system which, starting from some state, repeatedly returns back to arbitrary vicinity of the initial state. Zermelo states the contradiction of this result to be the monotonic decrease of H-theorem (monotonic entropy increase).

In the explanation of the paradox, Boltzmann refers to the following two important features of his theory that are not included into the Poincaré

theorem: probabilistic consideration of the different states of a system and its evolution, and the coarse-graining of the distribution function of the system. For a macroscopically large number of particles ( $\sim 10^{23}$ ), a probability to return to an initial volume  $A$  is immensely small. The coarse-graining procedure for the distribution function neglects the events of very small probability. Particularly, all rare (with small probability) fluctuations returning to any non-equilibrium initial state are neglected in the process of deriving the kinetic equation. This makes the kinetic relaxation irreversible. Boltzmann makes first estimates of the recurrence time for molecules in  $1 \text{ cm}^3$  at the normal density and temperature. The time that is necessary to return the system of the molecules to the initial state with an accuracy of  $10^{-7}$  cm is  $10^{10^{10}}$  (Boltzmann (1897)).

### 22.1.3 *Paradox of reversibility*

This paradox was formulated by Loschmidt who links some value of entropy  $S_j$  to a corresponding state of the system  $z_j$ . If  $S$  increases from the value  $S_i$  to  $S_f > S_i$  when the system evolves from  $z_i$  to  $z_f$ , then the entropy  $S_f$  should decrease to the value  $S_i < S_f$  on the reverse system evolution  $z_f \rightarrow z_i$ , in contradiction to the H-theorem.

In fact, as was also explained by Boltzmann, any kind of evolution of the system must be considered in a probabilistic way and different paths have different probabilities. In the derivation of the kinetic equation small probability transitions are neglected that lead to the breaking of symmetry with respect to the reverse  $t \rightarrow -t$ .

### 22.1.4 *Boltzmann's comments*

It is worthwhile to mention a few other comments by Boltzmann that will be used in other sections of this chapter and that are important in understanding the origin of statistical mechanics.

Boltzmann has mentioned that Poincaré recurrence theorem does not say anything about the recurrence time. Moreover, this time can be arbitrarily large as it was not understood in (Zermelo (1896)) objections. At the same time, as was commented in (Boltzmann (1897)), neglecting the low probability of events does not mean their impossibility of happening, and the same should be said about the fluctuation of molecules. Boltzmann's comment inferred or assumed an existence of a finite time  $t^*$  such that events which most probably could appear at  $t \gg t^*$  would be neglected. Boltzmann estimated that  $t^*$  is of the order of a time between collisions (*Note 22.3*).

To better understand the origin of the H-theorem, Boltzmann proposed the urn-model with exchange of black and white balls (Boltzmann (1898a)) that was developed in (Ehrenfest (1911)) and then, in a modified version, rigorously solved by Kac (Kac (1957, 1959)).

## 22.2 Chaos and the paradoxes

The theory of chaos helps us to understand the origin of randomness from the dynamics and occurrence of statistical laws in systems. The chaos exists even in systems of two degrees of freedom and we do not need a large number of particles to generate random behaviour. It is also important that the Poincaré recurrence theorem has no connection to the origin of statistical properties in systems although these statistical properties impose the distribution of the Poincaré cycles  $P_{\text{rec}}(t)$ . For any chaotic trajectory the sequence of recurrence time intervals  $t_1, t_2, \dots$  is a probabilistic sequence described by  $P_{\text{rec}}(t)$ . The irreversibility appears in the following way.

Consider a small phase domain  $A_0$  at  $t = 0$  of a ‘good’ shape, say a sphere, and look at its evolution with time. Assume that the system is of the Anosov type and there is a uniform mixing in phase space. After a not small time the boundary of the drop will be of an extremely complicated shape and the probability of the newly shaped domain  $A_t$  to return to the previous ‘shell’  $A_0$  is extremely small. The irreversibility occurs after the coarse-graining of the phase volume. Small details of the system’s state in phase volume disappear and after while any exact predictability of the future system’s state becomes impossible.

In the same way, the coarse-graining can resolve the paradox of reversibility. The coarse-graining makes it impossible to reverse the trajectories from a high probability state to a low probability one. Consider that a group of trajectories exits from a small domain  $A_0$ , and let  $A$  be another domain such that the coarse-grained volume  $\Delta \equiv \Gamma(A) \geq \Gamma(A_0)$ . We should also introduce a scale of coarse-graining and let it be  $\Delta$ . This means that we have lost the individual properties of trajectories inside  $A$ . Therefore, within  $A$  we cannot distinguish the trajectories that started at  $A_0$  and arrive to  $A$  from those trajectories that follow different paths. Reversing the trajectories from  $A$  into backward paths, we reverse, in this way, not only the trajectories that arrive from  $A_0$  but also many other trajectories that fill other domains of phase space. In the case of a positive Lyapunov exponent there are many trajectories in  $A$  that do not arrive from  $A_0$ .

The coarse-graining leads to a loss of information about trajectories and the mixing leads to a fast filling of the domain of observation by trajectories from almost all phase space.

Despite this fairly clear picture there exists a question without an answer: how does a system perform the self coarse-graining, and how can one discover accidentally a rare transition or a state of exponentially small probability (Note 22.4)?

## 22.3 Anomalous properties of the Sinai and Bunimovich billiards

In this section we would like to provide two examples to illuminate a specific phenomenon of chaotic dynamics: *There may exist a zero measure domain that cannot be neglected in the constructing of kinetics.*

In the Sinai billiard (Sections 9.2 and 12.1) all trajectories are chaotic except for a zero measure set that particularly includes bouncing trajectories, i.e. all phase space has one ergodic component excluding a domain of zero measure. Nevertheless, the excluded area generates *scars* in the phase space as is seen from Fig. 9.3. The bouncing segment of a trajectory can be arbitrarily long depending on the angle. The trajectories that bounce an infinitely long time have zero measure and their existence makes scars in the phase space. A similar situation appears for the Bunimovich (stadium) billiard (Fig. 9.5) where there exists a positive Lyapunov exponent (Bunimovich (1979)) for almost all trajectories except for a set of zero measure. Any chaotic trajectory has infinitely long segments of bounces and the corresponding scars in the phase plane.

Despite zero measure of scars, but because of them, the distribution of Poincaré recurrences is strongly different from what exists for the Anosov-type systems. Simulations show (see Fig. 22.1) that for both billiards (compare to (12.10))

$$P_{\text{rec}}(t) = \begin{cases} e^{-ht}, & t \lesssim t^*, \\ \frac{1}{t^\gamma}, & t \gtrsim t^*, \end{cases} \quad (22.2)$$

where  $h$  is the Kolmogorov-Sinai entropy,  $t^*$  is a crossover time that depends on the geometry,  $\gamma \cong 3$  (see for example (Zaslavsky and Edelman (1997) and references therein)). The result (22.2) does not yet have a rigorous proof (see estimate in Bunimovich (1985)). Particularly, we stress a fairly sharp crossover from the exponential decay to the power law for both billiards as in Fig. 12.2.

To study diffusion or moments dynamics in the Sinai billiard, we should consider the corresponding Lorentz gas model, i.e. a unit cell that is periodically continued in  $x$  and  $y$  directions (see Fig. 9.4). For a point ball with distribution function  $F(x, y, t)$  the moments are

$$\langle R^{2m} \rangle = \int_{-\infty}^{\infty} (x^2 + y^2)^m F(x, y, t) dx dy. \quad (22.3)$$

Qualitative estimates lead to

$$\langle R^2 \rangle \sim \text{const} \cdot t \ln t, \quad (22.4)$$

while numerical analysis show for  $t \rightarrow \infty$

$$\langle R^{2m} \rangle \sim (t \ln t)(t \ln t)^{3(m-1)/2}, \quad (22.5)$$

which strongly deviate from the Gaussian law (Note 22.5).

Diffusion in the stadium billiard can be considered in two different variations (see Fig. 22.1). In the first case that corresponds to the infinite horizon,

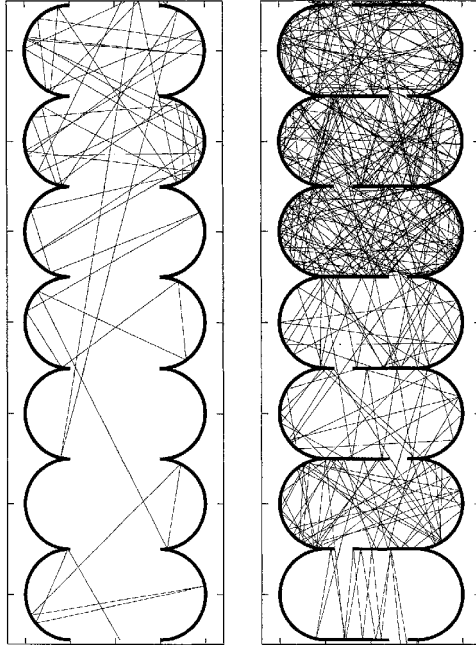


FIG. 22.1. Diffusion in the periodically continued Bunimovich billiards with different openings: infinite horizon (left) and finite horizon (right).

i.e. a possibility of arbitrary long flights, simulations show

$$\langle y^{2m} \rangle = \int_{-\infty}^{\infty} y^{2m} F(y, t) dy \sim t^{\mu m}, \quad (t \rightarrow \infty) \quad (22.6)$$

with  $\mu = 1.05$  and  $F(y, t)$  as a distribution function. In the case of finite horizon (Fig. 22.1, right)  $\mu = 1$ , i.e. the transport is normal or very close to the normal.

Both examples show that long flights can significantly influence kinetics and transport. At the same time the origin of flights is imposed by a zero measure domain in phase space that cannot be neglected (*Note 22.6*).

We return to this issue at the end of the chapter.

## 22.4 Maxwell's Demon and Chaos

*Maxwell's Demon* is a paradigm imported for a deeper understanding of the main principles of thermodynamics. We use the notion 'kinetics' when speaking about microscopic picture of the considered system and the notion 'thermodynamics'

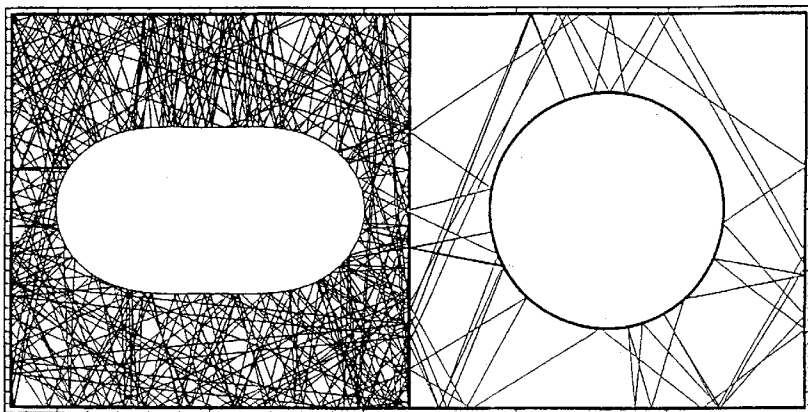


FIG. 22.2. Two billiards coupled through a small hole size 0.2. The shape of the scatterer is a Cassini oval in the left half. In the figure we present one trajectory that bounces in the Cassini and Sinai billiards.

or ‘transport’ when speaking about the moments of the distribution function obtained from the kinetics (*Note 22.6*).

In the *Theory of Heat* (1871), Maxwell proposed a conceptual device that could make molecules select one of two equal chambers connected through a hole. This device (Demon), located at the hole, should work against the thermodynamic law that causes the gas of molecules in two contacting volumes to be in equilibrium. The problem, however, leaves an ambiguity in regard to its precise definition as it involves a non-physical element as a part of the full construction. In contemporary physics, this element is specified, which helps the Maxwell’s Demon to acquire a different, realistic visualization:

- (i) The Demon can be considered as a device which is able to work with information and transfer the information into action (thinking device).
- (ii) The Demon is a measuring device, and its actions depend on the results of the measurement.

Both concepts give rise to rich physical discussions on the possibilities of computing devices, irreversibility of computations, natural limitations of the measurement process, role of quantum effects, and the quantum uncertainty.

The existence of chaos or pseudochaos provides a new direction for studying the Maxwell’s Demon problem, based on its complete dynamical formulation and avoiding any types of elements that cannot be formulated as equations of motion. In his original publication, Maxwell wrote that in statistical consideration ‘...we are compelled to adopt... the statistical method of calculations and to abandon the strict dynamical method in which we follow every motion by

calculus.’ Here we are just going in the opposite direction, i.e. we follow the *strict dynamics*, as is shown, for example, in Fig. 22.2.

A general idea of the proposed approach to the problem can be fairly simply formulated. Consider two separate dynamical systems with mixing properties of the trajectories such that a statistical equilibrium can be achieved in each of the systems. Let us make a weak contact between the systems, which brings the coupled sub-systems to a new equilibrium state. One may ask the question: Does the new equilibrium for each sub-system correspond to what we commonly define as thermodynamical equilibrium (equal pressures, temperatures, etc.)?

In Fig. 22.2, a prototype of the dynamical model is introduced, consisting of two billiard-like systems with mixing motion inside each and with the contact of billiards through a hole. A point particle is bouncing inside the billiards with absolutely elastic reflections from the billiards’ walls. As both billiards have mixing properties, a stationary distribution function is expected. It can be a probability measure to find a particle in one or another part of the system in the infinite time limit. For the ergodic motion the infinite time limit can be replaced by an ensemble average in the phase space of a system. Can the equilibrium in the described billiard-like system be of the same kind as the one we usually call thermodynamic equilibrium? Or, in other words, can the Hamiltonian chaotic dynamics explain, in principle, the origin of the thermodynamics law, or do we need some additional constraints? In the following section we will show a negative answer to this question, considering an appropriate ‘design’ of the billiard-like system with chaotic dynamics.

Actually, the main aim of this discussion is to determine what kind of random process corresponds to the dynamical chaotic motion. It is known from the previous chapters that this problem is quite complicated. For the Hamiltonian systems of general type, the motion is not ergodic. To obtain a domain of ergodic motion, one needs to extract from the entire phase space a (multi-) fractal set of islands with regular motion. The properties of the rest of the phase space, called the *stochastic sea*, are not well understood as those of the islands’ boundaries. This part of the phase space is non-uniform. It is filled by another kind of fractal objects, *cantori*, which have zero measure and strongly influence the transport of particles, creating a ‘stickiness’ of the islands’ boundaries.

## 22.5 Maxwell’s Demon as a dynamical model

We call the *Maxwell Demon system* a dynamical system that can create a non-equilibrium distribution of particles between two contacted chambers for an arbitrarily long time. The notion of equilibrium has the thermodynamic meaning, i.e. difference of pressures, or temperatures, etc. in different chambers. Neither any random nor ‘thinking’ element is included into the model.

A crucial feature in construction of the dynamical model of the Maxwell’s Demon is to use the dynamical traps that lead to incomplete randomness and long-lasting fluctuations. Such a model was presented in Fig. 22.2 where the

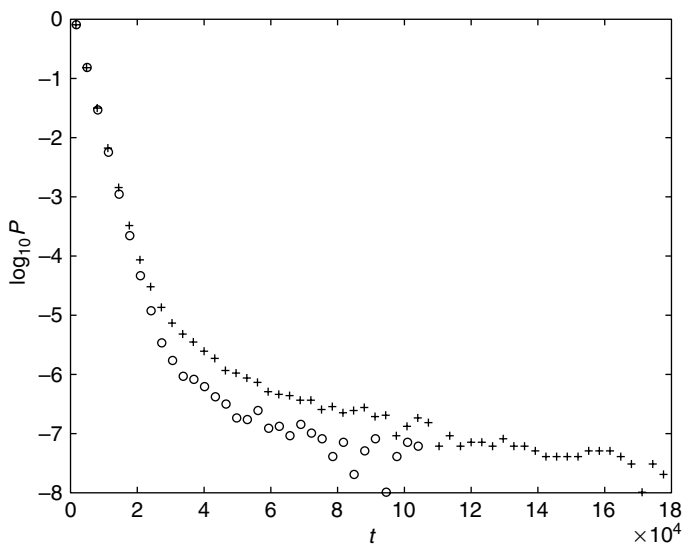


FIG. 22.3. Distribution of Poincaré recurrences to a hole in the partition from the left (circles) and right (crosses) chambers. The difference persists for a time  $1.16 \times 10^{10}$ . The data are accumulated from 37 orbits.

Cassini billiard part was taken with special parameters of the inner scatterer. Due to these parameters the islands' boundaries in phase space were very sticky (see the details in Zaslavsky and Edelman (1997)). The result of computations of Poincaré recurrences to the hole in the left (circles) and right (crosses) chambers are shown in Fig. 22.3.

These recurrences are actually residence times in a chamber before the escape to another chamber. There are evident differences in the distributions that imply a difference in moments of the distribution  $P(t)$  and a difference in the corresponding thermodynamical properties of the chambers. A more evident difference can be obtained for another example (see Fig. 22.4) where the rhombus billiard replaces the Cassini oval (*Note 22.8*).

As was mentioned above, for the Sinai billiard part only, the recurrence exponent  $\gamma = 3$  and for the rhombus billiard only,  $\gamma \gtrsim 2$ . When the hole is open, the recurrences to each chamber are distributed in a different way (see Fig. 22.5). Our next step will be to get pressure in each chamber when the hole is open.

The pressure from one particle can be considered as a mean value for the transferred momentum per unit length of the chamber's divider:

$$pr(t) = \left\langle \frac{\Delta p}{\Delta t} \right\rangle. \quad (22.7)$$



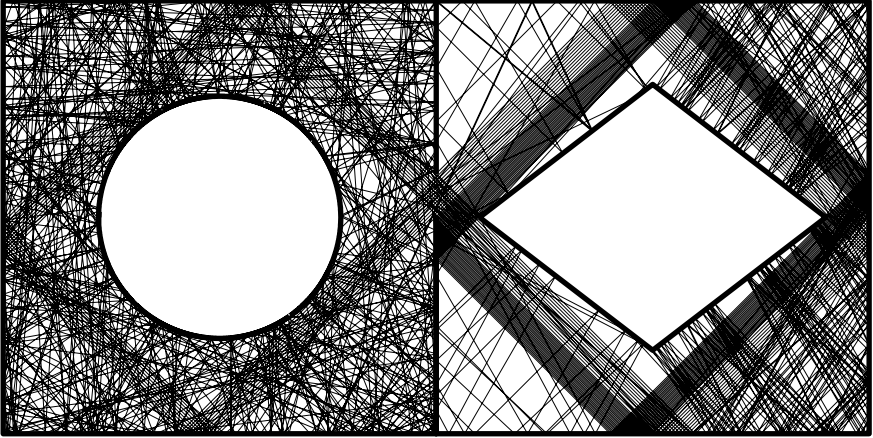


FIG. 22.4. A model of the Maxwell's Demon device with two chambers and scatterers as a circle and a rhombus.

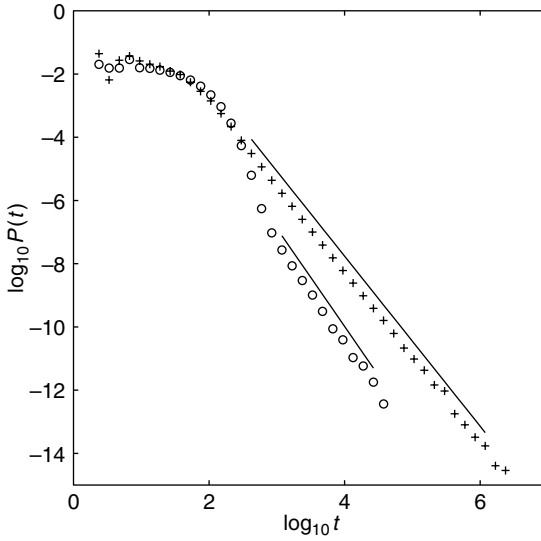


FIG. 22.5. Distribution of the Poincaré recurrences for the left (circles) and right (crosses) chambers of the model of Maxwell's Demon in Fig. 22.4.

The expression (22.7) is a ‘coarse-grained’ pressure over some time  $\Delta t$ , and its value depends on a macroscopic time and on how the coarse-graining is performed. Let  $\Delta t^\pm$  be the time intervals that a trajectory (particle) spends in a chamber with the rhombus or circle correspondingly between two successive

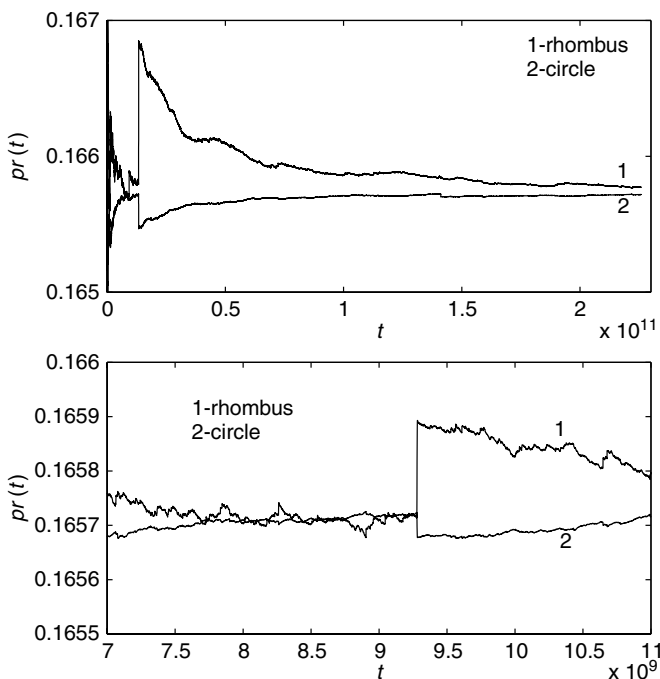


FIG. 22.6. Time behaviour of the pressure  $pr(t)$  obtained by the  $\Delta t$ -averaging.

crossings of the hole. One can calculate the cumulative momentums transfer  $\Delta p$  and the corresponding pressures will be called  $\Delta t$ -average. These results are shown in Fig. 22.6 with a very clear sign that a particle in a chamber with rhombus reveals larger amplitude fluctuations and less uniformity than in the chamber with the circle.

For this example, we consider  $\Delta t \sim 10^6$ . While it follows from Fig. 22.6 that there is a convergence of the pressures from the left and from the right to a common value, there are *immense fluctuations* without a finite time of their relaxation. As we see from Fig. 22.6, the fluctuations can last up to the full time of observations, which is  $\sim 10^{11}$  in our simulations. The longer time we consider, the longer lasting fluctuations can be observed. In Section 4.1 we called them *persistent fluctuations*.

The considered systems have unusual behaviour and do not follow the thermodynamic laws in a common sense. These systems possess the polynomial complexity and the features typical for the Maxwell's Demon. The most interesting fact about these systems is that they are either close to some natural systems (wave propagation in non-uniform wave guides) or close to the behaviour of some Hamiltonian systems with non-zero Lyapunov exponents when the dynamics is sticky, especially in some problems of plasma physics. It is important to underline that we consider pure dynamical models within a dynamical consideration.

## 22.6 Comments on the application of Ergodic Theory

The results of the previous sections show that the chaotic or pseudochaotic dynamics in real systems does not always provide a finite relaxation time to the equilibrium or fast decay of fluctuations, and that chaotic systems are not completely random in the sense originally prescribed for statistical systems. These properties may require rethinking some of the fundamental assumptions of what is necessary to work out thermodynamic laws, if we put aside the thermodynamic limit:  $N$  (number of particles)  $\rightarrow \infty$ ,  $V$  (volume)  $\rightarrow \infty$  but

$$\lim_{N, V \rightarrow \infty} \frac{N}{V} = \text{const.} \quad (22.8)$$

Within the type of analysis performed in this book we should mention some specific features of dynamical systems that may be related to fairly realistic models, and at the same time, make it impossible to apply the most typical assumptions of the ergodic theory: ergodicity (4.12)

$$\bar{f} = \lim_{t \rightarrow \infty} \frac{1}{t} \int_0^t f(x, t') dt' = \langle f(x, t) \rangle = \int d\Gamma(x) f(x, t) \rho(x, t) \quad (22.9)$$

and mixing (4.13)

$$\lim_{t \rightarrow \infty} \langle f(x(t + \tau)) \cdot g(x(\tau)) \rangle - \langle f(x) \rangle \langle g(x) \rangle = 0. \quad (22.10)$$

Here are some general comments:

- (a) The limit  $t \rightarrow \infty$  may not exist for all functions  $f(x, t)$ .
- (b) The limit  $t \rightarrow \infty$  may not exist for all initial conditions  $x(t = 0)$ .
- (c) The limit  $t \rightarrow \infty$  may not exist at all for (22.9) or (22.10), or for both.
- (d) The measure  $\rho(x, t) d\Gamma(x)$  in (22.9) and (22.10) for which the limit does exist, may not be the natural (physical) one.
- (e) Some zero measure sets cannot be excluded from the consideration.
- (f) Convergence for the limit  $t \rightarrow \infty$  can be arbitrarily slow which makes the limit senseless from the physical point of view.
- (g) Lyapunov exponents distribution can include  $\sigma_L = 0$  as the lower band.

All these comments deserve to be carefully reconsidered for the realistic Hamiltonian systems. We believe that their illumination plays not only a fundamental theoretical role, but is also important for numerous applications.

## 22.7 Comments on dynamical cooling and chaos erasing

The described construction of the dynamical system that can reveal the features of the Maxwell's Demon for some appropriate values of control parameters is a result of the non-uniformity of phase space of chaos and existence of dynamical traps.

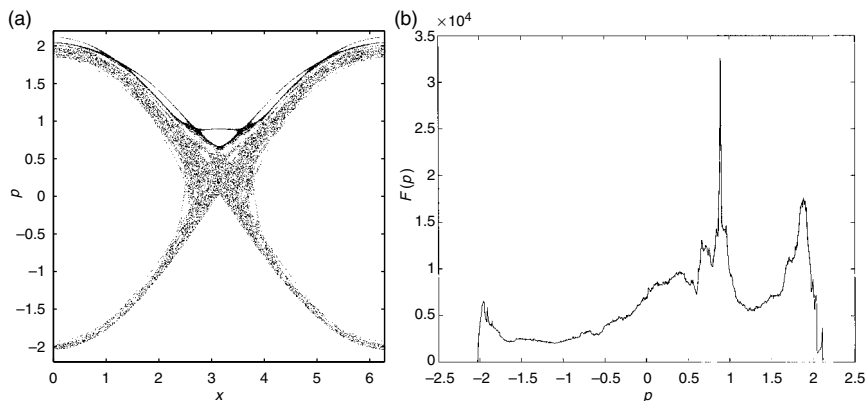


FIG. 22.7. Stochastic layer trap (dark area in (a)) for the perturbed pendulum model and the corresponding strongly asymmetric distribution of momentum  $F(p)$  in (b):  $\epsilon = 0.181$ ;  $\nu = 5.4$ ;  $t = 6 \times 10^6 \times 2\pi/\nu$ .

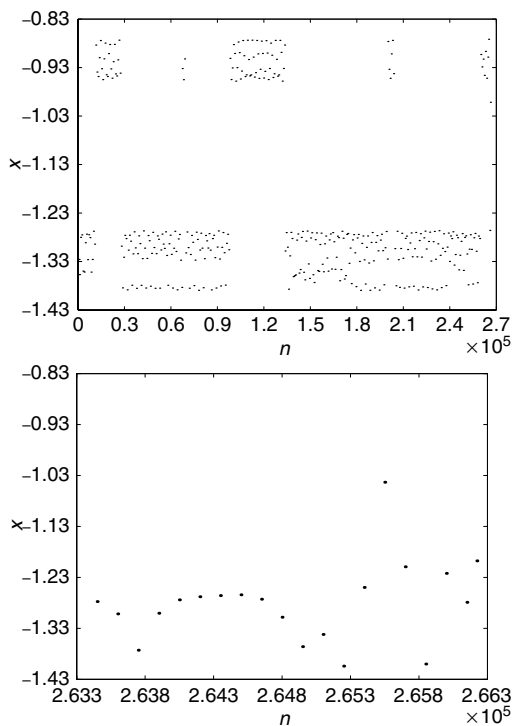


FIG. 22.8. A long trapped trajectory for about  $10^5$  iterations of the standard map ( $K = 6.908745$ ) is ‘cool’ (top) until it escapes (bottom).

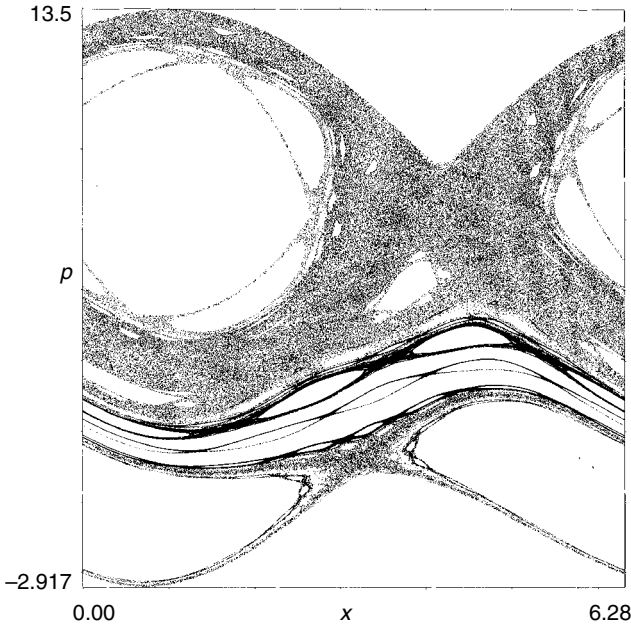


FIG. 22.9. Phase portrait for the perturbed pendulum (6.1) with  $k = 1$ ,  $\epsilon = 8.1$ ,  $\nu = 8.59$ .

Long flights of random trajectories can be considered as the trajectory entrapment into a small domain of phase space. An example in Fig. 22.7 displays such entrapment and the corresponding phase space domain. It is clear from the figure being trapped that the trajectory sharply reduces the dispersion along the momentum (or more accurately, along the perpendicular direction to the stochastic jet). More effective entrapment is demonstrated in Fig. 22.8 for the standard map (Zaslavsky (2002a)), which shows a kind of regularity of the dynamics within the trapping domain. This property of the chaotic dynamics can be called *dynamical cooling*. The main idea of the cooling (Zaslavsky and Abdullaev (1995); Zaslavsky and Edelman (2000)) is to tune the control parameter in such a way that creates effective dynamical traps and immensely reduces fluctuations, i.e. cooling the trajectories for a fairly long time. As a result, a strongly asymmetric distribution function of momentum  $F(p)$  occurs. The example in Fig. 22.7 corresponds to a stochastic layer for the perturbed pendulum:

$$\ddot{x} + \omega_0^2 \sin x = -\epsilon \omega_0^2 \sin(x - \nu t).$$

A sticky trajectory that corresponds to the ballistic mode can be captured into a fairly narrow layer for a time of the order  $10^7$ , preventing a relaxation

to the uniform distribution. The right part of Fig. 22.7 shows  $F(p)$  with a strong peak that corresponds to the appearance of a *preferential direction* (Note 22.9).

The fluctuations are not reduced for ever; they appear after a long time. The phenomenon of entrapment of trajectories into phase space domain with immensely reduced fluctuations in some direction is also called *erasing of chaos*. Fig. 22.9 shows the phase space of the perturbed pendulum (6.1) for some special values of parameters. The dark strip of the upper stochastic layer indicates a long stay of the trajectory in this place. That means a lowering of fluctuations and erasing of chaos due to the particle trapping in the sticky domain of phase space.

## Notes

### Note 22.1

There are numerous different discussions of the derivation of kinetic equations and their foundations (Ehrenfest (1911); Kac (1958, 1959); Prigogine (1962); Krylov (1979); Chirikov (1981)). In this section we refer to the original works (Boltzmann (1872, 1895, 1897, 1898a)) and a paper of Zermelo (1896). With respect to the connection between chaos and the problem of the foundation of statistical mechanics, we follow our publications (Zaslavsky (1985, 1999, 2002)).

### Note 22.2

In this paper (Boltzmann (1872)) the Maxwellian distribution was the equilibrium, and the kinetic equation was derived that led to the  $H$ -theorem. In this paper of 1872 Boltzmann did not actually use the notation  $H$ , and it appeared a few years later together with formulation of the result as the  $H$ -theorem.

### Note 22.3

Boltzmann also mentioned that in the Zermelo paper (1896) the rigorous results of Poincaré were applied in a non-rigorous way.

### Note 22.4

Some discussion of this issue can be found in Krylov (1979).

### Note 22.5

For estimates of (22.4), see Bunimovich (1979, 1985); Machta (1983); Machta and Zwanzig (1983); Zacherl *et al.* (1986); Machta (1986). The result (22.5) for higher moments is in Zaslavsky and Edelman (1997). For the experimental observation of stickiness in optic billiards, see Kaplan *et al.* (2001, 2004), where the 'soft walls' billiard (Turaev and Rom-Kedar (1998)) was realized.

### Note 22.6

See more properties of these billiards in Zaslavsky and Edelman (2004), where the existence of log-periodicity is also shown in the stadium billiard with infinite horizon.

*Note 22.7*

For the principle publications related to the Maxwell's Demon, see the collection of papers in Leff and Rex (1990). The material of this section follows Zaslavsky (1995) and Zaslavsky and Edelman (1997).

*Note 22.8*

All data for the Maxwell's Demon model with a rhombus billiard are from Zaslavsky and Edelman (2004).

*Note 22.9*

This type of phenomenon is typically used for stochastic ratchets (Mateos (2000)) or for the current generation using the broken symmetry due to a time-space non-uniformity (Flach *et al.* (2000); Denisov and Flach (2001)).

## 23

### CHAOTIC ADVECTION (DYNAMICS OF TRACERS)

The dynamics of fluids can be presented by a vector field  $\mathbf{v}(\mathbf{r}, t)$  that defines a velocity of fluid at any time instant  $t$  at the point  $\mathbf{r}$ . Small particles (tracers) being put into fluid can move in such a way that their velocities  $\dot{\mathbf{r}}(t)$  coincide with the fluid velocity  $\mathbf{v}(\mathbf{r}, t)$  at the same point and the same time, that is,

$$\dot{\mathbf{r}}(t) = \mathbf{v}(\mathbf{r}, t). \quad (23.1)$$

Such particle dynamics is called *Lagrangian dynamics* or *advection*. Chaotic dynamics of tracers is also known as *Lagrangian turbulence*. In the case of stationary flow  $\mathbf{v} = \mathbf{v}(\mathbf{r})$  and incompressibility, that is,

$$\operatorname{div} \mathbf{v} = 0 \quad (23.2)$$

trajectories of particles coincide with field lines, that is, streamlines, and the corresponding equation

$$\dot{\mathbf{r}}(t) = \mathbf{v}(\mathbf{r}) \quad (23.3)$$

is the same as (2.31). It was shown in Chapter 2 that the system (23.3) can be presented in a Hamiltonian form if the condition (23.2) is valid.

In this chapter we consider some properties of advection that demonstrate a specific chaos in fluids and fractional kinetics of Lagrangian particles (*Note 23.1*).

#### 23.1 Beltrami flows with $q$ -symmetry

As was mentioned in Section (2.42), stationary flow  $\mathbf{v}$  satisfies the Beltrami condition:

$$\mathbf{v} \times \operatorname{curl} \mathbf{v} = 0 \quad (23.4)$$

or

$$c\mathbf{v} = \operatorname{curl} \mathbf{v} \quad (23.5)$$

with an arbitrary scalar function  $c = c(\mathbf{r})$ . Such field  $\mathbf{v}$  will be called the *Beltrami flow* or *helical flow* (*Note 23.2*).



Here is an example of the Beltrami flow with a plane-symmetry:

$$\begin{aligned} v_x &= -\frac{\partial \Psi}{\partial y} + \epsilon \sin z, \\ v_y &= \frac{\partial \Psi}{\partial x} - \epsilon \cos z, \\ v_z &= \Psi, \end{aligned} \tag{23.6}$$

where  $\epsilon$  is a parameter, and function  $\Psi = \Psi(x, y)$  satisfies the two-dimensional Helmholtz equation

$$\Delta \Psi + \Psi = 0. \tag{23.7}$$

It is easy to check that the velocity field (23.6) has the properties (23.2) and (23.5) with  $c = -1$ .

The advection equations (23.3) can be written in the form

$$\frac{dx}{dz} = -\frac{1}{\Psi} \frac{\partial H}{\partial y}, \quad \frac{dy}{dz} = \frac{1}{\Psi} \frac{\partial H}{\partial x} \tag{23.8}$$

with

$$H = H(x, y, z) = \Psi(x, y) - \epsilon(x \cos z + y \sin z). \tag{23.9}$$

The system (23.8) can be considered as a generalized Hamiltonian system since we can introduce new ‘time’  $\tau$  as:

$$\frac{d\tau}{dz} = \frac{1}{\Psi(x, y)}, \tag{23.10}$$

which leads to the Hamiltonian equation of a system with 1 1/2 degrees of freedom:

$$\begin{aligned} \frac{dx}{d\tau} &= -\frac{\partial}{\partial y} H(x, y, z(\tau, x, y)), \\ \frac{dy}{d\tau} &= \frac{\partial}{\partial x} H(x, y, z(\tau, x, y)). \end{aligned} \tag{23.11}$$

A special case of  $\Psi$

$$\Psi_q = \Psi_0 \sum_{j=1}^q \cos(\mathbf{r} \cdot \mathbf{e}_j), \quad \left( \mathbf{e}_j = \left( \cos \frac{2\pi}{q} j, \sin \frac{2\pi}{q} j \right) \right), \quad q \in \mathbb{N} \tag{23.12}$$

will be called helical flow with  $q$ -symmetry. For  $q = 1, 2$  we have one-dimensional flow, for  $q = 3, 4, 6$ -flow with a crystal symmetry, and for  $q = 5, 7, 8, \dots$ -flow with quasi-crystal symmetry, or simply, quasi-symmetry). The case  $q = 4$  corresponds to the ABC-flow (see Section 2.5).

A more general solution of (23.7), based on  $q$  unit vectors  $\mathbf{e}_j$ , can be written as

$$\Psi_q = \sum_{j=1}^q A_j \cos(\mathbf{r} \cdot \mathbf{e}_j + \phi_j) \quad (23.13)$$

with constants  $\{A_j\}$ ,  $\{\phi_j\}$  and an arbitrary orientation of  $\mathbf{e}_j$ . ABC-flow (2.44) is a particular case of (23.6) with a special choice of constants  $\{A_j\}$ ,  $\{\phi_j\}$  (see Problem 23.1).

For  $\epsilon = 0$  the advection equations are integrable. They describe a two-dimensional dynamics in  $(x, y)$  plane with a symmetry defined by  $\Psi(x, y)$ . Perturbation with  $\epsilon \neq 0$  creates zones of chaotic dynamics that form a kind of stochastic web with helical symmetry (see details in Zaslavsky *et al.* (1988); Zaslavsky *et al.* (1991)). An example of such zones is given in Fig. 23.1, which corresponds to the equations

$$\begin{aligned} \dot{x} &= -\sin y + \epsilon \sin z, \\ \dot{y} &= \sin x + \epsilon \cos z, \\ \dot{z} &= \cos x + \cos y. \end{aligned} \quad (23.14)$$

Points on the plane  $z = 0$  in Fig. 23.1 are obtained as the points of intersection of a trajectory with the plane  $z = 0$  of a unit cell:  $x, y, z \bmod 2\pi$ . Closed orbits correspond to invariant cylinders along  $z$ , while the chaotic zone near the destroyed saddles belongs to the only trajectory which performs a random walk along the stochastic web. This web signifies a three-dimensional connected channel of finite measure along which there exists three-dimensional mixing. The pattern is different in different planes of section  $z = \text{const}$ , and that is why we do not see that the web is a connected net. It was also shown in (Zaslavsky *et al.* (1988)) that the width  $\delta r$  of the web is  $\delta r \sim \epsilon$ .

Diffusion along the stochastic web depends on  $\epsilon$  and it can correspond to fractional kinetics with

$$\langle |\mathbf{r}| \rangle \sim t^{\mu/2} \quad (23.15)$$

and values of  $\mu = \mu(\epsilon) \geq 1$ . Figure 23.2 (Beloshapkin *et al.* (1989)) demonstrates flights for  $q = 4$  (Note 23.3).

## 23.2 Compressible helical flows

It was shown in (Arnold (1965, 1986)) that solutions of the advection equation (23.3) under the divergence-free condition (23.2) and Beltrami flow (23.5) can be classified in two categories: (a) for the smooth  $c \neq \text{const}$  and nowhere zero, the topology of orbits is trivial in the sense that the equations (23.3) are integrable and orbits are coils of the invariant tori or invariant cylinders; (b) for the case  $c = \text{const}$  the topology of orbits is non-trivial in the sense that

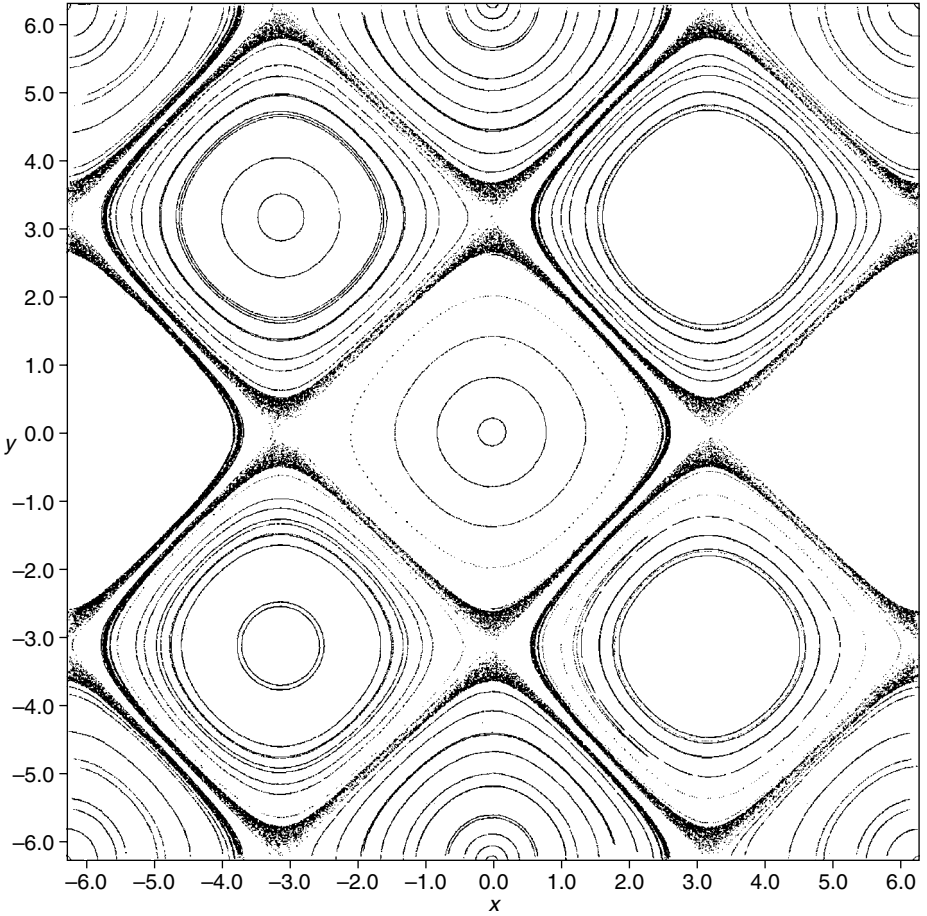


FIG. 23.1. Poincaré section of trajectories in  $z = 0$  plane for the flow (23.7) with square symmetry ( $q = 4$ ) and  $\epsilon = 0.05$ . A thin stochastic web forms a connection grid similar to the cubic lattice.

some of the orbits are chaotic. The statement (a) follows from the Beltrami condition (23.5) that

$$\operatorname{div} c \mathbf{v} = \mathbf{v} \cdot \nabla c + c \operatorname{div} \mathbf{v} = 0. \quad (23.16)$$

Because of  $\operatorname{div} \mathbf{v} = 0$  one has  $\nabla c \cdot \mathbf{v} = 0$  or due to (23.3),  $\dot{\mathbf{r}} \cdot \nabla c = 0$  and that means

$$\frac{dc}{dt} = \dot{\mathbf{r}} \cdot \nabla c = 0, \quad (23.17)$$

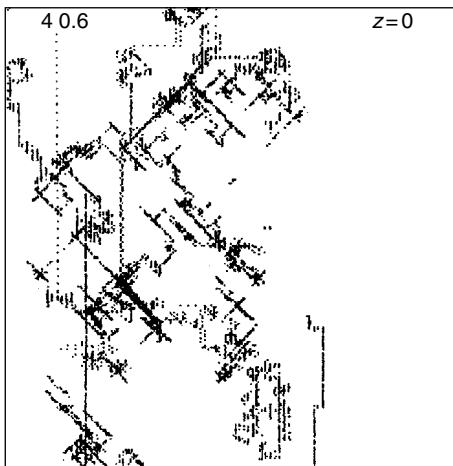


FIG. 23.2. Poincaré section of a trajectory on  $(x, y)$  plane at  $z = \pi/4$  for equations (23.14) with  $\epsilon = 0.6$ .

which is a condition for  $c$  to be the first integral. For the case (b) the equations (23.3) can be rewritten in the Hamiltonian form which reveals the chaotic dynamics in three-dimensional space as a generic situation.

The described situation appears to be paradoxical from the physical point of view because the general situation (non-uniform  $c$ ) leads to a non-general (integrable) particle motion. In other words, the sharp transition from non-integrability to integrability for any small non-uniformity of  $c$  does not appear acceptable from the physical point of view.

The simplest way to reduce the paradox is to lift the incompressibility condition and to consider the general compressible situation of

$$\operatorname{div} \rho \mathbf{v} = 0. \quad (23.18)$$

Then  $c$  is not an integral of motion and  $c/\rho = \text{const}$  due to (23.16). In this new situation (23.2) is replaced by (23.17) or its equivalent (23.16) (*Note 23.4*).

Consider, for simplicity, the case  $c = c(z)$  and rewrite the advection equation (23.3) in the form

$$\frac{d}{d\tau} \mathbf{r} = c \mathbf{v}, \quad (23.19)$$

where a new variable  $\tau$  is introduced, instead of  $t$ , by the equation

$$\frac{dt}{d\tau} = c(z(t; x_0, y_0, z_0)) \quad (23.20)$$

with initial conditions  $x_0, y_0, z_0$  at  $t = 0$  and restriction  $c \neq 0, \infty$  at any finite point  $(x, y, z)$ .

Three equations (23.19) can be written in Hamiltonian form, using the condition (23.16) or (23.18), similar to Section 2.4. The choice of Hamiltonian representation is not unique, but it does not influence the phase space structure and the physical results for the advection.

Let us write

$$\frac{dx}{dz} = \frac{v_x}{v_z}, \quad \frac{dy}{dz} = \frac{v_y}{v_z} \quad (23.21)$$

instead of equation (23.19) and consider  $x = x(z)$ ,  $y = y(z)$  as independent phase-space variables. A change from equation (23.21) to a Hamiltonian form of the equations can be done using some transformation from  $(x, y)$  to  $(x, p)$  variables with

$$p(x, y, z) = c(z) \int_0^y v_z(x, y', z) dy'. \quad (23.22)$$

Let us define

$$H = H(x, p, z) = c(z) \left\{ \int_0^y v_x(x, y', z) dy' - \int_0^x v_y(x', 0, z) dx' \right\}. \quad (23.23)$$

Then it follows from equations (23.21)–(23.23) that

$$\frac{dx}{dz} = \frac{\partial H}{\partial p}, \quad \frac{dp}{dz} = -\frac{\partial H}{\partial x}, \quad (23.24)$$

i.e.  $H$  is the Hamiltonian function for canonically conjugate pair  $(x, p)$  and  $z$  plays the role of time variable. Again, we consider  $x = x(z)$ ,  $p = p(z)$  as independent variables instead of the pair  $(x, y)$ . The first equation in (23.24) follows directly from (23.23) and definition (23.22). To prove the second one, consider the expression:

$$\frac{\partial H}{\partial x} = c(z) \left\{ \int_0^y \frac{\partial v_x(x, y', z)}{\partial x} dy' - v_y(x, 0, z) \right\} \quad (23.25)$$

and use condition (23.18) which gives

$$\begin{aligned} \frac{\partial H}{\partial x} &= - \int_0^y c(z) \frac{\partial v_y(x, y', z)}{\partial y'} dy' \\ &\quad - \int_0^y \frac{\partial}{\partial z} [c(z) v_z(x, y', z)] dy' - c(z) v_y(x, 0, z) \\ &= -c(z) v_y(x, y, z) - \int_0^y \frac{\partial}{\partial z} [c(z) v_z(x, y', z)] dy'. \end{aligned} \quad (23.26)$$

From equations (23.22) and (23.21) we have

$$\begin{aligned}\frac{dp}{dz} &= c(z)v_z \frac{dy}{dz} + \int_0^y \frac{\partial}{\partial z} [c(z)v_z(x, y', z)] dy' \\ &= c(z)v_y(x, y, z) + \int_0^y \frac{\partial}{\partial z} [c(z)v_z(x, y', z)] dy'.\end{aligned}\quad (23.27)$$

Comparison of (23.26) and (23.27) proves the second equation (23.24). There are other Hamiltonian representations which may be convenient for different situations depending on the considered flow.

The existence of a local Hamiltonian form for the advection equation (23.19) in the compressible case permits us to apply Hamiltonian dynamics theory. In particular, we can immediately state that a generic three-dimensional helical compressible flow generates advection with chaotic trajectories in analogy to the statement that Hamiltonian systems with  $1\frac{1}{2}$  degrees of freedom possess, typically, chaotic trajectories. Moreover, we expect the existence of an infinite number of islands (tubes) which are isolated from the stochastic sea and are filled by invariant curves (cylinders) according to the KAM-theory. The Hamiltonian type of chaos means also the absence of attractors in the presence of compressibility.

Consider an example of the compressible flow (Morgulis *et al.* (1995)):

$$\begin{aligned}v_x &= -4 \frac{dW}{d\zeta} \sin x - 4W \sin y + \epsilon \sin \zeta, \\ v_y &= -4 \frac{dW}{d\zeta} \sin y + 4W \sin x + \epsilon \cos \zeta, \\ v_z &= 4 \frac{W}{c} (\cos x + \cos y),\end{aligned}\quad (23.28)$$

where  $\epsilon$  is a constant, the variable  $\zeta$  is introduced instead of  $z$  by the equation

$$\frac{d\zeta}{dz} = c(z) \quad (23.29)$$

and  $W = W(\zeta)$  is a solution of the equation

$$W'' + \left(1 - \frac{1}{c^2}\right) W = 0. \quad (23.30)$$

For the case of  $c = 1$  and  $W = \text{const}$ , the system (23.28) converts to a particular case of the ABC-flow. We can say that equation (23.28) is a compressible analogue of the ABC-flow. Field (23.28) satisfies equation (23.5) with an arbitrary helicity parameter function  $c(z)$ .

The advection equation (23.3) that corresponds to equation (23.28) can be written as

$$\begin{aligned}\dot{x} &= -4 \frac{dW}{d\zeta} \sin x - 4W \sin y + \epsilon \sin \zeta, \\ \dot{y} &= -4 \frac{dW}{d\zeta} \sin y + 4W \sin x + \epsilon \cos \zeta, \\ \dot{z} &= 4 \frac{W}{c} (\cos x + \cos y) = \frac{1}{c} \dot{\zeta},\end{aligned}\tag{23.31}$$

where we use the condition (23.29). For the incompressible uniform case ( $c = 1$ ,  $W = \text{const}$ ), the system (23.31) is reduced to the ABC-flow

$$\begin{aligned}\dot{x} &= -4W \sin y + \epsilon \sin z, \\ \dot{y} &= 4W \sin x + \epsilon \cos z, \\ \dot{z} &= 4W (\cos x + \cos y).\end{aligned}\tag{23.32}$$

We will consider the non-uniformity of the helicity parameter (and density) in the form

$$c = c(\zeta) = \left[ 1 + \frac{4}{\ell^2} + \frac{6}{\ell^2 \cosh^2(\zeta/\ell)} \right]^{-1/2}\tag{23.33}$$

with a characteristic length scale  $\ell$  of the non-uniformity. The corresponding solution of equation (23.30) has a soliton shape

$$W = \frac{1}{\cosh^2(\zeta/\ell)}.\tag{23.34}$$

The uniform case corresponds to the limit  $\ell \rightarrow \infty$ , i.e.  $c \rightarrow 1$ ,  $W \rightarrow 1$ , which is also the case of incompressible flow. Thus, advection governed by the equations (23.31), (23.33), and (23.34) corresponds to the *compressible ABC-flow*, and we can observe changes of the advection pattern when the compressible flow approaches the incompressible limit by smooth change of the only parameter  $\ell$ .

In Fig. 23.3 we present a typical trajectory in a slab geometry using  $\zeta$ -variable instead of  $z$ . The trajectory is bounded in  $\zeta$ . More detailed insight about trajectories comes from Fig. 23.4. Parameter  $\ell$  provides a characteristic length scale of the non-uniformity of the helicity parameter  $c(z)$ . One can consider  $\ell \sim 1$  as a strong non-uniformity case. The corresponding Poincaré map of trajectories is given in Fig. 23.4 for the system (23.31), with domain  $x \in (-2\pi, 2\pi)$ ;  $y \in (-2\pi, 2\pi)$ ;  $z(-\infty, \infty)$ , and a fairly large number of initial conditions. The phase portrait in the plane  $z = 0$  (Fig. 23.4(a)) displays invariant curves and a domain of chaotic dynamics that covers the main part of the plane. Magnification of a fragment of the  $(x, y)$ -plane is shown in Fig. 23.4(b) that demonstrates connectedness of different chaotic areas. The plane  $(\zeta, x)$  is shown

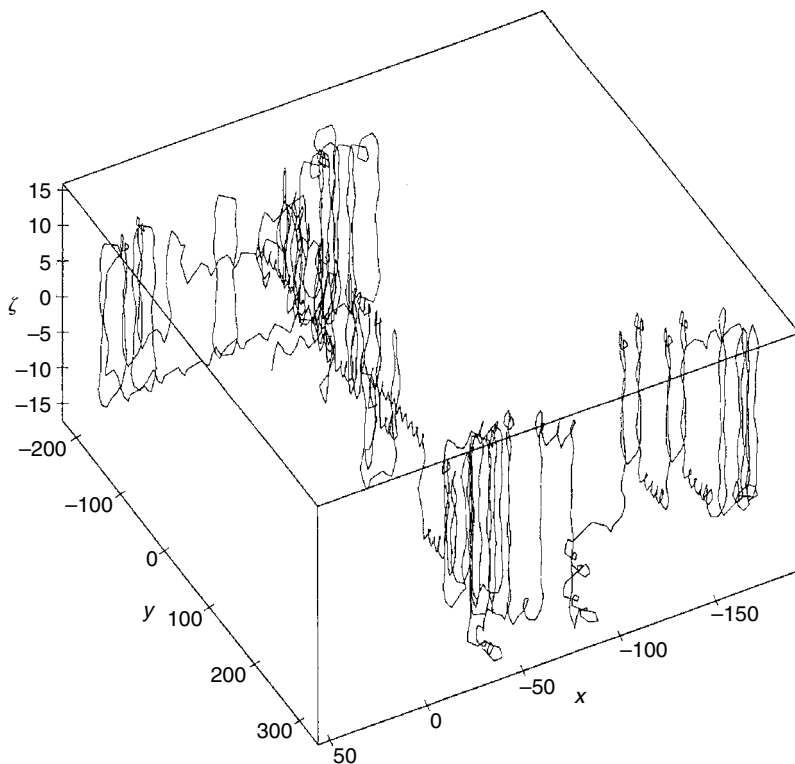


FIG. 23.3. A sample of a trajectory for the compressible ABC-flow with  $\epsilon = 0.9$ ,  $\ell = 12$ .

in Fig. 23.4(c) for  $y = -\pi/2$ . It is clearly seen that the dynamics along  $\zeta$  (or along  $z$ ) is bounded by invariant curves which makes the compressible case strongly different from the incompressible one. Upper and lower parts of the chaotic dynamics in Fig. 23.4(c) are not disjointed and their connection appears for different values of  $y$  (see Fig. 23.4(d)).

Comparing Fig. 23.4(a) to Fig. 23.1, we conclude that in spite of the small value of  $\epsilon = 0.05$ , the area of chaotic dynamics increases in the compressible case. Even the decrease in  $\epsilon$  does not sufficiently change the pattern, although the process of mixing slows down. In this comparison we mean the absence of big islands at compressible ABC-flow for small  $\epsilon$  if one compares them to the sizes of islands for the ABC-flow with the same  $\epsilon$ .

The case of large values of  $\ell$  can be referred to as the adiabatic case. An example is given in Fig. 23.5. Surprisingly, it shows that almost all the area of motion belongs to the stochastic sea, and the size of the islands becomes very small. Comparing Fig. 23.5 and Fig. 23.1, we conclude that compressibility enormously increases the mixing domain, especially in the adiabatic case. More



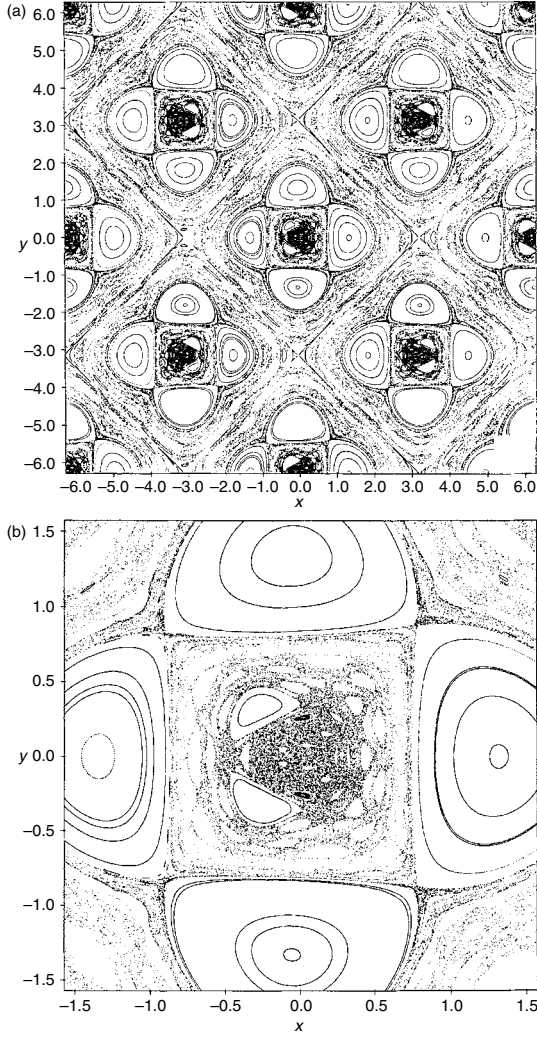
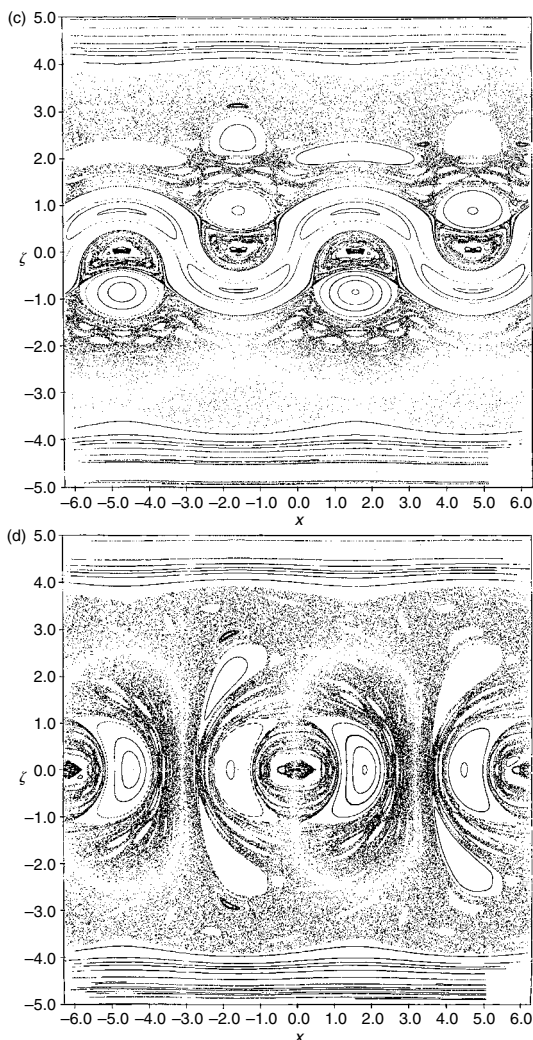


FIG. 23.4. Poincaré section of trajectories for the compressible ABC-flow with  $\epsilon = 0.95$ ,  $\ell = 1.1$ . (a) A full cell in the  $(x, y)$  plane. (b) Magnification of the central part of (a). (c) The same in the  $(\zeta, x)$  plane;  $y = -\pi/2$ . (d) The same in the  $(\zeta, x)$  plane;  $y = -\pi$ .

FIG. 23.4. (*Continued*)

precisely, for small  $\epsilon$  the chaotic region in the compressible ABC-flow is of the order one in  $(x, y)$ -plane. On the other hand, the area of chaotic advection in the unit  $(x, y)$ -cell of the incompressible ABC-flow is of the order  $\epsilon$  (*Note 23.5*).

### 23.3 Compressible flow with quasi-symmetry

For the sake of completeness, let us provide a solution of the Beltrami equation (23.5) with a quasi-symmetry of order  $q$  in  $(x, y)$  plane (*Note 23.6*). Assume  $c = c(z)$  and  $\zeta$  is given by (23.29). Then the advection in compressible flow with

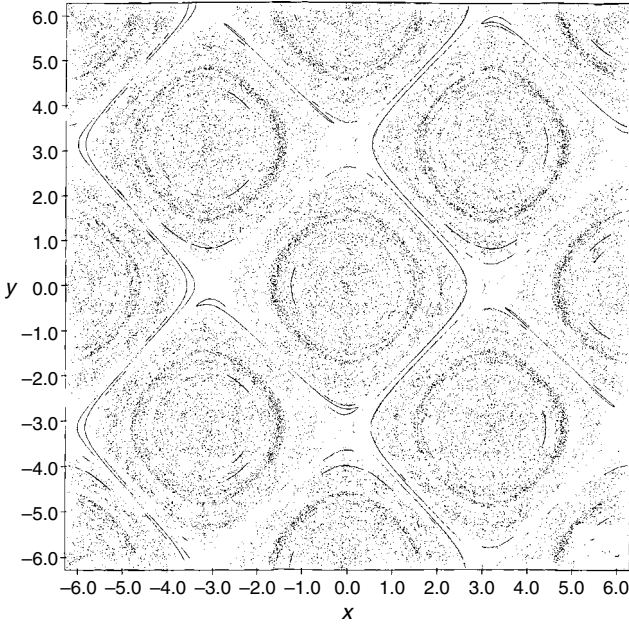


FIG. 23.5. Same as in Fig. 23.4(a) but for adiabatic case with  $\ell = 20$  and  $\epsilon = 0.05$ .

$q$ -symmetry and generating function  $\Psi_q$  from (23.12) is defined by the equations

$$\begin{aligned}\dot{x} = v_x &= \frac{2}{k^2} \frac{dW}{d\zeta} \frac{\partial \Psi_q}{\partial x} + \frac{2}{k^2} W \frac{\partial \Psi_q}{\partial y} + \epsilon \sin \zeta, \\ \dot{y} = v_y &= \frac{2}{k^2} \frac{dW}{d\zeta} \frac{\partial \Psi_q}{\partial y} - \frac{2}{k^2} W \frac{\partial \Psi_q}{\partial x} + \epsilon \cos \zeta, \\ \dot{z} = v_z &= 2 \left( \frac{W}{c} \right) \Psi_q.\end{aligned}\tag{23.35}$$

It is easy to check that the vector field  $\mathbf{v} = (v_x, v_y, v_z)$  in (23.35) is a solution of (23.5), i.e. the solution has been expressed through the generating function  $\Psi_q$ , arbitrary function  $c(z)$ , and the solution of the equation for  $W$

$$\frac{d^2 W}{d\zeta^2} + \left( 1 - \frac{k^2}{c^2} \right) W = 0\tag{23.36}$$

similar to (23.30) up to a constant  $k^2$ .

As an example let  $c = k$  and  $2W/c = \text{const} = 1$  (the value one for the constant is taken without loss of generality). Then  $\zeta = kz$  and due to (23.29) and (23.36) the solution for  $v$  can be written as

$$\begin{aligned} v_x &= \frac{1}{k} \frac{\partial \Psi_q}{\partial y} + \epsilon \sin kz, \\ v_y &= -\frac{1}{k} \frac{\partial \Psi_q}{\partial x} + \epsilon \cos kz, \\ v_z &= \Psi_q. \end{aligned} \tag{23.37}$$

These equations correspond to (23.6).

Now we can write down a simple example for the non-uniform Beltrami flow using the representation (23.35). Let

$$1 - \frac{c^2}{c^2} = -\frac{4}{\ell^2} + \frac{6}{\ell^2 \cosh^2 \zeta/\ell}, \tag{23.38}$$

where  $\ell$  is a scale parameter along  $z$ . Solution of equation (23.36) for the case (23.38) is simply

$$W_0 = \frac{\text{const}}{\cosh^2 \zeta/\ell}, \tag{23.39}$$

which has a shape of a soliton. If  $\ell \rightarrow \infty$  then  $x \rightarrow c_0 = k$  and the problem can be reduced to the known helical flow (23.37) (there are also some other possibilities). This situation makes the solution (23.39) convenient for different physical applications.

Let us consider a simple square-symmetric generating function

$$\Psi_4 = 2(\cos kx + \cos ky). \tag{23.40}$$

Then in accordance with (23.35) and (23.39) we have

$$\begin{aligned} v_x &= -\frac{4}{k^2} \frac{dW_0}{d\zeta} \sin kx - \frac{4}{k^2} W_0 \sin ky + \epsilon \sin \zeta, \\ v_y &= -\frac{4}{k^2} \frac{dW_0}{d\zeta} \sin ky + \frac{4}{k^2} W_0 \sin ky + \epsilon \cos \zeta, \\ v_z &= 4 \left( \frac{W_0}{c} \right) (\cos kx + \cos ky), \end{aligned} \tag{23.41}$$

where the connection between  $z$  and  $\zeta$  can be calculated by simple integration from the definition (23.23)

$$z = \int c^{-1} d\zeta = k^{-1} \int d\zeta \left( 1 + \frac{4}{\ell^2} - \frac{6/\ell^2}{\text{ch}^2 \zeta / \ell} \right)^{1/2}. \quad (23.42)$$

For  $W_0 = \text{const}$  the equations (23.41) describe the ABC-flow. One can consider the flow (23.41) as an example of compressible generalization of the ABC-flow with a special profile of density.

The advection equation can be rewritten now in a symmetrized form using variable  $\zeta$  instead of  $z$ :

$$\begin{aligned} \dot{x} = v_x &= -\frac{4}{k^2} \frac{dW_0}{d\zeta} \sin kx - \frac{4}{k^2} W_0 \sin ky + \epsilon \sin \zeta, \\ \dot{y} = v_y &= -\frac{4}{k^2} \frac{dW_0}{d\zeta} \sin kx + \frac{4}{k^2} W_0 \sin kx + \epsilon \cos \zeta, \\ \dot{\zeta} = c\dot{z} = cv_z &= 4W_0(\cos kx + \cos ky) \end{aligned} \quad (23.43)$$

that coincides with (23.31) considered in Section 23.2 with  $c = k = 1$ .

## Notes

### Note 23.1

The chaos of field lines was considered a fairly long time ago with application to the magnetic field configurations in plasma devices (see Rosenbluth *et al.* (1966); Filonenko *et al.* (1967)). The notion of Lagrangian turbulence had been coined by Aref (1984). See more in books by Ottino (1989) and Zaslavsky *et al.* (1991).

### Note 23.2

The interest in Beltrami flows was stimulated by the problem of Lagrangian turbulence and its application to the fast magnetic dynamo (Arnold (1965); Henon (1966); Childress (1970); Dombre *et al.* (1986); Zaslavsky *et al.* (1988)). Another aspect of this flow was related to the patterns with quasi-symmetry in flows (see Zaslavsky *et al.* (1991); Beloshapkin *et al.* (1989)).

### Note 23.3

Details of simulations of transport for the ABC-flow can be found in Chernikov *et al.* (1990). In Zaslavsky *et al.* (1993) renormalization properties of hierarchical islands were studied.

### Note 23.4

The material of this section follows Morgulis *et al.* (1995); Govorukhin *et al.* (1999).

*Note 23.5*

An interesting case appears for  $\epsilon = 0$  that corresponds to a stratified flow with

$$\begin{aligned}\dot{x} &= -4 \frac{dW}{d\zeta} \sin x - 4W \sin y, \\ \dot{y} &= -4 \frac{dW}{d\zeta} \sin y + 4W \sin x, \\ \dot{z} &= 4 \frac{W}{c} (\cos x + \cos y).\end{aligned}$$

The set of equations seems to be non-integrable while the situation is not described yet (see simulations in Govorukhin *et al.* (1999)).

*Note 23.6*

For the details of constructing this solution and for more general case, see Morgulis *et al.* (1995).

**Problems**

*23.1* In (23.13) find the constants  $A_1, A_2, A_3, A_4; \varphi_1, \varphi_2, \varphi_3, \varphi_4; \epsilon$ , and orientation of vectors  $\mathbf{e}_1, \mathbf{e}_2, \mathbf{e}_3, \mathbf{e}_4$  such that for  $q = 4$  the flow (23.6) coincides with ABC-flow (2.44).

*This page intentionally left blank*

## ADVECTION BY POINT VORTICES

A system of point vortices is a specific type of flow with singularities at the points of the vortices location. Being an exact solution of the Euler equation, a set of point vortices is a convenient model to study different problems of fluid dynamics and turbulence. Such types of models occur in other areas of physics: condensed matter, statistical physics, plasma physics, oceanography, meteorology, etc. Advection of tracers by point vortices is an important and constructive way for the resolution and diagnostic of the vortices states. At the same time, systems with point vortices present a special and interesting types of Hamiltonian dynamics as well as dynamics of advected particles. In this chapter we demonstrate how the fractional kinetics and anomalous transport appear for advection of tracers and vortices (*Note 24.1*).

**24.1 Basic equations for point vortices and for advection**

We consider two-dimensional incompressible flow with velocity

$$\mathbf{v} = (v_x, v_y), \quad \operatorname{div} \mathbf{v} = 0 \quad (24.1)$$

and the stream function  $\Psi = \Psi(x, y, t)$  that satisfies the condition

$$\Delta \Psi = \frac{\partial^2 \Psi}{\partial x^2} + \frac{\partial^2 \Psi}{\partial y^2} = 0 \quad (24.2)$$

and

$$v_x = \frac{\partial \Psi(x, y, t)}{\partial y}, \quad v_y = -\frac{\partial \Psi(x, y, t)}{\partial x} \quad (24.3)$$

(compare to 23.6).

It is convenient to introduce complex coordinates  $z = x + iy$  and  $z^* = x - iy$ . The advection is defined by the equation (23.3) or

$$\dot{x} = v_x = \frac{\partial \Psi}{\partial y}, \quad \dot{y} = v_y = -\frac{\partial \Psi}{\partial x}, \quad (24.4)$$



that is, the stream function  $\Psi$  is also a Hamiltonian. In complex coordinates, equations (24.4) can be written as

$$\begin{aligned}\dot{z} &= [z, \Psi] = -2i \frac{\partial \Psi}{\partial z^*}, \\ \dot{z}^* &= [z^*, \Psi] = 2i \frac{\partial \Psi}{\partial z},\end{aligned}\tag{24.5}$$

where

$$[a, b] = 2i \left( \frac{\partial a}{\partial z^*} \frac{\partial b}{\partial z} - \frac{\partial a}{\partial z} \frac{\partial b}{\partial z^*} \right)\tag{24.6}$$

are the Poisson brackets.

The Hamiltonian (stream function) for the system of  $M$  point vortices, directed perpendicularly to the plane  $(x, y)$ , is

$$\Psi(z, z^*, t) \equiv H = -\frac{1}{4\pi} \sum_{m=1}^M k_m \ln |z - z_m|^2,\tag{24.7}$$

where  $z_m(t) \equiv x_m(t) + iy_m(t)$  are coordinates and  $k_m$  is the strength of the  $m$ -th vortex. It is also assumed that there are no walls or other obstacles and that the flow has zero velocity at infinity. The corresponding advection equations (24.5) take the form

$$\begin{aligned}\dot{z} &= -\frac{1}{2\pi i} \sum_{m=1}^M \frac{k_m}{z^* - z_m^*(t)}, \\ \dot{z}^* &= \frac{1}{2\pi i} \sum_{m=1}^M \frac{k_m}{z - z_m(t)},\end{aligned}\tag{24.8}$$

where  $(z, z^*)$  are coordinates of the advected particle. As soon as vortices trajectories  $(z_m(t), z_m^*(t))$ ,  $\forall m$  are specified, the advection equations (24.8) are completely defined.

Equations (24.8) are symmetric with respect to the coordinate  $z$  of the advected particle and a vortex coordinate  $z_m$ , i.e. the advected particle can be interpreted as a ‘passive’ point vortex with a strength  $k = 1$ . In general, the system of  $M$  vortices is defined by the stream function

$$\Psi_M \equiv H_M = -\frac{1}{4\pi} \sum_{m,n=1}^M k_m k_n \cdot \ln |z_m - z_n|\tag{24.9}$$

and the corresponding equations of motion are

$$\begin{aligned}\dot{z}_m &= [z_m, H_M] = -\frac{2i}{k_m} \frac{\partial H_M}{\partial z_m^*} = -\frac{1}{2\pi i} \sum_{\substack{n=1 \\ n \neq m}}^M \frac{k_n}{z_m^* - z_n^*}, \quad (m = 1, \dots, M), \\ \dot{z}_m^* &= [z_m^*, H_M] = \frac{2i}{k_m^*} \frac{\partial H_M}{\partial z_m} = \frac{1}{2\pi i} \sum_{\substack{n=1 \\ n \neq m}}^M \frac{k_n}{z_m - z_n}, \quad (m = 1, \dots, M).\end{aligned}\tag{24.10}$$

These equations coincide with (24.8) when we omit the subscript  $m$  and put  $k_m = 1$ .

The advection problem can be formulated now as following: for a given set of  $M$  point vortices and the initial conditions  $\{z_m(0), z_m^*(0)\}$ ,  $(m = 1, \dots, M)$  the equations (24.10) should be solved and the solutions

$$z_m(t) = z_m(t; z_1(0), z_1^*(0), \dots, z_M(0), z_M^*(0)), \quad \forall m \tag{24.11}$$

with the corresponding  $z_m^*(t)$  should be defined and put into the equations (24.8). Then, the equations (24.8) should be solved for given functions  $z_m(t), z_m^*(t), (\forall m)$ .

The system (24.10) of  $M$  point vortices possesses some remarkable properties. Besides the ‘energy’  $H_M$  integral of motion, the following expressions are also the dynamical integrals:

$$\begin{aligned}Q + iP &= \sum_{m=1}^M k_m z_m, \\ L^2 &= \sum_{m=1}^M k_m |z_m|^2.\end{aligned}\tag{24.12}$$

Between the quantities  $(H, P, Q, L^2)$ , only three integrals are in involution, that is, commuting with each other. These integrals can be taken as the following ones:  $H, P^2 + Q^2, L^2$ .

Due to this, the system of three point vortices is always integrable. In the case of all  $k_{1,2,3}$  are of the same sign and for some cases of  $k_{1,2,3}$  of different signs the system performs a periodic motion that is a rotation around the *centre of vorticity* defined by the condition

$$Q + iP = \sum_{j=1}^3 k_j z_j = 0. \tag{24.13}$$

The case  $M > 3$  corresponds to, generally speaking, non-integrable dynamics (*Note 24.2*).

In some cases it is convenient to rewrite (24.9) in the form

$$H = -\frac{1}{2\pi} \ln \Lambda \quad (24.14)$$

with

$$\Lambda = \prod_{m>n=1}^M |z_m - z_n|^{k_m k_n} \equiv e^{-2\pi H}. \quad (24.15)$$

We will discuss in more detail the case of  $M = 3$  with  $k_1 = k_2 = k_3 = k = 1$ . Then the parameter

$$\Lambda = |z_1 - z_2||z_2 - z_3||z_3 - z_1| \quad (24.16)$$

is a geometric factor since  $|z_m - z_n|$  is a distance between two vortices located at points  $z_m$  and  $z_n$ .

## 24.2 Advection in three vortices

Let us start from a brief description of the dynamics of three vortices of equal strength  $k = 1$  (*Note 24.3*). Then

$$\begin{aligned} Q^2 + P^2 &= \sum_{m,n=1}^3 z_m z_n^*, \\ L^2 &= \sum_{j=1}^3 z_j z_j^* \end{aligned} \quad (24.17)$$

as follows from (24.12). Two square forms (24.17) can be diagonalized simultaneously by a transfer from the variables  $(z_j, z_j^*)$ ,  $j = 1, 2, 3$  to the variables  $(Q_n, P_n)$ :

$$Q_n + iP_n = \left(\frac{L}{3^{1/2}}\right) \sum_{m=1}^3 e^{i(2\pi n/3)(m-1)} z_m, \quad (n = 0, 1, 2). \quad (24.18)$$

For the pair  $(Q_0, P_0) = (L/3^{1/2})(Q, P)$  we can put  $P_0 = Q_0 = 0$  by a choice of special frame of reference (24.13). New variables are canonical and satisfy the commutation rules

$$[Q_n, P_m] = \delta_{nm}, \quad [Q_n, Q_m] = 0, \quad [P_n, P_m] = 0, \quad (n, m = 0, 1, 2). \quad (24.19)$$

For the rest of the two pairs  $(Q_n, P_n)$ ,  $n = 1, 2$  it is convenient to use polar coordinates  $(J_n, \theta_n)$  instead:

$$Q_n + iP_n = (2J_n)^{1/2} e^{i\theta_n}, \quad (n = 1, 2). \quad (24.20)$$

Use of (24.20) to invert (24.18) gives

$$z_j = \left( \frac{L}{3^{1/2}} \right) \sum_{n=1,2} (2J_n)^{1/2} e^{-2\pi i n(j-1)/3}, \quad (j = 1, 2, 3) \quad (24.21)$$

with

$$L^2 = 2(J_1 + J_2) \quad (24.22)$$

and Hamiltonian

$$H = -\frac{1}{4\pi} \ln[8(J_1^3 + J_2^3 - 2J_1^{3/2} J_2^{3/2} \cos 3(\theta_2 - \theta_1))]. \quad (24.23)$$

One more canonical transform

$$\begin{aligned} I_1 &= \frac{(J_2 - J_1)}{2}, & \phi_1 &= \theta_2 - \theta_1, \\ I_2 &= \frac{(J_2 + J_1)}{2}, & \phi_2 &= \theta_2 + \theta_1 \end{aligned} \quad (24.24)$$

helps to integrate the dynamics. The new form of the Hamiltonian

$$H = -\frac{1}{4\pi} \ln[16(I_2(I_2^2 + 3I_1^2) - (I_2^2 - I_1^2)^{3/2} \cos 3\phi_1)] \quad (24.25)$$

does not depend on  $\phi_2$  and thus  $I_2$  is an integral of motion. Since  $(I_1, \phi_1)$  is a canonical pair,

$$\dot{I}_1 = -\frac{\partial H}{\partial \phi_1} = \frac{12}{\pi} e^{4\pi H} (I_2^2 - I_1^2)^{3/2} \sin 3\phi_1 \quad (24.26)$$

and one can get with the help of (24.25) and notation (24.14)

$$(\dot{I})^2 = P(I; \Lambda), \quad I = \frac{I_1^2}{I_2^2} \quad (24.27)$$

with a polynomial of fourth order  $P(I; \Lambda)$  (see Problem 24.3).

From the definition of  $H$  in (24.23) and  $\Lambda$  in (24.14) it follows that

$$0 < \Lambda < 1 \quad (24.28)$$

and there exists a critical value

$$\Lambda_c = \frac{1}{\sqrt{2}} \quad (24.29)$$

(see Problem 24.3) of a degeneracy of roots of  $P(I; \Lambda)$ . For the latter case the dynamics of vortices is similar to the soliton-like aperiodic solution

$$I = \left[ 1 + (2\sqrt{3}) \cosh \left( \frac{3\sqrt{3}}{2\pi L^2} (t - t_0) \right) \right]^{-1} \quad (24.30)$$

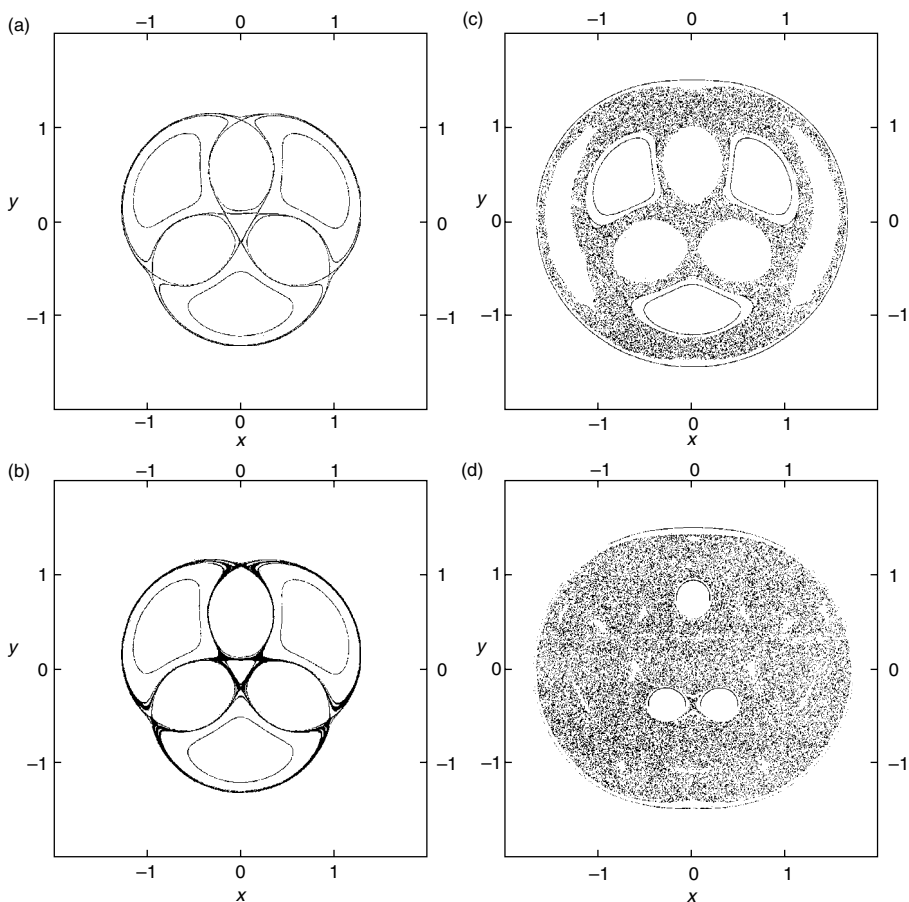
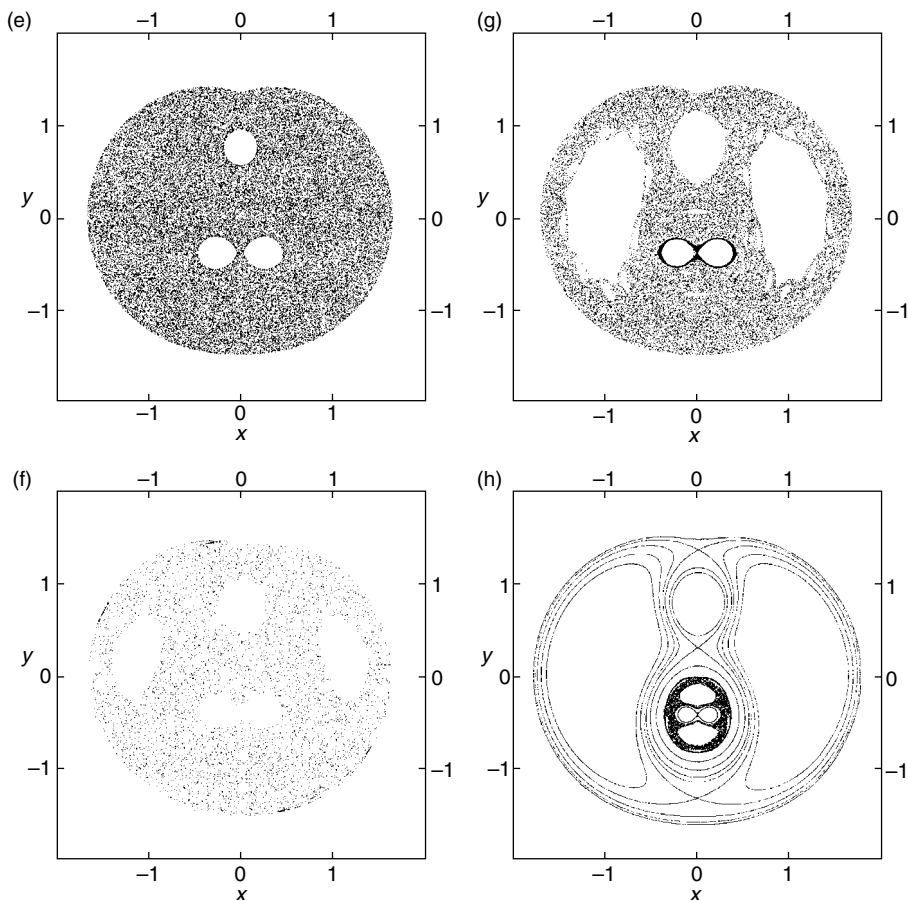


FIG. 24.1. Poincaré sections of passive particle trajectories: (a) Regular advection for  $\Lambda = 1$  (vortices from uniformly equilateral rotating triangle). (b) Destruction of separatrices and onset of chaotic advection,  $\Lambda = 1 - 9.6 \times 10^{-7}$ . (c)  $\Lambda = 0.990656$ ; a large mixing region already exists. (d) Typical advection pattern,  $\Lambda = 0.752192$ . Arcs inside vortex cores are narrow resonant islands; (see Fig. 24.2 for details). (e) and (f) show strong chaotization for  $\Lambda \approx \Lambda_c$ ; (e)  $\Lambda = 0.707109 > \Lambda_c$ ; (f)  $\Lambda = 0.707107$ ; (g)  $\Lambda = 0.605247$ ; a permeable barrier of a sticky boundary layer separates the vortex pair from the rest of the mixing region; (h)  $\Lambda = 0.353088$ .

FIG. 24.1. (*Continued*)

(see Problem 24.6). For all other values of  $\Lambda \neq \Lambda_c$  the dynamics of vortices is periodic (see Problem 24.4) and at the same time there is a periodic rotation of the system of vortices as a whole system with some frequency  $\Omega(\Lambda)$  (for details, see Kuznetsov and Zaslavsky (1998)).

Now the way to study advection is constructively well defined: from the solution of (24.27) we determine  $J_{1,2}(t)$  following a linear transform (24.24), and then  $z_j(t)$ , ( $j = 1, 2, 3$ ) following (24.21). The expressions  $z_j(t)$  should be substituted into equations for a tracer (24.8). In the case of one static vortex with a coordinate  $z_p$  we have from (24.8):

$$\dot{\zeta} = -\frac{k_p}{2\pi i} \frac{1}{\zeta^*}, \quad \zeta = z - z_p \quad (24.31)$$

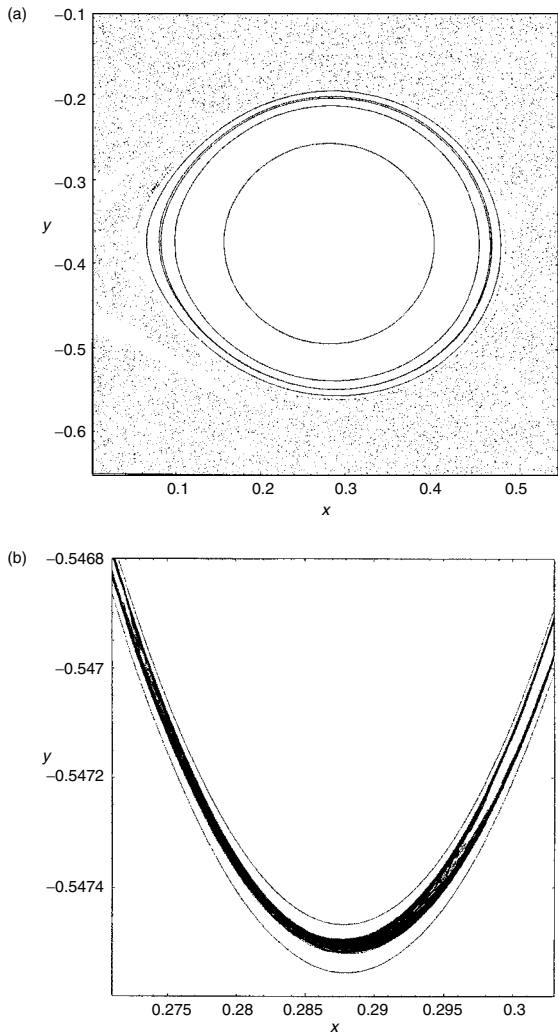


FIG. 24.2. (a) KAM curves inside a vortex core,  $\Lambda = 0.752192$ . The homoclinic orbit (second from outside) is in fact a narrow stochastic layer with a complex structure. (b) Magnification of the piece of this layer in the vicinity of the  $X$  point. Two nearby KAM curves are shown for contrast.

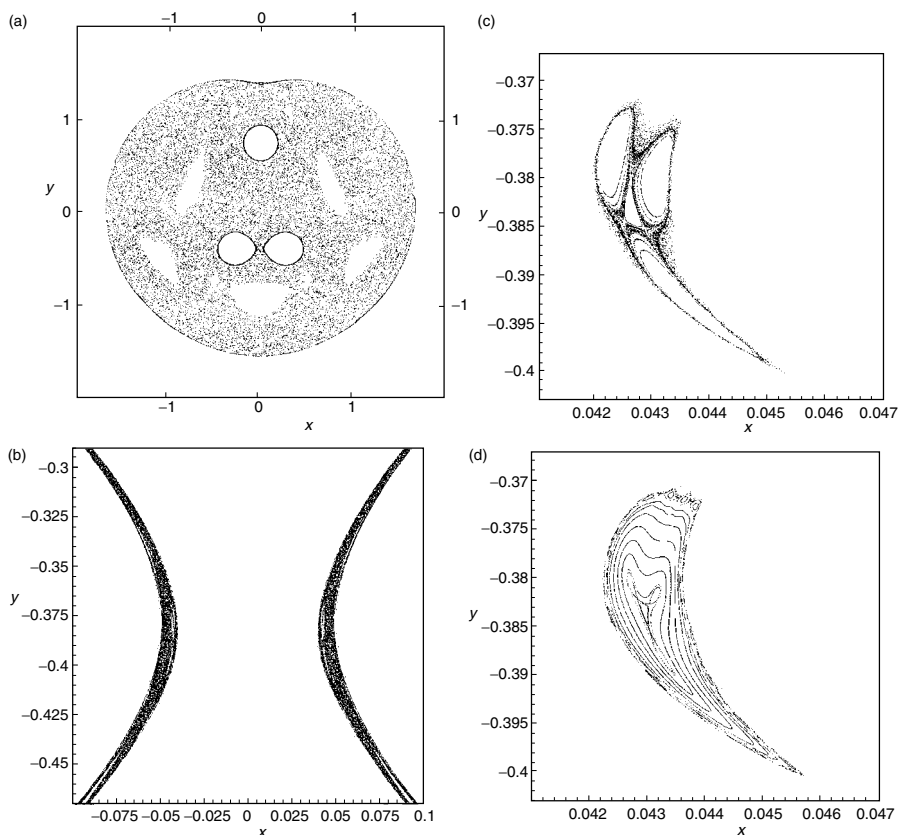


FIG. 24.3. (a) Stickiness of the vortex core boundaries,  $\Lambda = 0.71666$ . (b) Magnification of the central part. Thin white areas inside the bands are regular island structures. Their zoom (stretched in the  $x$  direction) is shown for two close vortex geometries. (c)  $\Lambda = 0.71682$ ; (d)  $\Lambda = 0.716917$ .

with a solution

$$\zeta = \zeta_0 \exp(i\omega t) \quad (24.32)$$

and frequency

$$\omega = \frac{k_p}{2\pi|\zeta_0|^2}, \quad |\zeta|^2 = \text{const} = |\zeta_0|^2, \quad (24.33)$$

where  $|\zeta_0|$  is a radius of rotation of the tracer around the vortex. The smaller the radius, the larger the frequency of rotation. This property leads to a ‘rigidity’ of a domain near a vortex, that is, the regular rotation is hard to perturb in



the very vicinity of the vortex. This specific feature will be demonstrated for the advection in a 3-vortex system.

Different regimes of the advection in 3-vortex with equal strength are presented in Fig. 24.1. In the cases (c), (d), (e), and (f) the holes in stochastic sea correspond to the vortex cores which are KAM zones (islands) of stability. A resonant island inside a core is shown in Fig. 24.2. The vortex cores are sticky. The stickiness is easy to see from Fig. 24.1(f) and from Fig. 24.3. An effective radius of cores  $\zeta_c$  is defined by a formula

$$\zeta_c = \left[ \frac{\pi/\sqrt{3}}{18(\ln \ln |\Lambda - \Lambda_c|^{-1} + c)} \right]^{1/2}, \quad (24.34)$$

where  $c$  is a constant and  $|\Lambda - \Lambda_c| \ll 1$ . This case corresponds to a large area of stochastic sea (*Note 24.4*).

Concluding this section we have to accept the tracer dynamics in the 3-vortex system as a typical type of dynamical system with 1 1/2 degrees of freedom and with a typical phase space structure of stochastic sea and resonant islands. An unusual part of the phase space topology is the presence of non-removable and

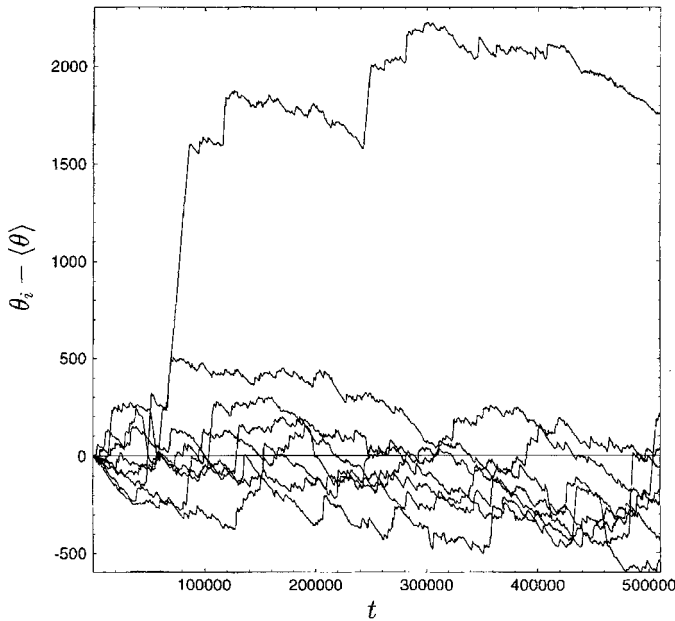


FIG. 24.4. Time evolution of the azimuthal coordinate  $\theta(t) - \langle \theta \rangle$  for eight typical tracer trajectories.

almost non-deformable cores around the vortices (see double-logarithm dependence on  $\Lambda$  in (24.34)). We will see that only these cores appear to create coherent structures in the case of advection in many-vortex systems.

### 24.3 Transport of advected particles (vortices)

The behaviour of tracers or advected particles in different flows is a convenient way of visualization of trajectories in phase space. From the physical point of view, we have an ‘intermediate’ type of system between laminar and turbulent regimes. From the mathematical point, we have a class of systems with multiplicity or degeneracy of Hamiltonians (*Note 24.5*). In this section we present some data of simulations that demonstrate different features of fractional kinetics of tracers: flights, powerwise distribution of recurrences, superdiffusion, etc.

In the 3-vortex system, considered in Section 24.3, the phase space of advection is compact (see Fig. 24.1) and the transport of tracers can be studied along the angle  $\theta$  of rotation of tracers around the centre of vorticity defined in (24.13).

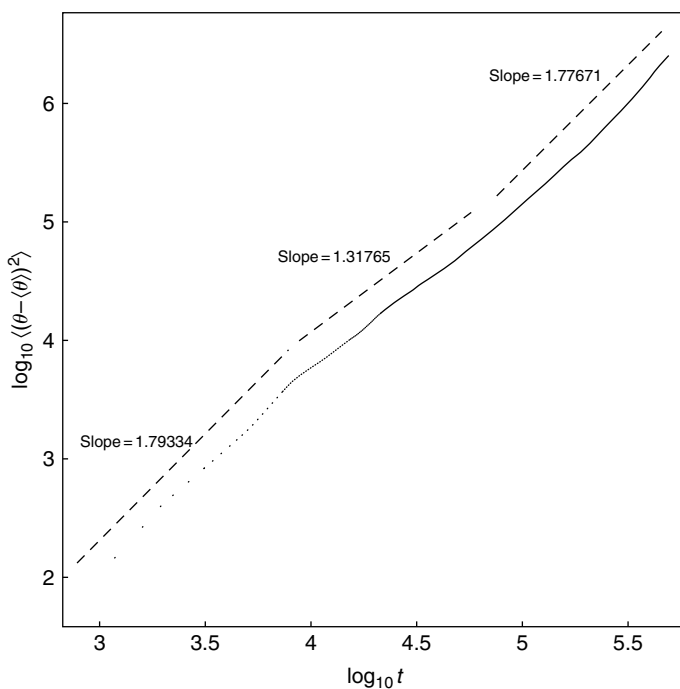


FIG. 24.5. Superdiffusion of the tracers in an angular direction. Oscillation of slopes corresponds to the log-periodicity.

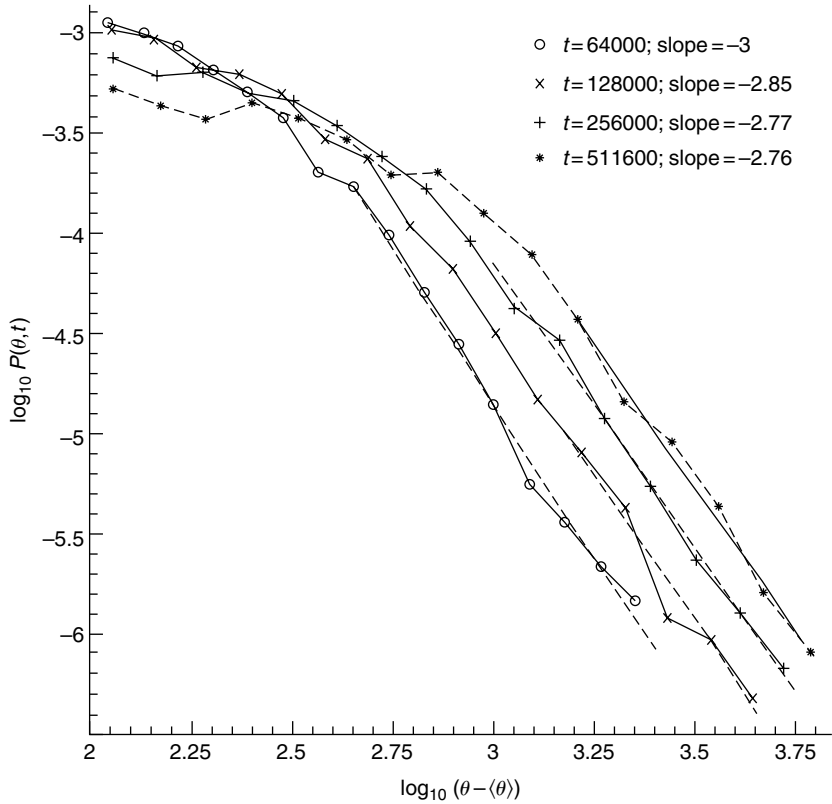


FIG. 24.6. Self-similarity of the distribution function  $P(\theta, t)$  for different time instants.  $\gamma \approx 0.6$ .

We assume that the complex coordinate of a tracer is written as

$$z(t) = |z|e^{i\theta} \tag{24.35}$$

in a frame of reference that rotates together with whole 3-vortex system. Samples of trajectories in Fig. 24.4 show many flights during which the angular displacement  $\theta(t) - \theta(0)$  is a linear function of time. The length of flights can be exceptionally long. Two other pictures in Figs. 24.5 and 24.6 show a second moment  $\langle (\theta - \langle \theta \rangle)^2 \rangle$  over truncated distribution function  $P(\theta, t)$  and its self-similar structure:

$$P(\theta, t) \sim \frac{1}{t^\gamma} P(\xi), \quad \xi = \frac{\theta(t) - \langle \theta \rangle}{t^\gamma}. \tag{24.36}$$

It follows from Fig. 24.5 that transport exponent  $\mu$  in

$$\langle (\theta - \langle \theta \rangle)^2 \rangle = \text{const} \cdot t^\mu \quad (24.37)$$

oscillates near value  $\mu \approx 1.6$ . The tails in Fig. 24.6 have a power law

$$P(\theta - \langle \theta \rangle) \sim \frac{1}{(\theta - \langle \theta \rangle)^\delta} \quad (24.38)$$

with  $\delta \approx 2.8$ . Finally, for the distributon of Poincaré recurrences we obtain

$$P_{\text{rec}}(t) \sim \frac{1}{t^{\gamma_{\text{rec}}}} \quad (24.39)$$

with  $\gamma_{\text{rec}} \approx 2.7$  that satisfies approximately the condition  $\gamma_{\text{rec}} = \mu + 1$  (*Note 24.6*).

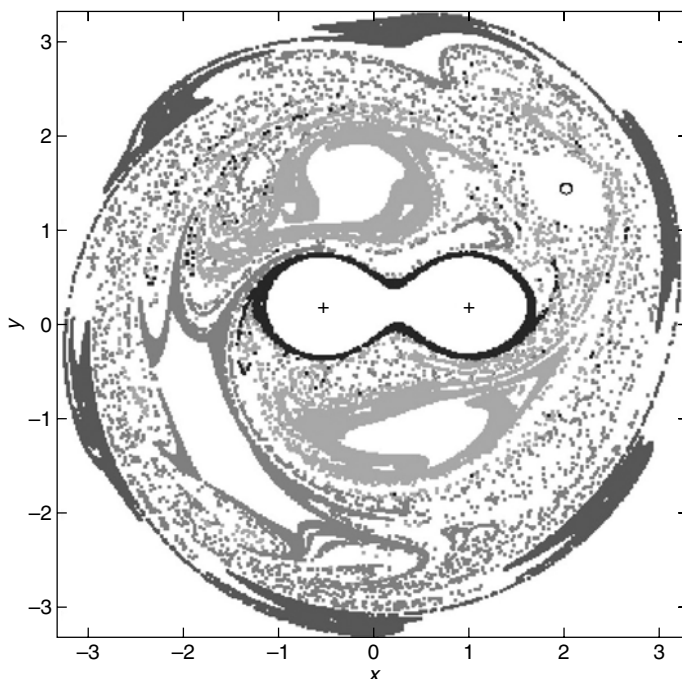


FIG. 24.7. Points on the Poincaré section coloured by the values of averaged velocity. In dark grey the points correspond to  $0.595 < \omega < 0.605$ . In light and lighter grey the points correspond respectively to  $0.81 < \omega < 0.83$  and to  $1.22 < \omega < 1.25$ . In black the points with speeds  $\omega > 1.8$ . The constants of motion are  $K = 0$ ,  $\Lambda = 0.9$ . Vortex strengths are  $(-0.2, 1, 1)$ . The period of the motion is  $T = 10.73$ .  $K = 1.8L^2 - Q^2 - P^2$ .

Another presentation of the data was obtained in (Leoncini *et al.* (2001)) for 3 vortices of different signs. Dots of the Poincaré section were marked by different colours depending on the angular velocity  $\omega$  of the tracer at the point. In Fig. 24.7 the locations of two vortices with positive strength are marked by '+' and location of the negative one by a small circle. The figure shows that tracers in the vicinity of islands and the external boundary exhibit an almost constant value of the velocity  $\omega$ . This demonstrates the stickiness, that is, the rotation around islands with almost constant velocity.

When the number of point vortices  $M > 3$ , the vortex dynamics can be chaotic. Such motion of vortices does not represent a realistic flow but, as was mentioned above, it corresponds to an intermediate situation, and a study of particle advection in such systems has different interesting directions (*Note 24.7*). There is particular and important interest in finding coherent structures created within the chaotic flow of many point vortices. For example, such a coherent structure can be a vortex pair, i.e. an intermittent state created by two of the same sign vortices that approach close to each other. Passive particles, in their chaotic motion, can 'recognize' these coherent structures. Some evidence of this statement is presented below.

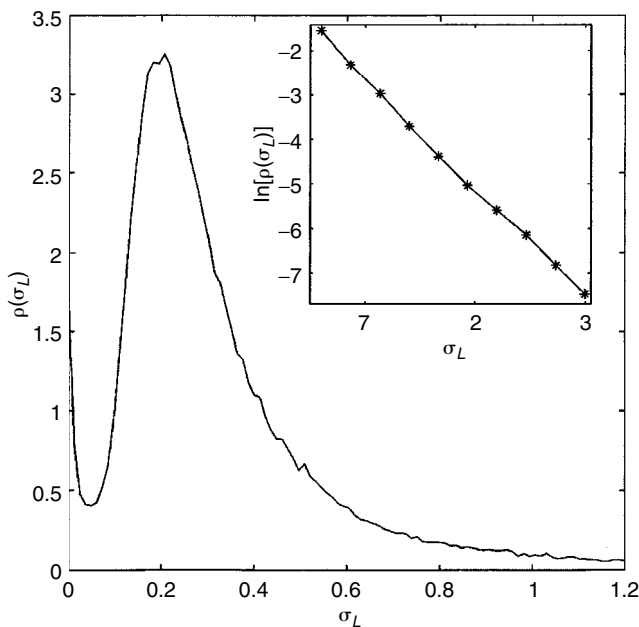


FIG. 24.8. Distribution function  $\rho(\sigma_L)$  of the finite time Lyapunov exponents. Data obtained with four different trajectories during the time  $5 \times 10^6$  from 328,220 records.

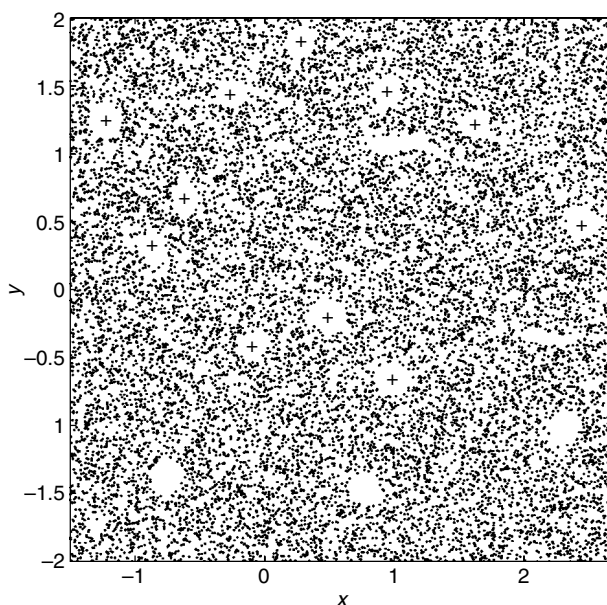


FIG. 24.9. A snapshot of location of  $9 \times 10^4$  tracers. The vortices are marked by '+' at the centres of the cores impermeable for tracers.

First, consider a distribution function  $\rho(\sigma_L)$  of finite time of Lyapunov exponents  $\sigma_L$ :

$$\sigma_L = \frac{1}{\Delta t} \ln \left( \frac{\epsilon}{\delta} \right), \quad \delta \ll \epsilon \ll 1. \quad (24.40)$$

Here  $\delta$  and  $\epsilon$  are some fixed numbers and  $\Delta t$  is a time that two tracers are  $\epsilon$ -separated being initially at distance  $\delta \ll \epsilon$ . An example of  $\rho(\sigma_L)$  is shown in Fig. 24.8 (Leoncini and Zaslavsky, 2002) for tracers in system 4-point vortices, which performs chaotic motion. The values of  $\sigma_L$  are concentrated near  $\sigma_L \sim 0.25$  and  $\rho(\sigma_L) \sim \exp(-\sigma_L/\sigma_0)$  with  $\sigma_0 \approx 0.4$  and  $\sigma_L > 0.2$ . But there is a dip at  $\sigma_L \sim 0.05$  and the value of  $\sigma_L \ll 0.05$  is not negligible (*Note 24.8*).

The system of 16 same sign vortices considered in (Leoncini and Zaslavsky (2002)) moves more randomly than system of 4 vortices and the advection in such a system mixes more uniformly in the phase space (see Fig. 24.9 with well indicated vortex cores). A direct determination of coherent structures created by vortices may be very difficult and ambiguous since the chaotic dynamics of vortices by themselves. Another way is to find long jets for tracers and to visualize the vortex dynamics during a span time of the jet. The jet is 'captured' when close tracers do not split apart for a fairly long time. This means that

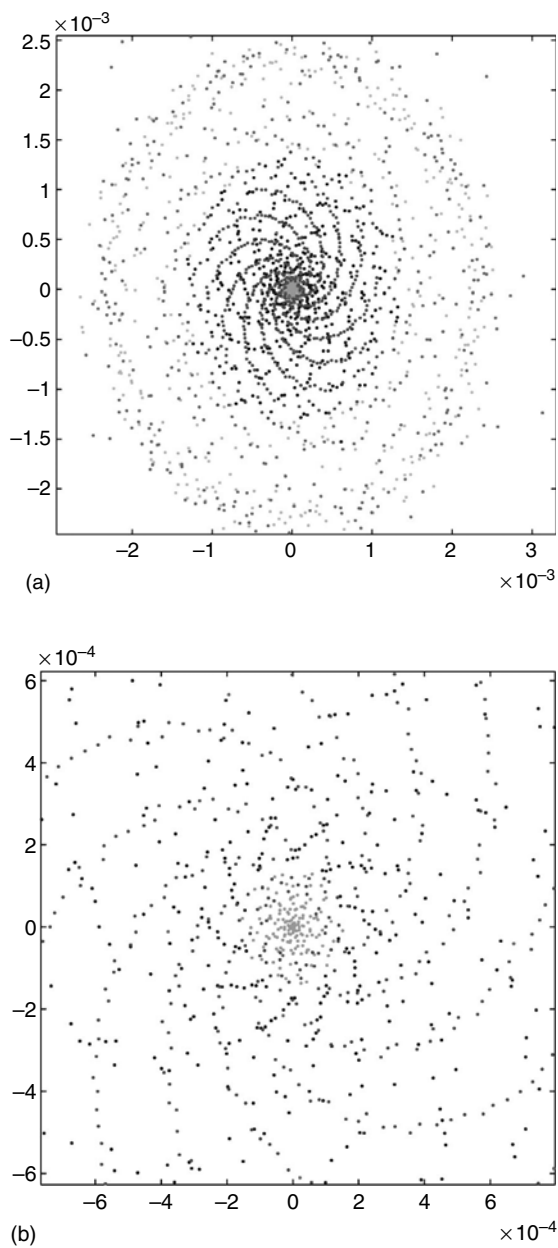


FIG. 24.10. A tracer in a jet regime for the chaotic flow of 16 vortices. The points indicate the tracer locations with equal small time interval  $\Delta t$ . Part (b) is a magnification of (a) for about an order. It shows a kind of self-similarity of a regular structure of vortices.

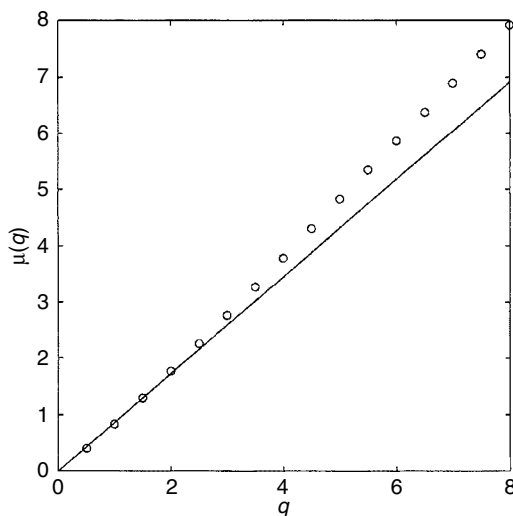


FIG. 24.11. Transport exponent of tracers in the 16-vortex flow.

these two tracers are passing a vortex cluster (configuration) with a very small finite time Lyapunov exponent. This kind of configurations are responsible for the peak near  $\sigma_L = 0$  in Fig. 24.8. An example of a jet is shown in Fig. 24.10 (*Note 24.9*).

More detailed analysis shows that two vortices are making a closely staying pair for a very long time. During this time the pair rotates and some tracers are captured in the very vicinity of the vortex cores.

The moments of tracers dynamics can be obtained from the standard equation for the length of the trajectories

$$\langle |s(t) - \langle s(t) \rangle|^q \rangle \sim t^{\mu(q)} \quad (24.41)$$

(see Fig. 24.11) that show  $\mu(2) \approx 1.77$ , and for large  $q > 2$  the slope is  $\mu(q) \approx 1.95q/2$ , i.e. very close to ballistic dynamics. Similar properties are observed for the dynamics of one vortex in the 16-vortex flow. This shows a kind of equivalence of the kinetics at large time scale for a vortex in a large set of vortices and for an advected vortex.

## Notes

### *Note 24.1*

The literature on the dynamics of point vortices is immense. The basic equation can be found in Lamb (1945) or Meleshko and Konstantinov (1999).



Applications for different systems are described in Pismen (1999), and for Hamiltonian dynamics in Kozlov (1998).

*Note 24.2*

Non-integrability for  $M > 3$  vortices was shown in Novikov and Sedov (1978). Integration for a system of three vortices was performed in Novikov (1975) and in a more complete form in Aref and Pomphrey (1980). The close to the collapse case and different scenarios of the approach to the collapse are in Leoncini *et al.* (2000). Different special cases of integrability are in Meleshko and Konstantinov (1999).

*Note 24.3*

For the details see Aref and Pomphrey (1980) and Kuznetsov and Zaslavsky (1998). We follow the notations of the last reference.

*Note 24.4*

Figures 24.1 through 24.3 are taken from Kuznetsov and Zaslavsky (1998). The vortex cores were first observed in simulations (Crisanti *et al.* (1992)). Their theory and the formula (24.34) were derived in Kuznetsov and Zaslavsky (1998).

The case of 3 vortices dynamics with different signs of their strength  $k_j$  and a possibility to collapse was considered in Aref (1979). Different scenarios of the collapse in the 3-vortex system were described in Leoncini *et al.* (2000); see also references therein.

*Note 24.5*

A discussion of degeneracy is related to the ABC-flow and its generalizations (Zaslavsky *et al.* (1991); Zaslavsky *et al.* (1993)) with respect to the appearance of stochastic webs for advected particles. For multiplicity of Hamiltonians, see examples in Sinai and Khanin (1992); Zaks *et al.* (1996); Zaks and Straube (2002).

*Note 24.6*

All results of simulations presented in Figs. 24.4 through 24.6 follow Kuznetsov and Zaslavsky (2000). Their detailed analysis is in the same papers.

*Note 24.7*

See more in papers by Babiano *et al.* (1994) and Provencale (1999). The material presented below follows Leoncini and Zaslavsky (2002).

*Note 24.8*

The central peak in the frequency spectrum for the standard map was observed in Beloshapkin and Zaslavsky (1983) attributing it to the stickiness.

*Note 24.9*

Figures 24.9 through 24.11 are from Leoncini and Zaslavsky (2002).

## Problems

More complicated problems are marked by (\*).

*24.1* Show that the transform of variables  $(Q_n, P_n) \rightarrow (J_n, \vartheta_n)$  in (24.20) is canonical and find the Poisson brackets for  $(J_n, \vartheta_n)$ ,  $n = 1, 2$ .

24.2 Show that the transform of variables (24.24) is canonical.

24.3 Show that the equation (24.27) is equivalent to

$$\left(\frac{dI}{d\tau}\right)^2 = -I[I^3 + 6I^2 + 3(3 - 8\Lambda^2)I + 8\Lambda^2(2\Lambda^2 - 1)]$$

with

$$\tau = \frac{3t}{2\pi L^2 \Lambda^2}$$

and

$$I = \left(\frac{I_1}{I_2}\right)^2.$$

24.4\* Integrate the equation (1) of the Problem 24.3 and find a period of non-linear oscillations  $T = T(\Lambda)$  in the following cases:

- (a)  $\Lambda \ll 1$ ;
- (b)  $\Lambda = 1 - \delta$ , where  $\delta \ll 1$ ;
- (c)  $\Lambda = \Lambda_c \pm \delta$ , where  $\delta \ll 1$  and  $\Lambda_c = 1/\sqrt{2}$ .

24.5 Find solutions of equation (1) of Problem 24.3 for three cases of  $\Lambda$  indicated in Problem 24.4.

24.6 Derive the solution (24.30) for  $\Lambda = \Lambda_c$ .

*This page intentionally left blank*

## APPENDICES

### Appendix A Elliptic integrals and elliptic functions

Here are elliptic integrals of the first kind

$$F(\phi, \kappa) = \int_0^\phi \frac{d\alpha}{(1 - \kappa^2 \sin^2 \alpha)^{1/2}} = \int_0^{\sin \phi} \frac{dx}{(1 - x^2)^{1/2}(1 - \kappa^2 x^2)^{1/2}} \quad (\text{A1.1})$$

and the second kind

$$E(\phi, \kappa) = \int_0^\phi (1 - \kappa^2 \sin^2 \alpha)^{1/2} d\alpha = \int_0^{\sin \phi} (1 - \kappa^2 x^2)^{1/2} (1 - x^2)^{1/2} dx. \quad (\text{A1.2})$$

Expressions  $F(\pi/2, \kappa)$ ,  $E(\pi/2, \kappa)$  are called full elliptic integrals of the corresponding kind. Their asymptotics are

$$\begin{aligned} F\left(\frac{\pi}{2}, \kappa\right) &\approx \left(\frac{\pi}{2}\right) \left(1 + \frac{1}{4}\kappa^2 + \cdots\right), & \kappa^2 \ll 1, \\ E\left(\frac{\pi}{2}, \kappa\right) &\approx \left(\frac{\pi}{2}\right) \left(1 - \frac{1}{4}\kappa^2 + \cdots\right), & \kappa^2 \ll 1 \end{aligned} \quad (\text{A1.3})$$

and

$$\begin{aligned} F\left(\frac{\pi}{2}, \kappa\right) &\approx \ln \left[ \frac{4}{(1 - \kappa^2)^{1/2}} \right] + \cdots, & 1 - \kappa^2 \ll 1, \\ E\left(\frac{\pi}{2}, \kappa\right) &\approx 1 + \frac{1}{2}(1 - \kappa^2) \left[ \ln \left( \frac{4}{(1 - \kappa^2)^{1/2}} \right) - \frac{1}{2} \right] + \cdots, & 1 - \kappa^2 \ll 1. \end{aligned} \quad (\text{A1.4})$$

Functions of  $u$

$$\operatorname{sn} u = \sin \phi, \quad \operatorname{cn} u = \cos \phi, \quad \operatorname{dn} u = (1 - \kappa^2 \sin^2 \phi)^{1/2}, \quad (\text{A1.5})$$

where  $\phi$  is the same as in (A1.1) and (A1.2), are called Jacobi elliptic functions or simply elliptic functions. Their Fourier expansions are:

$$\begin{aligned} \operatorname{sn} u &= \frac{2\pi}{\kappa F(\pi/2, \kappa)} \sum_{n=1}^{\infty} \frac{q^{n-1/2}}{1 - q^{2n-1}} \sin \left[ (2n-1) \frac{\pi u}{2F(\pi/2, \kappa)} \right], \\ \operatorname{cn} u &= \frac{2\pi}{\kappa F(\pi/2, \kappa)} \sum_{n=1}^{\infty} \frac{q^{n-1/2}}{1 + q^{2n-1}} \cos \left[ (2n-1) \frac{\pi u}{2F(\pi/2, \kappa)} \right], \\ \operatorname{dn} u &= \frac{\pi}{2F(\pi/2, \kappa)} \left[ 1 + \sum_{n=1}^{\infty} \frac{q^n}{1 + q^{2n}} \cos \frac{n\pi u}{F(\pi/2, \kappa)} \right] \end{aligned} \quad (\text{A1.6})$$

where

$$q = \exp \left\{ -\frac{\pi F(\pi/2, (1 - \kappa^2)^{1/2})}{F(\pi/2, \kappa)} \right\}. \quad (\text{A1.7})$$

There are the following functional relations:

$$\begin{aligned} \operatorname{sn}^2 u + \operatorname{cn}^2 u &= 1, \\ \operatorname{dn}^2 u + \kappa^2 \operatorname{sn}^2 u &= 1 \end{aligned} \quad (\text{A1.8})$$

and

$$\begin{aligned} \frac{d}{du} \operatorname{sn} u &= \operatorname{cn} u \cdot \operatorname{dn} u, \\ \frac{d}{du} \operatorname{cn} u &= -\operatorname{sn} u \cdot \operatorname{dn} u. \end{aligned} \quad (\text{A1.9})$$

More information can be found in (Abramowitz and Stegun, 1972) or in (Gradshteyn and Ryzhik, 1980).

## Appendix B Spectrum of the Kepler problem

Here we show how the spectral decomposition can work in the problems where the unperturbed dynamics corresponds to the Kepler problem.

Particle dynamics is defined by the equation (in polar coordinates  $r, \phi$ ):

$$1 + \epsilon_0 \cos \phi = \frac{a}{r} (1 - \epsilon_0^2). \quad (\text{A2.1})$$

Here  $\epsilon_0$  is eccentricity and  $a$  is large semiaxis:

$$a = \frac{\alpha}{2|E|}, \quad \epsilon_0 = \left( 1 - \frac{2}{m\alpha^2} |E| L^2 \right) \quad (\text{A2.2})$$

with  $\alpha = |e_1 e_2|$ ,  $e_{1,2}$  are charges,  $m$  is reduced mass,  $E$  is total energy,  $L = mr^2 \dot{\phi}$  angular momentum. It is known (Landau and Lifshits, 1976) that the Kepler dynamics can be presented in a parameter form

$$r = a(1 - \epsilon_0 \cos \xi), \quad t = \left( \frac{ma^3}{\alpha} \right)^{1/3} (\xi - \epsilon_0 \sin \xi). \quad (\text{A2.3})$$

One full elliptic rotation corresponds to the change of  $\xi$  from 0 to  $2\pi$ , and the frequency is

$$\omega(|E|) = \left( \frac{\alpha}{ma^3} \right)^{1/2} = \frac{(2|E|)^{3/2}}{\alpha m^{1/2}}. \quad (\text{A2.4})$$

For the cartesian coordinates  $(x, y)$  we have

$$x = a(\cos \xi - \epsilon_0), \quad y = a(1 - \epsilon_0^2)^{1/2} \sin \xi \quad (\text{A2.5})$$

with  $\xi = \xi(t)$  from (A2.3). The Fourier expansion can be written as

$$\begin{aligned} x &= \sum_n x_n e^{-i\omega n t}, \\ y &= \sum_n y_n e^{-i\omega n t}. \end{aligned} \quad (\text{A2.6})$$

It follows from the definition

$$\begin{aligned} x_n &= \frac{i\dot{x}_n}{n\omega} = \frac{i}{n\omega} \frac{2}{T} \int_0^T e^{i\omega n t} \dot{x} dt = -\frac{ia}{\pi n} \int_0^{2\pi} e^{in(\xi - \epsilon_0 \sin \xi)} \sin \xi d\xi, \\ y_n &= \frac{ia(1 - \epsilon_0^2)^{1/2}}{\pi n} \int_0^{2\pi} e^{in(\xi - \epsilon_0 \sin \xi)} \cos \xi d\xi, \end{aligned} \quad (\text{A2.7})$$

where  $T = 2\pi/\omega(|E|)$ . We can use an integral presentation of the Bessel function

$$J_n(x) = \frac{1}{\pi} \int_0^{2\pi} e^{i(n\xi - x \sin \xi)} d\xi = \frac{1}{\pi} \int_0^\pi \cos(n\xi - x \sin \xi) d\xi.$$

Then (A2.7) gives

$$x_n = \frac{2a}{n} J'_n(n\epsilon_0), \quad y_n = \frac{2ia}{n\epsilon_0} (1 - \epsilon_0^2)^{1/2} J_n(n\epsilon_0). \quad (\text{A2.8})$$

It follows asymptotics (see Landau and Lifshits (1975))

$$J_n(n\epsilon_0) \sim \frac{2}{\pi^{1/2}} \left(\frac{2}{n}\right)^{1/3} \Phi \left[ \left(\frac{n}{2}\right)^{3/2} (1 - \epsilon_0^2) \right], \quad n \gg 1, \quad 1 - \epsilon_0 \ll 1, \quad (\text{A2.9})$$

where

$$\Phi(z) = \frac{1}{\pi^{1/2}} \int_0^\infty \cos \left( \frac{\xi^3}{3} + z\xi \right) d\xi \quad (\text{A2.10})$$

is the Eiry function. For large  $z > 0$

$$\Phi(z) \sim \frac{1}{2z^{1/4}} \exp \left( -\frac{2}{3} z^{3/2} \right) \quad (\text{A2.11})$$

and (A2.9) transforms into

$$J_n(n\epsilon_0) \sim \frac{2^{2/3}}{\pi^{1/2}} \frac{1}{n^{3/2}} \frac{1}{(1 - \epsilon_0^2)^{1/4}} \exp \left( -\frac{n}{N} \right), \quad (n \gg N) \quad (\text{A2.12})$$

with

$$N = \frac{3}{(1 - \epsilon_0^2)^{3/2}} \gg 1. \quad (\text{A2.13})$$

The spectrum is effectively cut for the harmonics  $n > N \gg 1$ , i.e. when  $\epsilon_0 \rightarrow 1$ . The same property is valid for the harmonics  $x_n, y_n$  in (A2.8). The dimensionless parameter  $N$  defines the spectral width.

## Appendix C Fractional integro-differentiation

This and the following appendix consist of some useful information related to the fractional calculus. For more details, see Gelfand and Shilov (1964), Miller and Ross (1993), Samko *et al.* (1987), and Podlubny (1999). Different applications are collected in Hilfer (2000).

Fractional integration of order  $\beta$  is defined by the operators

$$\begin{aligned} I_{a+}^{\beta} f(t) &= \frac{1}{\Gamma(\beta)} \int_a^t f(\tau)(t-\tau)^{\beta-1} d\tau, & (\beta > 0), \\ I_{b-}^{\beta} f(t) &= \frac{1}{\Gamma(\beta)} \int_t^b f(\tau)(\tau-t)^{\beta-1} d\tau, & (\beta > 0). \end{aligned} \quad (\text{A3.1})$$

There is no constraint on the limits  $(a, b)$  and one can use different types of definitions. The first and second definitions are also called left and right integration. Any of them can be used for applications, and choice of a specific definition is only a matter of boundary, or initial conditions, or convenience. We unite everywhere  $a = -\infty$ ,  $b = \infty$  and simplify the notations (A3.1):

$$\begin{aligned} I_{\beta} f(t) &\equiv \frac{1}{\Gamma(\beta)} \int_{-\infty}^t f(\tau)(t-\tau)^{\beta-1} d\tau, & (\beta > 0), \\ I_{\beta} f(-t) &\equiv \frac{1}{\Gamma(\beta)} \int_t^{\infty} f(\tau)(\tau-t)^{\beta-1} d\tau, & (\beta > 0). \end{aligned} \quad (\text{A3.2})$$

The definitions (A3.2) can be written in a compact form:

$$\begin{aligned} I_{\beta} f(t) &= f(t) * \frac{t_+^{\beta-1}}{\Gamma(\beta)}, \\ I_{\beta} f(-t) &= f(t) * \frac{t_-^{\beta-1}}{\Gamma(\beta)}, \end{aligned} \quad (\text{A3.3})$$

where  $*$  means convolution and:

$$\begin{aligned} t_+^{\beta-1} &= \begin{cases} t^{\beta-1}, & t > 0, \\ 0, & t < 0, \end{cases} \\ t_-^{\beta-1} &= \begin{cases} t^{\beta-1}, & t < 0, \\ 0, & t > 0. \end{cases} \end{aligned} \quad (\text{A3.4})$$

The fractional derivative could be defined as the inverse operator to  $I_{\beta}$ , i.e.

$$\frac{d^{\beta}}{dt^{\beta}} = I_{-\beta}, \quad I_{\beta} = \frac{d^{-\beta}}{dt^{-\beta}}. \quad (\text{A3.5})$$

Their explicit form is:

$$\begin{aligned} \frac{d^{\beta} f(t)}{dt^{\beta}} &= \frac{1}{\Gamma(1-\beta)} \frac{d}{dt} \int_{-\infty}^t \frac{f(\tau) d\tau}{(t-\tau)^{\beta}}, \\ \frac{d^{\beta} f(t)}{d(-t)^{\beta}} &= \frac{-1}{\Gamma(1-\beta)} \frac{d}{dt} \int_t^{\infty} \frac{f(\tau) d\tau}{(\tau-t)^{\beta}}, & (0 < \beta < 1). \end{aligned} \quad (\text{A3.6})$$

The expressions (A3.1), (A3.2) and (A3.6) are called Riemann–Liouville integrals and derivatives respectively. Also, the first equation in (A3.6) corresponds to the left derivative and the second one to the right derivative.

For arbitrary  $\beta$  we have the definition:

$$\begin{aligned} \frac{d^\beta}{dt^\beta} f(t) &= \frac{1}{\Gamma(n-\beta)} \frac{d^n}{dt^n} \int_{-\infty}^t \frac{f(\tau) d\tau}{(t-\tau)^{\beta-n+1}}, \\ \frac{d^\beta}{d(-t)^\beta} f(t) &= \frac{(-1)^n}{\Gamma(n-\beta)} \frac{d^n}{d(-t)^n} \int_t^\infty \frac{f(\tau) d\tau}{(\tau-t)^{\beta-n+1}}, \end{aligned} \quad (\text{A3.7})$$

where  $n = [\beta] + 1$  and  $[\beta]$  is an integer part of  $\beta > 0$ .

The notation for the general case of the Riemann–Liouville derivatives are:

$${}_a \mathcal{D}_t^\beta f(t) = \frac{1}{\Gamma(n-\beta)} \left( \frac{d}{dt} \right)^n \int_a^t (t-\tau)^{n-\beta-1} f(\tau) d\tau, \quad (n-1 < \beta < n) \quad (\text{A3.8})$$

for the left derivative and

$${}_t \mathcal{D}_b^\beta f(t) = \frac{1}{\Gamma(n-\beta)} \left( -\frac{d}{dt} \right)^n \int_t^b (\tau-t)^{n-\beta-1} f(\tau) d\tau, \quad (n-1 < \beta < n) \quad (\text{A3.9})$$

for the right derivative.

Definitions (A3.8) and (A3.9) are not the only possible ones. Use of any definition of the fractional derivative depends on the initial or boundary condition and on the type of the problem to be solved. We provide the following three other definitions important for applications.

**Caputo derivative.** This derivative appears due to some practical needs (Caputo, 1967):

$$\begin{aligned} {}_a \overline{\mathcal{D}}_t^\beta &= \frac{1}{\Gamma(\beta-n)} \int_a^t (t-\tau)^{n-\beta-1} f(\tau) d\tau, \\ {}_t \overline{\mathcal{D}}_b^\beta &= \frac{1}{\Gamma(\beta-n)} \int_t^b (\tau-t)^{n-\beta-1} f(\tau) d\tau, \quad 0 \leq n-1 < \beta < n. \end{aligned} \quad (\text{A3.10})$$

The differences between  ${}_a \mathcal{D}_t^\beta$  and  ${}_a \overline{\mathcal{D}}_t^\beta$  will be indicated later.

**Grünwald–Letnikov derivative.** The main idea of this derivative is to get it as a limit of finite difference (see Samko *et al.*, 1987; Podlubny, 1999). The quantity

$${}_a \Delta_{\Delta t}^\beta f(t) = \sum_{k=0}^{[(t-a)/\Delta t]} (-1)^k \binom{\beta}{k} f(t - k\Delta t), \quad (\text{A3.11})$$

where  $[\dots]$  means the integer part is a fractional generalization of finite difference of the order  $(\Delta t)^\beta$ . We also use a notation:

$$\binom{n}{r} = \frac{n(n-1) \cdots (n-r+1)}{r!} = \frac{\Gamma(n+1)}{\Gamma(n-r+1)\Gamma(r+1)}.$$



This expression can be generalized by replacing  $n$  with a non-integer number. Then the number of terms in (A3.11) goes to infinity as  $\Delta t \rightarrow 0$ .

For integer  $\beta$  the expression (A3.11) gives:

$$\begin{aligned} {}_a\Delta_{\Delta t}^1 f(t) &= f(t) - f(t - \Delta t), \\ {}_a\Delta_{\Delta t}^2 f(t) &= f(t) - 2f(t - \Delta t) + f(t - 2\Delta t), \text{ etc.} \end{aligned}$$

The following expression gives the Grünwald–Letnikov derivative

$${}_a\mathcal{D}_t^\beta f(t) = \lim_{\Delta t \rightarrow 0} \frac{1}{(\Delta t)^\beta} {}_a\Delta_{\Delta t}^\beta f(t), \quad (\text{A3.12})$$

which coincides with Riemann–Liouville derivative for a wide class of functions. The formula (A3.11) is important for numerical integrators. More information about the generalization of finite differences can be found in Lubich (1986), Gorenflo (1997), Gorenflo and Mainardi (1997).

**Riesz derivative.** This is a symmetrized derivative which can be considered as a fractional generalization of Laplacian

$$(-\Delta)^{\alpha/2} \equiv \frac{d}{d|x|^\alpha} = -\frac{1}{2 \cos(\pi\alpha/2)} \left[ \frac{d^\alpha}{dx^\alpha} + \frac{d^\alpha}{d(-x)^\alpha} \right], \quad (\alpha \neq 1), \quad (\text{A3.13})$$

which in a regularized form reads:

$$\begin{aligned} \frac{d^\alpha}{d|x|^\alpha} f(x) &= -\frac{1}{K(\alpha)} \int_{0+}^{\infty} \frac{dy}{y^{\alpha+1}} [f(x-y) - 2f(x) + f(x+y)], \quad 0 < \alpha < 2, \\ K(\alpha) &= \begin{cases} 2\Gamma(-\alpha) \cos\left(\frac{\pi\alpha}{2}\right), & \alpha \neq 1 \\ -\pi, & \alpha = 1. \end{cases} \end{aligned} \quad (\text{A3.14})$$

The following formula is valid for all types of derivatives:

$$\frac{d^{\alpha+\beta}}{dt^{\alpha+\beta}} = \frac{d^\alpha}{dt^\alpha} \frac{d^\beta}{dt^\beta} = \frac{d^\beta}{dt^\beta} \frac{d^\alpha}{dt^\alpha}. \quad (\text{A3.15})$$

For a power function the Riemann–Liouville derivative is

$$\frac{d^\alpha}{dt^\alpha} t^\beta = \frac{\Gamma(1+\beta)}{\Gamma(1+\beta-\alpha)} t^{\beta-\alpha}. \quad (\text{A3.16})$$

Particularly

$$\frac{d^\alpha}{dt^\alpha} 1 = \frac{t^{-\alpha}}{\Gamma(1-\alpha)}, \quad t > 0 \quad (\text{A3.17})$$

and

$$\lim_{\alpha \rightarrow 1} \frac{d^\alpha}{dt^\alpha} 1 = \delta(t). \quad (\text{A3.18})$$

Contrary to that for the Caputo derivative

$${}_a\overline{\mathcal{D}}_t^\beta 1 = 0. \quad (\text{A3.19})$$

## Appendix D Formulas of fractional calculus

Here we provide some useful formulas of operating with fractional derivatives (for more details see Podlubny (1999) and Samko *et al.* (1987)).

Let us denote:

$$[g(x) \cdot f(x)] = \int_{-\infty}^{\infty} g(x)f(x)dx \quad (\text{A4.1})$$

as the scalar product of  $g(x)$  and  $f(x)$ . The following formula is equivalent to integration by parts:

$$\left[ g(x) \cdot \frac{d^\alpha}{dx^\alpha} f(x) \right] = \left[ f(x) \cdot \frac{d^\alpha}{d(-x)^\alpha} g(x) \right]. \quad (\text{A4.2})$$

It can be used to prove that

$$\int_{-\infty}^{\infty} dx \frac{d^\alpha}{dx^\alpha} f(x) = \int_{-\infty}^{\infty} dx \frac{d^\alpha}{d(-x)^\alpha} f(x) = \int_{-\infty}^{\infty} dx \frac{d^\alpha}{d|x|^\alpha} f(x) \equiv 0. \quad (\text{A4.3})$$

**Fourier transform.** The Fourier transform will be defined as

$$g(q) = \int_{-\infty}^{\infty} g(x)e^{iqx}dx \quad (\text{A4.4})$$

with a notation

$$g(x) \xrightarrow{F} g(q). \quad (\text{A4.5})$$

Then

$$\begin{aligned} \frac{d^\alpha}{dx^\alpha} g(x) &\xrightarrow{F} (-iq)^\alpha g(q), \\ \frac{d^\alpha}{d(-x)^\alpha} g(x) &\xrightarrow{F} (iq)^\alpha g(q) \end{aligned} \quad (\text{A4.6})$$

and for the Riesz derivative

$$\frac{d^\alpha}{d|x|^\alpha} g(x) \xrightarrow{F} -|q|^\alpha g(q) \quad (\text{A4.7})$$

if  $g(q=0) \neq 0$ . The usual convolution formula is also valid, that is, if

$$f(t) * g(t) = \int_{-\infty}^{\infty} f(t-\tau)g(\tau)d\tau \quad (\text{A4.8})$$

then

$$f(t) * \frac{d^\beta}{dt^\beta} g(t) \xrightarrow{F} (i\omega)^\beta f(\omega)g(\omega). \quad (\text{A4.9})$$

The same formulas (A4.5)–(A4.9) are valid for the Grünwald–Letnikov and Caputo derivatives with a condition to have  $a = -\infty$  as the lower limit of the integrand.

For the Riesz derivative

$$(-\Delta)^{\alpha/2} \xrightarrow{F} |k|^\alpha, \quad (\text{A4.10})$$

which has a correct sign for  $\alpha = 2$ .

**Laplace transform.** We define the Laplace transform of  $f(t)$  as

$$f(p) = \int_0^\infty e^{-pt} f(t) dt \quad (\text{A4.11})$$

and a notation

$$f(t) \xrightarrow{L} f(p). \quad (\text{A4.12})$$

The inverse formula is

$$f(t) = \int_{c-i\infty}^{c+i\infty} e^{pt} f(p) dp. \quad (\text{A4.13})$$

A difference between the lower limit of integrand in the Fourier and Laplace transforms makes differences for different fractional derivatives.

For the Riemann–Liouville derivative

$${}_0\mathcal{D}_t^\beta f(t) \xrightarrow{L} p^\beta f(p) - \sum_{m=0}^{n-1} p^m [{}_0\mathcal{D}_t^{\beta-m-1} f(t)]_{t=0}, \quad (n-1 < \beta < n). \quad (\text{A4.14})$$

The second term of (A4.14) has a problem of practical use since there is an absence of physical interpretation of the initial or boundary conditions for fractional derivatives (see more in Podlubny, 1999).

For the Caputo derivative

$${}_0\overline{\mathcal{D}}_t^\beta f(t) \xrightarrow{L} p^\beta f(p) - \sum_{m=0}^{n-1} p^{\beta-m-1} f^{(m)}(0), \quad (n-1 < \beta < n). \quad (\text{A4.15})$$

This derivative does not have the problem of initial or boundary conditions since all values  $f^{(m)}(0)$  can be given a physical meaning.

For the Grünwald–Letnikov derivative

$${}_0\overline{\mathcal{D}}_t^\beta f(t) \xrightarrow{L} p^\beta f(p) \quad (\text{A4.16})$$

similar to the Fourier transform.

Differentiation of a product  $f(t)g(t)$  is given by the Leibniz formula. Its generalization for the fractional derivative case is

$${}_a\mathcal{D}_t^\beta (f(t)g(t)) = \sum_{m=0}^{\infty} \binom{\beta}{m} f^{(m)}(t) {}_a\mathcal{D}_t^{\beta-m} g(t). \quad (\text{A4.17})$$

**Mittag–Leffler function.** This is an important function for fractional calculus since it appears in solutions of fractional differential equations (see references in Samko *et al.* (1987) and Podlubny (1999)). Its definition is

$$E_\alpha(z) = \sum_{k=0}^{\infty} \frac{z^k}{\Gamma(\alpha k + 1)}. \quad (\text{A4.18})$$

Particularly

$$\begin{aligned} E_1(z) &= e^z, \\ E_{1/2}(-z) &= e^{z^2} \operatorname{erfc}(z) = \frac{2}{\pi^{1/2}} e^{z^2} \int_z^\infty e^{-y^2} dy. \end{aligned} \quad (\text{A4.19})$$

The two-parameter function of the Mittag-Leffler type is defined as

$$E_{\alpha,\beta}(z) = \sum_{k=0}^{\infty} \frac{z^k}{\Gamma(\alpha z + \beta)}, \quad \alpha, \beta > 0. \quad (\text{A4.20})$$

Particularly

$$\begin{aligned} E_{\alpha,1}(z) &= E_\alpha(z), \\ E_{1,1}(z) &= E_1(z) = e^z, \\ E_{1,2}(z) &= \frac{e^z - 1}{z}, \\ E_{2,1}(z^2) &= \cosh(z), \\ E_{2,2}(z^2) &= \frac{1}{z} \sinh(z). \end{aligned} \quad (\text{A4.21})$$

The functions  $E_\alpha(z)$  and  $E_{\alpha,\beta}(z)$  can be used to solve some simple equations with fractional derivatives using a formal expansion into series. As an example, consider the equation

$${}_0\mathcal{D}_t^\beta y(t) - sy(t) = f(t) \quad (\text{A4.22})$$

and initial conditions

$$[{}_0\mathcal{D}_t^{\beta-m} y(t)]_{t=0} = b_k, \quad (k = 1, 2, \dots, n), \quad n-1 < \beta < n. \quad (\text{A4.23})$$

The solution of (A4.22) that satisfies the conditions (A4.23), is

$$y(t) = \sum_{k=1}^n b_k t^{\beta-k} E_{\beta,\beta-k+1}(st^\beta) + \int_0^t (t-\tau)^{\beta-1} E_{\beta,\beta}(s(t-\tau)^\beta) f(\tau) d\tau. \quad (\text{A4.24})$$

*This page intentionally left blank*

## REFERENCES

- Abdullaev, S. S. and G. M. Zaslavsky (1996). *Phys. Plasmas*, **3**, 516.
- Abdullaev, S. S. and K. H. Spatschek (1999). *Phys. Rev.*, **E 60**, R6287.
- Abel, M., L. Biferale, M. Cencini, M. Falcone, D. Vergni, and A. Vulpiani (2000). *Physica*, **D 147**, 12.
- Abramowitz, M. and I. A. Stegun (1972). ‘Handbook of Mathematical Functions’, U.S. Dept. of Commerce, NBS, *Appl. Math. Ser.*, **55**.
- Adler, R. C., A. C. Konheim, and M. H. McAndrews (1965). *Trans. Am. Math. Soc.*, **114**, 309.
- Adler, R., B. Kitchens, and C. Tresser (2001). *Ergodic Theory and Dynamical Systems*, **21**, 959.
- Afanas’ev, V. V., A. A. Chernikov, R. Z. Sagdeev, and G. M. Zaslavsky (1990). *Phys. Lett.*, **A 144**, 229.
- Afanasiev, V. V., R. Z. Sagdeev, and G. M. Zaslavsky (1991). *Chaos*, **1**, 143.
- Afraimovich, V. (1997). *Chaos*, **7**, 12.
- Afraimovich, V., and G. M. Zaslavsky (1997). *Phys. Rev.*, **E 55**, 5418.
- Afraimovich, V., and G. M. Zaslavsky (1998). in ‘*Chaos, Kinetics and Nonlinear Dynamics in Fluids and Plasmas*’, Eds. S. Benkadda and G. M. Zaslavsky (Springer, Berlin), p. 59.
- Afraimovich, V., M. Courbage, B. Fernandez, and A. Morante (2002). in *Mathematical Problems of nonlinear Dynamics*, Eds. L. M. Lerman and L. P. Shilnikov (Nizhny Novgorod University Press, Nizhny Novgorod), p. 9.
- Afraimovich, V. and Sze-Bi Hsu (2003). ‘*Lectures on Chaotic Dynamical Systems*’, Amer. Math. Soc., Providence.
- Afraimovich, V. and G. M. Zaslavsky (2003). *Chaos*, **13**, 519.
- Aizawa, Y. (1989). *Progr. Theor. Phys.*, **81**, 249.
- Aizawa, Y., Y. Kikuchi, T. Harayama, K. Yamamoto, M. Ota, and K. Tanaka (1989). *Progr. Theor. Phys. Suppl.*, **98**, 36.
- Anosov, D. V. (1963). *Doklady Akad. Nauk, SSSR* **151**, 1250.
- Anosov, D. V. and Ya. G. Sinai (1967). *Uspekhi Math. Nauk*, **22**, 107.
- Aref, H. (1979). *Phys. Fluids*, **22**, 393.
- Aref, H., and N. Pomphrey (1980). *Phys. Lett.*, **A 78**, 297.
- Aref, H., and N. Pomphrey (1982). *Proc. Roy. Soc. London*, **A 380**, 359.
- Aref, H. (1984). *J. Fluid Mech.*, **143**, 1.
- Arnold, V. I. (1961). *Izvestia Akad. Nauk SSSR Math.*, **25**, 21.
- Arnold, V. I. (1963). *Russ. Math. Surveys*, **18**, 9, 85.
- Arnold, V. I. (1964). *Dokl. Akad. Nauk SSSR*, **156**, 9.
- Arnold, V. I. (1965). *C.R. Acad. Sci. Paris*, **261**, 17.

- Arnold, V. I. (1978). *'Mathematical Methods of Classical Mechanics'*. Springer, Berlin.
- Arnold, V. I. (1986). *Selecta Math. Soviet*, **5**, 327.
- Arnold, V. I. (1988). *Physica*, **D 33**, 21.
- Arnold, V. I. (1992). *'Ordinary Differential Equations'*. Springer, New York.
- Arnold, V. I., V. V. Kozlov, and A. I. Neishtadt (1993). *'Mathematical Aspects of Classical and Celestial Mechanics'*. Springer, Berlin.
- Artuso, R., I. Guarneri, and L. Rebuzzini (2000). *Chaos*, **10**, 189.
- Artuso, R., G. Casati, and I. Guarneri (1997). *Phys. Rev.*, **E 55**, 6384.
- Ashwin P., W. Chambers, and G. Petkov (1997). *Intern. J. Bifurcations and Chaos*, **7**, 2603.
- Aubry, S. (1983). *Physica*, **D 7**, 240.
- Aurell, E., G. Boffetta, A. Crisanti, G. Paladin, and A. Vulpiani (1997). *J. Phys.*, **A 30**, 1.
- Babiano, A., G. Boffetta, A. Provenzale, and A. Vulpiani (1994). *Phys. Fluids*, **6**, 2465.
- Badii, R., and A. Politi (1997). *'Complexity'*. Cambridge University Press, Cambridge.
- Ball, P. (1999). *'The Self-Made Tapestry: Pattern Formation in Nature'*. Oxford University Press, New York.
- Barkai, E. (2001). *Phys. Rev.*, **E 63**, 046118.
- Beloshapkin, V. V. and G. M. Zaslavsky (1983). *Phys. Lett.*, **A 97**, 121.
- Beloshapkin, V. V., A. A. Chernikov, M. Ya. Natenzon, B. A. Petrovichev, R. Z. Sagdeev, and G. M. Zaslavsky (1989). *Nature*, **337**, 113.
- Beloshapkin, V. V., A. G. Tretyakov, and G. M. Zaslavsky (1994). *Comm. Pure and Appl. Math.*, **47**, 39.
- Belov, N. V. (1976). *'Structural Mineralogy'* (in Russian). Nauka, Moscow.
- Benenti, G., G. Casati, S. Montangero, and D. Shepelyansky (2001). *Phys. Rev. Lett.*, **87**, 227901.
- Benkadda, S., S. Kassibrakis, R. B. White, and G. M. Zaslavsky (1997). *Phys. Rev.*, **E 55**, 4909.
- Benkadda, S., S. Kassibrakis, R. B. White, and G. M. Zaslavsky (1999). *Phys. Rev.*, **E 59**, 3761.
- Berger, J. M., and B. B. Mandelbrot (1963). *IBM J. Res. Dev.*, **7**, 224.
- Besicovitch, A. S. (1929). *Math. Ann.*, **101**, 161.
- Besicovitch, A. S. (1934). *J. London Math. Soc.*, **9**, 126.
- Biler, P., T. Funaki, and W. A. Woyczynski (1998). *J. Diff. Equations*, **148**, 9.
- Boffetta, G., A. Celani, and M. Vergassola (2000). *Phys. Rev.*, **E 61**, R29.
- Boffetta, G., M. Cencini, M. Falconi, and A. Vulpiani (2002). *Phys. Reports*, **356**, 367.
- Boltzmann, L. (1872). *Wien. Ber.*, **66**, 275.
- Boltzmann, L. (1895, 1898). *'Vorlesung en über Gastheorie, I, II'*. Leipzig, J. A. Barth. Translation: Boltzmann, L., 1964, 'Lectures on Gas Theory'. University of California Press, Berkeley.

- Boltzmann, L. (1897). *Wied. Ann.*, **60**, 392.
- Boltzmann, L. (1898a). *Math. Ann.*, **50**, 325.
- Bouchaud, J. P. and A. Georges (1990). *Phys. Rep.*, **95**, 127.
- Bowen, R. (1972). *Amer. J. Math.*, **94**, 413.
- Bowen, R. (1973). *Trans. Amer. Math. Soc.*, **84**, 125.
- Brudno, A. A. (1983). *Trans. Moscow Math. Soc.*, **44**, 127.
- Bunimovich, L. A. and Ya. G. Sinai (1973). *Math. USSR-Sb.*, **90**, 407.
- Bunimovich, L. A. (1979). *Comm. Math. Phys.*, **65**, 295.
- Bunimovich, L. A. and Ya. G. Sinai (1981). *Commun. Math. Phys.*, **78**, 479.
- Bunimovich, L. A. (1985). *Sov. Phys. JETP*, **62**, 842.
- Bunimovich, L. A., Ya. G. Sinai, and N. I. Chernov (1991). *Russ. Math. Surv.*, **46**, 47.
- Caputo, M. (1967). *Geophys. J.R. Astr. Soc.*, **13**, 529.
- Carathéodory, C. (1914). *Göttingen Nachr.*, 406.
- Carreras, B. A., V. E. Lynch, D. E. Newman, and G. M. Zaslavsky (1999). *Phys. Rev.*, **E 60**, 4770.
- Carreras, B. A., V. E. Lynch, and G. M. Zaslavsky (2001). *Phys. Plasmas*, **8**, 5096.
- Carreras, B. A., V. E. Lynch, L. Garcia, M. Edelman, and G. M. Zaslavsky (2003). *Chaos*, **13**, 1175.
- Cary, J. R., D. E. Escande, and J. L. Tennyson (1986). *Phys. Rev.*, **A 34**, 4256.
- Casati, G. and T. Prosen (1999). *Phys. Rev. Lett.*, **83**, 4729.
- Chaikovsky, D. K. and G. M. Zaslavsky (1991). *Chaos*, **1**, 463.
- Chandrasekhar, S. (1943). *Rev. Mod. Phys.*, **15**, 1.
- Chernikov, A. A., M. Ya. Natenzon, B. A. Petrovichev, R. Z. Sagdeev, and G. M. Zaslavsky (1987). *Phys. Lett.*, **A 122**, 39.
- Chernikov, A. A., B. A. Petrovichev, A. Rogalsky, R. Z. Sagdeev, and G. M. Zaslavsky (1988). *Phys. Lett.*, **A 129**, 3377.
- Chernikov, A. A., B. A. Petrovichev, A. Rogalsky, R. Z. Sagdeev, and G. M. Zaslavsky (1990). *Phys. Lett.*, **A 144**, 127.
- Chernikov, A. A. and A. V. Rogalsky (1994). *Chaos*, **4**, 35.
- Chernov, N., and L.-S. Young (2000). in ‘*Encyclopedia of Mathematical Science*’, Ed. D. Szasz, **101**, 51.
- Childress, S. (1970). *J. Math. Phys.*, **11**, 3063.
- Chirikov, B. V. (1959). *Atomnaya Energiya*, **6**, 630.
- Chirikov, B. V. (1979). *Phys. Rep.*, **52**, 263.
- Chirikov, B. V. and D. L. Shepelyansky (1984). *Physica*, **D 13**, 395.
- Chua, L. O. and T. Lin (1998). *IEEE Trans.*, **35**, 648.
- Cohen, A. and I. Procaccia (1985). *Phys. Rev.*, **A 31**, 1872.
- Compte, A. (1996). *Phys. Rev.*, **E 53** 4191.
- Cornfeld, I. P., S. V. Fomin, and Ya. G. Sinai (1982). ‘*Ergodic Theory*’. Springer, New York.
- Crisanti, A., M. Falcioni, A. Provenzale, P. Tanga, and A. Vulpiani (1992). *Phys. Fluids*, **A 4**, 1805.



- Critchlow, K. (1999). ‘*Islamic Patterns*’. Inner Traditions, Rochester, Vermont.
- Dana, I. (1995). *Phys. Lett.*, **A 197**, 413.
- Dana, I. and M. Amit (1995). *Phys. Rev.*, **E 51**, R2731.
- Davies, A. C. (1995). *Phil. Trans. R. Soc.*, **A 353**, 85.
- Delshams, A., R. de la Llave, and T. M. Seara (2003). *Electron. Res. Announc.*, **9**, 125.
- Denisov, S. and S. Flach (2001). *Phys. Rev.*, **E 64**, 056236.
- Dombre, T., U. Frisch, J. M. Green, M. Henon, A. Mehr, and A. M. Soward (1986). *J. Fluid Mech.*, **167**, 353.
- Dorfman, J. R. (1999). ‘*An Introduction to Chaos in Nonequilibrium Statistical Mechanics*’. Cambridge University Press, Cambridge, MA.
- Douady, S. and Y. Couder (1992). *Phys. Rev. Lett.*, **68**, 2098.
- Douady, S. and Y. Couder (1996). *J. Theor. Biol.*, **178**, 255.
- Douglas, J. F. (2000). in ‘*Applications of Fractional Calculus in Physics*’, Ed. R. Hilfer. World Scientific, Singapore, p. 241.
- Douglas, J. F., S.-Q. Wang, and K. F. Freed (1986). *Macromolecules*, **19**, 2207.
- Douglas, J. F., S.-Q. Wang, and K. F. Freed (1987). *Macromolecules*, **20**, 543.
- Dubrovin, B. A., A. T. Fomenko, and S. P. Novikov (1984). ‘*Modern Geometry — Methods and Applications*’. Springer, New York.
- Dumont, J. and C. Reiter (2002). *Chaos, Solitons, and Fractals*, **11**, 1287.
- Dumont, J. P., F. J. Meiss, K. C. Jones, C. A. Reiter, and L. M. Vislocky (2001). *Chaos, Solitons, and Fractals*, **12**, 761.
- Ehrenfest, P. and T. Ehrenfest (1911). ‘*Encyklopädie d. Mathem. Wiss.*’, **Bd 4**, s. 4. Translation: ‘The Conceptual Foundations of Statistical Approach in Mechanics’. Cornell University Press, Ithaca, 1959.
- Einstein, A. (1905). *Ann. Phys.*, **17**, 549.
- Einstein, A. (1917). *Verhandl. Dtsch. Phys. Ges.*, **19**, 82.
- Evans, T. E., R. A. Moyer, and P. Monat (2002). *Physics of Plasmas*, **9**, 4957.
- Feller, W. (1949). *Trans. Amer. Math. Soc.*, **67**, 98.
- Feller, W. (1957). ‘*An Introduction to Probability Theory and Its Applications*’. John Wiley, New York.
- Fermi, E. (1949). *Phys. Rev.*, **75**, 1169.
- Field, M. and M. Golubitsky (1992). ‘*Symmetry in Chaos*’. Oxford University Press, New York.
- Filonenko, N. N., R. Z. Sagdeev, and G. M. Zaslavsky (1967). *Nucl. Fusion*, **7**, 253.
- Flach, S., O. Yevtushenko, and Y. Zolotaryuk (2000). *Phys. Rev. Lett.*, **84**, 2358.
- Fogedby, H. C. (1994). *Phys. Rev.*, **E 50**, 1657.
- Fokker, A. D. (1914). *Ann. Physik*, **43**, 810.
- Frisch, U. and G. Parisi (1985). in ‘*Turbulence and Predictability of Geophysical Flows and Climate Dynamics*’, Eds. M. Ghill, R. Benzi, and G. Parisi. North-Holland, Amsterdam, p. 84.
- Fukuyama, A. H., Momota, R. Itatani, and T. Takizuka (1977). *Phys. Rev. Lett.*, **38**, 701.

- Galperin, G. A. and A. N. Zemlyakov (1990). '*Mathematical Billiards*'. Nauka, Moscow in Russian.
- Gardner, M. (1977). *Scientific American*, **236**, 110.
- Gaspard, P. and X.-J. Wang (1953). *Physics Reports*, **235**, 291.
- Geisel, T. (1984). *Europhys. News*, **15**, 5.
- Geisel, T. (1995). in '*Lévy Flights and Related Topics in Physics*', Eds. M. F. Shlesinger, G. M. Zaslavsky, and U. Frisch. Springer, Berlin, p. 153.
- Geisel, T., J. Nierwetberg, and A. Zacherl (1987a). *Phys. Rev. Lett.*, **54**, 616.
- Geisel, T., A. Zacherl, and G. Radons (1987b). *Phys. Rev. Lett.*, **59**, 2503.
- Gelfand, I. M., and G. E. Shilov (1964). '*Generalized Functions*'. Academic, New York, Vol. 1.
- Gnedenko, B. V., and A. N. Kolmogorov (1954). '*Limit Distributions for Sums of Independent Variables*'. Addison-Wesley, Cambridge, MA.
- Gollub, J. (1995). *Proc. Natl. Acad. Sci., USA*, **92**, 6705.
- Gorenflo, R. (1997). in '*Fractals and Fractional Calculus in Continuum Mechanics*', Eds. A. Carpinteri and F. Mainardi. Springer, New York, p. 277.
- Gorenflo, R. and F. Mainardi (1997). *ibid.*, p. 233.
- Govorukhin, V. N., A. Morgulis, V. I. Yudovich, and G. M. Zaslavsky (1999). *Phys. Rev.*, **E 60**, 2788.
- Gradshteyn, I. S. and I. M. Ryzhik (1980). '*Table of Integrals, Series, and Products*'. Academic, New York.
- Grassberger, P., I. Procaccia, and M. Hentschel (1983). *Lect. Notes Phys.*, **179**, 212.
- Grassberger, P. and I. Procaccia (1983). *Physica*, **D 9**, 189.
- Grassberger, P. and I. Procaccia (1984). *Physica*, **D 13**, 34.
- Greene, J. M. (1979). *J. Math. Phys.*, **20**, 1183.
- Greene, J. M., R. S. MacKay, F. Vivaldi, and M. J. Feigenbaum (1981). *Physica*, **D 3**, 468.
- Grunbaum, B. and G. C. Shepard (1987). '*Tiling and Patterns*'. W. H. Freeman, New York.
- Gutkin, E. (1986). *Physica*, **D 19**, 311.
- Gutkin, E. (1996). *J. Stat. Phys.*, **83**, 7.
- Gutkin, E. (2003). *Regular and Chaotic Dynamics*, **8**, 1.
- Halsey, T. C., M. H. Jensen, L. P. Kadanoff, I. Procaccia, and B. I. Schraiman (1986). *Phys. Rev.*, **A 33**, 1141.
- Hanson, J. D., J. R. Cary, and J. D. Meiss (1985). *J. Stat. Phys.*, **39**, 327.
- Hargittai, I., ed. (1992). '*Five-Fold Symmetry*'. World Scientific, Singapore.
- Hausdorff, F. (1919). *Math. Ann.*, **79**, 157.
- Hedlund, G. A. and M. Morse (1938). *Amer. J. Math.*, **60**, 815.
- Henon, M. (1966). *C.R. Acad. Sci., Paris*, **262**, 312.
- Hentschel, H. G. E. and I. Procaccia (1983). *Physica*, **D 8**, 435.
- Hilfer, R. (1993). *Phys. Rev.*, **E 48**, 2466.
- Hilfer, R. (1995a). *Chaos, Solitons, and Fractals*, **5**, 1475.
- Hilfer, R. (1995b). *Physica*, **A 221**, 89.

- Hilfer, R. (2000). in 'Application of Fractional Calculus in Physics'. Ed. R. Hilfer. World Scientific, Singapore.
- Hohenberg, P. C. and B. I. Halperin (1977). *Rev. Mod. Phys.*, **49**, 435.
- Hopf, E. (1940). *Math. Ann.*, **117**, 590.
- Horita, T., H. Hata, R. Ishizaki, and H. Mori (1990). *Progr. Theor. Phys.*, **83**, 1065.
- Horton, W. and Y.-H. Ichikawa (1996). 'Chaos and Structures in Nonlinear Plasmas'. World Scientific, Singapore.
- Hughes, B. D., M. F. Shlesinger, and E. W. Montroll (1981). *Proc. Natl. Acad. Sci., USA*, **78**, 3287.
- Hughes, B. D., E. W. Montroll, and M. F. Shlesinger (1982). *J. Stat. Phys.*, **28**, 111.
- Ichikawa, Y. H., T. Kamimura, and T. Hatori (1987). *Physica*, **D 29**, 247.
- Iomin, A., D. Gangardt, and S. Fishman (1998). *Phys. Rev.*, **E 57**, 4054.
- Isichenko, M. B. (1992). *Rev. Mod. Phys.*, **64**, 961.
- Ivanov, P. Ch., B. Podobnik, Y. Lee, and H. E. Stanley (2001). *Physica*, **A 229**, 154.
- Jensen, M. H., L. P. Kadanoff, A. Libshaber, I. Procaccia, and J. Stavans (1985). *Phys. Rev. Lett.*, **55**, 439.
- Kac, M. (1958). 'Probability and Related Topics in Physical Sciences'. Interscience, New York.
- Kac, M. (1959). 'Statistical Independence in Probability, Analysis, and Number Theory'. The Mathematical Association of America.
- Kadanoff, L. P. (1981). *Phys. Rev. Lett.*, **47**, 1641.
- Kadanoff, L. P. (1993). 'From Order to Chaos'. World Scientific, Singapore.
- Kadanoff, L. P. (2000). 'Statistical Physics'. World Scientific, Singapore.
- Kaplan, A., N. Friedman, M. Andersen, and N. Davidson (2001). *Phys. Rev. Lett.*, **87**, 274101.
- Kaplan, A., N. Friedman, M. Andersen, M. Andersen, and N. Davidson (2004). *Physica*, **D 187**, 136.
- Karney, C. F. F. (1983). *Physica*, **D 8**, 360.
- Kassibrakis, S., S. Benkadda, R. B. White, and G. M. Zaslavsky (1998). in 'Chaos, Kinetics and Nonlinear Dynamics in Fluids and Plasmas'. Eds. S. Benkadda and G. M. Zaslavsky. Springer, Berlin, p. 403.
- Katok, A. (1980). *Isr. J. Math.*, **35**, 301.
- Kenkre, V. M., E. W. Montroll, and M. F. Shlesinger (1973). *J. Stat. Phys.*, **9**, 45.
- Kepler, J. (1619). 'Harmonics Mundi Libri Quinque'. (Five books on the harmony of the world), Joannes Plancus, Lincii Austria.
- Kerckhoff, S., H. Masur, and J. Smillie (1986). *Ann. Math.*, **124**, 293.
- Khinchin, A. Ya. (1964). 'Continued Fractions'. University of Chicago Press, Chicago, IL.
- Kolmogorov, A. N. (1938). *Usp. Mat. Nauk*, **5**, 5.
- Kolmogorov, A. N. (1954). *Doklady Akad. Nauk SSSR*, **98**, 527.
- Kolmogorov, A. N. (1958). *Doklady Akad. Nauk SSSR*, **119**, 861.

- Kolmogorov, A. N. and V. M. Tikhomirov (1959). *Uspekhi Mat. Nauk*, **14**, 3.
- Kouptsov, K. L., J. H. Lowenstein, and F. Vivaldi (2002). *Nonlinearity*, **15**, 1795.
- Kozlov, V. V. (1983). *Uspekhi Matem. Nauk*, **38**, 3.
- Kozlov, V. V. (1996). *Symmetries, Topology, and Resonances in Hamiltonian Mechanics*. Springer, Berlin.
- Kozlov, V. V. (1998). *General Theory of Vortices* (in Russian). Udmurt University, Izhevsk.
- Krylov, N. S. (1979). *Works on the Foundation of Statistical Physics, Moscow-Leningrad, Academy of Sciences 1950'*. English translation Princeton University Press, New York.
- Kuznetsov, L. I. and G. M. Zaslavsky (1997). *Phys. Reports*, **288**, 457.
- Kuznetsov, L. and G. M. Zaslavsky (1998). *Phys. Rev.*, **E 58**, 7330.
- Kuznetsov, L. and G. M. Zaslavsky (2000). *Phys. Rev.*, **E 61**, 3777.
- Kuznetsov, L. and G. M. Zaslavsky (2002). *Phys. Rev.*, **E 66**, 046212.
- Lamb, H. (1945). *Hydrodynamics*. Dover, New York.
- Lamb, J. S. W. (1993). *J. Phys.*, **A 26**, 2921.
- Lamb, J. S. W. and G. R. W. Quispel (1994). *Physica*, **D 73**, 277.
- Landau, L. D. (1937). *Zhurn. Eks. Teor. Fiz.*, **7**, 203.
- Landau, L. D. and E. M. Lifshits (1975). *The Classical Theory of Fields*. Pergamon Press.
- Landau, L. D. and E. M. Lifshits (1976). *Mechanics*. Pergamon Press, Oxford.
- Lazutkin, V. F., I. G. Schakhmanski, and M. B. Tabanov (1989). *Physica*, **D 40**, 235.
- Ledrappier, F. and L.-S. Young (1985). *Ann. of Math.*, **122**, 509, 540.
- Leff, H. S. and A. F. Rex (1990). *Maxwell's Demon*. Princeton University Press, Princeton.
- Leoncini, X., L. Kuznetsov, and G. M. Zaslavsky (2000). *Phys. Fluids*, **12**, 1911.
- Leoncini, X., L. Kuznetsov, and G. M. Zaslavsky (2001). *Phys. Rev.*, **E 63**, 036224.
- Leoncini, X., and G. M. Zaslavsky (2002). *Phys. Rev.*, **E 165**, 046216.
- Lepri, S., L. Rondoni, and G. Benettin (2000). *J. Stat. Phys.*, **99**, 857.
- Lévy, P. (1937). *Theorie de L'Addition des Variables Aleatoires*. Gautier-Villier, Paris.
- Liboff, R. (1998). *Kinetic Theory*. Wiley, New York.
- Lichtenberg, A. and M. Lieberman (1983). *Regular and Chaotic Motion*. Springer, Berlin.
- Lowenstein, J. H. (1991). *Chaos*, **1**, 473.
- Lowenstein, J. H. (1992). *Chaos*, **2**, 413.
- Lowenstein, J. H. (1993). *Phys. Rev.*, **E 47**, R3811.
- Lowenstein, J. H. (1994a). *Chaos*, **4**, 397.
- Lowenstein, J. H. (1994b). *Phys. Rev.*, **E 49**, 232.
- Lowenstein, J. H. and F. Vivaldi (1998). *Nonlinearity*, **11**, 1321.
- Lowenstein, J. H. and F. Vivaldi (2000). *Chaos*, **10**, 747.
- Lubich, Ch. (1986). *SIAM J. Math. Anal.*, **17**, 704.

- Luo, A. (2004). *Appl. Mech. Rev.* **57**, 161.
- Lyubomudrov, O., M. Edelman, and G. M. Zaslavsky (2003). *Intern. J. Modern Phys.*, **B 17**, 4149.
- Machta, J. (1983). *J. Stat. Phys.*, **32**, 555.
- Machta, J. and R. Zwanzig (1983). *Phys. Rev. Lett.*, **48**, 1959.
- MacKay, R. S. (1983). *Physica*, **D 7**, 283.
- MacKay, R. S., J. D. Meiss, and I. C. Percival (1984). *Physica*, **D 13**, 55.
- Makovicky, E. (1992). see Hargittai, 1992, p. 67.
- Mandelbrot, B. (1982). *'The Fractal Geometry of Nature'*. Freeman, San Francisco.
- Mandelbrot, B. and J. W. Van Ness (1968). *SIAM Review*, **10**, 422.
- Margulis, G. A. (1969). *Funkts. Anal. i Prilozh.*, **3**, 80.
- Margulis, G. A. (1970). *Funkts. Anal. i Prilozh.*, **4**, 62.
- Mateos, J. L. (2000). *Phys. Rev. Lett.*, **84**, 258.
- Mather, J. N. (1982). *Topology*, **21**, 457.
- Meerschaert, M. M. and H. P. Scheffler (2000). *'Limit Theorems for Sums of Independent Random Vectors: Heavy Tails in Theory and Practice'*. Wiley, New York.
- Meerschaert, M. M., D. A. Benson, and B. Baeumer (2001). *Phys. Rev.*, **E 63**, 021112.
- Meiss, J. D. (1986). *Phys. Rev.*, **A 34**, 2375.
- Meiss, J. D. (1992). *Rev. Mod. Phys.*, **64**, 795.
- Meiss, J. D. (1997). *Chaos*, **7**, 39.
- Meleshko, V. V. and M. Yu. Konstantinov (2002). *'Vortex Dynamics Chaotic Phenomena'*. World Scientific, Singapore.
- Melnikov, V. K. (1963). *Dokl. Akad. Nauk SSSR*, **148**, 1257.
- Metzler, R. and J. Klafter (2000). *Phys. Rep.*, **339**, 1.
- Miller, K. S. and B. Ross (1993). *An Introduction to the Fractional Differential Equations*. John Wiley and Sons, NY.
- Milnor, J. (1988). *Complex Systems*, **2**, 357.
- Milovanov, A. V. (2001). *Phys. Rev.*, **E 63**, 047301.
- Montroll, E. W. and M. F. Shlesinger (1984). in *'Studies in Statistical Mechanics'*, Eds. J. Lebowitz and E. Montroll. North-Holland, Amsterdam, Vol. 11, p. 1.
- Montroll, E. W. and G. H. Weiss (1965). *J. Math. Phys.*, **6**, 167.
- Morgulis, A., V. I. Yudovich, and G. M. Zaslavsky (1995). *Comm. Pure and Appl. Math.*, **48**, 571.
- Moser, J. K. (1962). *Nachr. Acad. Wiss., Göttingen, Math. Phys.*, **K1 (11a)**, 1.
- Moser, J. K. (1967). *Math. Ann.*, **169**, 136.
- Natenzon, M. Ya., A. I. Neishtadt, R. Z. Sagdeev, G. K. Seryakov, and G. M. Zaslavsky (1990). *Phys. Lett.*, **A 145**, 255.
- Neishtadt, A. I. (1975). *J. Appl. Math. Mech.*, **39**, 594.
- Neishtadt, A. I., D. K. Chaikovsky, and A. A. Chernikov (1991). *Zhurn. Eksp. Teor. Fiz.*, **99**, 763.
- Neishtadt, A. I., V. V. Sidorenko, and D. V. Treschev (1997). *Chaos*, **7**, 2.

- Nekhoroshev, N. N. (1977). *Uspekhi Matem. Nauk*, **32**, 5.
- Niemeijer, Th. and J. M. J. van Leeuwen (1976). in '*Phase Transitions and Critical Phenomena*', Eds. C. Domb and M. S. Green. Academic Press, London, Vol. 6, p. 425.
- Nigmatullin (1986). *Phys. Stat. Solidi B*, **133**, 425.
- Novikov, E. A. (1975). *JETP*, **41**, 937.
- Novikov, E. A. and Ya. B. Sedov (1978). *Sov. Phys. JETP*, **48**, 440.
- Obberhettinger, F. (1974). *Tables of Mellin Transforms*. Springer, Berlin.
- Oceledec, V. I. (1968). *Trans. Moscow Math. Soc.*, **19**, 197.
- Ott, E. (1993). '*Chaos in Dynamical Systems*'. Cambridge University Press, Cambridge, MA.
- Ottino, J. (1989). '*The Kinematics of Mixing: Stretching, Chaos, Transport*'. Cambridge University Press, Cambridge, MA.
- Paladin, G. and A. Vulpiani (1987). *Phys. Reports*, **156**, 147.
- Paret, J. and P. Tabeling (1997). *Phys. Rev. Lett.*, **79**, 4162.
- Pekarsky, S. and V. Rom-Kedar (1997). *Phys. Lett.*, **A 225**, 274.
- Penrose, R. (1974). *Bull. Inst. Math. App.*, **10**, 266.
- Percival, I. (1974). *J. Phys.*, **A 7**, 794.
- Percival, I. (1979). *J. Phys.*, **A 12**, L57.
- Pesin, Ya. B. (1977). *Russ. Math. Surveys*, **32**, 55.
- Pesin, Ya. B. (1988). *Russ. Math. Surveys*, **43**, 111.
- Pesin, Ya. B. (1997). '*Dimension Theory in Dynamical Systems*'. University of Chicago Press, Chicago.
- Pesin, Ya. B. and H. Weiss (1997). *Chaos*, **7**, 89.
- Petrosky, T. J. (1986). *Phys. Lett.*, **A 117**, 328.
- Petrovichev, B. A., A. V. Rogalsky, R. Z. Sagdeev, and G. M. Zaslavsky (1990). *Phys. Lett.*, **150**, 391.
- Pismen, L. M. (1999). '*Vortices in Nonlinear Fields*'. Clarendon Press, Oxford.
- Planck, M. (1917). *Sitzber. Preuf. Akad. Wiss.*, p. 810.
- Podlubny, I. (1999). '*Fractional Differential Equations*'. Academic Press, San Diego.
- Prigogine, I. (1962). '*Non-Equilibrium Statistical Mechanics*'. Wiley, New York.
- Procaccia, I. (1985). *Phys. Scripta*, **9**, 40.
- Provenzale, A. (1999). *Annu. Rev. Fluid Mech.*, **31**, 55.
- Rakhlin, D. A. (2000). *Phys. Rev.*, **E 63**, 011112-1.
- Rechester, A. B. and R. B. White (1980). *Phys. Rev. Lett.*, **44**, 1586.
- Rechester, A. B., M. N. Rosenbluth, and R. B. White (1981). *Phys. Rev.*, **A 23**, 2664.
- Reichl, L. E. (1992). '*The Transition to Chaos*'. Springer, New York.
- Rényi, A. (1957). *Trans. 2nd Prague Conf. on Information Theory, Statistical Decision Functions, and Random Processes*, 545.
- Rényi, A. (1970). '*Probability Theory*'. North-Holland, Amsterdam.
- Richardson, L. (1961). *General Systems Yearbook*, **6**, 139.
- Richens, P. J. and M. Berry (1981). *Physica*, **D 2**, 495.

- Risken, H. (1989). *'The Fokker-Planck Equation: Methods of Solution and Applications'*. Springer, Berlin.
- Rom-Kedar, V., A. Leonard, and S. Wiggins (1990). *J. Fluid Mech.*, **214**, 347.
- Rom-Kedar, V. (1994). *Nonlinearity*, **7**, 441.
- Rom-Kedar, V. (1995). *Chaos*, **5**, 385.
- Rom-Kedar, V. and G. M. Zaslavsky (1999). *Chaos*, **9**, 697.
- Rosenbluth, M., R. Z. Sagdeev, J. B. Taylor, and G. M. Zaslavsky (1966). *Nucl. Fusion*, **6**, 297.
- Sagdeev, R. Z. and G. M. Zaslavsky (1987). *Nuovo Cimento*, **97**, 119.
- Sagdeev, R. Z., D. A. Usikov, and G. M. Zaslavsky (1988). *'Nonlinear Physics: From the Pendulum to Turbulence and Chaos'*. Harwood Acad. Publ., New York.
- Saichev, A. I. and W. A. Woyczynski (1997). *'Distributions in the Physical and Engineering Sciences'*. Birkhäuser, Boston, Vol. 1.
- Saichev, A. I. and G. M. Zaslavsky (1997). *Chaos*, **7**, 753.
- Samko, S. G., A. A. Kilbas, and O. I. Marichev (1987). *Fractional Integrals and Derivatives and Their Applications*. Nauka i Tekhnika, Minsk. Translation by Harwood Academic Publ., Schur, 1993.
- Sapoval, B., Th. Gobron, and A. Margolina (1991). *Phys. Rev. Lett.*, **67**, 2974.
- Shannon, C. E. (1960). in *'Information and Decision Processes'*, Ed. R. Machol. McGraw-Hill, New York, p. 93.
- Schertzer, D., M. Larcheveque, J. Duan, V. V. Yanovsky, and S. Lovejoy (2001). *J. Math. Phys.*, **42**, 200.
- Schrödinger, E. (1944). *'What is Life?'*. Cambridge University Press, Cambridge.
- Schwägerl, M., and J. Krug (1991). *Physica*, **D 52**, 143.
- Senechal, M. (1995). *'Quasi-Crystals and Geometry'*. Cambridge University Press, Cambridge.
- Shechtman, D., I. Blech, K. Gratias, and J. W. Cahn (1984). *Phys. Rev. Lett.*, **53**, 1951.
- Shlesinger, M. F. (1988). *Annu. Rev. Phys. Chem.*, **39**, 269.
- Shlesinger, M. F. and B. D. Hughes (1981). *Physica*, **A 109**, 597.
- Shlesinger, M. F., B. D. Hughes, and E. W. Montroll (1981). in *'6th International Symposium On Noise in Physical Systems'*, Eds. R. Meijer, R. Mountain, R. Soulen. *National Bureau of Stand. Pub.* **61**, 18.
- Shlesinger, M. F. and J. Klafter (1989). *J. Phys. Chem.*, **93**, 7023.
- Shlesinger, M. F. and B. J. West (1991). *Phys. Rev. Lett.*, **67**, 2106.
- Shlesinger, M. F., B. J. West, and J. Klafter (1987). *Phys. Rev. Lett.*, **58**, 1100.
- Shlesinger, M. F., G. M. Zaslavsky, and U. Frisch (1995a). *'Lévy Flights and Related Topics in Physics'*. Springer, Berlin.
- Shlesinger, M. F., J. Klafter, and G. Zumofen (1995b). *Fractals*, **3**, 491.
- Shlesinger, M. F., G. M. Zaslavsky, and J. Klafter (1993). *Nature*, **363**, 31.
- Sinai, Ya. G. (1959). *Doklady Akad. Nauk SSSR*, **124**, 768.
- Sinai, Ya. G. (1961). *Soviet Math. Dokl.*, **2**, 106.

- Sinai, Ya. G. (1963). *Dokl. Akad. Nauk SSSR*, **153**, 1261 [Sov. Math. 4, 1818].
- Sinai, Ya. G. (1966). *Izvestia Akad. Nauk SSSR, Math.*, **30**, 15.
- Sinai, Ya. G. (1970). *Russ. Math. Surv.*, **25**, 137.
- Sinai, Ya. G. and K. M. Khanin (1992). *Funct. Anal. Appl.*, **26**, 155.
- Sinai, Ya. G. (1994). '*Topics in Ergodic Theory*'. Princeton University Press, Princeton.
- Smoluchowski, M. V. (1912). *Phys. Zeits.*, **13**, 1069.
- Smoluchowski, M. V. (1913). *Phys. Zeits.*, **14**, 261.
- Smoluchowski, M. V. (1915). *Wien. Ber.*, **124**, 339.
- Sornette, D. (1998). *Phys. Rep.*, **297**, 239.
- Suzuki, M. (1983). *Progr. Theor. Phys.*, **69**, 65.
- Takens, F. (1983). in '*Distinguishing Deterministic and Random Systems*', Eds. G. I. Barenblatt, G. Ioss, and D. D. Joseph. Pittman, New York, p. 314.
- Taylor, J. B. (1969). *Culham Lab. Prog. Report CLM-PR-12*.
- Tikhomirov, V. M. (1963). *Uspekhi Mat. Nauk*, **18**, 55.
- Treschev, D. V. (1996). *Chaos*, **6**, 6.
- Treschev, D. V. (1997). *Physica*, **D 116**, 21.
- Treschev, D. V. (2002). *J. Nonlin. Sci.*, **12**, 27.
- Turaev, D. and V. Rom-Kedar (1998). *Non-linearity*, **11**, 575.
- Uchaikin, V. V. and V. M. Zolotarev (1999). '*Chance and Stability*'. VSP, Utrecht.
- Uchaikin, V. V. (2000). *J. Theor. Phys.*, **39**, 2087.
- Uchaikin, V. V. (2003). *JETP*, **97**, 810.
- Ulam, S. M. (1961). '*Proceedings of the Fourth Berkeley Symposium on Mathematical Statistics and Probability*', **3**, 315 (Berkeley, Los Angeles).
- Vedenov, A. A., E. P. Velikhov, and R. Z. Sagdeev (1961). *Nucl. Fusion*, **1**, 82.
- Weiss, G. H. (1994). '*Aspects and Applications of the Random Walk*'. North-Holland, Amsterdam.
- Weitzner, H. and G. M. Zaslavsky (2001). *Chaos*, **11**, 384.
- Weitzner, H. and G. M. Zaslavsky (2003). *Comm. Nonlinear Sci. and Numerical Simulation*, **8**, 273.
- West, B. J., M. Bologna, and P. Grigolini (2000). '*Physics of Fractal Operators*'. Springer, New York.
- West, B. J. and P. Grigolini (2000). in '*Applications of Fractional Calculus in Physics*', Ed. R. Hilfer. World Scientific, Singapore, p. 171.
- Weyl, H. (1952). '*Symmetry*'. Princeton University Press, New Jersey.
- White, R. B., S. Benkadda, S. Kassibrakis, and G. M. Zaslavsky (1998). *Chaos*, **8**, 757.
- Wilson, K. and J. Kogut (1974). *Phys. Reports*, **12**, 75.
- Yanovsky, V. V., A. V. Chechkin, D. Schertzer, and A. V. Tur (2000). *Physica*, **A 282**, 13.
- Young, L.-S. (1995). in '*Real and Complex Dynamics*', Eds. Branner and Hjorth. Kluwer, p. 293.
- Young, L.-S. (1998a). *Ann. Math.*, **147**, 585.



- Young, L.-S. (1998b). *Notices Amer. Math. Society*, **45**, 1318.
- Young, L.-S. (2002). *J. Stat. Phys.*, **108**, 733.
- Young, L.-S. (2003). In ‘*Entropy*’, Eds. A. Greven, G. Keller, and G. Warnecke. p. 313.
- Young, W., A. Pumir, and Y. Pomeau (1989). *Phys. Fluids*, **A 1**, 462.
- Zacherl, A., T. Geisel, and J. Nierwetberg (1986). *Phys. Lett.*, **A 114**, 317.
- Zaks, M. A., A. S. Pikovsky, and J. Kurths (1996). *Phys. Rev. Lett.*, **77**, 1996.
- Zaks, M. A. and A. V. Straube (2002). *Phys. Rev. Lett.*, **89**, 244101.
- Zaslavsky, G. M. and B. V. Chirikov (1964). *Doklady Akad. Nauk SSSR*, **159**, 306 (Translation: *Sov. Phys. Dokl.* 9, **989**, 1965).
- Zaslavsky, G. M. and R. Z. Sagdeev (1967). *Sov. Phys. JETP*, **25**, 718.
- Zaslavsky, G. M. and N. N. Filonenko (1968). *Sov. Phys. JETP*, **25**, 851.
- Zaslavsky, G. M. (1970). *Statistical Irreversibility in Nonlinear Systems* (in Russian). Nauka, Moscow. Translated by UKAEA Culham Laboratory, 1976, reprint CTO/1048.
- Zaslavsky, G. M. and B. V. Chirikov (1972). *Sov. Phys. Usp.*, **14**, 549.
- Zaslavsky, G. M. (1981). *Phys. Reports*, **80**, 157.
- Zaslavsky, G. M. (1985). ‘*Chaos in Dynamic Systems*’. Harwood Acad. Publ., Amsterdam.
- Zaslavsky, G. M., M. Yu. Zakharov, R. Z. Sagdeev, D. A. Usikov, and A. A. Chernikov (1986). *Sov. Phys. JETP*, **64**, 294.
- Zaslavsky, G. M., R. Z. Sagdeev, and A. A. Chernikov (1988). *JETP*, **67**, 270.
- Zaslavsky, G. M., M. Yu. Zakharov, A. I. Neishtadt, R. Z. Sagdeev, D. A. Usikov, and A. A. Chernikov (1989). *Sov. Phys. JETP*, **69**, 1563.
- Zaslavsky, G. M., R. Z. Sagdeev, D. A. Usikov, and A. A. Chernikov (1991). *Weak Chaos and Quasi-regular Patterns*. Cambridge University Press, Cambridge.
- Zaslavsky, G. M. (1992). in ‘*Topological Aspects of the Dynamics of Fluids and Plasmas*’, Eds. H. K. Moffatt, G. M. Zaslavsky, P. Comte, and M. Tabor. Kluwer, Dordrecht, p. 481.
- Zaslavsky, G. M., D. Stevens, and H. Weitzner (1993). *Phys. Rev.*, **E 48**, 1683.
- Zaslavsky, G. M. (1994a). *Physica*, **D 76**, 110.
- Zaslavsky, G. M. (1994b). *Chaos*, **4**, 25.
- Zaslavsky, G. M. (1994c). *Chaos*, **4**, 589.
- Zaslavsky, G. M. (1995). *Chaos*, **5**, 653.
- Zaslavsky, G. M. and S. S. Abdullaev (1995). *Phys. Rev.*, **E 51**, 3901.
- Zaslavsky, G. M. and M. Edelman (1997). *Phys. Rev.*, **E 56**, 5310.
- Zaslavsky, G. M. and S. S. Abdullaev (1997). *Chaos*, **7**, 182.
- Zaslavsky, G. M. and B. Niyazov (1997). *Phys. Rep.*, **283**, 73.
- Zaslavsky, G. M., M. Edelman, and B. Niyazov (1997). *Chaos*, **7**, 159.
- Zaslavsky, G. M. (1998). ‘*Physics of Chaos in Hamiltonian Systems*’. Imperial College Press, London.
- Zaslavsky, G. M. (1999). *Physics Today*, **52**, 39.
- Zaslavsky, G. M. and M. Edelman (2000). *Chaos*, **10**, 135.

- Zaslavsky, G. M. (2000a). in ‘*Application of Fractional Calculus in Physics*’, Ed. R. Hilfer. World Scientific, Singapore, p. 203.
- Zaslavsky, G. M. (2000b). *Physica*, **A 288**, 431.
- Zaslavsky, G. M. and M. Edelman (2001). *Chaos*, **11**, 295.
- Zaslavsky, G. M. (2002a). *Physica*, **D 168–169**, 292.
- Zaslavsky, G. M. (2002b). *Physics Reports*, **371**, 461.
- Zaslavsky, G. M. and M. Edelman (2003). in ‘*Perspectives and Problems in Nonlinear Science*’, Eds. E. Kaplan *et al.* Springer, New York, p. 421.
- Zaslavsky, G. M. and M. Edelman (2004). *Physica*, **D 193**, 128.
- Zermelo, E. (1896). *Ann. Phys.*, **57**, 485.
- Zolotarev, V. M. (1986). ‘*One-Dimensional Stable Distributions*’. American Mathematical Society, Providence, RI.
- Zolotarev, V. M. (1997). ‘*Modern Theory of Summation of Random Variables*’. VSP, Utrecht.
- Zolotarev, V. M., V. V. Uchaikin, and V. V. Saenko (1999). *JETP*, **88**, 780.
- Zorich, A. (1997). *Ergodic Theory and Dynamical Systems*, **17**, 1477.

*This page intentionally left blank*

# INDEX

- ABC-flow 20, 21
- ABC-flow, compressible 364
- Accelerator mode 147
- Accelerator mode island 141, 143, 145, 147
- Action 9, 24
- Action-angle variables 8, 24
- Advection 357, 373
- Anosov system 46, 54
- Arnold diffusion 97, 99, 122
- Asymptotics 183
- Asymptotics, intermediate 185
- Balance equation 262
- Ballistic mode 151
- Barrier, dynamical 153
- Beltrami flow 20, 357
- Bernoulli scaling 201, 240
- Billiard 142
- Billiard, Cassini 236
- Billiard, square-with-slit 290
- Billiard, Bunimovich 143, 189, 344
- Billiard, irrational 287
- Billiard, polygonal 287
- Billiard, rhombic 303
- Billiard, Sinai 58, 143, 188, 344
- Billiard, square-in-square 302
- Billiard, stadium 189
- Boltzmann 215
- Boltzmann H-theorem 214, 227, 341
- Boltzmann's comments 343
- Boundary layer, island 266
- Bowen theorem 178
- Canonical equations 3, 18, 20
- Cantor 152, 153
- Chaos, definition 53
- Chaos erasing 352
- Chaos of field lines 19, 21
- Chaos, strong 64
- Chaos, weak 97
- Chaotic dynamics, definition 37, 53
- Chirikov overlapping criteria 54
- Characteristic function 230, 232
- Coarse-graining 38, 48, 318
- Collision time 216
- Complexity 315, 316
- Complexity, directional 338, 340
- Complexity function 325
- Complexity function, flight 331
- Complexity function, local 326
- Complexity,  $(\epsilon, n)$ - 329
- Complexity,  $(\epsilon, t, s)$ - 331
- Complexity,  $\epsilon$ - 325
- Complexity, mixed 335
- Complexity, non-local 317
- Complexity, polynomial 289, 335
- Complexity, symbolic 317
- Complexity, topological 318
- Conservation, phase volume 5, 6
- Continued fraction 291
- Continued fractions, scaling 294
- Continuous time random walk (CTRW) 276, 279
- Contour, basic 24
- Cooling 352, 354
- Correlation, decay 40, 46
- Correlation, function 40
- Cover, finite 318
- Cover, minimal 318
- Critical exponents 209, 249, 253, 258
- Crystal, aperiodic 122
- CTRW 276, 279
- Cycle, Poincaré 173, 178
- Cycle, quasi- 178
- Decoration 114
- Degeneracy 33
- Derivative, Caputo 397
- Derivative, fractional 396, 397
- Derivative, Riemann–Liouville 397
- Derivative, Riesz 284, 398
- Detailed balance principle 220, 248
- Difference, finite 397
- Diffusion anomalous 251
- Diffusion coefficient 219
- Diffusion equation 219
- Diffusion, Rechester–White 225
- Diffusion time 216
- Dimension, box 160
- Dimension, complex 169

- Dimension, correlation 166
- Dimension, directional 338
- Dimension, fractal 161
- Dimension, generalized fractal 161
- Dimension, Hausdorff 160
- Dimension, multifractal 164
- Dimension, Renyi 165
- Dimension spectral function 164, 268
- Distinguishable trajectories,  $(\epsilon, t)$  327
- Distribution function 37
- Distribution function, coarse-grained 179
- Distribution, truncated 226
- Divergence,  $\epsilon$ - 328
- Duality of dynamics 265
- Dynamical barrier 153
- Dynamical cooling 352, 354
- Elliptic point 8, 130
- Ensemble average 40
- Entropy 48, 53
- Entropy function 333
- Entropy function,  $(\epsilon, t, s)$ - 334
- Entropy function, directional 338
- Entropy, Boltzmann's 222, 223
- Entropy, directional 338
- Entropy, information 166
- Entropy, Kolmogorov–Sinai (KS) 49, 50
- Entropy, topological 51, 320
- Entropy, metric 50, 320
- Equation, Fokker–Plank–Kolmogorov (FPK) 217
- Equation, FFPK 245, 248
- Equation, Montroll–Weiss 278
- Ergodic layer 78
- Ergodic, theorem 352
- Ergodicity 39, 352
- Escape time 155, 193
- Exit time 193
- Exponent, transport 196
- Exponent, critical 249, 253, 258
- Exponent, recurrence 177
- Feller theorems 234
- Field lines 18
- Finite horizon 303, 305
- Five-fold symmetry 102, 110, 112, 117, 119, 120
- Flight 239, 295
- Flight complexity function 331
- Flight length 331
- Flight, Lévy 235
- Flights, parabolic 237
- Flow, compressible ABC- 364
- Fluctuation, immence 351
- Fluctuations, persistent 41, 351
- Fractal Brownian motion 282
- Fractal dimensions 160
- Fractal, Koch 171, 306
- Fractality 159
- Fractal time 201
- Fractional derivative 397
- Fractional difference 397
- Fractional integration by parts 399
- Fractional integro-differentiation 396
- Fractional kinetic equation (FKE) 245, 273, 279
- Fractional kinetic equation, solutions 273
- Fractional kinetics (FK) 245, 296
- Frequency of oscillations 24
- Function, Mittag–Leffler 400
- Generating function 8, 369
- Granular structure 303
- H-theorem 223, 227
- Hamiltonian 3, 20
- Hamiltonian, averaged 104, 129
- Hamiltonian, equation 3
- Hamiltonian, quadratic 10
- Hamiltonian system, generalized 18
- Helical flow 357
- Helical flow, compressible 359
- Heteroclinic structure 77, 79
- Homoclinic structure 77, 79, 267
- Hyperbolic point 9, 130
- Hyperbolic system 46
- Incompressibility 619
- Increment, instability 42
- Indistinguishable trajectories,  $(\epsilon, t)$  326
- Indistinguishable trajectories,  $\epsilon$ - 319, 326
- Information entropy 166
- Instability, local 42
- Integrability 26
- Integrability, complete 26
- Interaction of resonances 55, 73
- Interval exchange transform (IET) 289
- Invariants of motion 23
- Invariant surfaces 24
- Irrational trajectory 291
- Irreversibility 215, 219
- Island, tangled 145
- Islands 29, 140
- Islands, accelerator mode 145
- Islands, ballistic mode 151
- Islands, hierarchy 190, 192
- Isolines 105, 107
- Isolines, thick 107, 117

- Jacobian matrix 43, 63
- Jet 387
- Kac lemma 174, 234
- KAM-theory 3, 32, 125
- KAM-tori 133, 135
- Kinetics, multifractional 267
- Koch island 171
- Kolmogorov condition 219, 223, 248
- Kozlov condition 26, 27
- Lagrangian turbulence 357, 370
- Landau–Lifshits equation 17
- Lévy distribution 230
- Lévy flight 229, 235
- Lévy index 231
- Lévy process 229, 231
- Lévy walks 279
- Liouville equation 6, 215
- Liouville–Arnold theorem 23, 26
- Log-periodicity 169, 243, 263, 297, 299
- Lorentz gas 144
- Lorentz gas, generalized (GLG) 287
- Lyapunov exponent 43, 53
- Lyapunov exponent, zero 287
- Lyapunov number 43
- Magnetic moments dynamics 17
- Map, Arnold cat 45
- Map, Chirikov–Taylor 61
- Map, Kepler 68, 69
- Map, Poincaré 58
- Map, saw-tooth 306
- Map, separatrix 76
- Map, standard 61
- Map, universal 60
- Map, web 64, 65
- Map, Zeno 57
- Master equation 280
- Maxwell’s Demon 346, 350, 356
- Measure, natural 37
- Measure, physical 38
- Mellin transform 242
- Melnikov integral 78, 79, 85, 94
- Mittay–Leffler function 274, 400
- Mixing 39
- Mixing, weak 39, 41
- Moments, evolution 226, 250
- Moments, truncated 226
- Multifractal space-time 207
- Multifractal spectra 164
- Multifractal time 207
- Non-ergodicity, dynamics 189, 258
- Non-degeneracy condition 33, 99, 126
- Non-degeneracy, isoenergetic 33
- Non-integrable system 27
- Non-linearity parameter 32, 126
- Number of states 322
- Oscillator, kicked 64, 98
- Oscillators, coupled 91, 94
- Paradox, Loschmidt 343
- Paradox, reversibility 343
- Paradox, St Petersburg 201
- Paradox, Zermelo 186, 342
- Partitioning 48
- Patterns, ornamental 119
- Pendulum 13
- Pendulum, perturbed 73, 82, 126
- Periodic orbits 26
- Perturbation parameter 23
- Pesin formula 53
- Phase flow 5
- Phase portrait 6
- Phase volume 5
- Phase volume, enveloped 53
- Phyllotaxis 122
- Poisson bracket 4
- Polygon, rational 287
- Potential well, infinite 16
- Probability of  $\epsilon$ -divergence 328
- Pseudochaos 287
- Quasi-crystal, one-dimensional 107, 111, 123
- Quasi-symmetry 118
- Quasilinear theory 55
- Random phase approximation 226
- Random walk, continues time 276, 279
- Ray propagation 289
- Recurrences 173, 180
- Recurrences distribution 177
- Recurrences, Poincaré 173
- Recurrences, multifractal 204
- Recurrences time distribution 174, 179
- Recurrences time, mean 175, 179
- Renormalization 162, 189, 201
- Renormalization group (RG) 162
- Renormalization, discrete 263
- Renormalization group equation 203, 242
- Renormalization group, hidden 83, 88, 91
- Renormalization group of kinetics (RGK) 261
- Renormalization of resonances 89
- Renormalization transform 85, 162, 190, 195, 202

- Residence frequency 205
- Residence time 205
- Resonance 28, 29
- Resonance, condition 28, 29
- Resonance, non-linear 29
- Resonances interaction 55, 73
- Resonant, island 31
- Resonant, islands chain 32
- Riddling 308
- Riemann invariants 337
- Rotation number 152, 153
  
- Saddle point 9
- Saddle points distribution 107
- Scaling, space-time 261
- Scars 345
- Separation,  $(\epsilon, n)$  319, 330
- Separation,  $\Delta\Gamma$ - 322
- Separatrix 7, 13
- Separatrix destruction 77, 78
- Separatrix map 76, 77, 82
- Separatrix splitting 77
- Seven-fold symmetry 103, 113
- Sierpinski carpet 160
- Simulations, principles 257
- Singular zone 154
- Skeleton Hamiltonian 104
- Smoluchowski formula 177
- Space-time windows 250
- Spectral decomposition 10, 15, 25
- Spectrum 10
- Spectrum, Kepler problem 394
- Spectrum, multifractal 164
- Stationary point 7, 8
- Stickiness 183, 237
- Sticky domain 183
- Sticky islands hierarchy 184
- Sticky set 192, 238
- Stochastic jet 198
- Stochastic layer 61, 78, 81
- Stochastic layer width 80, 82
- Stochastic sea 63, 140
- Stochastic web 66, 97
- Stochastic web width 114, 134
- Stream function 20
- Streamlines 20
- Stretching condition 45
- Sub-symmetry 109
- Subdiffusion 251, 281
- Superdiffusion 251, 281
- Survival probability 181
- Symmetry, crystal 100
- Symmetry, pentagonal 111
- Symmetry, q- 110, 111
- Symmetry, q-fold 110, 111
- Symmetry, quasi-crystal 99
- Symmetry, seven-fold 103, 111, 113
  
- Targeting 185
- Tiling 111
- Tiling, chaos assisted 118
- Tiling, dynamical genetaror 111
- Tiling, seven-fold symmetric 113
- Tiling, brickwall 113
- Tiling, hexagonaly 113
- Tiling, Penrose 112
- Tiling, periodic (crystalline) 107
- Tiling, quasi-symmetric 111, 112
- Tiling, symmetric 112
- Time, correlation decay 40, 46
- Topological pressure 169
- Topological, transitivity 42
- Torus, invariant 24, 26
- Trajectory, irrational 291
- Trajectory, rational 291
- Transfer probability 218
- Transport 221, 250
- Transport exponent 196, 251
- Transport, anomalous 251, 335, 383
- Transport, anisotropic 284
- Transport, directional 284
- Transport, normal 221
- Trap 187, 189
- Trap, absolute 187
- Trap, dynamical 187
- Trap, hierarchical islands 189, 191
- Trap, net- 154
- Trap, quasi- 187
- Trap, stochastic layer 196
- Trapping time 181, 183
- Travelling wave 337
- Truncated distribution 225, 226
- Truncated momentum 226
  
- Vortices, point 373
- Vorticity center 375
- Vortices advection 373
- Vortices transport 386
  
- Wave guide 289
- Weak chaos 97
- Web, finite 135, 137
- Web, Arnold 97
- Web, infinite 66, 99

- Web, skeleton 98, 102
- Web, stochastic 66, 97
- Web, symmetry 100
- Web, with crystal symmetry 107
- Web, with quasi-crystal symmetry 107
- Web-tori 127, 135
- Weierstrass random walk (WRW)  
201, 240
- Weyl problem 118
- Windows, space and time 250